

Interpenetrating Polymer Networks

ADVANCES IN CHEMISTRY SERIES **239**

Interpenetrating Polymer Networks

D. Klempner, EDITOR
University of Detroit Mercy

L. H. Sperling, EDITOR
Lehigh University

L. A. Utracki, EDITOR
National Research Council

Developed from a symposium sponsored
by the Division of Polymeric Materials: Science and Engineering,
of the American Chemical Society,
at the Fourth Chemical Congress of North America
(202nd National Meeting of the American Chemical Society),
New York, New York,
August 25–30, 1991



American Chemical Society, Washington, DC 1994



Interpenetrating polymer networks

Library of Congress Cataloging-in-Publication Data

Interpenetrating polymer networks / Les Sperling, Daniel Klempner, L. A. Utracki.

p. cm.—(Advances in chemistry series; 239)

Includes bibliographical references and index.

ISBN 0-8412-2528-1

1. Polymer networks. I. Sperling, L. H. (Leslie Howard), 1932- .
II. Klempner, Daniel. III. Utracki, L. A. 1931- . IV. Series.

QD1.A355 no. 239


[QD328.P67]

540 s—dc20

[668.9]

93-23106

CIP

The paper used in this publication meets the minimum requirements of American National Standard for Information Sciences—Permanence of Paper for Printed Library Materials, ANSI Z39.48-1984. 

Copyright © 1994

American Chemical Society

All Rights Reserved. The appearance of the code at the bottom of the first page of each chapter in this volume indicates the copyright owner's consent that reprographic copies of the chapter may be made for personal or internal use or for the personal or internal use of specific clients. This consent is given on the condition, however, that the copier pay the stated per-copy fee through the Copyright Clearance Center, Inc., 27 Congress Street, Salem, MA 01970, for copying beyond that permitted by Sections 107 or 108 of the U.S. Copyright Law. This consent does not extend to copying or transmission by any means—graphic or electronic—for any other purpose, such as for general distribution, for advertising or promotional purposes, for creating a new collective work, for resale, or for information storage and retrieval systems. The copying fee for each chapter is indicated in the code at the bottom of the first page of the chapter.

The citation of trade names and/or names of manufacturers in this publication is not to be construed as an endorsement or as approval by ACS of the commercial products or services referenced herein; nor should the mere reference herein to any drawing, specification, chemical process, or other data be regarded as a license or as a conveyance of any right or permission to the holder, reader, or any other person or corporation, to manufacture, reproduce, use, or sell any patented invention or copyrighted work that may in any way be related thereto. Registered names, trademarks, etc., used in this publication, even without specific indication thereof, are not to be considered unprotected by law.

PRINTED IN THE UNITED STATES OF AMERICA

**American Chemical Society
Library**

**1155 16th St., N.W.
Washington, D.C. 20036**

1993 Advisory Board

Advances in Chemistry Series

M. Joan Comstock, *Series Editor*

V. Dean Adams

University of Nevada—Reno

Robert J. Alaimo

Procter & Gamble
Pharmaceuticals, Inc.

Mark Arnold

University of Iowa

David Baker

University of Tennessee

Arindam Bose

Pfizer Central Research

Robert F. Brady, Jr.

Naval Research Laboratory

Margaret A. Cavanaugh

National Science Foundation

Dennis W. Hess

Lehigh University

Hiroshi Ito

IBM Almaden Research Center

Madeleine M. Joullie

University of Pennsylvania

Gretchen S. Kohl

Dow-Corning Corporation

Bonnie Lawlor

Institute for Scientific Information

Douglas R. Lloyd

The University of Texas at Austin

Robert McGorin

Kraft General Foods

Julius J. Menn

Plant Sciences Institute,
U.S. Department of Agriculture

Vincent Pecoraro

University of Michigan

Marshall Phillips

Delmont Laboratories

George W. Roberts

North Carolina State University

A. Truman Schwartz

Macalaster College

John R. Shapley

University of Illinois
at Urbana-Champaign

L. Somasundaram

DuPont

Peter Willett

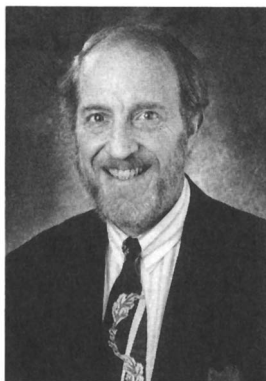
University of Sheffield (England)

FOREWORD

The ADVANCES IN CHEMISTRY SERIES was founded in 1949 by the American Chemical Society as an outlet for symposia and collections of data in special areas of topical interest that could not be accommodated in the Society's journals. It provides a medium for symposia that would otherwise be fragmented because their papers would be distributed among several journals or not published at all.

Papers are reviewed critically according to ACS editorial standards and receive the careful attention and processing characteristic of ACS publications. Volumes in the ADVANCES IN CHEMISTRY SERIES maintain the integrity of the symposia on which they are based; however, verbatim reproductions of previously published papers are not accepted. Papers may include reports of research as well as reviews, because symposia may embrace both types of presentation.

ABOUT THE EDITORS



DANIEL KLEMPNER is a professor of polymer chemistry and engineering at the University of Detroit Mercy; associate director of Polymer Technologies, Inc. (also known as the Polymer Institute), a subsidiary of the University of Detroit Mercy; and director of the university's Center of Excellence in Environmental Engineering and Science (CE³S) in Detroit, Michigan. He received his B.S. in chemistry from Rensselaer Polytechnic Institute in 1964, his M.S. in chemistry from Williams College in 1968, and his Ph.D. in physical chemistry from the State University of New York at Albany in 1970. From 1964 to 1968 he was an engineer for Sprague Electric Company, where he studied electrical properties of polymers. From 1970 to 1972 he was a visiting scientist in the polymer science and engineering program of the University of Massachusetts, where he carried out high-pressure X-ray studies on polymers. In 1972 he joined the faculty of the University of Detroit. He conducts extensive research in polymer science and engineering, focusing especially on interpenetrating polymer networks, polymer alloys, polyurethanes, structure-property relationships, high-temperature polymers, flammability of polymers, coatings, elastomers, foams, medical applications of polymers, and environmental studies on polymers. He has more than 120 publications, has written or authored 15 books, and holds several patents. His research is heavily supported by federal and industrial grants and contracts. He is an active consultant for industry and the legal profession.

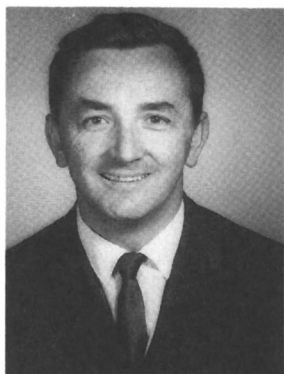


L. H. SPERLING serves an interdisciplinary role at Lehigh University, being a member of both the Chemical Engineering Department and the Materials Science and Engineering Department. He serves as director of the Engineering Polymers Laboratory of the Materials Research Center, is chairman of the Polymer Education Committee of the Center for Polymer Science and Engineering, and is also a member of the Polymer Interfaces Center.

Sperling has conducted research in the field of interpenetrating polymer networks since arriving at Lehigh University in 1967, and he also has broad interests in physical polymer science, especially in the areas of polymer chain diffusion, film formation, and the molecular aspects of fracture in plastics. Other recent areas of research include sound and vibration damping with polymers and IPNs, the use of triglyceride oils in IPNs, and the general area of renewable resources. This is the ninth book he has written or edited. In addition, he has written some 250 scientific papers and holds five patents.

Sperling's teaching efforts include polymer blends and composites, physical polymer science, and a range of other chemical engineering and materials areas. In addition, he has offered a number of short course programs, both in the United States and in Europe.

Sperling was a Ph.D. student of W. R. Krigbaum at Duke University and a postdoctoral research associate of A. V. Tobolsky at Princeton University before joining Lehigh University. He also was employed by Buckeye Cellulose Corporation in Memphis, Tennessee from 1958 to 1965. In addition to his efforts in polymers, Sperling is active in the American Wine Society and has published a number of works on wine making, especially in the area of fruit wine making.



L. A. UTRACKI is a senior research officer and past head of the Industrial Polymers Section of the National Research Council of Canada, Industrial Materials Institute in Montreal. He was born and educated (Chem.Eng., M.Eng., Dr.Sci., Privat Dozent/Doctorat d'Etat) in Poland and conducted postdoctoral work at the University of Southern California (1960–1962). Since 1968, he has worked at Shawinigan Chemicals, McGill University, and C.I.L. Inc. He is author of more than 300 technical papers, patents, books, and book chapters. His research activities cover thermodynamics, rheology, and polymer processing. He served as president of the Canadian Rheology Group and the Polymer Processing Society (International). He was member of the Society of Plastics Engineers EPSDIV board of directors. His name is listed in *American Men and Women of Science* and in *Who's Who in Science and Engineering*. Utracki organized the monograph book series *Progress in Polymer Processing* (published by the Polymer Processing Society) and served for three years as the series editor. He has been a member of several editorial boards, co-editor of *Current Topics in Polymer Science*, editor of *Polymer Blends and Networks*, and frequent guest editor of the Society of Plastics Engineers journals, *Polymer Composites* and *Polymer Engineering and Sciences*.

PREFACE

AT LEAST 20 INDUSTRIAL PRODUCTS have been publicly identified as containing interpenetrating polymer networks (IPNs). These products include such diverse materials as tough plastics, sound- and vibration-damping compounds, ion-exchange resins, artificial teeth, and burn dressings. As a composition of matter, the IPNs are younger cousins to polymer blends, blocks, and grafts, all members of the larger class of multicomponent polymer materials. Each of these materials is based on combinations of two or more polymers. In IPNs, the polymers are cross-linked. Most, but not all, of the multicomponent polymer materials are phase separated because of the very small entropy of mixing. Cross-linking of the polymers provides a mechanism for controlling domain sizes and shapes and also reduces creep and flow.

Although very much IPN research is (and should be) industrially oriented, a surprising fraction of the research is fundamental in nature, taking place in universities and research institutes. Thus, many of us have found that IPNs are a very fertile ground for graduate theses, which contribute basic information about the synthesis, gelation, morphology, mechanical behavior, permeability, and adhesive nature of these complex materials.

This book is the written record of the first international symposium devoted entirely to IPNs held at the joint meeting of the 4th Chemical Congress of North America and the American Chemical Society meeting. The IPN symposium, which ran for two and a half days, had an overflow participation, with papers also scheduled in the poster session. The big surprise to the organizers was the extent of the international participation, with papers submitted from France, Japan, Canada, Australia, the People's Republic of China, Belgium, Russia, Ukraine, Holland, Korea, England, Israel, and Poland as well as the United States.

There are many people and organizations to thank for making this book possible. The ACS Petroleum Research Fund, the Polymeric Materials: Science and Engineering Division of the ACS, Lehigh University, University of Detroit Mercy, and the National Research Council of Canada all contributed financially to the symposium. Although secretaries everywhere contributed to the production of the

manuscripts, special thanks is due to Virginia Newhard, who handled much of the extensive correspondence and mass mailings related to the symposium.

We dedicate this book to polymer scientists and engineers everywhere, who are building a most important interdisciplinary field for the betterment of humanity.

D. KLEMPNER
University of Detroit Mercy
Detroit, MI 48221

L. H. SPERLING
Lehigh University
Bethlehem, PA 18015

L. A. UTRACKI
National Research Council
Boucherville, Quebec, Canada J4B 6Y4

January 1993

Interpenetrating Polymer Networks: An Overview

L. H. Sperling

Department of Chemical Engineering, Department of Materials Science and Engineering, Center for Polymer Science and Engineering, Materials Research Center Whitaker Laboratory 5, Lehigh University, Bethlehem, PA 18015

Interpenetrating polymer networks (IPNs) are combinations of two or more network polymers, synthesized in juxtaposition. Several methods of synthesis, particularly sequential IPNs and simultaneous interpenetrating networks, are described. As with polymer blends, blocks, and grafts, phase separation takes place during polymerization, but the rules are different. Applications to the plastics and rubber industry are described, along with historical aspects.

INTERPENETRATING POLYMER NETWORKS (IPNs) are defined as a combination of two or more polymers in network form that are synthesized in juxtaposition. Thus, there is some type of “interpenetration.” However, the term interpenetrating polymer network was coined before current aspects of phase separation and morphology were understood. Now we know that most IPNs do not interpenetrate on a molecular scale; they may, however, form finely divided phases of only tens of nanometers in size. Many IPNs exhibit dual phase continuity, which means that two or more polymers in the system form phases that are continuous on a macroscopic scale.

When two or more polymers are mixed, the resulting composition can be called a multicomponent polymer material. There are several ways to mix two kinds of polymer molecules; see Figure 1. Simple mixing, as in an extruder, results in a polymer blend. If the chains are bonded together, graft or block copolymers result: Bonding between some portion of the backbone of polymer I and the end of polymer II, the result is called a graft copolymer; chains

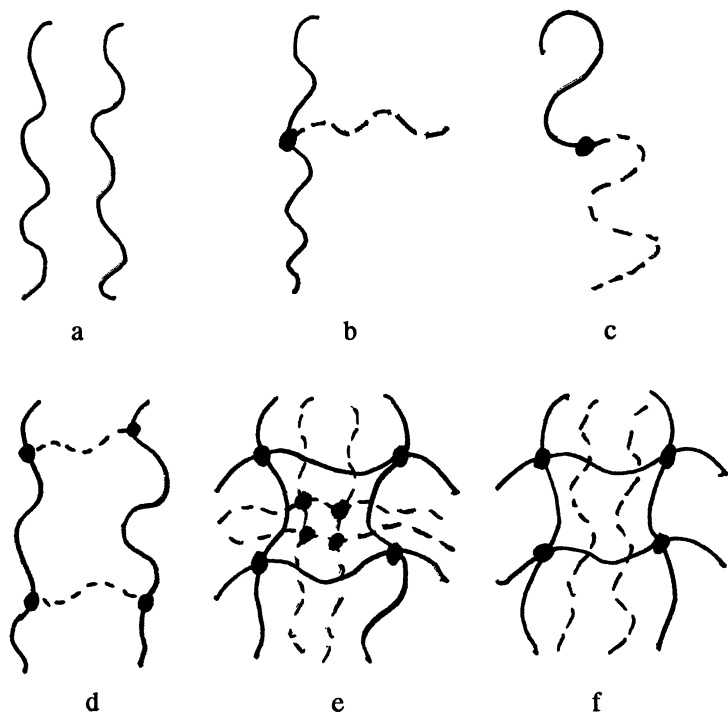


Figure 1. Six basic combinations of two polymers. *a*, Polymer blend, no bonding between chains; *b*, a graft copolymer; *c*, a block copolymer; *d*, an AB-graft copolymer; *e*, an IPN; *f*, a SIPN. Structures *a-c* are thermoplastic; structures *d-f* are thermoset.

bonded end to end result in block copolymers. Other types of copolymers include AB-cross-linked copolymers, where two polymers make up one network, and the IPNs, and semi-IPNs (SIPNs), which are the subject of this chapter and book.

In many ways, IPNs are related most closely to block copolymers. In the block copolymer systems, the length of the block determines the size of the domains. Correspondingly, the cross-link level (length of chain between cross-links) plays a major role in determining the domain size of IPNs. Short blocks or short chain segments between cross-links both make for small domains under many conditions. However, there are some important differences. Short block lengths are important because they increase miscibility between component polymers. For the case of IPNs, there is growing evidence that cross-links decrease the miscibility of the system relative to the corresponding blend, for systems in which the linear component polymers are miscible.

This chapter updates three earlier reviews of IPNs (1–3). Other recent major reviews include the book edited by Klempner and Frisch (4), the book

written by Lipatov and Sergeeva (5), and the book edited by Frisch and Klemperer (6). Although IPNs have been included in several recent symposia (7–11), this ACS symposium is the first major international symposium devoted entirely to IPNs. Until 1979, the total literature on IPNs consisted of about 125 papers and 75 patents (1). Presently, the annual production of papers and patents is at least these numbers. Although most of these papers and patents now recognize the IPN literature and use some IPN terminology, one objective of the present symposium and book is to encourage everyone to recognize the current status of IPN development. In addition, through the exchange in ideas only possible in a symposium (and book) of this type, the field will be encouraged to further growth.

Kinds of IPNs

IPNs can be made in many different ways. Brief definitions of some of the more important IPN materials are as follows (1):

- **Sequential IPN.** Polymer network I is made. Monomer II plus cross-linker and activator are swollen into network I and polymerized in situ; *see* Figure 2A. The sequential IPNs include many possible materials where the synthesis of one network follows the other.
- **Simultaneous interpenetrating network (SIN).** The monomers or prepolymers plus cross-linkers and activators of both networks are mixed. The reactions are carried out simultaneously, but by noninterfering reactions. An example involves chain and step polymerization kinetics; *see* Figure 2B.
- **Latex IPN.** The IPNs are made in the form of latexes, frequently with a core and shell structure. A variation is to mix two different latexes and then form a film, which cross-links both polymers. This variation is sometimes called an interpenetrating elastomer network (IEN).
- **Gradient IPN.** Gradient IPNs are materials in which the overall composition or cross-link density of the material varies from location to location on the macroscopic level. For example, a film can be made with network I predominantly on one surface, network II on the other surface, and a gradient in composition throughout the interior.
- **Thermoplastic IPN.** Thermoplastic IPN materials are hybrids between polymer blends and IPNs that involve physical cross-links rather than chemical cross-links. Thus, these materials flow at elevated temperatures, similar to the thermoplastic elastomers, and at use temperature, they are cross-linked and

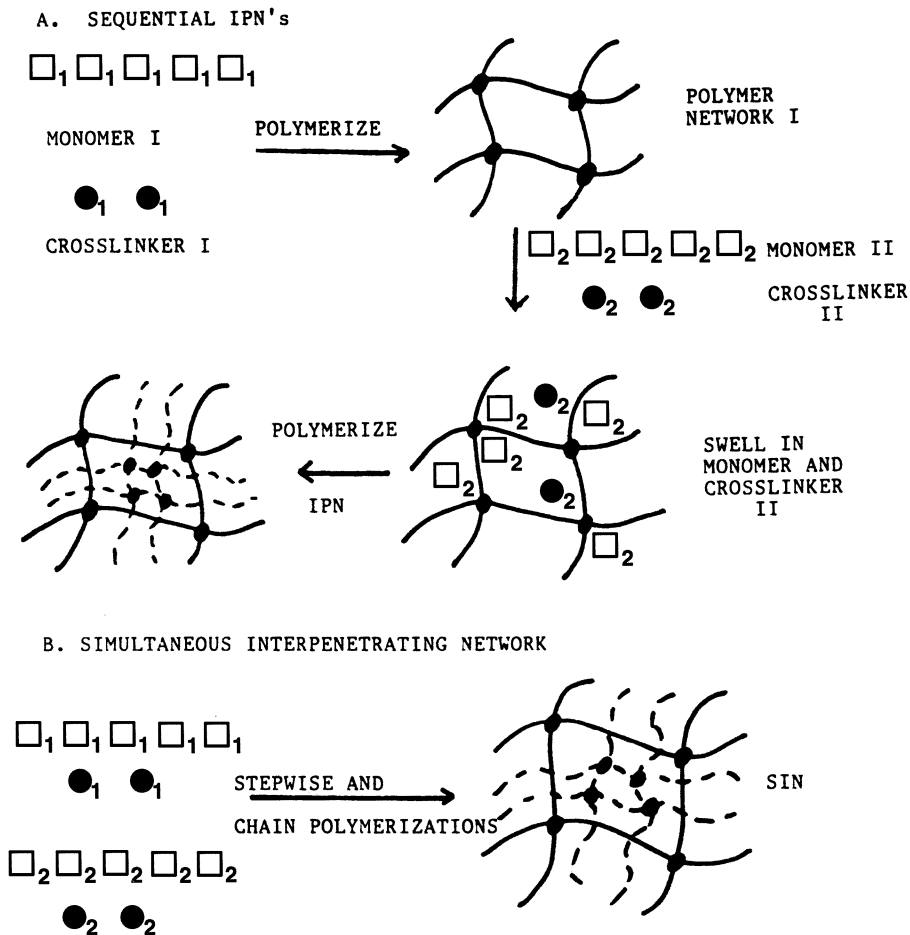


Figure 2. Basic synthesis methods for IPNs. A, Sequential IPNs; B, simultaneous interpenetrating polymer networks (SINs).

behave like IPNs. Types of cross-links include block copolymer morphologies, ionic groups, and semicrystallinity.

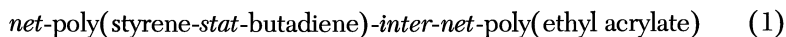
- **Semi-IPN.** Compositions in which one or more polymers are cross-linked and one or more polymers are linear or branched are semi-IPN (SIPN).

Although the preceding definitions are idealized and simple, many combinations may be envisioned that form the basis for a broad scientific as well as patent literature.

Nomenclature

At the present time, no organized, widely accepted nomenclature for IPNs exists. The IUPAC Commission on Macromolecular Nomenclature is addressing this issue. The following, in significant measure, is a summary of some of their proposed nomenclature, now in subcommittee (Mita, I.; Jenkins, A. D.; Kroschwitz, J. I.; Papisov, I. M.; Stepto, R. F. T.; Sperling, L. H., in preparation). Some of the suggested prefixes and connectives include *cyclo-* (cyclic), *star-* (starlike), *net-* (network), and *m-net-* (micronetwork). (I often used *cross-* for cross-linked.) *m-net-* includes internally cross-linked single macromolecules such as the globular proteins and gels that involve only a few chains. An example of a common network is *net*-polybutadiene, a network of polybutadiene. A careful distinction must be drawn between a cross-linked polymer—a polymer that contains cross-links (which may still be soluble)—and a polymer network, which is cross-linked so all of the chains in the macroscopic sample are bonded together (which is insoluble). Amazingly, up to now there is no IUPAC approved nomenclature for even simple cross-linked polymers.

For multipolymer assemblies, some proposed connectives include *-blend-* (polymer blend), *-inter-* (IPN), *-s-inter-* (SIPN), and *-compl-* (interpolymer complex). An interpolymer complex is defined as an assembly of two or more different polymers, the different molecules of which are held together by a cooperative system(s) of noncovalent intermolecular bonds. An example is poly(acrylic acid)-*compl*-poly(4-vinyl pyridine). The difference between interpolymer complexes and thermoplastic IPNs is that thermoplastic IPNs have two different polymers that are each independently physically cross-linked. An example of an IPN in the new nomenclature might be written



which is an IPN of a statistical copolymer of styrene and butadiene [perhaps styrene-butadiene rubber (SBR)] and cross-linked poly(ethyl acrylate). Note that connectives like *-stat-* (statistical copolymer), *-alt-* (alternating copolymer), and *-co-* (unspecified copolymer) are IUPAC recommended nomenclature (12, 13).

Literature Review. Are IPNs More or Less Miscible Than Blends?

Starting with the 1960s, several research groups discovered that if two immiscible polymers were formed into an IPN, the glass-transition temperatures of the two polymers were shifted inward (14, 15). This shift was interpreted as an increase in the miscibility of the two polymers caused by the presence of cross-links. This concept was extended by Sperling and co-

workers, who used the Fox equation for copolymers (treating each phase as a miscible copolymer system) to determine the composition of the two phases (16). At that time theory held that the cross-links in IPNs played a role similar to junction points in block copolymers in increasing the miscibility (17), although a quantitative theory was never developed.

Also, the size of the phase domains of IPNs was discovered to be smaller than expected for the corresponding blends; often on the order of 20–80 nm. The development of rather broad interphases between the two phases was noted and led to the observation that the two components were mixing over a 5–10-nm range. Thus, the shifts in the glass-transition temperature might have been caused by the interphase mixing rather than by thermodynamic changes.

At this time, whether an IPN forms a lower or an upper critical solution temperature phase diagram is unknown because no complete phase diagram for an IPN has ever been reported. Thus, the effect of temperature on IPN miscibility is unknown. This factor is important because, like many other polymer systems, polymerization is carried out at elevated temperatures and properties are measured at lower temperatures. Thus, if an IPN were more miscible at higher temperature, its nonequilibrium properties might be measured at some lower temperature and yield the apparent effect of increased miscibility.

IPNs undergo both nucleation and growth and spinodal decomposition kinetics of phase separation (18–21). Spinodal decomposition kinetics often predominates; see Figure 3 (22). The theory is described in a single paper by Binder and Frisch (23). Nucleation and growth kinetics tend to produce spheres of the second phase within the matrix of the first phase. These spheres grow by increasing their diameter. Spinodal decomposition tends to produce interconnected cylinders of the second phase within the matrix of the first phase. These cylinders grow by increasing their wave amplitude. Later, coarsening and coalescence may cause important changes. However, these changes may be impeded by cross-links, which keep the domains small. Provided gelation precedes phase separation during polymerization, phase separation might be restricted by the cross-links for both kinetic methods, which increases apparent miscibility.

Note that all of the compositions that exhibit inward glass-transition temperature shifts were immiscible in both the blend and IPN states. The only conclusion drawn (very tentatively and perhaps erroneously) under these circumstances was that a better dispersion was achieved in the IPN than in the blend.

In the 1980s, quite a different approach was taken because the thermodynamic requirements for polymer–polymer miscibility were much better understood and a number of miscible polymer pairs had been investigated. Naturally, a comparison of the miscibility of IPNs with the miscibility of the blends was of interest. This time, the comparison started with compositions

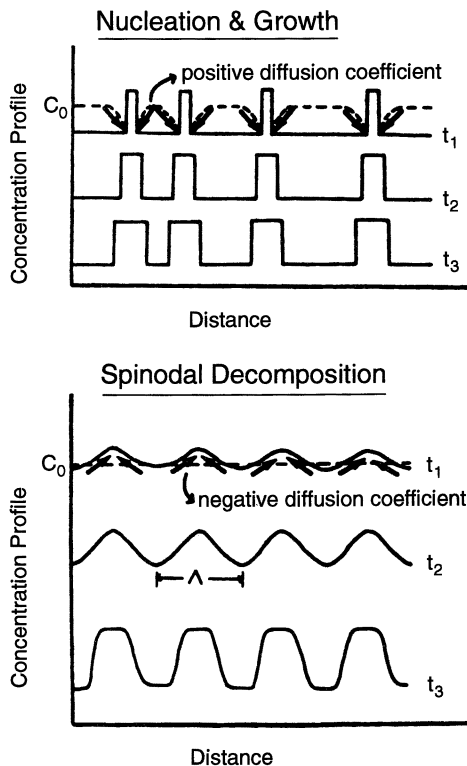


Figure 3. Illustration of the kinetic mechanisms of phase domain formation. (Reproduced with permission from reference 37. Copyright 1988 VCH Publishers, Inc.)

that were known to be miscible in the blend. The results of a comparison of six systems are shown in Table I.

In system 1, polystyrene-H-*inter-net*-polystyrene-D semi-II IPNs were studied by small-angle neutron scattering (SANS) (25). The H stands for natural hydrogen (ordinary) material and the D stands for deuterated material. Because deuterium scatters differently than hydrogen, it serves as a probe material. The reasons for immiscibility of the IPN were (1) a positive thermodynamic, binary interaction parameter, χ , value (which leads to phase separation in the blends at 8×10^5 g/mol in the blend) and (2) an unfavorable contribution to the free energy from the elastic stretching of the first-formed portion of the network. This system is actually a three-dimensional rubber elasticity problem, where the chains have fewer conformations available than if they were formed in the relaxed state.

The second reason for immiscibility is particular to networks. All networks formed under conditions where the first-formed polymer is soluble in

Table I. IPN Miscibility

No.	System	Method of Measurement ^a	Blend Miscibility	IPN Miscibility	Comments	Ref.
1.	Linear PSH-cross-PSD semi-II Phenolic-EVA copolymer	SANS	Miscible to 8×10^5 g/mol	Miscible to 3×10^5 – 4×10^4 or 4×10^4 – 1×10^4 g/mol	Semi-II IPN somewhat less miscible	24, 25
2.		FTIR ^a (EVA carbonyl)	Single phase	Cross-linking phenolic leads to phase separation	IPN less miscible	28
3.	Cross-PSD-linear PVME semi-II	SANS	Single phase	Moderately cross-linked PSD and above phase separate	IPN less miscible	29
4.	PSD-PVME cross-linked and grafted by γ -radiation	SANS	Single phase	Spinodal temperature increases from 140 to 430 °C with 125 Mrad	IPN-Graft more miscible	30
5.	PPO-PS blends, SIPNs, and IPNs	DSC, DMS, and TEM	Single phase	Single phase	All compositions miscible	32
6.	PVME-PS sequential IPNs	DSC, DMS	Single phase	Mid-range compositions phase separate	IPNs less miscible	31

^a SANS, small-angle neutron scattering; FTIR, Fourier transform IR spectroscopy; DSC, differential scanning calorimetry; DMS, dynamic mechanical spectroscopy; TEM, transmission electron microscopy.

the remaining monomer will be subject to some elastic deformation. There is some basis for concluding that the first-formed polymer in a single network is different from that formed later; frequently the first-formed polymer behaves as if it were more continuous in space (26, 27). All SINs as well as IPNs are subject to this unfavorable contribution to the free energy; thus, all such compositions of matter will have one term that opposes mixing and that is absent in the corresponding blend.

For system 2, Coleman et al. (28) comment that partial segregation based on a fractionation of molecular weights takes place. Ethylene-vinyl acetate (EVA) prefers to associate with the lower end of the resole molecular weight distribution for a more favorable entropic contribution. This association leads to a more or less pure phenolic phase and a mixed resole-EVA phase.

Systems 3, 4, and 6 (29–31) all describe systems of poly(vinyl methyl ether) (PVME) and polystyrene. Whereas system 3 is a semi-II IPN, the radiation cross-linked system 4 has presumably equal numbers of grafts and cross-links. Interestingly, system 4 is the only modern study to show the IPN as more miscible than the blend. Both systems 3 and 6 show that the IPN is less miscible, as do the other studies, where applicable. Perhaps the grafts contribute to the increased miscibility. In this way, graft copolymers would be expected to behave like block copolymers. System 4 was cross-linked after polymerization, and thus does not suffer from the unfavorable contribution to the free energy caused by rubber elastic forces.

System 5 (32) is based on poly(2,6-dimethyl phenylene ether) (PPE) and polystyrene and is one of the most miscible of the polymer blends from a thermodynamic point of view. In this case, the IPN as well as both SIPNs were found to be miscible.

The overall conclusion from these studies is that IPNs may be less miscible (and certainly less homogeneous) than the corresponding blends. Each of these blends is miscible, whereas those studied in the 1970s were all immiscible. At this time, the two findings are not necessarily contradictory. The presence of cross-links may indeed cause small domains with large interphases; thus, some mixing occurs, whereas less mixing occurs in the blend. Whether this kind of mixing will eventually have a thermodynamic basis is unknown. If the polymer blend is miscible, the one identifiable special force toward demixing seems to be the rubber elasticity chain deformation contribution.

There is, however, an alternate approach. Work done by de Gennes (33) points out that AB-cross-linked polymers, described by system 4 in Table I, may be more miscible than corresponding blends because the chains must be extended to enable phase separation. Daoud et al. (34, 35) state that the behavior of the AB-cross-linked polymers should be very different from the SIPNs shown in Table I.

The case for full IPNs can be inferred to be more like that of the AB-cross-linked polymers. Both network chains must be extended (lower entropy) to enable phase separation. This theory assumes that phase separation takes place long after gelation, when the networks are already formed, or the equivalent, which is that the kinetics of phase separation are much slower than the kinetics of polymerization. If the reverse process is true, then the networks will tend to be less miscible than the corresponding blend, the cross-links holding the polymers apart.

Phase Diagrams for IPNs

So far, no complete phase diagram for an IPN has been published. Questions that might be asked include the effect of cross-link density and composition; each has a significant effect. However, a phase diagram implies thermodynamic equilibrium and should be independent of exact method of synthesis. What kinds of phase diagrams exist? Which kinds would be of interest?

Some of the better known types of phase diagram are shown in Figure 4. Most of the research on polymer-I–polymer-II phase diagrams has been temperature–composition diagrams where most polymer blends have been shown to exhibit lower critical solution temperatures; *see* Figure 4a. Another phase diagram of interest is the pressure–composition phase diagram, where hydrostatic pressure was applied during the polymerization. From a strict point of view, pressure should be maintained during the actual measurements, assuming equilibrium. However, final observations were all made at 1-atm pressure, assuming kinetic changes to be slow. Pressure–composition phase diagrams were investigated by Lee and Kim (36), who concluded that hydrostatic pressure up to 0.2 MPa during polymerization increased the miscibility of the final product. Thermodynamically, this means that the one-phase system is denser than the two-phase system because hydrostatic pressure causes a decrease in the volume, as is illustrated in Figure 4b.

However, the phase diagram most needed universally for polymer blends, blocks, grafts, and IPNs alike is the polymer-I–polymer-II–monomer-II system under isothermal and isobaric conditions, where monomer II is converted into polymer II; Figure 4d. Research to date on ternary phase diagrams for two polymers and the monomer of one of them is summarized in Table II (37). There is an excruciating need for more studies on this type of phase diagram. Schematically, the polymer-I–polymer-II–monomer-II diagram is identical to the polymer-I–polymer-II–solvent situation (Figure 4c). In this case, monomer II is the “solvent.” For SINs, two polymers and two monomers (or prepolymers) are simultaneously present, but in ever-changing concentration.

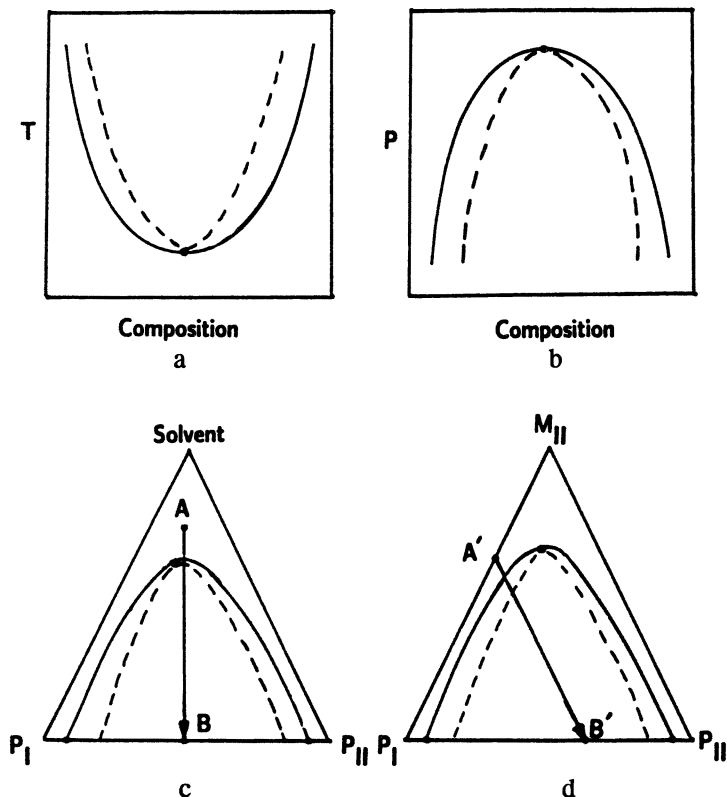


Figure 4. Phase diagrams for multicomponent polymer materials. *a*, Lower critical solution temperature; *b*, upper critical solution pressure; *c*, ternary phase diagram including a solvent undergoing evaporation from *A* to *B*; *d*, monomer II polymerizing from *A'* to *B'*. (Reproduced with permission from reference 13. Copyright 1992 John Wiley & Sons, Inc.)

Domain Shapes and Sizes

Polymerization of IPNs may result in four distinct stages of morphology development (18, 19). At first, monomer II may be soluble in polymer (or network) I. During this first stage of polymerization, polymer II also remains soluble. At this stage, the polymerizing system may be optically clear. As polymerization proceeds to stage 2, it suddenly clouds up, which indicates phase separation. This phase separation may be nucleation- and growth-controlled spheres; see Figure 5 (21). In stage 3 of continued polymerization, interconnected cylinders develop and increase in number during the latter stages of polymerization, indicative of spinodal decomposition. In stage 4, the

**Table II. Ternary Phase Diagrams
for Polymer I–Polymer II–Monomer II**

<i>Group</i>	<i>Institute</i>	<i>System</i>
Reiss et al. (38)	Ecole Nationale Superieure de Chimie de Mulhouse	Polybutadiene– polystyrene–styrene blocks and blends
Rosen et al. (39)	Carnegie Mellon University	Polybutadiene– polystyrene–styrene graft copolymers
Thompson et al. (40)	Univ. of Maine at Ontario	Poly(methyl methacrylate)– polystyrene–styrene blend
Lipatov et al. (18)	Academy of Science of the Ukrainian SSR	Poly(<i>n</i> -butyl acrylate)– polystyrene–styrene, semi-II IPN
Walsh et al. (41)	Imperial College	Poly(<i>n</i> -butyl acrylate)– poly(vinyl chloride)– vinyl chloride blend
Purvis et al. (42)	Rohm and Haas Co.	Polyurethane– poly(methyl methacrylate)– methyl methacrylate blend
Sperling et al. (22)	Lehigh University	Polybutadiene–polystyrene– styrene full IPN

SOURCE: Reproduced with permission from reference 37. Copyright 1988 VCH Publishers, Inc.)

morphology may become less distinct because the high viscosity of the system very significantly reduces diffusion toward the equilibrium state. The progress of morphology development shown in Figure 5 is modeled in Figure 6 (21).

The morphology of an IPN depends on the cross-linking level of networks I and II. There are several cases to consider; *see* Figure 7 (43). If there are no cross-links, a solution graft copolymer exists. If the solution is *stirred* during the polymerization, a phase inversion takes place. For the polybutadiene-*blend*-polystyrene system, high-impact polystyrene (HIPS) results (Figure 7, upper left). If the system is not stirred, it does not undergo phase inversion and polybutadiene remains the continuous phase (Figure 7, upper right).

If the polymers are cross-linked, there are several additional cases to be considered. First and most general, the following question must be asked: Did phase separation or gelation happen first? This question is particularly important for simultaneous interpenetrating networks. If phase separation occurs before gelation, then the phase domain sizes will tend to be large. When gelation finally occurs, it will tend to keep the domains apart. If gelation happens first, the presence of cross-links will tend to keep the domains much smaller. Here, spinodal coarsening and aging are suppressed. Obviously, if both polymers reach gelation at different times, further questions must be asked about the time sequence of events.

For the sequential IPNs, the presence of a cross-linked network I always guarantees that gelation happens before phase separation because (in the simplest case) gelation has happened before monomer II is added. Figure 7, middle left, illustrates a semi-I IPN, with the polybutadiene cross-linked. If only polymer II is cross-linked, then a quite different situation exists. Figure 7, middle right, shows a semi-II IPN in which phase separation preceded gelation of polymer II. Note the relationship between the upper right and middle right morphologies; both are coarse, polymer I is continuous, and polymer II is discontinuous.

For the full sequential IPNs, the domains are always finely divided. It was noted experimentally that increasing the cross-link density decreased the domain size. Here, the cross-link density on the lower right of Figure 7 is twice that of the lower left. Although the morphology as seen in these two

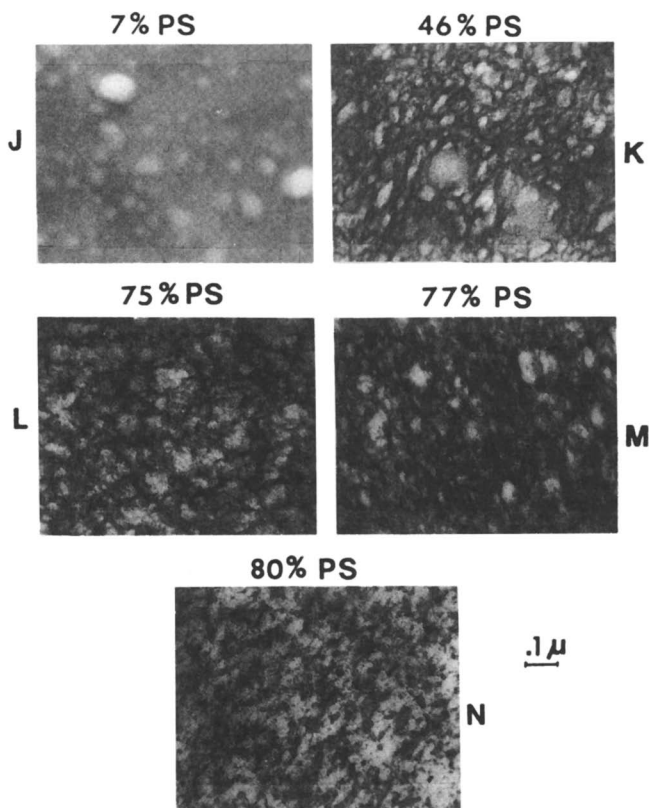


Figure 5. Transmission electron micrograph of a polymerizing polybutadiene-polystyrene IPN, as the polystyrene (PS) is being polymerized. Osmium tetroxide strains the polybutadiene. As the PS is formed, first spheres and then cylinders form, which indicates a change from nucleation and growth to spinodal decomposition kinetics; Figure 3. (Reproduced with permission from reference 21. Copyright 1984 A. M. Fernandez.)

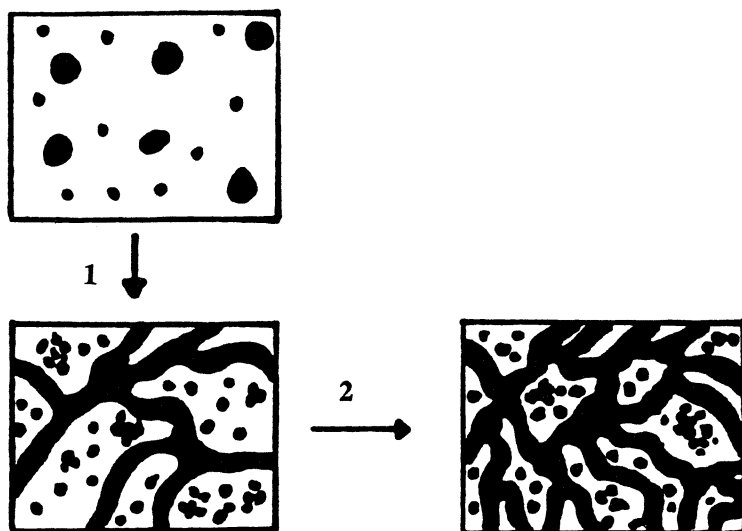


Figure 6. Model of the electron micrographs of Figure 5. (Reproduced with permission from reference 21. Copyright 1984 A. M. Fernandez.)

electron micrographs seems to be spheres of polystyrene in a matrix of polybutadiene, they are now thought to be interconnected cylinders; the “spherical” appearance is merely the cross-sectioning effects of thin slicing the material for transmission electron microscopy. Burford et al. (44) recently obtained direct evidence of the formation of cylinders in this system; see Figure 8.

Donatelli et al. (45) and Yeo et al. (46) derived equations for estimating the domain size in sequential IPNs. The domain diameter of polymer II, D_2 , is related to the interfacial tension, γ , the absolute temperature, T , the gas constant, R , and the concentration of effective network chains ν_1 and ν_2 , and the volume fractions v_1 and v_2 for networks I and II, respectively. The Donatelli equation may be written (47)

$$D_2 = \frac{2\gamma v_2}{RT\nu_1 v_1 \left[1/\nu_1^{2/3} - \frac{1}{2} \right]} \quad (2)$$

and the Yeo equation may be written

$$D_2 = \frac{4\gamma}{RT(A\nu_1 + B\nu_2)} \quad (3)$$

where

$$A = \frac{1}{2}(1/v_2)(3v_1^{1/3} - 3v_1^{4/3} - v_1 \ln v_1) \quad (4a)$$

and

$$B = \frac{1}{2}(\ln v_2 - 3v_2^{2/3} + 3) \quad (4b)$$

γ is related algebraically to the thermodynamic interaction parameter, χ_1 . The advantage of the Yeo equation is that the derivation removed some of the

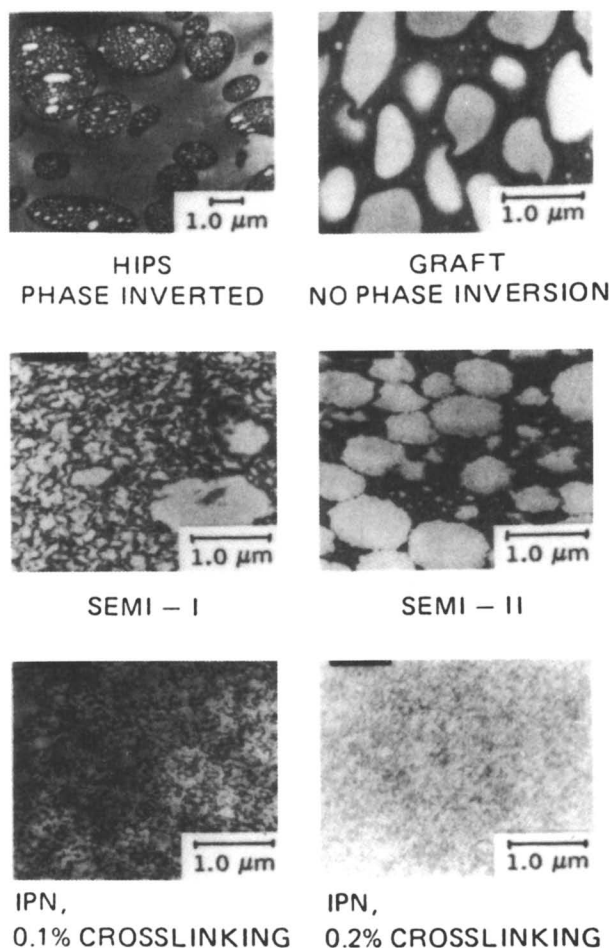


Figure 7. Six morphologies of polystyrene-SBR blends, SIPNs, and IPNs, as described in the text. (Reproduced from reference 43. Copyright 1976 American Chemical Society.)

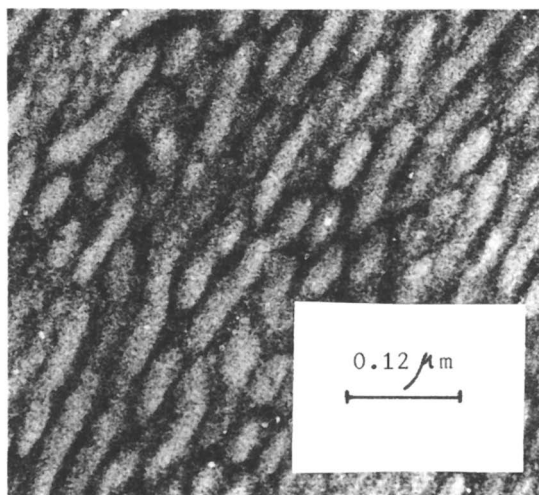


Figure 8. Transmission electron micrographs that show cylindrical structures. (Reproduced with permission from reference 44. Copyright 1979 Plenum Publishing Corp.)

approximations inherent in the Donatelli equation. Surprisingly, both equations give nearly the same numerical results for many systems of interest and both agree substantially with experimental results.

Both eqs 2 and 3 assume spheres of polymer II embedded in a continuous matrix of polymer I. As previously mentioned, current thought is that these spheres are really cylinders. Surprisingly, eqs 2 and 3 provide the approximate corresponding dimension of the cylinders.

The results of many investigations on sequential IPNs lead to the following generalizations:

1. Polymer I tends to be continuous in space for all compositions. Mid-range and high concentrations of polymer II tend to have dual phase continuity that is most likely interconnected cylinders for polymer II.
2. Phase separation probably proceeds through a brief period of nucleation and growth, followed by a region of spinodal decomposition.
3. Domain sizes vary from about 100 nm for highly immiscible systems to about 10 nm for microheterogeneous systems. For the purposes of eqs 1 and 2, immiscibility is defined as having large values of interfacial tension. Thermodynamically, γ can be related to the free energy of mixing.

4. The domain size decreases with increasing cross-link density. For many compositions, the effect is about 10 times as large for cross-links in network I as for network II.
5. For domains in the size range of 50–100 nm, a potential application is for tough or impact-resistant plastics. For domain sizes of about 10 nm, sound and vibration damping materials should be considered.

If the domains are 10–20 nm in size, they are actually smaller than the primary polymer chains that make up the system.

The morphology is as important for the development of good damping properties as it is important for the development of tough plastics. Dual phase continuity leads to an increase in the area under the loss modulus–temperature curve in the vicinity of the glass transitions (48). For very small domain sizes, only one broad glass transition is observed. For tough, impact-resistant plastics, where the domains are larger and the two polymers are better separated, two distinct glass transitions are often observed.

Supporting Evidence for Dual Phase Continuity. Dual phase continuity is defined as the continuity of both polymer I and polymer II domains throughout the macroscopic sample. In terms of spinodal decomposition concepts, the most usual physical situation is expected to be a system of interconnected cylinders of polymer II stretching through a matrix of polymer I.

We already showed direct evidence for the cylinders (or ellipsoids of revolution) in one case; *see* Figure 8. Supporting evidence comes from measurements of the modulus of these materials (43), which is much higher than would be expected for dispersed spheres. For example, 50% dispersed glassy spheres in a rubbery matrix raises the modulus only a factor of 2; this is a lower bound case based on the Takayanagi models. On the other hand, a 50:50 system with dual phase continuity is an upper bound case: The modulus is raised to half that of the glassy phase. Values close to the Takayanagi upper bound model were observed.

Co-Continuous Networks. The concept of co-continuous networks must be kept separate from the concept of dual phase continuity. Many (but not all) IPNs have co-continuous networks, which means that a Maxwell demon could traverse the entire macroscopic sample by stepping consecutively on the covalent bonds of either network. Such a system might be miscible or phase separated. If the system is phase separated, dual phase continuity might be true, but should not be implied. For example, single network chains of polymer II might traverse a polymer I phase and be

trapped mechanically. The shape of the polymer II domains might be spherical.

Although many IPNs have both co-continuous networks *and* dual phase continuity, researchers should assume neither case without experimental evidence.

Phase Inversion. Phase inversion is usually defined as a transposition of the continuous and discontinuous phases. Important aspects include the volume fraction, v , of each phase, and the viscosity, η , of each phase. Phase inversion requirements have been studied by Jordhamo et al. (49) and Paul and Barlow (50), and improved by Metelkin and Blecht (51). The simplest relationship can be written (49)

$$\frac{v_1}{v_2} \times \frac{\eta_2}{\eta_1} > 1 \quad \text{phase 1 continuous}$$

$$\approx 1 \quad \text{dual phase continuity or phase inversion}$$

$$< 1 \quad \text{phase 2 continuous}$$

where the subscripts 1 and 2 represent phases 1 and 2, respectively. Experimental data confirm the general relationship; see Figure 9 (49). Shearing is generally required to bring about a phase inversion. Quiescent systems rarely

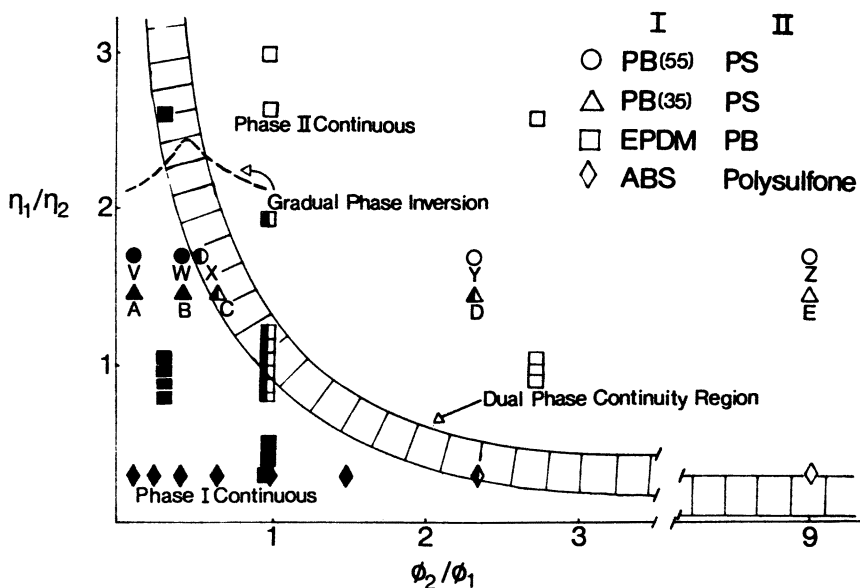


Figure 9. Phase continuity diagram for blends and IPNs undergoing phase inversion during polymerization, or under shear. (Reproduced with permission from reference 49. Copyright 1986.)

phase invert. Equation 5 is a relationship that holds at or near zero shear rate, and its validity is further limited to nearly equiviscous systems. More general relationships were recently presented by Utracki (52).

Phase inversion is most important for polymer blends, the so-called solution graft copolymers (HIPS is a key example), SINs, and the thermoplastic IPNs. In each of the important cases, a polymerization or cross-linking is in progress while the material is undergoing shear. For a number of industrial materials, especially the thermoplastic IPNs, one of the components is being cross-linked. The reaction is stopped when eq 3 equals 1, and dual phase continuity achieved.

Finally, the theoretical work of Termonia (53) indicates that network dominance in a sequential IPN is due to the lower extensibility of the first polymerized network for idealized networks.

Thermoplastic IPNs. The thermoplastic IPNs may undergo cross-linking, neutralization of ionic groups, or development of crystallinity during shear. Studies of some of the basic phenomena underlying phase inversion were investigated by Siegfried et al. (54). Siegfried et al. described a series of thermoplastic IPNs prepared from Kraton rubber, polystyrene-*block*-poly(ethylene-*stat*-butylene)-*block*-polystyrene (SEBS), and poly(styrene-*stat*-sodium methacrylate). These materials were called chemically blended thermoplastic IPNs because the styrene-methacrylic acid mix was swollen into the block copolymer and polymerized in situ. The corresponding mechanically blended system was made by separately synthesizing the two polymers and mechanically blending the two together later. In general, chemically blended and mechanically blended thermoplastic IPNs are expected to have different properties.

Davison and Gergen (55, 56) made mechanically blended thermoplastic IPNs from SEBS and polyamides, polyesters, or polycarbonates. These and other thermoplastic IPNs seem to have the very special property of dual phase continuity.

The most important commercial system involves ethylene-propylene-diene monomer (EPDM) in combination with isotactic polypropylene (PP). The EPDM is blended with the PP under conditions where the EPDM undergoes cross-linking through the diene moiety. The reaction is stopped when eq 5 equals unity. The result is a series of leathery materials that have great energy-absorbing capacity. End uses include automotive bumpers.

Table III (2) summarizes some of the patent literature concerning the EPDM-PP thermoplastic IPNs. Each patent represents a different approach to the same problem: how to achieve and control dual phase continuity.

This new class of IPN was invented by Fischer (57) in the early 1970s. Fischer blended *i*-PP and EPDM, and partly cross-linked the EPDM during the shearing action. The result is described in systems 1, 2, and 3 of Table III. These ideas were carried further by Coran and Patel (58-61) who

Table III. Polypropylene-EPDM or Polyethylene Thermoplastic IPN Patents

No.	Major Feature	Company	U.S. Patent No.
1.	EPDM precured then blended	Uniroyal	3,758,643
2.	EPDM blended then cured	Uniroyal	3,806,558
3.	EPDM of high molecular weight	Uniroyal	3,835,201
4.	Dynamically fully cured	Monsanto	4,130,535
5.	High ethylene length index (with PE)	Goodrich	4,046,840
6.	High ethylene sequence index (with PP)	Goodrich	4,036,912
7.	70-85% (by weight) of ethylene EPDM with dicyclopentadiene	Uniroyal	4,031,169
8.	Dual phase continuity	Exxon	4,132,698

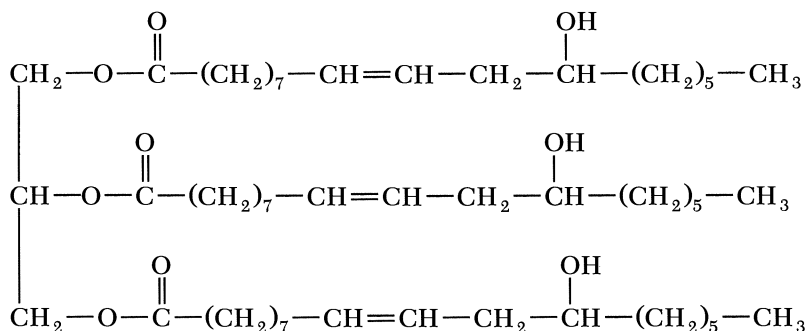
SOURCE: Reprinted from reference 2. Copyright 1986 American Chemical Society.

learned to prepare thermoplastic vulcanizates with the rubber completely cured; *see* Table III, system 4. If the EPDM is prepared with long ethylene sequences so that it crystallizes slightly, no cross-linking at all is required; *see* Table III, systems 5, 6, and 7. This thermoplastic IPN is based on two semicrystalline polymers. When both melt, the material flows. Dual phase continuity is emphasized in system 8.

Triglyceride Oil-Based IPNs

A brief description of the triglyceride-based IPNs will be given. As with many other IPN developments, a strong international character pervades the scene. All of the triglyceride oils are renewable resources. Castor oil is widely used commercially for paints and adhesives. Other oils derived from wild plants seem to offer unusual industrial and economic opportunities. The oil content of the seeds ranges from 30-45%, in the commercially acceptable range.

Research on castor oil-polystyrene IPNs began in 1974 as a cooperative research program between the Universidad Industrial de Santander, in Bucaramanga, Colombia, and Lehigh University in the United States. Castor oil is a triglyceride that has a hydroxyl group on each of its acid residues:



The hydroxyl group can be reacted to form urethanes or esters, and hence a polymer network. The glass-transition temperatures of castor oil polyesters are on the order of $-50\text{ }^{\circ}\text{C}$ (62). A series of tough plastics and reinforced elastomers was made. For demonstration purposes, a pair of shoe heels was fabricated in 1978 that has outlasted its leather sole counterparts.

This research was subsequently broadened to include lesquerella oil, a hydroxy-bearing oil plant native to Arizona, and vernonia oil, which contains oxirane (epoxy) groups and is native to Kenya and India. More importantly, many other laboratories began research on these IPNs. For example, a group long interested in vernonia oil is led by Dr. F. O. Ayorinde of Howard University (63). Research on castor oil-based IPNs has been carried out by Tan and Xie (64) and also Song and Donghua (65) in the People's Republic of China, Patel et al. (66) in India, and Liang et al. (67) in Taiwan.

Most recently, Dirlikov et al. (68) at Eastern Michigan University have become interested in vernonia oil as well. Dirlikov is interested in reactive diluents for high-solids coating formulations and for modification of epoxy resins. Barrett and Sperling (69) are making SIPNs of castor oil with poly(ethylene terephthalate) (PET) to increase the crystallization rate of the PET. The research to date has been reviewed recently (70).

The double bond in castor oil serves excellently in staining with osmium tetroxide for transmission electron microscopy; *see* Figure 10 (62). Here,

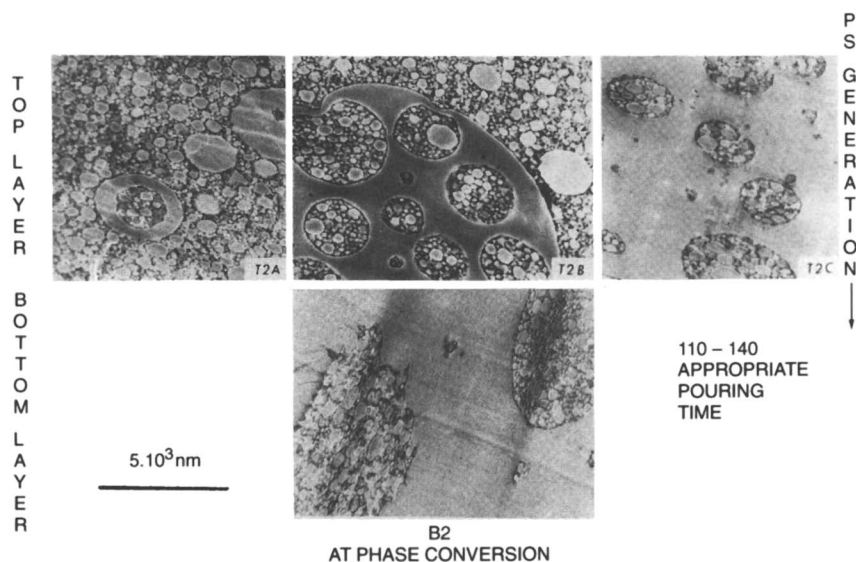


Figure 10. Castor oil-polyester-polystyrene SIN phase inversion. Osmium tetroxide stains the castor oil-rich phase. (Reproduced from reference 62. Copyright 1979 American Chemical Society.)

castor oil–polyester compositions are made into SINs with polystyrene. Figure 10 shows the phase inversion process that results in a continuous polystyrene phase and droplets of castor oil–polyester. Within the droplets of castor oil–polyester, however, there are smaller domains of polystyrene. These phase-within-a-phase-within-a-phase systems may be cylindrical in nature and may be formed through spinodal decomposition relatively late in the polymerization.

Sound and Vibration Damping with IPNs

Sound and vibration damping are important in the world today for the automotive industry, appliances, aircraft, tall buildings, and submarine technology. One of the most important methods of damping involves polymeric materials which are often in the glass-transition range (7).

There are two basic engineering mechanisms for the use of polymers in damping: extensional damping, where a polymer is placed as a free layer on a resonating vibrating system, and constrained layer damping, where a stiff material is placed on top of the polymer to increase the shearing action. Sometimes a simple sandwich arrangement is used, where two thin layers of sheet metal (the bread) have a thin layer of polymer between them (the jelly), which is very effective. Extensional dampers tend to work best when the polymer is at the low temperature (stiff) end of the glass-transition range, whereas constrained layer dampers tend to work best at the high-temperature (rubbery) end of the transition.

A simple example of constrained layer damping is for earthquake protection of tall buildings. Here, the girders are arranged with constrained layer damping sections. The frequency is low, generally below 1 Hz—the time to complete one back and forth sway of the entire building.

Why IPNs? Many IPNs exhibit a microheterogeneous morphology; *see* Figure 11. When the domains are on the order of 10–20 nm, the whole system is substantially all interphase material. Subsequently, the glass-transition temperature, T_g , tends to be very broad and stretches the range between the two polymers. Although other multicomponent materials can be made to do the same thing, it seems especially easy with IPNs. Using the time–temperature superposition principle, a broad temperature transition also means a broad active frequency range of damping. Such materials are excellent for outdoor applications, aircraft, and variable temperature machinery.

The number of IPN research teams interested in damping is astonishing; *see* Table IV (37). Table IV includes a commercial material (71), vinyl–phenolic, useful particularly at elevated temperatures.

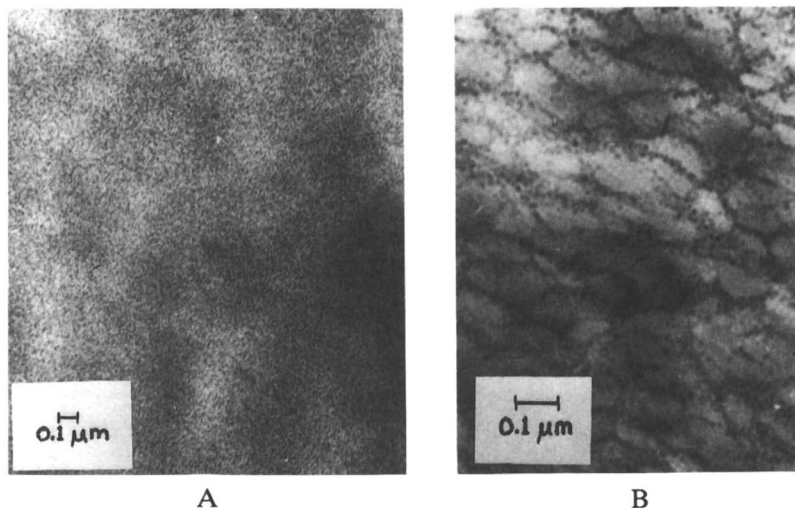


Figure 11. Two types of IPN phase domains. A, Microheterogeneous [poly(ethyl acrylate)-poly(methyl methacrylate)]; B, cellular structure [poly(ethyl acrylate)-polystyrene]. (Reproduced from reference 147. Copyright 1972 American Chemical Society.)

Damping Optimization. The measurement of damping effectiveness involves several terms: the storage modulus, E' , the loss modulus, E'' , and their ratio, $E''/E' = \tan \delta$. What is the definition of the best damper? Should it be the polymer with the highest $\tan \delta$ or E'' ? That question might be answerable if the engineering specification is for a monofrequency isotherm-temperature problem, which is rather rare in practice. To the extent that a range of frequencies and temperatures must be dealt with, broader (but controlled) widths of the glass-transition temperatures are required.

If indeed we are working with an IPN, (or other multicomponent polymer material) to broaden the transition, how shall success be determined? A recent discovery showed that the area under the loss modulus-temperature curves in the glass-transition region is controlled by the structure of the mer or mers and can be quantified through a group contribution analysis (7, 72-74, 98-101). This theory applies for one-phase systems such as homopolymers, statistical copolymers, and miscible or nearly miscible IPNs. The data were treated by plotting the linear loss modulus versus temperature and correcting for background, as shown in Figure 12 (100).

When the IPNs phase separate, however, aspects of morphology had to be considered (91). The loss area, LA, the area under the linear loss modulus-temperature curve, could be increased by proper morphology control; see Figure 13 (99). Dual phase continuity or large volumes of higher T_g

Table IV. Research Teams in the Area of Sound and Vibration Damping with IPNs

<i>Group</i>	<i>Institute</i>	<i>IPNs Studied^a</i>	<i>Ref.</i>
Sperling and Thomas	Lehigh University	Full, semi-, and filled IPNs based on acrylic polymers	72–81
Hourston	University of Lancaster	1. Polyurethane–acrylic polymer based on full and semi-SINs.	82–86
		2. poly(vinyl isobutyl ether)–poly(methyl acrylate)	87
		3. polyurethane–modified polyester-based semi-II SINs	88
		4. Latex IPNs based on acrylic polymers	89, 90
Fox	Naval Research Laboratory	Polyurethane/poly(<i>n</i> -butyl acrylate- <i>stat</i> - <i>n</i> -butyl methacrylate)-based IPNs and SINs	91
Klempner and Frisch	University of Detroit	Polyurethane–epoxy-based SINs	92
	University of Toronto	Polyurethane–epoxy-based semi-II SINs	93
Meyer	Louis Pasteur University	Polyurethane–poly(methyl methacrylate) semi- and full SINs	94, 95
Satgurunthan and Campbell	Courtaulds Research	Acrylics	— ^b
Sorathia and Yeager	David Taylor Research Center, U.S. Navy	Polyurethane–epoxy	96
Yamamoto and Takahashi	Hitachi Chem. Co.	Vinyl–phenolic	71
Ting	Naval Res. Lab. (Orlando)	Polyurethane–epoxy	97

^a IPNs, sequential interpenetrating polymer networks; SINs, simultaneous interpenetrating polymer networks; Full, both components in IPNs were cross-linked; semi-I (or -II), component 1 (or 2) in IPNs was cross-linked.

^b R. Satgurunthan and A. M. Campbell, private communication.

SOURCE: Reproduced with permission from reference 37. Copyright 1988.

polymer dispersed in the lower T_g polymer seemed to increase LA. Lower cross-linking levels also increased LA; see Table V (99).

The corresponding values for $\tan \delta$ –temperature plots, TA, are clearly important also. However, the areas are not “fundamental” from a polymer physics point of view because they involve the ratio E''/E' . The storage

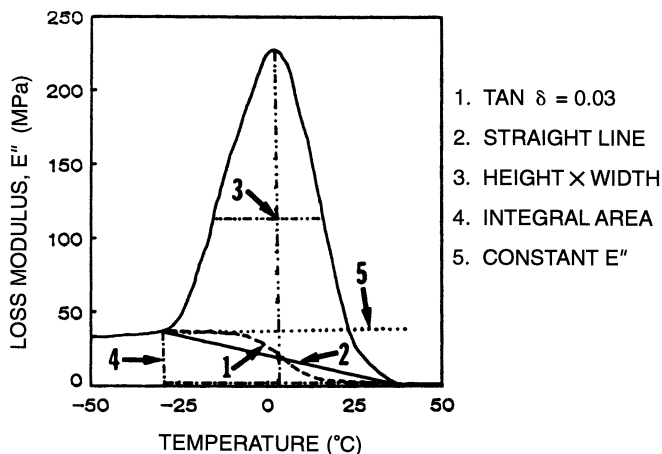


Figure 12. Methods of correcting the linear loss modulus for instrumental and chemical structure background. Curves 1 and 2 were used at Lehigh University. (Reproduced with permission from reference 100. Copyright 1991 John Wiley & Sons, Inc.)

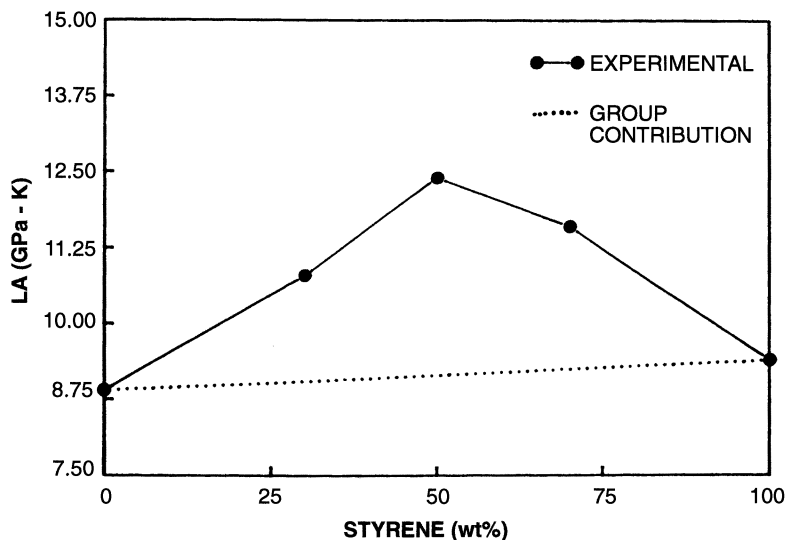


Figure 13. For sequential IPNs of cross-poly(vinyl methyl ether)-inter-cross-polystyrene, the loss area goes through a maximum when dual phase continuity exists. (Reproduced with permission from reference 48. Copyright Society of Plastics Engineers.)

Table V. Summary of General Conclusions Regarding TA and LA

<i>Effect</i>	<i>tan δ Area (TA)</i>	<i>Loss Modulus Area (LA)</i>
Decrease cross-link density	↑	↑
Increase network II (glassy) composition	↓	↑
Decrease miscibility/mixing	Goes through maxima	

SOURCE: Reproduced with permission from reference 48. Copyright Society of Plastics Engineers.

modulus, E' , decreases by 3 orders of magnitude through the glass-transition temperature range, but so far has defied theoretical prediction of its exact shape.

Polyurethane-Based IPNs

Although several papers on IPNs have already described the use of polyurethane-based compositions (32, 62–69), the importance of polyurethane-based IPNs needs special emphasis. Such materials are relatively easy to synthesize and have outstanding properties. The polyurethane elastomers may serve as network I in a sequential IPN synthesis or, in prepolymer form, may serve as one component in simultaneous interpenetrating networks. Several methods of synthesis between the classical sequential and simultaneous methods have been worked out.

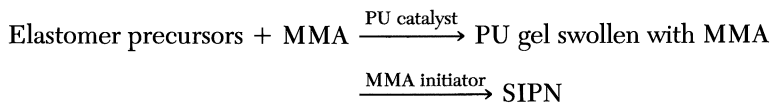
One of the more interesting series of papers is by Meyer and co-workers (94, 95, 102–104), who investigated the composition *cross-polyurethane-inter-cross-poly(methyl methacrylate)*. In general, the synthesis involved an aromatic triisocyanate and a polyether glycol catalyzed by stannous octanoate. The poly(methyl methacrylate) (PMMA) network resulted from an AIBN-initiated (azobisisobutyronitrile-initiated) free radical polymerization with a trimethacrylate cross-linker. All of the components were mixed together. The polyurethane (PU) network was allowed to form first at room temperature, followed by heating to initiate the polymerization of the methyl methacrylate (MMA) monomer. The resulting IPNs exhibited two loss peaks in $\tan \delta$ -temperature studies, but the glass-transition temperatures were shifted inward significantly and broadened. Thus Meyer et al. concluded that these materials exhibited incomplete phase separation.

More recently, Jin and Meyer (105) studied the kinetics of reaction of these IPNs via Fourier transform infrared spectroscopy (FTIR). The PU

network was formed at room temperature again; then the PMMA was free radical polymerized at 60 °C. The authors adopted the term “in situ” sequential IPNs for such materials to emphasize that all the reagents are introduced simultaneously, but that the networks are formed sequentially. This formulation is an example of kinetics partway between sequential and simultaneous syntheses.

Continued work by Jin et al. (106) showed that the polyurethane has two effects on the formation of the acrylic phase: (1) By conferring a very high viscosity on the reaction medium from the very beginning of the polymerization process, an initial high reaction rate and early gelation effect is induced. (2) the polyurethane clearly acts as a diluent and keeps the T_g of the reaction medium below the T_g of the PMMA; hence, complete monomer to polymer conversion at 50–70 °C is allowed. Polymerization usually stops at or just beyond the point of glassification, due to slowed diffusion processes (107).

In an early series of six papers, Allen et al. (108–113) carried out an interstitial polymerization of vinyl monomers within PU gels. The reaction scheme was as follows:



Allen et al. pointed out that the maximum swelling capacity of the gel should not be exceeded (taking into account χ_1) or macrosyneresis will occur. On the other hand, the cross-link density must be high enough to prevent macroscopic phase separation on polymerization of the MMA. For all of the systems considered by Allen et al., the PU was gelled at room temperature and the MMA was initiated at elevated temperatures, in a manner similar to the work of Meyer et al. (105, 106).

Although the focus of these papers has been on the polyurethane, note that each of these papers also has poly(methyl methacrylate) as the mate polymer. This pair develops excellent mechanical behavior over a wide range of compositions.

Other workers interested in polyurethane-based IPNs include Frisch et al. (114), Hourston et al. (84, 85), Klemperer et al. (92, 115), Fox et al. (91, 116), Akay et al. (117), Hourston and Zia (118), Lipatov et al. (119), Mai and Johari (120), Hur et al. (121, 122), Ting et al. (123), and Sorathia et al. (124). Hur et al. (122) present a brief review of these materials.

Applications of IPN Technology

The IPNs have many applications, both proposed and in practice. Some commercial materials are shown in Table VI (2). Although most applications involve bulk polymeric materials, ion exchange resins make a particularly

Table VI. IPN Commercial Materials

<i>Manufacturer</i>	<i>Trade Name</i>	<i>Composition</i>	<i>Application</i>
Shell Chemical Company	Kraton IPN	SEBS-polyester	Automotive parts
Petrarch Systems Inc.	Rimplast	Silicone rubber-PU	Gears or medical
ICI Americas Inc.	ITP	PU-polyester-styrene	Sheet molding compounds
DSM N.V.	Kelburon	PP-EP rubber-PE	Automotive parts
Shell Research B.V. Reichold Chemical Co.	TPR	Rubber-PP EPDM-PP	Tough plastic Auto bumper parts and wire and cable
Rohm & Haas	—	Anionic-cationic	Ion exchange resins
Monsanto	Santoprene	EPDM-PP	Tires, hoses, belts, and gaskets
Du Pont	Somel	EPDM-PP	Outdoor weathering
BFGoodrich	Telcar	EPDM-PP or PE	Tubing, liners, and wire and cable
Exxon	Vistalon	EPDM-PP	Paintable automotive parts
Freeman Chemical	Acpol	Acrylic-urethane-polystyrene	Sheeting molding compounds
Dentsply International	Trubyte Bioform	Acrylic-based	Artificial teeth
Hitachi Chemical	—	Vinyl-phenolics	Damping compounds

SOURCE: Reproduced from reference 2. Copyright 1986 American Chemical Society.

interesting application. IPN ion exchange resins usually have anionically and cationically charged networks within the same suspension particle, whereas other types have charged networks on different particles. One way to produce such a particle is to have a mixture of monomer I, cross-linker, and a suitable solvent that dissolves the monomer, but not the polymer. Under conditions of dense cross-linking, polymer I precipitates to a reticulated or macroporous form. Monomer II plus cross-linker are then swollen into the pores and polymerized. If we assume that, in the end, the two polymers can be positively or negatively charged by further reactions, an IPN ion exchange

resin can be made (125). For the best results (1), the ionic charges should be close to one another, but not in juxtaposition.

As previously mentioned, Hitachi Chemical has a new high-temperature sound and vibration damping material (71). Aspects of these developments will be discussed elsewhere in this volume.

Although many IPNs are combinations of a plastic and an elastomer, glassy-glassy IPNs have also found applications. An outstanding example is artificial teeth made by Dentsply. According to Dentsply patents (126), the material is substantially a homo-IPN of poly(methyl methacrylate). A homo-IPN is an IPN where both network polymers are based on the same monomer. Polymer network I is suspension polymerized and dispersed in monomer II plus cross-linker and activator. Some, but not all, of the monomer II mix swells into the suspension particles. The remaining mix is fully dense. The monomer II mix is then polymerized to make a type of sequential homo-IPN.

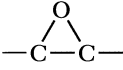
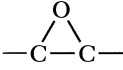
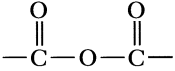
There are two advantages claimed in the patents and advertising literature for the IPN over an hypothetical product made from either a linear PMMA or a single network: (1) Swelling by solvents is reduced (salad oil is a wonderful plasticizer for linear PMMA) and (2) the dentist can grind the IPN better because the product is removed as a fine powder, whereas the single network or linear material tends to burn or char under the burr. The reason a fine powder forms is perhaps because the polymer I suspension-sized particles "remember" their interface and fracture along those surfaces.

There are many new or proposed applications. One especially interesting composition is a gradient IPN used for constant rate of delivery medication. In this case, a polymer network I is made into suspension-sized particles. Two extra ingredients are dissolved into the network: the drug to be delivered and one of the components of a condensation polymer (127). The particles are then rolled in the second component of the condensation polymer, which swell into the suspension particle. As it diffuses, the second component meets the first component and reacts to form a network. A list of the two mating component monomers is given in Table VII (128).

Exciting prospective IPN materials include a flexible solid electrolyte (129), improved molding properties for poly(ethylene terephthalate) and sulfone-epoxy resin granules (130), high-temperature polymers as SIPNs (131), adhesive bonding of denture basis resins to plastic denture teeth (132) and hydrogels based on gelatin and polyacrylamide (133), latex printing ink compositions (134), and latex binders for nonwoven products (135). Thus, not all application of IPNs involve mechanical behavior.

An interesting commercial series of latex IPNs and related materials known as Hevea Plus is based on natural rubber (NR) latex and PMMA. Hourston and Romaine (136) continued earlier latex IPN work (90, 137) by synthesizing natural rubber-PMMA latex IPNs and SIPNs. Transmission electron microscopy studies on cast film indicated a core-shell structure for

Table VII. Gradient IPN Polymer II Components

<i>Function A</i>	<i>Function B</i>	<i>Reaction Product</i>
—OH	—NCO —COOH —COCl	Polyurethane Polyester Polyester
—NH ₂ , >NH	—NCO —COOH —COCl	Polyurea Polyamide Polyamide
		Epoxy resin
—COOH		Epoxy resin
—NCO		Polyamide

SOURCE: Reference 128.

an 80:20 NR:PMMA IPN with the PMMA as the core. Stress-strain studies support the notion that these materials are reinforced elastomers with tensile strengths of 5–8 MPa for 90:10 NR:PMMA compositions.

History of IPNs

The patent literature shows that IPNs were invented over and over again, beginning in 1914. Each time, the idea was lost and reinvented. In the same sense that Columbus was the *last* person to discover America, this author hopes that IPNs will never have to be rediscovered another time.

The first known person to invent an IPN was Aylsworth, who in 1914 combined the then new phenol–formaldehyde compositions with natural rubber and sulfur (138, 139). Jonas Aylsworth was Thomas Edison's chief chemist. Edison had switched from the cylinder-type record to the platter and used the new phenol–formaldehyde materials. (Edison was then working in West Orange, New Jersey; Leo Baekeland, inventor of the phenol–formaldehyde resins, was working across the river in Yonkers, New York.) However, the new phonograph records were brittle and had to be made very thick.

In effect, by adding natural rubber and sulfur, Aylsworth made the world's first rubber-toughened plastic, decades before rubber-toughened styrenics were commercial. Thus, credit should be placed where it is fully deserved. There is evidence that Aylsworth's composition was used for toughening phonograph records and other materials from 1914 to 1929, when Edison left the phonograph record business, and then the idea was lost.

The patent (138), however, does not mention IPNs, polymer networks, or even use the term polymer. The year 1914 was six years prior to H.

Staudinger's enunciation of the macromolecular hypothesis, which was the first statement that certain colloids had the structure of long chains.

The next known discovery of IPNs was by Staudinger (son of H. Staudinger) and Hutchinson as revealed in a patent with a 1941 application date (140). To smooth the surfaces of transparent plastic sheeting for esthetic reasons, Staudinger and Hutchinson took sheets of cross-linked polystyrene or PMMA and swelled the sheets with the same monomer mix as network I. After polymerization, the swelled sheets were stretched to reduce the waviness or surface imperfections of the original material.

The next independent invention of IPNs was by Solt in 1955 (141). Solt developed cationic–anionic ion exchange resins using suspension-sized particles and both networks oppositely charged. The idea of both charges on the *same* particle (rather than different particles) was that the exchange efficiency would be improved if both charges were in juxtaposition, but still separated in space. Indeed, the charges must be separated, even by a fraction of a nanometer, to prevent coacervation.

The term “interpenetrating polymer networks” was coined by Millar (142) in 1960. Several investigating teams found IPNs independently in the 1960s. Early work by Shibayama and Suzuki (143), Lipatov and Sergeeva (144), Frisch et al. (145), and Sperling and Friedman (146) set the pace for modern development, founding the field of IPNs.

Concluding Comments

Interpenetrating polymer networks and related materials represent one of the fastest growing fields in polymer science. Although most of these materials are phase separated, the presence of cross-links reduces the phase domain size and provides a method of controlling properties. Many of these materials possess dual phase continuity. Although combinations of elastomers with plastics produce both tough plastics and reinforced elastomers, depending on the composition, IPNs see applications as damping materials and as ion exchange materials.

Outlook

The outlook for IPNs is exceedingly bright. These new materials have the following advantages:

1. IPNs form a series of tough plastics, broad-temperature damping materials, and reinforced elastomers that can be used wherever thermosets are required.
2. The presence of cross-links in a multiphase material gives an added mode of control over the morphology, especially in the

development of finely divided domains or dual phase continuity.

3. The thermoplastic IPNs and the gradient IPNs provide a series of physical and mechanical properties that may be difficult to match with other polymers or combinations of polymers.

Acknowledgments

Financial assistance has been provided over the years by the National Science Foundation, the Office of Naval Research, Wright-Patterson Air Force Base, Air Force Office of Scientific Research, Aberdeen Proving Ground, Naval Air Development Center, Edgewood Arsenal, Enichem, 3M, and Pfizer Hospital Products Group, Inc. This review would not have been possible without generations of graduate students, postdoctoral research associates, and undergraduates, who toiled day and night in the author's laboratory, and my very many wonderful associates in the field of IPNs.

References

1. Sperling, L. H. *Interpenetrating Polymer Networks and Related Materials*; Plenum: New York, 1981.
2. Sperling, L. H. In *Multicomponent Polymer Materials*; Paul, D. R.; Sperling, L. H., Eds.; Advances in Chemistry 211; American Chemical Society: Washington, DC, 1986.
3. Sperling, L. H. In *Multiphase Macromolecular Systems*; Culbertson, B. M., Ed.; Contemporary Topics in Polymer Science; Plenum: New York, 1989; Vol. 6.
4. *Advances in Interpenetrating Polymer Networks*; Klempner, D.; Frisch, K. C., Eds.; Technomic: Lancaster, PA, 1989, Vol. I; 1990, Vol. II.
5. Lipatov, Yu. S.; Sergeeva, L. M. *Interpenetrating Polymeric Networks*; Naukova Dumka: Kiev, 1979.
6. *Recent Developments in Polyurethanes and Interpenetrating Polymer Networks*; Frisch, K. C., Jr.; Klempner, D., Eds.; Technomic: Lancaster, PA, 1988.
7. *Sound and Vibration Damping with Polymers*; Corsaro, R. D.; Sperling, L. H., Eds.; ACS Symposium Series 424; American Chemical Society: Washington, DC, 1990.
8. *Polymers for Advanced Technologies*; Lewin, M., Ed.; VCH: New York, 1988.
9. *Multicomponent Polymer Materials*; Paul, D. R.; Sperling, L. H., Eds.; Advances in Chemistry 211; American Chemical Society: Washington DC 1986.
10. *Multicomponent Macromolecular Systems*; Culbertson, B. M., Ed.; Contemporary Topics in Polymer Science; Plenum: New York, 1989; Vol. 6.
11. Dickie, R. A.; Labana, S. S.; Bauer, R. S. *Cross-Linked Polymers: Chemistry, Properties, and Applications*; ACS Symposium Series 367; American Chemical Society: Washington, DC, 1988.
12. Ring, W.; Mita, I.; Jenkins, A. D.; Bikales, N. M. *Pure Appl. Chem.* **1985**, *57*, 1427.
13. Sperling, L. H. *Introduction to Physical Polymer Science*, 2nd ed.; Wiley-Interscience: New York, 1992; Chapter 2.
14. Kim, S. C.; Klempner, D.; Frisch, K. C.; Frisch, H. L. *Macromolecules* **1976**, *9*, 263.

15. Yenwo, G. M.; Sperling, L. H.; Pulido, J.; Manson, J. A.; Conde, A. *Polym. Eng. Sci.* **1977**, *17*, 251.
16. Scarito, P. R.; Sperling, L. H. *Polym. Eng. Sci.* **1979**, *19*, 297.
17. Krause, S. *Macromolecules* **1970**, *3*, 84.
18. Lipatov, Y. S.; Grigor'yeva, O. P.; Kovernik, G. P.; Shilov, V. V.; Sergeyeveva, L. M. *Makromol. Chem.* **1985**, *186*, 1401.
19. Sperling, L. H.; Heck, C. S.; An, J. H. In *Multiphase Polymers: Blends and Ionomers*; Utracki, L. A.; Weiss, R. A., Eds.; ACS Symposium Series 395; American Chemical Society: Washington, DC, 1989.
20. An, J. H.; Sperling, L. H. In *Cross-Linked Polymers: Chemistry, Properties, and Applications*; Dickie, R. A.; Labana, S. S.; Bauer, R. S., Eds.; ACS Symposium Series 367; American Chemical Society: Washington, DC, 1988.
21. Fernandez, A. M. Ph.D. Thesis, Lehigh University, Bethlehem, PA, 1984.
22. An, J. H.; Sperling, L. H. In *Cross-Linked Polymers: Chemistry, Properties, and Applications*; Dickie, R. A.; Labana, S. S.; Bauer, R. S., Eds.; ACS Symposium Series 367; American Chemical Society: Washington, DC, 1988.
23. Binder, K.; Frisch, H. L. *J. Chem. Phys.* **1984**, *81*, 2126.
24. Bates, F. S.; Wignall, G. D. *Phys. Rev. Lett.* **1986**, *57*, 1429.
25. Briber, R. M.; Bauer, B. J. *Macromolecules* **1991**, *24*, 1899.
26. Siegfried, D. L.; Thomas, D. A.; Sperling, L. H. In *Polymer Alloys II*; Frisch, K. C.; Klempner, D., Eds.; Plenum: New York, 1980.
27. Misra, S. C.; Manson, J. A.; Sperling, L. H. In *Epoxy Resin Chemistry*; Bauer, R. S., Ed.; ACS Symposium Series 114; American Chemical Society: Washington, DC, 1979; Chapter 12.
28. Coleman, M. M.; Serman, C. J.; Painter, P. C. *Macromolecules* **1987**, *20*, 226.
29. Bauer, B. J.; Briber, R. M.; Han, C. C. *Macromolecules* **1989**, *22*, 940.
30. Briber, R. M.; Bauer, B. J. *Macromolecules* **1988**, *21*, 3296.
31. Fay, J. J.; Murphy, C. J.; Thomas, D. A.; Sperling, L. H. In *Sound and Vibration Damping with Polymers*; Corsaro, R. D.; Sperling, L. H., Eds.; ACS Symposium Series 424; American Chemical Society: Washington, DC, 1990.
32. Frisch, H. L.; Klempner, D.; Yoon, H. K.; Frisch, K. C. *Macromolecules* **1980**, *13*, 1016.
33. deGennes, P. G. *J. Phys.* **1979**, *40*, L-69.
34. Daoud, M. Seminar at Lehigh University, April 1992.
35. Bettachy, A.; Derouiche, A.; Benhamou, M.; Daoud, M. *J. Phys. I* **1991**, *1*, 153.
36. Lee, D. S.; Kim, S. C. *Macromolecules* **1984**, *17*, 268.
37. Sperling, L. H. In *Polymers for Advanced Technologies*; Lewin, M., Ed.; VCH: New York, 1988.
38. Graillard, P.; Ossenbach-Sauter, M.; Riess, G. In *Polymer Compatibility and Incompatibility*; Solc, K., Eds.; MMI Press: New York, 1981.
39. Ludwico, W. A.; Rosen, S. L. *Polym. Sci. Technol.* **1977**, *10*, 401.
40. Parent, R. D.; Thompson, E. V. In *Multiphase Polymers*; Cooper, S. L.; Ester, G. M., Eds.; Advances in Chemistry 176; American Chemical Society: Washington, DC, 1979; Chapter 20.
41. Walsh, D. J.; Sham, C. K. *Polymer* **1984**, *25*, 1023.
42. Purvis, M. T.; Yanai, H. S. In *Polymer Compatibility and Incompatibility*; Solc, K., Ed.; MMI Press: Harwood, Switzerland, 1982; p 261.
43. Donatelli, A. A.; Sperling, L. H.; Thomas, D. A. *Macromolecules* **1976**, *9*, 671, 676.
44. Burford, R.; Chaplin, R.; Mai, Y. M. In *Multiphase Macromolecular Systems*; Culbertson, B. M., Ed.; Contemporary Topics in Polymer Science; Plenum: New York, 1989; Vol. 6.

45. Donatelli, A. A.; Sperling, L. H.; Thomas, D. A. *J. Appl. Polym. Sci.* **1977**, *21*, 1189.
46. Yeo, J. K.; Sperling, L. H.; Thomas, D. A. *Polymer* **1983**, *24*, 307.
47. Michel, J.; Hargest, S. C.; Sperling, L. H. *J. Appl. Polym. Sci.* **1981**, *26*, 743.
48. Fay, J. J.; Murphy, C. J.; Thomas, D. A.; Sperling, L. H. *Polym. Eng. Sci.*, in press.
49. Jordhamo, G. M.; Manson, J. A.; Sperling, L. H. *Polym. Eng. Sci.* **1986**, *26*, 517.
50. Paul, D. R.; Barlow, J. W. *J. Macromol. Sci. Chem.* **1980**, *C18*, 109.
51. Metelkin, V. I.; Blecht, V. S. *Kolloid Zh.* **1984**, *46*, 476.
52. Utracki, L. A. *J. Rheol.* **1991**, *35*, 1615.
53. Termonia, Y. *Macromolecules* **1991**, *24*, 1392.
54. Siegfried, D. L.; Thomas, D. A.; Sperling, L. H. *J. Appl. Polym. Sci.* **1981**, *26*, 177.
55. Davison, S.; Gergen, W. P. U.S. Patent 4,041,103, 1977.
56. Gergen, W. P.; Davison, S. U.S. Patent 4,101,605, 1978.
57. Fischer, W. K. U.S. Patent 3,806,558, 1974.
58. Coran, A. Y.; Das, B.; Patel, R. P. U.S. Patent 4,130,535, 1978.
59. Coran, A. Y.; Patel, R. *Rubber Chem. Technol.* **1980**, *53*, 141.
60. Coran, A. Y.; Patel, R. *Rubber Chem. Technol.* **1981**, *54*, 91.
61. Coran, A. Y.; Patel, R. *Rubber Chem. Technol.* **1982**, *55*, 1063.
62. Devia, N.; Manson, J. A.; Sperling, L. H.; Conde, A. *Macromolecules* **1979**, *12*, 360.
63. Afolabi, O. A.; Aluko, M. E.; Wang, G. C.; Anderson, W. A.; Ayorinde, F. O. *J. Am. Oil Chem. Soc.* **1989**, *66*, 7.
64. Tan, P.; Xie, H. *Hecheng Xiangjiao Gongye* **1984**, *1*, 180.
65. Song, M.; Donghua, Z. *Plastics Industry* **1987**, *2*, 42.
66. Patel, P.; Shah, T.; Suthar, B. *J. Appl. Polym. Sci.* **1990**, *40*, 1037.
67. Liang, J. L.; Liu, H. T.; Ku, W. H.; Wang, G. M. Abstracts of Papers, IUPAC International Symposium on Polymers for Advanced Technologies, August, 1987, Jerusalem, Israel.
68. Dirlikov S. K.; Frischinger, I.; Islam, M. S.; Graham, J. *Polym. Mat. Sci. Eng. (Prepr.)* **1990**, *62*, 217.
69. Barrett, L. W.; Sperling, L. H. *Polym. Mat. Sci. Eng. (Prepr.)* **1991**, *65*, 180.
70. Sperling, L. H.; Carraher, C. E.; Qureshi, S. P.; Manson, J. A.; Barrett, L. W. In *Biotechnology and Polymers*; Gebelein, C. G., Ed.; Plenum: New York, 1991.
71. Yamamoto, K.; Takahashi, A. In *Sound and Vibration Damping with Polymers*; Corsaro, R. D.; Sperling, L. H., Eds.; ACS Symposium Series 424; American Chemical Society: Washington, DC, 1990.
72. Fradkin, D. G.; Foster, J. N.; Sperling, L. H.; Thomas, D. A. *Rubber Chem. Technol.* **1986**, *59*, 255.
73. Chang, M. C. O.; Thomas, D. A.; Sperling, L. H. *J. Appl. Polym. Sci.* **1987**, *34*, 409.
74. Chang, M. C. O.; Thomas, D. A.; Sperling, L. H. *J. Polym. Sci., Polym. Phys. Ed.* **1988**, *26*, 1627.
75. Sperling, L. H.; Chiu, T. W.; Gramlich, R. G.; Thomas, D. A. *J. Paint Technol.* **1974**, *46*, 47.
76. Grat, J. A.; Thomas, D. A.; Hickey, E. C.; Sperling, L. H. *J. Appl. Polym. Sci.* **1975**, *19*, 1731.
77. Sperling, L. H.; Thomas, D. A. U.S. Patent 3,833,404, 1974.
78. Lorenz, J. E.; Thomas, D. A.; Sperling, L. H. In *Emulsion Polymerization*; Pirmra, I.; Gardon, J. L., Eds.; ACS Symposium Series 24; American Chemical Society: Washington, DC, 1976; Chapter 20.

79. Fradkin, D. G.; Foster, J. N.; Sperling, L. H.; Thomas, D. A. *Polym. Eng. Sci.* **1986**, *26*, 730.
80. Foster, J. N.; Sperling, L. H.; Thomas, D. A. *J. Appl. Polym. Sci.* **1987**, *33*, 2637.
81. Chang, M. C. O.; Thomas, D. A.; Sperling, L. H. *Polym. Mat. Sci. Eng.* **1986**, *55*, 350.
82. Hourston, D. J.; Zia, Y. *J. Appl. Polym. Sci.* **1983**, *28*, 2139, 3475, 3849.
83. Hourston, D. J.; Zia, Y. *J. Appl. Polym. Sci.* **1984**, *29*, 629, 2951, 2963.
84. Hourston, D. J.; McCluskey, J. A. *J. Appl. Polym. Sci.* **1986**, *31*, 645.
85. Hourston, D. J.; Huson, M. G.; McCluskey, J. A. *J. Appl. Polym. Sci.* **1986**, *31*, 709.
86. Hourston, D. J.; Huson, M. G.; McCluskey, J. A. *J. Appl. Polym. Sci.* **1986**, *32*, 3881.
87. Hourston, D. J.; McCluskey, J. A. *Polymer* **1979**, *20*, 1573.
88. Hourston, D. J.; Zia, Y. *Polymer* **1979**, *20*, 1497.
89. Hourston, D. J.; Satgurunathan, R. *J. Appl. Polym. Sci.* **1984**, *29*, 2969.
90. Hourston, D. J.; Satgurunathan, R.; Varma, H. *J. Appl. Polym. Sci.* **1986**, *31*, 1955.
91. Fox, R. B.; Bitner, J. L.; Hinkle, J. A.; Carter, W. *Polym. Eng. Sci.* **1985**, *25*, 157.
92. Klempner, D.; Wang, C. L.; Ashtiani, M.; Frisch, K. C. *J. Appl. Polym. Sci.* **1986**, *32*, 4197.
93. Wong, D. T. H.; Williams, H. L. *J. Appl. Polym. Sci.* **1983**, *28*, 2187.
94. Hermant, I.; Danyanidu, M.; Meyer, G. C. *Polymer* **1983**, *24*, 1419.
95. Morin, A.; Djomo, H.; Meyer, G. C. *Polym. Eng. Sci.* **1983**, *23*, 394.
96. Sorathia, U.; Yeager, L. In *Sound and Vibration Damping with Polymers*; ACS Symposium Series 424; American Chemical Society: Washington, DC, 1990.
97. Ting, R. Y.; Capps, R. N. In *Sound and Vibration Damping with Polymers*; ACS Symposium Series 424; American Chemical Society: Washington, DC, 1990.
98. Fay, J. J.; Murphy, C. J.; Thomas, D. A.; Sperling, L. H. In *Sound and Vibration Damping with Polymers*; Corsaro, R. D.; Sperling, L. H., Eds.; ACS Symposium Series 424; American Chemical Society: Washington, DC, 1990.
99. Fay, J. J.; Thomas, D. A.; Sperling, L. H. *Polym. Eng. Sci.* **1991**, *31*, 1731.
100. Fay, J. J.; Thomas, D. A.; Sperling, L. H. *J. Appl. Polym. Sci.* **1991**, *43*, 1617.
101. Sperling, L. H.; Fay, J. *J. Polym. Adv. Technol.* **1991**, *2*, 49.
102. Djomo, H.; Widmaier, J. M.; Meyer, G. C. *Polymer* **1983**, *24*, 1415.
103. Hermant, I.; Meyer, G. C. *Eur. Polym. J.* **1984**, *20*, 85.
104. Jehl, D.; Widmaier, J. M.; Meyer, G. C. *Eur. Polym. J.* **1983**, *19*, 597.
105. Jin, S. R.; Meyer, G. C. *Polymer* **1986**, *27*, 592.
106. Jin, S. R.; Widmaier, J. M.; Meyer, G. C. *Polymer* **1988**, *29*, 346.
107. Gillham, J. K. *Encyclopedia of Polymer Science and Engineering*, 2nd ed.; Wiley-Interscience: New York, 1986; Vol. 4, p 519.
108. Allen, G.; Bowden, M. J.; Blundell, D. J.; Hutchinson, F. G.; Jeffs, G. M.; Vyvoda, J. *Polymer* **1973**, *14*, 597.
109. Allen, G.; Bowden, M. J.; Blundell, D. J.; Jeffs, G. M.; Vyvoda, J.; White, T. *Polymer* **1973**, *14*, 604.
110. Allen, G.; Bowden, M. J.; Lewis, G.; Blundell, D. J.; Jeffs, G. M. *Polymer* **1974**, *15*, 13.
111. Allen, G.; Bowden, M. J.; Lewis, G.; Blundell, D. J.; Jeffs, G. M.; Vyvoda, J. *Polymer* **1974**, *15*, 19.
112. Allen, G.; Bowden, M. J.; Todd, S. M.; Blundell, D. J.; Jeffs, G. M.; Davies, W. E. A. *Polymer* **1974**, *15*, 28.

113. Blundell, D. J.; Longman, G. W.; Wignall, G. D.; Bowden, M. J. *Polymer* **1974**, *15*, 33.
114. Frisch, H. L.; Frisch, K. C.; Klempner, D. *Pure Appl. Chem.* **1981**, *53*, 1557.
115. Klempner, D.; Berkowski, F.; Frisch, K. C. *Rubber World* **1985**, *187*, 16.
116. Fox, R. B.; Fay, J. J.; Sorathia, U.; Sperling, L. H. In *Sound and Vibration Damping with Polymers*; Corsaro, R. D.; Sperling, L. H., Eds.; ACS Symposium Series 424; American Chemical Society: Washington, DC, 1990; Chapter 19.
117. Akay, M.; Rollins, S. N.; Riordan, E. *Polymer* **1988**, *29*, 37.
118. Hourston, D. J.; Zia, Y. *J. Appl. Polym. Sci.* **1983**, *28*, 3745.
119. Lipatov, Y.; Karabanova, L.; Sergeeva, L.; Gorbach, L.; Skiba, S. *Vysokomol. Soedin, Ser. B* **1986**, *29*, 274.
120. Mai, C.; Johari, G. P. *J. Polym. Sci., Polym. Phys. Ed.* **1987**, *25*, 1903.
121. Hur, T.; Manson, J. A.; Hertzberg, R. W. In *Cross-Linked Polymers*; Dickie, R. A.; Labana, S. S.; Bauer, R. S., Eds.; ACS Symposium Series 367; American Chemical Society: Washington, DC, 1988.
122. Hur, T.; Manson, J. A.; Hertzberg, R. W.; Sperling, L. H. *J. Appl. Polym. Sci.* **1990**, *39*, 1933.
123. Ting, R. Y.; Capps, R. N.; Klempner, D. In *Sound and Vibration Damping with Polymers*; Corsaro, R. D.; Sperling, L. H., Eds.; ACS Symposium Series 424; American Chemical Society: Washington, DC, 1990; Chapter 20.
124. Sorathia, U.; Yeager, W.; Dapp, T. In *Sound and Vibration Damping with Polymers*; Corsaro, R. D.; Sperling, L. H., Eds.; ACS Symposium Series 424; American Chemical Society: Washington, DC, 1990; Chapter 21.
125. Barrett, J. H.; Clemens, D. H. U.S. Patent 3,966,489, 1976.
126. Roemer, F. D.; Tateosian, L. H. European Patent 0,014,515, 1984.
127. Mueller, K. F.; Heiber, S. J. *J. Appl. Polym. Sci.* **1982**, *27*, 4043.
128. Mueller, K. F.; Heiber, S. J. U.S. Patent 4,423,099, 1983.
129. Mason, C. F. Europe Patent 390307 A2, 1990.
130. Nishino, S.; Hagiwara, I.; Abe, K. Japan Patent 03000742 A2, 1991.
131. Pater, R. H. *Polym. Eng. Sci.* **1991**, *31*, 20, 28.
132. Suzuki, S.; Sakoh, M.; Shiba, A. *J. Biomed. Mater. Res.* **1990**, *24*, 1091.
133. Chatterjii, P. R. *J. Appl. Polym. Sci.* **1990**, *40*, 401.
134. Lindeman, M. K.; Deacon, K. U.S. Patent 4,686,260, 1987.
135. Lindeman, M. K.; Deacon, K. U.S. Patent 4,683,165, 1987.
136. Hourston, D. J.; Romaine, J. *J. Appl. Polym. Sci.* **1990**, *39*, 1587.
137. Hourston, D. J.; Satgurunathan, R.; Varma, H. *J. Appl. Polym. Sci.* **1987**, *34*, 901.
138. Aylsworth, J. W. U.S. Patent 1,111,284, 1914.
139. Sperling, L. H. *Polymer News* **1987**, *12*, 332.
140. Staudinger, J. J. P.; Hutchinson, H. M. U.S. Patent 2,539,377, 1951.
141. Solt, G. S. British Patent 728,508, 1955.
142. Millar, J. R. *J. Chem. Soc.* **1960**, 1311.
143. Shibayama, K.; Suzuki, Y. *Rubber Chem. Tech.* **1967**, *40*, 476.
144. Lipatov, Yu. S.; Sergeeva, C. M. *Russ. Chem. Rev.* **1967**, *45(1)*, 63.
145. Frisch, H. L.; Klempner, D.; Frisch, K. C. *J. Polym. Sci., Polym. Phys. Ed.* **1969**, *7(11)*, 775.
146. Sperling, L. H.; Friedman, D. W. *J. Polym. Sci.* **1969**, *A-2(7)*, 425.
147. Huelck, V.; Thomas, D. A.; Sperling, L. H. *Macromolecules* **1972**, *5*, 340.

RECEIVED for review November 26, 1991. ACCEPTED revised manuscript September 15, 1992.

Interpenetrating Polymer Networks as Energy-Absorbing Materials

Daniel Sophiea, Daniel Klempler, Vahid Sendjarevic, B. Suthar, and K. C. Frisch

Polymer Technologies, Inc., University of Detroit Mercy,
4001 West McNichols Road, P.O. Box 19900, Detroit, MI 49219-3599

Polyurethane-poly(vinyl chloride) pseudo-IPN (interpenetrating polymer network) elastomers, polyurethane-poly(vinyl ester) IPN foams, and polyurethane-epoxy-unsaturated polyester two- and three-component IPN foams and elastomers were studied by dynamic mechanical spectroscopy sound absorption (impedance tube technique), compressive hysteresis, resilience (ball rebound), and other measurements. The IPN systems were tailored to possess broad glass-transition temperatures, and the effects of this broad viscoelastic region on the energy-absorbing properties were determined. Materials with broad transitions resulted in enhanced mechanical-energy-absorbing properties, but not always improved absorption of airborne noise. The results suggest that sound attenuation can be more a function of cell morphology rather than polymer morphology.

Sound and Vibration Damping

The ability of polymers to damp vibration and absorb sound is a function of their viscoelastic nature, specifically their glass-transition behavior. Four mechanisms of sound attenuation can occur: (1) scattering by inhomogeneities, (2) mode conversion at boundaries, (3) redirection, and (4) intrinsic absorption by conversion to heat with viscoelastic materials (1). In solid elastomers vibration damping through intrinsic absorption depends on Young's modulus, which is expressed as $E^* = E' - iE''$, where E^* is the complex modulus, E' is the storage modulus, and E'' is the loss modulus. When a viscoelastic polymer is adhered to a vibrating substrate, internal friction

created by segmental chain motions results in heat buildup within the polymer and absorption of the vibrational waves. In a free viscoelastic layer on a vibrating substrate, the composite loss factor is given by

$$(\tan \delta)_{\text{composite}} = k(E_2^*/E_1^*)(h_2/h_1)^2 \tan \delta_2 \quad (1)$$

where E^* and h are the Young's modulus and thickness, respectively, subscripts 1 and 2 refer to the substrate and viscoelastic layer, respectively, and k is a constant. In a constrained layer configuration the composite loss factor is given by

$$(\tan \delta)_{\text{composite}} = k(E_3^*/E_2^*)(h_3/h_1) \tan \delta_2 \quad (2)$$

where subscripts 1, 2, and 3 refer to the substrate, viscoelastic layer, and constraining layer, respectively. Therefore, damping is dependent on the material loss factor, the material modulus, the substrate modulus, and the constraining layer modulus. The deformation of the viscoelastic material is described as extensional in the configuration in eq 1 and a combination of extensional and shear in the configuration in eq 2. Damping through a viscoelastic polymer affixed to a vibrating surface is, therefore, efficient due to the forced extensional and shear deformations imposed on the viscoelastic material.

Sound absorption through solid elastomers is not as efficient. Sound waves (acoustics) refer to wave propagation through fluids (air or liquid) as opposed to vibrations through solids. In fluids, the shear modulus equals zero and, therefore, propagation occurs through longitudinal waves only. For a coating of solid viscoelastic polymer, Jarzynski (1) showed that incidental longitudinal waves may generate longitudinal and shear waves within the coating (mode conversion) as well as other modes of wave propagation that result from scattering. Also, by making inclusions (such as microcells or large voids) in the materials, the incident longitudinal waves may be converted to shear waves. In this manner, viscoelastic foams may actually absorb sound and vibrational energy. The inclusion of voids within a viscoelastic material increases the likelihood of sound attenuation through more of the mechanisms stated previously. That is, viscoelastic foams may attenuate sound through intrinsic conversion to heat and mode conversion (like viscoelastic solids) as well as through scattering by inhomogeneities.

Simplified Theory of Damping. The ability of materials to damp vibrations is characterized by dynamic mechanical terms. The storage modulus (E') and loss modulus (E'') are the quantities of energy stored through elastic behavior and energy lost through conversion to heat via molecular friction, respectively. When a polymer is in its viscoelastic region (*see* Figure 1),

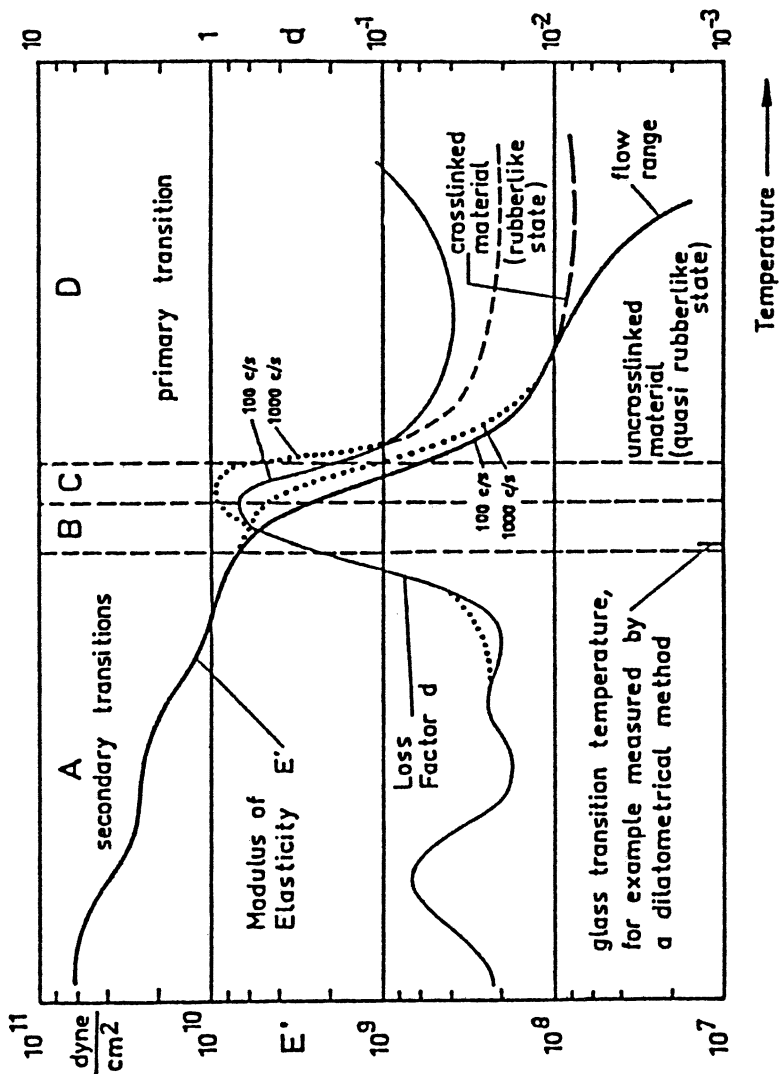


Figure 1. Modulus of elasticity and loss factor of viscoelastic material as a function of temperature (2).

which is the transition (relaxation) between the hard glassy state and the soft rubbery state, it exhibits the highest level of damping. In this region, the glass-transition region (T_g), there is a distribution of phases. When the material is forced to vibrate (as is done with a shaker during dynamic mechanical measurement or when adhered to a vibrating substrate), some molecules exhibit viscous flow while others remain rigid. Molecular friction rises, which results in heat buildup and a decreased amount of transmitted energy.

The expressions are as follows:

$$E^* = E' - iE'' \quad (3)$$

$$\tan \delta = E''/E' \quad (4)$$

$$H = \pi E''/\epsilon_0^2 \quad (5)$$

where H is the actual heat gained by the material for each cycle and ϵ_0^2 represents the magnitude of deformation.

When vibration-damping polymers are formulated, it is desirable to maximize E'' ; however, there is a limit. Maximizing E'' results in lower elastic response and, therefore, poor physical and mechanical properties may result.

Keskkula et al. (3) were able to quantify damping performance by expressing it as the area under the $\tan \delta$ versus temperature curve. Although this quantification is better than reporting the maximum value or width of the $\tan \delta$ peak, it is often difficult to determine because the sample fails or becomes too soft to allow the instrument to record at elevated temperature. A better method is to express the area under the linear loss modulus curve as the damping function (4) or the loss area (LA) (5, 6). The loss area as derived along with tA , the area under the $\tan \delta$ -temperature curve, by Chang, Thomas, and Sperling (5, 6) is given by

$$LA = \int_{T_G}^{T_R} E'' dT \cong (E'_G - E'_R) R / (Ea)_{\text{avg}} [\pi/2] T_g^2 \quad (6)$$

where E'_G and E'_R are the storage moduli in the glassy and rubbery states, respectively, T_G and T_R are the glassy and rubbery temperatures just below and above the T_g , $(Ea)_{\text{avg}}$ is the average activation energy of the relaxation process, and R is the gas constant. Also,

$$tA = \int_{T_G}^{T_R} \tan \delta dT \cong (\ln E'_G - \ln E'_R) R / (Ea)_{\text{avg}} [\pi/2] T_g^2 \quad (7)$$

Evaluation of damping performance was furthered (5, 6) by the application of group contribution analysis as shown in Figure 2. The LA obeys a

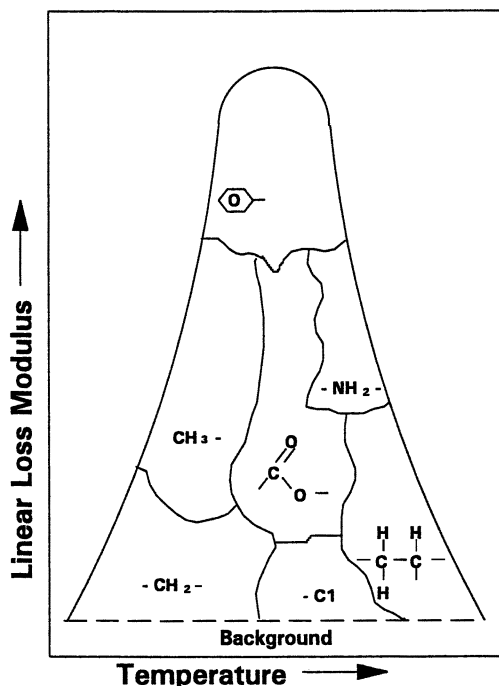


Figure 2. The idea of group contribution analysis for dynamic mechanical spectroscopy (E'' vs. temperature plot) (7).

simple mixing rule based on the weight averages of the individual polymers species in an interpenetrating polymer (IPN); that is,

$$(LA)_{IPN} = W_I(LA)_I + W_{II}(LA)_{II} \quad (8)$$

where W_I and W_{II} are the weight fractions of polymer components I and II, respectively (Figure 3). Also note that tA does not exhibit this simple additivity principle because it is dependent on the ratio E''/E' and $1/E'$ is not expected to obey additivity (5) (Figure 4). From this information and assuming that the total loss area is a combination of the weight additive contribution of the individual structural repeat units,

$$LA = \sum_{i=1}^{\mu} (LA)_i M_i/M - \sum_{i=1}^{\mu} G_i/M \quad (9)$$

where M_i is the molecular weight of the i th group in the mer, M in the molecular weight of the whole mer, G_i is the molar loss constant for the i th group, $(LA)_i$ is the loss area contributed by the i th group, and n represents the number of units in the mer. The molar loss constants and contribution to

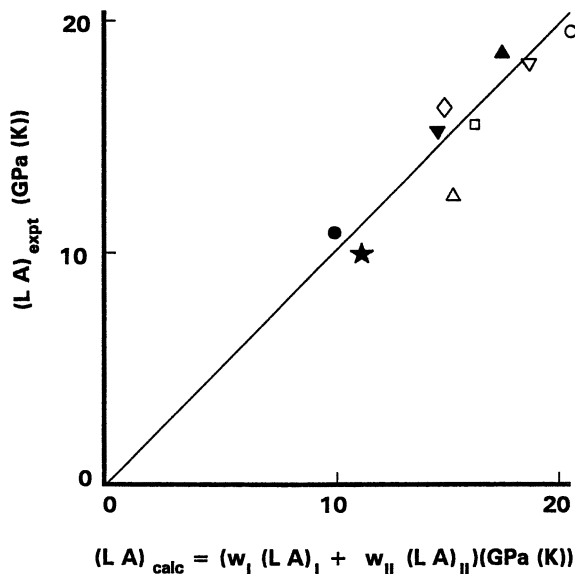


Figure 3. Test of additivity of the homopolymer LAs to predict corresponding IPN areas: ★, IPN-1; ○, IPN-2; ●, IPN-3; ○, IPN-4; ▽, IPN-5; △, IPN-6; □, IPN-7; ◇, IPN-8; ▲, IPN-9; ▼, IPN-10 (7).

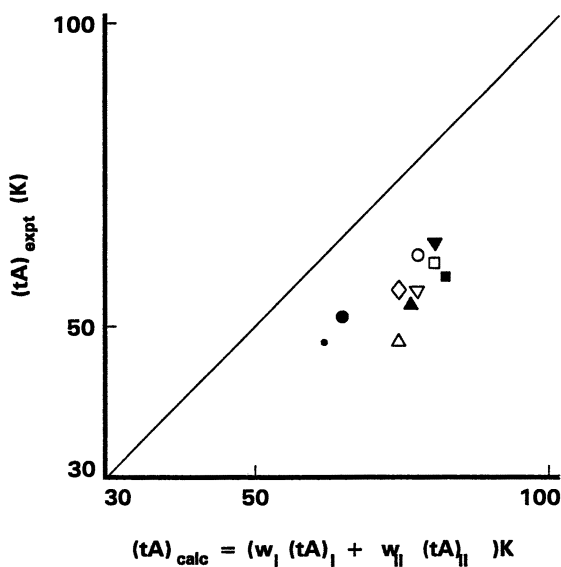


Figure 4. Test of additivity of the homopolymer tAs in predicting the corresponding IPN areas: □, IPN-1; ○, IPN-2; ●, IPN-3; △, IPN-4; ▽, IPN-5; ◇, IPN-6; ■, IPN-7; ●, IPN-8; ▲, IPN-9; ▼, IPN-10 (7).

the loss area have been reported for a significant number of structural groups (8). Group contribution analysis, however, may be unable to predict the LA of filled polymers and composites (9) because the analysis is based only on molecular structure. Additionally, group contribution analysis may not accurately be able to predict LA of partially miscible (microheterogeneous) IPNs that exist in a “forced” phase state (10); that is, group contribution analysis contradicts current thought on controlling IPN morphology to enhance energy-damping properties. Further experimental work is required to determine the effect of the degree of phase separation on the LA values, an area where IPNs are uniquely suitable.

Acoustic Theory. As previously stated, absorption of impinging acoustic waves by a solid viscoelastic material is not efficient. To improve performance, open-cell porous materials are primarily used to allow the waves to enter the foam, reverberate, and eventually dissipate or become absorbed. Most commercial sound-absorbing foams are of this type and perform with increasing efficiency at higher frequencies. The ability to quantify the relative amounts of energy actually absorbed through conversion to heat as opposed to decay is not yet possible. Chen and Williams (11) report that relevant parameters for sound absorption by a homogeneous, isotropic porous material are porosity (H), specific flow resistance (R^*), structural factors (m), frequency of the applied sound, and the geometry of the foam sample such as length, width, thickness, and density. For inhomogeneous, nonisotropic materials such as IPNs the parameters would also include cell orientation and morphology.

Another method of preparing sound-absorbing materials is to incorporate heavy fillers such as lead or rubber into the foams. The filler is thought to work in one or all of the three following ways: (1) it can resonate by absorbing some of the impinging sound waves; (2) it can reflect impinging sound waves back through the polymer, thereby allowing the foam to absorb more energy while also redirecting and dissipating it; (3) each filler particle can act as a “miniature constrained-layer system”.

When inhomogeneities that are macroscopic (such as previously described) are present, the acoustic wave that propagates through one medium encounters the boundary layer of the other: Some energy is transmitted and some is reflected (12) (Figure 5). The sound power transmission coefficient (T) is given by

$$T = 4Z_1Z_2/(Z_1 + Z_2)^2 \quad (10)$$

where Z is the acoustic impedance and the subscripts refer to the two media. The acoustic impedance is defined as the ratio of acoustic pressure to the particle velocity associated with wave motion.

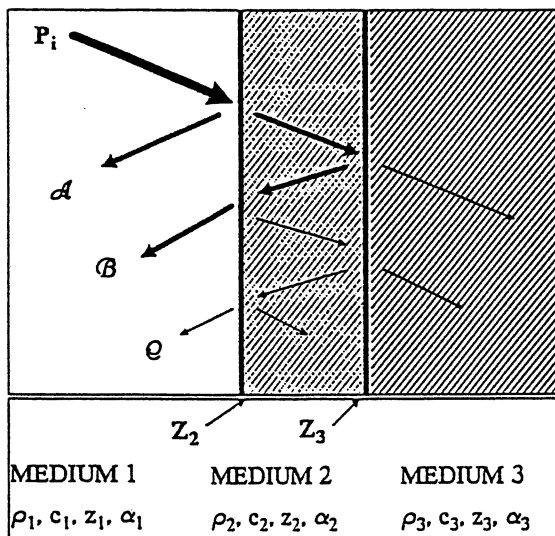


Figure 5. Major echoes reflected from a single finite layer of material. (Reproduced from reference 12. Copyright 1990 American Chemical Society.)

Hilyard and MacFarland (13) recently described both concepts of airborne noise insulation and structure-borne noise isolation with respect to polymeric foams. For airborne noise, which is typically responsible for automobile noise above 500 Hz, acoustic wave transmission is dependent on two factors: the acoustic impedance at each interface of a panel and composite and the attenuation of acoustic wave propagation through the foam. Again, the foam modulus, density, and air flow resistivity govern these factors. The transmission loss (TL) (14–16) is given as the ratio of sound pressure in the incident and transmitted fields, P_i and P_t , respectively:

$$\text{system TL} = 10 \log [P_i/P_t]^2 \quad (11)$$

$$\text{panel TL} = 10 \log [1 + (\omega M_1/\rho_0 C_0)^2] \quad (12)$$

$$\text{composite TL} = \text{system TL} - \text{panel TL} \quad (13)$$

where ω is the angular frequency, M_1 is the mass density, and $\rho_0 C_0$ is the acoustic impedance.

IPNs as Damping Materials. Effective ways to broaden or shift the T_g range include the use of plasticizers and fillers, blending, grafting, copolymerization, or the formation of IPNs.

IPNs are an intimate mixture of two or more cross-linked polymers in which one network is formed in the presence of another (17). IPNs can be formed simultaneously (18–20), sequentially (7, 21, 22), or by the latex technique (2, 23). Ideally, interpenetration occurs only through physical cross-links (catenane-type structures) and mixing is on a molecular (monomer) scale as long as no covalent bonds exist between the differing polymers. In this case, a single phase material results when dynamic mechanical measurements are used. However, these materials possess some level of phase separation (domain size on the order of 5.0 nm) as evidenced by transmission electron microscopy (TEM). If mixing is incomplete (domain sizes of greater than 30 nm), such as when cross-linking occurs after phase separation, then two phases result. However, microheterogeneous morphologies (domain sizes of 5.0–30 nm) can occur and result in broad glass-transition regions (Figure 6) with respect to temperature and frequency. The advantages that IPNs present over other transition-broadening techniques include more control over the resulting morphology, longer phase stability (due to cross-linking), and broader glass-transition regions.

The use of IPNs as energy-damping materials was first reported by Huelck et al. (24). Latex IPNs based on poly(ethyl acrylate) and poly(methyl methacrylate) were observed to exhibit high $\tan \delta$ values that stayed high over a broad temperature range (Figure 7). Because the polymer components

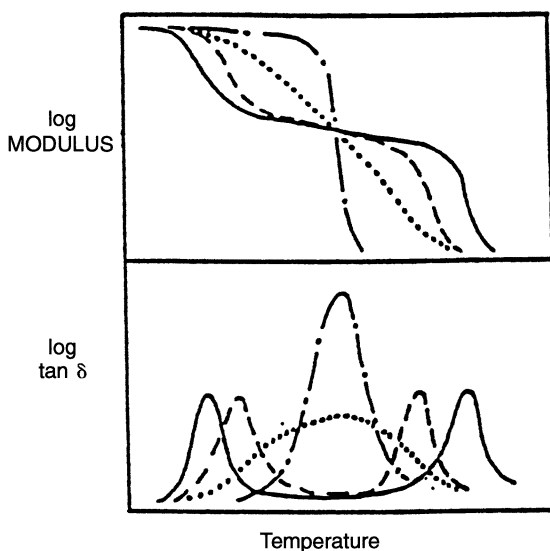


Figure 6. Generalized mechanical loss and modulus behavior for different types of polymer blends. Case 1 (dashed-dotted line), miscible; case 2 (dashed line), limited miscibility; case 3 (dotted line), microheterogeneous; case 4 (solid line), heterogeneous.

**American Chemical Society
Library**

1155 16th St., N.W.
Washington, D.C. 20036

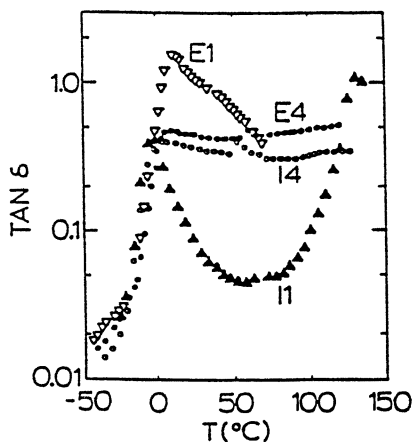


Figure 7. Temperature dependence of $\tan \delta$ for four IPNs: E1, 74% PEA:26% PS; E4, 72% PEA:28% PMMA; I1, 25% PS:75% PEA; I4, 27% PMMA:73% PEA. The components of the IPNs were synthesized in the order as listed. Reproduced from reference 26.

were isomers, it was reasoned that the heat of mixing would be near zero and, therefore, the IPN must lie near the phase boundary; that is, the IPNs exhibited a microheterogeneous morphology.

Further work led to the development of "silent paint", which is a latex IPN based on *cross*-poly(ethyl methacrylate)-*intercross*-poly(*n*-butyl acrylate) constrained with epoxy resin (25) and a constrained layer configuration prepared from the IPN itself (26). These IPNs were prepared by the sequential method. Monomer II was only allowed to swell the outer regions of network I, which was a soft viscoelastic material before curing. In this manner an IPN was formed that had a hard outer surface and a soft viscoelastic core.

Recent Types of IPN Materials Being Studied for Energy-Damping Applications. Klempner et al. studied a series of polyurethane-epoxy (PU-E) full and semi-IPNs (27, 28). The vibration-damping performance of the elastomers, which was characterized by $\tan \delta$ measurements (Rheovibron), was tailored to exhibit highest performance centered around room temperature. Further work led to the development of PU-E IPN cellular plastic foams (29, 30). These viscoelastic materials were based on elastomer formulations that exhibited broad and high $\tan \delta$ versus temperature peaks centered around room temperature. The sound attenuation properties were characterized by the impedance tube technique (standing wave apparatus). The IPN foams, some of which are high density, did not absorb more energy than the lower density foams, which suggests the importance of cell structure. Although most of the IPN foams exhibited higher sound absorption properties than PU foams, no direct correlation could be made with respect to damping performance.

Chang et al. (31) broadened the concept of group contribution analysis by comparing theoretical damping performance to experimental data for

homopolymers, statistical copolymers, and IPNs based on acrylic, vinyl, and styrenic monomers. Fay et al. (32) studied the effect of the loss modulus on the damping behavior of poly(vinyl methyl ether)–polystyrene blends and IPNs. Other studies include kinetic aspects of IPN formation that influence damping performance (33) and the effects of fillers on PU–E IPNs (34).

Recent findings (35) suggest that for airborne sound attenuation by foams, the effects of cell structure may be more significant due to scattering than due to intrinsic absorption (viscoelastic foam morphology). A polyimide foam with low density (less than 1% solid polymer), highly irregular-shaped open cells, and very high glass-transition temperature (T_g) exhibited significantly higher sound absorption coefficients (impedance tube technique) than did a viscoelastic open-cell polyurethane foam with a density 10 times greater (Figure 8). No correlation was found between sound absorption and ball rebound, hysteresis, or compressive measurements (Table I). The polyimide foam (36) was compared to toluene diisocyanate-based urethane foams that are characterized as highly resilient, semiflexible, or viscoelastic.

IPN Studies

Polyurethane–Poly(vinyl chloride) Semi-IPNs. Pseudo- or semi-interpenetrating polymer networks (SIPNs) were prepared from various polyurethanes (PU) and poly(vinyl chloride) (PVC). These SIPNs are a class

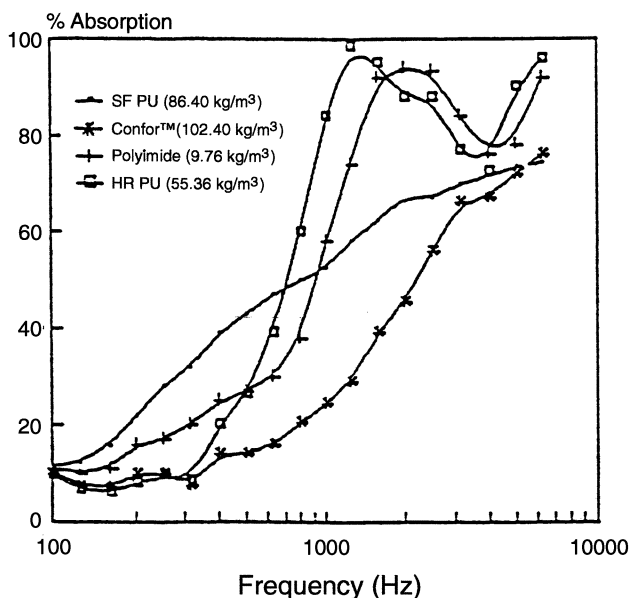


Figure 8. Sound absorption of various foams parallel to foam rise (foam thickness is 2.54 cm).

of sequential IPN in which only one component is in network form. The polyurethane was based on a mixture of two polyols: poly(ϵ -caprolactone diol) (PCL) and poly(oxypropylene diol) (PPG). PCL is miscible in all proportions with PVC (37) and when it is included in polyurethanes as the soft segment, PU-PVC alloys that form are more homogeneous. PPG diol is immiscible with PVC and results in phase separation between the polyurethane and PVC. To obtain SIPNs with microheterogeneous morphologies, the polyurethanes were based on a mixture of these two polyols. The microheterogeneous morphologies result in broadened T_g and frequency damping ranges (38).

The materials used in this study are listed in Table II. Dynamic mechanical spectroscopy (DMS) was carried out on a dynamic mechanical thermal analyzer (Rheovibron DDV-II-C type, Toyo Baldwin Co., Ltd.) from -60 to

Table I. Properties of Foam Employed for Normal Incidence Sound Absorption Measurement

<i>Property</i>	<i>HR^a</i>	<i>SF^b</i>	<i>VE^c</i>	<i>Polyamide</i>
Density (kg/m ³)	55.36	86.40	102.40	9.76
Ball rebound (%)	55	20	2.3	32
Hysteresis (%)	18.5	63.6	-100	—
Compressive stress (kPa)				
25% deformation	2.28	37.74	1.93	10.49
65% deformation	6.07	85.49	4.49	31.40

^a HR, high-resilience.

^b SF, semi-flexible.

^c VE, viscoelastic commercial foam CONFOR supplied by Specialty Composites Corporation (company data).

Table II. Materials Used in IPN Studies

<i>Chemical Composition</i>	<i>Trade Name</i>	<i>Supplier</i>	<i>Molecular Weight (g/mol)</i>	<i>Equivalent Weight</i>	<i>Designation</i>
Poly(oxypropylene glycol)	Pluracol P-2010	BASF	1,992	996	PPG-2000
Poly(ϵ -caprolactone glycol)	Tone 0240	Union Carbide	1,996	998	PCL-2000
4,4'-Diphenylmethane diisocyanate	Mondur M	Mobay	250	125	MDI
Triethanolamine	—	Matheson	149	49.7	TEOA
Poly(vinyl chloride)	VC-106 PM	Borden	58,000	—	PVC
Dibutyltin dilaurate	Dabco T-12	Air Products	—	—	T-12
Tetrahydrofuran	—	Fisher	—	—	THF
Barium-cobalt-zinc salt	BC-103	Scientific Interstab	—	—	BC-103

100 °C at a heating rate of 1–3 °C/min and 110 Hz. Tensile testing (Instron Table Model 1130 Universal Tester) was carried out according to ASTM D-1708 at a strain rate of 50 mm/min using microdie-cut samples. To study the phase behavior and to determine the lower critical solution temperature (if any exists), annealing was carried out on samples equal in size to samples required for DMS analysis (4 × 4 × 0.25 mm). Samples were wrapped in poly(tetrafluoroethylene) sheets and then in aluminum foil and annealed in an electronically controlled oil bath. Next the samples were quenched in liquid nitrogen and the dynamic mechanical spectra were then obtained. Turbidity was determined visually by viewing through the 1-mm-thick specimens over printed white paper. Pure cast PVC was used as a control and any reduction in clarity was designated turbid. The DMS data were used as a measure of miscibility and energy damping properties. Composition and turbidity are given in Table III.

IPNs prepared from 100% PCL-based PU and PVC were homogeneous as evidenced by single, composition-dependent $\tan \delta$ maxima (shown for a single composition in Figure 9); that is, the glass-transition (T_g) temperatures exhibited simple additivity (by weight) when plotted against composition. The IPNs were annealed at temperatures up to 200 °C and various lengths of time to induce phase separation, although none was observed (Figure 10). Annealing above 200 °C resulted in severe degradation of the films; therefore, no lower critical solution temperature (LCST) could be found.

All SIPNs prepared from 80% PCL:20% PPG-based polyurethane and PVC also exhibited single transitions (shown for a single composition in Figure 11). The transitions, however, are significantly broader than those of the IPNs based on 100% PCL, which suggests a broader distribution of phase sizes (Table IV). This suggests a co-continuous microheterogeneous morphology in which the intermediate compositions lie near the phase boundary. From a practical standpoint, this morphology is ideal for damping considerations. Broader T_g ranges equate to higher damping efficiency over both broader temperature and frequency ranges. The time–temperature superposition principle that uses the Williams–Landel–Ferry (WLF) equation enables a demonstration that increasing the glass-transition range by 10 °C corresponds to an increased frequency-damping range of 5–6 decades.

Annealing under various temperature and time conditions resulted in two distinguishable phases of intermediate composition (Figure 12), although phase separation was not complete. A phase diagram (Figure 13) was derived from these data and showed that an LCST exists at 120 °C. Note that the interval between annealing temperatures was 20 °C.

All IPNs based on 100% PCL and 80% PCL:20% PPG-based PU were clear, whereas the individual polyurethanes were turbid because of PCL crystallinity. The clarity of the IPNs partly may be due to similar refractive indices for PVC (9.6) and PU (9.5–9.6) rather than solely due to miscibility.

Table III. Composition and Turbidity of Pseudo-IPNs

Sample Code	Prepolymer Composition (%)	PU (wt%)	PVC (wt%)	Turbidity ^a
A-1	100 PCL	100	0	T
A-2	100 PCL	80	20	C
A-3	100 PCL	60	40	C
A-4	100 PCL	50	50	C
A-5	100 PCL	40	60	C
A-6	100 PCL	20	80	C
B-1	80 PCL:20 PPG	100	0	T
B-2	80 PCL:20 PPG	80	20	C
B-3	80 PCL:20 PPG	60	40	C
B-4	80 PCL:20 PPG	50	50	C
B-5	80 PCL:20 PPG	40	60	C
C-1	70 PCL:30 PPG	100	0	T
C-2	70 PCL:30 PPG	80	20	C
C-3	70 PCL:30 PPG	60	40	C
C-4	70 PCL:30 PPG	50	50	C
C-5	70 PCL:30 PPG	40	60	C
C-6	70 PCL:30 PPG	20	80	C
C-7	70 PCL:30 PPG	0	100	C
D-1	60 PCL:40 PPG	100	0	T
D-2	60 PCL:40 PPG	80	20	C
D-3	60 PCL:40 PPG	60	40	C
D-4	60 PCL:40 PPG	50	50	C
D-5	60 PCL:40 PPG	40	60	ST
D-6	60 PCL:40 PPG	20	80	ST
E-1	50 PCL:50 PPG	100	0	T
E-2	50 PCL:50 PPG	80	20	ST
E-3	50 PCL:50 PPG	60	40	ST
E-4	50 PCL:50 PPG	50	50	ST
E-5	50 PCL:50 PPG	40	60	ST
E-6	50 PCL:50 PPG	20	80	ST
F-1	50 PCL:50 PPG	100	0	T
F-2	50 PCL:50 PPG	80	20	T
F-3	50 PCL:50 PPG	60	40	T
F-4	50 PCL:50 PPG	50	50	T
F-5	50 PCL:50 PPG	40	60	T
F-6	50 PCL:50 PPG	20	80	T

^a T indicates turbid; C indicates clear; ST indicates semi-turbid.

Higher quantities of PPG such as in PU based on 70% PCL:30% PPG exhibited decreased linearity of the T_g versus composition curve, as expected. These IPNs exhibited the highest level of damping. Intermediate compositions lay on or near the spinode, which was evidenced by an LCST of 80–100 °C, nearly the temperature at which the materials were cured. These

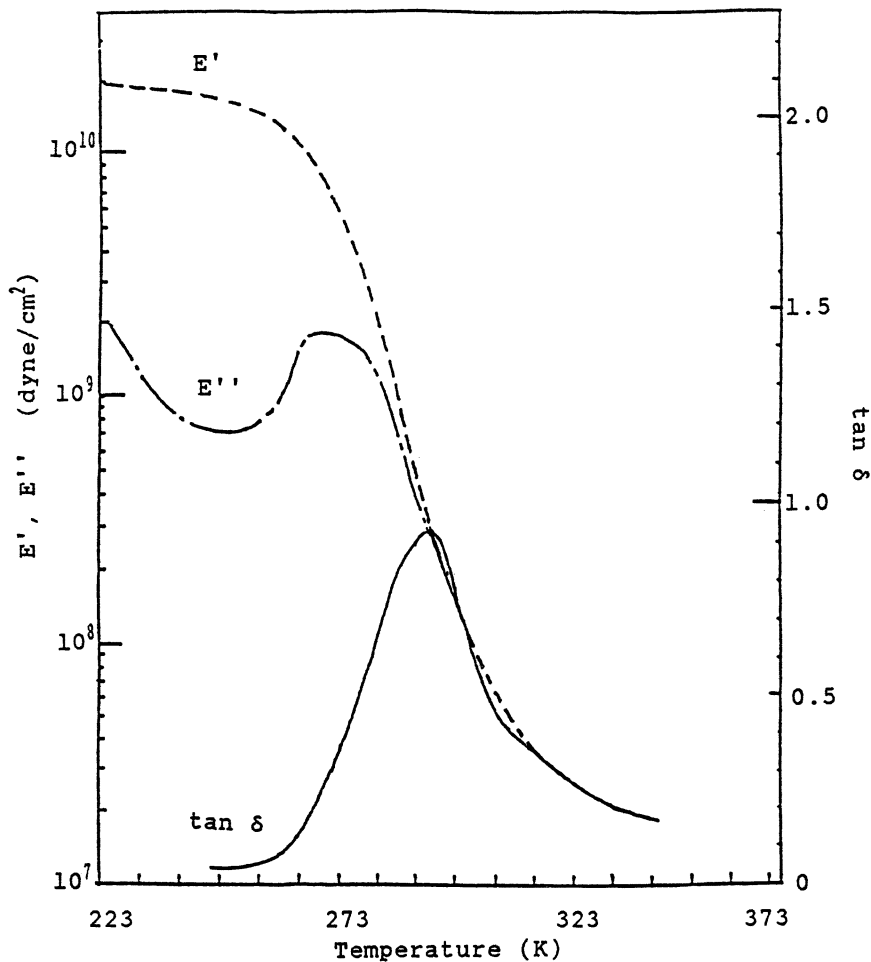


Figure 9. Dynamic mechanical spectrum of pseudo-IPN composed of 50% polyurethane (100% PCL-based) and 50% PVC.

materials did not appear to phase separate over time when kept for more than 1 year at uncontrolled ambient conditions. This lack of phase separation suggests that cross-linking of the PU component inhibited phase separation to some degree. On the other hand, IPNs that contained 40% or more PPG-based urethane exhibited two phases, which suggests that even with kinetically controlled mixing, phase separation processes occurred sooner and controlled the overall morphology. The level of cross-linking, the rate of urethane gelation, or the rate of solvent removal are factors that may influence the balance between thermodynamic processes (phase separation) and kinetic processes (“forced miscibility”). Other parameters that effect this

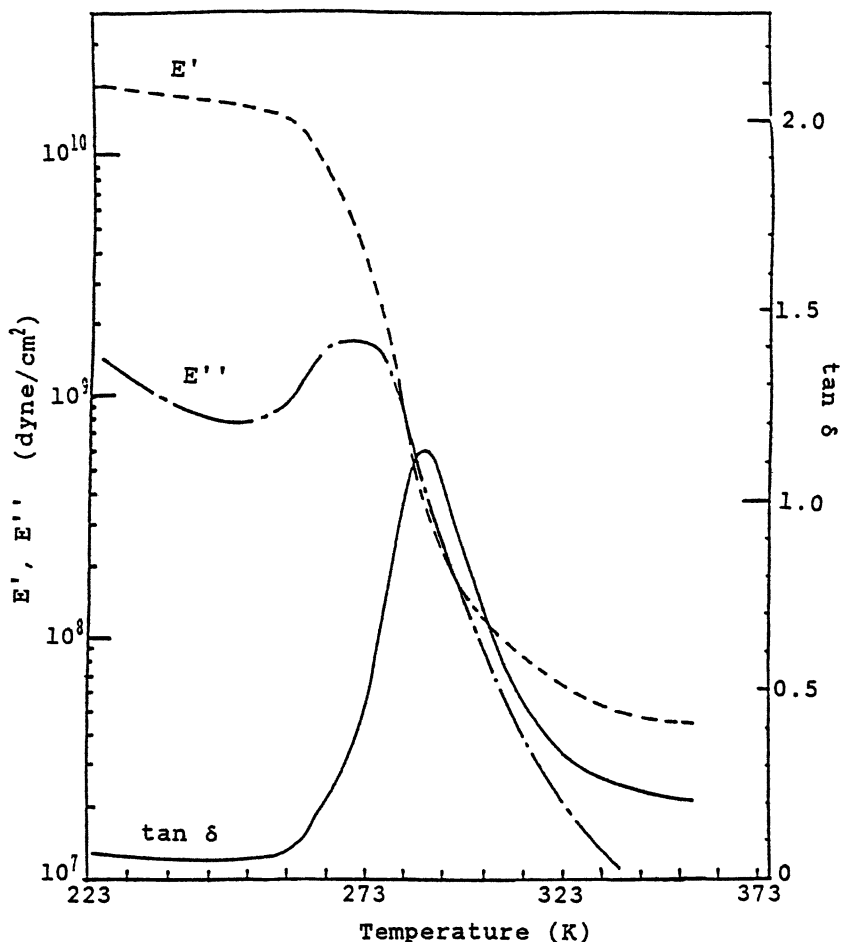


Figure 10. Dynamic mechanical spectrum of pseudo-IPNs composed of 50% polyurethane (100% PCL-based) and 50% PVC, annealed at 200 °C for 20 min.

balance and that are now being investigated include reaction temperature and pressure.

Polyurethane–Poly(vinyl ester) Hybrid-IPN Foams. In this study, polyurethane and polyurethane–poly(vinyl ester) (PVE) hybrid-interpenetrating polymer network foams were prepared and low-frequency (100–500 Hz) sound absorption measurements and dynamic mechanical analysis (DMA) were performed (39).

The purpose of this study was twofold: (1) to determine the low-frequency sound absorption properties of filled and unfilled polyurethane-based IPNs

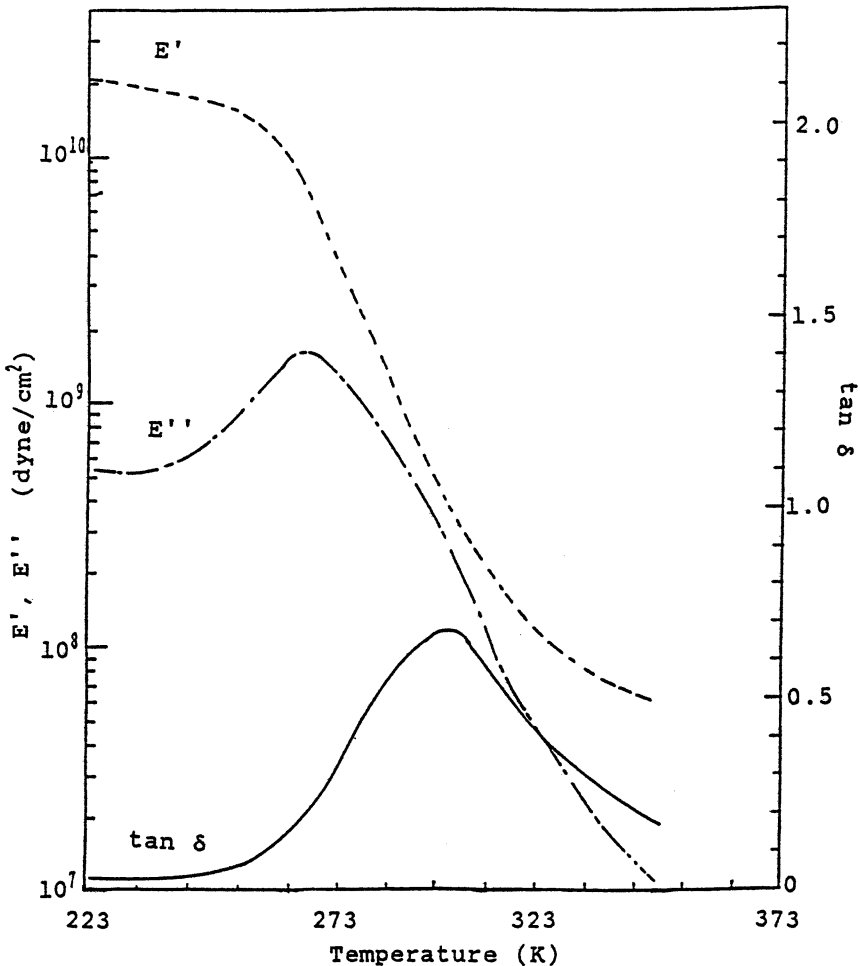


Figure 11. Dynamic mechanical spectrum of pseudo-IPNs composed of 50% polyurethane (80% PCL:20% PPG-based) and 50% PVC.

and (2) to investigate the relationship between viscoelastic response (damping curves) and sound absorption properties. The effect of cell structure, cell orientation, density, and foam thickness were determined as well.

The foams (Table V) were prepared by the one-shot free-rise method at room temperature using a high-speed constant-torque mixer. The PVE used (Derakane 470-36) contains 36% styrene in a low molecular weight (470) resin based on isophthalic ester. The polyurethane foams based on toluene diisocyanate (TDI; T-80, Dow Chemical, and 80:20 mixture of 2,4- to 2,6-toluene diisocyanate) were post-cured at 70 °C for 16 h. The density (ASTM D 1622), Bashore rebound (resilience, ASTM D 3574 H), compressive

Table IV. Dynamic Mechanical Data of Pseudo-IPNs

<i>Sample Code</i>	<i>Temp. at E'' max (°C)</i>	<i>Temp. at tan δ max (°C)</i>	<i>Height of tan δ Peak</i>	<i>Half-Width of tan δ Peak</i>
A-1-a, turbid sample	-33, -2	-25	0.49	51
A-1-b, clear after heating	-31, 0	-22	1.58	17
A-2	-19	-6	1.05	25
A-3	-3	16	0.85	36
A-4	10	34	0.91	37
A-5	20	45	0.76	51
A-6	49	86	0.68	53
B-1-a, turbid sample	-36, -5	-29	0.67	16
B-1-b, clear after heating	-39, -2	-25	1.69	18
B-2	-20	-3	1.01	30
B-3	-9	18	0.68	52
B-4	4	39	0.68	54
B-5	13	63	0.53	86
B-6	50	94	0.61	50
B-7	77	98	0.97	37
C-1, a turbid sample	-30	-16	0.99	32
C-1-b clear after heating	-33	-17	1.49	26
C-2	-20	0	1.00	35
C-3	-8	21	0.68	60
C-4	5	48	0.57	77
C-5	20	66	0.53	61
C-6	64	92	0.80	40

hysteresis at 25 and 65% deformation, and dynamic mechanical properties (DuPont, DMA 900 series) were measured. Sound absorption coefficients were measured by the impedance tube technique using Bruel and Kjaer equipment (standing wave apparatus tube 400z, beat frequency oscillator type 1014, and frequency spectrometer type 2112). Because low frequencies were of interest, only the large-diameter tube (101.6 mm) was used. The thickness of all foams was 25.4 mm. The properties of the foams are given in Table VI. Three isocyanate-polyol combinations were used to prepare the PU foams: TDI-Pluracol 726, TDI-Pluracol 1003, and 4,4'-diphenylmethane diisocyanate-Pluracol 1003 (MDI-Pluracol 1003). Note that these IPNs are of the intercross or hybrid type due to the probable reactions of isocyanate with the hydroxy groups and, to a lesser extent, with the acid groups on PVE. The overall polyol:diisocyanate equivalence ratio is believed to be lower than ideal.

The sound absorption coefficients of the three PU foam compositions are shown in Figure 14 and their respective loss modulus curves are shown in Figure 15. Note that the curves are offset with respect to relative log E'' for clarity. The PU based on MDI and Pluracol 1003 exhibited the broadest

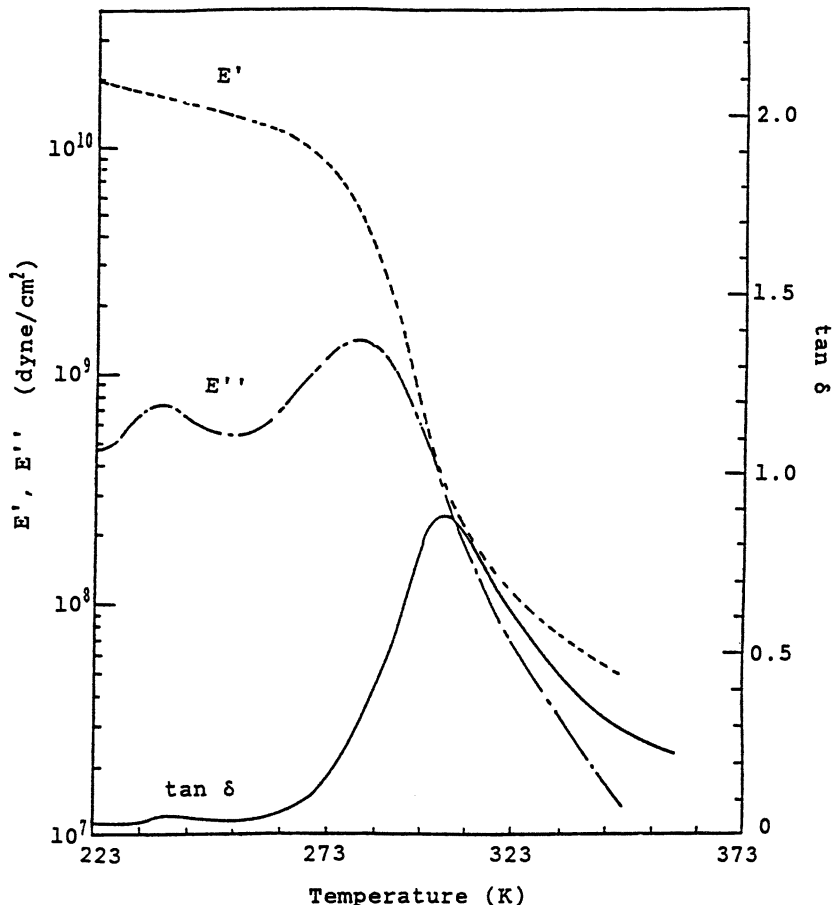


Figure 12. Dynamic mechanical spectrum of pseudo-IPNs composed of 50% polyurethane (80% PCL:20% PPG-based) and 50% PVC, annealed at 200 °C for 15 min.

transition and highest sound absorption coefficients (SAC), although differences in density were not accounted for.

The sound absorption coefficients (Figure 16) of TDI-Pluracol 726-based PU and PU-PVE IPNs exhibited a maximum at PU:PVE = 90:10 and the coefficients decreased at nearly all frequencies for PU:PVE = 80:20. Note that the SAC of pure PU and PU:PVE = 80:20 are nearly identical. This behavior may be due to phase separation; that is, at a composition of PU:PVE = 90:10, a microheterogeneous morphology probably exists because there is too little PVE component to result in complete phase separation (Figure 17). At PU:PVE = 80:20, phase separation resulted, as evidenced by DMA loss modulus versus temperature curves, and the sound absorption

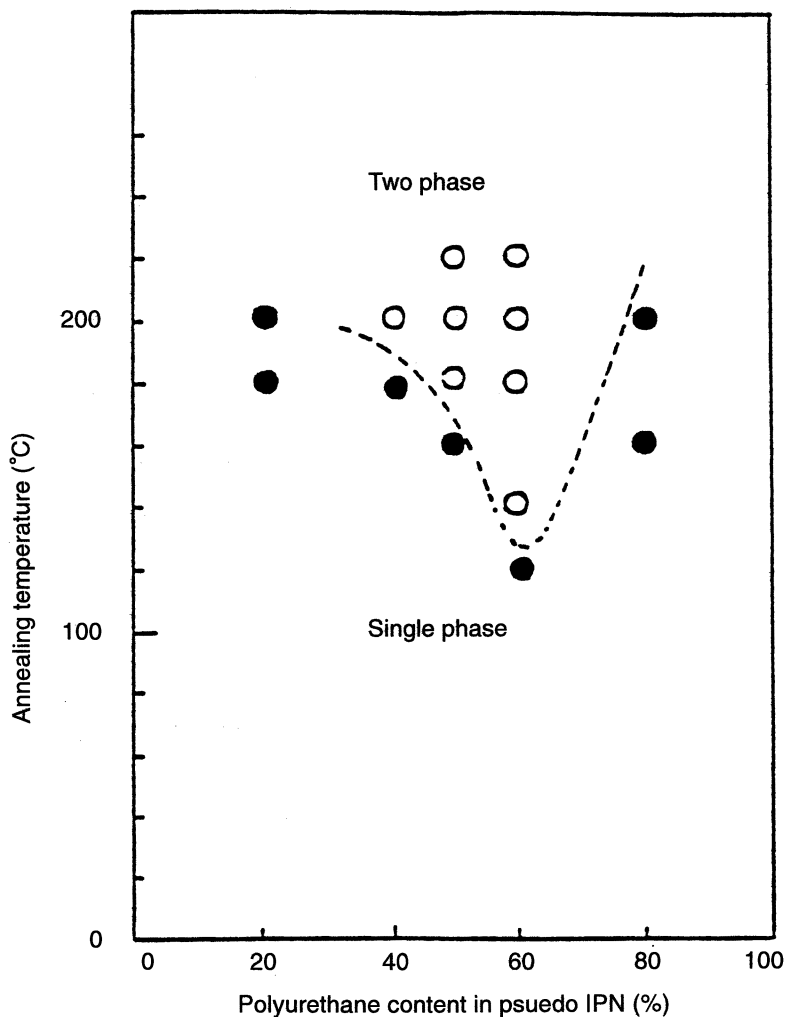


Figure 13. Phase diagram of pseudo-IPNs composed of polyurethane (80% PCL:20% PPG-based) and PVC.

characteristics are similar to the PU control. This situation suggests that the IPN morphology and, in particular, the degree of PU-PVE phase separation may influence the sound absorption properties similar to its influence on damping properties in viscoelastic materials.

There are two considerations necessary: one is related to these experiments and the other is related to acoustics. First, these results reflect only one SAC measurement taken for each foam. Although three specimens of each formulation were prepared, only enough material was available for these

Table V. Six Formulations of Flexible Polyurethane and Polyurethane-Poly(vinyl ester) IPN Foams

<i>Designation</i>	<i>1</i>	<i>2</i>	<i>3</i>	<i>4</i>	<i>5</i>	<i>6</i>
PU-PVE ratio	100	100	100	90:10	90:10	90:10
Pluracol 726	100	—	—	100	—	—
Pluracol 1003	—	95	95	—	95	95
Voranol 220-530	—	5	5	—	5	5
Water	1.5	1.5	1.5	3.5	1.5	—
DC-5043	1.0	—	—	1.0	—	—
DC-190	1.0	—	—	1.0	—	—
Dabco 33LV	0.40	0.20	0.20	0.40	0.20	0.20
Dabco T-9	0.05	—	—	—	—	—
Dabco T-12	—	0.15	0.15	0.15	0.15	0.15
CFC-11	—	—	5	—	—	—
Isonate 2143L	—	—	39.5	—	—	—
Lupranate T-80	24.6	23.8	—	45	23.8	—
Isocyanate index	105	105	105	105	105	105
Derakane 470-36	—	—	—	16.6	14.1	15.8
DMA	—	—	—	0.80	0.80	0.80
Co-octoate	—	—	—	0.01	0.10	0.10
MEKP	—	—	—	0.17	0.14	0.16

Table VI. Properties of Six Flexible Polyurethane and PU-PVE IPN Foams

<i>Property</i>	<i>1</i>	<i>2</i>	<i>3</i>	<i>4</i>	<i>5</i>	<i>6</i>
PU-PVE ratio	100	100	100	90:10	90:10	90:10
Polyol	Pluracol 726	Pluracol 1003	Pluracol 1003	Pluracol 726	Pluracol 1003	Pluracol 1003
Isocyanate	TDI	TDI	MDI	TDI	TDI	MDI
Density (kg/m ³)	63.43	66.15	62.79	40.85	126.8	91.14
Ball rebound (%)	35	43	31	31	28	13
Hysteresis (%)	—	40.0	50.3	53.9	49.2	63.7
Compressive stress (kPa)						
25% deformation	—	8.3	11.0	4.1	15.1	15.7
65% deformation	—	15.9	11.9	9.4	63.3	40.3

measurements after all other characterizations were performed and no statistics could be gathered. Second, repeated observations at the University of Detroit Mercy and by others indicate that IPN morphology may or may not influence sound attenuation. This ambivalence can be due to various factors. First, the measurement of SAC is the measure of actual sound attenuation and includes contributions from scattering, redirection, mode conversion, and intrinsic absorption. On the other hand, IPN (or any alloy) morphology should only contribute to the intrinsic absorption contribution. Thus if the

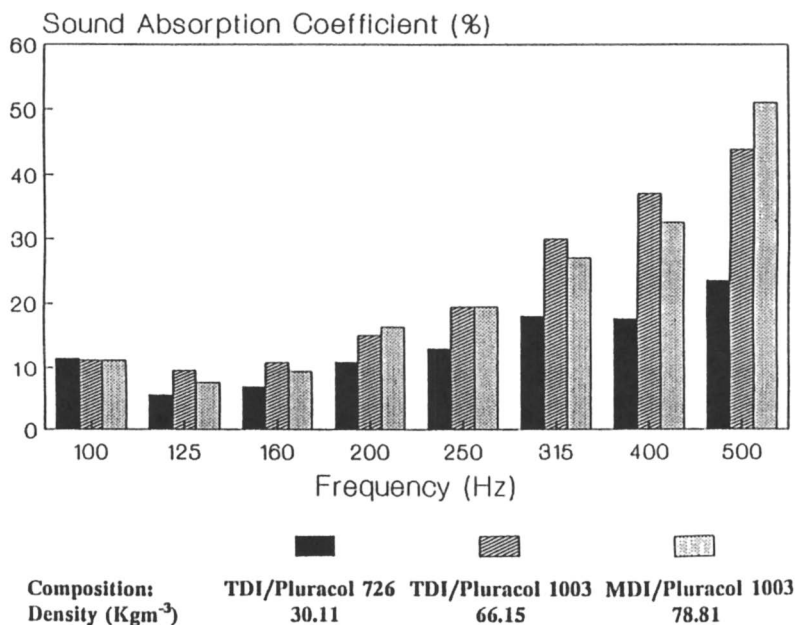


Figure 14. Effect of chemical structure on sound absorption coefficients of PU foams.

other parameters are large in magnitude, the effects of morphology will not be as great, or may even be undetectable. If the other contributions are small in magnitude, then morphology may have a higher net effect on the overall SAC. Second, the sound absorption properties are dependent on the characteristic of the impinging sound waves. In damping vibrations, the viscoelastic polymer is forced to vibrate because it is in direct contact with the vibrating metal surface and energy transfer from metal to polymer is high. Efficient absorption can occur. When airborne waves contact foam cell walls, the sound pressure must be high enough to induce energy transfer. The behavior of the previous IPNs is similar to IPNs based on TDI and Pluracol 1003, although different morphologies exist. The pure PU exhibits similar sound absorption coefficients to both PU:PVE = 90:10 and PU:PVE = 80:20 IPNs (Figure 18). DMA results suggest that the PU and its respective IPNs possess microheterogeneous morphologies (Figure 19), as evidenced by relatively broad loss modulus versus temperature transition ranges.

IPNs based on MDI and Pluracol 1003 exhibit similar sound absorption properties (Figure 20) to the respective PU, even with different densities.

The effect of fillers on a single IPN composition (PU:PVE = 80:20) based on MDI and Pluracol 1003 is shown in Figure 21. Note that zinc powder and 40-mesh rubber powder resulted in some decrease in sound

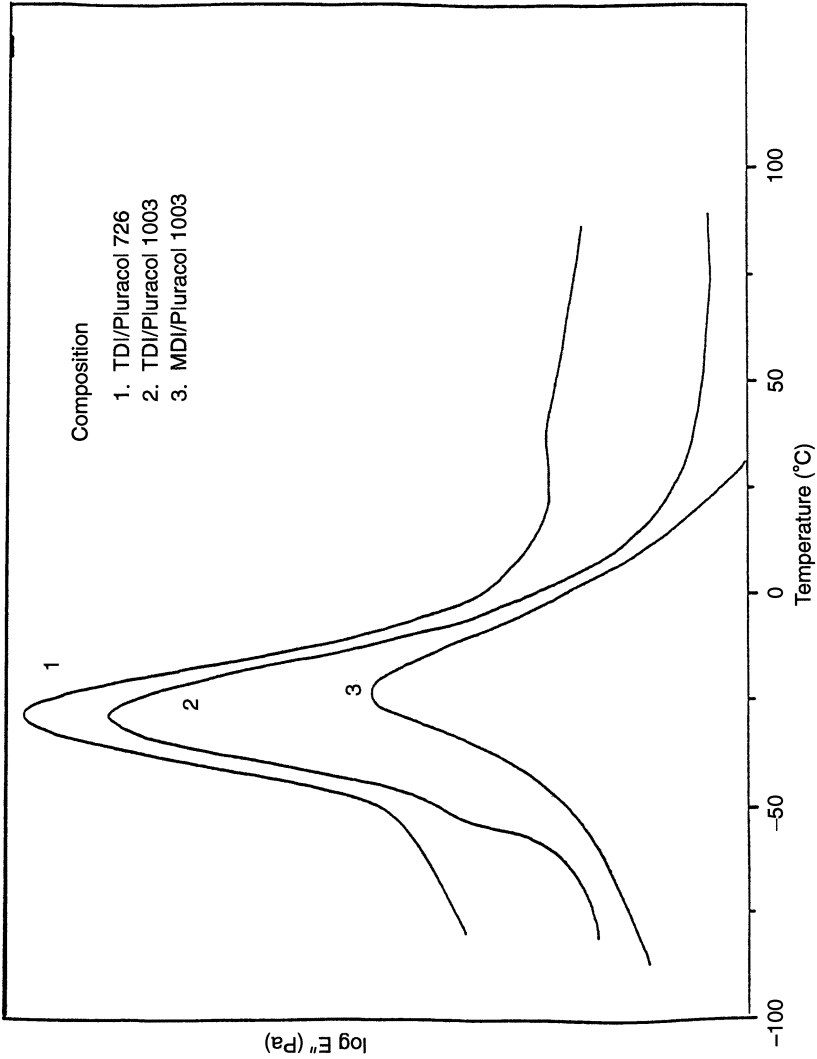


Figure 15. Loss modulus curves of PU foams.

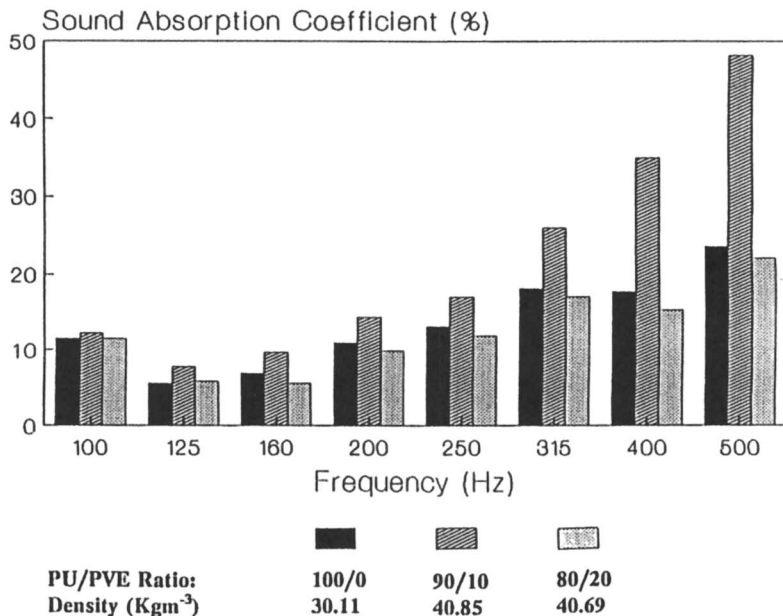


Figure 16. Sound absorption coefficients of TDI-Pluracol 726-based PU and PU-PVE IPN foams.

absorption coefficients at low frequencies, whereas rubber (10-mesh size) enhanced the property.

Polyurethane-Epoxy-Unsaturated Polyester Two- and Three-Component IPNs. In this study two- and three-component IPN elastomers and foams were prepared from polyurethane, epoxy (E), and unsaturated polyester (UPE) by the simultaneous technique (40). The energy-absorbing ability of the elastomers were demonstrated by dynamic mechanical spectroscopy (Rheovibron), ball rebound, and hysteresis measurements. Foams formulations that were based on high damping elastomers were also tested for sound absorption properties. The effects of graphite, rubber, and plasticizers on the IPN foams and elastomers were examined.

The materials used are given in Table VII. Polyol (Niax 31-28), epoxy (DER-330), and chain extender (Isonol-100) were vacuum dried overnight at 80 °C. All other materials were used as received.

For preparation of the polyurethanes, ethylene-oxide-capped PPG containing 21 wt% grafted polyacrylonitrile (Niax 31-28, Union Carbide; MW = 6000) was blended with a carbodiimide-modified diphenylmethane diisocyanate (Isonate-143L, Dow Chemical) *N,N'*-bis(2-hydroxypropyl)aniline (Isonol-100, Dow Chemical) and dibutyltin dilaurate (Dabco T-12, Air Products).

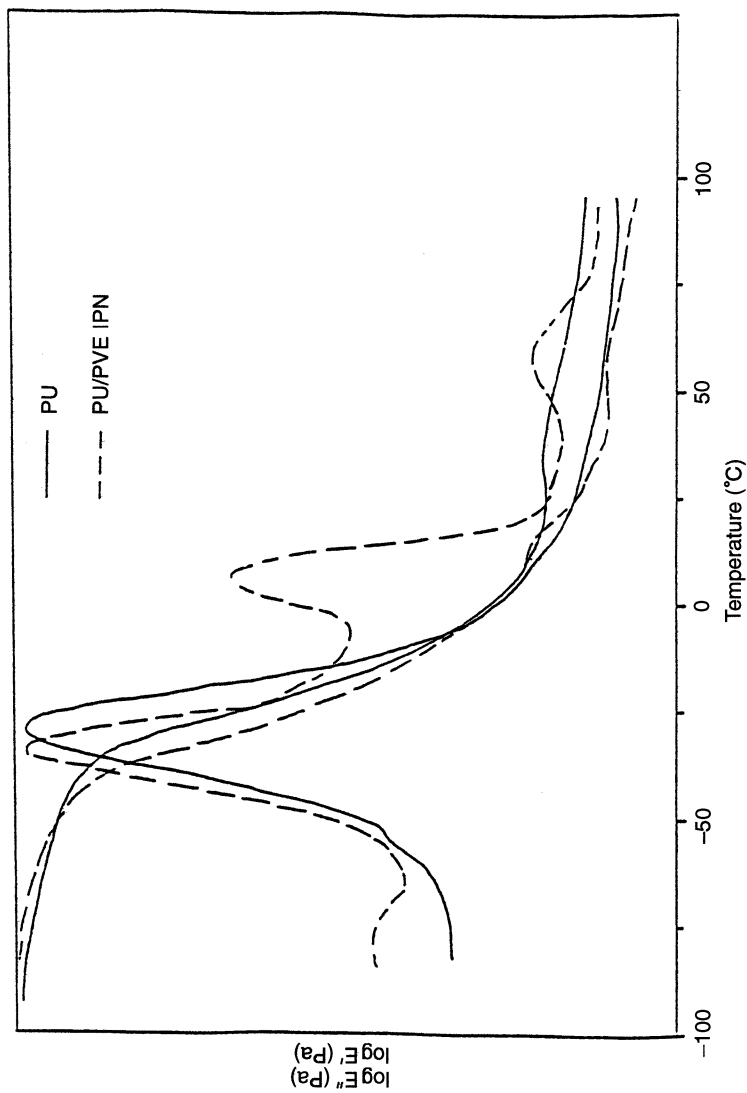


Figure 17. Comparison of loss modulus and storage modulus of TDI-Pluracol 726-based PU and PU-PVE (80:20 wt%) IPN.

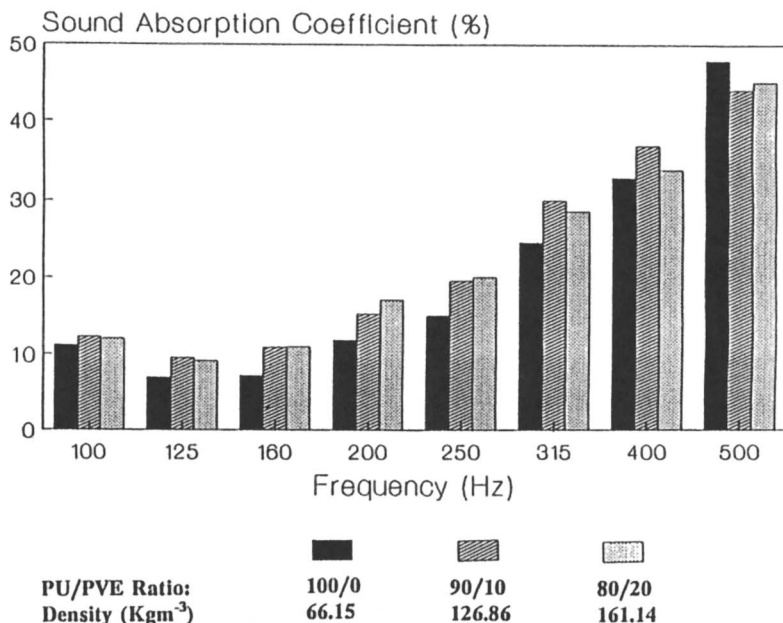


Figure 18. Sound absorption coefficients of TDI-Pluracol 1003-based PU and PU-PVE IPN foams.

The IPN elastomers (formulations shown in Tables VIII-X) were synthesized by mixing two components. In the case of two-component PU-E IPN elastomers, one component contained Niax 31-28, Isonol-100, Dabco T-12, and epoxy catalyst (BF_3 etherate; Eastman Chemical). The other component contained epoxy resin (DER-330, Dow Chemical) and Isonate-143L. In the case of three-component IPN elastomers, unsaturated polyester and *t*-butyl perbenzoate catalyst (TBPB) were premixed in component one and epoxy resin was mixed in component two.

The blend was mixed for 60 s at ambient temperature, then poured into a hot mold (100 °C) and cured for 30 min on a platen press under a pressure of approximately 2.8 MPa. The elastomers were then post-cured in an oven at 100 °C for 16 h and conditioned at 25 °C and 50% relative humidity for 3 days prior to testing.

PU foams were prepared by the one-shot free-rise method. A homogeneous liquid mixture of Niax 31-28, Isonol-100, silicone surfactant DC-193 (Dow Corning), Dabco T-12, Niax A-1 (Union Carbide), trichlorofluoromethane (Freon 11A, DuPont), and water was mixed thoroughly with Isonate-143L, then poured into an open cold mold, and allowed to free rise.

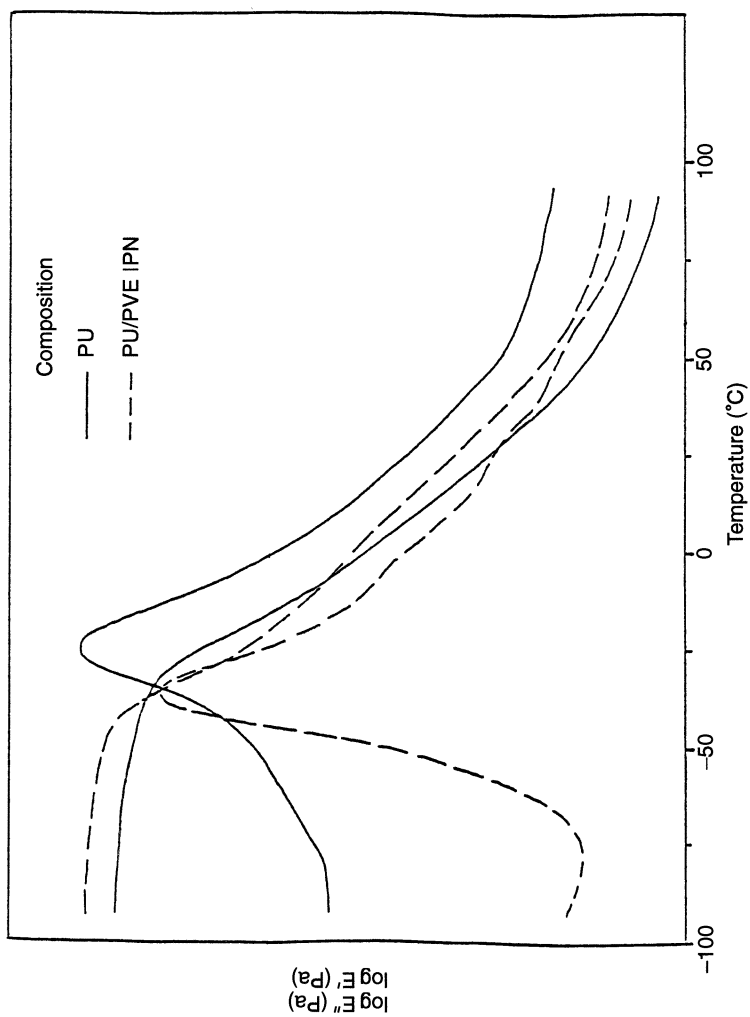


Figure 19. Comparison of loss modulus and storage modulus of TDI-Pluracol 1003-based PU-PVE (80:20 wt%) IPN.

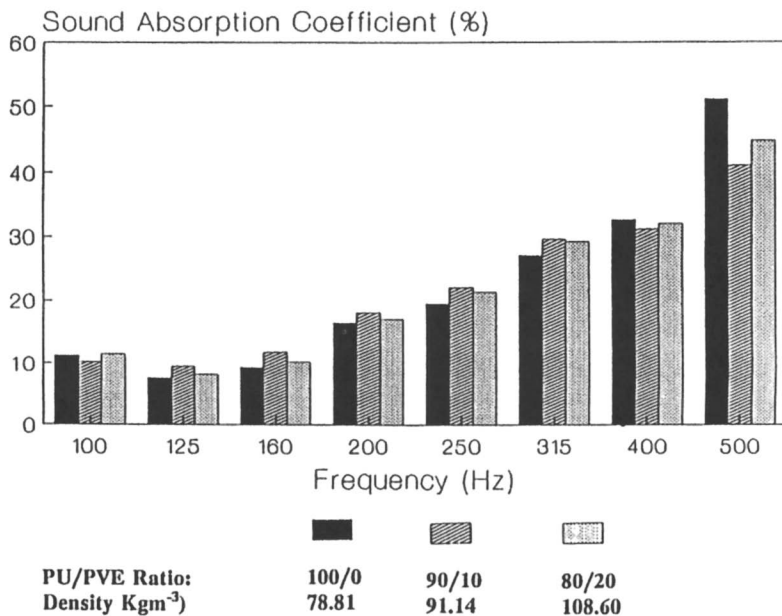


Figure 20. Sound absorption coefficients of MDI-Pluracol 1003-based PU-PVE IPN foams.

Two-Component IPN Elastomers. The two-component polyurethane-epoxy IPNs (Tables VIII-X) were formulated in compositions ranging from 60:40 to 40:60, respectively, with and without various fillers. Again, these IPNs are better characterized as intercross-IPNs due to the probability of some diisocyanate reacting with terminal hydroxy or epoxy groups. The isocyanate index was again less than ideal and was not determined. The unfilled IPN (No. 2, Table VIII) exhibited a microheterogeneous, co-continuous morphology as evidenced by a broad loss tangent curve that was larger in total area than the pure PU component. Only a single DMS reading was taken on each specimen. Also, due to the tendency of the material to become very soft at elevated temperatures, the total area under the $\tan \delta$ versus temperature curve was difficult to determine. However, the recorded values are believed to represent the most accurate values possible.

The fillers, which included various grades of graphite, mica powder, and plasticizer (Benzoflex 988) (Tables XI-XII), also resulted in significant differences in the total loss area. The breadth and position of the $\tan \delta$ maxima were effected also.

In general, graphite filler (all grades) resulted in lower $\tan \delta$ maximum values and broader damping ranges.

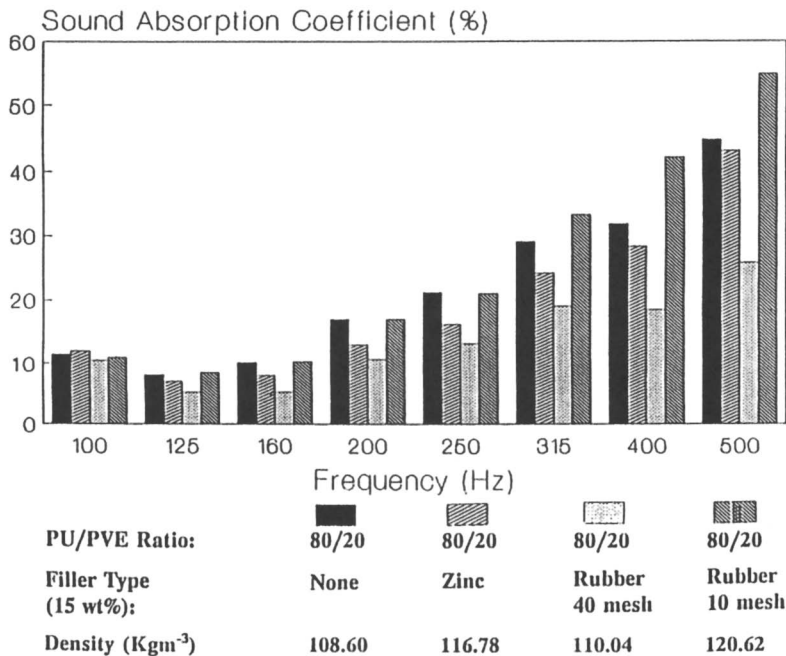


Figure 21. Effect of zinc and rubber fillers on sound absorption coefficients of MDI-Pluracol 1003-based PU-PVE IPN foams.

Three-Component IPN Elastomers. Three-component IPNs based on polyurethane, epoxy, and unsaturated polyester (PU-E-PVE) (Table XIII) were prepared to further broaden the glass-transition region because unsaturated polyester is immiscible with both the urethane and epoxy components. The loss tangent curves stayed high over a significantly broader temperature range and thus no specific value could be ascribed to $\tan \delta$ maximum; rather a range was reported.

Two-Component IPN Foams. Two-component IPN foams that consisted of polyurethane and epoxy were prepared based on the elastomer formulations that exhibited the broadest and highest $\tan \delta$ curves. The foam formulations and properties are given in Tables XIV and XV.

In general, the IPN foams possessed greater mechanical energy absorption with respect to the polyurethane foam as evidenced by hysteresis and ball rebound. This observation agrees with the expected morphology, based on the elastomer studies in which the IPNs possessed a broader glass-transition region. Less enhancement in sound absorption resulted (Figure 22),

Table VII. Materials

<i>Designation</i>	<i>Description</i>	<i>Supplier</i>
Isonate-143L	Carbodiimide modified diphenylmethane diisocyanate	Dow Chemical Co.
Niax 31-28	Graft copolymer of poly(oxypropylene) (oxyethylene) adduct of glycerol	Union Carbide
Isonol-100	<i>N,N'</i> -Bis(2-hydroxypropyl) aniline	Dow Chemical Co.
DER-330	Diglycidyl ether of bisphenol A	Dow Chemical Co.
Unsaturated polyester	Unsaturated polyester	Budd Chemical
T-12	Dibutyltin dilaurate	Air Products
Niax A-1	70% Bis(2-dimethylaminoethyl)ether solution in dipropylene glycol	Union Carbide
BF ₃ C(C ₂ H ₅) ₂	Boron trifluoride etherate	Eastman Chemical
TBPB	(±)-Butyl perbenzoate	Aldrich
DMP-30	2,4,6-Tris(dimethylamino methyl) phenol	Rohm & Haas
XU-213	BCl ₃ -Amine complex	Ciba-Giegy
Freon-11A	Trichlorofluoromethane	DuPont
DC-193	Silicone copolymer surfactant	Dow Corning
L-540	Silicone copolymer surfactant	Union Carbide
L-5303	Silicone copolymer surfactant	Union Carbide
L-548	Silicone copolymer surfactant	Union Carbide
1,4-BD	1,4-Butanediol rubber powder	BASF
Santicizer 141	2-Ethylhexyl diphenyl phosphate	Monsanto
Santicizer 148	Isodecyl diphenyl phosphate	Monsanto
Santicizer 160	Butyl benzyl phthalate	Monsanto
Stan-Flux LV	Aromatic processing oil	Harwick Chemical
Benzolfex 988	—	Velsicol Chemical
TCP	Tricresyl phosphate	C.P. Hall Co.
Sundex 748 T	Aromatic oil plasticizer	Sun Graphite
Graphite flake No. 1	Size: -20 mesh + 80 mesh	Asbury Graphite Mills
Graphite flake No. 2	Size: -50 mesh + 200 mesh	Asbury Graphite Mills
Graphite flake No. 3	Size: -80 mesh down	Asbury Graphite Mills
Dicaperl FP 1010	Hollow glass sphere filler	Grefco Inc.

especially at low frequencies. Density and cell structure had a more important effect on the sound absorption.

These experiments also show the effect of several fillers: graphite, rubber powder, and various plasticizers. Graphite (20 wt%), rubber powder (10 wt%), butyl benzyl phthalate (Santicizer 160, 20 wt%), and isodecyl diphenyl phosphate (Santicizer 148, 20 wt%) all resulted in a slight increase in sound absorption properties with respect to their IPN and PU control foams. However, the fillers did not contribute significantly to the hysteresis or ball rebound values.

Table VIII. Formulations of Polyurethane–Epoxy Two-Component IPN Elastomers

<i>Component</i>	<i>1</i>	<i>2</i>	<i>3</i>	<i>4</i>	<i>5</i>	<i>6</i>	<i>7</i>	<i>8</i>	<i>9</i>
Polyurethane									
Isonate 143L	6.48	3.89	3.89	3.89	3.89	3.89	3.89	3.89	3.89
Niax 31-28	62.24	37.35	37.35	37.35	37.35	37.35	37.35	37.35	37.35
Isonol-100	1.27	0.76	0.76	0.76	0.76	0.76	0.76	0.76	0.76
T-12	0.06	0.06	0.06	0.06	0.06	0.06	0.06	0.06	0.06
Epoxy									
DER-330	—	28.0	28.0	28.0	28.0	28.0	28.0	28.0	28.0
BF ₃ Etherate	—	0.6	0.6	0.6	0.6	0.6	0.6	0.6	0.6
Fillers									
Graphite No. 1	—	—	7.0	—	—	—	—	—	—
Graphite No. 2	—	—	—	7.0	—	—	—	—	3.5
Graphite No. 3	—	—	—	—	7.0	—	—	—	—
Dicaperl	—	—	—	—	—	7.0	—	—	—
FP 1010	—	—	—	—	—	—	7.0	—	—
Plasticizer									
Benzoflex 988	—	—	—	—	—	—	7.0	35.0	35.0
PU–epoxy ratio	100:0	60:40	60:40	60:40	60:40	60:40	60:40	60:40	60:40

NOTE: All values (except ratios) are grams.

Table IX. Formulations of Polyurethane–Epoxy Two-Component IPN Elastomers

<i>Component</i>	<i>10</i>	<i>11</i>	<i>12</i>	<i>13</i>	<i>14</i>	<i>15</i>	<i>16</i>	<i>17</i>
Polyurethane								
Isonate 143L	3.89	3.89	3.89	3.89	3.24	3.24	2.59	2.59
Niax 31-28	37.35	37.35	37.35	37.35	31.12	31.12	24.9	24.9
Isonol-100	0.76	0.76	0.76	0.76	0.64	0.64	0.51	0.51
T-12	0.06	0.06	0.06	0.06	0.04	0.04	0.04	0.04
Epoxy								
DER-330	28.0	28.0	28.0	28.0	35.0	35.0	42.0	42.0
BF ₃ Etherate	0.6	0.6	0.6	0.6	0.6	0.6	0.6	0.6
Plasticizers								
Benzoflex 988	—	—	—	—	21.0	—	21.0	—
Santicizer 160	35.0	—	—	—	—	14.0	—	14.0
Stanflux LV	—	7.0	14.0	—	—	—	—	—
Sundex 748T	—	—	—	7.0	—	—	—	—
PU–epoxy ratio	60:40	60:40	60:40	60:40	50:50	50:50	40:60	40:60

NOTE: All values (except ratios) are grams.

Table X. Formulations of Polyurethane–Epoxy–Unsaturated Polyester Three-Component IPN Elastomers

<i>Component</i>	<i>18</i>	<i>19</i>	<i>20</i>	<i>21</i>
Polyurethane				
Isonate 143L	3.24	3.24	2.60	2.60
Niax 31-28	31.12	31.12	24.9	24.9
Isonol-100	0.63	0.63	0.50	0.50
T-12	0.065	0.065	0.052	0.052
Epoxy				
DER-330	14.0	17.50	14.0	7.0
BF ₃ Etherate	0.30	0.40	0.30	0.15
Unsaturated Polyester Resin				
Polyester resin	21.0	17.50	28.0	35.0
TBPB	0.066	0.055	0.088	0.110
PU–E–UPE ratio	50:20:30	50:25:25	40:20:40	40:10:50

NOTE: All values (except ratios) are grams.

Table XI. Comparison of Dynamic Mechanical Spectroscopy Results for IPN Elastomers

<i>Sample Number</i>	<i>System</i>	<i>tan δ max</i>	<i>Temp. (°C) at tan δ max</i>	<i>Temp. Range (°C)</i>	<i>Area Under tan δ Curve</i>
1	100% Polyurethane	0.96	−24	−43–20	35.16
2	60:40 PU:E	0.65	40	−20–108	43.90
3	60:40 PU:E + 10% graphite No. 1	0.71	32	−40–128	49.77
4	60:40 PU:E + 10% graphite No. 2	0.68	32	−40–120	45.62
5	60:40 PU:E + 10% graphite No. 3	0.68	30	−40–104	47.08
6	60:40 PU:E + 10% dicaperl	0.65	48	−20–100	41.57
7	60:40 PU:E + 10% Benzoflex	0.85	20–24	−40–40	36.39
8	60:40 PU:E + 50% Benzoflex	1.70	0	−36–12 ^a	—
9	60:40 PU:E + 10% graphite No. 2 + 50% Benzoflex	1.20	5	−40–32 ^a	—

^a Actual temperature range is greater than the specified by +5–20 °C.

Summary

Two- and three-component IPN elastomers and foams were prepared and characterized by dynamic mechanical spectroscopy, hysteresis, ball rebound, sound absorption, and ultimate property measurements. The IPNs studied

Table XII. Comparison of Dynamic Mechanical Spectroscopy Results for IPN Elastomers

Sample Number	System	$\tan \delta$ max	Temp. (°C) at $\tan \delta$ max	Temp. Range (°C)	Area Under Curve $\tan \delta$
10	60:40 PU:E + 50% Santicizer 160	1.65	-7	-40-4 ^a	—
11	60:40 PU:E + 10% Stanflux	1.20	8	-26-34 ^a	—
12	60:40 PU:E + 20% Stanflux	0.93	16	-40-64 ^a	50.73
13	60:40 PU:E + 10% Sundex	0.72	40	-40-60 ^a	—
14	50:50 PU:E + 30% Benzoflex	0.80	24-28	-12-60 ^a	34.25
15	50:50 PU:E + 20% Santicizer-160	0.90	12	-28-44	31.10
16	40:60 PU:E + 30% Benzoflex	1.20	20	-39-56	42.71
17	40:60 PU:E + 20% Santicizer-160	1.34	20	-12-71	48.03

^a Actual temperature range is greater than the specified by +20-40 °C.

Table XIII. Comparison of Dynamic Mechanical Spectroscopy Results for IPN Elastomers

Sample Number	System	$\tan \delta$ max	Temp. (°C) at $\tan \delta$ max	Temp. Range ^a (°C)
18	50:20:30 PU:E:UPE	0.75	60 ^b	-32-80
19	50:25:25 PU:E:UPE	0.81	8 ^b	-36-68
20	40:20:40 PU:E:UPE	0.72	52-68	-32-100
21	40:10:50 PU:E:UPE	1.02	68-100	-32-120

^a Beyond instrument range.

^b $\tan \delta$ never returned to its pretransition value. Samples became too soft to continue measurements.

were PU-PVC SIPN elastomers, PU-PVE hybrid IPN foams, and PU-E-PVE IPN foams and elastomers.

Enhanced mechanical energy absorption was shown to result when the IPNs possess a microheterogeneous morphology. Viscoelastic foams that possess broad glass-transition temperatures centered around use temperature do not, however, necessarily absorb or attenuate airborne sound more effectively than nonviscoelastic foams. Cell morphology (geometry, size, orientation) can affect the sound-absorbing properties at least as much as polymer

Table XIV. Formulations of Polyurethane and IPN Foams

<i>Designation</i>	1	2	3	4	5	6	7	8	9	10
Isonate 143L	25	25	7.5	17.4	21.4	21.4	25	17.5	24	24
Niax 31-28	100	100	60	50	50	50	100	60	50	50
Water	1.05	1.05	0.77	0.76	0.95	0.95	1.05	0.77	0.90	0.90
1,4-BD	—	—	—	—	—	—	—	—	1.12	1.12
A-1	0.06	0.06	0.06	0.06	0.06	0.06	0.06	0.06	0.06	0.06
T-12	0.02	0.02	0.02	0.02	0.02	0.02	0.02	0.02	0.02	0.02
DC-193	0.5	0.5	0.1	0.1	0.5	0.5	0.5	0.1	0.2	0.2
L-540	0.5	0.5	0.3	0.3	0.5	0.5	0.5	0.3	0.3	0.3
DER 330	—	—	8.6	29.2	48.2	48.2	—	8.6	32.5	32.5
XU-213	—	—	0.25	0.40	0.72	0.72	—	0.25	0.49	0.49
DMP-30	—	—	0.12	0.22	0.36	0.36	—	0.12	0.24	0.24
Freon 11A	15	15	20	20	20	20	20	20	26	26
Plasticizer	—	—	—	—	—	—	—	17.4 ^a	22 ^b	22 ^a
Filler	—	25 ^c	—	—	—	24 ^c	12.5 ^d	—	—	—
PU:epoxy	100:0	100:0	90:10	70:30	60:40	60:40	100:0	90:10	70:30	70:30
Filler (%)	—	20	—	—	—	20	10	—	—	—
Plasticizer (%)	—	—	—	—	—	—	—	20	20	20

NOTE: All values (except ratios and percents where indicated) are in grams.

^a Santicizer 160.

^b Santicizer 148.

^c Graphite.

^d Rubber powder.

Table XV. Polyurethane and Polyurethane–Epoxy IPN Foam Properties

<i>Formulation and PU: Epoxy Ratio</i>	<i>Hysteresis (%)</i>	<i>Density (kg/m³)</i>	<i>Rebound (%)</i>	<i>Tensile Strength (kPa)</i>	<i>Elongation (%)</i>	<i>Stress at 50% Compression (kPa)</i>
1 100:0	28	54.5	35	158	120	15
2 100:0 + 20 graphite	31	68.9	32	138	107	16
3 90:10	39	38.4	20	140	100	21
4 70:30	47	41.7	8	114	130	13
5 60:40	73	49.7	8	89	150	15
6 60:40 + 20 graphite	69	64.1	6	58	95	12
7 100:0 + 10 RP ^a	35	68.9	39	207	124	15
8 90:10 + 20 S160 ^b	27	51.3	18	50	90	10
9 70:30 + 20 S148 ^c	30	46.5	3	37	116	17
10 70:30 + 20 S160 ^b	37	59.3	6	75	116	10

^a Rubber powder.

^b Santicizer 160.

^c Santicizer 148.

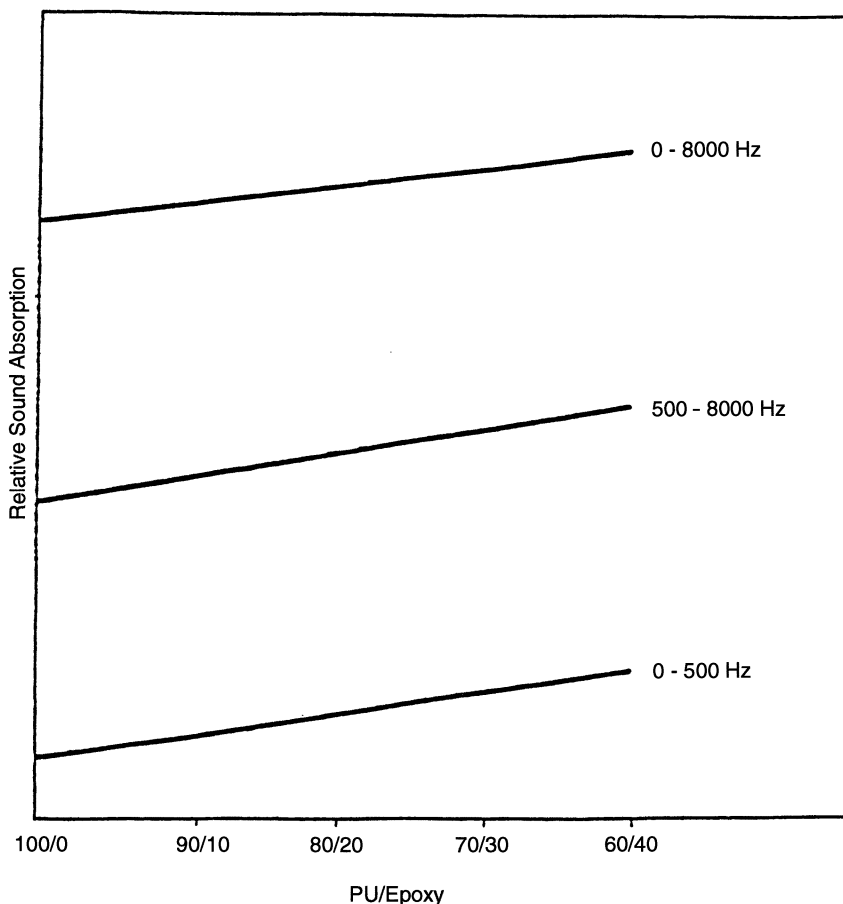


Figure 22. Total change in relative sound absorption from 100:0 to 60:40 PU:epoxy ratio.

density or foam thickness as further evidenced by comparison with previous studies on polyimide foams.

Fillers may have positive or negative effects on sound absorption properties of polymeric foams. Fillers that did not alter the polymer morphology contributed to the improved sound attenuation due to scattering and mode conversion.

Outlook

Research in damping technology utilizing IPNs will continue to receive attention from both academia and industry. Currently, vibration-damping relationships are well understood for both the viscoelastic materials and their

composites. The relationships for acoustic absorption are less understood from a practical aspect. The effects of morphology, chemical structure, macroscopic structure such as voids, and their effects on sound absorption by foams require more research. New materials will capitalize on IPN formation to control the morphology and optimize damping and absorption for specific applications.

Attempts should be made to separate the contributions of sound attenuation in cellular materials into scattering, mode conversion, redirection, and absorption. Also, the ability to predict the required sound pressure level at which to transfer energy into the viscoelastic material would be beneficial in solving this problem.

Acknowledgments

The authors gratefully acknowledge Dutch State Mines for supporting the work on PU-PVC pseudo-IPNs and the U.S. Army for supporting the studies on PU-PVE IPNs under contracts with the Army Research Office and the Construction Engineering Research Laboratory of the Army Corps of Engineers.

References

1. Jarzynski, J. In *Sound and Vibration Damping with Polymers*; Corsaro, R. D.; Sperling, L. H., Eds.; American Chemical Society: Washington, DC, 1990.
2. Sperling, L. H. *Interpenetrating Polymer Networks and Related Materials*; Plenum: New York, 1981.
3. Keskkula, H.; Turley, S. G.; Boyer, R. F. *J. Appl. Polym. Sci.* **1971**, *15*, 351.
4. Fradkin, D. G.; Foster, J. N.; Sperling, L. H.; Thomas, D. A. *Rubber Chem. Technol.* **1986**, *59*, 255.
5. Fradkin, D. G.; Foster, J. N.; Sperling, L. H.; Thomas, D. A. *Polym. Eng. Sci.* **1986**, *26*, 730.
6. Chang, M. C. O.; Thomas, D. A.; Sperling, L. H. *J. Appl. Polym. Sci.* **1987**, *34*, 409.
7. Chang, M. C. O.; Thomas, D. A.; Sperling, L. H. *J. Polym. Sci., Polym. Phys. Ed.* **1988**, *26*(8), 1627-1640.
8. Fay, J. J.; Murphy, C. J.; Thomas, D. A.; Sperling, L. H. In *Sound and Vibration Damping with Polymers*; Corsaro, R. D.; Sperling L. H., Eds.; American Chemical Society: Washington, DC, 1990.
9. Foster, J. N.; Sperling, L. H.; Thomas, D. A. *J. Appl. Polym. Sci.* **1987**, *33*, 2637.
10. Lipatov, Y. S. In *Advances in Interpenetrating Polymer Networks*; Klemmner, D.; Frisch, K. C., Eds.; Technomic: Lancaster, PA, 1989.
11. Chen, A.; Williams, H. L. *J. Appl. Polym. Sci.* **1976**, *20*, 3387.
12. Corsaro, R. D.; Covey, J. F.; Young, R. M.; Spryn, G. In *Sound and Vibration Damping with Polymers*; Corsaro, R. D.; Sperling, L. H., Eds.; American Chemical Society: Washington, DC, 1990.
13. Hilyard, N. C.; MacFarland, D. *Automotive Polym. Design* **1991**, *7*.
14. Beranek, L. L.; Work, G. L. *J. Acoust. Soc. Am.* **1949**, *21*(4), 419.
15. Mangiaretto, R. A. *J. Acoust. Soc. Am.* **1963**, *35*(7), 1023.

16. Au, A. C. K.; Byrne, K. D. *J. Acoust. Soc. Am* **1987**, *82*(4), 1325.
17. Sperling, L. H. In *Comprehensive Polymer Science*; Allen, G., Ed.; Pergamon: New York, 1989; Vol. 6, p 423.
18. Frisch, K. C.; Klempner, D.; Frisch, H. L. *Polym. Eng. Sci.* **1982**, *22*(18), 1143.
19. Xiao, H. X.; Frisch, K. C.; Frisch, H. L. *J. Polym. Sci., Polym. Chem. Ed.* **1982**, *21*, 2547.
20. Kim, S. C.; Klempner, D.; Frisch, K. C.; Radigan, W.; Frisch, H. L. *Macromolecules* **1976**, *9*, 258.
21. Omoto, M.; Kusters, J.; Sophiea, D.; Klempner, D.; Frisch, K. C. *Polym. Mater. Sci. Eng.* **1988**, *58*, 459.
22. Chang, M. C. O.; Thomas, D. A.; Sperling, L. H. *Polym. Mater. Sci. Eng.* **1986**, *55*, 350-354.
23. Grates, J. A.; Thomas, D. A.; Hickey, E. C.; Sperling, L. H. *J. Appl. Polym. Sci.* **1975**, *6*, 1731-1743.
24. Huelck, V.; Thomas, D. A.; Sperling, L. H. *Macromolecules* **1972**, *5*, 348.
25. Sperling, L. H.; Chiu, T. W.; Gramlich, R. G.; Thomas, D. A. *J. Paint Technol.* **1974**, *46*, 4.
26. Sperling, L. H.; Thomas, D. A. U.S. Patent 3,833,404, 1974.
27. Klempner, D.; Berkowski, L.; Frisch, K. C.; Hsieh, K. H.; Ting, R. *Polym. Mater. Sci. Eng.* **1985**, *52*, 57.
28. Klempner, D.; Berkowski, L.; Frisch, K. C.; Hsieh, K. H.; Ting, R. *Rubber World* **1985**, *192*, 16.
29. Klempner, D.; Wang, C. L.; Ashtiani, M.; Frisch, K. C. *J. Appl. Polym. Sci.* **1986**, *32*, 4187.
30. Klempner, D.; Frisch, K. C.; Sedghi, B.; Raza, I.; Muni, B. *Cell. Polym.* **1987**, *6*, 1.
31. Chang, M. C.; Thomas, D. A.; Sperling, L. H. *J. Polym. Sci., Polym. Phys. Ed.* **1988**, *26*(8), 1627.
32. Fay, J. J.; Murphy, C. J.; Thomas, D. A.; Sperling, L. H. *Polym. Mater. Sci. Eng.* **1989**, *60*, 649.
33. Tabka, T.; Widmaier, J. M.; Meyer, G. C. *Polym. Mater. Sci. Eng.* **1989**, *60*, 659.
34. Ting, R. Y.; Capps, R. N.; Klempner, D. *Polym. Mater. Sci. Eng.* **1989**, *60*, 654.
35. Lee, D. K.; Chen, L.; Sendijarevic, A.; Sendijarevic, V.; Frisch, K. C.; Klempner, D. *J. Cell. Plast.* **1991**, *27*, 135.
36. Gagliani, J.; Long, J. V. U.S. Patent 3,966,652, 1976.
37. Bonk, H. W.; Sardonapoli, A. A.; Ulrich, H.; Sayigh, A. A. *J. Elastoplast.* **1971**, *3*, 157.
38. Sophiea, D. Ph.D. Dissertation, University of Detroit Mercy, 1991.
39. Klempner, D.; Sophiea, D.; Suthar, B.; Frisch, K. C.; Sendijarevic, V. *Polym. Mater. Sci. Eng.* **1991**, *65*, 82.
40. Klempner, D.; Muni, B.; Okoroafor, M.; Frisch, K. C. In *Advances in IPNs*; Klempner, D.; Frisch, K. C., Eds.; Technomic: Lancaster, PA, 1989.

RECEIVED for review December 9, 1991. ACCEPTED revised manuscript July 23, 1992.

Thermodynamics and Kinetics of Phase Separation

L. A. Utracki

National Research Council of Canada, Industrial Materials Institute,
75 de Mortagne, Boucherville, Quebec, Canada J4B 6Y4

The morphology of multiphase polymeric systems, polymer alloys, blends, and interpenetrating polymer networks depends on kinetics of polymerization and cross-linking (in reactive systems), composition, degree of polymerization and branching, miscibility (defined in terms of equilibrium thermodynamics), dynamics of phase separation, and flow conditions. In this review, the latter three aspects are briefly discussed.

POLYMER BLENDS are defined as mixtures of high molecular weight ingredients, polymers, copolymers, or elastomers (1). Dependent on Gibbs free energy of mixing, ΔG_m , polymer blends are either miscible, $\Delta G_m < 0$, or immiscible, $\Delta G_m \geq 0$. A *polymer alloy* is an immiscible polymer blend that has a modified interface and morphology. The process of modification is known as *compatibilization*. Most polymer alloys and blends (PAB) are prepared by mechanical mixing or compounding. With increasing frequency, compatibilization is achieved through the reactive process. The morphology of PAB depends on the concentration and chemical nature of the ingredients, as well as on the compatibilization and compounding methods. Both dispersed and co-continuous structures with phase dimensions varying from 0.1 to 10 μm have been prepared (2–5).

Interpenetrating polymer networks (IPNs) are defined as materials that contain two or more polymers in network form, each chemically cross-linked (6, 7). The thickness of the network strand usually varies from 10 to 1000 nm. IPNs are prepared as either *sequential*, *simultaneous* (SIN), or *latex* type. In the sequential case, the first cross-linked polymer is swollen by

monomer of the second polymer, which is then polymerized and cross-linked. Depending on the kinetics and extent of swelling, as well as on the rate of subsequent polymerization, cross-linking, and phase separation, IPNs with different structure and properties can be generated. By contrast, SINs are prepared by simultaneous polymerization of a mixture of two monomers. Like the case of sequential IPN, here also the morphology and properties depend on the component miscibility, as well as relative kinetics of polymerization, cross-linking and phase separation. Latex IPNs are made by emulsion polymerization and the IPN structure is limited to each latex particle.

IPNs have been used as (i) impact resistant polymers, (ii) reinforced elastomers, (iii) sound and vibration damping materials, (iv) rubber blends, (v) electrical insulators, (vi) diffusion-selective compositions, (vii) coatings, and (viii) ion exchangers (6). The advantageous properties of IPNs originate from co-continuity and excellent compatibilization (obtained by co-reactions) that result in fine dispersions. Often the IPNs do not possess co-continuity of networks (required by the cited definition); rather, one phase forms fine droplets dispersed in another phase, and the diameters range from $d = 10$ to 100 nm. However, because the system has been prepared via the standard methods of IPN preparation, it is labeled as such (8–10).

Thus, there are two classes of multiphase polymeric mixtures, PABs and IPNs, that very much resemble each other. Historically, the principal difference has been the method of preparation (mechanical blending for PAB versus polymerization and cross-linking for IPN) and the resultant difference in dispersion (PAB with $d < 100$ nm is difficult to prepare). Today, however, there is more and more chemistry involved in PAB preparation (for compatibilization as well as for stabilization of morphology, e.g., by low degree of cross-linking). Furthermore, owing to environmental concerns, there is increased pressure to make IPNs recyclable (i.e., to reduce the density of chemical cross-links). This concern led to recognition of a new class of polymeric mixtures: the thermoplastic IPNs.

A *thermoplastic IPN* is a material that contains two or more physically cross-linked polymers, each in network form. Here the cross-links originate in crystals, ion clusters, hard blocks of block copolymer, and so forth. Thus, for example, blends of (i) polyethylene (PE) or polypropylene (PP) with ethylene-propylene rubber (EPR or EPDM), (ii) PP with polyamide-66 (PA-66), (iii) maleated styrene-butadiene-styrene (SBS) or poly(styrene-*stat*-sodium methacrylate) copolymer with PA-66, (iv) “molecular composites” (blends of rigid macromolecules in a thermoplastic matrix) prepared through dissolution of rigid-rod polymer in monomer of a second polymer and then polymerization (5, 6), can all be labeled as either PAB or thermoplastic IPN. In principle, both phases of IPN should be in a network form; that is, they should be co-continuous. However, in view of the previously discussed case of IPNs, this criterion is not *sine qua non*. Finally, there are *semi-IPNs* that have one chemically cross-linked polymer and the other polymer remains

linear. A blend of PA–cross-linked poly(phenylene ether) (PPE) can serve as an example.

Thus, the IPN nomenclature covers a whole spectrum of materials from the original thermoset IPN to physical mixtures of thermoplastic resins that are traditionally classified as polymer blends or alloys. The clear distinction between PAB and IPN is becoming increasingly fuzzy. A brief summary of the definitions is given in Table I. In principle, IPNs should be considered a special class of polymer alloys that is characterized by fine dispersion and co-continuity of phases.

Both PAB and IPN are subject to the same physical laws. Park et al. (11) observed that in SIN the degree of dispersion depends on such factors as composition, polymer–polymer miscibility, relative rates of polymerization and of cross-linking, the degree of cross-linking and polymerization at the time of gelation, and, finally, the kinetics of phase separation.

On the basis of the equilibrium thermodynamics, Donatelli et al. (8, 9) developed relations that allow for calculation of the dispersed phase diameter in sequential IPNs:

$$d_2 = 4\nu_{12}\phi_2/RTx_1\phi_1(2\phi_1^{-2/3} - 1) \quad (1)$$

where ν_{12} is the interfacial tension coefficient, $\phi_1 = 1 - \phi_2$ is the volume fraction of the matrix phase with the cross-link density equal to x_1 , R is the gas constant, and ϕ_2 is the volume fraction of the dispersed phase. An example of the predictive capability of eq 1 is shown in Figure 1 (12, 13). Equation 1 was later generalized by Yeo et al. (12) to describe the drop formation in any IPN system.

Table I. Summary of Blend and IPN Definitions

<i>Material</i>	<i>Definitions</i>	<i>Phases</i>		
		<i>TS</i>	<i>TP</i>	<i>Continuity</i>
Polymer blend	A mixture of polymers or copolymers	^a	^a	Not required
Polymer alloy	A compatibilized or modified blend	^a	^a	Not required
IPN (and SIN)	A mixture of finely dispersed, chemically cross-linked polymers in network form	Yes	No	Required
Thermoplastic IPN	A mixture of physically cross-linked polymers in network form	No	Yes	Required
Semi-IPN	A mixture of at least two polymers in network form, where only one polymer is chemically cross-linked; the other is linear	^b	^b	Required

^a The polymer (or copolymer) may have either thermoset (TS) or thermoplastic (TP) character.

^b One phase is TS; the other is TP.

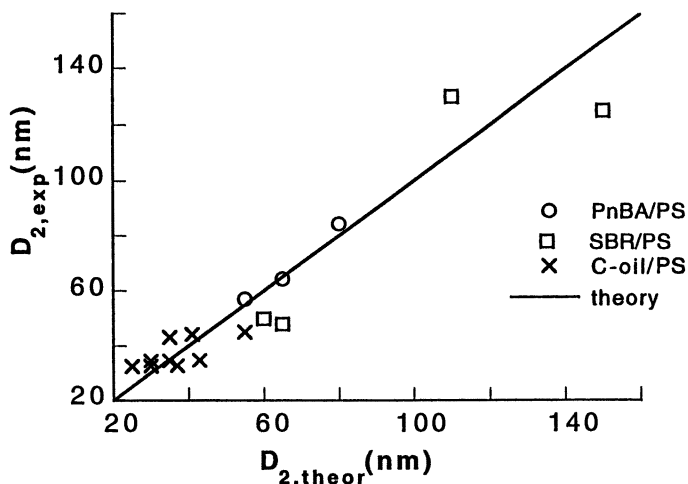


Figure 1. Measured vs. calculated diameters of dispersed drops in IPNs; poly(cross-(n-butyl acrylate))-inter-poly(cross-styrene) (PnBA/PS) (12), styrene-butadiene rubber-polystyrene (SBR/PS) (12), and castor oil-polystyrene (C-oil/PS) (13).

To interpret PAB glass-transition temperature, T_g , Utracki and Jukes (14) proposed the relation

$$\phi_1 \ln(T_g/T_{g1}) + k\phi_2 \ln(T_g/T_{g2}) = 0 \quad (2)$$

where k is a measure of the degree of dispersion (or miscibility) that is usually determined by computer fit to the experimental data. Because assignment of index 1 and 2 is arbitrary, from the symmetry principle for $k \neq 1$, two branches of the dependence are expected: one branch corresponds to k and the other branch corresponds to $1/k$.

Equation 2 is expected to be applicable to IPNs. In Figure 2 the Yenwo et al. (13) data for compositional variation of a castor oil-polystyrene IPN are presented. Judging by the two well-separated values of T_g in the mid-composition range, the system is immiscible. The two broken lines (one for eq 2 parameter $k = 0.133$ and the other symmetrical for $1/k$) were computed from eq 2. The relation 2, derived for T_g versus composition dependence in polymer blends, describes this dependence in IPNs quite well.

Assuming that the effect of chemical cross-linking on T_g is small, the following relation was proposed (6):

$$T_g/T_{g0} = 1 + A\phi_c/(1 - \phi_c) \quad (3)$$

where $A = 1-1.2$ is a dimensionless parameter of the equation and ϕ_c is the volume fraction of cross-linked monomer units.

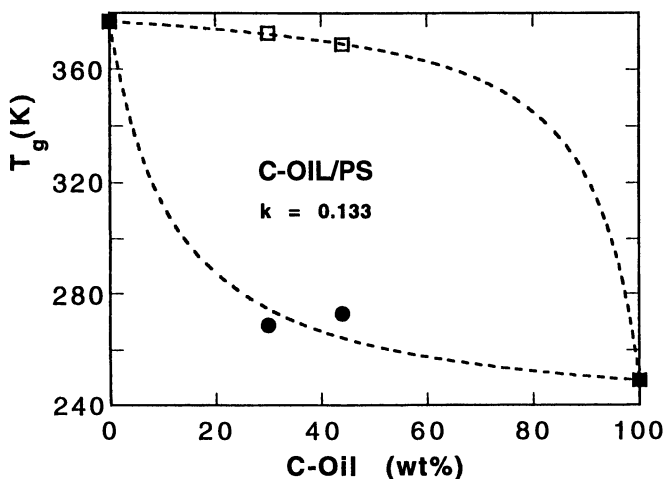


Figure 2. Composition dependence of the glass-transition temperature of castor oil-polystyrene IPN. Points are experimental (13); the lines are computed from eq 2.

In the following text the equilibrium thermodynamics and the dynamics of phase separation will be discussed. The aim is to indicate their implications as far as morphology of PAB and IPN is concerned. The influence of flow will also be mentioned.

Equilibrium Thermodynamics

Conditions for Phase Separation. In a closed, single-phase system contained in volume, V , with n_i moles of i th species at temperature, T , and pressure, P , the infinitesimal change of the Gibbs free energy is given by:

$$dG = V dP - S dT + \sum \mu_i dn_i; \quad \mu_i = (\partial G / \partial n_i) |_{P, T, n_i} \quad (4)$$

where S is the system entropy and μ_i is the chemical potential of specimen i . The equilibrium thermodynamics allows one to predict phase separation (15) on the basis of excess functions, $\Delta F = F - F_0$, for $F = G, H, S, \mu_i, \dots$, where F and F_0 are intrinsic functions in the mixture and pure state, respectively (H is the enthalpy).

As shown in Figure 3, there are three regions of miscibility:

1. Single-phase, miscible region on the outside of the binodal.
2. Metastable phase region, between the binodal and spinodal.
3. Phase-separated (or spinodal) region enclosed by the spinodal.

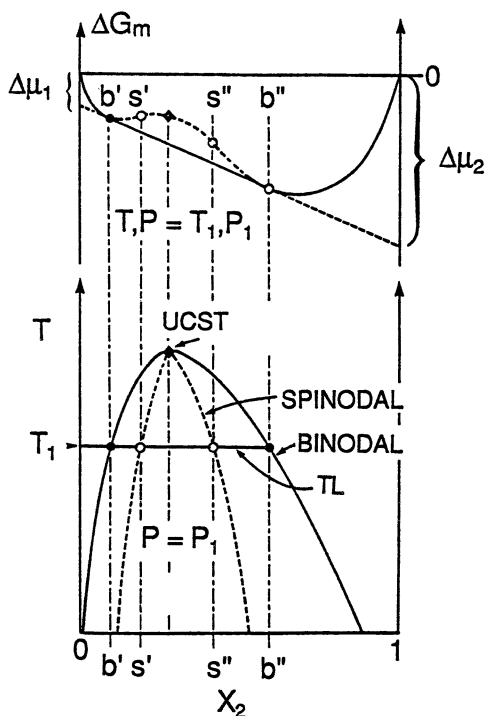


Figure 3. Construction of phase diagram for two-component systems. Upper part: Gibbs free energy of mixing vs. composition at constant temperature and pressure; $T = T_1$, $P = P_1$. The intercept of the tangential line provides a measure of the chemical potential. Lower part: Phase diagram at constant pressure, $P = P_1$; that is, a plot of the phase separation temperature vs. composition. Solid (binodal, b) and dotted (spinodal, s) lines represent collections of b points and s points, respectively. UCST stands for upper critical solution temperature. Symbols b', b'', s', and s'' indicate, respectively, the binodal and spinodal points at temperature T_1 .

All three regions meet at the critical point, either lower critical solution temperature (LCST) or upper critical solution temperature (UCST). At the binodal point the chemical potential of each specimen i has the same value in both phases, $\mu'_i = \mu''_i$ (here the superscripts prime and double prime indicate the two phases at equilibrium). At the spinodal and at the critical point, respectively, the second and the third derivative of ΔG_m (with respect to concentration) must be equal to zero. Furthermore, for the phase to be located in the stable region, the fourth derivative must be positive: $(\partial^4 \Delta G_m / \partial \phi_2^4)_{P, T} > 0$.

To compute the phase diagram requires knowledge of how ΔG_m varies with independent variables, P , T , composition, molecular weight, and polydispersity.

Huggins–Flory Theory of Miscibility. In 1941 the following equation was published independently by Huggins (16) and by Flory (17):

$$\Delta G_m / RTV = \underbrace{\sum(\phi_i \ln \phi_i) / V_i}_{\text{configurational entropy, } \Delta S_{\text{conf}}} + \underbrace{\chi_{ij} \phi_i \phi_j}_{\text{heat of mixing, } \Delta H_m} \quad (5)$$

where

$$\chi_{ij} = z \Delta w_{ij} r_1 / k_B TV_1$$

and V is the total volume of the system, V_i and ϕ_i are, respectively, the molar volume and volume fraction of specimen i , χ_{ij} is the thermodynamic binary interaction parameter, z is the lattice coordination number, Δw_{12} is the energy change due to formation of 1–2 interaction pairs, r_1 is the site fraction of specimen 1 ($r_1 \approx V_1/V$), and k_B is the Boltzmann constant.

In eq 5 the first term represents the athermal (*configurational* or, according to present terminology, *conformational*) entropy of mixing, whereas the second (originating from the “zeroth approximation” heat of mixing) is directly related to the van Laar–Hildebrand enthalpy of mixing in the theory of regular solutions:

$$\Delta H_m = V\phi_1\phi_2(\delta_1 - \delta_2)^2 \geq 0 \quad (6)$$

where δ_i represents the Hildebrand solubility parameter.

Application of the aforementioned critical conditions to eq 5 (i.e., take second and third derivatives of ΔG_m with respect to concentration and equate the result to zero) allows the critical values of the solubility parameter to be expressed as

$$\chi_{12,c} = (r_1^{-1/2} + r_2^{-1/2})^2 / 2 \quad (7)$$

where r_1 and r_2 are proportional to degrees of polymerization of components 1 and 2, respectively. Thus:

For mixtures of low molecular weight liquids, ($r_1 \sim r_2 \sim 1$),
 $\chi_{12,c} = 2$.

For polymer solutions ($r_1 \sim 1$, $r_2 \rightarrow \infty$), $\chi_{12,c} = 1/2$.

For mixtures of polymers ($r_1 \sim r_2 \rightarrow \infty$), $\chi_{12,c} = 0$.

Two comments should be made regarding the applicability of eq 5 to polymer mixtures:

1. Because in the first term $|\phi_i \ln \phi_i| \ll 1$ and polymer molar volume $V_i > 1000$, ΔS_{conf} is negligibly small for polymer blends.

2. Equation 6 specifies that enthalpy of mixing is never negative, $\Delta H_m \geq 0$, but because $\Delta S_{\text{conf}} \approx 0$, then eq 5 predicts that all polymer blends are immiscible.

However, there are at least 400 miscible polymer blends (1). Evidently the assumptions on which the Huggins–Flory equation is based are not adequate for these systems and another approach must be taken.

Newer Theories. During the intervening 50 years a number of modifications to the Huggins–Flory equation as well as several new theories have been proposed (1). The modifications attempted to include the free volume and specific interaction effects. The contribution of these to the total binary interaction parameter is schematically shown in Figure 4 (18). The newer theories include surface interactions (19), continuous thermodynamics (20), and strong interactions (21). For more detailed discussion of this topic, see reference 1.

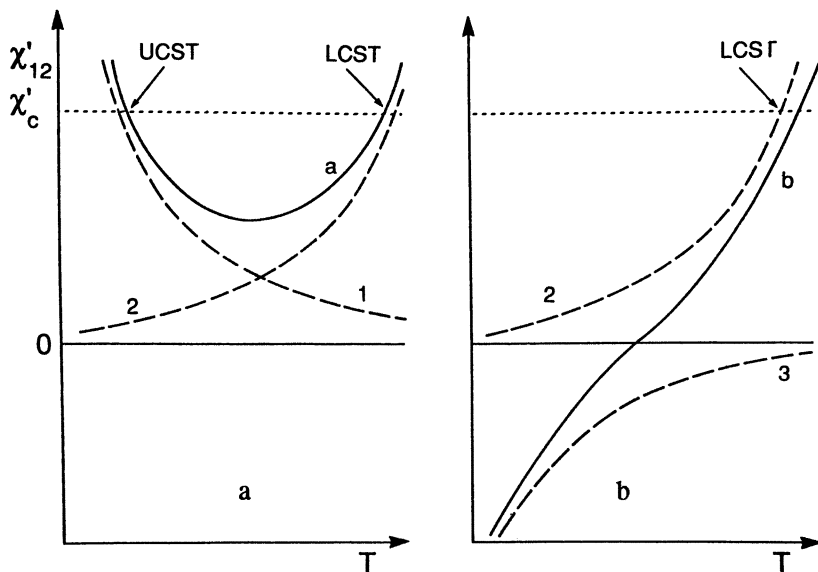


Figure 4. Schematic of binary interaction parameter vs. temperature dependence that shows contributions from (1) dispersion forces, (2) free volume, and (3) specific interactions. Solid lines represent the total effect. Dotted line χ_c indicates critical value of the interaction parameter. The graph on the left is usually found for solutions, whereas the graph on the right is found for polymer blends. (Reproduced from reference 18. Copyright 1978 American Chemical Society.)

Two approaches have been particularly successful for polymer mixtures.

Koningsveld. Because ΔS_{conf} is negligibly small, from eq 5 (22, 23),

$$\Delta G_m/RTV \approx \chi_{ij}\phi_i\phi_j \quad \text{where } \chi_{ij} = \sum_{i=0}^2 \left[\sum_{j=-1}^1 a_{ij}T^j \right] \phi_2^i \quad (8)$$

(a_{ij} are empirical parameters). Note that in eq 8 the Huggins–Flory assumption that the thermodynamic binary interaction parameter χ originates exclusively from the enthalpic effects has been relaxed. In the Koningsveld formalism χ is considered an empirical function of composition and temperature (and pressure) that represents both the entropic and enthalpic contribution to the free energy of mixing. Equation 8 can describe the isobaric phase diagram provided that at least five empirical parameters a_{ij} (two that describe the temperature and three that describe the concentration dependence) are known. An example of the $\chi = \chi(T, \phi)$ dependence is presented in Figure 5.

Nies and Stroeks. Nies and Stroeks (25, 26) modified the Simha–Somcynsky equation of state to introduce two binary interaction parameters: volumetric and energetic. The new theory reproduced the complicated changes in the critical temperature, an accomplishment no other theory could match. The phase behavior with UCST and LCST for a series of polystyrenes with different molecular weight was theoretically predicted with accuracy of ± 3 °C. Good agreement with experimental data was obtained down to the fourth derivative of ΔG_m (see Figure 4 in reference 26).

Interactions. Neither the configurational entropy nor the dispersive and free volume contributions can be used alone for interpretation of polymer–polymer miscibility. To explain this behavior, the effects of specific interactions and intramolecular repulsions must be considered.

Specific Interactions. Several types of specific interactions have been identified (1):

1. π -hydrogen bonding, as in poly(phenylene ether)–polystyrene (PPE–PS) blends.
2. Hydrogen bonding between vinyl =CH— and =CO ester (or other polar) group, as in poly(vinyl methyl ether) (PVME)–PS, or poly(vinyl chloride)–polycaprolactone (PVC–PCL) blends.
3. Direct hydrogen bonding as in poly(hydroxy ether) of bisphenol A (Phenoxy)–PCL, or in poly(ethylene oxide)–polyacrylic acid (PEO–PAA) blends.

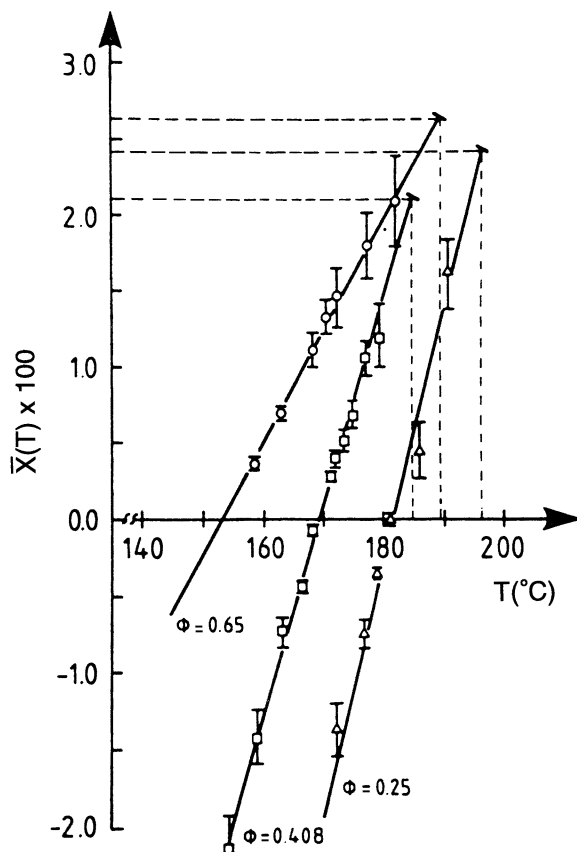


Figure 5. An average interaction parameter, $\bar{\chi}$, vs. temperature for indicated volume fraction of PVME in its blends with PS. Dotted lines represent spinodal conditions. (Reproduced with permission from reference 24. Copyright 1983 American Institute of Physics.)

4. Electron donor–acceptor complexes.
5. Ionic interactions between ions or between ions and dipoles.

Repulsive Interactions. Another source of miscibility is the presence of strong repulsive interactions within the macromolecule. Interactions with another polymer may reduce the internal stresses and thus be energetically favorable. This idea is particularly useful to explain the *window of miscibility* in homopolymer–copolymer blends (27, 28).

If the configurational entropy of polymer blends is vanishingly small, then Huggins–Flory eq 5 can be written as

$$\Delta G_m/RT \approx \Delta H_m = (V_A + V_B)B\phi_A\phi_B; \quad \chi_A = BV_A/RT \quad (9)$$

where B is a redefined binary interaction parameter.

The assumption that entropy is limited to configurational effects is very strong indeed, and as Greenhill et al. (29) found, not always valid. In Figure 6a the enthalpy of mixing versus composition for a series of low molecular weight analogs of poly(methyl methacrylate) (PMMA) or polystyrene (PS) blends with acrylic esters is presented. Evidently, the mixture of the low molecular weight analog of PS with that of poly(*n*-butylacrylate) (PnBA) shows the most negative value of ΔH_m ; that is, the negative value of the binary interaction parameter. Thus, if the entropy is limited to configurational entropy, $\Delta S_m(\text{conf}) \approx 0$, then the polymeric homologues of this system should be miscible. However, as Figure 6b indicates, this is not the case. Here, the dynamic mechanical loss tangent data indicate two, well-separated (glass) transition temperatures—evidence of phase separation.

There is little doubt that in polymer blends the configurational entropy is small, but other entropic effects remain. Thus, following the Koningsveld postulate, one must relax the restrictive consequences of eq 6 and consider the parameters χ and B to have both enthalpic and entropic character. Under these circumstances, treatment of polymer A as a copolymer of mers 1 and 2, and treatment of polymer B as made of mer 3 enables the free energy of mixing to be written as

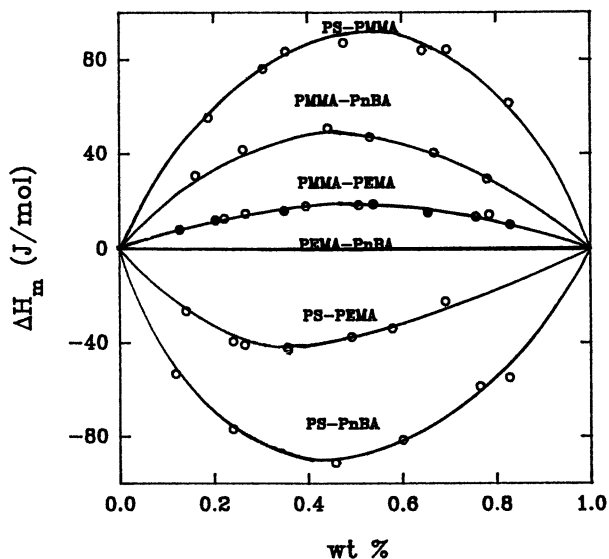
$$\Delta G_m/RT = (V_A + V_B) \sum_{i>j} B_{ij} \phi_i \phi_j - V_A B_{12} \phi'_1 \phi'_2 \quad (10)$$

where $\phi'_1 + \phi'_2 = 1$ represents composition of polymer A. From eqs 9 and 10,

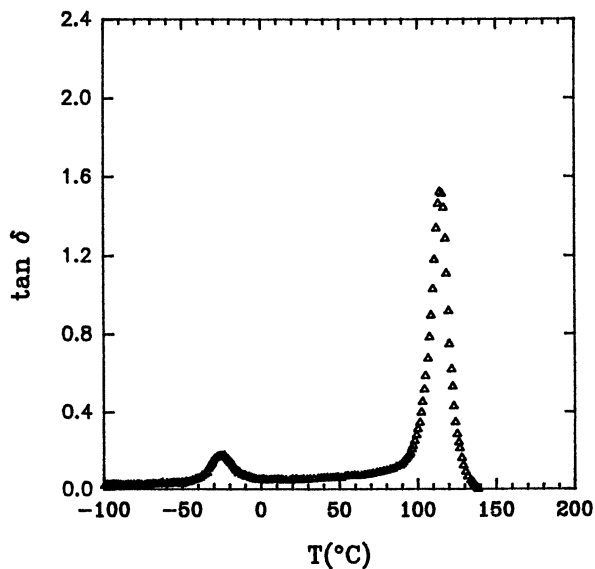
$$B = B_{13} \phi'_1 + B_{23} \phi'_2 - B_{12} \phi'_1 \phi'_2 \quad (11)$$

Thus, the larger the positive value of $B_{12} > 0$ (i.e., the larger the repulsive interactions within polymer A), the more negative is the overall interaction parameter B , and the blend is more miscible. Ellis applied this concept to mixtures of aliphatic and aromatic polyamides, PA; he treated the PAs as copolymers of aliphatic, aromatic, and amide “mers.” A good description of the miscibility of the blends was obtained (28).

In the preceding discussion of equilibrium thermodynamic properties of polymer–polymer systems, linear macromolecules were implicitly assumed. The listed relations can also be used for cross-linked systems, provided that the interaction parameters are appropriately adjusted. Owing to reduction of the entropic contribution to the free energy of mixing, ΔG_m , the cross-linking decreases miscibility that results in an increase of the binary thermodynamic interaction parameter: $\chi(\text{cross-linked}) > \chi(\text{linear})$. Thus, in general, the cross-linked systems are less miscible, but at the same time less prone to morphological changes, viz. phase separation or coarsening. Note that in the foregoing reasoning it is implicitly assumed that cross-linking does not change molecular conformation of the two polymeric components. This assumption is valid for most systems.



a



b

Figure 6. Experimental values of the excess heat of mixing vs. composition for low molecular weight analogs of PS or PMMA blended with either polymethacrylates or polyacrylates (a). Note that the system identified as PS-PnBA shows the most negative heat of mixing (i.e., strong miscibility). Tensile loss tangent vs. temperature for PS-PnBA semi-IPN (b). The two loss peaks indicate immiscibility. Data from reference 29.

Dynamics of Phase Separation

Although equilibrium thermodynamics describes the overall tendency for the system to stay miscible or to phase separate, the dynamics allows for determination of the rate of the process, interdiffusion coefficient, and binary thermodynamic interaction parameter, as well as for prediction of the blend structure. Dependent on the depth of quenching (i.e., the distance of the temperature jump from the miscible to immiscible region), two types of phase separation are distinguished: spinodal decomposition (SD) and nucleation and growth (NG). The morphologies generated by these two mechanisms are illustrated in Figure 7 (30). These mechanisms originate from quite different, time-dependent concentration fluctuations and are presented schematically in Figure 8 (1, 31).

Cahn–Hilliard Theory. In 1958, Cahn and Hilliard (32) proposed an approximate, mean field theory of phase separation in metallic alloys that allowed for calculation of the short time spinodal decomposition. Owing to the large radius of gyration of polymer molecules, $\langle r_g^2 \rangle$, and slow diffusion in polymer blends, the theory was found to be particularly suitable to describe these systems. The theory expresses time (t) dependence of the virtual structure function (determined by the time-dependent, spatial concentration variation of one component in the mixture) as:

$$S(q) = S_0 \exp\{R(q)t\}; \quad R(q) = -Mq^2[(\partial^2 G/\partial\phi^2) + 2q^2\kappa_s] \quad (12)$$

where M is the Onsager-type mobility factor and κ_s is the gradient energy coefficient that arises from effects of localized composition fluctuation (i.e., related to the interfacial effects). In scattering experiments, the wave vector, q , can be expressed as a function of the wavelength, λ_s , and the scattering angle θ :

$$q = (4\pi/\lambda_s) \sin(\theta/2) = 2\pi/\Lambda \quad (13)$$

where Λ is the wavelength of the concentration fluctuation (see Figure 7). Furthermore, extrapolation of the rate of concentration fluctuation function, $R(q)/q^2$, to zero wave vector allows for determination of the mutual diffusion (or interdiffusion) coefficient:

$$D = D_{\text{app}} = \lim_{q \rightarrow 0} R(q)/q^2 = \lim_{t \rightarrow 0} 2R(q_m)/q_m^2 \quad (14)$$

In eq 14 the second method of determination of apparent interdiffusion coefficient, $D_{\text{app}} = D_M$, is also indicated. Here q_m is the wave vector at which the scattering intensity is at maximum (33). From eqs 12 and 14 it is evident that D_{app} changes sign at the spinodal: D_{app} is positive on the

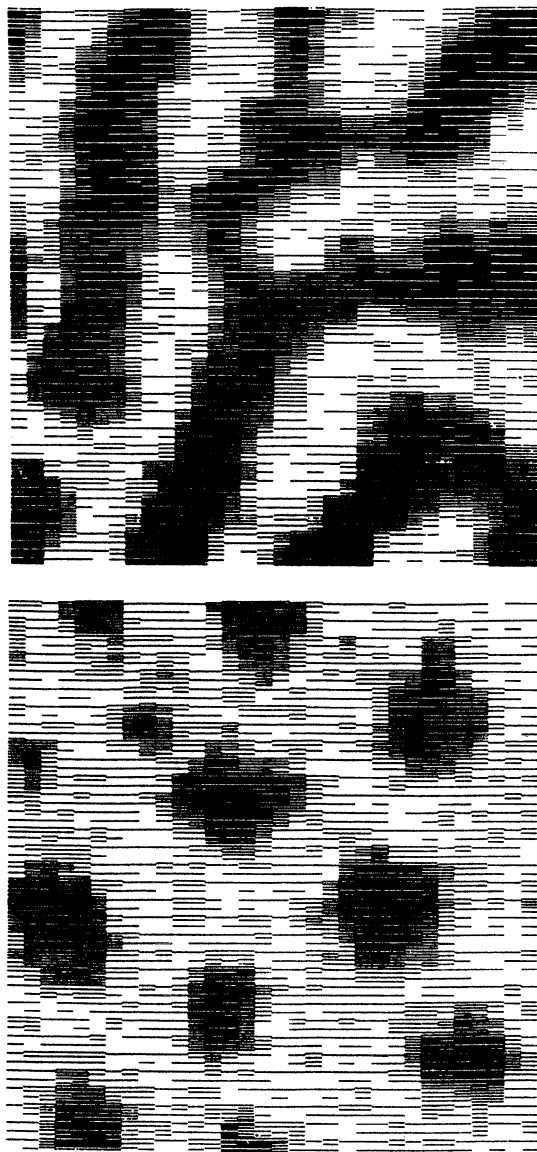


Figure 7. Computer-simulated concentration distribution engendered in phase separation by the nucleation and growth (left) and the spinodal decomposition mechanisms (right). (Reproduced with permission from reference 30. Copyright 1983 American Institute of Physics.)

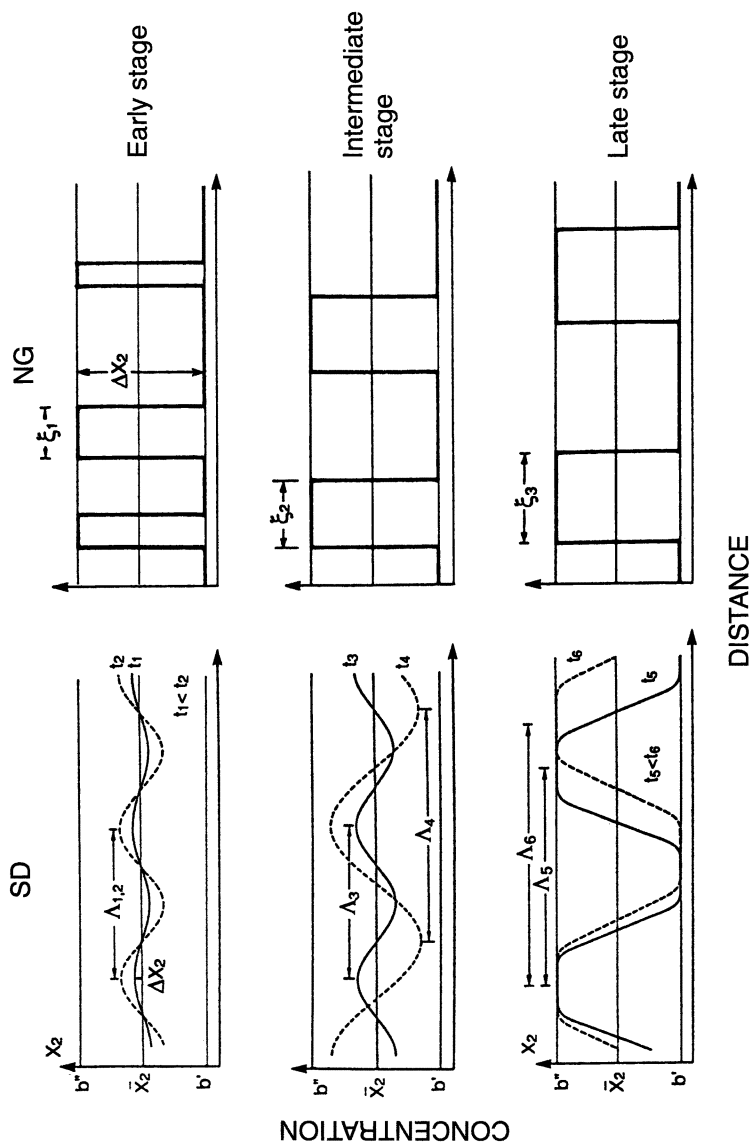


Figure 8. Schematic representation of the early (top), intermediate (middle), and late (bottom) stage of phase separation via the spinodal decomposition (left) and nucleation and growth (right) mechanisms (1). (Reproduced with permission from reference 31. Copyright 1986 The Society of Polymer Science, Japan.)

outside, zero at the spinodal, and negative within the spinodal region. Therefore, within the spinodal region the molecules diffuse *uphill*, from low to high concentration. This is the mechanism responsible for the initial phase coarsening.

From D_M one can calculate the binary interaction parameter χ (31):

$$D_M = 2\phi_1\phi_2(\chi_s - \chi)(N_1D_1^*\phi_2 + N_2D_2^*\phi_1) \quad (15a)$$

$$\chi_s = (1/N_1\phi_1 + 1/N_2\phi_2)/2 \quad (15b)$$

In eq 15a, the symbol D_i^* represents the “tracer” diffusion coefficient (defined in terms of a single molecule of polymer 1 diffusing through polymer 2). An example of the temperature dependence of χ at different concentrations was shown in Figure 5.

The “random phase approximation” (34) allows the parameter κ_s to be expressed in terms of the statistical segment length, b_i , its molar volume, V_i , and volume fraction in the mixture, ϕ_i :

$$\kappa_s = (RT/36) \sum b_i^2/V_i\phi_i \quad (16)$$

At the early stage of spinodal decomposition, when the system temperature, T , is near the spinodal temperature, $T \rightarrow T_s$, and the interfacial tension factor κ_s is small, eq 12 predicts that (35):

$$\begin{aligned} R(q)/q^2 &= -M[D + 2q^2\kappa_s] \\ \therefore R(q)/q^2 &= D_s[(T - T_s)(\partial \ln \chi/\partial T)_{T_s} - q^2\langle r_0^2 \rangle/36] \end{aligned} \quad (17)$$

where D_s is the self-diffusion coefficient—a measure of a single molecule that diffuses in an identical matrix. Derivation of eq 17 assumed that the two monodisperse polymers have the same degree of polymerization, Kuhn statistical segment length, and self-diffusion coefficient. These assumptions are equivalent to postulating validity of the mean-field Ising model.

To illustrate the experimental observations, the scattering pattern that results from SD is shown in Figure 9. The data are usually recorded as scattering intensity versus scattering angle (given by the radial position in Figure 9) converted into the q wave vector. An example of such a plot is shown in Figure 10.

Determination of the Structure Factor. There is a simple correlation between the virtual structure function, $S(q, t)$, and the scattering intensity, $I(q, t)$:

$$\begin{aligned} I(q, t) &= I_b + KS^2(q, t) \\ \therefore I(q, t) &= (KS_\infty + I_b) + K(S_0 - S_\infty) \exp\{2R(q)t\} \\ I(q, t) &= I_\infty + (I_o + I_\infty) \exp\{2R(q)t\} \end{aligned} \quad (18)$$

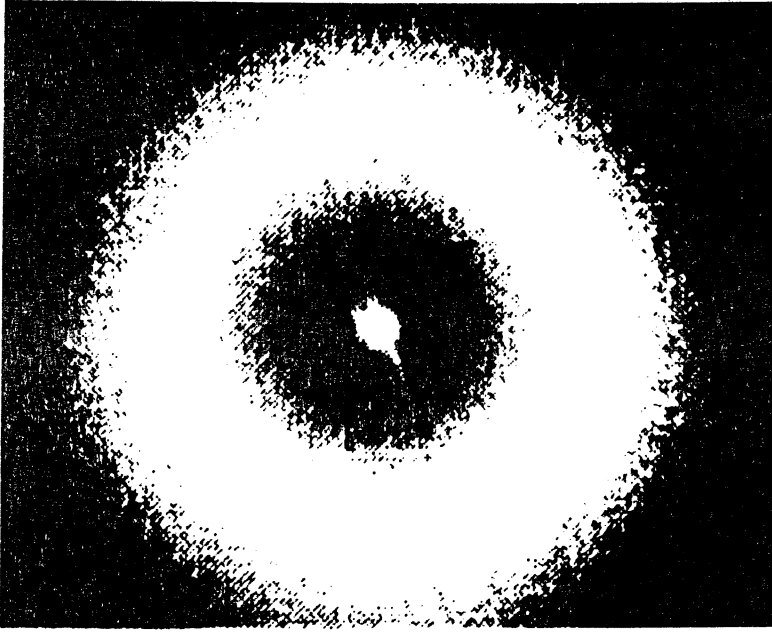


Figure 9. Observed scattering pattern that results from phase separation of a polybutadiene-polystyrene blend by the SD mechanism. Note that in SD the maximum scattering angle is always greater than zero.

where I_b is the background scattering, K is constant, and S_0 and S_∞ are, respectively, the structure factor at time $t = 0$ and at equilibrium. To extract the concentration fluctuation function $R(q)$, eq 18 suggests a semilogarithmic plot $\ln [I(q, t) - I_\infty]$ versus t , such as presented in Figure 11 (35).

An alternative relation was proposed by Sato and Han (36):

$$\left\{ t / (I(q, t) - I_0) \right\}^{1/3} = A [1 - R(q)t/3 + \dots] \\ A = 1 / [2(I_0 - I_\infty)R(q)]^{1/3} \quad (19)$$

The authors noted that eq 19 provides better precision in determination of $R(q, t)$ than the customarily used method of plotting $\ln I(q, t)$ versus t . As evident from Figure 12 the PS-PVME isothermal data follow the proposed dependence quite well (36).

Spinodal Decomposition. The interpretation of spinodal decomposition is based on eq 17. Thus, a plot of $R(q)/q^2$ versus q^2 should result in a linear dependence. Such a dependence is shown in Figure 13 (37). On the other hand, near the spinodal temperature, T_s (where κ_s is negligibly small),

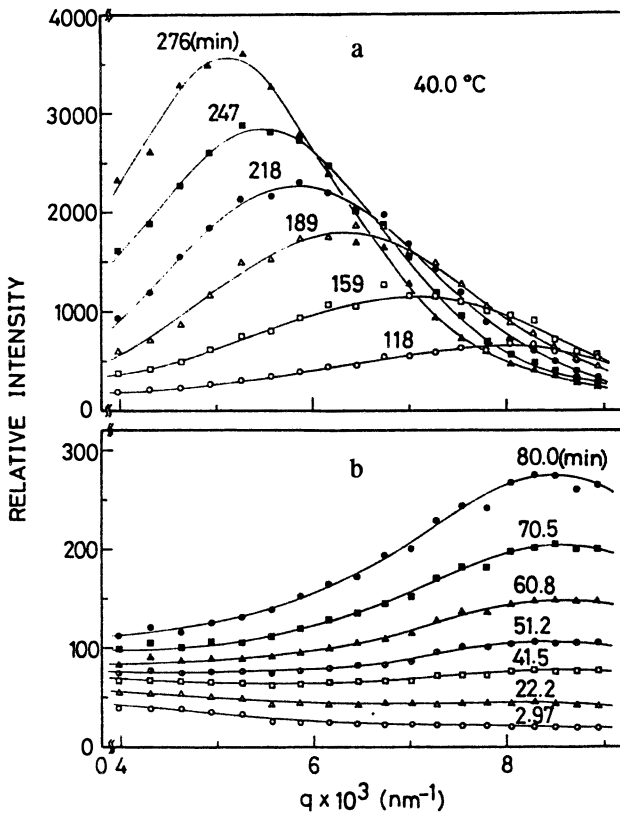


Figure 10. Variation of light scattering intensity during phase separation in a polybutadiene-polystyrene blend by the spinodal decomposition (SD) mechanism, as observed by the time-resolved light scattering photometer. Variation of light scattering during early stage, $t > 80$ min (b) and variation of scattering profiles at later stages (a). (Reproduced with permission from reference 33. Copyright 1987 Carl Hanser Verlag.)

the data at small wave vectors should be free of the q^4 term. In this case, a plot of $R(q)$ versus q^2 should result in a linear dependence that starts at the origin of the axes as illustrated in Figure 14 (36).

Figure 15 indicates that the Cahn-Hilliard theory can describe SD in both (mixing and demixing) directions. Furthermore, the mutual diffusion coefficient indicates that the temperature dependence of the process is continuous across the spinodal (36).

As shown in Figures 9 and 10, within the SD region the scattering intensity versus q vector goes through a local maximum at $q = q_m$. It has been observed that:

$$1/q_m = 1 + 0.05(tD/\zeta^2) \quad (20)$$

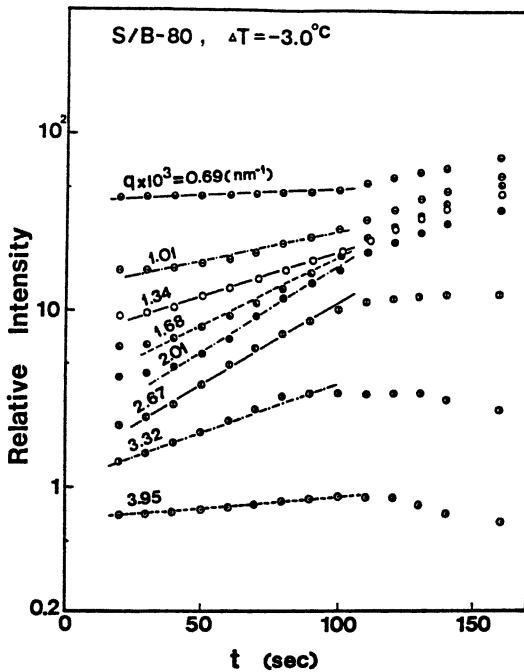


Figure 11. Variation of the scattering intensity with time at early stage of SD phase separation in polybutadiene-polystyrene blend. (Reproduced with permission from reference 33. Copyright 1987 Carl Hanser Verlag.)

where ζ is the concentration correlation length (38). The dependence was found to be universally valid for binary liquids, inorganic glasses, metal alloys, and polymer blends. A more recent observation indicates that the universality may be limited to non-entangling systems (39).

During the SD phase separation, the concentration fluctuation can be expressed as:

$$(\phi - \bar{\phi})^2 \cong S^2(q, t) = I(q, t) \quad (21)$$

where ϕ and $\bar{\phi}$ are, respectively, the volume fraction of one polymer in the phase-separated phase and its average value. From eqs 12 and 21 the rate of concentration variation can be expressed as

$$\partial\phi/\partial t = \partial S(q)/\partial t = 2S(q)[R(q) + (\partial R(q)/\partial t)t] \quad (22)$$

Because at the early stage of SD, the function $R(q)$ varies linearly with depth of quenching, $T - T_s$, the rate is also expected to follow this dependence. An example of cited data (40) is presented in Figure 16.

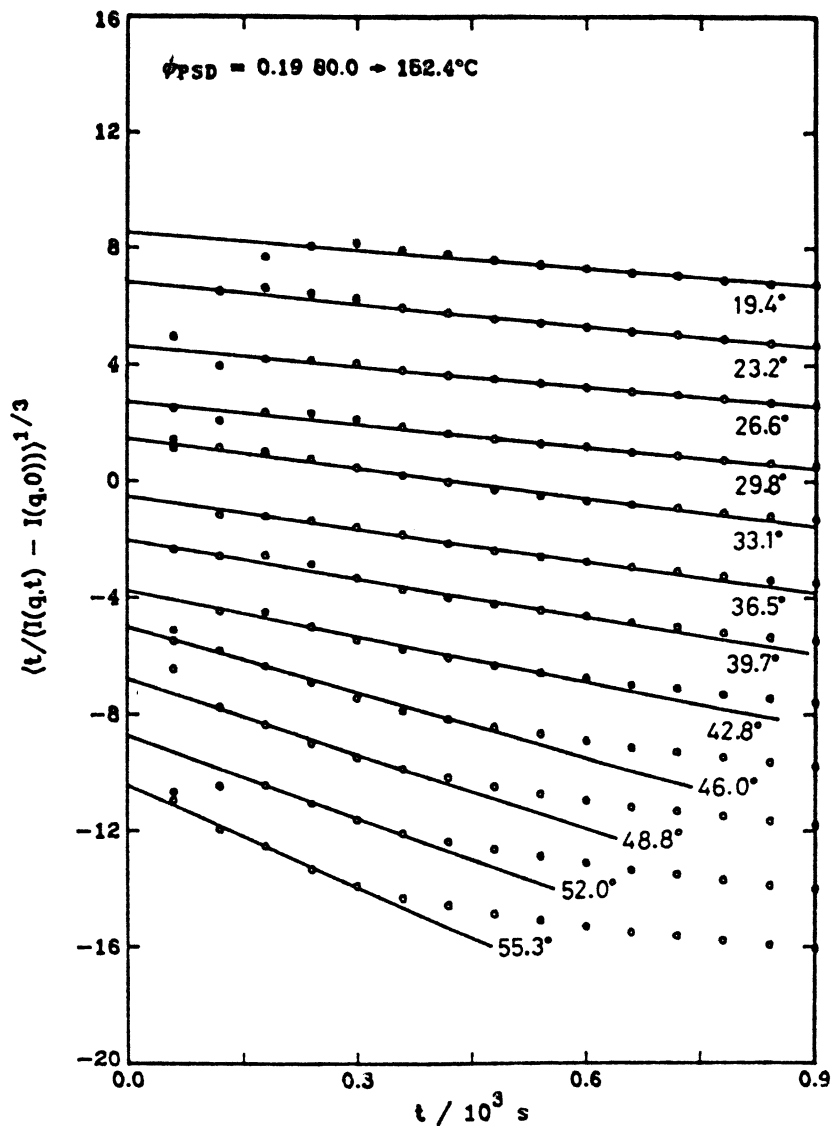


Figure 12. Light scattering intensity vs. time for a deuterated polystyrene-poly(vinyl methyl ether) blend (PSD-PVME) plotted according to eq 19. For clarity each data set but the first was vertically displaced. (Reproduced with permission from reference 36. Copyright 1988 American Institute of Physics.)

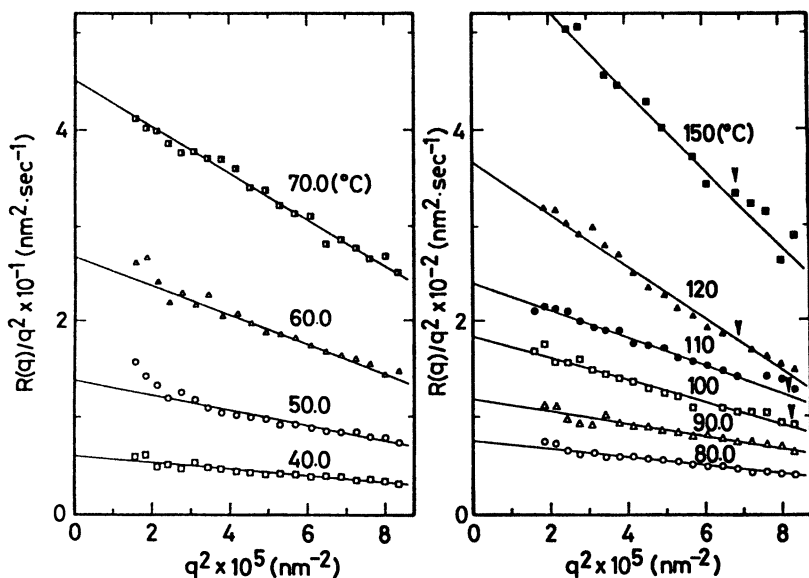


Figure 13. Plot of $R(q)/q^2$ vs. q^2 for early stage demixing in styrene-butadiene-styrene three-block copolymer blended with polybutadiene at the indicated temperatures. The apparent mutual diffusion coefficient, D_{app} , is given by the intercept of the straight lines with the y axis. (Reproduced with permission from reference 37. Copyright 1985 American Institute of Physics.)

Nucleation and Growth. Numerical simulation of the phase separation by Petschek and Metiu (30) led to the correct prediction of SD and NG. The change of the mechanism followed from the assumed changes of the initial and final temperature and concentration. Thus, the same physical laws control both mechanisms of phase separation.

The off-critical shallow quenching into the metastable region results in phase separation by the NG mechanism. In contrast to SD, in NG (owing to irregularity of structure) the dependence of scattering intensity versus q does not go through a local maximum (for SD shown in Figures 9 and 10), but rather monotonically decreases with q . Furthermore, as evident from data in Figure 17, the time dependencies of $I(q = \text{constant})$ versus t for SD and NG regions are quite different: in the SD region, the dependence is exponential; in the NG region the dependence is a power-law type (33).

The Cahn-Hilliard theory provides a good description of SD for polymer blends, especially within the linear range of small q and t . However, eq 12 overemphasizes the difference in the mechanism of phase separation at the spinodal point; for $\partial^2 G/\partial\phi^2 < 0$ (i.e., within the SD region) the system spontaneously decomposes, whereas for $\partial^2 G/\partial\phi^2 > 0$ (NG region) the system will not phase separate. To describe the phase separation by the NG mechanism another approach must be found.

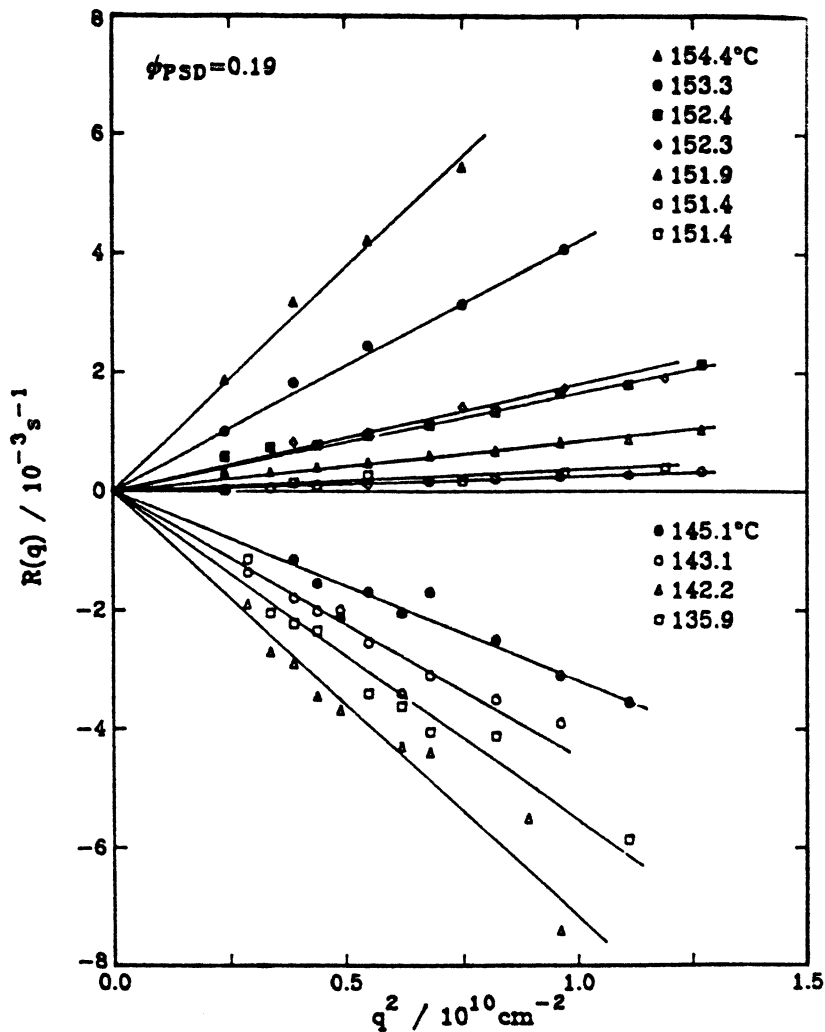


Figure 14. $R(q)$ vs. q^2 for deuterated polystyrene-poly(vinyl methyl ether) blend (PSD-PVME) at the indicated temperatures. The upper part is quenched from 80 °C; the lower part is reverse-quenched from 149.9 °C. Note the negative slopes of the dependence for data within the spinodal region, $T > T_s \approx 151.2$ °C, which indicates uphill diffusion. (Reproduced with permission from reference 36. Copyright 1988 American Institute of Physics.)

Such an approach was recently used by Matsuda (41), who assumed that the activation energy of the formation of critical nuclei has contributions from the free energy of mixing as well as from the interfacial energy:

$$\Delta E_{aN} = (4/3) \Delta G_m \pi r_N^3 + 4\pi r_N^2 \nu = (16\pi/3) \nu^3 \Delta G_m^2 \quad (23)$$

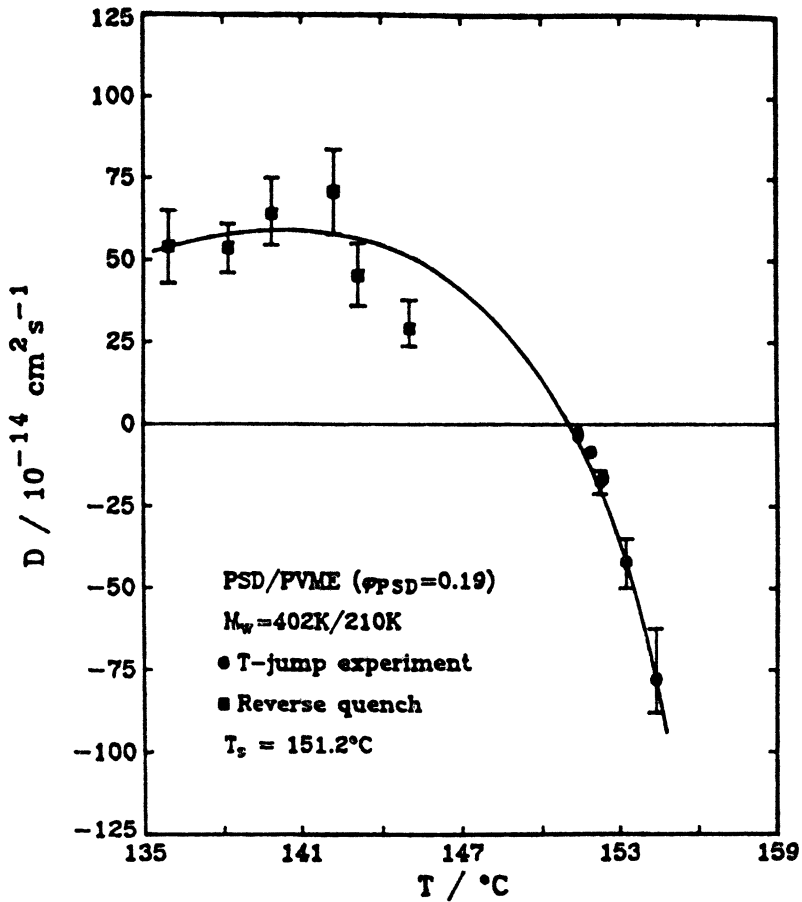


Figure 15. Temperature dependence of the mutual diffusion coefficient for polystyrene–poly(vinyl methyl ether) blend (PSD:PVME = 19:81); $D(T_s = 151.2^\circ\text{C}) = 0$. Note that the interdiffusion coefficient within the spinodal region is negative. (Reproduced with permission from reference 36. Copyright 1988 American Institute of Physics.)

where r_N is the critical radius of the nucleus and ν is the interfacial tension coefficient. If the nucleation process follows a simple exponential rule,

$$dN/dt = k_N \exp\{-\Delta E_{aN}/k_B T\} \quad (24)$$

and the growth rate of nuclei depends on the concentration gradient,

$$\partial\phi/\partial t = D \nabla^2\phi \quad (25)$$

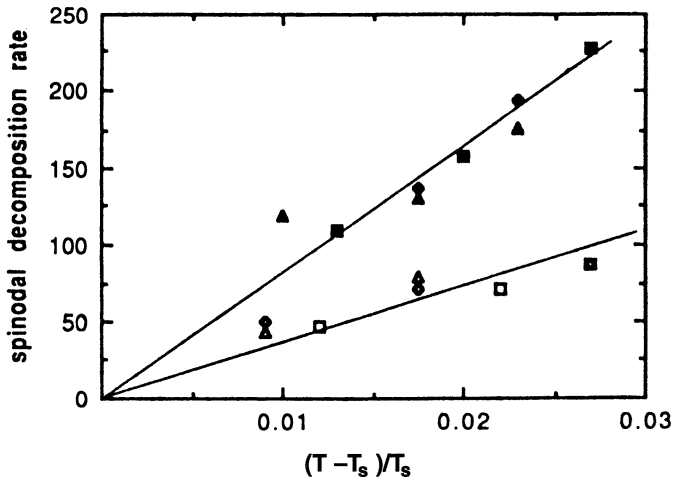


Figure 16. Initial rates of SD for polystyrene–poly(vinyl methyl ether) blends (PS–PVME). (Reproduced from reference 40. Copyright 1991 American Chemical Society.)

then the rate of growth of the drop radius can be expressed as:

$$\partial r_N / \partial t = (1 / \Delta \phi r_N^2) \int_{r_{N0}}^{r_{Nt}} [\partial \phi(r, t) / \partial t] r_N^2 dr_N \quad (26)$$

For the PS–cyclohexane system, r_N was found to vary with polymer concentration from 0.5 to 9000 μm . The rate of the relative growth of the reduced drop radius, $\bar{r} = r / r_N$ (illustrated in Figure 18) depends on the concentration as well as on the volume ratio of the two phases (41).

Coarsening. The later stages of phase separation are complicated by breakdown of the SD structures and growth of drops, known as coarsening. Siggia (42) distinguished three regions of phase coarsening:

1. Early stage, $d_0 \leq d \leq 5d_0$, that obeys the Ostwald ripening mechanism, $d \propto t^{1/3}$.
2. The flow stage, $k_B T / \nu \leq d^2 \leq \nu / g \Delta \rho$, where $d \propto t$ (Tomotika's mechanism).
3. Gravitational or divergent.

The initial diameter of the segregated region, d_0 , depends on the depth of quenching. For PS–PVME at 94–82 °C, Voigt-Martin et al. (43) calculated $d_0 = 2\text{--}9$ nm.

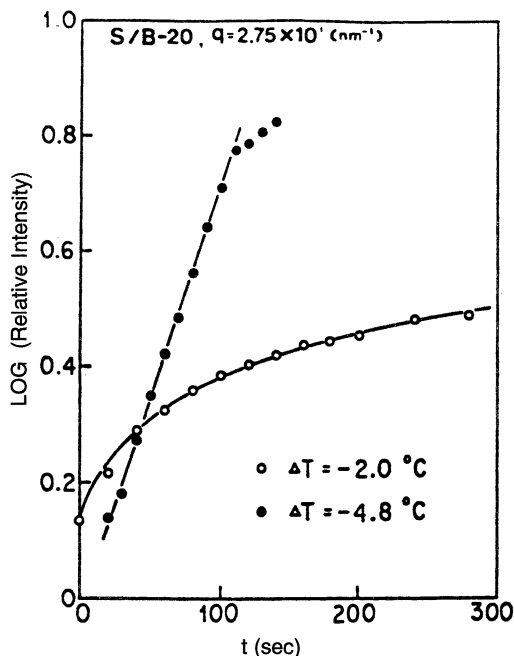


Figure 17. Time dependence of the scattering intensity for polybutadiene-polystyrene blends at the wave vector $q = 2750 \text{ nm}^{-1}$ for SD (filled circles) and for NG (open circles). (Reproduced with permission from reference 33. Copyright 1987 Carl Hanser Verlag.)

The Ostwald ripening process is enhanced by imposition of flow (44):

$$\left(\frac{d}{d_0}\right)^n = 1 + Kt \quad \text{where } n = 3-3/2 \quad (27)$$

Flow also broadens the particle size distribution.

The coarsening is observed directly in the scattering intensity versus wave vector plot. When the coordinates for maximum intensity are defined as $I_m = I(q_m, t)$, then the time dependence of I_m and q_m is expected to follow the “power law” relations:

$$I_m \approx t^\beta \quad q_m \approx t^{-n} \quad \text{with } \beta \geq 3n \quad (28)$$

Under special circumstances the coarsening process progresses only to a certain stage and then the structure is “pinned”. This process is illustrated in Figure 19 for three concentrations of a poly(styrene-*stat*-butadiene) blend with polyisoprene; SBR:PI = 1:4, 3:7 and 1:1 (45). Because $q_m = 2\pi/\Lambda_m$ as the composition approaches a 1:1 ratio, the pinning occurs at longer coarsen-

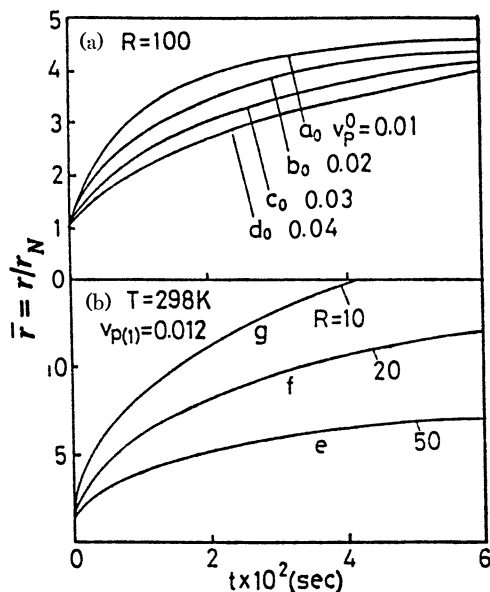


Figure 18. Time dependence of the average drop size; at different polymer volume fraction, ϕ_p (a) and at different ratio of the two-phase volume, \bar{R} (b). (Reproduced with permission from reference 41. Copyright 1991.)

ing times and at more advanced stages. The pinning originates in the transition from dynamic percolation to cluster formations, when the thermodynamic freezes the molecular diffusion, caused by a high kinetic barrier (proportional to χNRT) (45).

Rheological Considerations

The main task in the manufacture of high-performance multiphase polymeric systems (blends, alloys, IPNs, composites, or filled polymers) is control of morphology. For different applications, different morphologies are required. For example, a blend for containers with high gas or liquid barrier properties should have a layered morphology; to toughen engineering resins, a fine dispersion of drops is desired. However, in most cases for the preparation of a multicomponent system it is desirable to generate material with high modulus and high maximum strain at break. These criteria can be accomplished by securing a co-continuous structure. Phase co-continuity may be generated by chemical (IPN), thermodynamic (SD), or rheological (phase inversion) means. As an example, the temperature dependence of the storage modulus for homopolymers and two blends with different structures is presented in Figure 20 (46).

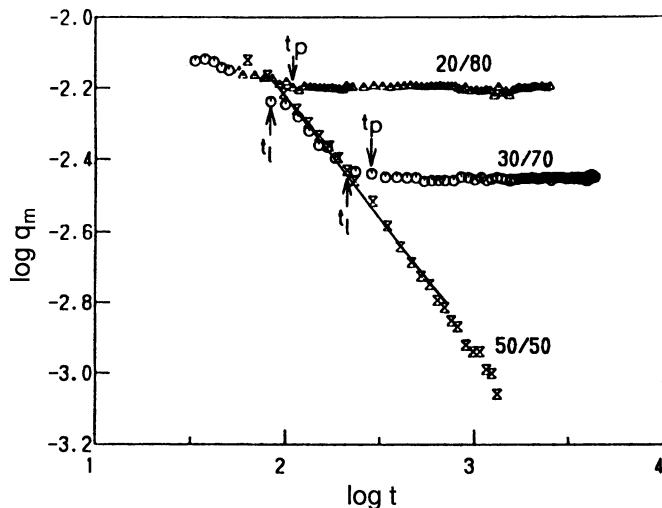


Figure 19. Time dependence of q_m for the critical (50:50) and off-critical SBR-PI mixtures at 60 °C. t_p is the time of pinning. (Reproduced with permission from reference 45. Copyright 1989.)

In the context of this review two aspects of rheology must be considered: (1) the interrelation between rheology and thermodynamics and (2) the interrelation between rheology and morphology. The first relationship contains two elements: the effect of the phase separation on rheology and the effect of flow on phase separation. Furthermore, there are two aspects of the interrelation between morphology and flow: the phase inversion and the flow imposed structures.

From the point of view of blend morphology, the flow should be evaluated for the presence of vorticity, type of strain, and homogeneity of stress field. For example, small strain dynamic flow in a cone-and-plate geometry engenders the least amount of structure modification. By contrast, steady-state extensional flow leads to the most extensive modification of blend structure. Different types of flow are summarized in Table II.

Influence of Thermodynamics on Rheology. For linear viscoelastic functions near phase separation, Larson and Fredrikson derived (47) the equations

$$G'(\omega) \approx \omega^2 \Delta^{-5/2}; \quad \psi_1 \approx \psi_2 \approx \Delta^{-5/2} \quad (29a)$$

$$G''(\omega) \approx \omega \Delta^{-3/2}; \quad \eta(\dot{\gamma}) \approx \Delta^{-3/2} \quad (29b)$$

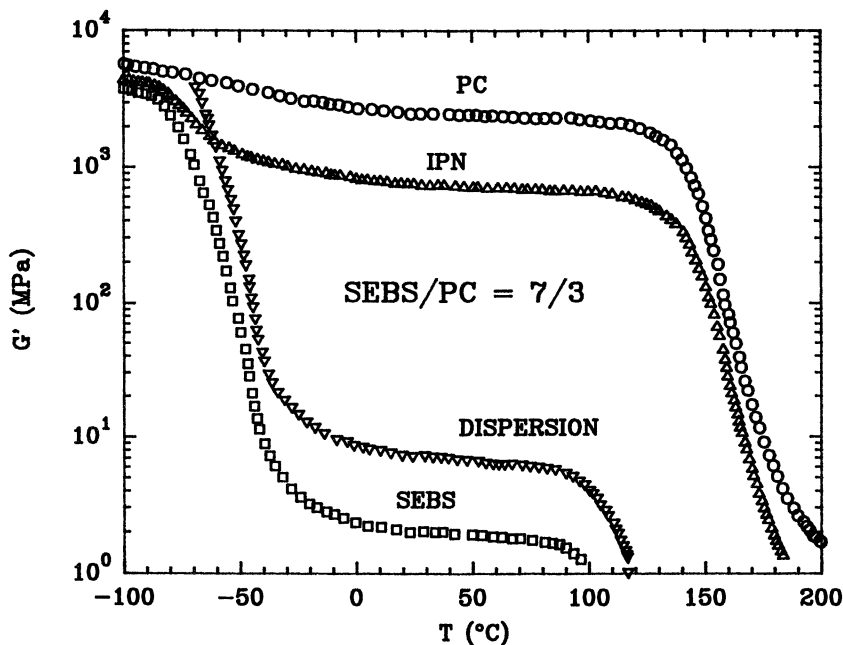


Figure 20. Storage shear modulus vs. temperature for hydrogenated styrene-butadiene-styrene three-block copolymer (SEBS), polycarbonate, (PC), and their blend SEBS:PC = 70:30 wt%. The blend marked "DISPERSION" contains PC as a dispersed phase, whereas in the blend marked "IPN", both phases are co-continuous (thermoplastic IPN). (Reproduced with permission from reference 46. Copyright 1984 Huethig (Heidelberg)).

Table II. Classification of Flow Type

Flow	Vorticity	Strain	Stress Homogeneity
Shear			
Steady state	Yes	Large	Only for cone and plate geometry
Dynamic	Yes	Small	
Extensional			
Steady state	No	Large	Yes
Dynamic	No	Small	Yes

where $\Delta = 2[(\chi N)_s - (\chi N)]$ is a measure of thermodynamic distance from the spinodal. The theory indicates that at the spinodal the linear viscoelastic functions go to infinity; in other words, the system becomes rheologically nonlinear (47). Numerically, near the spinodal, the theory predicts that the ratio $\psi_2/\psi_1 \cong -1.35$, instead of the usual $\psi_2/\psi_1 = -0.05$ to -0.20 . Equation 29 is valid at low strains; for large strains (such as those encountered in steady-state shear or extensional flow) the basic assumption loses its validity;

the system becomes perturbed and eq 29 overestimates the effects. As the authors noted, their theory predicts stronger influence of thermodynamic criticality than the earlier mean field theories for small molecule mixtures.

All the data for diverse liquid systems indicate that when phase separation is approached, the viscosity should increase with the correlation length; viz. Figure 21 (48). Both the rate of the increase and the absolute magnitude vary from one system to another. The effect depends on the deformation rate and is more pronounced in high molecular weight systems.

Influence of Rheology on Thermodynamics. In a sense, the situation discussed in this section is a mirror image of the situation treated in the preceding one. Previously the question was “How does approach to the critical conditions affect the flow properties of miscible blends?” Now the question is “How does shearing the phase-separated liquids affect the critical conditions?”

The response of heterogeneous systems to a stress field allows them to be placed in two categories: (i) those in which stress induces irreversible changes (e.g., precipitation, denaturation of protein, crystallization, etc.) and (ii) those in which the changes are reversible. The classification is not perfect because the type and magnitude of the stress field can be crucial, but it does provide a guide: In most cases, miscibility in the first type of system is reduced by stress, whereas miscibility in the second is increased. In other words, if a system can be irreversibly modified by rheological means, its solubility will be reduced. Prediction of which one of the reversible systems will show en-

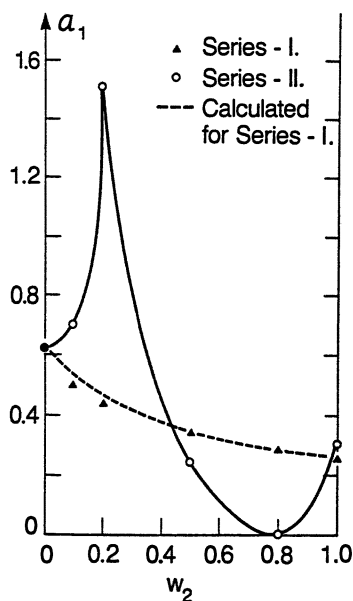


Figure 21. The temperature gradient of viscosity, a_1 , vs. composition for miscible (triangles) and immiscible (circles) blends of polyethylenes. The broken line is theoretical. (Reproduced with permission from reference 48. Copyright 1987 Society of Plastics Engineers.)

hanced and which will show reduced miscibility is more difficult; for example, a solution of polystyrene in *tert*-butyl acetate belongs to the first category, whereas the same solution in dioctyl phthalate belongs to the second category (1).

Strain compatibilization at low, steady-state stress was considered by Lyngaae-Jørgensen (49), from whose work a relation between shear stress, σ , and its effect on the spinodal was derived (1):

$$\sigma_{cr}^2 = a_0 T (T_s - T); \quad T \leq T_s \quad (30)$$

where a_0 is a material parameter. An example of the experimental values of strains required to increase T_s by $\Delta T_s = 3$ –12 °C and those calculated from eq 30 are presented in Table III. Thus, in this case the flow enhanced the blend miscibility. For systems with LCST the spinodal point is shifted to higher temperature. Values of $a_0 = 0.26$ and 0.53 (kPa/K)² were calculated for block copolymers and poly(styrene-*co*-acrylonitrile)–poly(methyl methacrylate) blends, respectively. This result may indicate that the homogenization mechanism is similar for block polymers and blends.

Owing to the deformability of droplets, emulsions as well as polymer blends are elastic. The stored elastic energy may be responsible for drops bursting and the resulting homogenization. Following this idea Mazich (50) studied the effects of shear on spinodal temperature variation in PS–PVME blends at constant storage modulus, $G'(\omega) = 400$ –780 Pa (50). Mazich's results are summarized in Figure 22. The effect amounts to an increase of the miscible region by $T_{sN_1} - T_s = 1$ to 7 °C (T_{sN_1} is the T_s value at constant normal stress, $N_1 \cong 2G'$).

The homogenizing effect of flow is not limited to shear. In a planar extensional flow at $\dot{\epsilon} = 0.013$ –26 s⁻¹ the phase-separated PS–PVME was homogenized at temperatures 3–6 °C above T_s . The critical parameter of homogenization was found to be the strain: $\epsilon_c = \dot{\epsilon} t_c = 44 \pm 14$, where t_c is the critical time to achieve miscibility at various ϕ , T , and $\dot{\epsilon}$. The constancy of ϵ_c indicates that the main mechanism of flow-induced miscibility is related

Table III. Planar Flow Strain Effect on Spinodal Temperature

Strain, ϵ		ΔT_s (°C)
Experimental	Calculated from eq 30	
32 ± 7	30	3
63 ± 4	61	6
88 ± 3	104	9
174 ± 4	161	12

SOURCE: Reproduced with permission from reference 51. Copyright 1986 Springer-Verlag New York, Inc.

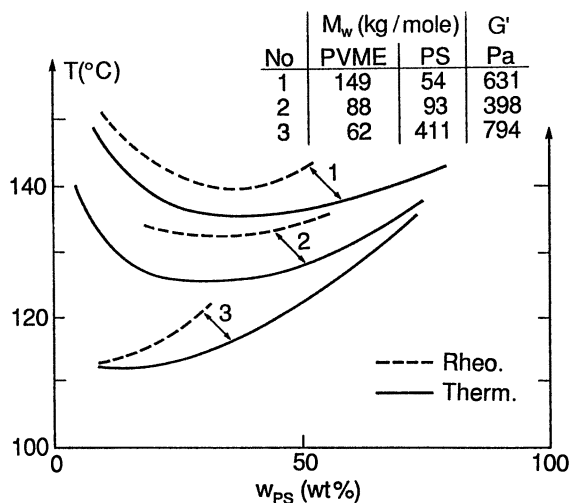


Figure 22. Phase diagrams (for three PVME–PS blends) determined under equilibrium (solid lines) and during dynamic shearing (50).

to deformation; after cessation of flow, the deformation dissipates and the homogenized blend phase separates within 20–70 s (51).

By contrast, large stresses can cause demixing in colloidal (e.g., denaturation of proteins) and polymeric systems. In polymeric systems, precipitation from poor solvent solution, shear crystallization, and stress-related phase separation are known. For example, PS–PVME under planar stresses at $\sigma_{11} < 10$ MPa shows the previously discussed strain compatibilization (see Table III), whereas at $\sigma_{11} \geq 30$ MPa it exhibits stress demixing (51). The stress demixing seems to be related to stress-induced extension of macromolecular coils that leads to negative entropy of mixing.

The blend morphology depends primarily on the viscosity ratio, λ , and the capillarity number, κ :

$$\lambda \equiv \eta_1/\eta_2 \quad \text{and} \quad \kappa \equiv d\sigma/\nu_{12} \quad (31)$$

where η_1 and η_2 represent the viscosity of the dispersed and matrix phases, respectively, d is the drop diameter, σ is the deforming stress, and ν_{12} the interfacial tension coefficient (1).

In shear field the drops can be deformed only if $\lambda < 3.8$ and $\kappa > 0.1$. For $\kappa > 4$ the drops deform affinely with matrix into fibrillar structures, which upon cessation of flow disintegrate (under the influence of the capillary forces) into mini-drops. The diameter of these drops is about twice as large as that of the initial fibers.

Three factors complicate this simple image:

1. The processes are kinetic and the time scale of the event depends on the system properties.

2. The theoretical description is valid only for infinitely diluted Newtonian systems.
3. For concentrations of the dispersed phase that exceed 0.5 vol%, coalescence effects must be taken into account.

More detailed discussion of this topic can be found in references 1 and 52.

Phase Inversion. There are two expressions that predict the phase inversion concentration from the viscosity ratio (D):

$$\phi_{1I}/\phi_{2I} = \eta_1/\eta_2 \equiv \lambda \quad \text{or} \quad \phi_{2I} = 1/(1 + \lambda) \quad (32a)$$

$$\phi_{2I} = 1/[1 + \lambda F(\lambda)] \quad (32b)$$

with

$$F(\lambda) = 1 + 2.25(\log \lambda) + 1.81(\log \lambda)^2$$

where $\phi_{1I} = 1 - \phi_{2I}$ is the volume fraction of liquid 1 at the phase inversion. Equation 32a, proposed by Paul and Barlow (53), is empirical, whereas eq 32b was derived from the filament instability equation by Metelkin and Blekht (54). The viscosity ratio λ should be taken at the shear stress used to prepare the blends. Jordhamo et al. (55) found the Paul and Barlow dependence valid for several liquid–liquid systems. However, as the viscosity ratio increases, both dependencies in eq 32 predict far too rapid a change of ϕ_{2I} (56).

To generate co-continuous structure in a thermoplastic polymer blend (i.e., to generate thermoplastic IPN) the components' viscosity ratio must be adjusted in such a way as to ascertain that the phase inversion occurs at the commercially viable composition. The alternative is to stop the phase inversion process at the moment when the phase percolation reaches its maximum. However, adjusting the viscosity ratio leads to stable IPN morphology (several commercial polymer blends are known to possess such a structure), whereas stopping the phase inversion is kinetic; any further processing may result in the change of morphology from co-continuous to disperse with an associated reduction of performance (for example, see Figure 20).

New Theory. By analogy with emulsions, adding polymer 1 to polymer 2 or polymer 2 to polymer 1 should increase the viscosity: $\eta(A) = \eta(\phi_1)$ and $\eta(B) = \eta(\phi_2)$. Because polymer 2 constitutes the matrix in blend A, whereas in blend B, polymer 1 constitute the matrix, at concentration $\phi_{1I} = 1 - \phi_{2I}$ the phase inversion is expected. As the viscosities in both A and B systems increase at the inversion concentration they must reach a common, maximum value.

The easiest way to express the viscosity–concentration behavior is by means of the relative viscosity, $\eta_r \equiv \eta/\eta^0$, where η^0 is the matrix viscosity.

Krieger and Dougherty (57) derived the simple dependence:

$$\eta_r = (1 - \phi/\phi_m)^{-[\eta]\phi_m} \quad (33)$$

where $[\eta]$ is the intrinsic viscosity and ϕ_m is the maximum packing volume fraction. Equation 33 allowed the computation of $\eta(A) = \eta_2^0 \eta_r(\phi_1)$ and $\eta(B) = \eta_1^0 \eta_r(\phi_1)$ curves shown in Figure 23. The solid line represents $\eta(B) = \eta_1^0 \eta_r(\phi_2)$ with $\eta_1^0 = 1$, whereas the other lines represent $\eta(A) = \eta_2^0 \eta_r(\phi_1)$ with $\eta_2^0 = 0.05, 0.5, 5, 50, 500$, and 5000 . The six points of intersection represent the isoviscous conditions for dispersion of liquid 1 in liquid 2 and liquid 2 in liquid 1; in other words, the conditions for phase inversion. At the isoviscous point,

$$\lambda = [(\phi_m - \phi_{2I})/(\phi_m - \phi_{1I})]^{[\eta]\phi_m} \quad (34)$$

Equation 34 provides a new relation between λ and the inversion concentration. Taking the logarithm of eq 34 and expanding it into the MacLaurin series leads to

$$\log \lambda = [\eta](\phi_{1I} - \phi_{2I}) = [\eta](1 - 2\phi_{2I})$$

or

$$\phi_{2I} = (1 - \log \lambda / [\eta]) / 2 \quad (35)$$

For $0 \leq |\log \lambda| < 1$, eq 35 provides a good approximation.

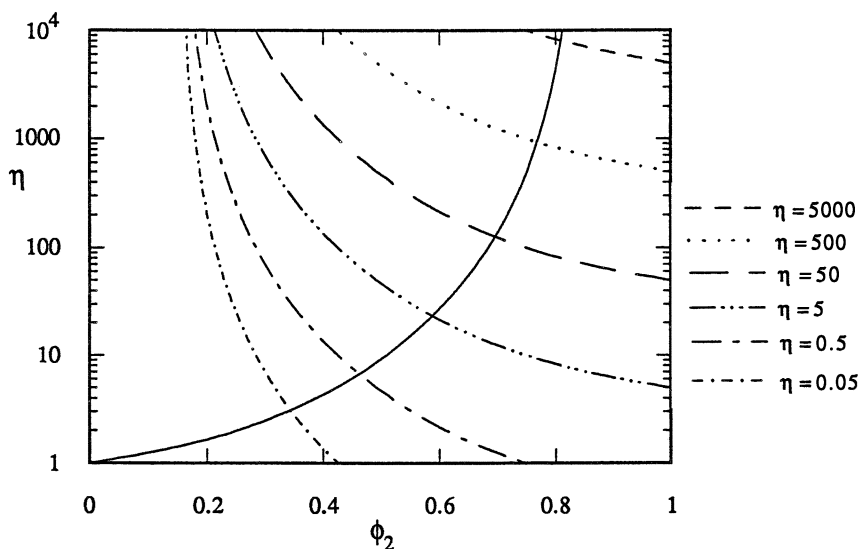


Figure 23. Concentration dependence of emulsion viscosity. The solid line represents $\eta = \eta_r(\phi_2)$; the other lines represent the same dependence for $\eta = \eta_2^0 \eta_r(\phi_1)$. The intercepts correspond to the isoviscous conditions that define the phase inversion concentration, $\phi_{2I} = 1 - \phi_{1I}$.

In shear flow, for $\lambda > 4$ the dispersed drops deform elastically but do not break (1, 58). Here the phase inversion may occur only through coalescence of tightly packed drops at the concentration that corresponds to the maximum packing volume fraction, ϕ_m (59). In extension, drop deformation was observed in a very wide range, up to $\lambda \leq 2000$ (1, 60, 61).

Experimental Verification. Extensive studies of the relationship between the morphology of the blends and the compounding parameters were undertaken (1, 62, 63). Within the range of $0.3 \leq \lambda \leq 4$ (defined in terms of the mixer torque ratios, instead of η) these data are well represented by eq 35 with $[\eta] = 1.9$.

In Figure 24 other experimental data of ϕ_{2I} variation with the viscosity ratio, λ , for thermoplastic blends is presented. The numbers denote the following polymers refer to: 1, acrylonitrile-butadiene-styrene (ABS)-poly-sulfone (PSO) (64); 2, EPDM-polybutadiene (PB) (55); 3 and 4, PS-PB (55); 5, PS-PMMA (65); 6 high-density polyethylene (HDPE)-PS (66); 7, PC-PP (67); 8, low-density polyethylene (LDPE)-PS (68); 9, PS-PMMA (61); 10, PMMA-PE (61); 11, PS-PB (61); 12, 13, and 14, PS-PE (69); 15, PP-linear low-density polyethylene (LLDPE) (70); 16, natural rubber (NR)/HDPE (71); 17 and 18, PP/LLDPE (72). The horizontal and vertical lines represent the conditions between which the phase inversion was observed. Clearly eqs 34 and 35 provide good approximation.

In a recent publication it was demonstrated that onset of phase co-continuity occurs at a nearly constant value of volume fraction, $\phi_{cc} = 0.19 \pm 0.09$, that corresponds to the three-dimensional (3D) percolation threshold, $\phi_{cr} = 0.16$ (59). For one dimension (1D) the percolation threshold depends on the direction: $\phi_{cr\parallel} = 0$ and $\phi_{cr\perp} = 0.25$. Thus, the theoretical values of the maximum packing volume fraction for polymer blends depend on the type of deformation field, $\phi_m = 1 - \phi_{cr} \cong 0.84$ in shear and $\phi_m = 1.0$ in elongational flow field, respectively. Consequently, the phase co-continuity in blends prepared in extension is observed in a much broader range of composition than in shear (73).

Concentration Dependence of Blend Viscosity. Polymer blend viscosity can be expressed as the sum of two terms:

$$\log \eta = \log \eta_L + \Delta \log \eta^E \quad (36)$$

The first term in eq 36 originates from the interlayer slip (74):

$$\log \eta_L = -\log \left[1 + \beta_{12} (\phi_1 \phi_2)^{1/2} \right] - \log (\phi_1 / \eta_1 + \phi_2 / \eta_2) \quad (37)$$

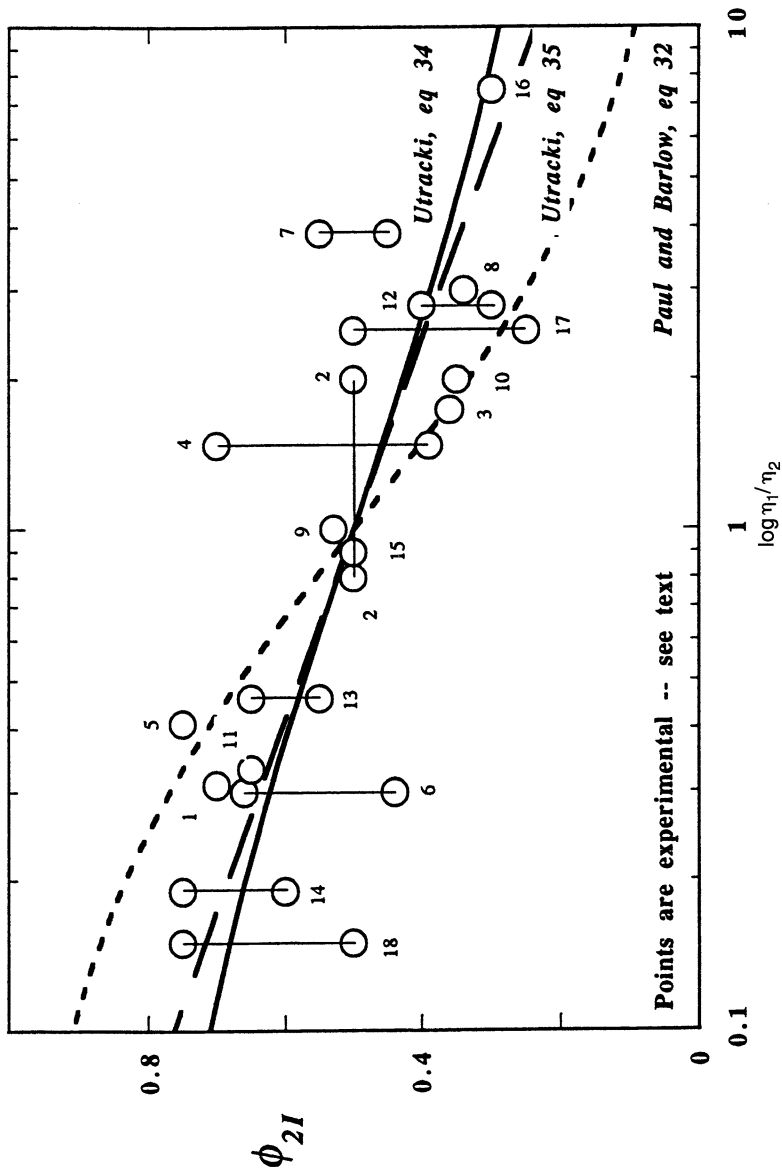


Figure 24. Experimental ϕ_{21} vs. $\log \lambda$ dependence for mechanically prepared thermoplastics blends. The dotted, solid, and broken lines represent eqs 32a, 34, and 35, respectively. The values $[\eta] = 1.9$ and $\phi_m = 0.84$ were used.

where $\beta_{12} = \beta_{12}(\sigma_{12})$ is the interlayer slip factor, whereas the second term, $\Delta \log \eta^E$, is an excess term derived from the concept of the emulsionlike behavior of PABs (75):

$$\Delta \log \eta^E = \eta_{\max} \left\{ 1 - \left[\frac{(\phi_1 - \phi_{1I})^2}{(\phi_1 \phi_{21}^2 + \phi_2 \phi_{1I}^2)} \right] \right\} \quad (38)$$

where η_{\max} is a measure of the effect.

Because ϕ_{iI} can be calculated from $\lambda \equiv \eta_1/\eta_2$, eqs 36–38 have two adjustable parameters, η_{\max} and β . To examine their usefulness, over 30 polymer blends were analyzed. Examples presented in Figures 25 (76) and 26 (77) indicate that for immiscible polymer blends, eqs 36–38 well describe and η versus ϕ relation.

From the η - ϕ data analysis the following observations were made:

1. The interlayer slip parameter β increases with temperature and with shear stress, but decreases upon addition of a compatibilizer.
2. The emulsion effect (as measured by the η_{\max}) decreases with temperature and shear stress, but increases with the molecular weight and compatibilizer content.
3. Comparison of the dynamic (dyn) and steady state (ss) shear flows at the same level of stress reveals that $\beta(\text{dyn}) < \beta(\text{ss})$, whereas $\eta_{\max}(\text{dyn}) > \eta_{\max}(\text{ss})$.

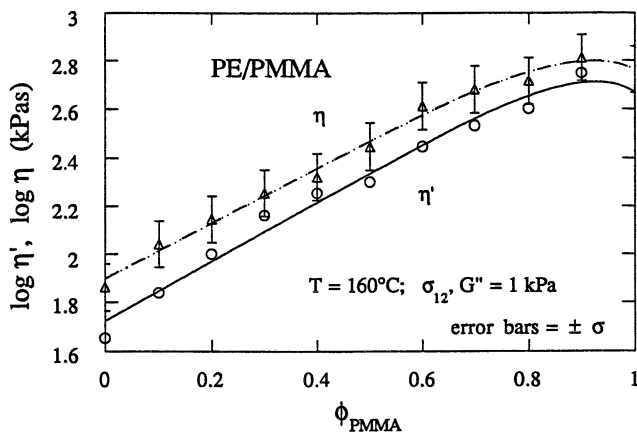


Figure 25. Concentration dependence of dynamic, η' , and steady-state, η , shear viscosity at 160 °C of PE blended with PMMA. Points are experimental and the error bars indicate standard error of measurements (76). The curves were computed from eqs 36–38 with parameters $\beta = 0.001$ and $\eta_{\max} = 0.4$.

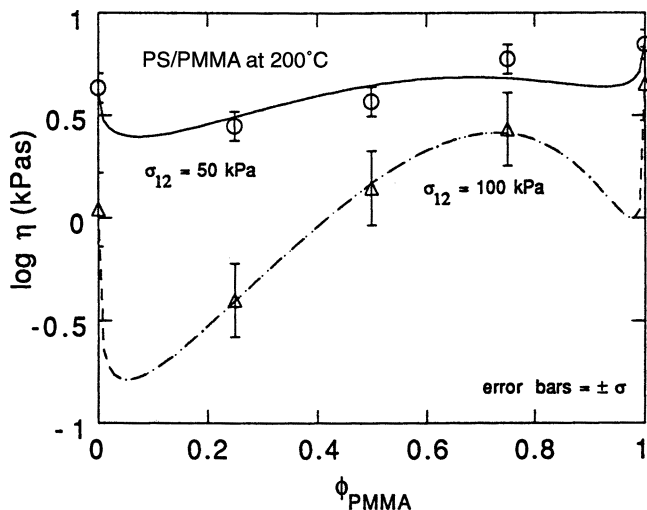


Figure 26. Concentration dependence of constant stress shear viscosity at 200 °C of PS-PMMA blends. Points are experimental and the error bars indicate standard error of measurements (77). The curves were computed from eqs 36–38 with parameters $\beta_{12} = 4.6$ and 42 and $\eta_{max} = 0.45$ and 1.36 for $\sigma_{12} = 50$ and 100 kPa, respectively.

Flow-Imposed Morphology. In polymer blends the morphology changes with stress and strain. The interrelation between the morphology and flow is best described in terms of the apparent yield stress and the strain-induced modification.

Yield Stress. The yield stress can be accounted for by means of the relation

$$\eta = (\sigma_{app} - \sigma_y) / \dot{\gamma} \quad (39)$$

where σ_{app} and σ_y are, respectively, the apparent and the yield stress. In numerous polymer blends σ_y was found to depend on time or rate of deformation, $\dot{\gamma}$:

$$\sigma_y = \sigma_y^\infty [1 - \exp\{-\tau \dot{\gamma}\}]^u \quad (40)$$

where σ_y^∞ , τ , and u are parameters (1).

Dispersion (Mechanical Compatibilization). In Figure 27 the effect of shearing on the relative magnitude of drop size is presented. It is evident that as the rate of shear increases, the dispersed phase drop size decreases.

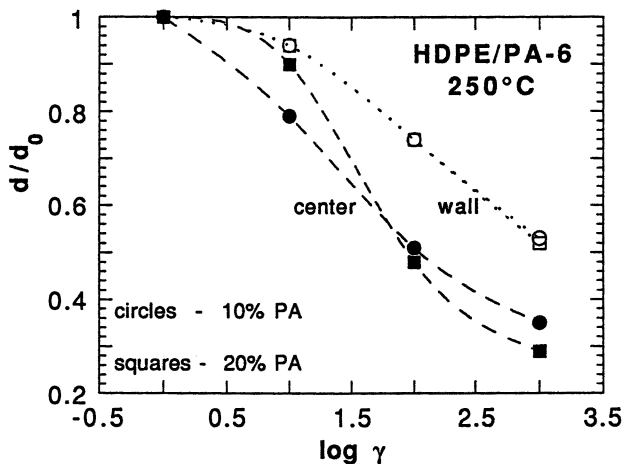


Figure 27. Relative drop size vs. rate of shear for HDPE/PA-6 blend that contains 10 and 20 wt% PA-6. The open symbols indicate the diameters found near the die wall; the filled symbols represent diameters found near the flow center line.

Encapsulation of One Phase by Another. This phenomenon is usually observed in steady-state flow through a tube (see Figure 28). Encapsulation originates in the relative magnitude of shear viscosity and elasticity of the phases. The less viscous or more elastic phase tends to migrate toward the high shear stress area near the tube wall, encapsulating the more viscous or less elastic phase.

Fibrillation. The optimum conditions for elongation of dispersed drops are (i) steady-state extensional flow (e.g., flow through a convergence), (ii) low viscosity of the dispersed liquid, (iii) low concentration of the dispersed phase (to prevent coalescence), and (iv) rapid quenching, for preservation of the fibrillar structure. Under these circumstances up to 61,500 microfibrils per fiber cross-section were observed (78).

When deformed drops are unable to relax and regain their spherical shape, long fibrils with large aspect ratio, $p \rightarrow \infty$, can be generated. An example is presented in Figure 29, where extrusion of PA-6 well below the melting point prevented fiber breakup (79). Another more recent example is fibrillation of liquid crystal polymers (LCP) in thermoplastic matrixes (80).

Coalescence. During convergent flow the flow lines approach each other and create favorable conditions for coalescence. This is indeed observed in the micrograph presented in Figure 29, where fibrillation was accompanied by drop coalescence. Shear-induced coalescence is also well known (81).

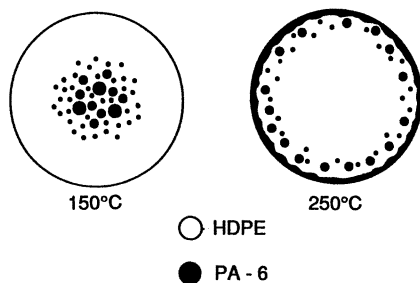


Figure 28. Schematic representation of the PA-6:HDPE = 1:9 morphology after extrusion through a capillary at $T = 150$ and 250 °C (note that melting of PA-6 occurs at $T_m \approx 219$ °C).

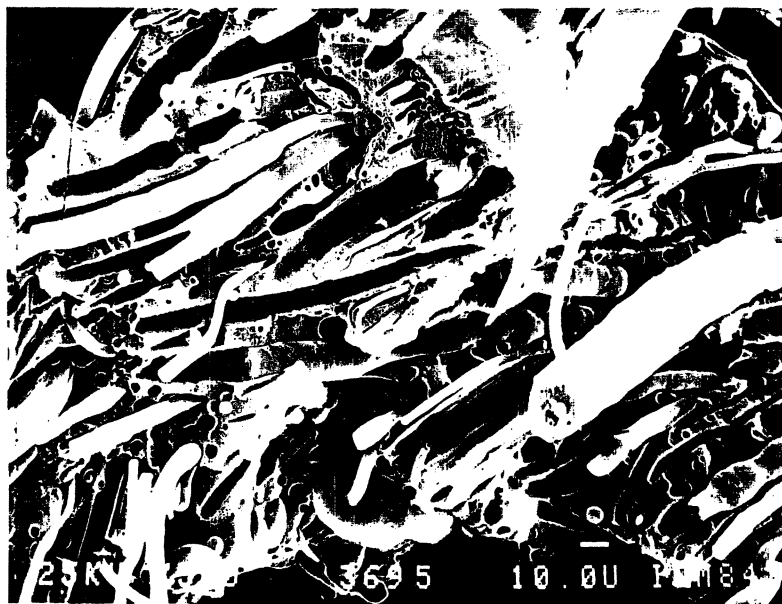


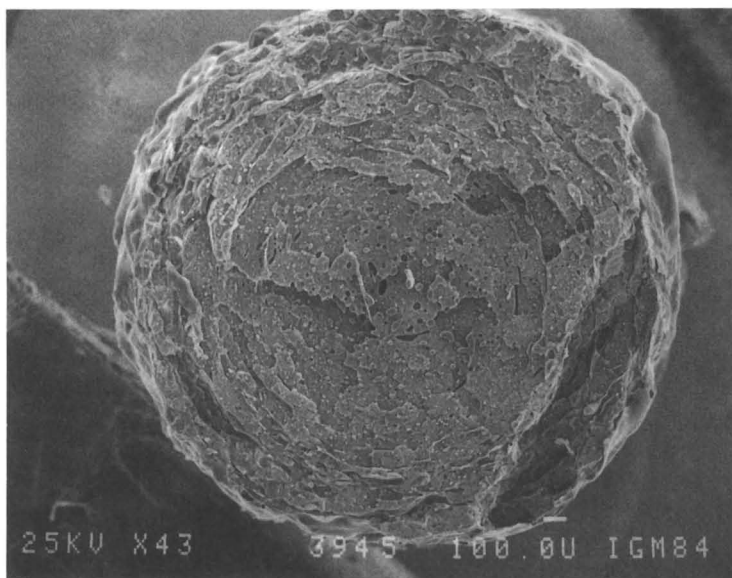
Figure 29. Scanning electron micrograph of PA-6:HDPE = 3:7 blend, a crystalline–crystalline thermoplastic IPN, extruded through a convergent die at 150 °C; that is, 69 °C below T_m of PA-6. (Reproduced with permission from reference 79. Copyright 1986 Society of Plastics Engineers.)

Interlayer Slip. Assuming a telescopic pipe flow with interlayer slip, Lin derived the relation (74)

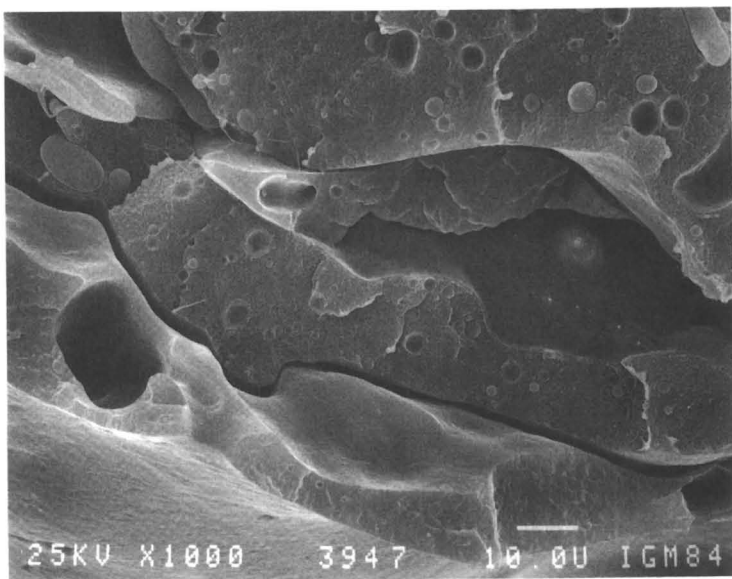
$$1/\eta = \left[1 - (\beta_{12}/\sigma_{12})(w_1 w_2)^{1/2} \right] [w_1/\eta_1 + w_2/\eta_2] \quad (41)$$

In this dependence, β_{12} represents the specific slip factor and w_i is the weight fraction of polymer i (see also eq 37). Evidence for interlayer slip can be found in many micrographs of immiscible systems; viz. Figure 30.

One of the consequences of flow modification of morphology is that measurements carried out under different flow conditions characterize mate-



a



b

Figure 30. Scanning electron micrograph of PA-6:HDPE = 3:7 blend extruded through a convergent die at 250 °C. Note the tree-ring structure of the extrudate (a) and interlayer fractures that occur after crystallization (b). (Reproduced with permission from reference 79. Copyright 1986 Society of Plastics Engineers.)

rials with differing structures; that is, *different materials*. For example, measuring shear viscosity under a low-strain dynamic field yields a different dependence than obtained from large-strain capillary flow. An example is shown in Figure 31. Here the shear flow data for a 50:50 wt% polycarbonate-linear low density polyethylene (PC-LLDPE) blend, determined in dynamic oscillatory (low-strain) mode (solid points), are compared with data measured under the steady-state capillary flow conditions (open points; the solid line was computed from eq 41) (82). Obviously, there is a large difference of rheological response between the two sets of data. Thus, if the measurements are to be performed for characterization of a blend, the capillary instrument (which modifies the morphology and thus gives false information) should be avoided.

These few types of flow-induced changes in blend morphology provide only an example of the variety of modification that occurs during flow while measuring or processing multiphase polymeric materials. Because the molten thermoplastic IPNs (polymer alloys) may be subjected to flow-induced morphological changes, the knowledge of rheology is of critical importance.

Owing to slow rate of cooling, the observed morphology frequently is part-way toward a steady-state structure. Thus, to observe the effects of flow or to preserve the morphology created during the processing (i.e., performance), stabilization of the system may be required. There are several

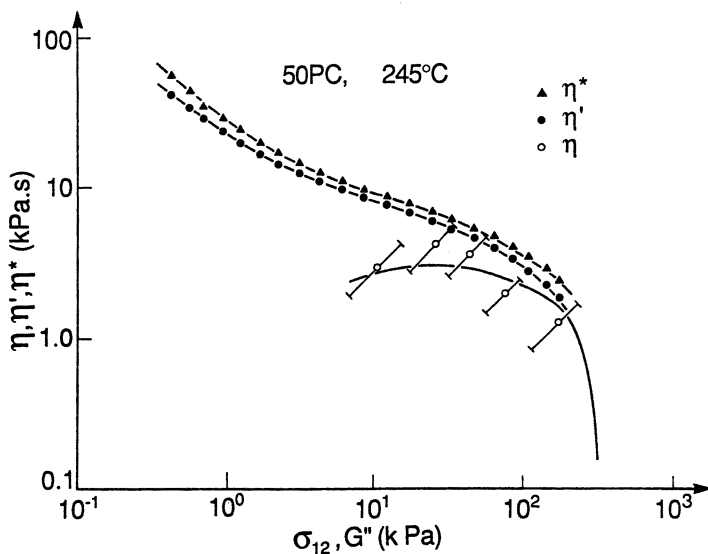


Figure 31. The dynamic (solid points) and capillary shear viscosities for a 50:50 PC:LLDPE blend at 245 °C. The solid line was computed from Lin's eq 41. (Reproduced with permission from reference 82. Copyright 1990 Society of Plastics Engineers.)

chemical and physical methods known to science and industry. Among these methods, quenching and crystallization are most common, but radiation cross-linking is used with increasing frequency (83).

Summary and Conclusions

1. IPNs as compatibilized mixtures of macromolecular species constitute a subgroup of polymer alloys.
2. The morphology of IPNs depends on the interplay between reaction kinetics, miscibility, dynamics of phase separation, and flow.
3. The miscibility of high molecular weight specimens depends on the presence of specific (attractive) or repulsive interactions.
4. The dynamics of phase separation can be followed by scattering methods.
5. The early stage of phase separation depends on interdiffusion.
6. Later stages of phase separation depend on coalescence.
7. At the late stage, flow controls the morphology.
8. In uncross-linked polymer systems the concentration at phase inversion is determined by relative viscosity of the polymers (measured under conditions of blend preparation) and the type of flow.
9. In polymeric systems the phase inversion occurs within a wide concentration range. The range depends on the type of flow field and is larger for extensional than for shear flow.
10. To a great extent the morphology controls flow behavior and product performance.
11. The final morphology of a polymer–polymer two-phase system depends on the flow field and the rate of quenching.
12. Cooling rate, as well as other methods of morphology fixation, has an important influence on the final structure and performance of polymer blends.

Nomenclature

Abbreviations

ABS	acrylonitrile–butadiene–styrene
C-oil	castor oil

EPDM	ethylene-propylene-diene terpolymer
EPR	ethylene-propylene rubber
EVA	ethylene-vinyl acetate copolymer
HDPE	high-density polyethylene
HIPS	high-impact polystyrene
LDPE	low-density polyethylene
LLDPE	linear low-density polyethylene
NG	nucleation and growth
NR	natural rubber
PA	polyamide
PAA	poly(acrylic acid)
PAB	polymer alloys and blends
PB	polybutadiene
PC	polycarbonate
PCL	polycaprolactone
PE	polyethylene
PEO	poly(ethylene oxide)
Phenoxy	poly(hydroxy ether) of bisphenol A
PI	polyisoprene
PMMA	poly(methyl methacrylate)
PnBA	poly(<i>n</i> -butyl acrylate)
PP	polypropylene
PPE	poly(phenylene ether)
PS, PSD	polystyrene, deuterated PS
PSO	polysulfone
PVC	poly(vinyl chloride)
PVME	poly(vinyl methyl ether)
RMS	Rheometrics Mechanical Spectrometer
RSR	Rheometrics Stress Rheometer
SBR	styrene-butadiene rubber
SBS	styrene-butadiene-styrene three-block copolymer
SEBS	styrene-ethylene/butene-styrene three-block copolymer
SEC	size-exclusion chromatography
SIN	simultaneous interpenetrating polymer networks
TP	thermoplastic resin
TS	thermoset resin

Symbols

a, b, k, K, n, u, β	equation constants
\bar{r}	reduced drop radius
$\langle r_0^2 \rangle$	unperturbed, average radius of gyration
$B = \chi RT/V$	reduced binary thermodynamic interaction parameter
b	binodal

b_i	segment length
d	droplet diameter
D, D_M, D_S	diffusion, interdiffusion, and self-diffusion coefficients
ΔE	activation energy
ΔG_m	Gibbs free energy of mixing
$\Delta \bar{G}_m$	reduced Gibbs free energy of mixing
ΔH_m	heat of mixing
F	intrinsic thermodynamic function
G	Gibbs free energy
G''	loss shear modulus
G'	storage shear modulus
H	enthalpy
k_B	Boltzmann constant
M	Onsager-type mobility factor
M_n	number-average molecular weight
M_w	weight-average molecular weight
M_z	z-average molecular weight
n_i	number of moles per unit volume
$N_1 = \sigma_{11} - \sigma_{22}$	first normal stress difference
P	pressure
q	wave vector
R	ideal gas constant
$R(q)$	fluctuation function
r_N	radius of the critical nucleus
S	entropy
s	spinodal
$S(q), S_0$	virtual structure function
T	temperature
t	time
T_g	glass transition temperature
UCST	upper critical solubility temperature
V	volume
β_{12}	interlayer slip factor
χ	binary thermodynamic interaction parameter
Δ	thermodynamic distance from the spinodal; $\Delta \equiv 2[(\chi N)_s - (\chi N)]$
ϵ	Hencky strain in extension
$\dot{\epsilon}$	rate of straining in extension
ϕ_1, ϕ_2	volume fractions of the dispersed and matrix phase
ϕ_c	volume fraction of the cross-linked monomer units
ϕ_{cr}	percolation threshold volume fraction
ϕ_i	volume fraction of phase i at phase inversion
ϕ_m	maximum packing volume fraction
γ	shear strain

$\dot{\gamma}$	shear rate
η	viscosity
η'	dynamic viscosity
η^*	complex viscosity
η_1, η_2	viscosity of the dispersed and matrix phase
η_r	relative viscosity
$[\eta]$	intrinsic viscosity
$\kappa = \sigma d / \nu_{12}$	capillarity (or Taylor) number
κ_s	gradient energy coefficient
Λ	distortion wavelength
$\lambda = \eta_1 / \eta_2$	viscosity ratio
λ_s	wavelength
ν_{12}	interfacial tension coefficient between phase 1 and 2
σ	stress
σ_{11}	extensional stress
$\sigma_{11} - \sigma_{22}$	first normal stress difference
σ_{12}	shear stress
σ_y	yield stress
σ_y^0	permanent yield stress
τ	relaxation time
ω	angular frequency
ψ_1, ψ_2	first and second normal stress difference coefficients
ζ	concentration correlation length

References

1. Utracki, L. A. *Polymer Alloys and Blends*; Hanser Publishers: Munich, Germany, 1989.
2. Utracki, L. A. *Int. Polym. Process.* **1987**, 2, 3.
3. Utracki, L. A.; Favis, B. D. "Polymer Alloys and Blends." In *Handbook of Polymer Science and Technology*; Cheremisinoff, N. P., Ed.; Marcel Dekker: New York, 1989; Vol. 4.
4. *Two Phase Polymer Systems*; Progress in Polymer Processing Series; Utracki, L. A., Ed.; Hanser Publishers: Munich, Germany, 1991.
5. Utracki, L. A. *Polym. Networks Blends* **1991**, 1, 61.
6. Sperling, L. H. *Interpenetrating Polymer Networks and Related Materials*; Plenum: New York, 1981.
7. Fox, R. B.; Fay, J. J.; Sorathia, U.; Sperling, L. H. In *Sound and Vibration Damping with Polymers*; Corsaro, R. D.; Sperling, L. H., Eds.; ACS Symposium Series 424; American Chemical Society: Washington, DC, 1990.
8. Donatelli, A. A.; Sperling, L. H.; Thomas, D. A. *Macromolecules* **1976**, 9, 671.
9. Donatelli, A. A.; Sperling, L. H. *J. Appl. Polym. Sci.* **1977**, 21, 1189.
10. Michel, J.; Hargest, S. C.; Sperling, L. H. *J. Appl. Polym. Sci.* **1980**, 26, 743.
11. Park, I. H.; Lee, J. H.; Kim, S. C. *Polym. Bull.* **1983**, 10, 126.
12. Yeo, J. K.; Sperling, L. H.; Thomas, D. A. *Polym. Eng. Sci.* **1981**, 21, 696; **1982**, 22, 190; *J. Appl. Polym. Sci.* **1981**, 26, 3283; *Polymer* **1983**, 24, 307.

13. Yenwo, G. M.; Sperling, L. H.; Pulido, J.; Manson, J. A.; Conde, A. *Polym. Eng. Sci.* **1977**, *17*, 251.
14. Utracki, L. A.; Jukes, J. A. *J. Vinyl Technol.* **1984**, *6*, 85.
15. Tompa, H. *Polymer Solutions*; Butterworth: London, England, 1956.
16. Huggins, M. L. *J. Chem. Phys.* **1941**, *9*, 440.
17. Flory, P. J. *J. Chem. Phys.* **1941**, *9*, 660.
18. Patterson, D. D.; Robard, A. *Macromolecules* **1978**, *11*, 690.
19. Huggins, M. L. *J. Phys. Chem* **1976**, *80*, 1317.
20. Rätzsch, M. T.; Kehlen, H. *Prog. Polym. Sci.* **1989**, *14*, 1.
21. Walker, J. S.; Vause, C. A. In *8th Symp. Thermodynamic Properties*; Sengers, J. V., Ed.; American Society of Mechanical Engineers: New York, 1982; Vol. 1, p 411.
22. Koningsveld, R.; Kleintjens, L. A.; Schoffaleers, H. M. *Pure Appl. Chem.* **1974**, *39*, 1.
23. Qian, C.; Mumby, S. J.; Eichinger, B. E. *J. Polym. Sci., Polym. Phys. Ed.* **1991**, *29*, 635.
24. Herkt-Matzky, C.; Schelten, J. *J. Phys. Rev. Lett.* **1983**, *51*, 896.
25. Nies, E.; Stroeks, A. *Macromolecules* **1990**, *23*, 4088.
26. Stroeks, A.; Nies, E. *Macromolecules* **1990**, *23*, 4092.
27. Barlow, J. W.; Paul, D. R. *Polym. Eng. Sci.* **1987**, *27*, 1482.
28. Ellis, T. S. *Polym. Eng. Sci.* **1990**, *30*, 998.
29. Greenhill, D. A.; Hourston, D. J.; Waters, J. A. In *Sound and Vibration Damping with Polymers*; Corsaro, R. D.; Sperling, L. H., Eds.; American Chemical Society: Washington, DC, 1990.
30. Petschek, R.; Metiu, H. *J. Chem. Phys.* **1983**, *79*, 3443.
31. Hashimoto, T.; Takebe, T.; Suehiro, S. *Polym. J.* **1986**, *18*, 123.
32. Cahn, J. W.; Hilliard, J. E. *J. Chem. Phys.* **1958**, *28*, 258.
33. Hashimoto, T. In *Current Topics in Polymer Science*; Ottenbrite, R.; Utracki, L. A.; Inoue, S., Eds.; Carl Hanser Verlag: Munich, Germany, 1987.
34. Brochard, F.; Jouffroy, J.; Levisson, P. *Macromolecules* **1983**, *16*, 1638.
35. Binder, K. *J. Chem. Phys.* **1983**, *79*, 6387.
36. Sato, T.; Han, C. C. *J. Chem. Phys.* **1988**, *88*, 2057.
37. Izumitani, T.; Hashimoto, T. *J. Chem. Phys.* **1985**, *83*, 3694.
38. Snyder, H. L.; Meakin, P. *J. Chem. Phys.* **1983**, *79*, 5588.
39. Hashimoto, T. *Phase Transitions* **1988**, *12*, 47.
40. Larbi, F. B. C.; Halary, J.-L.; Monnerie, L. *Macromolecules* **1991**, *24*, 867.
41. Matsuda, S. *Polym. J.* **1991**, *23*, 435.
42. Siggia, E. D. *Phys. Rev. A* **1979**, *20*, 595.
43. Voigt-Martin, I. G.; Leister, K.-H.; Rosenau, R.; Koningsveld, R. *J. Polym. Sci., Polym. Phys. Ed.* **1986**, *24*, 723.
44. Ratke, L.; Theringer, W. K. *Acta Metall.* **1985**, *33*, 1793.
45. Takenaka, M.; Tanaka, K.; Hashimoto, T. In *Contemporary Topics in Polymer Science*; Culberston, W. M., Ed.; Plenum: New York, 1989; Vol. 6.
46. Gergen, W. P. *Kautsch. Gummi* **1984**, *37*, 284.
47. Larson, R. G.; Fredrikson, G. H. *Macromolecules* **1987**, *15*, 1278.
48. Utracki, L. A.; Schlund, B. *Polym. Eng. Sci.* **1987**, *27*, 367, 1512.
49. Lyngaae-Jørgensen, J. In *Processing, Structure and Properties of Block Copolymers*; Folkesm, M. J., Ed.; Elsevier Applied Science Publishers: London, England, 1985.
50. Mazich, K. A. Ph.D. Thesis, Northwestern University, 1983.
51. Katsaros, J. D.; Malone, M. F.; Winter, H. H. *Polym. Bull.* **1986**, *16*, 83; Katsaros, J. D. Ph.D. Thesis, University of Massachusetts, 1987.

52. Utracki, L. A.; Shi, C.-K. *Polym. Eng. Sci.* **1992**, 32, 1824, 1834, 1846.
53. Paul, D. R.; Barlow, J. W. *J. Macromol. Sci., Rev. Macromol. Chem.* **1980**, C18, 109.
54. Metelkin, V. I.; Blekht, V. S. *Kolloid. Zh.* **1984**, 46, 476.
55. Jordhamo, G. M.; Manson, J. A.; Sperling, L. H. *Polym. Eng. Sci.* **1986**, 26, 517.
56. Utracki, L. A. In *Multiphase Polymers: Blends and Ionomers*; Utracki, L. A.; Weiss, R. A.; Eds.; ACS Symposium Series 395; American Chemical Society: Washington, DC, 1989; Chap. 7.
57. Krieger, I. M.; Dougherty, T. J. *Trans. Soc. Rheol.* **1959**, 3, 137.
58. Berger, W.; Kammer, H. W.; Kummerlöwe, C. *Makromol. Chem. Suppl.* **1984**, 8, 101.
59. Lyngaae-Jørgensen, J.; Utracki, L. A. *Makromol. Chem., Macromol. Symp.* **1991**, 48/49, 189.
60. Grace, H. P. *Chem. Eng. Commun.* **1982**, 14, 225.
61. Dreval, V. Ye.; Vinogradov, G. V.; Plotnikova, E. P.; Zabugina, M. P.; Krasnikova, N. P.; Kotova, E. V.; Pelzbauer, Z. *Rheol. Acta* **1983**, 22, 102.
62. Avgeropoulos, G. N.; Weissert, F. C.; Biddison, P. N.; Böhm, G. G. A. *Rubber Chem. Technol.* **1976**, 49, 93.
63. Miles, I. S.; Zurek, Z. *Polym. Eng. Sci.* **1988**, 28, 796.
64. Inguli, A. F.; Alter, H. L. U.S. Patent 3,636,140, 1972.
65. Utracki, L. A.; Sammut, P.; Lyngaae-Jørgensen, J.; Valenza, A. *SPE Tech. Pap.* **1991**, 37, 978.
66. Thorsteinsson, F. M.Sc. Thesis, Technical University of Denmark, Lyngby, 1989.
67. Favis, B. D.; Chalifoux, J. P. *Polymer* **1988**, 29, 1761.
68. Utracki, L. A.; Sammut, P. *Polym. Eng. Sci.* **1990**, 30, 1019.
69. Elemans, P. H. M. Ph.D. Thesis, Delft University of Technology, 1986.
70. Levij, M.; Maurer, F. H. J. *Polym. Eng. Sci.* **1988**, 28, 670.
71. Akhtar, S.; Kuriakose, B.; De, P. P.; De, S. K. *Plast. Rubber Process. Appl.* **1987**, 7, 11.
72. Dumoulin, M. M. Ph.D. Thesis, Ecole Polytechnique, Montreal, 1988.
73. Valenza, A.; Demma, G. B.; Acierno, D. *Polym. Networks Blends* **1993**, 3, 1.
74. Lin, C.-C. *Polym. J.* **1979**, 11, 185.
75. Utracki, L. A. *J. Rheol.* **1991**, 35, 1615.
76. Martinez, C. B.; Williams, M. C. *J. Rheol.* **1980**, 24, 421.
77. Lyngaae-Jørgensen, J. In *Polymer Alloys III*; Klempner, D.; Frisch, K. C., Eds.; Plenum: New York, 1983.
78. Tsebrenko, M. V.; Rezanova, N. M.; Vinogradov, G. V. *Nov. Reol. Polim., 11 Mater. Vses. Simp. Rheol.* **1982**, 2, 136.
79. Utracki, L. A.; Dumoulin, M. M.; Thoma, P. *Polym. Eng. Sci.* **1986**, 26, 34.
80. Sukhadia, A. M.; Datta, A.; Baird, D. G. *SPE Tech. Pap.* **1991**, 37, 1008.
81. Utracki, L. A. *Coll. Interface Sci.* **1973**, 42, 185.
82. Utracki, L. A.; Sammut, P. *Polym. Eng. Sci.* **1990**, 30, 1027.
83. *Radiation Processing of Polymers*; Progress in Polymer Processing Series; Singh, A.; Silverman, J., Eds.; Hanser Publishers: Munich, Germany, 1991; Vol. 3.

RECEIVED for review October 30, 1991. ACCEPTED revised manuscript October 13, 1992.

Equilibrium and Nonequilibrium Microphase Structures of Interpenetrating Polymer Networks

Yuri S. Lipatov

Institute of Macromolecular Chemistry, Ukrainian Academy of Sciences,
253160, Kiev, Ukraine

Formulation of a new approach to the structure of interpenetrating polymer networks (IPNs) is the objective of this review of the author's experimental works. As a whole, IPNs are not thermodynamically equilibrium systems because, in the course of chemical reactions leading to gelation, simultaneous phase separation proceeds due to increased thermodynamic immiscibility. However, the phases that evolve preserve the inherent structure of the state of mixing at an earlier stage of the reaction, before the onset of phase separation. Thus, the IPN is considered to be in a state of quasi-equilibrium with the molecular level of mixing. As a consequence, the nonequilibrium microphase structure of the IPN is described as a microheterogeneous system with a lack of molecular mixing of the two constituent networks throughout the bulk, but with a limited level of forced molecular mixing in each of the phases.

PROPERTIES OF INTERPENETRATING POLYMER NETWORKS (IPNs) depend on both the thermodynamic miscibility of the constituent networks and the kinetic conditions of the cross-linking reaction. The principal work on IPNs has been done by Sperling (1) and Frisch et al. (2). Research has established that IPNs have a complex structure and morphology and frequently exhibit dual-phase continuity (3). Thermodynamic considerations have yielded equa-

tions that predict domain sizes in IPNs (4, 5), and the two-phase morphology was investigated by direct structural methods (6–9). A phenomenological theory was formulated for chemically quenched binary IPNs and the conditions of their phase stability were elucidated by Binder and Frisch (10). All of these results support the conclusion that IPNs cannot be considered as systems with a molecular level of mixing of the two networks. With some exceptions, IPNs have a heterogeneous structure and are multiphase systems. The structural heterogeneity in IPNs is caused by the thermodynamic immiscibility of the networks that arises at a definite degree of conversion in the course of the chemical reactions of polymerization and cross-linking. The thermodynamic immiscibility leads to microphase separation that proceeds in accordance with the spinodal mechanism (11). This chapter provides a review of the critical papers produced in Kiev on the microphase structure of IPNs. The principal features of the mechanism and the kinetics of IPN formation and microphase separation will be discussed.

Development of Thermodynamic Immiscibility in IPNs

The thermodynamic immiscibility of the constituent networks in an IPN begins at low degrees of conversion [both for full and semi-IPN (SIPN)]. For example, Figure 1 shows the phase diagrams of SIPNs based on a styrene–divinylbenzene copolymer and poly(butyl methacrylate). The regions that correspond to the two-phase SIPN (hatched areas) are much larger than the regions of the one-phase state. In the phase diagram, heterogeneous regions are separated from the homogeneous regions by a binodal curve. In the course of SIPN formation, the polymerizing system passes from point A to point A₁, which correspond to the initial mixture and to the SIPN, respectively. Phase separation occurs after the border of the two-phase region (point 0) is passed. An increase in the reaction temperature does not change the shape of the diagram; however, the area of the one-phase state slightly increases, which is typical for systems with an upper critical solution temperature. Analysis of the region of IPN compositions situated inside the triangle BB₁C shows that polymerization of mixtures with poly(butyl methacrylate) (PBMA) content above some critical value is accompanied by phase separation (12) almost from the very beginning. Figure 2 presents kinetic curves of the reaction of cross-linking polyurethane in the presence of poly(butyl methacrylate). The arrows indicate the onset time of phase separation. Microphase separation begins very early and depends on the kinetic conditions. Characteristics of the system are given in Table I.

These data show the dependence of phase separation time on the reaction conditions and composition of the system. From these data it follows that an interconnection exists between the kinetic conditions of reaction and

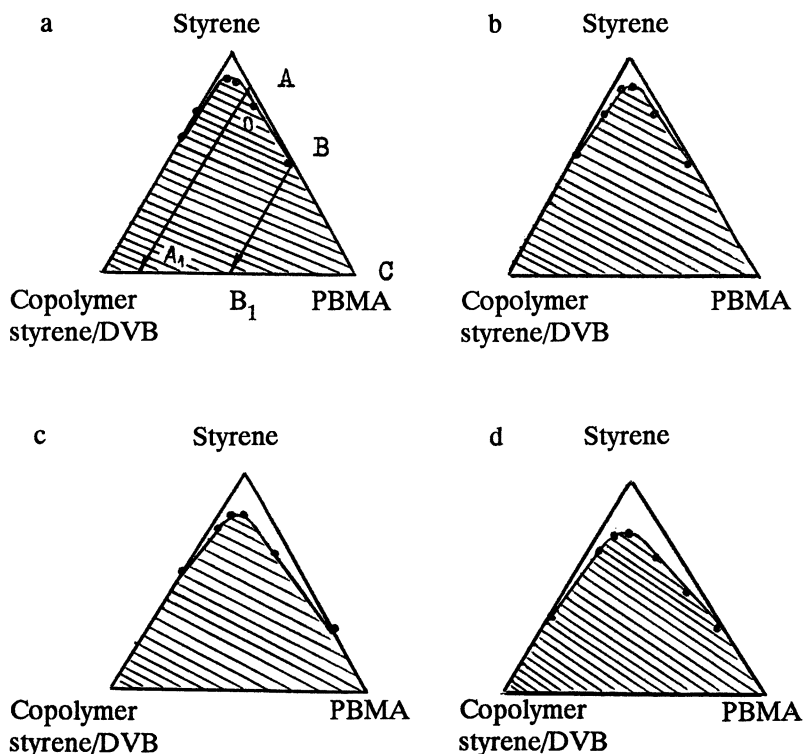


Figure 1. Phase diagrams of SIPN: styrene–divinylbenzene–poly(butyl methacrylate) network copolymer at temperatures of 333 (a), 343 (b), 353 (c), and 363 (d) K (12).

the properties of the phase-separated system. An absence of inflection points on the kinetic curves at the onset of microphase separation is noted. The lack of an inflection point often shows an absence of volume changes brought about by microphase separation, although the volume change itself does not affect the reaction rate. Such a situation may be possible only when phase separation leads to the appearance of two phases that have compositions very close to one another (a sign of spinodal decomposition).

The existence of a definite correlation between the kinetic conditions of chemical reactions leading to IPN formation and the degree of microphase separation has been shown in many cases (13). Concurrently, a definite mutual influence of the reaction mixture components on the kinetics of formation of constituent networks in IPNs exists: the rate of cross-linking of each network is dependent on the network ratio (Figure 3). The conversion degree of the components that form the IPN at the onset of phase separation also depends on the cross-linking level of each network.

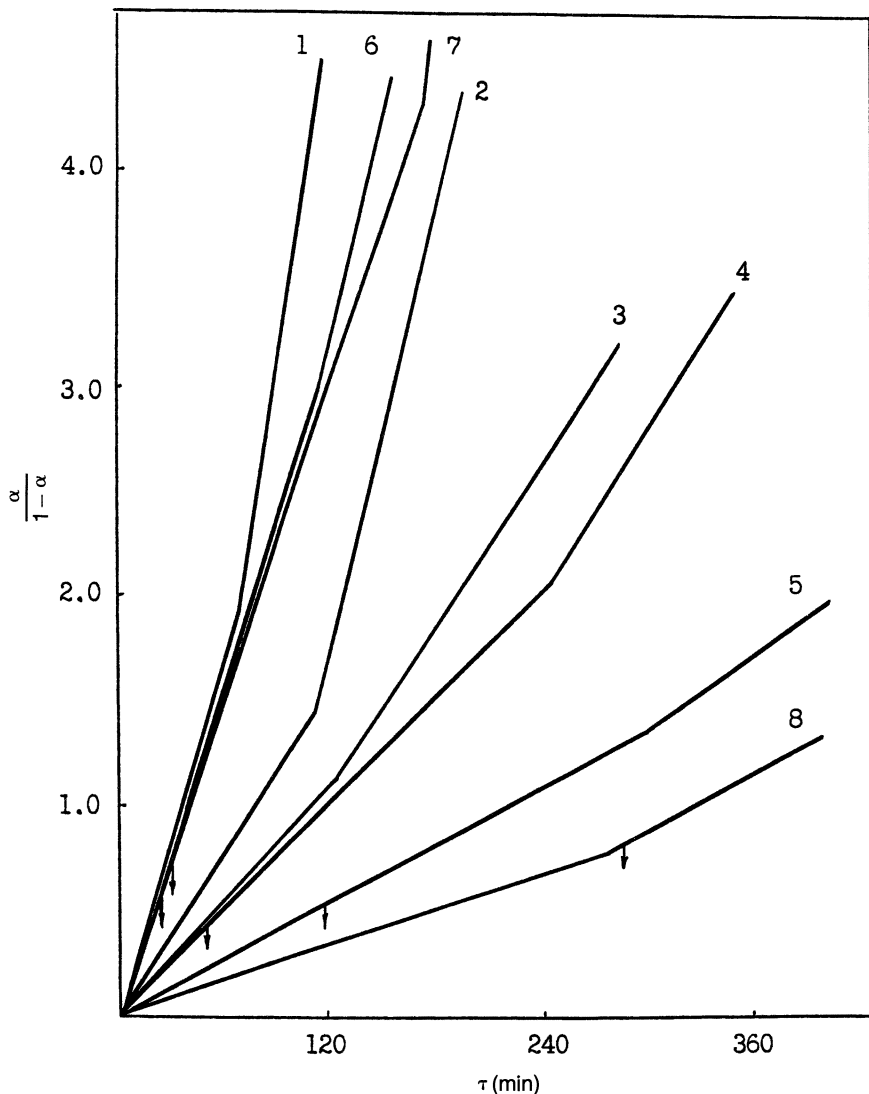


Figure 2. Kinetic curves of polyurethane formation in the presence of 15 wt% of PBMA. α is the conversion degree. For designations, see Table I. (Reproduced with permission from reference 13. Copyright 1990.)

Superposition of Chemical and Physical Kinetics

Both processes that accompany IPN formation—chemical reaction of cross-linking and physical process of microphase separation—proceed simultaneously in the time interval between the onset of phase separation and the gel point of each network. Such superposition results in a complicated IPN

Table I. Physicochemical Parameters of Eight SIPNs Based on PU–PBMA (85:15)

<i>Parameters</i>	<i>1</i>	<i>2</i>	<i>3</i>	<i>4</i>	<i>5</i>	<i>6</i>	<i>7</i>	<i>8</i>
Curing temperature, ± 1 (K)	333	333	313	333	333	333	353	313
Catalyst mass fraction, ± 0.001	0.005	0.010	0.010	0.010	0.005	0.050	0.010	0.010
Reaction rate constant, $\times 10^{-4}$ (kg/mol s)	3.46	7.63	1.90	2.62	1.3	8.1	7.05	0.73
Phase separation onset, ± 1 (min)	—	—	—	43	100	28	30	29
Conversion degree at phase separation, α	—	—	—	0.23	0.13	0.39	0.56	0.48
Conversion degree at anamorphose inflection point, α , ± 0.01	—	—	—	0.68	0.58	0.74	0.82	0.47
Glass-transition temperature of PU-enriched phase, ± 1 (K)	253	251	255	253	261	248	265	249
Glass-transition temperature of PBMA-enriched phase, ± 1 (K)	—	—	—	316	333	323	315	318
Segregation degree (SD)	—	—	—	0.33	0.32	0.35	0.32	0.34

NOTE: Data were taken from reference 3.

microphase structure. In this case, when curing occurs simultaneously with growth in conversion degree, the composition and molecular weights of the network fragments change with time. The onset of phase separation takes place when the thermodynamic interaction parameter, χ_{AB} , reaches a critical value or, more generally stated, when the free energy of mixing becomes positive. The rate at which this critical value is achieved depends on the rates of two independent curing reactions. After reaching the critical value, χ_{AB} continuously changes with increasing cross-link density. As a result, the thermodynamic immiscibility of the IPN components and the driving force for phase separation increase as well. Despite the nonequilibrium conditions for both chemical and physical processes and because of their superposition, the phase separation may be described as a spinodal decomposition. The experimental data show the corresponding relationships (11).

Incomplete Phase Separation

Both the chemical reactions and the phase separation proceed under nonequilibrium conditions. After some high degree of chemical conversion and cross-linking is reached, however, microphase separation is impeded and the system fixes at a nonequilibrium structure characterized by incomplete

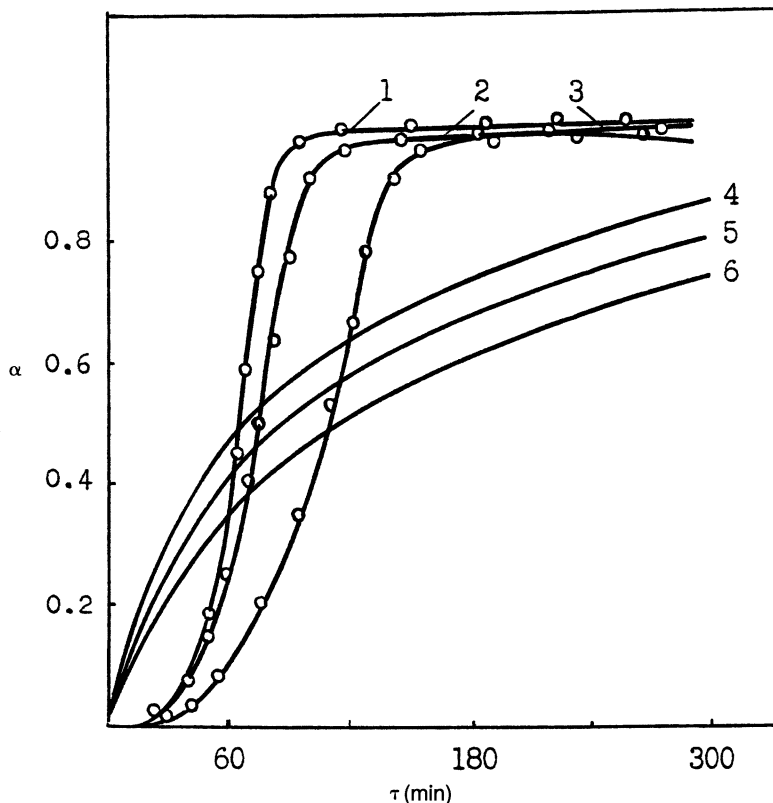


Figure 3. Kinetics of formation of simultaneous IPN: Curing polyurethane (curves 1–3) and polymerization of butyl methacrylate (curves 4–6) at various component ratios: 85:15 (curves 1 and 4); 75:25 (curves 2 and 5); 65:35 (curves 3 and 6). α is the degree of conversion of the components.

phase separation. Thus completion of the IPN polymerization evolves in two phases. The separated system may be characterized by the segregation degree (11), which can be calculated from small-angle X-ray scattering (SAXS) data or from the viscoelastic functions (14). Figure 4 shows schematically the temperature dependence of the mechanical losses in a two-phase polymer system with differing degrees of component segregation (miscibility). Case a corresponds to a mixture of two components where the phases are clearly separated and each phase is characterized by its own glass-transition temperature (maximum $\tan \delta$); case e corresponds to a fully miscible system. From the curve parameters the segregation degree may be estimated easily as

$$\alpha = \frac{[h_1 + h_2 - (l_1 h_1 + l_2 h_2 + l_m h_m)/L]}{(h_1^0 + h_2^0)} \quad (1)$$

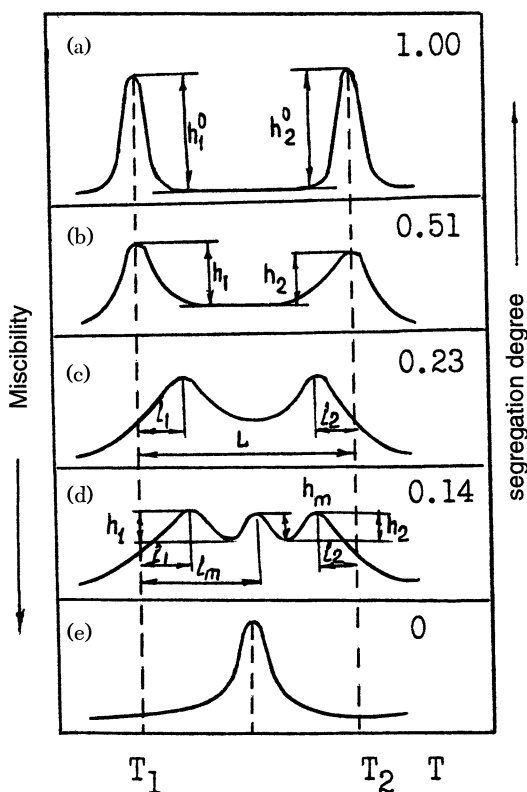


Figure 4. Temperature dependence of mechanical loss $\tan \delta$ at various degrees of component segregation. (Reproduced with permission from reference 14. Copyright 1985 Blackwell Scientific Publications, Ltd.)

where the significance of α can be gleaned from Figure 4. As illustrated in Figure 4, l_1 and l_2 represent the temperature shift of the lower and upper glass transitions, respectively. The quantities h_1 and h_2 represent the intensities of the transitions above the plateau region between the transitions. The superscript zero refers to the pure components. The quantity L is the initial temperature difference between the peaks. The subscript m refers to the temperature and intensity of an intermediate mixed phase peak, if any. Equation 1 is a semiempirical equation to determine the extent of phase separation; it is a more sophisticated model than the model used earlier by Curtius et al. (15). With reference to Figure 4, $l_m h_m = 0$ for parts a, b, and c because there is no mixed phase peak. The quantity $h_m l_m$ is finite only for part d. For part e, the equation does not apply because there is only one peak. Note that $l_1 h_1$ and $l_2 h_2$ are measures of the area under the peaks. When $l_1 + l_2 = L$, a microheterogeneous morphology emerges.

Table II. Dependence of Segregation Degree on Reaction Temperature for IPN Based on Poly(butyl methacrylate) (PBMA) and a Copolymer of Styrene–Divinylbenzene

<i>Component Ratio (PBMA:PS)</i>	333 °C	353 °C	363 °C
95:5	0.46	0.51	0.65
85:15	0.30	0.32	0.43
60:40	0.15	0.20	0.40

In general, the segregation degree α determines the fraction of the system mass that is phase separated: for fully separated systems, $\alpha = 1$; for miscible systems, $\alpha = 0$. Thus, α is an effective measure of phase separation. This value strongly depends on the kinetic conditions (Tables I and II). The comparatively low degrees of segregation in most IPNs (0.3–0.6) shows that a large fraction of the system mass is preserved in the unseparated state and distributed between two phases. Both phases represent mixtures of both components; each phase is enriched by the opposite component. This statement is illustrated in Figure 5. There are two distinguishable relaxation maxima that correspond to the two phases. The position of these maxima does not correspond to the transition temperatures of the pure components. Thus, the position of the two maxima depends on the reaction kinetics that govern phase separation. The dependence of the transitions on the kinetics of curing was observed for many systems. At the same time, it was found that the degree of phase separation is determined by the kinetic conditions and that increased reaction rates lead to a diminished degree of phase separation. An increase in the reaction rate decreases the time for the onset of phase separation. As the reaction rate of IPN formation increases, the segregation degree decreases (16). In some cases this inverse relationship may lead to incorrect conclusions about the miscibility of the two networks, as judged by their mechanical behavior.

Nonequilibrium Structure of IPNs

The microphase structure of IPNs may be described using the concept of the formation of various clusters: “physical” clusters due to phase separation of constituent networks under conditions of nonequilibrium phase transition and “chemical” clusters due to cross-linking. The real structure of an IPN should be considered as a multiphase structure that is determined by the coexistence of at least three “phases” (not in the true thermodynamic sense). Two phases are formed by the networks due to phase separation. Each phase may be considered as an independent IPN in which phase separation did not take place (the state of “forced” compatibility) (11) and in which mixing near the molecular level is preserved. The composition of these two phases is deter-

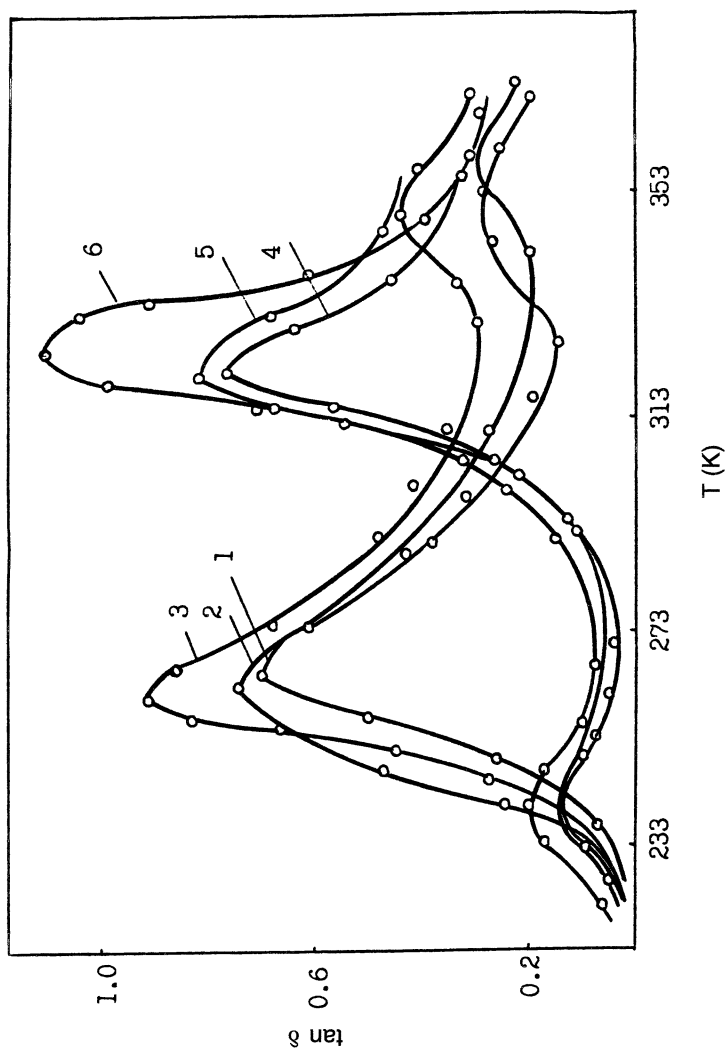


Figure 5. Temperature dependence of mechanical loss $\tan \delta$ of SIPN at various component ratios: PU-BMA (simultaneous curing) 85:15 (curve 1); 75:25 (curve 2); 65:36 (curve 3); PU-PBMA (introduction of PBMA into the reaction mixture): 85:15 (curve 4); 75:25 (curve 5); and 65:35 (curve 6).

mined by the reaction rate and the temperature. Each phase has an average composition that does not correspond to the ratio in the IPN. The third "phase" is the nonequilibrium transition zone from one phase to another; its dimension is dependent on the conditions of phase separation. This zone may be called the mesophase and may be considered a nonequilibrium IPN phase because the molecular level of mixing is also preserved. At spinodal decomposition conditions typically there is no sharp border between coexisting regions of phase separation. This transition zone may be chosen in such a way that its composition corresponds to the average composition of the IPN. The volume fraction of this zone depends on the conditions of IPN formation. The appearance of microregions of various composition constitutes the reason for the strong structural heterogeneity in IPNs.

In general, the microphase structure of IPNs may be described as nonequilibrium. However, in such a nonequilibrium IPN one can still distinguish various microregions that can be described as quasi-equilibrium; that is, microregions with a near molecular level of mixing of the constituent components. Only the thermodynamic stability of the IPNs is discussed here. The nonequilibrium state and thermodynamic instability of IPNs do not imply the instability of physical and mechanical properties because the relaxation time to establish true equilibrium is unattainable due to entanglements.

All the ideas connected with the nonequilibrium multiphase structure of IPNs are in a good agreement with a comparatively low segregation degree in IPNs. In such a way the whole structure of IPNs may be presented as a mesophase matrix with embedded microphase regions that represent two evolved phases. Such a structure model coincides with the spinodal mechanism of decomposition and many X-ray and electron microscopy studies (11, 17).

Thus, two thermodynamic states in IPNs can be distinguished. The IPN as a whole is a nonequilibrium system due to incomplete phase separation and thermodynamic immiscibility of the constituent networks. Figure 6 shows the free energy of mixing for a polyurethane–poly(ethyl acrylate) (PU–PEA) IPN; the positive values signify the lack of miscibility. However, the two phases may be considered as quasiequilibrium phases because they are the result of microphase separation and each phase preserves the composition that almost corresponds to the one-phase state; that is, the equilibrium state of molecular mixing. Because the level of mixing that was inherent to the state of mixing at earlier reaction stages is substantially preserved, which corresponds to the onset of phase separation, these phases are called quasiequilibrium phases. Thus, the nonequilibrium microphase structure of IPNs may be presented as a microheterogeneous two-phase system that lacks molecular mixing of two constituent networks throughout the bulk and with near molecular level of mixing in each phase and transition zone (mesophase).

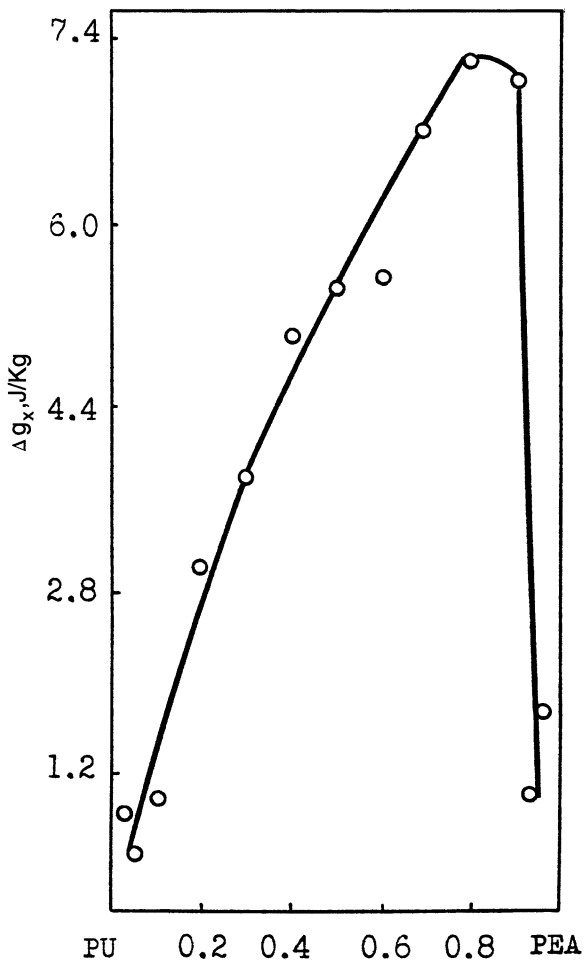


Figure 6. Concentration dependence of the free energy of mixing for a full IPN based on polyurethane and polyester acrylate.

Thermodynamic Description of Nonequilibrium Multiphase Structure

Depending on the kinetic condition of curing, various degrees of phase separation and various nonequilibrium states may be realized. To compare different systems, it is important to characterize these states by one parameter, χ_{AB} (18):

$$\chi_{AB} = Z \Delta W_{AB} / kT \quad (2)$$

where ΔW_{AB} is the exchange energy and Z is the coordination number of the lattice. For various nonequilibrium states of IPNs, the level of molecular interactions between chains may be different. Formally, the difference may be ascribed to different values of Z . The system is in the state of true thermodynamic equilibrium only if the free energy of mixing or χ_{AB} is negative. However, for immiscible systems like IPNs the free energy of mixing is positive (Figure 6) and χ_{AB} is positive as well. To compare various nonequilibrium states of IPN we can experimentally estimate the value $(\chi_{AB})_{\text{exp}}$. Various methods for the determination of χ_{AB} are described elsewhere (19). Now let us consider IPNs separated into two phases. Each quasiequilibrium phase may be considered as a solution of network A in network B or vice versa; that is, a miscible system. If phase separation is complete, we deal with an equilibrium system that consists of two equilibrium phases. For such a system

$$(\chi_{AB})_{\text{exp}} = (\chi_{AB})_{\text{I}}\phi_{\text{I}} + (\chi_{AB})_{\text{II}}\phi_{\text{II}} \quad (3)$$

where indices I and II relate to phases I and II and ϕ is their volume fraction, $\phi_{\text{I}} + \phi_{\text{II}} = 1$. If phase separation is incomplete, $(\chi_{AB})_{\text{exp}}$ may be written as

$$(\chi_{AB})_{\text{exp}} = (\chi_{AB})_{\text{I}}\phi_{\text{I}} + (\chi_{AB})_{\text{II}}\phi_{\text{II}} + (\chi_{AB})_{\text{m}}\phi_{\text{m}} \quad (4)$$

In this equation, $(\chi_{AB})_{\text{m}}$ is the interaction parameter for the transition zone (interphase) between the two phases. $(\chi_{AB})_{\text{m}}$ is the term that determines the free energy of interphase formation. For immiscible systems, $(\chi_{AB})_{\text{exp}}$ is positive (index m relates to mesophase; ϕ_{m} is the mesophase volume fraction). Generally, the two regions of microphase separation I and II are not in the state of true equilibrium and the system as a whole is also in a nonequilibrium state. Parameters $(\chi_{AB})_{\text{I}}$ and $(\chi_{AB})_{\text{II}}$ may be either positive or negative; $(\chi_{AB})_{\text{m}}$ is always positive. According to Helfand (20), $(\chi_{AB})_{\text{m}}$ characterizes the interaction at the interface between two phases (in the interphase layer). As is seen from eq 4, the experimental χ_{AB} is formed of three parts, each determined by the conditions of phase separation and by the deviation of the system from equilibrium.

Thus the nonequilibrium states may be described by a large number of values of three terms in eq 4. The experimental value of χ_{AB} is determined by the history of the system. The parameter $(\chi_{AB})_{\text{exp}} - \chi_{AB}$ has the physical meaning, a degree of which is a deviation of the system from its equilibrium state. This deviation enables a comparison of various IPNs of the same chemical nature that are obtained at different conditions and have different extents of phase separation.

Phase Composition and Phase Ratio in IPNs

To characterize the structure of an IPN in which the phase separation did not reach its equilibrium, the composition of each phase must be determined. This determination has been done for gradient IPNs based on cross-linked polyurethane and cross-linked copolymer of butyl methacrylate and dimethacrylate triethylene glycol (21). Various layers of the IPN sample were cut from the surface to the center of the block; each sample was 0.6 mm thick. For each layer, the free energy of mixing was calculated from the vapor sorption data (Figure 7). ΔG_m values are positive in all the layers and, therefore, the components are immiscible. This effect is supposed to be connected with the composition variations as well as with changing conditions

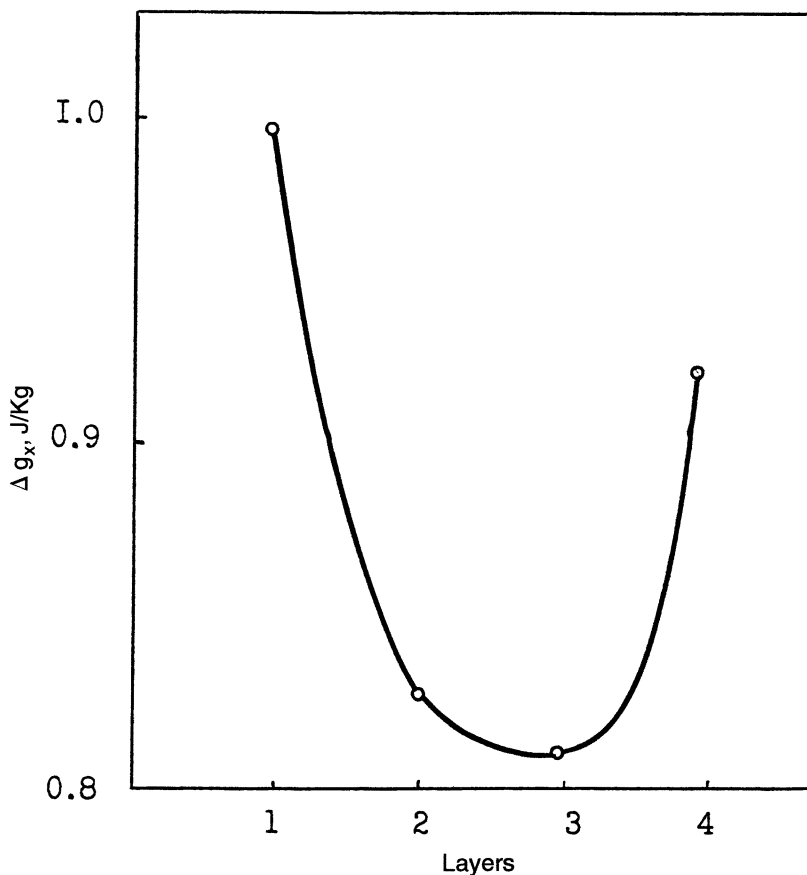


Figure 7. Free energy of component mixing in various layers of gradient IPN based on PU and PBMA. (Reproduced with permission from reference 22. Copyright 1992 American Institute of Physics.)

for phase separation during IPN formation in each layer. The different levels of immiscibility in various layers influence the structure formed after incomplete phase separation. Each arbitrary layer may be considered as an independent two-phase IPN with different composition of constituent phases.

Consideration of each phase as an independent quasiequilibrium IPN allows the composition and ratio of these phases to be estimated for each layer. For this purpose the Fox equation (22), which, in many cases, is valid for miscible polymer blends, is used:

$$1/T_g = \phi_1/T_{g1} + \phi_2/T_{g2} \quad (5)$$

Here ϕ_1 and ϕ_2 are the volume fractions of components, T_{g1} and T_{g2} are their glass-transition temperatures, and T_g is the glass-transition temperature of the miscible blend. In this case, the glass-transition temperature of one of the phases is enriched by one of the components. From corresponding data on glass-transition temperatures of IPN and gradient IPN layers, the volume fraction of polyurethane in the polyurethane-enriched phase and of copolymer in the acrylic copolymer-enriched phase were calculated according to the equations

$$\phi_1 = \frac{T_{g1}T_{g2} - T_g T_g^I}{T_g^I(T_{g2} - T_{g1})} \quad (6)$$

$$\phi_2 = (T_{g2}T_{g1} - T_{g2}T_g^{II})/T_g^{II}(T_{g1} - T_{g2}) \quad (7)$$

In this equation, T_g^I and T_g^{II} are, respectively, the glass-transition temperatures of the polyurethane and acrylic copolymer evolved phases. Consideration of these phases as quasiequilibrium and apparently one-phased with forced miscibility, these values were used to calculate the composition. From these data it was easy to calculate the ratio of phases in various layers. It was established that changing the ratio of network fractions in an IPN leads to differences both in the composition and ratio of evolved phases in each layer (21).

Thus the degree of network segregation in each layer is different compared with full nongradient IPNs of the same average composition. Thus, the gradient IPNs are truly multiphase nonequilibrium systems, and their properties depend not only on the composition gradient, but on the gradient of phase composition and phase ratio in each layer.

All the factors that determine the segregation degree in IPN as a function of reaction conditions lead to marked changes in viscoelastic properties of IPNs connected with the microheterogeneity of the systems (11).

References

1. Sperling, L. H. *Interpenetrating Polymer Networks and Related Materials*; Plenum: New York, 1981.

2. Frisch, H. L.; Klempner, D.; Frisch, K. C. *J. Polym. Sci., Polym. Chem. Ed.* **1970**, *A2*, 8921; Frisch, H. L.; Klempner, D. *Adv. Makromol. Chem.* **1971**, *2*, 149.
3. Sperling, L. H.; Widmaier, J. M. *Polym. Eng. Sci.* **1983**, *23*, 693.
4. Yeo, J. K.; Sperling, L. H.; Thomas, D. A. *Polymer* **1983**, *24*, 307.
5. Michel, J.; Hargest, S. C.; Sperling, L. H. *J. Appl. Polym. Sci.* **1981**, *26*, 743.
6. Shilov, V. V.; Lipatov, Y. S.; Karabanova, L.; Sergeeva, L. *J. Polym. Sci., Polym. Chem. Ed.* **1979**, *17*, 3083.
7. Sperling, L. H. *Polym. Eng. Sci.* **1984**, *24*, 1.
8. Schlick, S.; Harvey, R. D.; Alonso-Amigo, M.; Klempner, D. *Macromolecules* **1989**, *22*, 822.
9. Richards, R. W. *Makromol. Chem. Makromol. Symp.* **1990**, *40*, 209.
10. Binder, K.; Frisch, H. L. *J. Chem. Phys.* **1984**, *81*, 2126.
11. Lipatov, Y. S. In *Advances in Interpenetrating Polymer Networks*; Klempner, D.; Frisch, K. C., Eds.; Technomic: Lancaster, PA, 1989; Vol. 1, p 261.
12. Lipatov, Y. S.; Grigor'eva, O.; Kovernik, G.; Shilov, V.; Sergeeva, L. *Makromol. Chem.* **1985**, *186*, 1401.
13. Lipatov, Y. S. *J. Macromol. Sci. Rev. Macromol. Chem. Phys.* **1990**, *C30(2)*, 209.
14. Lipatov, Y. S. *Pure Appl. Chem.* **1985**, *57*, 1691.
15. Curtius, A. J.; Covitch, M. J.; Thomas, D. A.; Sperling, L. H. *Polym. Eng. Sci.* **1972**, *12*, 101.
16. Lipatov, Y. S.; Alekseeva, T.; Shilov, V. *Polym. Networks Blends* **1991**, *1*, 129.
17. McGary, B. In *Advances in Interpenetrating Polymer Networks*; Klempner, D.; Frisch, K. C. Eds.; Technomic: Lancaster, PA, 1989; Vol. 1, p 69.
18. Flory, P. *Principles of Polymer Chemistry*; Cornell University Press: Ithaca, New York, 1973.
19. Nesterov, A. E.; Lipatov, Y. S. *Thermodynamics of Polymer Solutions and Blends*; Naukova Dumka: Kiev, Ukraine, 1984.
20. Helfand, E. In *Polymer Compatibility and Incompatibility*; Harwood Academic Publishers: London, England, 1982; p 133.
21. Lipatov, Y. S.; Karabanova, L. V. *Polym. Int.* **1992**, *28*, 99.
22. Fox, T. G. *Bull. Am. Phys. Soc.* **1956**, *1*, 123.

RECEIVED for review September 10, 1991. ACCEPTED revised manuscript July 20, 1992.

Methacrylic-Allylic Interpenetrating Polymer Networks

C. Rouf¹, S. Derrough¹, J.-J. André², J.-M. Widmaier¹, and G. C. Meyer¹

¹Institut Charles Sadron (CNRS-ULP), Ecole d'Application des Hauts Polymères, 4, rue Boussingault, 67000 Strasbourg, France

²Institut Charles Sadron (CNRS-ULP), Centre de Recherche sur les Macromolécules, 6, rue Boussingault, 67083 Strasbourg, France

Classically, the simultaneous synthesis utilized to obtain interpenetrating polymer networks requires noninterfering polymerization modes to achieve distinct networks that are held together by only physical entanglements. In the absence of different mechanisms, a single copolymer network is formed, except for monomers with quite different reactivity ratios. Specific initiators that decompose at two different temperatures were used in an in situ sequential process to combine methyl methacrylate and diallyl carbonate of bisphenol A; both monomers are polymerizable under free-radical conditions. The monomer-to-polymer conversions were followed by Fourier transform infrared spectroscopy, and the absence of grafting between networks was deduced from electron spin resonance experiments.

INTERPENETRATING POLYMER NETWORKS (IPNs) are a special type of polymer blend (1–3) insofar as they are a combination of two or more polymers in network form. Therefore, IPNs require specific methods of mixing due to their cross-linked nature. Three basic techniques are described in the literature: latex blending (4–9), sequential polymerization (10–13), and simultaneous polymerization (14–17). Classically, simultaneous polymerization signifies that all the reactants of both systems are mixed together prior to initiation, but it does not give any information about the formation processes of the final networks. Several authors have tried to be more explicit in the definition: Fox et al. (18, 19) introduced the expression “sequential timing” in simultaneous IPNs, which specifies the interval of time between the onset

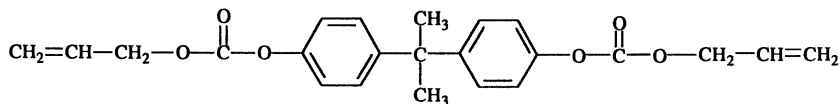
of the two independent reactions. In another approach, the simultaneous mixing of all the precursors is called *in situ* by Meyer and co-workers (20–22), and after this step, the initiation of both systems at once leads to “*in situ* simultaneous” IPNs (23), whereas the complete conversion of one system before the onset of the second yields “*in situ* sequential” IPNs. The expression “*in situ* sequential” is used hereafter, instead of simultaneous IPN.

In *in situ* IPNs, the reaction mechanisms that lead to the final networks must be different [e.g., polycondensation and free-radical polymerization (24–32)]; otherwise AB cross-linked polymers, which are quite different in behavior from IPNs, would be formed. However, if for some reason, two monomers that both polymerize by a free-radical mechanism must be combined as *in situ* IPNs, there exists an alternative means by which intersystem reactions may be avoided; namely, when the two monomers have quite different reactivities toward free radicals. This situation may occur with vinyl or acrylic C=C double bonds and allylic C=C double bonds, respectively. The allylic C=C double bonds are about 100 times less reactive than acrylic or methacrylic bonds (33). Additionally, cross-linking of a diallylic monomer takes place at the end of polymerization and requires a temperature higher than for a (meth)acrylic polymerization (34–38).

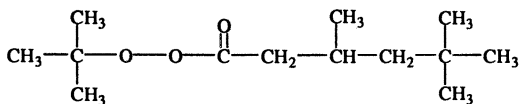
Furthermore, the use of two initiators, each specific to one system, leads to the elaboration of an entirely radical process of obtaining *in situ* sequential IPNs based on methyl methacrylate and diallyl carbonate of bisphenol A (DACBA). First, cross-linked poly(methyl methacrylate) (PMMA) is formed at a moderate temperature. Then, by just increasing the temperature after completion of the first polymerization, the formation of the allylic network follows. The specificity of the initiators toward their respective monomers was established by refractive index measurements. The kinetics of network formation was followed by Fourier transform infrared (FTIR) spectroscopy, and the nature of the propagating radicals during polymerization was determined by electron spin resonance (ESR) spectroscopy.

Experimental Details

The monomers, methyl methacrylate (MMA; Merck), 1,1,1-trimethylol propane trimethacrylate (TRIM; Degussa), diallyl carbonate of bisphenol A (DACBA; Pittsburgh Plate Glass Co.; *see* Chart I), were dried over molecular sieves, but not otherwise purified. The initiators, azobisisobutyronitrile (AIBN) and *t*-butylperoxy isononanoate (TBPIN) (Chart I), were used as received. The free-radical polymerization was carried out in the bulk. The monomer mixture was prepared by weighing the required amount of MMA, TRIM, DACBA, AIBN, and TBPIN, stirring thoroughly in a dry nitrogen atmosphere, and pouring into a glass mold to yield 3-mm-thick plates. AIBN and TBPIN were added in the amount of 1 and 3% by weight, respectively. The concentration of TRIM was 5% by weight



diallyl carbonate of bisphenol A (DACBA)



t-butyl peroxyisononanoate (TBPIN)

Chart I. Chemical structures of DACBA and TBPIN.

related to MMA. The weight ratio of the methacrylic monomers to the allylic monomer was 1:1 in the reaction mixtures. The mold was heated in a water bath at 60 °C for at least 3 h, then transferred into an oven for a further heating period at 95 °C.

The refractive index, n , of the reaction mixture was determined at 21 °C using a thermostated OPL (Optique et Précision de Levallois) refractometer. The conversion from monomer to polymer was followed by Fourier transform infrared (FTIR) spectroscopy on an apparatus (Nicolet 60SX) equipped with a heating chamber. For FTIR experiments, the mixture was injected in a cell formed by two NaCl windows separated by a 20- μm -thick gasket. The nature of the radicals present during the polymerization was investigated by electron spin resonance (ESR) spectroscopy. For such investigation, the reaction mixture was poured into 3-mm-diameter quartz test tubes and placed in the ESR cavity of a spectrometer (Bruker ER200D) with variable temperature control. Data handling was facilitated by a computer (HP 9000-360).

Results and Discussion

Under free-radical conditions, to form two distinct networks rather than a single copolymer network from the mixture of the constituents requires a sequential initiation of the monomers that may be accomplished by synthesis of the networks at two different temperatures, with adequate initiators that decompose at these temperatures. Obviously, methyl methacrylate must be polymerized first, using AIBN or benzoyl peroxide, which are classical initiators for this monomer. In practice, concentrations lower than 1% by

weight are used, and polymerizations are conducted typically in the temperature range of 50–80 °C. However, due to the relatively low reactivity of the allylic monomers, an unusually large amount of radical initiators is required to obtain polymerization within a reasonable time (33). Also, peroxidic initiators are preferred to azo initiators. Hence, by using only 1-wt% AIBN, the risk for an untimely initiation of the allylic monomer is rather low.

On the contrary, the decomposition into radicals of an initiator suitable for the polymerization of the allylic monomer would also initiate the polymerization of methyl methacrylate. To avoid this situation, a peroxidic initiator that decomposes at higher temperatures (but below the boiling temperature of the allylic monomer) must be used. TBPIN, which is supposed to form radicals only above 90 °C, is a suitable initiator for this purpose. Hence, the two free-radical initiators that we used for the process are AIBN and TBPIN, at 60 and 95 °C, respectively.

Refractive Index Measurements. The selectivity of the two free-radical initiators toward MMA and DACBA was checked through refractive index measurements. In the presence of 1 wt% AIBN, the refractive index of DACBA remained constant at $n = 1.537$, even after 7 h heating at 60 °C. The addition of 3 wt% TBPIN (i.e., when both initiators are present) and heating at 60 °C led to only 3% conversion of DACBA after 1 day and 10% conversion after 5 days. On the other hand, when MMA was mixed with 3 wt% TBPIN, no change in refractive index was observed under the same conditions of time and temperature. This result indicates that the azo radicals do not initiate DACBA, at least not during a period of time fully sufficient to polymerize MMA. Also, TBPIN does not decompose at 60 °C.

Due to the noticeable difference in refractive indexes between both monomers and their polymers, as well as between each polymer (Table I), it is possible to follow the polymerization of each monomer from the value of the refractive index of the reaction medium. The situation where the refractive index reaches a plateau and remains constant with constant 60 °C temperature indicates that only MMA polymerizes without the participation of DACBA. On the contrary, if the refractive index increases continuously, both monomers copolymerize to some extent.

Table I. Refractive Index

<i>Material</i>	<i>Monomer</i>	<i>Polymer</i>
MMA	1.414	1.502
DACBA	1.537	1.566

NOTE: Accuracy ± 0.001 . $T = 21^\circ\text{C}$.

The variation of the refractive index of the reaction mixture, heated at 60 °C, with time is displayed on Figure 1. The experimental plateau value ($n = 1.523$) was found to be equal, within accuracy limits, to the calculated value for a one-to-one mixture of poly(methyl methacrylate) and DACBA monomer. This value was calculated by assuming the additivity of refractive index of the constituents (Table I). From these results, we can conclude the specificity of each initiator and that only the methacrylic network is formed under these conditions.

Kinetics Measurements. Previously, Jin and Meyer (39) showed that Fourier transform infrared (FTIR) spectroscopy is an appropriate method for following the monomer-to-polymer conversion through absorbance measurements of a characteristic peak. The Beer-Lambert law allows the determination of the degree of conversion P :

$$P = (c_0 - c)/c_0 = (A_0 - A)/A_0$$

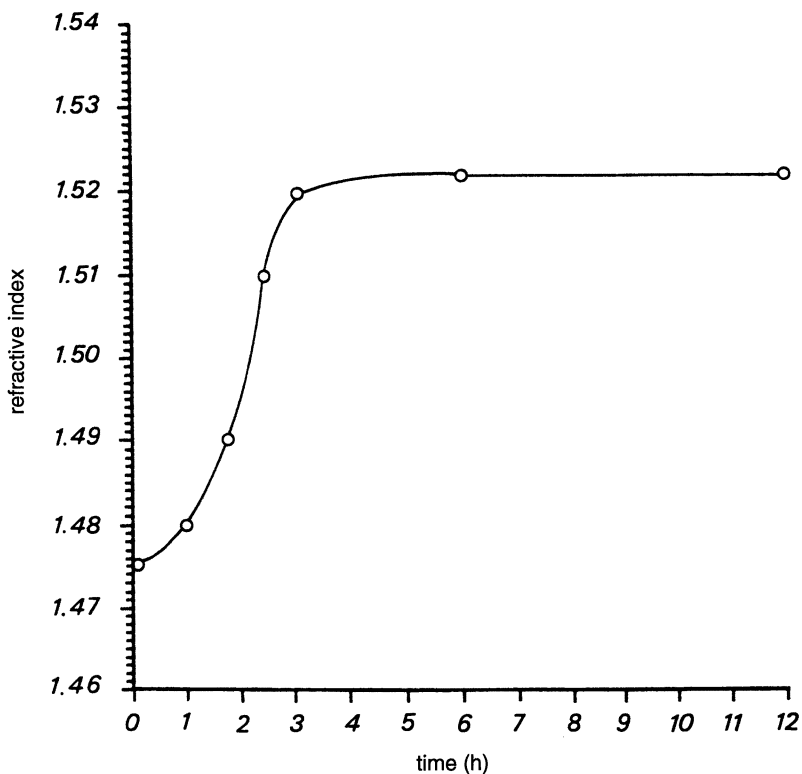


Figure 1. Variation of the refractive index of methyl methacrylate in the presence of AIBN and TBPIN. Reaction temperature: 60 °C.

where c_0 and A_0 are the initial concentration and initial absorbance, respectively, of the absorbing species. To avoid large errors in the degree of conversion due to variation of the sample thickness (shrinkage) or variation of the molar extinction coefficient (by changing temperature) during polymerization, the absorbance is referred to an internal calibration standard that corresponds to the asymmetric stretching peak of the $-\text{CH}_3$ groups at 2950 cm^{-1} . Finally, the degree of conversion can be expressed as

$$P = 1 - (A/A_0)(A_{\text{ref}}/A_{0,\text{ref}})$$

where $A_{0,\text{ref}}$ is the initial absorbance of the internal standard.

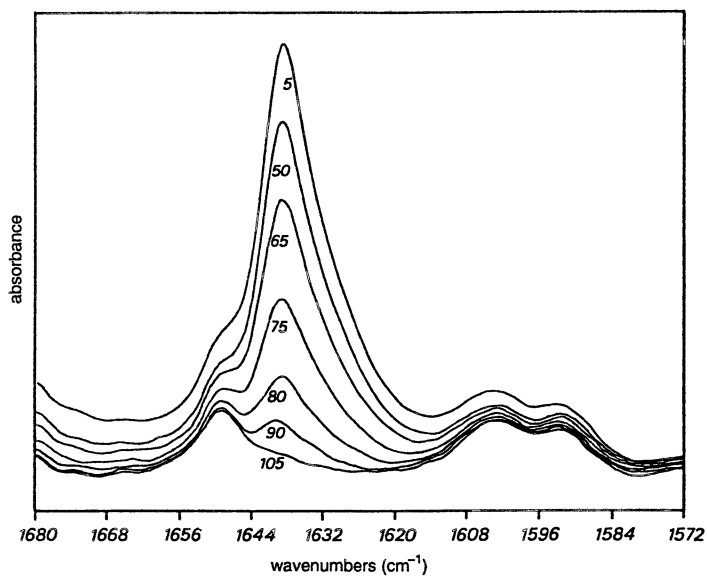
The polymerization at $60\text{ }^\circ\text{C}$ of a mixture of MMA, TRIM, and DACBA that contains AIBN and TBPIN was examined by FTIR, and the reaction conversion was estimated from the change of the normalized absorbance of the $\text{C}=\text{C}$ double-bond stretching mode in the $1630\text{--}1650\text{-cm}^{-1}$ region: the spectra (Figure 2a) display a strong peak at 1639 cm^{-1} , which is characteristic of MMA, with a shoulder at 1649 cm^{-1} , which corresponds to the allylic monomer (33, 37).

An accurate determination of the conversion is impossible because the two peaks overlap. Hence, another peak, related only to the conversion of the methacrylic $\text{C}=\text{C}$ double bond was sought. One may consider the peak located at 1324 cm^{-1} that corresponds to the asymmetric stretching of the $\text{C}-\text{O}-\text{C}$ bond, which is characteristic of α,β -unsaturated esters, and depends on the bond environment. During polymerization, the absorbance of this peak decreases in the same way as the classical $\text{C}=\text{C}$ bond (Figure 2b). A comparison of the conversion profiles taken from these two peaks is shown Figure 3 for the formation of the individual PMMA network.

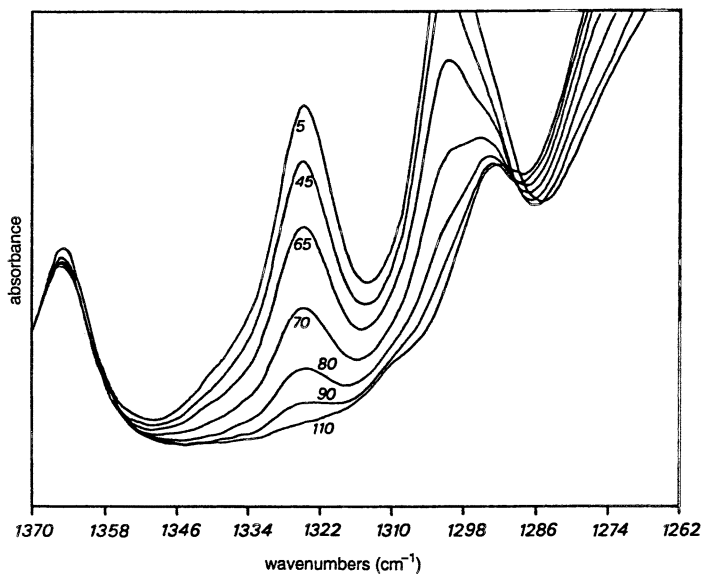
The conversion of MMA to PMMA from the absorbance change of the 1324-cm^{-1} peak can be calculated for the mixture of the two monomers. After complete conversion of MMA, the corresponding $\text{C}=\text{C}$ peak as well as the $\text{C}-\text{O}-\text{C}$ peak have disappeared. Meanwhile, the shoulder emerges from the main peak (1639 cm^{-1}) to give a single peak at 1649 cm^{-1} , and the intensity of this peak does not change until the reaction medium is heated to a temperature of $95\text{ }^\circ\text{C}$. Then, it slowly decreases, which reveals that DACBA is polymerizing.

Figure 4 shows the conversion versus time curve of a 50:50 (MMA + TRIM)–DACBA mixture. During the first 3 h, the temperature was set at $60\text{ }^\circ\text{C}$. One observes the typical curve of the (co)polymerization of MMA (20, 40, 41), which can be divided into three regimes: at low conversion, the rate of polymerization follows conventional kinetics; autoacceleration, known as the Trommsdorff effect, takes place; a pronounced decrease in polymerization rate is observed. A 96% end-conversion related to MMA was found.

The second part of the curve was recorded at $95\text{ }^\circ\text{C}$ and is similar in shape to the conversion curve of DACBA in bulk. The end-conversion for this



a



b

Figure 2. Variation of absorbance in the $1600\text{--}1700\text{-cm}^{-1}$ range (a) and in the $1250\text{--}1350\text{-cm}^{-1}$ range (b) of a 50:50 mixture of MMA and DACBA in the presence of AIBN and TBPIN. Reaction temperature: $60\text{ }^{\circ}\text{C}$. Numbers indicate reaction time in minutes.

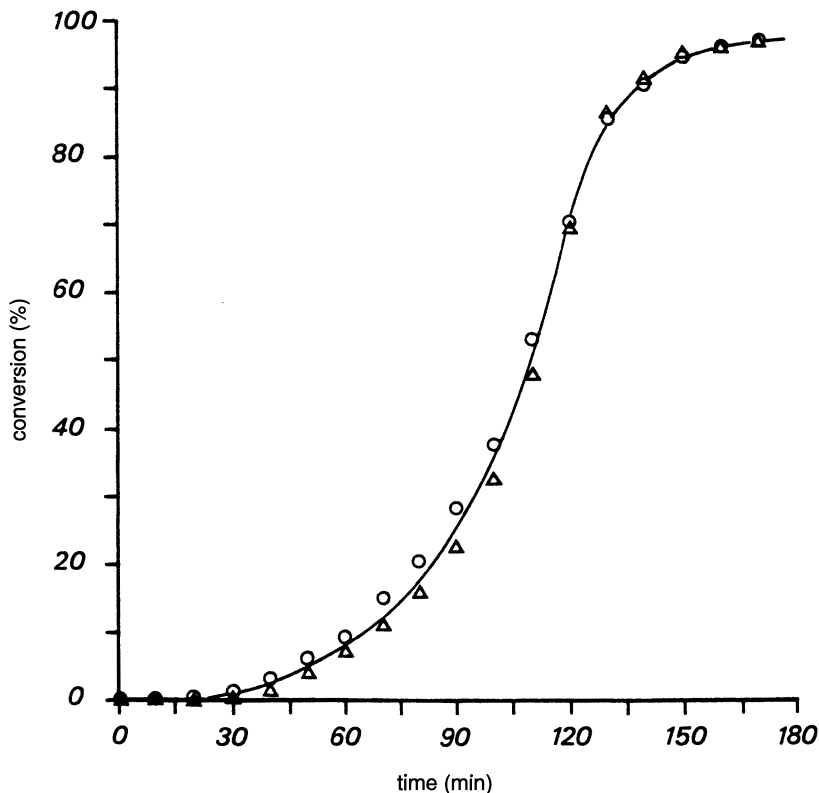


Figure 3. Conversion vs. time curves of MMA + TRIM copolymerization at 60 °C: ○, 1639-cm⁻¹ C=C double bond; △, 1324-cm⁻¹ C—O—C bond.

step was 64%, as in the bulk (65%), but the time necessary to reach this value increased from 4000 to ~ 7000 min, mainly due to the viscosity of the medium.

Electron Spin Resonance Spectroscopy. The FTIR experiments that confirm the refractive index measurements indicate that MMA does not copolymerize at 60 °C with DACBA and that, in a first approach, a pure network is formed. However, the possible action of propagating methacrylic radicals toward DACBA must be considered: such a transfer reaction to the allylic monomer actually introduces allylic mers into the PMMA. Also, because as radicals may be trapped during the course of polymerization (42–45), increasing the temperature from 60 to 95 °C, and consequently decreasing the viscosity, transforms these inactive radicals into active radicals and concurrently may initiate DACBA with the radicals issued from the

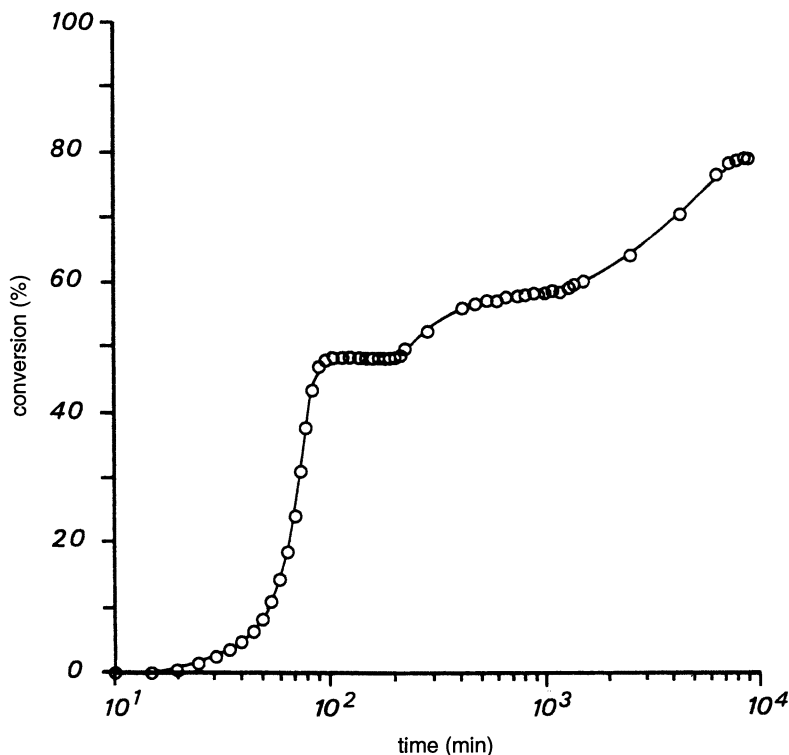


Figure 4. Conversion profile of the MMA + TRIM-DACBA system.

decomposition of TBPIN, which causes grafts between the methacrylic and the allylic networks.

To clarify the cross-action of radicals, ESR experiments were undertaken. ESR is a direct method for the determination of the nature and the concentration of radicals (46, 47). Preliminary measurements were made to identify the signal of the propagating DACBA radical.

The thermal polymerization of DACBA at 95 °C yields a four-line ESR signal that may be interpreted as a combination of two triplets (Figure 5). The relative intensities (1:3:3:1) indicate that two of the β -protons are equivalent. The hyperfine splittings of the α -protons and both β -protons are then ca. 12×10^{-4} T. This signal disappears rapidly due to the low reactivity of the monomer. However, in the presence of TBPIN at 95 °C, the previous signal is not found as TBPIN decomposes. The ESR spectra thus obtained is a combination of the signals of two populations of different mobility: the *t*-butoxy radical and the isononanoxy radical, which are characterized by a narrow line at 7.2×10^{-4} T and a broad line at 27×10^{-4} T, respectively. Also note that no signal appeared for experiments made at lower tempera-

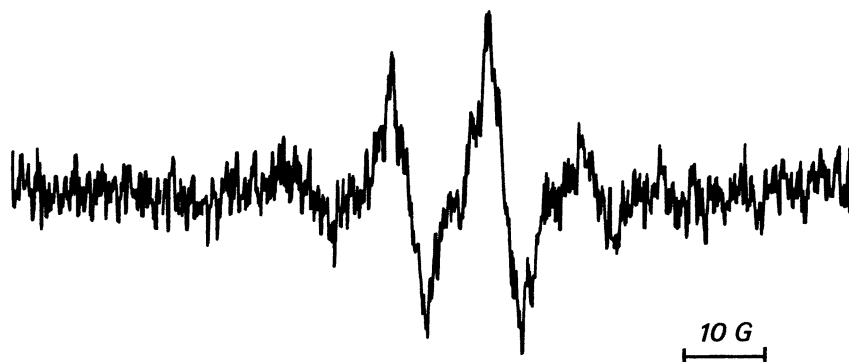


Figure 5. ESR spectrum of DACBA in bulk at 95 °C (g factor is 2.0049).

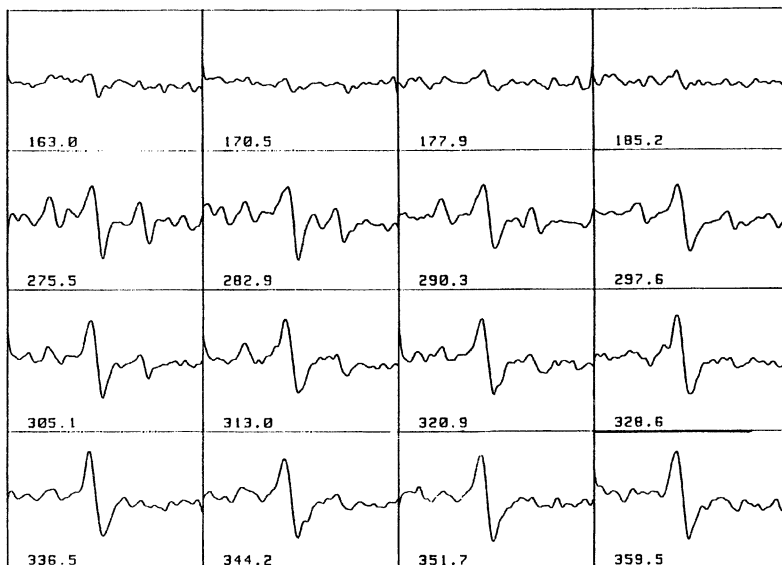
tures (60–80 °C), which thus confirms the absence of radicals at these temperatures.

The spectrum of propagating radicals throughout the process was recorded at different times (Figure 6). Initially, the temperature was set at 60 °C. A certain time was necessary until the concentration of radicals was sufficient for detection. In the early stage, the spectrum is characterized by 13 lines which are attributed to methacrylic radicals with two conformations (48). At high concentration, the exchange broadening between both conformations weakens the inner eight lines. Finally, after the gel point (Trommsdorff effect), the mobility decreases and the PMMA macroradical adopts a preferred conformation: the well-known nine-line spectrum (49–51). Gradual changes in the lineshape and in the radical concentration were observed in the final stage of polymerization. These changes were due to recombination and termination reactions.

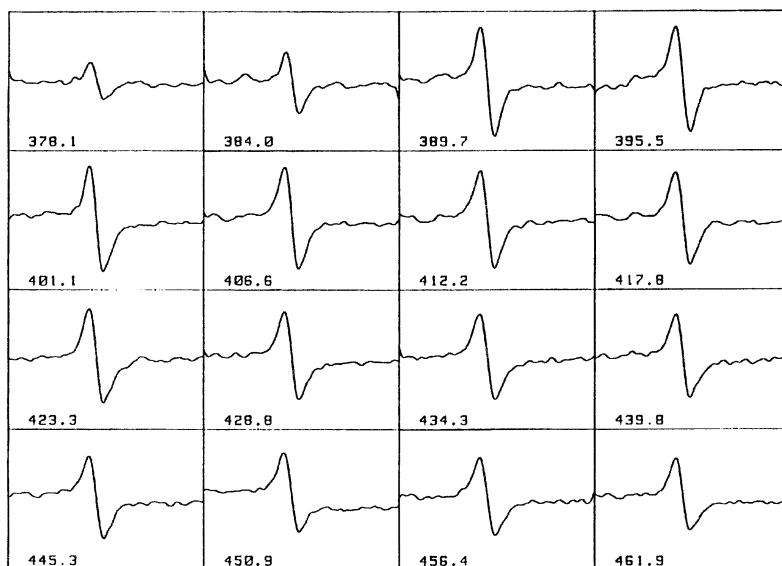
The most important point with regard to the experimental investigation at 60 °C is that the spectrum of DACBA is not found, which means that there is no transfer of the MMA macroradical to DACBA.

When the reaction mixture is heated to 95 °C, the spectrum that corresponds to only one of the two radicals issued from the decomposition of TBPIN at that temperature is observed. Due to the presence of the methacrylic network already formed and, consequently, to the high viscosity of the reaction medium, only the most mobile radical (i.e., the *t*-butoxy) was detected. The change of radical concentration in the medium is shown in Figure 7, where the intensity of the signal is plotted versus time: the concentration increases first as TBPIN decomposes; then, after reaching a peak value, the intensity of the signal decreases as the radicals are consumed by DACBA.

Two points were ascertained in these ESR experiments: (1) the specificity of each free-radical initiator used (AIBN toward MMA and TBPIN



a



b

Figure 6. ESR spectra recorded for the (MMA + TRIM)-DACBA system polymerized at 60 (a) and at 95 °C (b). Numbers indicate reaction time in minutes.

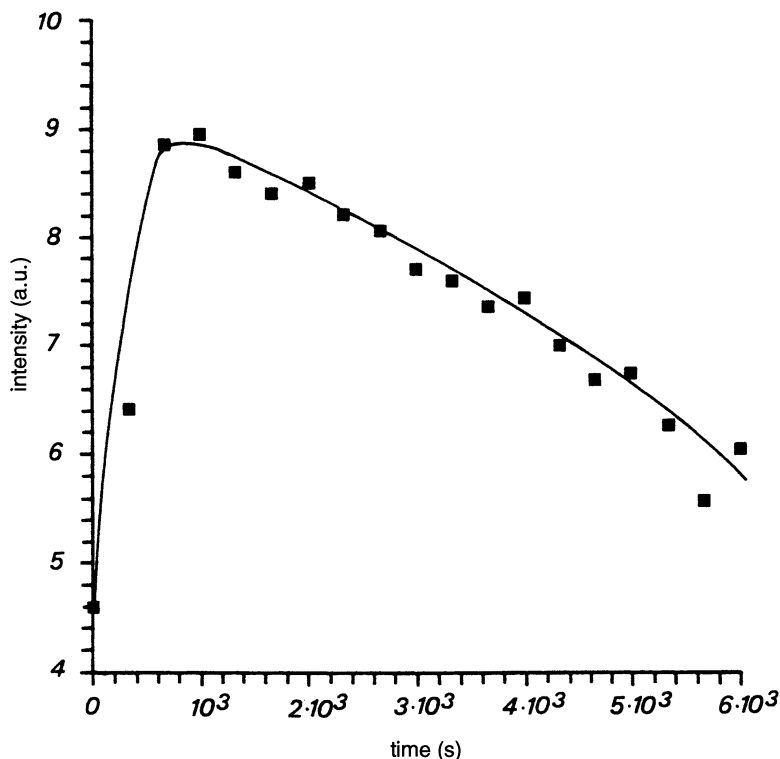


Figure 7. Variation of intensity of the *t*-butoxy signal of TBPIN with time at 95 °C.

toward DACBA, respectively) and (2) that the methacrylic radical does not transfer to the allylic monomer.

Summary and Conclusions

For the combination of methacrylic and allylic monomers, both polymerizable by free radicals, a new in situ sequential synthesis for obtaining interpenetrating polymer networks is proposed. With specific initiators (viz. AIBN at 60 °C and TBPIN at 95 °C), refractive index measurements and Fourier transform infrared spectroscopy show that neat networks are formed and the two monomers do not copolymerize. Electron spin resonance measurements lead to the conclusion that chemical links between the methacrylic network and the allylic network are unlikely.

This study concerns DACBA, a particular diallylic monomer that was chosen mainly for the presence of aromatic rings that, in association with methyl methacrylate, allow analysis through refractive index measurements.

However, the diallylic monomer that is most commercially developed is the diethyleneglycol bis(allyl carbonate) known as CR 39 resin, which is widely used to manufacture optical lenses and safety glasses. The CR 39 materials are more resistant to heat, to solvents, and to scratch than PMMA, but they exhibit limited impact resistance. To improve the toughness of CR 39, combinations with poly(butyl acrylate) (PBA) constitute an interesting solution. PBA is an elastomer at room temperature that can be made under free-radical conditions like PMMA; thus poly(butyl acrylate)-CR 39 IPNs can be formed. Toward this end, PMMA-DACBA IPNs have been synthesized and studied as a first step.

Acknowledgments

The authors wish to thank M. Bernard for performing the ESR experiments. G. C. Meyer would like to acknowledge the Petroleum Research Fund of the American Chemical Society for a travel grant.

References

1. Sperling, L. H. *Interpenetrating Polymer Networks and Related Materials*; Plenum: New York, 1981.
2. Klempler, D.; Berkowski, L. In *Encyclopedia of Polymer Science and Engineering*; Mark, H. F.; Bikales, N. H.; Overberger, C. G.; Menges, G., Eds.; Wiley: New York, 1987; Vol. 8.
3. Sperling, L. H. In *Comprehensive Polymer Science*; Allen, G.; Bevington, J. C., Eds.; Pergamon: Oxford, England, 1989; Vol. 6, p 423.
4. Sperling, L. H.; Chin, T. W.; Gramlich, R. G.; Thomas, D. A. *J. Appl. Polym. Sci.* **1973**, *17*, 2443.
5. Silverstein, M. S.; Narkis, M. *Polym. Eng. Sci.* **1985**, *25*, 257.
6. Silverstein, M. S.; Narkis, M. *J. Appl. Polym. Sci.* **1987**, *33*, 2529.
7. Hourston, D. J.; Satgurunathan, R.; Varma, H. *J. Appl. Polym. Sci.* **1987**, *33*, 215.
8. Hourston, D. J.; Satgurunathan, R.; Varma, H. C. *J. Appl. Polym. Sci.* **1987**, *34*, 901.
9. Sheu, R. H.; El-Aasser, M. S.; Vanderhoff, J. W. *J. Polym. Sci., Polym. Chem. Ed.* **1990**, *28*, 629.
10. Huelck, V.; Thomas, D. A.; Sperling, L. H. *Macromolecules* **1972**, *5*, 340, 348.
11. Hourston, D. J.; McCluskey, J. A. *J. Appl. Polym. Sci.* **1980**, *25*, 959.
12. McGarey, B.; Richards, R. W. *Polymer* **1986**, *27*, 1315.
13. Kotaka, T.; Nishi, S.; Adachi, H. In *Advances in Interpenetrating Polymer Networks*; Klempler, D.; Frisch, K. C., Eds.; Technomic: Lancaster, PA, 1990; Vol. 2, p 47.
14. Sperling, L. H.; Arnts, R. R. *J. Appl. Polym. Sci.* **1971**, *15*, 2317.
15. Frisch, K. C.; Klempler, D.; Xiao, H. X.; Cassidy, E.; Frisch, H. L. *Polym. Eng. Sci.* **1985**, *25*, 12.
16. Singh, S.; Frisch, H. L.; Ghiradella, H. *Macromolecules* **1990**, *23*, 375.
17. Nair, P. D.; Jayabalan, M.; Krishnamurthy, V. N. *J. Polym. Sci., Polym. Chem. Ed.* **1990**, *28*, 3775.
18. Fox, R. B.; Bitner, J. L.; Hinkley, J. A.; Carter, W. *Polym. Eng. Sci.* **1985**, *25*, 157.

19. Fox, R. B.; Moonay, D. J.; Armistead, J. P.; Roland, C. M. In *Multiphase Polymers: Blends and Ionomers*; Utracki, L. A.; Weiss, R. A., Eds.; ACS Symposium Series 395; American Chemical Society: Washington, DC, 1989; p 245.
20. Jin, S. R.; Widmaier, J. M.; Meyer, G. C. *Polymer* **1988**, *29*, 346.
21. He, X. W.; Widmaier, J. M.; Herz, J. E.; Meyer, G. C. *Polymer* **1989**, *30*, 364.
22. Tabka, M. T.; Widmaier, J. M.; Meyer, G. C. *Macromolecules* **1989**, *22*, 1826.
23. Tabka, M. T.; Widmaier, J. M.; Meyer, G. C. In *Sound and Vibration Damping with Polymers*; Corsaro, R. D.; Sperling, L. H., Eds.; ACS Symposium Series 424; American Chemical Society: Washington, DC, 1990; p 445.
24. Allen, G.; Bowden, M. J.; Lewis, G.; Blundell, D. J.; Jeffs, G. M. *Polymer* **1974**, *15*, 13.
25. Kim, S. C.; Klempner, D.; Frisch, K. C.; Radigan, W.; Frisch, H. L. *Macromolecules* **1976**, *9*, 263, 1187.
26. Djomo, H.; Morin, A.; Damyanidu, M.; Meyer, G. C. *Polymer* **1983**, *24*, 65.
27. Djomo, H.; Widmaier, J. M.; Meyer, G. C. *Polymer* **1983**, *24*, 1415.
28. Hourston, D. J.; McCluskey, J. A. *J. Appl. Polym. Sci.* **1986**, *31*, 645.
29. Ebdon, J. R.; Hourston, D. J.; Klein, P. G. *Polymer* **1986**, *27*, 1807.
30. Jin, S. R.; Widmaier, J. M.; Meyer, G. C. In *Polymers for Advanced Technologies*; Levin, M., Ed.; VCH Publishers: New York, 1988; p 697.
31. Hur, T.; Manson, J. A.; Hertzberg, R. W.; Sperling, L. H. *J. Appl. Polym. Sci.* **1990**, *39*, 1933.
32. Kim, S. K.; Kim, S. C. *Polym. Bull.* **1990**, *23*, 141.
33. Schildknecht, C. E. *Allyl Compounds and Their Polymers*; Wiley-Interscience: New York, 1973.
34. Schnarr, E.; Russell, K. E. *J. Polym. Sci., Polym. Chem. Ed.* **1980**, *18*, 913.
35. O'Donnell, J. H.; O'Sullivan, P. W. *Polym. Bull.* **1981**, *5*, 103.
36. Nikiforenko, V. S.; Alekseyev, N. N.; Zaitsev, Yu. S. *Vysokomol. Soedin, Ser. A* **1986**, *28*, 2063.
37. Portwood, T.; Stejny, J. *Nucl. Tracks* **1986**, *12*, 113.
38. Hill, D. J. T.; Londero, D. I.; O'Donnell, J. H.; Pomery, P. J. *Eur. Polym. J.* **1990**, *26*, 1157.
39. Jin, S. R.; Meyer, G. C. *Polymer* **1986**, *27*, 592.
40. Gulari, E.; McKeigue, K.; Ng, K. Y. S. *Macromolecules* **1984**, *17*, 1822.
41. Li, W. H.; Hamielec, A. E.; Crowe, C. M. *Polymer* **1989**, *30*, 1513.
42. Atherton, N. M.; Melville, H. W.; Whiffen, D. H. *J. Polym. Sci.* **1959**, *34*, 199.
43. Burnett, G. M.; Duncan, G. L. *Makromol. Chem.* **1962**, *51*, 154.
44. Zhu, S.; Tian, Y.; Hamielec, A. E.; Eaton, D. R. *Macromolecules* **1990**, *23*, 1144.
45. Zhu, S.; Tian, Y.; Hamielec, A. E.; Eaton, D. R. *Polymer* **1990**, *31*, 1726.
46. Bresler, S. E.; Kazbekov, E. N.; Shadrin, V. N. *Makromol. Chem.* **1974**, *175*, 2875.
47. Rånby, B.; Rabek, J. F. *ESR Spectroscopy in Polymer Research*; Springer: Heidelberg, Germany, 1977.
48. Kamachi, M.; Kohno, M.; Kuwae, Y.; Nozakura, S. *Polym. J.* **1982**, *14*, 749.
49. Shen, J.; Tian, Y.; Zeng, Y.; Qiu, Z. *Makromol. Chem., Rapid Commun.* **1987**, *8*, 615.
50. Garrett, R. W.; Hill, D. J. T.; O'Donnell, J. H.; Pomery, P. J.; Winzor, C. L. *Polym. Bull.* **1989**, *22*, 611.
51. Carswell, T. G.; Hill, D. J. T.; Hunter, D. S.; Pomery, P. J.; O'Donnell, J. H.; Winzor, C. L. *Eur. Polym. J.* **1990**, *26*, 541.

RECEIVED for review November 1, 1991. ACCEPTED revised manuscript July 21, 1992.

Synthesis and Characterization of Poly(organophosphazene) Interpenetrating Polymer Networks

K. B. Visser, I. Manners, and H. R. Allcock*

Department of Chemistry, The Pennsylvania State University,
University Park, PA 16802

Polyphosphazenes are a broad, novel class of inorganic-organic macromolecules with the general formula $[NPR_2]_n$. The physical properties of polyphosphazenes can be understood in terms of a highly flexible backbone, with various physical or chemical characteristics tailored by the incorporation of specific side groups. As part of this program to synthesize new materials with hybrid macromolecular properties, we report the synthesis and characterization of several interpenetrating polymer networks that contain the phosphazene polymers poly[bis(2-(2-methoxyethoxy)ethoxy)phosphazene] and poly[bis(propyloxybenzoate)phosphazene] with several organic polymers that include polystyrene, poly(methyl methacrylate), polyacrylonitrile, and poly(acrylic acid).

MOST INTERPENETRATING POLYMER NETWORKS are prepared using organic polymers. With the exception of polysiloxanes (1-8), little work has been published that describes the syntheses of interpenetrating polymer networks (IPNs) from inorganic-organic polymers. Inorganic-organic polymers generally have a high thermooxidative stability coupled with unusual combinations of properties that depend on the side groups attached to the backbone. Some common examples of inorganic-organic polymers include polysilanes, polysiloxanes, and polyphosphazenes, which are depicted in Chart I (9). The synthesis and characterization of some of the first IPNs that contain

* Corresponding author.

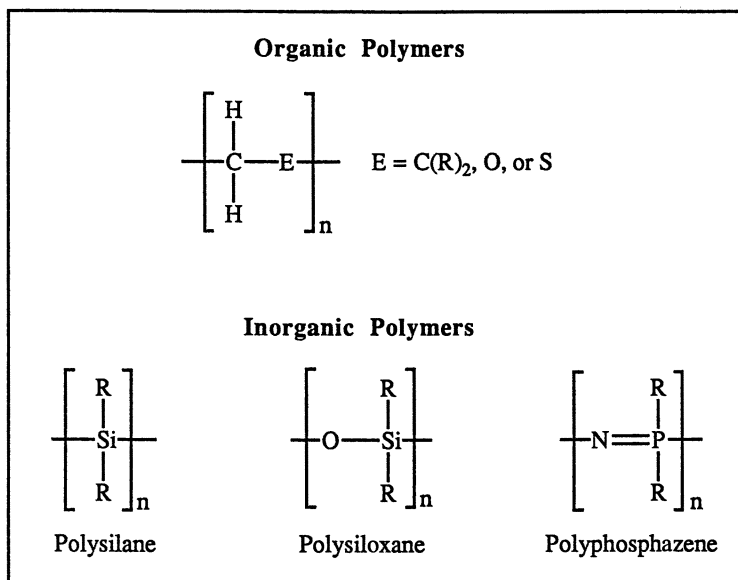


Chart I.

poly(organophosphazenes) with organic polymers (10, 11) are described herein.

Poly(organophosphazenes) are a unique class of inorganic–organic polymers that have alternating phosphorus and nitrogen atoms in the backbone and two organic, inorganic, or organometallic side groups attached to each phosphorus atom (12–16). The physical properties and applications of poly(organophosphazenes) can be tailored by the choice of the organic side group attached to the backbone. Due to this unique ability to tune properties and applications by the choice of side groups, polyphosphazenes are an excellent choice for the preparation of IPNs. Some advantages of the polyphosphazene system are as follows:

- Nonburning and flame retardancy
- Solvent and oil resistance
- Biomedical compatibility
- Materials flexibility (low glass-transition temperature, T_g)
- Easy tunability of molecular structure

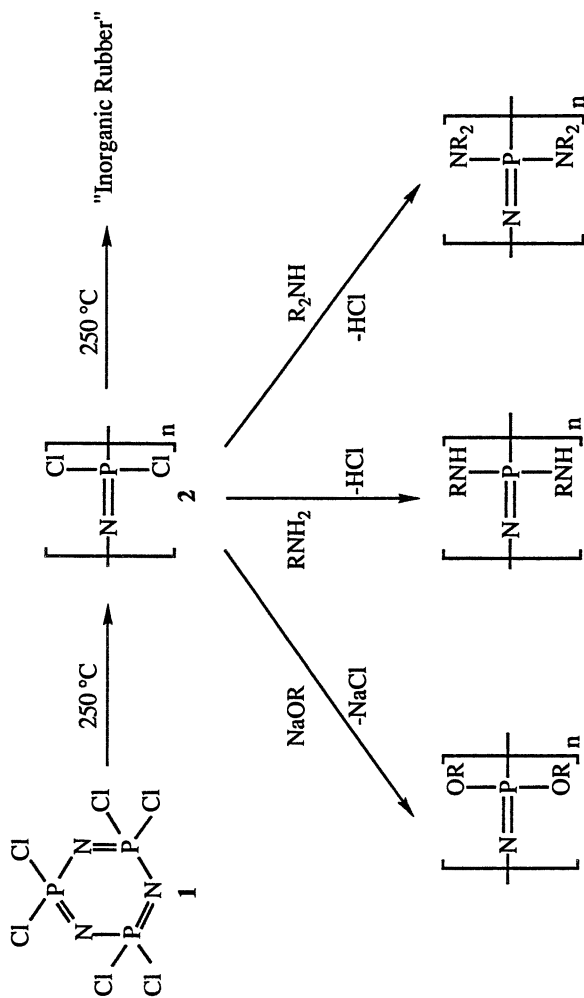
Polyphosphazenes are usually nonburning materials and may be highly flame retardant due to the fact that phosphorus in its highest valency state can interfere with the combustion pathway. A combination of phosphorus and nitrogen often yields compounds with enhanced flame retardant properties.

Some polyphosphazenes possess a high degree of solvent and oil resistance that makes them valuable materials for many industrial applications such as O-rings, gaskets, and fuel lines. Another advantage of the polyphosphazene system is that many of these materials have a high degree of biocompatibility, which depends on the side group structure: fluoroalkoxyphosphazenes are of particular interest. Some polyphosphazenes possess high flexibility and low glass-transition temperatures (T_g). This characteristic makes many phosphazene polymers useful as low-temperature elastomers and flexible thermoplastics. Probably the biggest advantage of the polyphosphazene system is the ease with which the polymeric molecular structure may be tuned to afford different properties and applications. This molecular tuning is accomplished by the linkage of different side groups to the polymer backbone (12–16). IPNs with combinations of poly(organophosphazenes) and other polymers combine the advantages of polyphosphazenes with the advantages of the other systems.

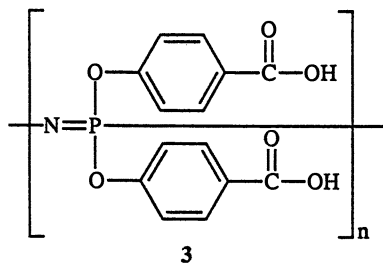
Poly(organophosphazenes) are prepared by the route summarized in Scheme 1. Commercially available hexachlorocyclotriphosphazene (**1**) undergoes a thermal ring opening polymerization at 250 °C to form poly(dichlorophosphazene) (**2**), a long-chain polymer with 15,000 or more repeating units. Poly(dichlorophosphazene) is hydrolytically sensitive, but the system may be stabilized against hydrolysis through halogen replacement reactions that use a wide variety of nucleophiles, including sodium alkoxides and aryloxides or primary and secondary amines. These substitution reactions yield a large number of stable poly(organophosphazene) derivatives, the properties and applications of which depend on the side group structure (17–19).

Chart II shows examples of phosphazene polymers with different side groups. Poly[bis(*p*-oxybenzoic acid)phosphazene] (**3**) is water soluble as its sodium salt and can be ionically cross-linked using calcium or other divalent or higher valency cation salts (20–22). Poly[bis((3-aminopropyl)pentamethyldisiloxane)phosphazene] (**4**) contains silicon atoms within the side groups and possesses elastomeric properties (23). Poly[bis(2-(2-methoxyethoxy)ethoxy)phosphazene] (**5**) is water soluble and is also an excellent solid solvent for salts such as lithium trifluoromethanesulfonate; it is being developed as a solid electrolyte material (24–28). When transannular ferrocenyl groups are attached to the polymer backbone, as seen in polymer **6**, the system is electroactive and may be used as an electrode mediator material (29).

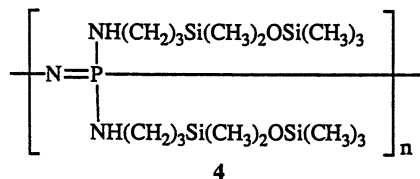
Some common applications for poly(organophosphazenes) include O-rings that are flexible at low temperature and have high solvent and oil resistance, oil seal gaskets, fuel lines, shock-absorber components with a high level of vibrational energy absorption, and carburetor and fuel injector components. As mentioned previously, polyphosphazenes are an excellent choice for these types of applications because of their nonburning characteristics, high flame retardancy, high levels of both solvent and oil resistance, and high degree of materials flexibility.



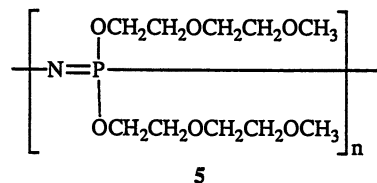
Scheme 1.



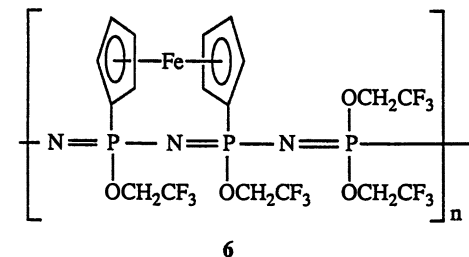
**Water Soluble as Sodium Salt,
Cross-linkable by Ca²⁺ Ions**



Elastomer



**Water-Soluble,
Solid Electrolyte**



Electroactive Material

Chart II.

Specific derivatives also are being developed for uses in the field of biomedicine. Figure 1 shows an example of a polyphosphazene–organic polymer IPN that is commercially available as a shock-absorbing denture liner. Poly(organophosphazenes) are employed for dental and oral surgical applications because of their of fungal resistance (30–33).

Syntheses of Poly(organophosphazenes)

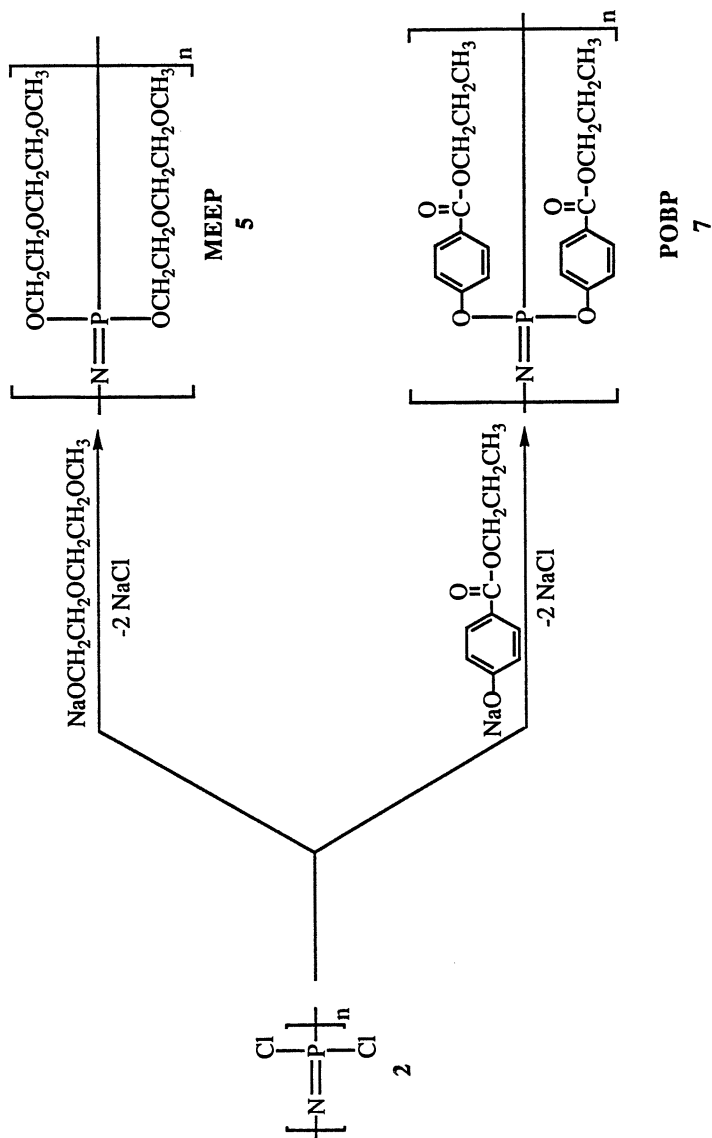
The phosphazene polymers used in this IPN study were synthesized as described in Scheme 2. Polymer **5** was prepared by allowing poly(dichlorophosphazene) (**2**) to react with the sodium salt of 2-(2-methoxyethoxy)ethanol.



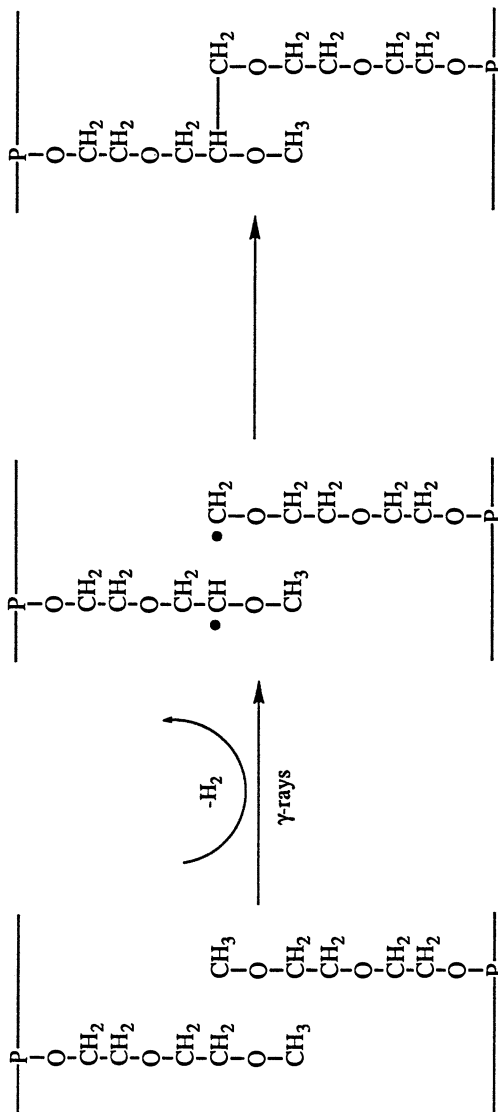
Figure 1. Poly(organophosphazene) shock-absorbing denture liner. (Photograph provided by L. Gettleman. See reference 51.)

The product polymer is poly[bis(2-(2-methoxyethoxy)ethoxy)phosphazene] (MEEP) (5). MEEP is an unusual, hydrophilic phosphazene polymer that is soluble in both water and organic solvents and has a T_g of $-84\text{ }^\circ\text{C}$ (24, 25). Polymer 7 was prepared by allowing poly(dichlorophosphazene) (2) to react with the sodium salt of propyl *p*-hydroxybenzoate. This synthesis yields poly[bis(propyl *p*-oxybenzoate)phosphazene] (POBP) (7), a hydrophobic, elastomeric polymer with a T_g of $-23\text{ }^\circ\text{C}$. This polymer is soluble in many organic solvents (21).

Both the POBP (7) and MEEP (5) undergo cross-linking when exposed to ^{60}Co gamma radiation (24, 25). Scheme 3 shows a proposed cross-linking mechanism of MEEP during exposure to ^{60}Co gamma radiation. (Materials were exposed to ^{60}Co gamma radiation at the Breazeale nuclear reactor on the campus of the Pennsylvania State University.) Radiation probably generates radicals on any of the five carbon atoms in the MEEP side chains. Transcombination of these radicals forms cross-links. Solid, uncross-linked MEEP has little resistance to viscous flow. However, after cross-linking, MEEP has an increased structural integrity and swells, without dissolving, in water or organic solvents. Figure 2 shows a sample of MEEP after cross-link-



Scheme 2.



Scheme 3.

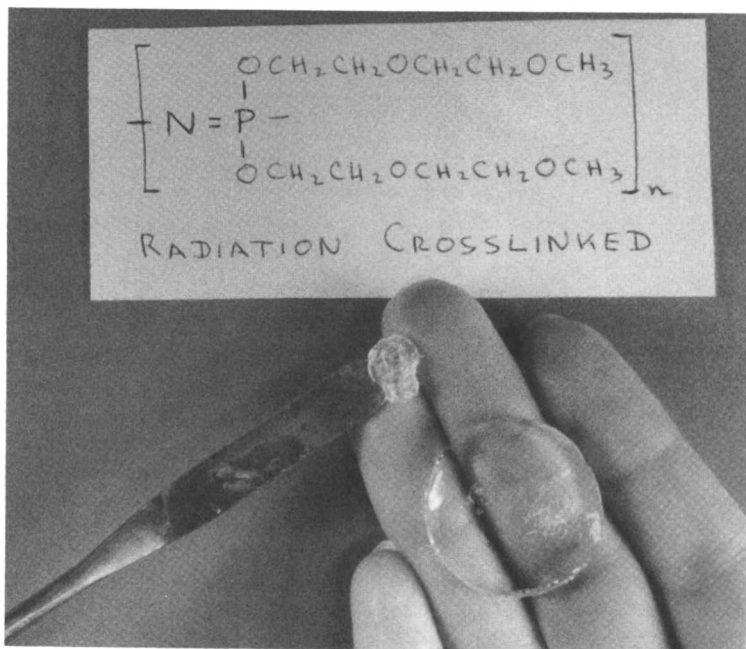


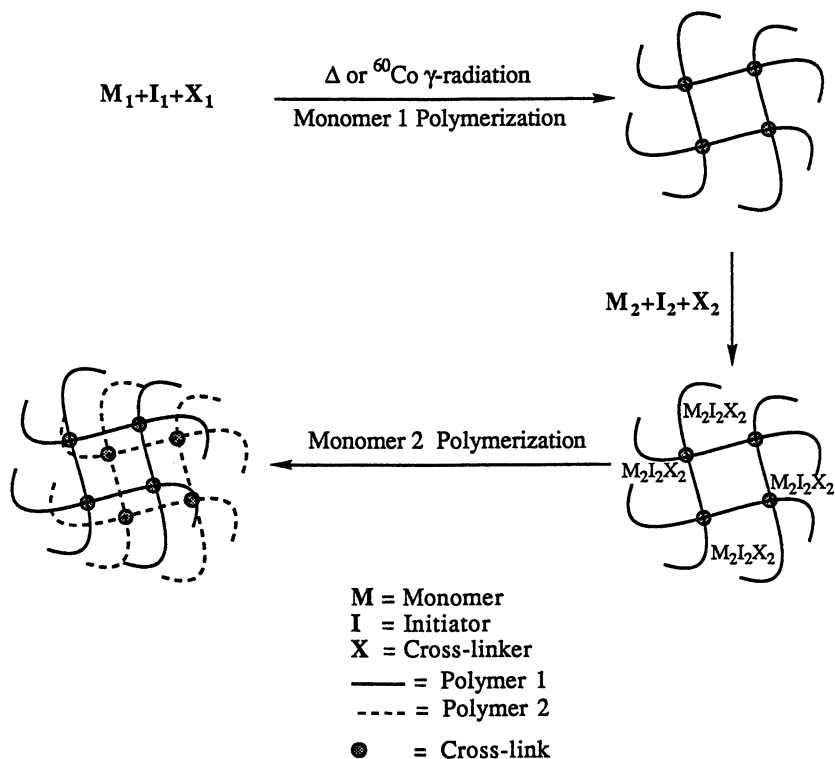
Figure 2. MEEP after cross-linking and after swelling in water for several hours. (Reproduced with permission from reference 25. Copyright 1988. Butterworth-Heinemann.)

ing and after the swelling of a cross-linked portion in water for several hours. Cross-linked MEEP is capable of swelling to over 10 times its original volume.

Synthesis of IPNs

In normal sequential IPN preparation, a monomer is first polymerized and cross-linked via either thermal or radiation techniques to form a cross-linked polymer matrix (34, 35). This cross-linked matrix is then allowed to imbibe a second monomer, a polymerization initiator, and a cross-linker to form a monomer-swollen cross-linked polymer matrix. The second monomer is then polymerized and cross-linked within the matrix of the first monomer to form the IPN. This general procedure for the preparation of a sequential IPN is shown in Scheme 4.

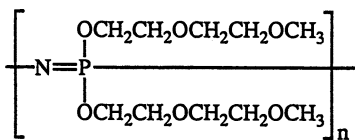
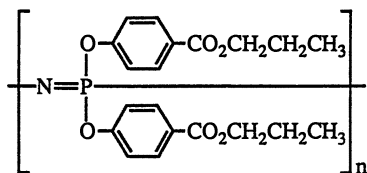
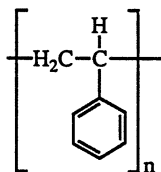
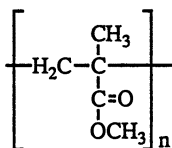
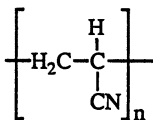
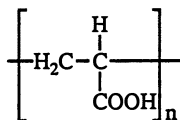
In all the IPN syntheses described here, a preformed phosphazene polymer, either MEEP (5) or POBP (7), was used as the initial cross-linked polymer system. The organic polymers prepared within the polyphosphazene matrix include polystyrene (PS) (8), poly(methyl methacrylate) (PMMA) (9),



Scheme 4.

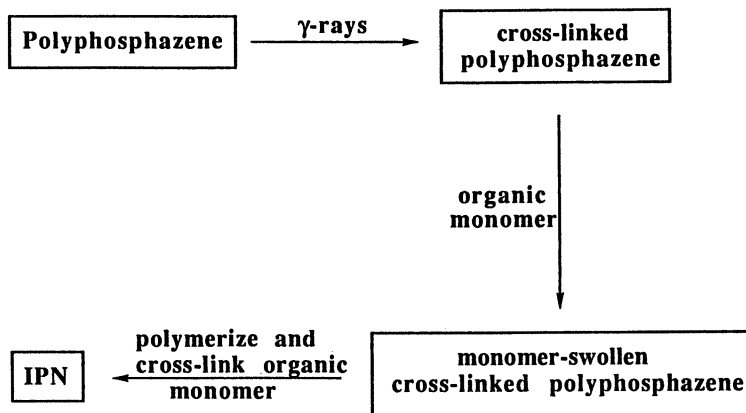
polyacrylonitrile (PAN) (10), and poly(acrylic acid) (PAA) (11). The structures of the component materials are depicted in Chart III. These organic polymers were chosen because they represent a cross section of common macromolecules. In addition, their ease of polymerization via thermal methods (for PS and PMMA) and by exposure to ^{60}Co gamma radiation (for PAN and PAA) made them an attractive choice.

Polyphosphazene-organic polymer IPNs were prepared as summarized in Scheme 5. The polymerized polyphosphazene was exposed to ^{60}Co gamma radiation (at the Breazeale nuclear reactor) to form a cross-linked polymer matrix. The cross-linked matrix was then allowed to swell in a mixture of the organic monomer, azobisisobutyronitrile (AIBN) initiator, and ethylene glycol dimethacrylate cross-linker until the swollen matrix increased approximately 10 times in volume. The imbibed organic monomer was then polymerized and cross-linked within the polyphosphazene matrix via either thermal techniques (PS and PMMA) or by exposure to additional ^{60}Co gamma radiation (PAN and PAA).

Poly(organophosphazenes)**MEEP (5)****POBP (7)****Organic Polymers****Polystyrene (PS) (8)****Poly(methyl methacrylate) (PMMA) (9)****Polyacrylonitrile (PAN) (10)****Poly(acrylic acid) (PAA) (11)***Chart III.*

The objective was to incorporate the maximum amount of organic polymer into the cross-linked poly(organophosphazene) matrix. The ratio of components within the IPN system was estimated using ^1H NMR spectroscopy, and the values are listed in Table I. The ratios ranged from a 1:1 ratio of polyphosphazene polymer to organic polymer in the MEEP-PS IPN to a 4.5:1 ratio of polyphosphazene to organic polymer in the IPN that contained POBP-PAN.

Following preparation, the IPNs were purified and characterized via conventional methods, including ^1H and ^{31}P NMR spectroscopy, Fourier transform infrared (FTIR) spectroscopy, differential scanning calorimetry (DSC), and transmission electron microscopy (TEM) (34, 35). FTIR and NMR analyses are useful mainly to confirm the presence of both macromolecular constituents in the IPN systems and to monitor the polymerization of the organic monomer by following the loss of vinyl protons.



Scheme 5.

Table I. IPN Component Ratios Based on NMR Integration

<i>Components</i>	<i>Ratio</i>
MEEP-PS (5, 8)	1:1
MEEP-PMMA (5, 9)	3:1
MEEP-PAN (5, 10)	1:1
MEEP-PAA (5, 11)	1:1
POBP-PS (7, 8)	2.5:1
POBP-PMMA (7, 9)	1.5:1
POBP-PAN (7, 10)	4.5:1
POBP-PAA (7, 11)	2:1

Characterization

DSC is an excellent technique to examine the miscibility of the components within an IPN system and to probe the intermolecular interactions that may exist between the component polymers. This examination may be accomplished by comparison of the T_g values of the IPN system with the T_g values of the component macromolecules. The displacement of the values of the IPN T_g s from the values of the component materials gives a general indication of both the degree of miscibility within the sample and of interactions that may take place between the component materials (34, 35). The T_g values for the IPN and the component materials are listed in Table II.

For example, an IPN that contains MEEP and polystyrene with glass-transition temperatures at -70 and $+57$ °C can be compared to the T_g s of the parent component materials that occur at -84 (MEEP) and $+100$ °C (PS). This displacement of 14 and 43 °C shows that a good degree of miscibility exists within the system and that strong intermolecular interactions probably exist between the component materials.

In a second example, an IPN that contains MEEP and PMMA has T_g s at -80 and $+112$ °C. These values may be compared to values of the component materials for which transition temperatures are at -84 (MEEP) and $+105$ °C [poly(methyl methacrylate)]. The displacement of the IPN T_g s by 4 and 7 °C from the T_g s of the component materials indicates that only a low degree of intercomponent interactions exist within this system.

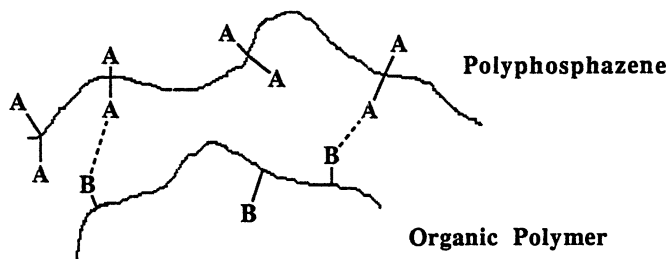
Finally, a single glass-transition temperature in a DSC thermogram indicates a high degree of miscibility within the IPN system and a high degree of intermolecular interactions between the component macromolecules. Two of the polyphosphazene-organic polymer IPNs studied contain a single T_g . MEEP-PAN and POBP-PAA showed single T_g s at $+34$ and $+54$ °C, respectively. These materials appear to enjoy a high degree of miscibility and presumably a high degree of intermolecular interaction.

Scheme 6 shows a representation of intermolecular interactions that might exist between a phosphazene polymer and an organic polymer within an IPN system. These interactions include hydrogen bonding, dipole-dipole interactions, and van der Waals forces. The interactions are shown in more detail in Chart IV. For example, a MEEP side group could undergo hydrogen bonding with the side unit of PAA through the etheric oxygen of the MEEP

Table II. DSC Data and T_g s of Individual Component Polymers

IPN	T_g^a (°C)
MEEP-PS (5, 8)	$-70, +57$
MEEP-PMMA (5, 9)	$-80, +112$
MEEP-PAN (5, 10)	$+34$
MEEP-PAA (5, 11)	$-41, +3.5$
POBP-PS (7, 8)	$-14, +92$
POBP-PMMA (7, 9)	$-14, +50$
POBP-PAN (7, 10)	$-9, +51$
POBP-PAA (7, 11)	$+54$

^a Component polymer T_g s (°C): MEEP (5) = -84 ; POBP (7) = -23 ; PS (8) = 100 ; PMMA (9) = 105 ; PAN (10) = 85 ; PAA (11) = 106 .



Scheme 6.

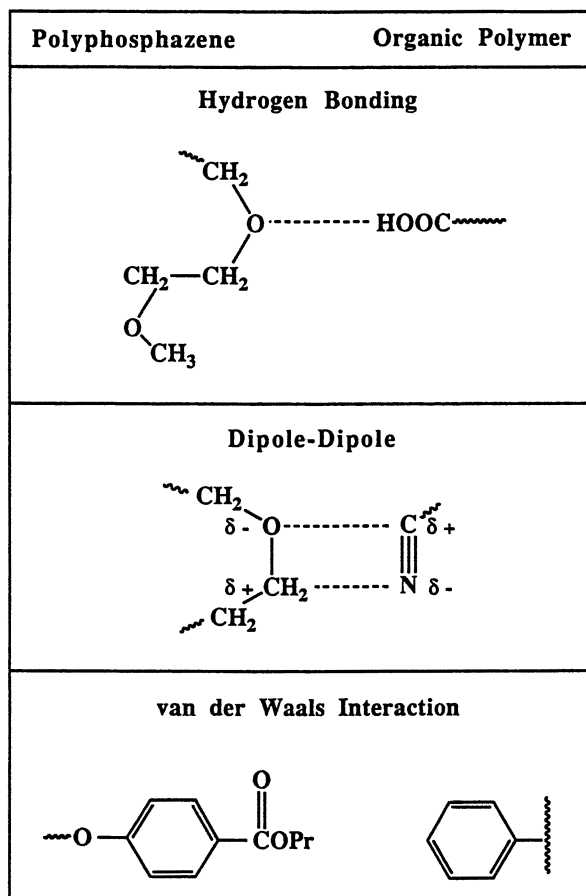
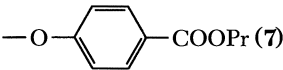
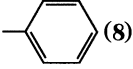


Chart IV.

and the acidic proton of the acrylic acid side group. MEEP could also undergo dipole-dipole interactions with PAN as depicted in Chart IV. Finally, any poly(organophosphazene) could, in principle, undergo van der Waals interactions with any organic polymer. A good example is POBP and PS.

Each poly(organophosphazene) and organic polymer combination is capable of undergoing one or more type of these different intermolecular interactions, as listed in Table III. MEEP is a hydrogen-bond acceptor and is capable of undergoing dipole-dipole interactions. POBP is also a hydrogen-bond acceptor and possesses hydrophobic qualities. Polystyrene is a hydrophobic material and may undergo van der Waals interactions, whereas PMMA is a hydrogen-bond acceptor and undergoes dipole-dipole interac-

Table III. Participating Side Groups and Possible Interactions

<i>Side Groups</i>	<i>Interactions</i>
Polyphosphazene	
$-\text{OCH}_2\text{CH}_2\text{OCH}_2\text{CH}_2\text{OCH}_3$ (5)	H-Bond acceptor Dipole-dipole
 (7)	H-Bond acceptor Hydrophobic
Organic Polymer	
 (8)	Hydrophobic
$-\text{COOMe}$ (9)	H-Bond acceptor Dipole-dipole
$-\text{C}\equiv\text{N}$ (10)	Dipole-dipole
$-\text{COOH}$ (11)	H-Bond donor Dipole-dipole

tions. PAN undergoes dipole-dipole interactions, whereas PAA is a hydrogen-bond donor and also experiences dipole-dipole interactions. These intermolecular interactions could increase the miscibility of the IPN components by binding the component polymers into a coherent material. However, even when favorable intermolecular interactions are built into the system, it may be impossible to predict the final miscibility of the IPN and whether or not these interactions will influence that miscibility (36-39).

Specific descriptions of typical polyphosphazene-organic polymer IPNs follow. In the first example, an IPN that contains MEEP and PAN is an amber, transparent, hard material that swells only slightly in water. This limited swelling behavior could be due to intermolecular interactions such as dipole-dipole interactions between the component materials or to the degree of cross-linking within the system. The DSC thermogram of the MEEP-PAN IPN, which is shown in Figure 3, contains a single, broad glass transition at +34 °C that indicates a high degree of miscibility within the system and favorable intermolecular interactions between the component polymers. The high degree of miscibility is reflected in the TEM micrograph shown in Figure 4, which shows a widely dispersed, almost weblike structure of light colored organic polymer throughout the darker phosphazene matrix. Due to the relatively high electron density of the polyphosphazene phosphorus-nitrogen backbone, no staining of the sample was required to prepare the TEM micrographs of poly(organophosphazenes).

A second example is an IPN that contains POBP and PS. This system forms a tough, opaque, white, elastomeric material that swells in organic solvents. The DSC thermogram for the POBP-PS system, depicted in Figure 5, shows two T_g s at +14 and +90 °C. These values are each displaced from those of the component materials by approximately 10 °C. Therefore, this

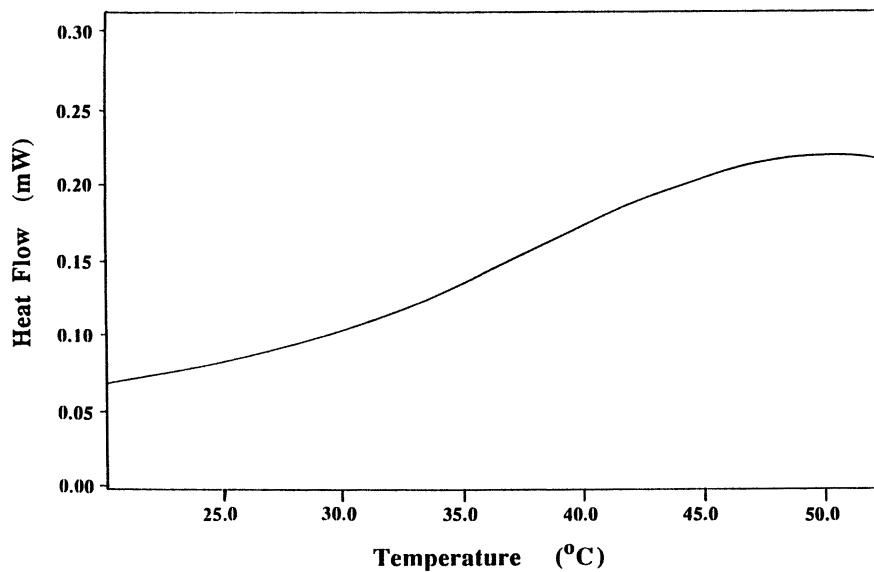


Figure 3. DSC thermogram of MEEP (5)-PAN (10) IPN.

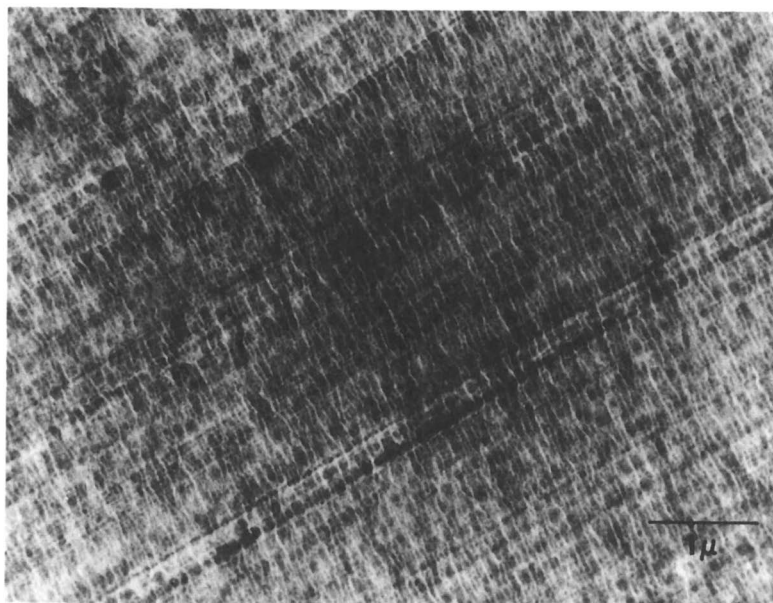


Figure 4. TEM micrograph of MEEP (5)-PAN (10) IPN.

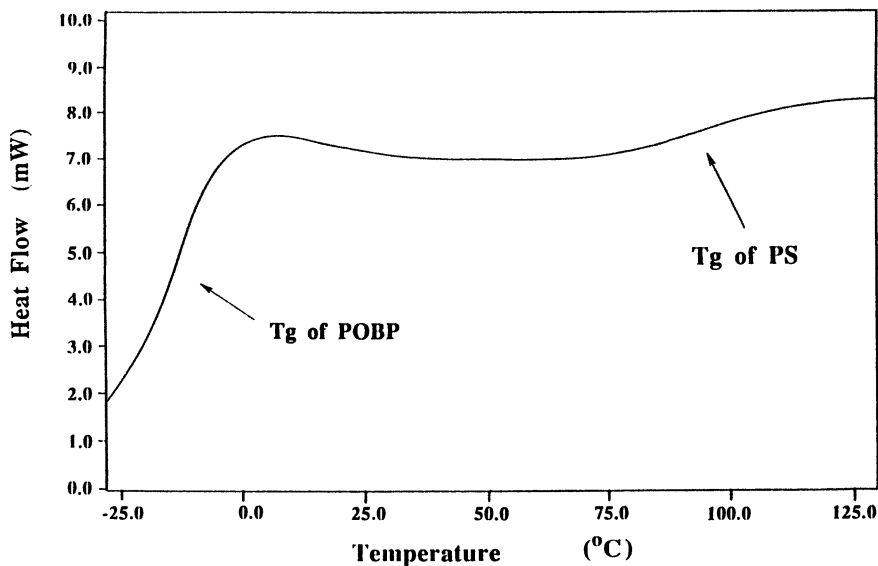


Figure 5. DSC thermogram of POBP (7)-PS (8) IPN.

system appears to be less miscible than the previous example. The lower degree of miscibility is also reflected in the TEM micrograph shown in Figure 6, where definite domains of the light colored organic polymer are evident dispersed throughout the darker colored polyphosphazene system.

Another example is an IPN composed of MEEP and PMMA. This IPN is a tough, opaque, white, elastomeric material that swells to a high degree in organic solvents. The DSC thermogram of the MEEP-PMMA system also shows two T_g s that occur at -80 and $+112$ °C. Both values are displaced ~ 5 °C from the component materials whose T_g values occur at -84 °C (MEEP) and $+105$ °C (PMMA). This small displacement indicates a very low degree of miscibility within the system and probably reflects the poor intermolecular interactions between the component materials. The low miscibility of the system is also evident from the TEM micrograph shown in Figure 7. Large domains of both the poly(organophosphazene) and the organic polymer throughout the IPN system are clearly evident.

A fourth example, is an IPN composed of POBP and PMMA. This material is opaque with a slight golden hue; it is also elastomeric and swells in organic solvents. The DSC thermogram of POBP-PMMA shows two T_g s at $+14$ and $+50$ °C. These values are displaced approximately 15 and 50 °C from those of their component polymers that occur at -23 (POBP) and $+105$ °C (PMMA). The larger degree of displacement indicates that this system is more miscible than the previous system. The increased miscibility is also obvious from the TEM micrograph, shown in Figure 8, where a definite

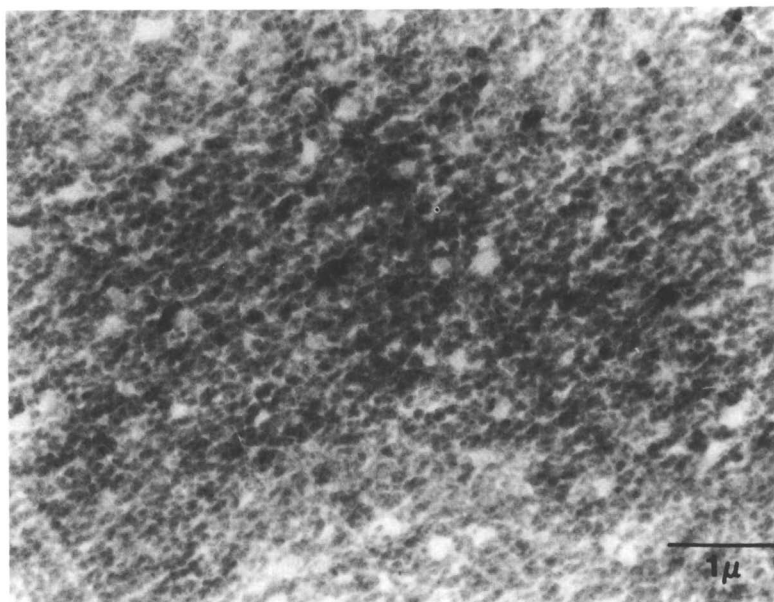


Figure 6. TEM micrograph of POBP (7)–PS (8) IPN.

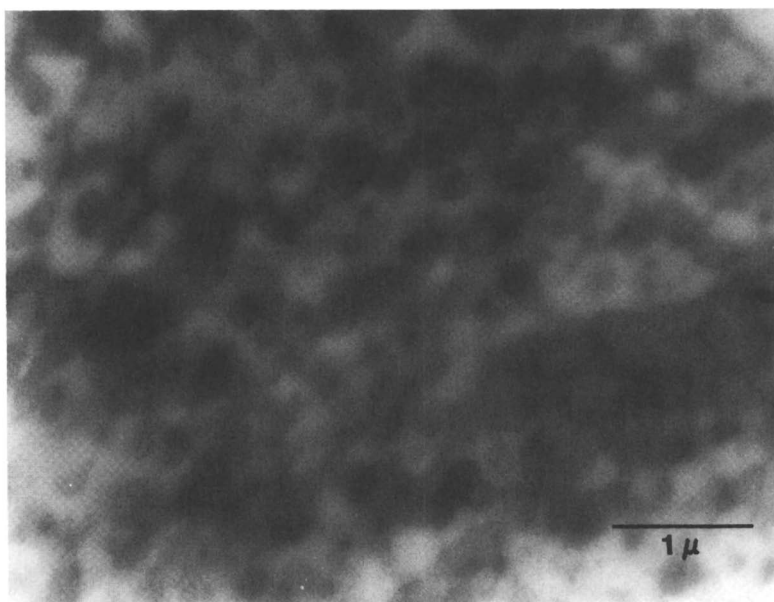


Figure 7. TEM micrograph of MEEP (5)–PMMA (9) IPN.

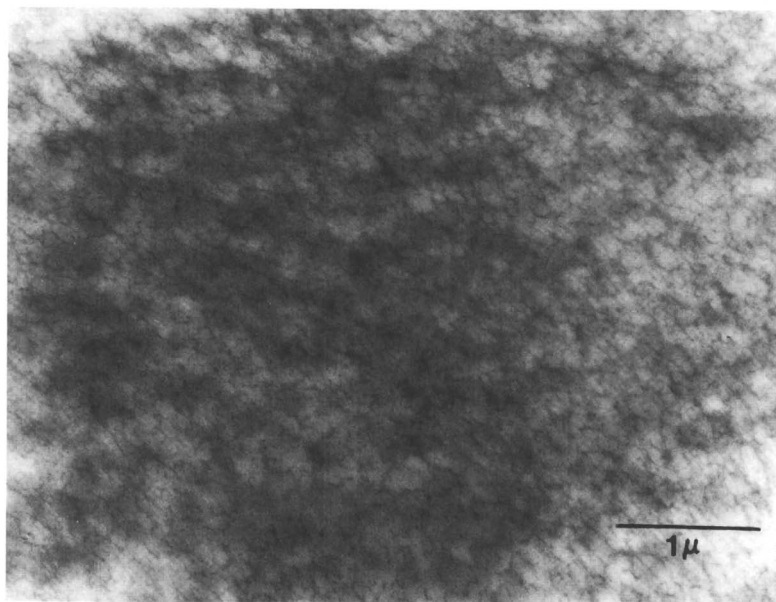


Figure 8. TEM micrograph of POBP (7)–PMMA (9) IPN.

domain structure of the light-colored organic polymer throughout the polyphosphazene matrix is evident.

The final example is an IPN that contains POBP and PAA and is a transparent, hard material that swells only slightly in organic solvents. The limited swelling behavior could reflect hydrogen bonding between the POBP and the acrylic acid side groups. This system shows a single T_g at +54 °C in the DSC thermogram that indicates a high degree of miscibility and good intermolecular interactions within the material. This behavior is also reflected in the TEM micrograph (Figure 9), which shows a domain structure of light-colored organic polymer bordered by an almost weblike structure of phosphazene polymer.

Summary

The synthesis and characterization of novel interpenetrating polymer networks composed of poly(organophosphazenes) and a selected series of organic polymers has been accomplished. Additionally, DSC and TEM methods were used to investigate the miscibility and phase structure in the new materials. When the miscibility is low, these IPNs show properties that are similar to the properties of the component polymers; when the components are highly miscible, these IPNs exhibit hybrid properties. Intermolecular

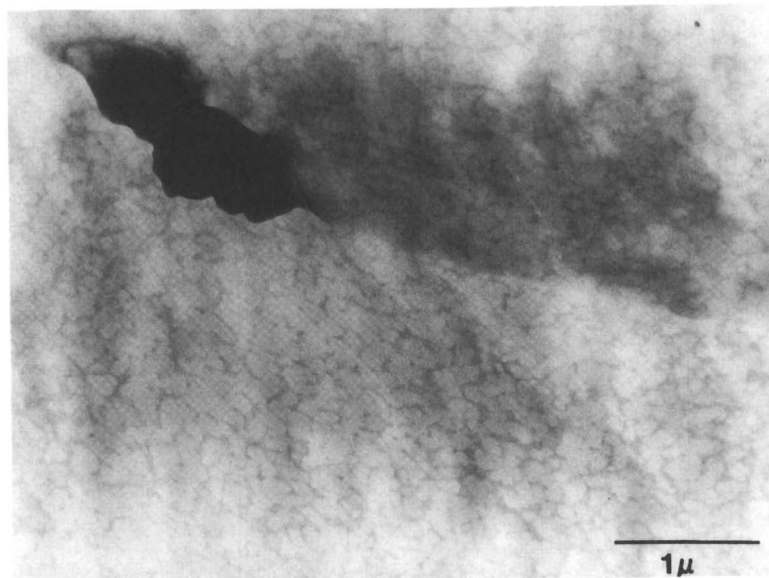


Figure 9. TEM micrograph of POBP (7)–PAA (11) IPN.

interactions, such as hydrogen bonding, dipole–dipole interactions, or van der Waals forces between the macromolecular components, could enhance miscibility within an IPN system. These phosphazene-containing IPNs are the first members of new classes of multicomponent polymeric materials that may possess unique technological and biomedical properties.

Future work in the area of polyphosphazene–organic or inorganic polymer IPNs includes the preparation of ion-specific poly(organophosphazene)–organic polymer IPNs that may be used as ionic filters of ion-exchange media. These types of materials could be used for both environmental and biomedical applications. The synthesis and characterization of IPNs composed of poly(organophosphazenes) and polysiloxanes is also being investigated.

Acknowledgment

This work was supported by the Office of Naval Research and the National Institutes of Health.

References

1. He, X. W.; Widmaier, J. M.; Herz, J. E.; Meyer, G. C. *Polymer* **1992**, *33*(4), 866–871.

2. Frisch, H. L.; Huang, M. W. *J. Polym. Sci., Polym. Chem. Ed.* **1991**, *29*(1), 131–133.
3. Mukae, K.; Bae, Y. H.; Okano, T.; Kim, S. W. *Polym. J. (Tokyo)* **1990**, *22*(3), 206–217.
4. Xiao, H.; Ping, Z. H.; Xie, J. W.; Yu, T. Y. *J. Polym. Sci., Polym. Chem. Ed.* **1990**, *28*(3), 585–594.
5. Mukae, K.; Bae, Y. H.; Okano, T.; Kim, S. W. *Polym. J. (Tokyo)* **1990**, *22*(3), 250–265.
6. Arkles, B.; Crosby, J. In *Silicon-Based Polymer Science*; Zeigler, J. M.; Fearon, F. W., Eds.; *Advances in Chemistry Series 224*; American Chemical Society: Washington, DC, 1990; pp 181–199.
7. Falcetta, J. J.; Friends, G. D.; Niu, G. C. C. Ger. Patent 2,518,904, 1975.
8. Clark, H. A. U.S. Patent 3,527,842, 1970.
9. Mark, J. E.; Allcock, H. R.; West, R. *Inorganic Polymers*; Prentice-Hall: Englewood Cliffs, NJ, 1992.
10. Allcock, H. R.; Visscher, K. B.; Manners, I. *Macromolecules* **1990**, *23*, 4885–4886.
11. Allcock, H. R.; Visscher, K. B.; Manners, I. *Chem. Mater.* **1992**, *4*, 1188.
12. Allcock, H. R. *Phosphorus-Nitrogen Compounds*; Academic: New York, 1972.
13. Penton, H. R. In *Inorganic and Organometallic Polymers*; Zeldin, M.; Wynne, K. J.; Allcock, H. R., Eds.; ACS Symposium Series 360; American Chemical Society: Washington, DC, 1988; pp 272–282.
14. Allcock, H. R. *Chem. Eng. News* **1985**, *63*(11), 22.
15. Allcock, H. R. *Angew. Chem.* **1977**, *16*, 147.
16. Allcock, H. R. In *Inorganic and Organometallic Polymers*; Zeldin, M.; Wynne, K. J.; Allcock, H. R., Eds.; ACS Symposium Series 360; American Chemical Society: Washington, DC, 1988.
17. Allcock, H. R.; Kugel, R. L. *J. Am. Chem. Soc.* **1965**, *87*, 4216.
18. Allcock, H. R.; Kugel, R. L. *Inorg. Chem.* **1966**, *5*, 1709.
19. Allcock, H. R.; Kugel, R. L. *Inorg. Chem.* **1966**, *5*, 1716.
20. Allcock, H. R.; Kwon, S. *Macromolecules* **1989**, *22*, 75–79.
21. Cohen, S.; Bano, M. C.; Visscher, K. B.; Chow, M.; Allcock, H. R.; Langer, R. *J. Am. Chem. Soc.* **1990**, *112*, 7832–7833.
22. Bano, M. C.; Cohen, S.; Visscher, K. B.; Allcock, H. R.; Langer, R. *Biotechnology* **1991**, *9*, 468–471.
23. Allcock, H. R.; Coggio, W. D. *Macromolecules* **1990**, *23*, 1626–1635.
24. Blonsky, P. M.; Shriver, D. F.; Austin, P. E.; Allcock, H. R. *J. Am. Chem. Soc.* **1984**, *106*, 6854.
25. Allcock, H. R.; Kwon, S.; Riding, G. H.; Fitzpatrick, R. J.; Bennett, J. L. *Biomaterials* **1988**, *9*, 509.
26. Allcock, H. R.; Fitzpatrick, R. J.; Gebura, M.; Kwon, S. *Polym. Prepr. (Am. Chem. Soc., Div. Polym. Chem.)* **1987**, *28*, 321.
27. Allcock, H. R.; Bennett, J. L.; Dembek, A. A.; Heyen, B. J.; Shriver, D. L. *Chem. Mater.* **1989**, *1*, 14–16.
28. Allcock, H. R.; Bennett, J. L.; Dembek, A. A.; Heyen, B. J.; Shriver, D. L. *Polym. Prepr. (Am. Chem. Soc., Div. Polym. Chem.)* **1989**, *30*, 437–438.
29. Allcock, H. R.; Dodge, J. A.; Manners, I.; Parvez, M.; Visscher, K. B. *Organometallic Chem.* **1991**, *10*, 3098–3104.
30. May, P.; Guerra, L. R. U.S. Patent 4,251,215, 1981.
31. Gettleman, L.; Farris, C. L.; Rawls, H. R.; LeBouef, R. J. U.S. Patent 4,432,730, 1984.

32. Gettleman, L.; Farris, C. L.; Rawls, H. R.; LeBouef, R. J. U.S. Patent 4,543,379, 1985.
33. Gettleman, L.; Gebert, P. H. U.S. Patent 4,661,065, 1987.
34. Sperling, L. H. *Interpenetrating Polymer Networks and Related Materials*; Plenum: New York, 1981.
35. Sperling, L. H. *CHEMTECH* **1988**, 104.
36. Coleman, M.; Painter, P. C. *Appl. Spectrosc. Rev.* **1984**, 20(3), 256-346.
37. Painter, P. C. *Macromolecules* **1988**, 21, 666.
38. Painter, P. C. *Macromolecules* **1988**, 22, 570.
39. Painter, P. C. *Macromolecules* **1989**, 22, 580.

RECEIVED for review October 9, 1991. ACCEPTED revised manuscript September 22, 1992.

Grafted Interpenetrating Polymer Networks

Barry J. Bauer, Robert M. Briber, and Brian Dickens

Polymers Division, Materials Science and Engineering Laboratory,
National Institute of Standards and Technology, Gaithersburg, MD 20899

A new class of interpenetrating polymer network (IPN) has been studied in which grafting reactions between the two components are varied. Small-angle neutron scattering of grafted and nongrafted IPNs shows that grafting greatly enhances the miscibility of the components. Five nonfunctionalized poly(methyl methacrylates) (PMMA) with alkacrylate, methacrylate, acrylate, and α -methylstyrene end groups were dissolved in styrene-divinylbenzene and polymerized. Small-angle X-ray scattering was used to characterize the extent of phase separation. The uniformity of the IPNs is strongly dependent on the grafting efficiency. Grafted and nongrafted IPNs were also made from the PMMA and polyethylene glycol diacrylates. Thermal studies showed one transition in the grafted samples and two distinct transitions in a nongrafted sample.

MISCIBLE POLYMER BLENDS ARE COMBINATIONS of two high molecular weight polymers that exist as a single phase; that is, the polymers dissolve in one another to form a polymer-polymer solution. Only a relatively few polymer pairs form miscible blends, largely because of the very low entropy of mixing of polymers. Although entropy of mixing always favors miscibility, it depends on the number of molecules per unit volume. Therefore, the larger the polymer molecules, the smaller the number of molecules per unit volume and the lower the entropy of mixing. Because the heat of mixing of polymer pairs is generally unfavorable, polymers generally do not form miscible blends.

Interpenetrating polymer networks (IPNs) are similar to polymer blends in that they are mixtures of two polymeric components. Unlike conventional

polymer blends, however, IPNs are made from components that are mixed while at least one of the polymers is in the form of a monomer. Whereas polymeric components have very little entropy of mixing, typical monomers are small molecules and hence have appreciable entropy of mixing. Therefore, many polymer–monomer combinations are miscible.

An important class of IPNs is sequential IPNs where there are two sequential, independent polymerizations. A polymer is formed through any conventional polymerization process and then swollen by or dissolved in a monomer of a different type. A second polymerization takes place and forms the second polymeric component in the presence of the first. During the second polymerization, entropy of mixing is lost as the molecules increase in size, and phase separation generally occurs, which results in the two-phase morphology common to IPNs. The phase separation occurs for the same reason that most polymer blends are immiscible: the unfavorable heat of mixing of most polymer pairs becomes larger than the effect of the entropy of mixing and causes the phase separation at some point during the second polymerization.

One or both of the polymerizations form a cross-linked network IPN component. It is difficult to judge the effects of the cross-links on the phase boundaries of the system when the two polymers are extremely immiscible because phase separation always occurs during the polymerization. The presence of cross-links may suggest that miscibility would be enhanced over that of a blend because the network acts as a mesh to restrict diffusion of the other polymer and thus to inhibit phase separation. On the other hand, the formation of the network during the second polymerization may exclude the linear chains of the other polymer and thereby cause phase separation.

To study the effects of cross-links on the phase separation in IPNs, it is therefore best to make the IPNs from polymers that are known to form miscible blends. Blends and IPNs of the polymers can then be studied by small-angle scattering techniques to measure thermodynamic parameters and to map out phase diagrams as a function of cross-link density (1).

The first attempts to synthesize miscible IPNs were made by Millar (2) in 1960. The IPNs were synthesized by initial polymerization of a polystyrene–divinylbenzene network (PS–DVB) and then swelling the network with more styrene and DVB and polymerization of the second network. Although this work is assumed to have produced two cocontinuous networks as a single phase, the two components are identical, and any phase separation would be difficult to detect. Seigfried et al. (3) modified this type of IPN slightly by the inclusion of small quantities of diene monomer in the second polymerization. This procedure allowed selective staining of the second network for microscopy. Indications that phase separation may have taken place during the second polymerization were present.

Frisch et al. (4) were first to successfully produce IPNs from polymers that form miscible blends. Polystyrene (PS) and polyphenylene oxide (PPO)

were made into IPNs by selectively cross-linking the components, and miscibility was maintained as judged by glass-transition temperature (T_g) measurements and microscopy. Because blends of these two polymers have a large, negative interaction parameter (5) and remain miscible under all conditions, there was no way to conclude whether the IPNs were more or less miscible than the blends.

Coleman et al. (6) used Fourier transform infrared (FTIR) spectroscopy to study blends of ethylene–vinyl acetate copolymers and various oligomers that could form a cross-linked phase. Although the blends were highly miscible due to hydrogen bonding interactions, phase separation occurred each time a network was formed through the condensation reaction.

Work at the National Institute of Standards and Technology (NIST) (1) on blends of deuterated polystyrene (PSD) and poly(vinyl methyl ether) (PVME) has shown that there is a very favorable interaction in this system at temperatures below 100 °C. However, semi-IPNs made by dissolving linear PVME in styrene–DVB mixtures and polymerizing at 70 °C phase separated upon polymerization (7).

Felisberti et al. (8) also showed that polymerization of styrene–DVB that contains dissolved PVME causes phase separation. Single-phase IPNs were produced by Felisberti et al. by lightly cross-linking functionalized PS in the presence of PVME with the polymers dissolved in solvent, but phase separation occurred as the cross-link density increased. Fay et al. (9) also made PS–PVME IPNs that were hazy, which suggested that phase separation had occurred. Control of the polymerization conditions enabled control of the resulting morphology, to yield large amounts of partial mixing. This result caused a very wide T_g range and good mechanical damping properties of the material.

IPNs made from standard polystyrene (PSH) and PSD were studied recently (10). These polymers form nearly athermal mixtures that allow easy study of the effects of linear chain molecular weight and the cross-link density. The interaction parameter between PSH and PSD is negligible compared to the effects of cross-links. An increase in the linear chain molecular weight or an increase in the cross-link density destabilizes the IPN and eventually causes phase separation.

In a related study (11), miscible PSD–PVME blends were cross-linked by gamma irradiation to produce many types of cross-links that include grafts between the two different polymers. These materials showed greatly increased miscibility compared to blends.

Frisch and Zhou (12) studied simultaneous full IPNs made from components that do not form miscible blends. In many of the IPNs, Frisch and Zhou found a single T_g , which they interpreted as the result of miscibility of the components of the IPN. Note, however, a single T_g would be found in systems where weak phase separation had occurred.

Radical polymerizations can result in chain transfer to polymer-forming grafted polymer structures (13). Some researchers have suggested that grafting one polymer type onto another in an IPN may effect the miscibility of the components (8). To examine the effect of grafting on IPN miscibility, IPNs with various amounts of grafting between components have been made and have been studied by small-angle scattering and thermal measurements (14, 15).

Theoretical Details

The thermodynamics of IPNs were first described by Binder and Frisch (16), who used classical rubber elasticity to describe the elastic contributions to the free energy by the polymer network. The equation has the form

$$\frac{\Delta f}{kT} = \frac{1}{2} A \nu (\lambda_x^2 + \lambda_y^2 + \lambda_z^2) - B \nu \ln(\lambda_x \lambda_y \lambda_z) \quad (1)$$

where Δf is the free energy, k is Boltzmann's constant, T is the temperature, λ_i is the extension ratio in the i th direction and is the ratio of the deformed length to the undeformed length, ν is the average number of elastically effective cross-links per unit volume, and A and B are characteristic constants. The scattering from the IPNs measures concentration fluctuations, so eq 2 is used to express the extension ratio in terms of ϕ , the volume fraction of the network, and ϕ_s , the volume fraction of the network where the chains are relaxed:

$$\lambda = (\phi_s / \phi)^{1/3} \quad (2)$$

These equations are an extension of the work of Flory and Rehner (17) on the swelling of networks.

The scattering from IPNs can be calculated from the foregoing thermodynamic relationships via a procedure described by Onuki (18). The resultant scattering for zero angle scattering is given by

$$\frac{\partial^2(\Delta f/kT)}{\partial \phi^2} = \frac{B}{v_a N_c \phi} + \frac{A \phi_s^{2/3}}{v_a N_c \phi^{5/3}} + \frac{1}{v_b N_b (1 - \phi)} - 2 \frac{\chi}{v_0} = \frac{k_n}{S(0)} \quad (3)$$

$S(0)$ is the zero angle scattering intensity, k_n is a contrast factor calculated from the polymeric repeat units, v_0 is a reference volume, N_c is the degree of polymerization between cross-links, N_b is the degree of polymerization of the linear chains, and χ is the Flory-Huggins interaction parameter. Equation 3 was derived for a semi-IPN; that is, a two-component IPN with one cross-linked polymer and one linear polymer.

The effect of cross-link density on the scattering intensity is shown by Figure 1 (10). Equation 3 indicates that a plot of inverse zero angle scattering versus inverse degree of polymerization between cross-links should be linear with a positive slope. The dashed line in Figure 1 is such a plot where the value of χ/v_0 is the value of the polymer blend; the symbols (Δ) represent experimental data and the solid line is a linear least squares fit of the data. Because $k_n/S(0)$ decreases in Figure 1 as $1/N_c$ increases, the scattered intensity increases with increased cross-link density. The point at which the intensity goes to infinity is the spinodal point for the system. Therefore, increased cross-link density pushes the system toward phase separation. Samples made with higher cross-link densities were phase separated.

Onuki has modified the original theory to include heterogeneities in the network (Onuki, A., personal communication). This modification changes the effect of cross-links from stabilization of the system to destabilization of the IPN. Bastide et al. (19) formulated a similar theory to explain scattering results from siloxane networks. Heterogeneities describe natural cross-link concentration fluctuations present even in model networks.

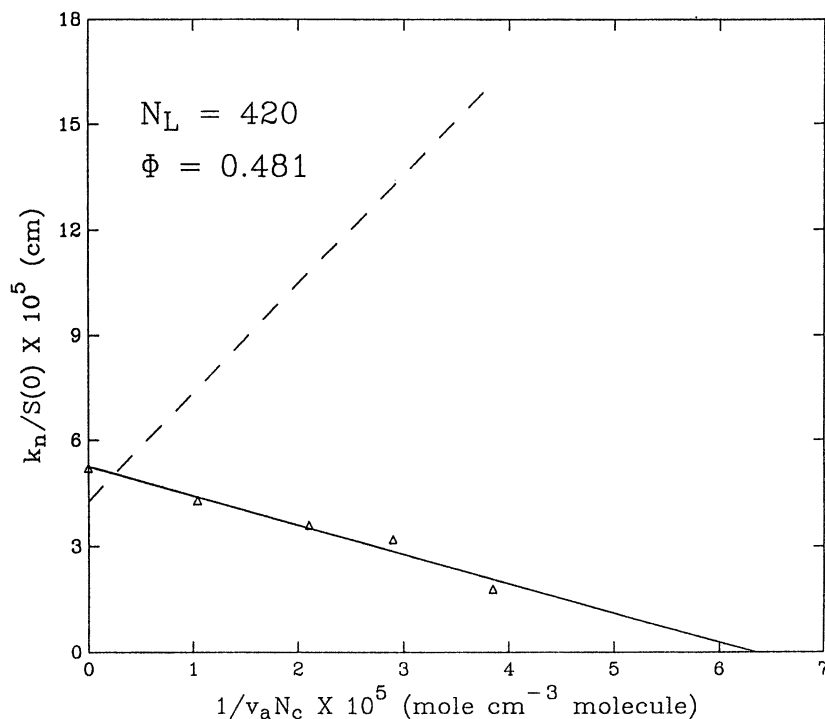


Figure 1. Small-angle neutron scattering plots for $k_n/S(0)$ versus $1/(\phi N_c)$ (solid line) for PSH-PSD semi-II IPNs. The values calculated from equation 3 (dashed line) are given for the same system.

Grafted polymers are more miscible than blends of ungrafted polymers. Although no theory for the scattering from grafted polymer networks exists, scattering from simple graft polymers has been studied extensively. Benoit and Hadziioannou (20) give equations for scattering from graft copolymers and from mixtures of block copolymers and homopolymers; their techniques can be used to predict the scattering from a graft copolymer–ungrafted polymer mixture.

Figure 2 is a plot of the spinodal value of χN versus polydispersity index, M_w/M_n , for polymers that are 100% grafted or 100% ungrafted. M_w and M_n are the weight average and number average molecular weights, respectively. A volume fraction of 0.5 of each component is present, N is the degree of polymerization of the graft (or the unattached chain), and χ is the interaction parameter. Because the scattering does not change significantly with the backbone length and number of grafts (20), the limiting case of the number of grafts going to infinity is taken.

The lower line in Figure 2 is the spinodal value of a polymer blend: one component has degree of polymerization N and the other component has

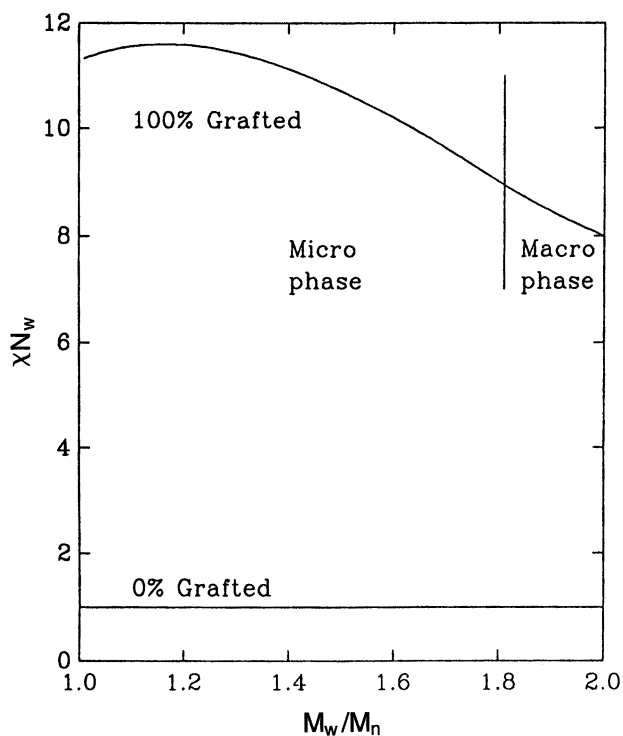


Figure 2. Spinodal values of χN_w for grafted and nongrafted polymers versus polydispersity index. The volume fraction of each component is 0.5.

infinite degree of polymerization. The upper line is the spinodal value for a 100% grafted copolymer. The graft copolymer has a much higher value of χN_w than an ungrafted sample of the same material at any polydispersity index. The graft copolymer is stabilized by a factor of 11.4 for the monodisperse case and 8.0 for a polydispersity of 2. Therefore, grafted IPNs are probably much more likely than ungrafted IPNs to be stable as a single phase.

The calculated scattering intensities can go to infinity in two ways (20). In polymer blends, the maximum scattering is at zero angle and any phase separation is macrophase separation, with characteristic sizes (commonly about 1000 nm) that are limited by kinetics. In grafted polymers, the maximum scattering occurs at a nonzero angle. Such samples separate into microphases if they are pushed into the two-phase region. The size scale is related to the inverse of the scattering angle at the peak maximum and is typically 10 nm.

Figure 2 shows that the phase separation, dependent on the polydispersity, can be either microphase or macrophase. A peak in the scattering of a grafted sample indicates efficient grafting and suggests that microphase separation would occur for the appropriate χN_w .

Experimental Details

Table I is a list of the characteristics of the poly(methyl methacrylate) (PMMA) and PSH macromonomers used to make grafted IPNs. All of the PMMA macromonomers have similar molecular weights and more than 90% functionalization with one of the chain ends being one of four copolymerizable groups; a fifth sample contains no end groups capable of radical copolymerization. The acrylate and methacrylate chain ends were attached through the ester linkages and the alkacrylate chain end was attached through the α -methylene group.

Seven samples were made for the small-angle neutron scattering (SANS) experiments and their compositions are listed in Table II. All samples were approximately 50 wt% of one of the two polymeric components. The first polymer was either PS or PMMA. All of the PMMA samples were macromono-

Table I. Characteristics of Macromonomers

<i>Polymer</i>	<i>Functionality</i>	M_w	M_n	<i>%End Group</i>
PS	Methacrylate	13,000		
PS	None	13,000		
PMMA	Alkacrylate	7,200	4,200	> 90
PMMA	Acrylate	7,100	4,600	95
PMMA	Methacrylate	4,600	3,800	96
PMMA	α -Methylstyrene	6,400	4,300	> 90
PMMA	None	7,900	3,600	—

Table II. SANS Samples

<i>Sample</i>	<i>Polymer I</i>	M_w	<i>DVB in II</i> (wt%)	<i>Graft</i>
1	PS	13,000	0.2	No
2	PS	13,000	0.5	No
3	PS	13,000	0.2	Yes
4	PS	13,000	0.5	Yes
5	PS	13,000	0.9	Yes
6	PMMA	7,200	0.5	Yes
7	PMMA	7,200	0.9	Yes

mers of the alkacrylate type, whereas the PS samples were either macromonomers of the methacrylate type of unfunctionalized. Both PS types had the same molecular weight and narrow molecular weight distributions. The cross-linked component in each sample of the semi-II IPNs was deuterated styrene, which provided the necessary contrast for the SANS experiment. The deuterated styrene was cross-linked with various amounts of divinylbenzene (DVB). The weight fraction of DVB listed in the table is based only on the second component.

Small-angle X-ray scattering (SAXS) samples were synthesized by a semi-II synthesis; 50-wt% PMMA macromonomer was dissolved in 50-wt% styrene-divinylbenzene. All samples contained 1-wt% divinylbenzene and 0.2-wt% azobis(isobutyronitrile) (AIBN) dissolved in the styrene. The samples were polymerized at 60 °C for 18.5 h and at 110 °C for 3 h. Extractions were done twice with toluene. Samples for neutron scattering were synthesized as SAXS except that 0.1-wt% AIBN free radical initiator was used. The samples were polymerized in place in neutron scattering cells in an oven at 130 °C for 16 h.

Gel permeation chromatography of the toluene extracts was carried out using ultraviolet and mass evaporative detectors to identify the amounts of PMMA macromonomer and polystyrene in the extract. Samples for the thermomechanical analysis (TMA) studies were made from 0–50-wt% PMMA macromonomer; the remainder of the sample was polyethylene glycol diacrylate that contained 1-wt% benzoyl peroxide. The TMA samples were polymerized into 1-mm-thick sheets at 60 °C for 24 h.

The SANS measurements were performed at the NIST small-angle neutron scattering facility (21). The wavelength of the incoming neutron beam was set to 0.6 nm with $\Delta\lambda/\lambda = 25\%$ by the use of a rotating velocity selector. The data were collected using a two-dimensional detector and corrected for empty cell scattering, incoherent scattering, and background. The scattering was put on an absolute intensity scale that used a secondary standard of silica gel.

The SAXS measurements were carried out at the NIST SAXS facility. Two-dimensional scattering data were corrected for empty cell scattering and dark current. All samples were isotropic and the results were circularly averaged.

The TMA was done with a thermomechanical analyzer (Perkin Elmer TMS-2). Sample thickness was monitored while the sample was being heated from –100 to 150 °C with a 10 °C/min heating rate. The rate of change in thickness with temperature is a measure of the thermal expansion coefficient, which has different values below and above T_g .

Results

Figure 3 is a plot of SANS scattering intensity versus the scattering vector $q = (4\pi/\lambda)\sin(\theta/2)$, where λ is the wavelength of the neutron beam and θ is the angle of the scattered beam. The top two curves are for the standard semi-II IPNs made from polystyrene that did not have macromonomer functionality and contained 0.5- and 0.2-wt% DVB, respectively. These results are in agreement with previous findings for such IPNs (10). If the DVB concentration were increased to 0.9 wt%, these samples would be phase separated.

The lower three curves in Figure 3 are for samples made with macromonomers that are capable of grafting to the PSD component. The presence of very low scattered intensity indicates that these macromonomers are much more homogeneous and further from a phase transition than equivalent samples made from unfunctionalized polymers. This status indicates that use of the macromonomer functionality, which allows grafting of the first polymer onto the network formed in the second step, greatly stabilizes the single-phase region. The solid triangle on the ordinate is the calculated value for zero angle scattering from an equivalent blend; that is, a

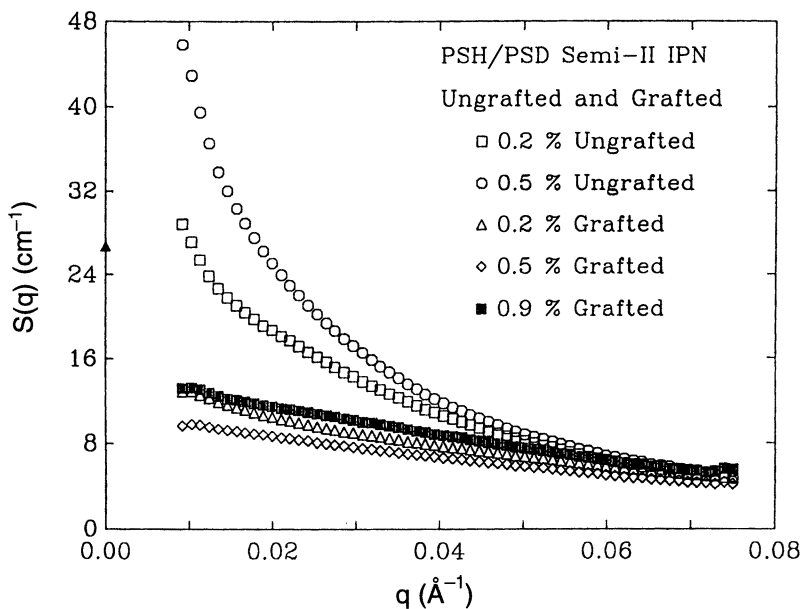


Figure 3. SANS scattering intensities for PSH-PSD grafted and ungrafted semi-II IPNs.

blend in which no cross-linking is present. Therefore, the semi-II IPN structure seems to push the polymers toward phase separation, whereas the grafted IPN structure made from the macromonomers favors the single phase.

Figure 4 gives the results for the grafted PMMA-PSD samples made with PMMA macromonomers. These scattering curves have prominent peaks. Previous work on blends cross-linked by exposure to gamma irradiation also gave scattering curves with similar peaks. These peaks were interpreted to be incipient microphase separation (11). There is no symbol on the ordinate to show where an equivalent blend would scatter because such a blend would be beyond the point of phase separation.

The SANS results from these model systems demonstrate that there are great differences in the microuniformity of samples made with and without macromonomers. The polymer pairs used in the SANS studies represent the two limits of grafting efficiency and it is, therefore, likely that mixtures of macromonomers and unfunctionalized polymers would produce morphologies between the two limiting cases.

Macromonomers can be made with a variety of end groups that are capable of copolymerization. The reactivity ratios of such a copolymerization will determine the uniformity of the resultant copolymers. Macromonomers generally have reactivity ratios similar to the ratios of small monomers of the same chemical nature as the macromonomer chain end (22).

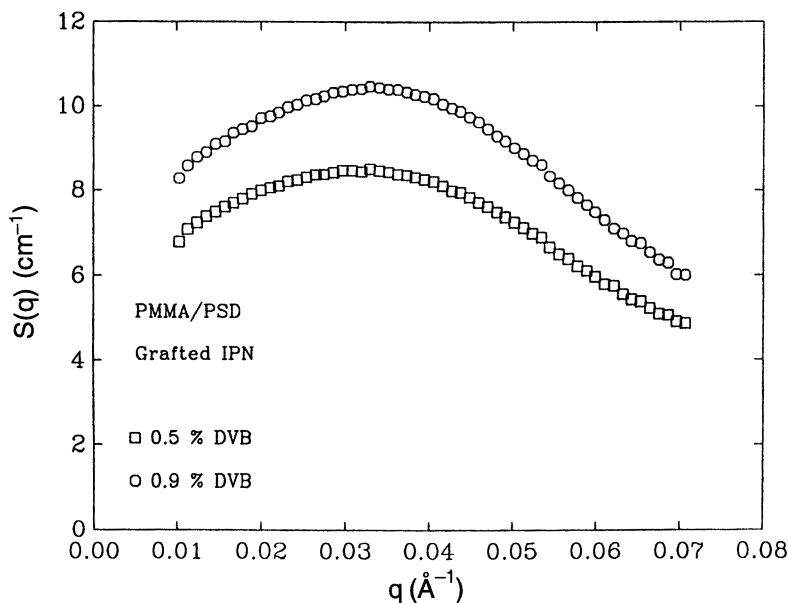


Figure 4. SANS scattering intensities for PMMA-PSD grafted semi-II IPNs.

SAXS is similar to SANS in that the range of scattering vector, q , is similar. The major difference between the two techniques is the factors that cause contrast to exist between the different components. Contrast in SANS can be conveniently obtained by replacing the hydrogen atoms in one component with deuterium atoms. Contrast in SAXS comes from differences in electron density, which are closely correlated with the mass density of the samples.

PS and PMMA have mass densities of approximately 1.05 (23) and 1.19 g/cm³ (24). Although the contrast factor in SANS is very large compared with the SAXS contrast, there is still a large enough density difference for SAXS experiments to give useful results (for much of the time covered by this work, construction at the reactor site temporarily stopped SANS experiments, so the SAXS technique was developed as a replacement).

In the five samples made, the only significant variable was the type of polymerizable end group on the macromonomer. Table III lists the composition of the SAXS samples. Samples made with alkacrylate, methacrylate, and acrylate groups were optically clear and appeared uniform. The α -methylstyrene sample was cloudy and the unfunctionalized sample was opaque; these conditions indicate ever stronger phase separation.

Figure 5 plots the scattering curves on a logarithmic scattering intensity scale shifted in the y axis for clarity. The α -methylstyrene sample has a very rapid dropoff in scattering intensity with angle, which indicates phase separation. The alkacrylate sample has a peak in the scattering intensity that is similar to the peak seen in the SANS data. As with the SANS results, these samples seem to be very uniform.

The four PMMA macromonomers differed only in the polymerizable end group, low molecular weight analogues of which are all known to copolymerize with styrene. The morphology of these samples was extremely varied, which indicates that slight differences in the polymerization kinetics may have produced profound differences in the morphology and hence properties.

Because the macromonomers have molecular weights many times larger than the styrene comonomer, a 50-wt% mixture means that styrene is present in a large molar excess. Therefore, only one reactivity ratio, r_2 , is important: the relative probability of a growing chain that contains the comonomer as

Table III. SAXS and Extraction Results of Grafted PS–PMMA IPNs

<i>End Group</i>	r_2 (<i>monomer</i>)	SAXS	% <i>Macromonomer Reacted</i>	<i>Optical Note</i>
Alkacrylate	0.5 (MMA) (26)	4	90	Clear
Methacrylate	0.5 (MMA) (26)	3	72	Clear
Acrylate	0.7 (MA) (27)	2	82	Clear
α -Methylstyrene	1.3 (α MS) (28)	1	36	Cloudy
None	∞	—	0	Opaque

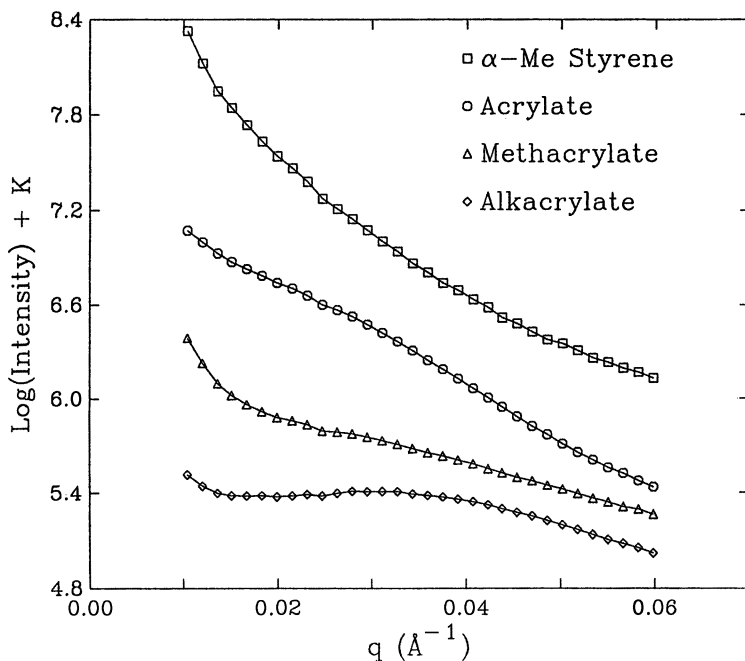


Figure 5. SAXS $\log(\text{scattering intensity})$ versus scattering vector q for PMMA-PS IPNs.

the terminal group to add a comonomer compared with addition of a macromonomer. A value less than 1 means that the macromonomer is preferentially incorporated, whereas a value greater than 1 means that the comonomer is preferentially added. Table III gives published values of reactivity ratios of styrene with small comonomers similar to the chain ends of the macromonomer used (MMA is methyl methacrylate, MA is methyl acrylate, and α MS is α -methylstyrene).

Extraction studies show that virtually all of the nonfunctionalized PMMA is not bonded to the PS network. The nonfunctionalized PMMA, therefore, did not become attached to the polystyrene network through grafting reactions such as chain transfer to the polymer. Only 36-wt% of the α MS-terminated PMMA was bonded to the network, whereas 72–90 wt% of the other polymers were bonded. This result is consistent with the expected reactivity ratios of the macromonomers. The sample that had the fewest grafted chains was very opaque and seemed to be strongly phase separated. The α MS-terminated PMMA, which had only 36% attached chains, was cloudy and translucent. This condition indicates phase separation to a lesser extent. The samples that had higher percentages of grafted chains seemed optically clear with no obvious phase separation.

Miscible blends and copolymers (25) that form a single phase produce materials that have T_g s between the T_g s of the individual components. To test the effect of macromonomers on the thermal properties, two samples were prepared from 35-wt% PMMA and 65-wt% poly(ethylene glycol) (PEG) 400 diacrylate: one sample was prepared with PMMA macromonomer and the other sample was unfunctionalized. The PMMAs were very similar in molecular weight (*see* Table I). The major difference was that one PMMA was a macromonomer with more than 96% alkacrylate functionality at one end, whereas the other PMMA had a hydroxy group at one end that made it incapable of copolymerization with the PEG 400 diacrylate. The samples were cured as previously described and a TMA was performed on each.

Figure 6 shows the TMA of the 35-wt% macromonomer sample that formed a grafted IPN. As described earlier, this sample displays a single transition. Figure 7 shows the results for a similar sample without the macromonomer functionality that forms an ungrafted IPN. Quite clearly, two thermal events take place. The lower transition is near the transition of the T_g of a pure PEG 400 diacrylate network, whereas the upper transition is near the transition of the PMMA macromonomer itself. The transitions could conceivably involve crystalline melting points, but because pure PEG networks and PMMA each only show T_g s, it seems more likely that the two transitions are T_g s. This sample seems to be strongly phase separated into domains of nearly pure components.

Summary

Small-angle scattering is a powerful tool for study of the effects of IPN structure on the miscibility of the two components. Previous work (7, 10) showed that conventional semi-II IPNs are destabilized compared to blends of the same two components.

Grafted IPNs are considerably more miscible than blends of the same polymers. Variation of the grafting efficiency greatly changes the resultant morphology of an IPN from very strong phase separation to high miscibility. The presence of a peak in the scattering data in some cases suggests that microphase separation may occur under the proper conditions.

These results suggest that controlling the chemistry of the IPN polymerization (i.e., cross-link density and grafting) can give a wide variety of morphologies and, hence, properties. Miscible polymers can be made to phase separate easily by increasing the cross-link density and avoiding grafting whereas immiscible polymers can be made miscible by providing functional groups that will result in grafting between the two polymers.

Control of the extent of phase separation from strong separation into nearly pure phases or weak separation with broad distributions of composi-

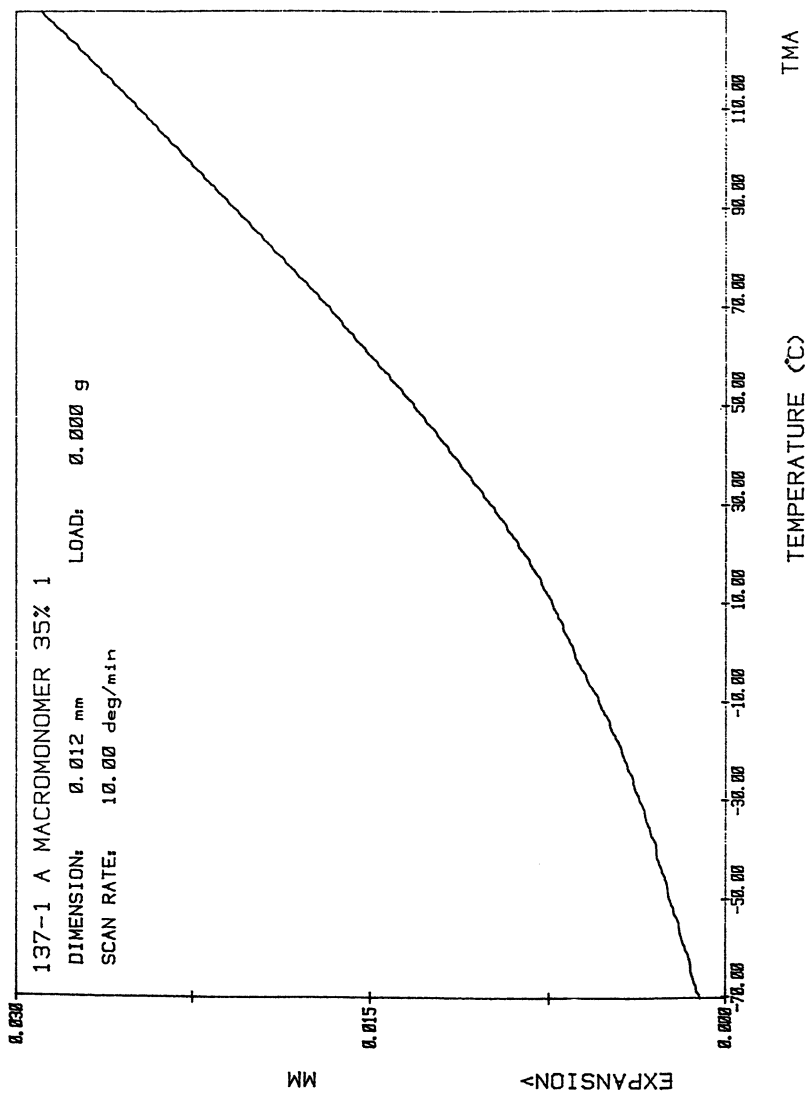


Figure 6. TMA scan of grafted semi-II IPN of PEO-PMMA.

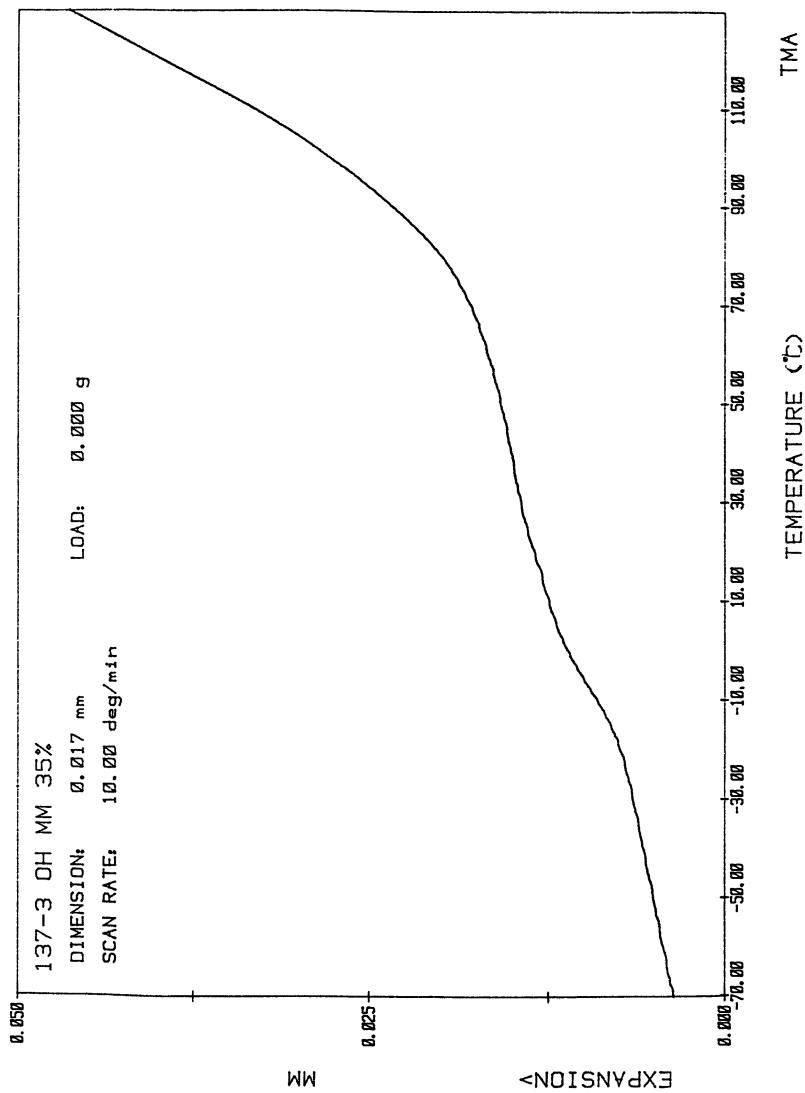


Figure 7. TMA scan of semi-II IPN of PEO-PMMA.

tions may be possible. Control of the characteristic size of phase separation from small microphase separated domains to much larger macrophase separation may also be possible.

These results raise questions concerning earlier studies. In the PS-PS IPNs made by Millar (2), if there is no grafting between the two polymeric components, it is likely that the IPNs are phase separated to some extent; if grafting did occur, the samples may have been single phase. However, making strongly grafted IPNs was not the intent of the study.

On the other hand, if IPNs are more miscible than blends of the same two polymers, unexpected grafting may have taken place. It is common to assume that the networks are independent in IPNs and that any grafting is inconsequential, but, as shown here, the resultant morphology will be strongly affected by grafting.

Acknowledgments

Samples and characterization were supplied by DuPont. Certain equipment, instruments, and materials are identified in this paper to adequately specify the experimental details. Such identification does not imply recommendation by the National Institute of Standards and Technology, nor does it imply the materials are necessarily the best available for the purpose.

References

1. Han, C. C.; Bauer, B. J.; Clark, J. C.; Muroga, Y.; Matushita, Y.; Okada, M.; Tran-Cong, Q.; Chang, T.; Sanchez, I. C. *Polymer* **1988**, *29*, 2002.
2. Millar, J. R. *J. Chem. Soc.* **1960**, 1311.
3. Seigfried, D. L.; Manson, J. A.; Sperling, L. H. *J. Polym. Sci., Polym. Phys. Ed.* **1978**, *16*, 583.
4. Frisch, H. L.; Klempner, D.; Yoon, H. K.; Frisch, K. C. *Macromolecules* **1980**, *13*, 1016.
5. Composto, R. J.; Kramer, E. J.; White, D. M. *Macromolecules* **1988**, *21*, 2580.
6. Coleman, M. M.; Serman, C. J.; Painter, P. C. *Macromolecules* **1987**, *20*, 226.
7. Bauer, B. J.; Briber, R. M.; Han, C. C. *Macromolecules* **1989**, *22*, 940.
8. Felisberti, M. I.; Freitas, L. L.; Stadler, R. *Polymer* **1990**, *31*, 1441.
9. Fay, J. J.; Murphy, C. J.; Thomas, D. A.; Sperling, L. H. *PMSE Proc.* **1989**, *60*, 649.
10. Briber, R. M.; Bauer, B. J. *Macromolecules* **1991**, *24*, 1899.
11. Briber, R. M.; Bauer, B. J. *Macromolecules* **1988**, *21*, 3296.
12. Frisch, H. L.; Zhou, P. *PMSE Proc.* **1991**, *64*, 52.
13. Dryfuss, P.; Quirk, R. P. In *Encyclopedia of Polymer Science and Engineering*; Kroschwitz, J. I., Ed.; Wiley Interscience: New York, 1987; Vol. 7, p 551.
14. Bauer, B. J.; Briber, R. M. *Polym. Prepr. (Am. Chem. Soc., Div. Polym. Chem.)* **1990**, *31(1)*, 578.
15. Bauer, B. J.; Briber, R. M.; Dickens, B. *PMSE Proc.* **1991**, *65*, 4.
16. Binder, K.; Frisch, H. L. *J. Chem. Phys.* **1984**, *81*, 2126.
17. Flory, P. J.; Rehner, J. Jr., *J. Chem. Phys.* **1943**, *11*, 521.

18. Onuki, A. In *Formation, Dynamics and Statistics of Patterns*; Kawasaki, K., Ed.; World Science Publishing: River Edge, NJ, 1989.
19. Bastide, J.; Liebler, L.; Prost, J. *Macromolecules* **1990**, *23*, 1821.
20. Benoit, H.; Hadziioannou, G. *Macromolecules* **1988**, *21*, 1449.
21. Glinka, C. *AIP Conf. Proc.* **1982**, *89*, 395.
22. Meijs, G. F.; Rizzardo, E. *J. Macromol. Sci., Rev. Macromol. Chem. Phys.* **1991**, *C30*, 305.
23. Rudd, J. F. In *Polymer Handbook*, 2nd ed.; Brandrup, J.; Immergut, E. H., Eds.; Wiley Interscience: New York, 1975; p V-59.
24. Wunderluch, W. In *Polymer Handbook*, 2nd ed.; Brandrup, J.; Immergut, E. H., Eds.; Wiley Interscience: New York, 1975; p V-55.
25. Roe, R.-L. In *Encyclopedia of Polymer Science and Engineering*; Kroschwitz, J. I., Ed.; Wiley Interscience: New York, 1987; Vol. 7, p 531.
26. Lewis, F. M.; Mayo, F. R.; Hulse, W. F. *J. Am. Chem. Soc.* **1945**, *67*, 1701.
27. Marvel, C. S.; Schwen, R. *J. Am. Chem. Soc.* **1957**, *79*, 6003.
28. O'Driscoll, K. F.; Gasparro, F. P. *J. Macromol. Sci., Chem.* **1967**, *A1*, 643.

RECEIVED for review November 26, 1991. ACCEPTED revised manuscript June 9, 1992.

Bifunctional Interpenetrating Polymer Networks

Spiro D. Alexandratos, Corinne E. Grady, Darrell W. Crick, and Robert Beauvais

Department of Chemistry, University of Tennessee, Knoxville, TN 37996

Interpenetrating polymer networks (IPNs) with two different functional groups on one of the two cross-linked networks have been synthesized. Bifunctional IPNs with imidazole and carboxylic acid groups are described and their binding affinity for copper and cobalt ions is quantified via Langmuir adsorption isotherm plots. The microenvironment within the imidazole-acid IPNs varies as the ratio of ligands changes along the series 1:0, 0.5:0.5, and 0:1. Binding constants for the foregoing IPNs are 3130, 1556, and 77 N⁻¹ for Cu(II) and 294, 189, and 26 N⁻¹ for Co(II), respectively. Conditions under which different ligands can cooperate synergistically in the complexation of substrates are being defined to enable design of highly selective chemical sensors and complexing agents for environmental separations.

THE MODIFICATION OF POLYMERS BY COVALENT BONDING OF LIGANDS on a support matrix has long been recognized as an important technique for the preparation of polymer-supported reagents (1). Such reagents are used for the complexation of ions and molecules from solutions (2) as well as in the synthesis of organic molecules such as proteins (3) and polysaccharides (4).

A number of procedures that are specific for targeted substrates have evolved for the preparation of polymeric reagents. Template polymerization creates cavities within a polymer matrix to produce selectivity based on size of the substrate (5). This shape-selectivity arises from polymerizing monomers around a template; the resulting cavities retain the dimensions of the template after the template is removed from the matrix. This approach has been

successful for molecular recognition (6) and shows promise in metal ion selectivity studies as well (7). Ligands with high levels of preorganization, such as crown ethers, have also been bonded to polymer matrices and retain much of their inherent selectivity (8).

Hard-soft acid-base theory (9) can provide the framework for choosing ligands that can be expected to display a certain ionic selectivity (10). In most cases, a single type of ligand is bonded to the polymer and its selectivity series then is determined. An alternate approach is to bond two types of ligands on a polymer and then define the conditions under which the ligands cooperate in complexing greater levels of metal ions than either individual could complex (11). In one example, ion exchange-coordination resins were synthesized with phosphonate monoester and diester ligands covalently bound on cross-linked polystyrene beads (12). This resin complexed far more Ag(I) than expected from results with the corresponding monofunctional resin (13).

The synthesis of bifunctional polymers to study the synergistic interaction of supported ligands required a new preparative technique due to the limited number of reactions that could immobilize well-defined pairs of ligands on polymers. The development of bifunctional interpenetrating polymer networks (IPNs) proved ideal for the synthesis of reagents with two types of ligands bound within a single matrix in bead, rather than granular, form. Polymers in bead form are important in rate studies due to their controlled particle size and shape; they are preferred in separations applications due to their adaptability to continuous processes and long-term stability.

IPNs have been defined as "a combination of two polymers both in network form, at least one of which is synthesized in the presence of the other" (14). The modification of the engineering properties displayed by a given polymer (tensile strength, flexibility, etc.) has been the primary objective of much research (15). The sequential method of IPN synthesis involves starting with a preformed cross-linked polymer, contacting it with a monomer solution, and forming the second network within the first. The final properties displayed by the sequential IPNs are dominated by the properties of the first network (16). The IPN morphology seen by electron microscopy is set by the cross-link density in the first network; changes in the degree of cross-linking in the second network have little effect (17). In a comprehensive study on the morphology of sequential IPNs, a number of such IPNs were synthesized, including two IPNs with equivalent levels of polystyrene and poly(ethyl acrylate): in one, the polystyrene was the initial matrix and the ethyl acrylate polymerized within it; in the other, the polyacrylate formed the initial matrix and styrene polymerized within it. In both cases, the initial matrix formed a continuous cellular structure with the second network found mainly within the cells (18). It is important to note that both networks were lightly cross-linked with 0.5 vol% tetraethylene glycol dimethacrylate; higher cross-link levels are expected to diminish the size of the cells. Dynamic mechanical spectroscopy on the same IPNs shows that the polystyrene-poly-

acrylate IPN is stiffer than the polyacrylate–polystyrene IPN, which confirms that the first network dominates the final IPN properties (19). The final properties also can depend on small changes in the synthesis: sequential IPNs of polyurethane–poly(methyl methacrylate), where the methacrylate network is initiated with azobis(4'-cyanovaleric acid), are more ductile than IPNs made with azobis(isobutyronitrile) (20).

IPN-modified polystyrene has been the subject of previous studies, including research by Millar, who formed a second polystyrene network within the original matrix (21), Sperling and Friedman, who modified the network with ethyl acrylate (22), and Kolarz, who used methyl methacrylate as the second network (23). IPNs also have been prepared as ion exchange resins. Polystyrene was functionalized with quaternary ammonium ligands within a polyethylene network (24), polystyrylsulfonic acid and polystyryltrimethylammonium ion ligands formed a network capable of both cation and anion exchange (25), and polystyryldimethylamine within polyacrylic acid formed a weak base–weak acid IPN (26).

The sequential synthesis of IPNs was adapted to the preparation of new dual-mechanism bifunctional polymers (27) that were developed as substrate-selective reagents. In the IPNs synthesized to date, polystyrene beads form the first matrix into which a second network with ion exchange or coordinating ligands or both is immobilized. Ideally, the selectivity of the bifunctional network will be greater than the selectivity of the corresponding monofunctional IPNs.

The objective of the current research is to define the manner in which bifunctional IPNs can be prepared and to understand whether their ability to complex substrates varies as a function of the ratio of ligands. Metal ions are used to probe the IPN environment. Binding constants, evaluated through Langmuir adsorption isotherms (28), are used to quantify changes in the microenvironment.

Experimental Details

The IPNs are synthesized from polystyrene beads that are cross-linked with 2% divinylbenzene (DVB). The 250–425- μm diameter polystyrene xerogel divinylbenzene beads were prepared by suspension polymerization wherein the organic phase consisted of 172 g of styrene, 6.50 g of technical grade DVB (55.4% *meta* and *para* isomers), 1.80 g of benzoyl peroxide, and 120 g of toluene as porogen.

Synthesis of the polystyrene–poly(*N*-vinylimidazole-*co*-acrylic acid) IPN is typical of the IPNs in this study. Monomer solution was prepared by dissolving 10.33 g of DVB, 16.99 g of *N*-vinylimidazole, 18.08 g of ethyl acrylate, and 1.55 g of azobis(isobutyronitrile) in enough toluene to give 85 mL of solution. The total concentration is 4.25 M in complexing monomers (2.125 M each in imidazole and acrylate; the *N*-vinylimidazole IPN is 4.25 M in imidazole alone). The solution was sparged with nitrogen for 5 min, then contacted overnight with 10 g of polystyrene. The beads swelled to 4.5 times their original volume. The second network was polymerized by adding the swollen beads to 134 g of an aqueous

solution of 1.5 wt% poly(vinyl alcohol) (based on the weight of monomers within the beads) and 70 g of CaCl_2 dihydrate. The mixture was stirred at 80 °C for 12 h, after which time the beads were washed with hot water and Soxhlet extracted with methanol for 17 h. The IPNs were then eluted with 1 L of H_2O , 1 N NaOH, H_2O , 1 N HCl, and H_2O . The ester groups were hydrolyzed to the acid by refluxing the beads in 250-mL of 2 N KOH in 90% aqueous dioxane for 72 h, then eluting with 2 L of H_2O , 1 L of 1 N HCl, and 1 L of H_2O . The imidazole IPN has a base capacity of 4.05 mequiv/g of dry resin, the carboxylate IPN has an acid capacity of 5.32 mequiv/g of dry resin, and the bifunctional IPN has acid–base capacities of 2.50/2.65 mequiv/g of dry resin. The analyses were made by acid or base titrations and confirmed by elemental analyses.

Metal ion solutions were prepared by dissolving varying amounts of metal nitrate and 0.06 equiv of acetic acid in 80 mL of H_2O , adjusting the pH to 5.00 with 6 N NaOH, and diluting the solution to 100 mL with water.

Binding isotherms were determined by contacting 1 mequiv of each IPN (0.2469-, 0.1880, and 0.1942 g of dry weight of the imidazole, acid, and bifunctional IPNs) with 10 mL of metal-containing buffer solution. The vials were shaken for 7 days on a wrist-action shaker to ensure that equilibrium had been reached. The concentration of metal remaining in solution was quantified with an atomic absorption spectrophotometer (Perkin-Elmer 3100). The wavelengths used for the analysis were 324.7 nm for Cu(II) and 240.7 nm for Co(II).

Results

Initial studies with bifunctional IPNs focused on the carboxylic acid ligand for ion exchange and the imidazole ligand for metal ion coordination. Acrylic acid was first tried as the monomer that would provide the ion exchange sites; ethyl acrylate was later found to be a better choice despite the fact that it necessitated a subsequent hydrolysis after IPN formation. The coordinating monomer was *N*-vinylimidazole.

The acid–base capacities of the imidazole, acid, and bifunctional IPNs were 0/4.05-, 5.32/0-, and 2.50/2.65-mequiv/g of dry resin, respectively. In each case, the calculated capacities based on monomer uptake were in agreement with experimental values, which indicates almost complete incorporation of monomer within the original polystyrene matrix. Fourier transform infrared (FTIR) analyses are consistent with IPN formation (29) as is a solid-state ^{13}C NMR study (Crick, D. W.; Alexandratos, S. D., in press, *Macromolecules*).

The binding constants for the imidazole, acid, and bifunctional IPNs were determined for Cu(II) and Co(II) in pH 5 acetate buffer solutions. The Cu(II) and Co(II) isotherms for the bifunctional IPN (Figure 1) are representative. Though the Cu(II) isotherm has not reached a well-defined plateau, no further data points were gathered because the inherent nonideality of the solutions at the required concentrations preclude their use in a Langmuir plot. The binding constants are calculated from an iterative solution of the

isotherm equation

$$r = (S_t c) / (K^{-1} + c) \quad (1)$$

where r is the milliequivalent complexed M^{n+} per gram of polymer, c is the corresponding milliequivalent M^{n+} in 1 mL of solution, S_t is the saturation capacity (milliequivalents per gram), and K is the binding constant (in units of reciprocal equivalents, i.e., normality). The binding constants for the IPNs are given in Table I. Note that the Cu(II) saturation capacity of the acid IPN (5.25 mequiv/g) is very close to the total capacity measured by base titration (5.32 mequiv/g), which indicates that IPN formation does not hinder ligand-substrate complexation.

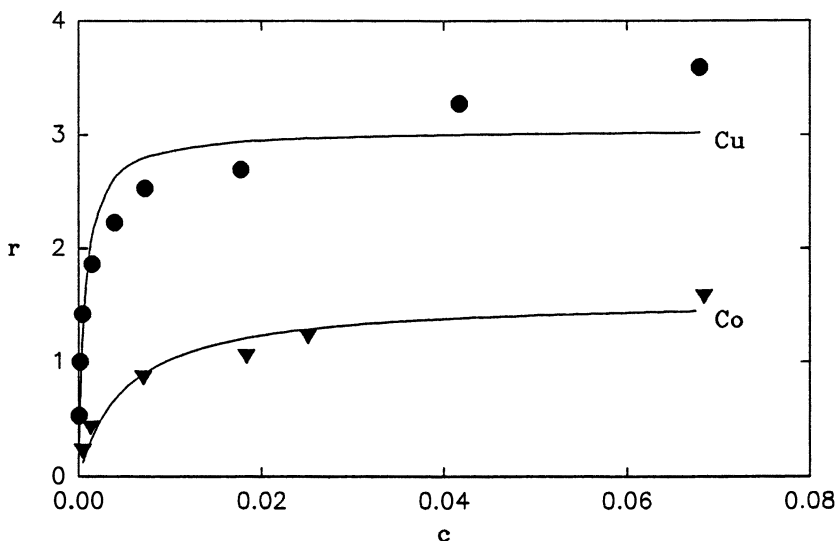


Figure 1. Adsorption isotherm plots for Cu(II) and Co(II) binding with the bifunctional poly(*N*-vinylimidazole-co-acrylic acid) polystyrene-based IPN.

Table I. Binding Constants (K) and Saturation Capacities (S_t) for the *N*-Vinylimidazole (VIm), Carboxylic Acid, and Bifunctional (VIm-Acid) IPNs for Cu(II) and Co(II) Complexation

IPN	$K(M^{-1})$	S_t (mequiv / g)
Cu(II) VIm	3130	2.37
Cu(II) Acid	77	5.25
Cu(II) VIm-acid	1556	3.05
Co(II) VIm	294	1.92
Co(II) Acid	26	3.06
Co(II) VIm-acid	189	1.56

Discussion

The substrate-complexing properties of ligands immobilized within a polymer network can be affected by the microenvironment formed by the polymer itself around the ligands (30). In the synthesis of IPNs and the study of their substrate recognition properties, it is important to define (1) whether different ligand ratios in the bifunctional IPNs are sensitive to variations in the structure of substrates and (2) what role the polymeric microenvironment plays in the complexation reaction. The role of polymeric microenvironments is addressed by the synthesis of a series of sequential IPNs from different initial supports [polystyrene, poly(methyl methacrylate), etc.] that will be reported in due course.

The results from the foregoing study show that bifunctional IPNs offer a different binding environment to metal ions than the monofunctional analogues. The use of copper and cobalt as the probe ions revealed that the bifunctional network is capable of distinguishing between different ions, depending on the inherent ligand ion affinities determined by monofunctional counterparts. Under the present conditions, the ligands interact with the metal ions in a noncooperative manner: the relationship between ligand ratio and binding constants is linear. The imidazole ligand has a binding constant that is 10 times greater for Cu(II) than for Co(II), and this selectivity is retained in the bifunctional IPN, though at a lower absolute value, which thus points to different binding environments for the two IPNs.

Current research is focused on definition of the conditions under which there is synergistic enhancement in the metal ion complexation reactions. Additional studies center on the microenvironmental effect, as previously defined, and on the influence of IPN morphology on substrate binding constants.

Acknowledgment

We gratefully acknowledge the support of the Department of Energy, Office of Basic Energy Sciences, through grant DE-FG05-86ER13591.

References

1. *Polymer-Supported Reactions in Organic Synthesis*; Hodge, P.; Sherrington, D. C., Eds.; Wiley: Chichester, United Kingdom, 1980.
2. *Syntheses and Separations Using Functional Polymers*; Sherrington, D. C.; Hodge, P., Eds.; Wiley: New York, 1988.
3. Merrifield, R. B. *J. Am. Chem. Soc.* **1964**, *86*, 304.
4. Frechet, J. M.; Schuerch, C. *J. Am. Chem. Soc.* **1971**, *93*, 492.
5. Nishide, H.; Tsuchida, E. *Makromol. Chem.* **1976**, *177*, 2295.
6. Wulff, G.; Grobe-Einsler, R.; Vesper, W.; Sarhan, A. *Makromol. Chem.* **1977**, *178*, 2817.

7. Kuchen, W.; Schram, J. *Angew. Chem. Int. Ed. Engl.* **1988**, *27*, 1695.
8. Warshawsky, A.; Kahana, N. *J. Am. Chem. Soc.* **1982**, *104*, 2663.
9. Pearson, R. G. *J. Am. Chem. Soc.* **1963**, *85*, 3533.
10. Hudson, M. J. In *Ion Exchange Technology*; Naden, D.; Streat, M., Eds.; Ellis Horwood: Chichester, United Kingdom, 1984.
11. Alexandratos, S. D. *Sep. Purification Methods* **1992**, *21*, 1.
12. Alexandratos, S. D.; Quillen, D. R.; Bates, M. E. *Macromolecules* **1987**, *20*, 1191.
13. Alexandratos, S. D.; Crick, D. W.; Quillen, D. R. *Ind. Eng. Chem. Res.* **1991**, *30*, 772.
14. Klemperer, D.; Berkowski, L. *Encyclopedia of Polymer Science and Engineering*, 2nd ed.; Wiley: New York, 1987; Vol. 8.
15. Sperling, L. H. *Interpenetrating Polymer Networks and Related Materials*; Plenum: New York, 1981.
16. Li, B.; Bi, X.; Zhang, D.; Wang, F. *Polymer* **1992**, *33*, 2740.
17. Donnatelli, A. E.; Sperling, L. H.; Thomas, D. A. *J. Appl. Polym. Sci.* **1977**, *21*, 1189.
18. Huelck, V.; Thomas, D. A.; Sperling, L. H. *Macromolecules* **1972**, *5*, 340.
19. Huelck, V.; Thomas, D. A.; Sperling, L. H. *Macromolecules* **1972**, *5*, 348.
20. Roha, M.; Wang, B. *J. Appl. Polym. Sci.* **1992**, *45*, 1367.
21. Millar, J. R. *J. Chem. Soc.* **1960**, 1311.
22. Sperling, L. H.; Friedman, D. W. *J. Polym. Sci., Polym. Phys. Ed.* **1969**, *7*, 425.
23. Kolarz, B. N. *Angew. Makromol. Chem.* **1980**, *90*, 167.
24. Czarczynska, H.; Trochimczuk, W. *J. Polym. Sci., Polym. Symp.* **1974**, *47*, 111.
25. Solt, G. S. Br. Patent 728,508, 1955.
26. Hatch, M. J. U.S. Patent 3,957,698, 1976.
27. Alexandratos, S. D.; Crick, D. W.; Quillen, D. R. *Ind. Eng. Chem. Res.* **1991**, *30*, 772.
28. Connors, K. A. *Binding Constants*; Wiley: New York, 1987.
29. Alexandratos, S. D.; Grady, C. E.; Crick, D. W. *Macromolecules* **1991**, *24*, 6365.
30. Warshawsky, A. *Isr. J. Chem.* **1979**, *18*, 318.

RECEIVED for review November 26, 1991. ACCEPTED revised manuscript September 10, 1992.

Hydrophilic–Hydrophobic Interpenetrating Polymer Networks and Semi-interpenetrating Polymer Networks

F. O. Eschbach and S. J. Huang

University of Connecticut, Institute of Materials Science, U-136,
Storrs, CT 06269–3136

Poly(2-hydroxyethyl methacrylate) (PHEMA) in the water-swollen state is a very soft hydrogel with high water content. Therefore, it is similar to natural tissues and is widely used as a biomaterial. Unfortunately, PHEMA hydrogels have low mechanical strength and tear resistance. The incorporation of hydrophobic polycaprolactone (PCL) improves the mechanical properties of the swollen networks and preserves their biocompatibility. Three ways to combine PHEMA and PCL were investigated. Semi-interpenetrating polymer networks of PHEMA and low molecular weight PCL diol were prepared. Interpenetrating polymer networks of PHEMA and high molecular weight PCL were synthesized using two different methods depending upon the relative composition (PHEMA:PCL). Mechanical, thermal, and swelling properties were investigated.

HYDROGELS ARE POLYMERIC NETWORKS HELD TOGETHER by cross-links or weaker cohesive forces such as hydrogen or ionic associations. These networks retain a large quantity of water within their structure without dissolving. Many natural materials of plant and animal origin are hydrogels. Because of their similarity to natural hydrogels, synthetic hydrogels hold promise for use as biomaterials. The first polymeric synthetic hydrogel intended for use as a biomaterial was poly(2-hydroxyethyl methacrylate) (PHEMA), which was first described and synthesized by Lim and Wichterle in 1960 (1). Currently, PHEMA hydrogels are widely used as biomaterials (2). High water content

and softness in the water-swollen state impart the quality of natural tissue to these materials (2, 3). Moreover, the high water permeability of these hydrogels allows easy purification before implantation. Likewise, diffusion of biofluids and nutrients through the hydrogel prosthesis after implantation is permitted. Unfortunately, PHEMA hydrogels possess low mechanical strength and tear easily when swollen in water. These adverse properties limit applications to low-strength uses such as contact lenses and suture coatings (2).

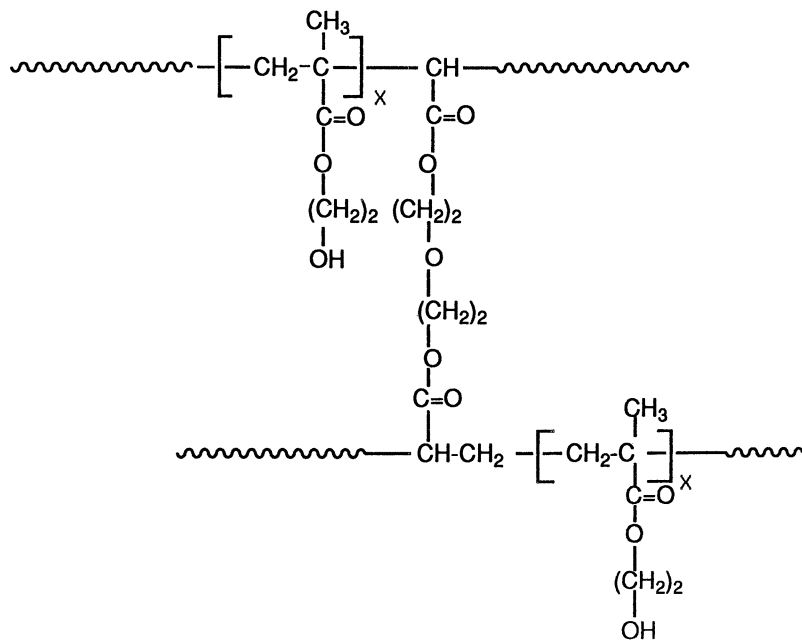
Various modifications of PHEMA hydrogels to improve their mechanical properties in the swollen state have been investigated. Mixed results were obtained from attempts to incorporate particulates such as glass beads (3, 4) and SiO_2 (5) as well as to copolymerize PHEMA with small amounts of maleic acid or maleic anhydride (6, 7). These methods resulted in poor water absorption in the modified PHEMA hydrogels. We successfully incorporated low molecular weight linear polycaprolactone (PCL) in the cross-linked PHEMA network. The resulting network showed improved mechanical properties in the swollen state (6–8) while high equilibrium water content and high permeability were maintained. Hence, the positive attributes that make PHEMA hydrogels exceedingly biocompatible were maintained. However, the incorporation of biodegradable PCL in the network resulted in a phase-separated biodegradable network that had mechanical integrity susceptible to change in aqueous media, due to the degradation of the PCL phase. Even though biodegradable hydrogels are of potential interest for some specific applications such as artificial tendons (8), the rate of degradation of the implant must be controlled to closely follow the healing process characterized by the formation of new connective tissue.

In this study we improved the mechanical properties of PHEMA hydrogels by independently cross-linking a hydrophobic network within the cross-linked PHEMA network. This mixture of two independently cross-linked polymers that cannot be physically separated is an interpenetrating polymer network (IPN) (9). If only one of the two polymers is cross-linked, the product is called a semi-interpenetrating polymer network (SIPN). The simultaneous interpenetration of two cross-linked polymers imparts the resultant network with outstanding mechanical properties (toughness, impact strength, tensile modulus). Synergistic mechanical and thermal behaviors also have been observed (10). The influence of polycaprolactone on the properties of the resultant modified PHEMA hydrogels SIPNs and IPNs was investigated. The networks were evaluated in terms of structural, mechanical, and thermal properties.

Experimental Details

Materials. IPNs and SIPNs that consist of a hydrophobic component and a hydrophilic component were investigated.

The hydrophilic network was a cross-linked PHEMA network (Structure 1) that was synthesized from the monomer 2-hydroxyethyl methacrylate (HEMA)

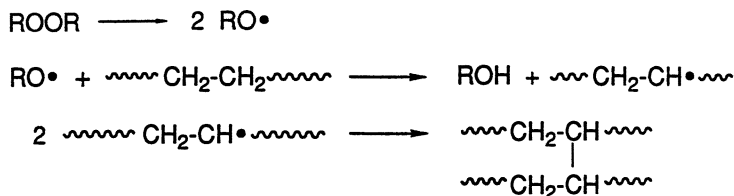


Structure 1. Cross-linked PHEMA network.

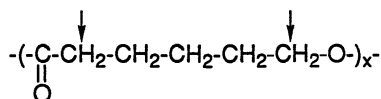
with ethylene glycol dimethacrylate (EGDMA) used as the cross-linking agent. The free radical initiator selected to cross-link the PHEMA network in the SIPNs was benzoyl peroxide. Azobis(isobutyronitrile) (AIBN) was selected to cross-link the PHEMA networks in the IPN.

The hydrophobic component was polycaprolactone (PCL). Low molecular weight PCL diol ($M_n = 2000$ g/mol) (Aldrich) was selected to synthesize the semi-interpenetrating polymer networks (SIPNs). The interpenetrating polymer networks (IPNs) were synthesized using high molecular weight PCL ($M_n = 42,000$ g/mol) (Aldrich) cross-linked with dicumyl peroxide. The mechanism of cross-linking polymers in the presence of peroxide free radical initiators is illustrated in Scheme 1. The hydrogens most likely to be abstracted by the peroxide radical from the PCL polymer chain are those located next to the carbonyl or next to the oxygen in the PCL repeat unit (Structure 2). Cross-links between the linear PCL polymer chains are established via carbon-carbon bonds. The cross-linking mechanism of PCL has been characterized previously in our laboratories (11, 12).

Synthesis. Synthesis of SIPNs. Polycaprolactone of low molecular weight ($M_n = 2000$ g/mol) was selected for the synthesis of the SIPNs. Two concentrations of PCL were investigated: 10 and 20% w/w, based on the weight of HEMA. PCL was dissolved in HEMA monomer at 70 °C at concentrations of 10 and 20% w/w based on the weight of HEMA. After the solution was cooled, 1% w/w of EGDMA and 1% w/w of benzoyl peroxide were added to the



Scheme 1. Cross-linking mechanism with peroxide free radical initiator.
(Reproduced with permission from reference 13. Copyright 1981.)



Structure 2. Hydrogen abstracted from PCL by peroxide free radical initiator.

mixture of HEMA and PCL. The mixed solution was injected with a syringe into molds fabricated from silicone gaskets sandwiched between two pieces of Mylar-lined glass plates. The clear solution was kept at 60 °C, above the melting point of PCL, for 1 h to ensure proper dispersion of the PCL phase and was subsequently cured at 90 °C for 1 h leading to a white opaque film. Soxhlet extraction with methylene chloride was performed on the SIPN that contained 10% w/w of PCL. The percentage of material extracted was 12% based on the weight of the dry sample.

Synthesis of IPNs. Two ways to synthesize IPN networks, dependent on the relative concentration of PHEMA and PCL, were investigated: sequential IPN and simultaneous IPNs.

Sequential IPN. For networks with a high content of cross-linked PCL, a sequential IPN was synthesized. The method adopted to synthesize this IPN is shown schematically in Figure 1. High molecular weight PCL ($M_n = 42,000$ g/mol) was mixed with 1% w/w of dicumyl peroxide in methylene chloride solvent. After evaporation of the solvent, PCL was cured at 130 °C for 5 h. The PCL network was then swollen in a mixed solution of HEMA (99% w/w), EGDMA (1% w/w), and AIBN (0.1% w/w) for 24 h. PHEMA was then cured at 90 °C for 1 h in situ. A PHEMA concentration of 10% w/w (based on the weight of cross-linked PCL) was obtained upon swelling of HEMA, EGDMA, and AIBN. Soxhlet extraction with methylene chloride was performed on the IPN. The percentage of material extracted was 30% based on the weight of the dry sample.

Simultaneous IPN. For networks with high content of PHEMA, a simultaneous IPN was synthesized. The method adopted to synthesize this IPN is shown schematically in Figure 2. HEMA, EGDMA 1% w/w, and high molecular weight PCL ($M_n = 42,000$ g/mol) were mixed above the melting point of PCL to form a homogenous solution. Two concentrations of PCL were investigated: 10 and 20% w/w based on the weight of HEMA. The free radical initiators AIBN (0.1% w/w) and dicumyl peroxide (1% w/w) were added after the solution was cooled. The mixed solution was injected with a syringe into molds fabricated from silicone gaskets sandwiched between two pieces of Mylar-lined glass plates. The

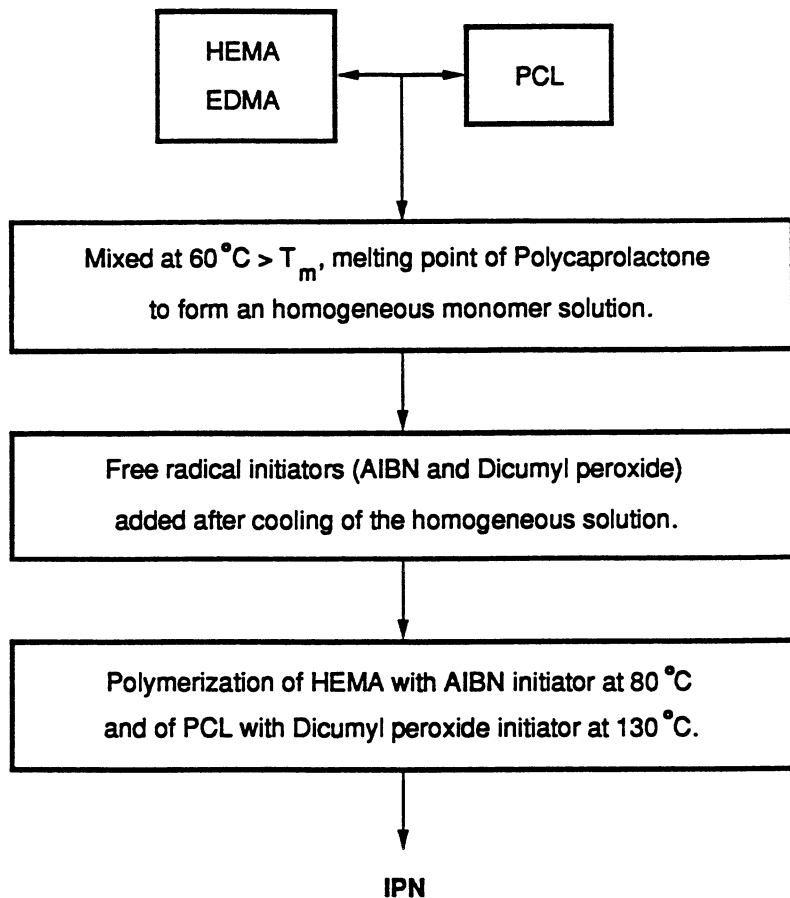


Figure 1. Sequential IPN synthesis scheme.

clear solution was kept at a 60 °C, above the melting point of PCL, for 1 h to ensure proper dispersion of the PCL phase. The PHEMA network was then polymerized with AIBN at 80 °C for 1 h and, in a second step, PCL was cross-linked with dicumyl peroxide at 150 °C for 5 h, which led to an opaque film. Two noncompeting methods were employed to independently cross-link one component in the presence of the other, which produced the intimate network characteristics of IPNs. Table I illustrates the selectivity of the free radical initiators chosen for this IPN synthesis approach. HEMA is very reactive and the carbon-carbon double bond will react with any type of free radical initiator; thus AIBN was chosen to cross-link PHEMA. PCL requires a stronger free radical initiator to be cross-linked. Radicals from a peroxide initiator will be reactive enough to abstract hydrogens from the main polymer chain. At 80 °C, AIBN has a half-life of approximately 1 h. Because 80 °C is below the self-accelerating decomposition temperature (SADT) of dicumyl peroxide (91 °C), heating the system at 80 °C cures the PHEMA network without cross-linking PCL. Then, by increasing the temperature above the SADT of dicumyl peroxide, the PCL

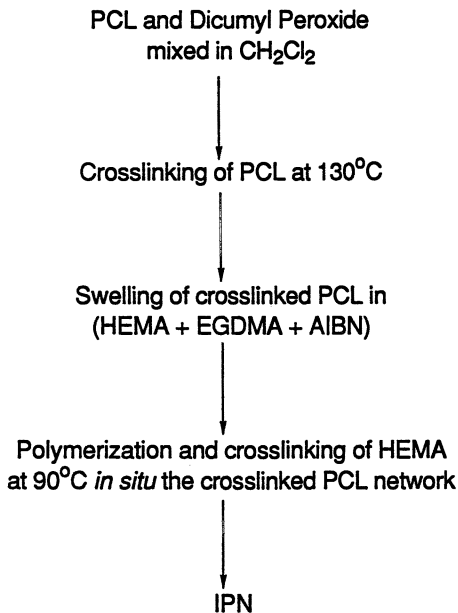


Figure 2. Simultaneous IPN synthesis scheme.

network is formed in a second step within the cross-linked PHEMA network. Soxhlet extraction with methylene chloride was performed on the IPN that contained 10% w/w of PCL. The percentage of material extracted was 9% based on the weight of the dry sample.

Characterization. The mechanical performances of the modified PHEMA networks both in the dry and swollen states were evaluated on a tensile tester (Instron model 1011). The SIPNs and simultaneous IPNs in the dry and swollen states met the requirements of the standard test for tensile properties of plastics (ASTM D-638, type II). The cross-linked PCL networks as well as the sequential IPNs were tested in the dry state and met the requirements of ASTM D-638, type V.

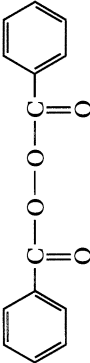
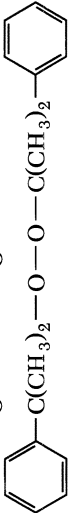
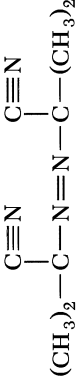
The thermal characterization of the networks was carried out on a differential scanning calorimeter (Perkin-Elmer DSC-7). The melting and glass transition temperatures of the networks as well as the crystallization of polycaprolactone in the IPNs and SIPNs were determined. The reported melting temperature was determined as the peak temperature.

The SIPNs and simultaneous IPNs were characterized in terms of equilibrium water content. Swelling experiments were performed by placing the samples in a bath of distilled water at 20 °C. Water absorption was determined by weighing the specimens at given time intervals until an asymptotic value of water uptake was reached.

Theory

The opacity of the PHEMA-PCL networks as well as previous scanning electron microscopy (SEM) results (6, 7) on PHEMA-PCL SIPNs confirms

Table I. Free Radical Initiators

<i>Free Radical</i>	SADT ^a (°C)	Temperature (°C)	Half-Life
	66	70 100	7.3 h 19.8 min
	91	132	115 h 13 h
	22	50 70 100	74 h 4.8 h 7.2 min

^a SADT, self-accelerating decomposition temperature.
SOURCE: Data are from reference 13.

phase separation between the two components. Several theoretical models of particulate-filled composites that cover a wide range of matrix–inclusion interactions were investigated in an attempt to interpret the mechanical behavior of the PHEMA–PCL networks in the dry state.

Stress-at-Break. The Nicolais–Narkis equation (eq 1) predicts the stress-at-break of nonadhering composites with a steady decrease of the stress-at-break of the composite with increasing particulate content (14). The Nicolais–Narkis equation was used to evaluate the stress-at-break of PHEMA–PCL nonadhesion particulate-filled composites:

$$\frac{\sigma_c}{\sigma_m} = 1 - 1.21(V_f)^{2/3} \quad (1)$$

where σ_c is the stress-at-break of the composite, σ_m is the stress-at-break of the matrix, and V_f is the volume fraction of the filler. The theoretical predictions of the Nicolais–Narkis equation were compared with the experimental stress-at-break of the SIPNs and sequential IPNs.

Tensile Modulus. Nielsen's equation (15, 16) predicts the shear or tensile moduli of particulate-filled composites. Nielsen's equation was used to evaluate the theoretical tensile modulus of PCL–PHEMA composites in the case of inclusions of PHEMA within the cross-linked PCL matrix:

$$\frac{E}{E_1} = \frac{1 + AB\Phi_2}{1 - B\Psi\Phi_2} \quad (2)$$

where E is the modulus of the composite and E_1 is the modulus of the matrix. The constant A is defined by

$$A = \frac{7 - 5\nu_1}{8 - 10\nu_1} \quad (3)$$

where ν_1 is defined as the Poisson's ratio of the matrix.

The constant B is defined by

$$B = \frac{(E_2/E_1) - 1}{(E_2/E_1) + A} \quad (4)$$

where E_1 is the modulus of the matrix and E_2 is the modulus of the filler. Φ_2 is the volume fraction of the particulate and Ψ is defined by

$$\Psi = 1 + \left(\frac{1 - \Phi_m}{\Phi_m^2} \right) \Phi_2 \quad (5)$$

where Φ_m is the maximum packing fraction of the particles.

Results and Discussion

SIPNs in the Dry State: Mechanical Characterization. Table II summarizes the mechanical properties of the networks in the dry state. The theoretical stress-at-break predicted by the Nicolais–Narkis equation of PHEMA–PCL particulate-filled composites was compared with the experimental stress-at-break of the SIPNs. In the Nicolais–Narkis equation, the stress-at-break of cross-linked PHEMA was used as the stress-at-break of the matrix ($\sigma_m = 56.5$ MPa, experimentally determined) with volume fractions of 0.1 and 0.2 as filler concentrations that correspond to the concentration of PCL in the SIPNs.

Figure 3 shows the experimental stress-at-break of a cross-linked PHEMA network and PHEMA–PCL SIPNs, that contain, respectively, 10 and 20% w/w of low molecular weight PCL diol (2000 g/mol). The effective loss of strength of the PHEMA–PCL composite with increasing content of PCL is more important than predicted by the Nicolais–Narkis equation. This observation suggests that the PCL domains behave like areas of stress concentration in the PHEMA matrix.

Table II. Mechanical Properties of PHEMA–PCL Network in the Dry State

<i>Material</i>	<i>Stress-at-Break (MPa)</i>	<i>Tensile Modulus (MPa)</i>
PHEMA		
SIPN	56.5 ± 13	1450 ± 350
10% w/w PCL	25.3 ± 5	1550 ± 205
SIPN		
20% w/w PCL	16.6 ± 2	522 ± 32

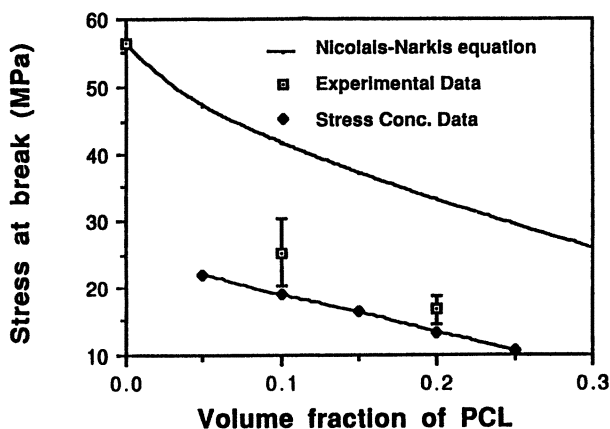


Figure 3. Stress-at-break of PHEMA–PCL SIPNs in the dry state.

Guild and Young developed a model for soft-particulate-filled composites subjected to stress concentration (17). Finite element analysis was carried out for a sphere centered in a cylinder of resin. A stress concentration factor was determined for various particle sizes that correspond to various module fractions of the filler. We used a concentration factor of 2 to predict the theoretical stress-at-break of nonadhesion-particulate-filled composites in the case of stress concentration between the matrix and the filler. Figure 3 illustrates the results. The location of the experimental data points between the two theoretical curves confirms the presence of stress concentration between PHEMA and PCL inclusions in the SIPNs.

Sequential IPN in the Dry State. Mechanical Characterization.

Table III summarizes the mechanical properties of the networks at each step of the sequential IPN synthesis scheme. The content of PHEMA in the sequential IPN was 10% w/w.

Stress-at-Break. The Nicolais–Narkis equation was used to predict the stress-at-break of cross-linked PCL particulate-filled composites with cross-linked PHEMA inclusions. The stress-at-break of cross-linked PCL was used as the stress-at-break of the matrix ($\sigma_m = 17$ MPa, experimentally determined) and a volume fraction of 0.1 was used as the concentration of the filler (cross-linked PHEMA). As shown on Figure 4, the strength of PCL increases upon cross-linking. No increase in the stress-at-break of the sequential IPN is observed. This result suggests phase separation between PCL and PHEMA in the IPN. However, the experimental stress-at-break of the IPN is higher than the stress-at-break predicted by the Nicolais–Narkis equation, which suggests good interaction between cross-linked PCL and cross-linked PHEMA.

Tensile Modulus. Nielsen's equation was used to predict the tensile modulus of cross-linked PCL particulate-filled composites with cross-linked PHEMA inclusions. The constant A was calculated by assuming a value of 0.3 for Poisson's ratio of cross-linked PCL ($\nu_1 = 0.3$). The constant B was calculated by considering cross-linked PCL as the matrix and cross-linked PHEMA as the filler. The modulus of cross-linked PCL was experimentally

Table III. Mechanical Properties of Sequential IPN

<i>Material</i>	<i>Stress-at-Break (MPa)</i>	<i>Tensile Modulus (MPa)</i>	<i>Strain-at-Break (%)</i>	<i>Strain at Necking (%)</i>
PCL	14.49 ± 1.11	233 ± 35	804 ± 354	23.3 ± 5.2
Cross-linked PCL 1% w/w of dicumyl peroxide	17.03 ± 0.47	285 ± 20	325 ± 68	9.6 ± 0.8
Sequential IPN (10% w/w of PHEMA)	15.8 ± 2.55	339 ± 49	149 ± 33	6.6 ± 1.1

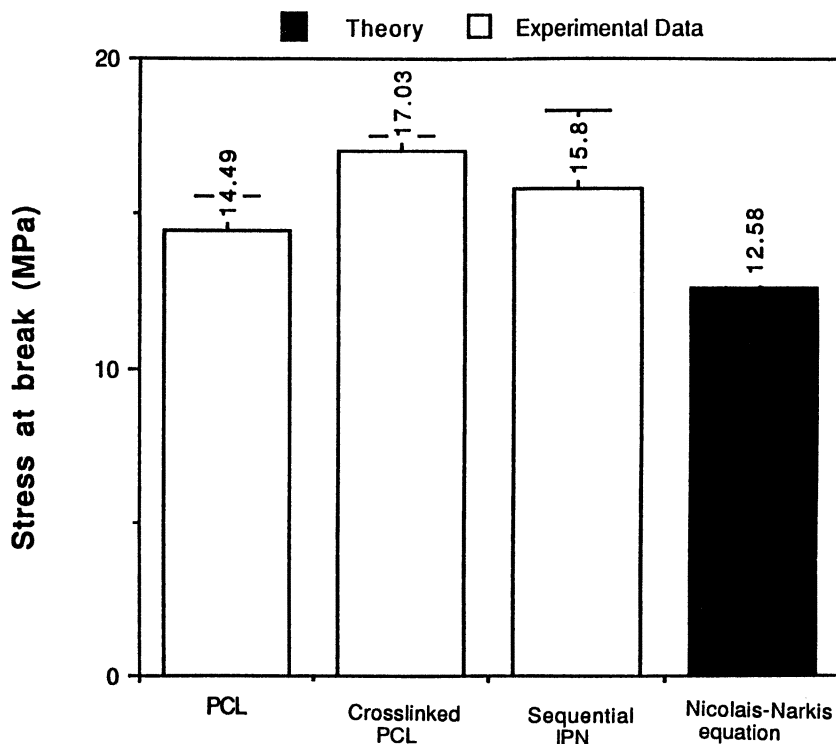


Figure 4. Stress-at-break of sequential IPN.

determined to be $E_1 = 285$ MPa (Table III). The modulus of cross-linked PHEMA in the dry state was experimentally determined to be $E_2 = 1450$ MPa (Table II). A value of 1 was used for the maximum packing fraction of PHEMA particulates, Φ_m . The experimental results and theoretical prediction of Nielsen's equation are shown Figure 5. The experimental tensile modulus increases at each step of the sequential IPN synthesis scheme. Each successive cross-linking reaction (PCL in a first step and PHEMA in a second step) leads to a tighter network. It should be noted that the experimental tensile modulus of the sequential IPN is higher than the modulus of particulate-filled composites as predicted by Nielsen's equation. This high value of tensile modulus can be explained by an increase in cross-link density that results from the interpenetration of the PCL and PHEMA networks in the IPN structure.

Strain-at-Break and Yielding Strain. The experimental results obtained for the strain-at-break and yielding strain (Table III and Figure 6) confirm the observations made for the tensile modulus. A gradual decrease in the strain-at-break and yielding strain (or strain at necking) is observed at each

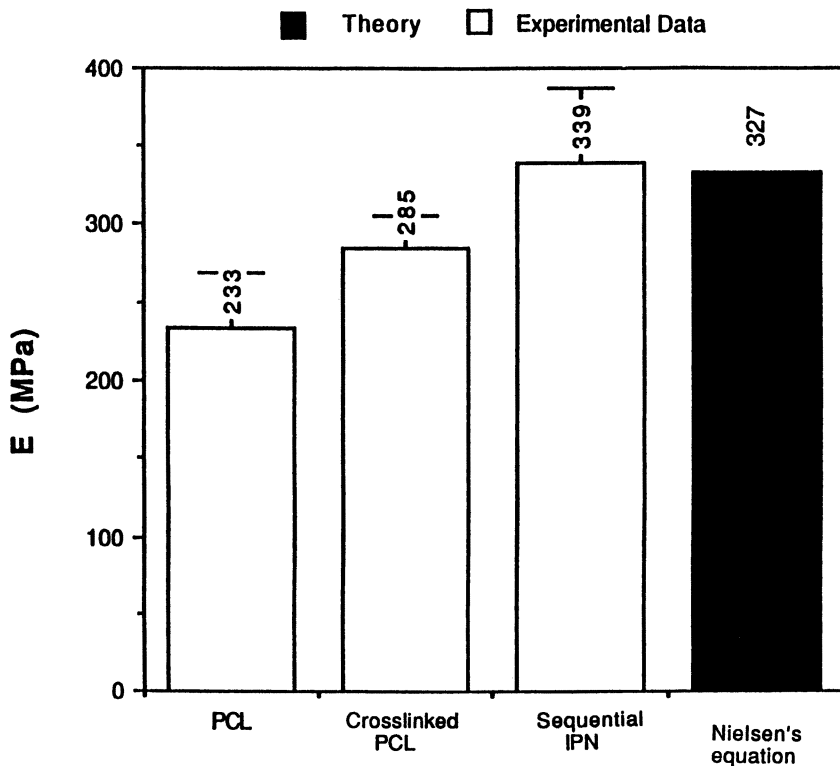
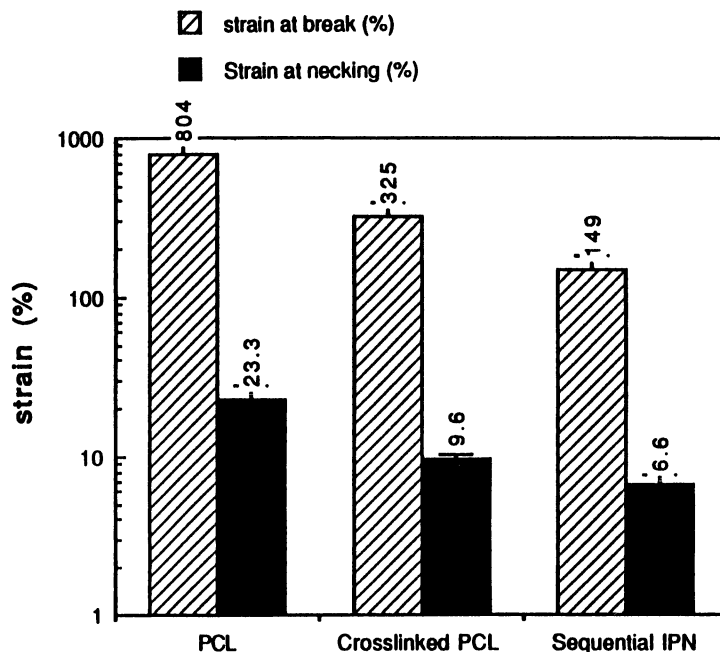


Figure 5. Tensile modulus of sequential IPN.

step of the sequential IPN synthesis scheme. This observation confirms the presence of a more constrained network. Figure 6 reports the ratio (strain at break:strain at necking) that is comparable for PCL (32.5) and cross-linked PCL (33.8). For the sequential IPN the strain-at-break is reduced to 22.5 times the strain at necking and confirms the introduction of the brittle PHEMA component to the network.

Thermal Characterization. Table IV shows the melting transition temperatures as well as the corresponding crystallinity of the PCL component for samples taken at each stage of the sequential IPN synthesis scheme. The melting transitions and heat of fusion were determined by DSC and a value of 142 J/g was used as the heat of fusion of 100% crystalline PCL (18). A drop of almost 50% in the crystallinity of PCL was observed upon cross-linking. The peak melting temperature of cross-linked PCL also decreased as a result of this decrease in crystallinity. There was no noticeable change in crystallinity between cross-linked PCL and the sequential IPN. This result confirms the assumption that AIBN will not initiate the cross-linking of PCL.



$$\frac{\text{(Strain at break)}}{\text{(Strain at necking)}} = \begin{matrix} 32.5 & 33.8 & 22.5 \end{matrix}$$

Figure 6. Strain-at-break and strain at yielding of sequential IPN.

Table IV. Crystallinity of PCL Network

Material	Melting Temperature (°C)	PCL Crystallinity (%)
PCL	59.8	70
Cross-linked PCL 1% w/w of Dicap	53.7	36
Sequential IPN 10% w/w PHEMA	47.7	33

The decrease in the melting temperature of the cross-linked PCL component in the sequential IPN can be explained by the miscibility of residual unreacted HEMA and PCL in the IPN network.

SIPNs and Simultaneous IPNs in the Swollen State. Mechanical Properties. Table V summarizes the mechanical properties of PHEMA hydrogel, SIPNs, and simultaneous IPNs swollen in distilled water at 20 °C. The samples were tested when the equilibrium water content of the networks was reached.

Table V. Mechanical Properties of PHEMA–PCL Networks Swollen in Water

<i>Material</i>	<i>Swelling in Water (%)</i>	<i>Stress at Break (kPa)</i>	<i>Tensile Modulus (kPa)</i>	<i>Strain at Break (%)</i>
PHEMA	55	607 ± 53	748 ± 41	68 ± 9
SIPN				
10% w/w PCL	45	1472 ± 30	1682 ± 90	80 ± 15
IPN				
10% w/w PCL	47	1303 ± 300	2339 ± 304	71 ± 15
IPN				
20% w/w PCL	39.5	2964 ± 214	6643 ± 761	75 ± 14

Stress-at-Break. Based on the stress-at-break of the PHEMA hydrogel, an increase of 142% in the stress-at-break of the swollen SIPN containing 10% w/w of PCL was observed. A 388% increase in stress-at-break was obtained with the swollen IPN that contained 20% w/w of PCL.

Tensile Modulus. The same trend was observed for the tensile modulus with an increase of 125% for the SIPN that contained 10% w/w of PCL, an increase of 212% for the IPN that contained 10% w/w of PCL, and an increase of 788% for the IPN that contained 20% w/w of PCL.

Strain-at-Break. Comparison of the SIPN and the simultaneous IPN, both of which contain the same amount of PCL (10% w/w) reveals that the tensile modulus of the IPN is higher than the modulus of the SIPN and the strain-at-break of the IPN is lower than the strain-at-break of the SIPN. These observations confirm that the IPN where both PCL and PHEMA are cross-linked is a tighter network than the corresponding SIPN that contains the same amount by weight of linear PCL.

Equilibrium Water Content. The networks were characterized in terms of equilibrium water content. It is important to verify that the incorporation of a hydrophobic component in the PHEMA network will not drastically affect the attributes of high water content that make PHEMA hydrogels extremely biocompatible. The swelling in water reported in Table V is defined as

$$\frac{\text{weight of swollen polymer at equilibrium} - \text{weight of dry polymer}}{\text{weight of dry polymer}}$$

It is of interest to note that for only 20% drop in equilibrium water content for the IPN that contains 20% w/w of PCL, the tensile modulus ($E = 6643$ kPa) is almost a factor of 10 higher compared to the PHEMA hydrogel ($E = 748$ kPa).

Summary

This study was motivated by the need for artificial tissue material. Previous work showed that the incorporation of low molecular weight PCL into soft PHEMA hydrogels was successful in strengthening the hydrogel (3–9). The approach presented here involves the synthesis of a more sophisticated network structure that holds promise for the development of truly mechanically useful artificial implants. The study of diverse hydrophobic polyester components and biodegradability and biocompatibility of the IPNs are under investigation.

Acknowledgments

The authors wish to thank P. A. Davis (Advanced Cardiovascular Systems), L. Nicolais, L. Ambrosio, and S. Iannace (University of Naples) for helpful discussions. Aid-in-Education from Hercules and the Kingsley High Technology are gratefully acknowledged.

References

1. Wichterle, O.; Lim, D. *Nature (London)* **1960**, *185*, 117–118.
2. *Hydrogels for Medical and Related Applications*; Andrade, A. D., Ed.; ACS Symposium Series 31; American Chemical Society: Washington, DC, 1976.
3. Nicolais, L.; Acierno, D.; Janacek, J. *Polym. Eng. Sci.* **1975**, *15*, 35–39.
4. Acierno, D.; Nicolais, L.; Vojta, V.; Janacek, J. *J. Polym. Sci., Polym. Phys. Ed.* **1975**, *13*, 703–714.
5. Ilavsky, M.; Hasa, J.; Janacek, J. *Int. J. Polym. Mater.* **1972**, *1*, 187.
6. Davis, P. A.; Huang, S. J.; Nicolais, L.; Ambrosio, L. In *High Performance Biomaterials*; Szycher, M., Ed.; Technomic Publishing: Lancaster, PA, 1991; pp 343–368.
7. Davis, P. A.; Ambrosio, L.; Huang, S. J. *J. Bioact. Compat. Polym.* **1988**, *3*, 205–218.
8. Davis, P. A. Ph.D. Thesis, University of Connecticut, Storrs, CT, 1990.
9. Sperling, L. H. *Interpenetrating Polymer Networks and Related Materials*; Plenum: New York, 1981.
10. Sperling, L. H. *Polym. Eng. Sci.* **1985**, *25*, 517–520.
11. Jarret, P. K.; Benedict, C. V.; Bell, J. P.; Cameron, J. A.; Huang, S. J. *Biomedical Applications of Polymers*; Hoffman, H.; Shalaby, S., Eds.; Plenum: New York, 1984; pp 181–192.
12. Jarret, P. K. Ph.D. Thesis, University of Connecticut, Storrs, CT, 1983.
13. Odian, G. *Principles of Polymerization*; Wiley: New York, 1981.
14. Nicolais, L.; Narkis, M. *Polym. Eng. Sci.* **1966**, *11*, 194.
15. Lewis, T. B.; Nielsen, L. E. *J. Appl. Polym. Sci.* **1970**, *14*, 1449.
16. Nielsen, L. E. *J. Appl. Phys.* **1970**, *41*, 4626.
17. Guild, F. J.; Young, R. J. *J. Mater. Sci.* **1989**, *24*, 2454–2460.
18. Wunderlich, B. *Macromolecular Physics*; Academic: New York, 1973; Vol. 3.

RECEIVED for review November 11, 1991. ACCEPTED revised manuscript October 15, 1992.

Simultaneous Interpenetrating Network Materials Derived from Reaction of Organostannane Dihalides

With Lignin and Hydroxyl-Capped Poly(ethylene oxide) and ABA Block Copolymers

Charles E. Carraher, Jr.¹, Dorothy C. Sterling¹, Thomas H. Ridgway², William Reiff³, and Bhoomin Pandya¹

¹Department of Chemistry, Florida Atlantic University, Boca Raton, FL 33431

²Department of Chemistry, University of Cincinnati, Cincinnati, OH 45221

³Mössbauer Spectroscopy Consultants, Burlington, MA 01803

Simultaneous interpenetrating network materials have been formed from the interfacial polycondensation of organotin halides with lignin and hydroxyl-capped poly(ethylene oxide) and ABA block copolymers where A is polyethylene glycol and B is poly(dimethylsiloxane). Structural characterization includes Fourier transform infrared spectroscopy, Mössbauer spectroscopy, elemental analysis, and electron ionization mass spectroscopy. Ion fragments that contain moieties from the organotin, lignin, and hydroxyl-capped coreactants are found.

LIGNIN RANKS SECOND ONLY TO SACCHARIDES AS A NATURAL, renewing material. Lignin is produced at an annual rate of about 2×10^{10} tons and is present in the biosphere in over 10 times this amount. Lignin is produced in mills at an annual rate of about 5×10^7 tons (1–3). Only about 2% of this lignin is isolated for further use; the remainder is discarded or burned as fuel. Lignin sulfonates are the most widely employed industrial surfactant (1), and they also have been reacted with a number of agents to take advantage of low

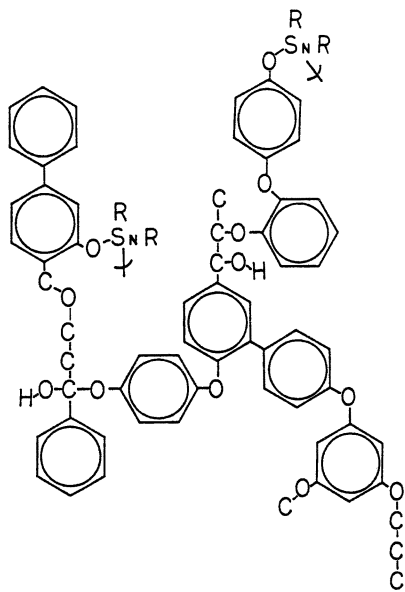
cost and high availability to produce feedstock. Lignin has been incorporated into phenol–formaldehyde resins (4–6) and reacted with isocyanates (7–12), alkene oxides (13–16), and epichlorohydrin-forming epoxy resins (17, 18). Even so, lignin remains a largely underused material.

We recently reported on the reaction between lignin and organostannane halides (19). As expected, products derived from reaction with dihalides were cross-linked, whereas products derived from monohalides were not. The products were “brick dustlike” in nature and showed no flexibility. This lack of flexibility was due to the rigid nature of the phenol groups present in the lignin and connected through hydrogen bonding. These products are depicted in structure 1 for materials derived from trialkyltin halides.

The present chapter reports attempts to produce flexible products by employing flexibilizing groups. Flexibilizing groups typically include methylene, ethylene oxide, and siloxane moieties (20). To increase the flexibility of lignin, hydroxyl-capped polyethylene glycol and hydroxyl-capped block copolymers of poly(ethylene oxide-*co*-dimethylsiloxane-*co*-ethylene oxide) were investigated as potential flexibilizing agents. The emphasis in this chapter is on structural results.

Experimental Details

Chemicals. Chemicals were used as received. Indulin AT, which is a purified (typically greater than 99%) form of lignin obtained from the krafting process, was a gift from Westva Company (Charleston, SC). The hydroxyl-capped compounds were all obtained from Petrarch (Briston, PA) and the organostannane dichlorides were obtained from Aldrich (Milwaukee, WI). The percentage



Structure 1. Portion of lignin product from reaction with dialkyltin chlorides.

of hydroxyl present in the lignin was determined by use of a modification of the procedure given in reference 21. The modifications are reported in reference 19. Analysis showed that the employed lignin had 1.14-mequiv/g phenolic hydroxyl and 8% catechol and other aromatic hydroxyls. The remainder of the lignin content was aliphatic hydroxyls with a total hydroxyl content of 3.30-mequiv/g or 59 hydroxyls for every 100 C₉ units. The employed lignin had a weight-average molecular weight of 3500 Da and a number-average molecular weight of 1600 Da. Structure 1 has a molecular weight of about 1600 Da for the lignin portion.

Reaction Procedure. A 1-qt emulsifying jar (Kimex) placed on a blender (Waring model 1120) with a no-load stirring rate of about 18,000 rpm was employed as the reaction system. The aqueous solution that contains the lignin and added base is placed in the reaction jar. The blender is turned on and the organic phase that contains the organostannane halide is introduced into the reaction jar. After a designated time, stirring is stopped and the blender jar contents are poured into a separatory funnel. The product is collected as a precipitate, washed repeatedly with water and the organic liquid, transferred to a preweighed glass Petri dish, and air dried.

Instrumentation. Potassium bromide pellets and a Fourier transform infrared (FTIR) spectrometer (Mattson Galaxy) were used to obtain infrared spectra. Mass spectroscopy (direct insertion probe, DIP) was carried out by a mass spectrometer (Kratos MS-50) operated in the electron ionization mode, 8-kV acceleration, and a 10-s per decade scan rate with variable probe temperature (Midwest Center for Mass Spectrometry, Lincoln, Nebraska) and a mass spectrometer (DuPont 21-491) at 1.8 kV. Elemental analysis was carried out by Galbraith Labs (Knoxville, TN). Mössbauer spectroscopy employed a tin-119-enriched BaSnO₃ source at 77 °K.

Solubilities were determined by placing about 3 mg of sample in approximately 5 mL of liquid.

Results and Discussion

To construct the reaction conditions under which the product should contain sufficient amounts of both the flexibilizing agent and the lignin, organostannane dichlorides were reacted with the candidate hydroxyl-capped monomers to form polymeric products:

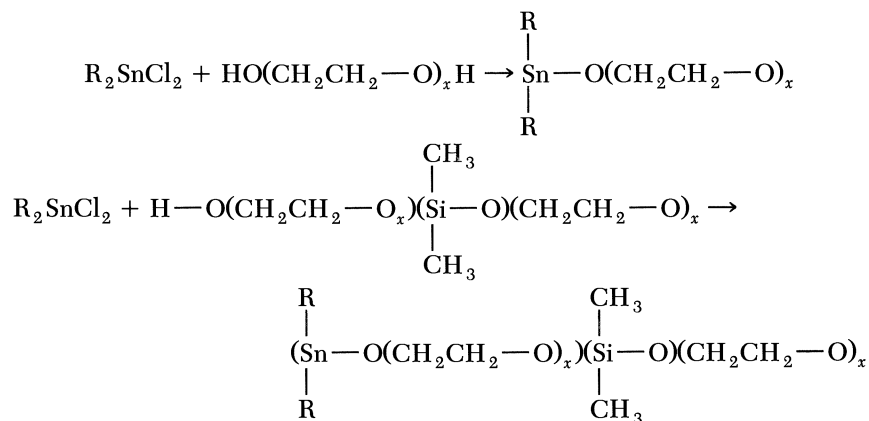


Table I. Reaction Results for Model and SIN Systems

<i>Reactants</i>	<i>Yield (g)</i>	<i>Yield (%)</i>	<i>Product Number</i>
Model System			
PEG(2000)-Bu ₂ SnCl ₂	0.5937	27	
PEG(2000)-La ₂ SnCl ₂	0.4167	17	
Silol(1250)-Bu ₂ SnCl ₂	0.0475	3	
Silol(2000)-Bu ₂ SnCl ₂	0.2196	10	
Lignin-Bu ₂ SnCl ₂	0.5311	38	2
Lignin-La ₂ SnCl ₂	1.8211	100	3
SIN System			
Silol(1250)-Bu ₂ SnCl ₂ -lignin	6.0216		6
Silol(2400)-Bu ₂ SnCl ₂ -lignin	7.6861		7
PEG(2000)-Bu ₂ SnCl ₂ -lignin	5.4155		4
PEG(2000)-La ₂ SnCl ₂ -lignin	3.0934		5

The results are shown in Table I. Similar reactions were carried out with lignin. Reaction was rapid, with yields of modified material produced within seconds (Table I). The yield was calculated assuming a hypothetical repeat unit that contained a single hydroxyl group. For instance, the average molecular weight for a single C₉ unit is 178 Da. For the AT material, the hydroxyl-based repeat unit molecular weight is 302 Da. For the dihaloorganostannanes, the repeat unit is assumed to have one organostannane moiety for every two hydroxyl-based repeat units.

Reactions that utilized organostannane dichlorides with a mixture of flexibilizing agent(s) and lignin were then run under the reaction conditions described in Table I. The products are believed to be intertwined with the lignin and flexibility polymers that are connected through reaction of the organostannane (Figure 1). The following connections are possible (where F is flexible moiety and L is lignin moiety).



The products may or may not be interpenetrating polymer networks (IPNs) because the exact nature of bonding is unknown.

The products do appear to be simultaneous interpenetrating networks (SINs), where connection of the two different polymers or like polymers occurs simultaneously.

Although a wide variety of organostannanes was used, emphasis will be placed on the product produced from the reaction of equal molar amounts (based on molar amounts of hydroxyl units) of hydroxyl-containing reactants and dibutyltin dichloride.

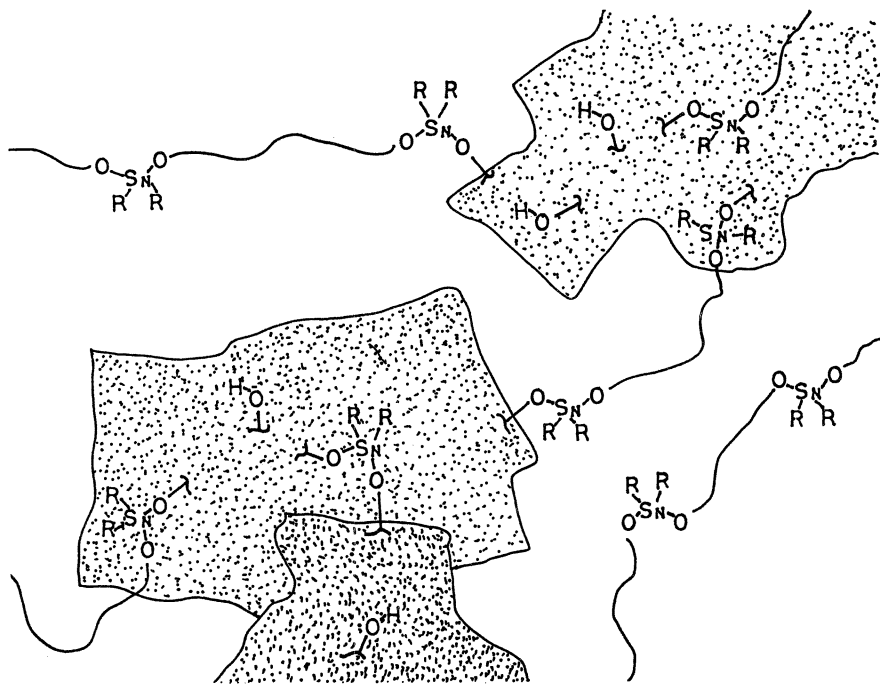


Figure 1. Simulation of the product produced from the reaction of organostannane dihalides with lignin and hydroxyl-capped flexibilizing agents.

Reaction Conditions. The organic phase consisted of 50 mL of CHCl_3 and the organostannane is added to rapidly (18,000 rpm, no load) stirred aqueous solutions (50 mL) of hydroxyl-containing reactants and added sodium hydroxide for 30 s stirring time at room temperature (ca 25 °C). (For the SIN reaction, 12 mequiv of each hydroxyl-containing reactant and 24 mequiv of sodium hydroxide and dibutyltin dichloride were used; half these values were used for the SIN product that contained dilauryltin dichloride).

Infrared spectral results are consistent with the presence of moieties derived from each of the three reactants. For unmodified lignin, a broad intense infrared band is present from about 3400 to 2800 cm^{-1} and is assigned to OH stretching in alcohols. The products show only a small band in this region that is consistent with the proposed substitution product. With reference to the siloxane-containing products, silicon-carbon vibrations should appear around 800 (Si—C stretch) and 1270–1250 cm^{-1} (Si— CH_3 deformation) (Table II). The second band is often partially hidden by the presence of a major band at 1269 cm^{-1} present in lignin (1271 cm^{-1}). Other silicon-associated bands are given in Table II. Bands associated with the formation of the Sn—O—R moiety are given in Table III.

Table II. Infrared Band Assignments for Silicon-Containing SIN Products

Band Assignment	Frequency (cm^{-1})	Products ^a	
		6 (1250 daltons)	7 (2400 daltons)
CH ₃ rock (from Si—CH ₃)	1266	sh	sh
Si—C stretch	857, 800	sh, +	+
CH ₃ —Si—CH ₃	700	sh	sh

^a Key: sh, shoulder; +, resolved.

Table III. Product Sn—O—R Band Assignment

Sn—O—R Stretch		Products ^a							
Frequency ± 5 (cm^{-1})	Band Type	1	2	3	4	5	6	7	Model Compound
665	Asymmetric	ur	ur	ur	ur	ur	ur	ur	+
598	Symmetric	ur	ur	ur	ur	ur	ur	ur	+
570	Symmetric	sh	sh	ur	ur	ur	ur	ur	+

^a Key: +, resolved; sh, shoulder; wk, weak; ur, unresolved.

Mass spectral results are also consistent with the presence of moieties from each of the three reactants. Tables IV–VIII focus on tin-containing ion fragments found in the polyethylene glycol containing product with a probe temperature of 400 °C.

In comparison to the lignin–organostannane products, new ion fragments (listed by the mass-to-charge ratio, m/e) are found at about 105 (OCH₂CH₂OCH₂CHO), 116–119 (H₂CCH₂OCH₂CH₂OCH₂CH₂; CH₂OCH₂CH₂OCH₂CH₂O), and 73 (H₃CCH₂OCH₂CH₂) characteristic of polyethylene glycol (PEG). New tin-containing fragments characteristic of the presence of PEG are found at 207 (BuSnOCH₂), 265 (C₄H₉SnOCH₂CH₂OCH₂CH), 280 (Bu₂SnOOCH₂), and 295 (Bu₂SnOOCH₂CH₂). None of these ions is of sufficient intensity to perform an isotope-ion fragmentation pattern check. The chemical bonding of the PEG and lignin structures by the tin-containing moiety is also indicated by the presence of specific ion fragments. Some of these ion fragments are given in Tables VI to VIII. Again, the ion fragment intensities for these tin-containing fragments are too low to develop a tin isotope relationship as contained in Table V.

Mössbauer spectroscopy is especially useful to describe environments of tin-containing materials. The Mössbauer results (Table IX) are consistent with the absence of significant Sn—Cl bound tin. The results indicate that the tin is bound in an organic matrix that is consistent with the presence of

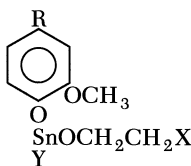
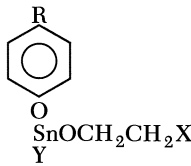
**Table IV. Tin-Containing Ion Fragments
(to $m/e = 315$) for the Products of
Dibutyltin Dichloride, Lignin, and
Hydroxyl-Capped Poly(ethylene oxide)**

m/e	% Relative Intensity	Possible Assignment
117	3.15	SnH(116)
118	2.66	Sn(118)
119	5.13	SnH(118)
119	2.25	Sn(119)
120	3.43	Sn(120)
121	6.17	SnH(120)
173	8.01	SnBu
174	5.15	SnBu
175	15.87	SnBu
176	6.30	SnBu
177	19.01	SnBu
178	2.34	SnBu
179	6.96	SnBu
208	6.30	BuSnCl, SnOPh
210	5.32	BuSnCl, SnOPh
211	10.71	BuSnCl, SnOPh
212	6.82	BuSnCl, SnOPh
213	12.86	BuSnCl, SnOPh
214	2.46	BuSnCl, SnOPh
215	4.57	BuSnCl, SnOPh
217	1.68	BuSnCl, SnOPh
231	1.85	Bu ₂ Sn
232	2.09	Bu ₂ Sn
233	2.60	Bu ₂ Sn
234	2.48	Bu ₂ Sn
235	2.45	Bu ₂ Sn
245	1.51	BuSnCl ₂
247	2.16	BuSnCl ₂
263	3.41	Bu ₂ SnCl, BuSnOPh
266	12.12	Bu ₂ SnCl, BuSnOPh
268	18.56	Bu ₂ SnCl, BuSnOPh
271	20.59	Bu ₂ SnCl, BuSnOPh
272	1.72	Bu ₂ SnCl, BuSnOPh
273	9.98	Bu ₂ SnCl, BuSnOPh
289	2.71	C ₃ H ₆ BuSnCl ₂
291	3.31	C ₃ H ₆ BuSnCl ₂
311	2.10	Bu ₂ SnOOCH ₂ CH ₂ O
313	5.00	Bu ₂ SnOOCH ₂ CH ₂ O
315	1.96	Bu ₂ SnOOCH ₂ CH ₂ O

Table V. Relative Isotopic Ion Fragmentation for Ion Fragments Derived from BuSn for the Product of Dibutyltin Dichloride, Lignin, and PEG

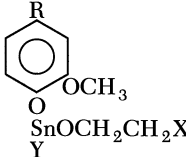
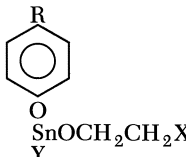
Sn (<i>m/e</i>)	116	117	118	119	120	122	124
Sn (expected) (%)	14	8	24	9	33	5	6
SnBu (<i>m/e</i>)	173	174	175	176	177	178	181
Sn (found) (%)	13	8	26	10	31	11	0

Table VI. Mass Fragments Found in Indulin AT–Dibutyltin Dichloride–PEG Product

Structure	<i>R</i> ^a	<i>X</i> (<i>m/e</i>)			
		—	<i>O</i> – <i>OH</i> – <i>OH</i> ₂	<i>OCH</i> ₂	<i>OCH</i> ₂ <i>CH</i> ₂
	H	288	303	317	331
	CH ₃	301	317	331	345 ^b
	CH ₃ CH ₂	315	331	345 ^b	360
	CH ₃ CH ₂ CH ₂	328–331	345 ^b	360	—
	Y	—	—	—	—
Y = H or absent					
Y = Butyl	H	345	360/361	—	388
	CH ₃	360	—	388	402
	CH ₃ CH ₂	371	388	402	416
	CH ₃ CH ₂ CH ₂	386	402	416	—
Y = 2-Butyl	H	401	418	—	—
	CH ₃	415	—	—	—
	CH ₃ CH ₂	429	—	—	—
	CH ₃ CH ₂ CH ₂	—	—	—	—
	H	257	272	288	301
	CH ₃	271	288	301	—
	CH ₃ CH ₂	—	301	—	—
	CH ₃ CH ₂ CH ₂	298	—	—	342
	Y	—	—	—	—
Y = H or absent					
Y = Butyl	H	—	331	345 ^b	301
	CH ₃	—	345 ^b	—	360
	CH ₃ CH ₂	342	360	371	386
	CH ₃ CH ₂ CH ₂	356	371	387	400
Y = 2-Butyl	H	371	387	401	415
	CH ₃	—	401	415	—
	CH ₃ CH ₂	399	415	—	—
	CH ₃ CH ₂ CH ₂	414	—	—	—

^a R group may be unsaturated.^b Possible background peak.

Table VII. Mass Fragments Found in Indulin AT–Dibutyltin Dichloride–Silol 1250 Product

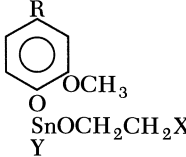
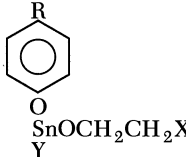
Structure	R^a	X (m/e)			
		—	O–OH–OH ₂	OCH ₂	OCH ₂ CH ₂
	H	287	—	318	—
	CH ₃	—	318	—	345
	CH ₃ CH ₂	315	—	345	361 ^b
	CH ₃ CH ₂ CH ₂	327	345	361 ^b	—
Y = H or absent					
Y = Butyl	H	345	361	—	387
	CH ₃	—	—	387	—
	CH ₃ CH ₂	—	387	—	416
	CH ₃ CH ₂ CH ₂	387	—	416	—
Y = 2-Butyl	H	—	418	—	—
	CH ₃	415	—	—	457
	CH ₃ CH ₂	429	—	457	473
	CH ₃ CH ₂ CH ₂	443	457	473	487
	H	257	273	287	298
	CH ₃	271	287	298	315
	CH ₃ CH ₂	285	298	315	327
	CH ₃ CH ₂ CH ₂	298	315	327	345
Y = H or absent					
Y = Butyl	H	314	330	345	356
	CH ₃	327	345	356	—
	CH ₃ CH ₂	342	356	—	386
	CH ₃ CH ₂ CH ₂	356	—	386	—
Y = 2-Butyl	H	—	387	—	415
	CH ₃	385	—	415	—
	CH ₃ CH ₂	—	415	—	—
	CH ₃ CH ₂ CH ₂	413	—	—	457

^a R group may be unsaturated.^b O group may be protonated.

the tin bound in a SIN matrix. Currently, differentiation between Sn—O—alkyl and Sn—O—aryl groupings is not possible.

Elemental analysis results help describe the complex product. The product produced from the siloxane (2400 daltons) block copolymer with polyethylene oxide (50% by weight PEG), lignin, and dibutyltin dichloride had 3.55%

Table VIII. Mass Fragments Found in Indulin AT–Dibutyltin Dichloride–Silol 2400 Product (400°C)

Structure	R^a	X (m/e)			
		—	O–OH–OH ₂	OCH ₂	OCH ₂ CH ₂
	H	287	—	315	—
	CH ₃	—	315	—	343
	CH ₃ CH ₂	315	—	343	—
	CH ₃ CH ₂ CH ₂	327	343	—	371
Y = H or absent					
Y = Butyl	H	343	—	—	387
	CH ₃	—	—	387	—
	CH ₃ CH ₂	371	387	—	416
	CH ₃ CH ₂ CH ₂	387	—	416	—
Y = 2-Butyl	H	—	416	—	—
	CH ₃	415	—	—	457
	CH ₃ CH ₂	—	—	457	—
	CH ₃ CH ₂ CH ₂	—	457	—	487
	H	257	273	287	299
	CH ₃	271	287	299	315
	CH ₃ CH ₂	285	299	315	327
	CH ₃ CH ₂ CH ₂	299	315	327	343
Y = H or absent					
Y = Butyl	H	313	—	344	—
	CH ₃	327	344	—	371
	CH ₃ CH ₂	341	—	371	387
	CH ₃ CH ₂ CH ₂	355	371	387	—
Y = 2-Butyl	H	371	387	—	415
	CH ₃	385	—	415	—
	CH ₃ CH ₂	—	415	—	—
	CH ₃ CH ₂ CH ₂	413	—	—	457

^a R group may be unsaturated.

Si and 6.49% Sn. This composition corresponds to a product that contains 18.8% block copolymer, 12.7% dibutyltin, and 68.5% lignin or for every 1 block copolymer, 7 dibutyltin moieties and 29 hydroxyl–lignin-containing units or 5.5 lignin molecules (assuming an average molecular weight per lignin molecule of 1600 Da). The assumption that each dibutyltin unit is doubly reacted translates to an average of two hydroxyl sites for each lignin molecule that is reacted.

In summary, spectral (Mössbauer, infrared, and mass) evidence is consistent with a complex product with various segments as pictured in Figure 1.

A thermal analysis study of the materials was accomplished. A description of selected results follows.

Lignin, under a nitrogen atmosphere, shows a complex differential scanning calorimetry (DSC) thermogram from ~ 50 to 450 °C. The product of lignin and dibutyltin dichloride shows a major exotherm in the 300 – 400 °C range with a maximum at ~ 360 – 370 °C. The corresponding product (except product that also contains PEG) shows a broad exotherm that is also in the range of 300 – 400 °C, but has a single maxima at about 345 °C.

The corresponding products (except products that contain the ethylene oxide–dimethylsiloxane–ethylene oxide block copolymers in place of the hydroxyl-terminated polyethylene oxide) show spectra similar to the polyethylene oxide-containing product with a maximum at 335 °C for the 1250-cm^{-1} block copolymer and 340 °C for the 2400 -dalton block copolymer.

The dilauryltin–PEG (2000)–lignin product softens when heated to about 224 °C, but the other products derived from dibutyltin dichloride do not soften until 300 °C. Most products do compress and form semiflexible sheets when pressure (about 2000 psi) is applied at room temperature. Selected results are summarized in Table X.

Table IX. Mössbauer Results for the Lignin–PEG– Bu_2SnCl_2 and Associated Compounds

<i>Compound</i>	ΔE (<i>mm/s</i>)	δ (<i>mm/s</i>)	$\Delta E / \delta$
	<i>Quad. Split.</i>	<i>Isomer Shift</i>	
Bu_2SnCl_2	3.42	1.61	
Lignin–PEG– Bu_2SnCl_2	2.97	1.23	2.46
Lignin– Bu_2SnCl_2	2.97	1.23	2.46

Table X. Film-Forming Characteristics of Organostannane Products Containing Flexibilizing Agents

<i>Products</i>	<i>Temperature</i> (°C)	<i>Pressure</i> (ft-lb)
AT–Dibutyltin–PEG	210	20
AT–Dilauryltin–PEG	180	4.5
AT–Dibutyltin–PEG–DMS–PEG 2400	220	10–15

Summary

The formation of simultaneous interpenetrating network (SIN) materials is indicated by FTIR and mass spectroscopy. Although non-SIN products are inflexible, the SIN products derived from coreactants that contain ethylene oxide and dimethylsilicone flexibilizing agents do offer some flexibility. Somewhat flexible films were formed by application of heat and pressure.

References

1. Glaser, W.; Kelley, S. *Encyclopedia of Polymer Science and Engineering*, 2nd ed.; Wiley: New York, 1988; Vol. 8, p 795.
2. Sperling, L.; Carraher, C. *Encyclopedia of Polymer Science and Engineering*, 2nd ed.; Wiley: New York, 1988; Vol. 12, p 658.
3. Sperling, L.; Carraher, C. *Renewable-Resource Materials*; Plenum: New York, 1986.
4. Muller, P.; Glaser, W. *J. Adhes.* **1984**, *17*, 157.
5. Muller, P.; Kelley, S.; Glaser, W. *J. Adhes.* **1984**, *17*, 185.
6. Dolenko, A.; Clarke, M. *For. Prod. J.* **1978**, *28C8*, 41.
7. Kratzl, K.; Buchtela, K.; Gratzl, J.; Zauner, J.; Ettingshausen, O. *Tappi J.* **1962**, *45(2)*, 117.
8. Hsu, O.; Glaser, W. *Wood Sci.* **1976**, *9(2)*, 97.
9. Glaser, W.; Hsu, O.; Reed, D.; Forte, R.; Wu, L. In *Urethane Chemistry and Applications*; Edwards, Kenneth N., Ed.; ACS Symposium Series 172; American Chemical Society: Washington, DC, 1981; p 311.
10. Saraf, V.; Glaser, W. *J. Appl. Polym. Sci.* **1984**, *29*, 1831.
11. Saraf, V.; Glaser, W.; Wilkes, G.; McGrath, J. *J. Appl. Polym. Sci.* **1985**, *30*, 2207.
12. Saraf, V.; Glaser, W.; Wilkes, G. *J. Appl. Polym. Sci.* **1985**, *30*, 3809.
13. Christian, D.; Look, M.; Nobell, A.; Armstrong, T. U.S. Patent 3,546,199, 1970.
14. Allan, G. U.S. Patent 3,476,795, 1969.
15. Glaser, W.; Barnett, C.; Rials, T.; Saraf, V. *J. Appl. Polym. Sci.* **1984**, *29*, 1815.
16. Wu, L.; Glaser, J. *J. Appl. Polym. Sci.* **1984**, *29*, 1111.
17. Tai, S.; Nakano, J.; Migita, N. *Mokuzai Gakkaishi* **1967**, *13*, 257.
18. Tai, A.; Nagata, M.; Nakano, J.; Migita, N. *Mokuzai Gakkaishi* **1967**, *13*, 102.
19. Carraher, C.; Sterling, D.; Ridgway, T.; Louda, J. W. *PMSE* **1991**, *62*, 241.
20. Seymour, R.; Carraher, C. *Structure and Property Relationships in Polymers*; Plenum: New York, 1984.
21. Critchfield, F. *Organic Functional Group Analysis*; MacMillan: New York, 1984; p 82.

RECEIVED for review November 11, 1991. ACCEPTED revised manuscript August 26, 1992.

Phenolic Interpenetrating Polymer Networks for Laminate Applications

K. Yamamoto

Hitachi Chemical Co., Ltd., Shimodate Research Laboratory, 1500 Ogawa, Shimodate, Ibaraki-ken 308, Japan

Interpenetrating polymer networks (IPNs) composed of phenolics and vinyl compounds have the properties, such as heat resistance and flexibility, of each component. Phenolic IPN varnishes prepared by dissolving phenolic prepolymers in monomeric acrylates are expected to have a rapid curing property, which will improve productivity in commercial applications. We have applied these IPN varnishes to paper-based phenolic laminates, which are important materials in the electronics industry. The curing time of prepared phenolic IPN varnishes was measured by differential scanning calorimetry. The curing rate was found to depend on the species of radical polymerization initiator and the ratio of the components. Various formulations of varnish were proposed and laminates were prepared on a laboratory scale. The resulting IPN laminate has advantages that include improved productivity, processability, and electrical properties compared with a conventional commercial product.

PHENOLIC-RESIN PAPER-BASED COPPER-CLAD LAMINATES (phenolic laminates) are important in the electronics industry because they have good electrical, chemical, and physical properties. Phenolic laminates also exhibit good processability and through-holes can be punched easily. In Japan, such laminates are widely used for consumer products such as televisions, air conditioners, audio sets, refrigerators, and tape players. The demand for phenolic laminate is expected to increase continuously at a rate of approximately 5% a year (1, 2). Currently, these materials are used mainly in Asian countries, especially Japan.

Although phenolic resin has the previously cited advantages, it does have the problematic properties, also. One problem is the brittleness of the resin, which necessitates modifications for industrial applications (3–10). Tung oil is commonly used as a flexibilizer for the phenolic laminates. However, the supply of tung oil is very unstable because it is a natural product and its growth and yield depend on the weather conditions. Another disadvantage of tung oil is that it lowers the reactivity of modified phenolic resin; that is, the curing time of phenolic resin modified with tung oil is so long that a huge manufacturing plant is necessary to mass-produce the laminate. Therefore, the development of the new flexibilizer for the laminate is greatly desirable.

We have previously synthesized phenolic interpenetrating polymer networks (IPNs) composed of phenolic and vinyl compounds to improve the brittleness of phenolic resins (11–15). These IPNs possess useful properties of each component, such as heat resistance and flexibility, that make them of potential interest for phenolic laminates. In a similar manner, by dissolving phenolic prepolymers in monomeric acrylates, phenolic IPN varnishes can be prepared, and these varnishes can be used to impregnated kraft paper to produce the laminates. The preparation of IPN varnishes is simple compared with tung-oil-modified phenolic varnish. IPN varnishes are expected to have rapid curing and have less potential for environmental pollution because they contain no removable solvent; instead monomeric acrylates act as the reactive solvent. These advantages of IPN varnishes offer the potential to improve productivity in commercial applications.

In the work described in this chapter, the curing time of various varnishes was measured with a differential scanning calorimeter (DSC). Then, laminates that employed the most promising IPN varnishes were prepared on a laboratory scale and compared with a conventional commercial product.

Experimental Methods

Preparation of IPN Varnishes. A list of the materials used is given in Table I. Phenolic novolac, epoxy, and flame retardants were dissolved in acrylates at 70 °C and radical polymerization initiators and curing catalysts were added to the mixture at 40 °C to obtain clear IPN varnishes (*see* Figure 1).

DSC Measurement. The curing time of the IPN varnishes was measured with a pressure-type DSC (DuPont 910) under 2-MPa nitrogen atmosphere. The temperature of the varnish was raised from 40 to 170 °C at a rate of 30 °C/min and held for 15 min at 170 °C. Figure 2 is an illustration of the DSC result for a typical IPN varnish. In Figure 2, time A is the time to complete the reaction after reaching 170 °C; time B is the time after setting the sample in the measurement cell to the first peak, peak 1.

Measurement of Gelation Time of IPN Varnishes. The gelation time of IPN varnishes was measured at 160 °C on a heated plate.

Table I. Materials and Suppliers

<i>Material</i>	<i>Chemical composition</i>	<i>Supplier</i>
Phenolic novolac HP800N	Phenolic novolac	Hitachi Chemical
Epoxy R 140P	Diglycidyl ether of bisphenol A	Mitsui Petrochemical
Acrylates		
BA	<i>n</i> -Butyl acrylate	Mitsubishi Rayon
ESB400A	Diglycidyl ether of tetrabromobisphenol A acrylic acid adducts	Synthesized
Flame retardants		
ESB 400	Diglycidyl ether of tetrabromobisphenol A	Sumitomo Chemical
ESB 400A	Diglycidyl ether of tetrabromobisphenol A acrylic acid adducts	Synthesized
TPP	Triphenyl phosphate	Daihachi Chemical
Curing catalysts		
2E4MZ	2-Ethyl-4-methylimidazole	Shikoku Chemical
BDMA	<i>N,N</i> -Dimethylbenzylamine	Wako Pure Chemical
Radical polymerization initiators		
AIBN	2,2'-azobis(isobutyronitrile)	Wako Pure Chemical
DCP	Dicumyl peroxide	Nippon Oil & Fats
3M	1,1'-Bis(<i>tert</i> -butylperoxy)-3,3,5-trimethylcyclohexane	Nippon Oil & Fats
PL	Lauroyl peroxide	Nippon Oil & Fats
PH	Cyclohexanone peroxide	Nippon Oil & Fats
PO	<i>t</i> -Butylperoxy (2-ethyl hexanoate)	Nippon Oil & Fats

Preparation of Laminate. The phenolic-IPN paper-based copper-clad laminate (IPN laminate) was prepared as follows (*see* Figure 3). Kraft paper was first treated with modified melamine varnish (which also acted as a flame retardant) and then was impregnated with an IPN varnish to obtain a preimpregnate (prepreg) for laminate. Seven prepreg sheets and a copper foil were laminated and then pressed under 2-MPa pressure at 170 °C for 2 min. To complete the curing reactions, the heating was continued for an additional 5 min at 170 °C under atmospheric pressure.

Evaluation of Laminate. The general properties of laminate were measured according to JIS standard C-6481 or the standard of Hitachi Chemical Co., Ltd. (*see* Table II).

Results and Discussion

Determination of Factors That Affect Curing. To determine the factors that affect curing, DSC measurement of various IPN varnishes was carried out. Generally speaking, the speed of curing is improved by

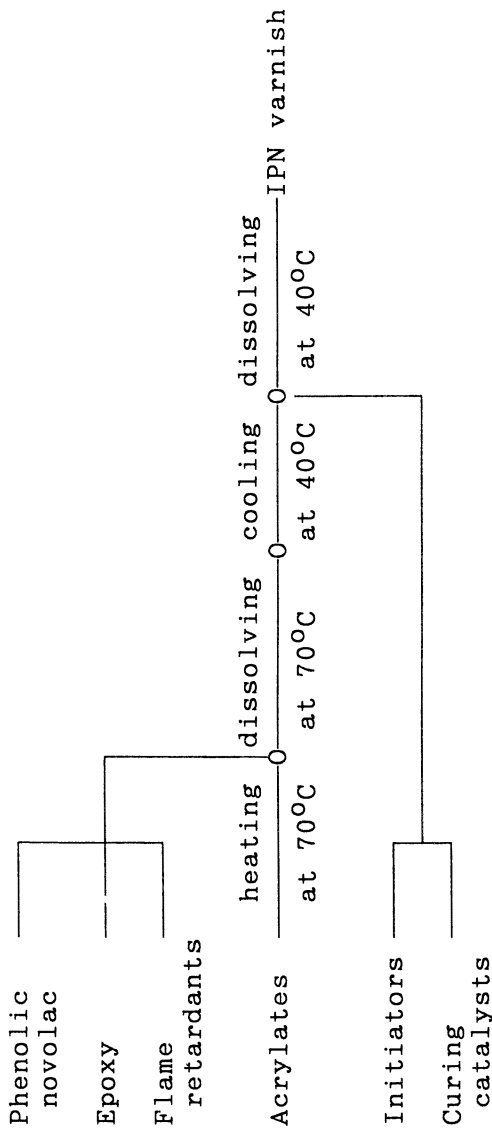
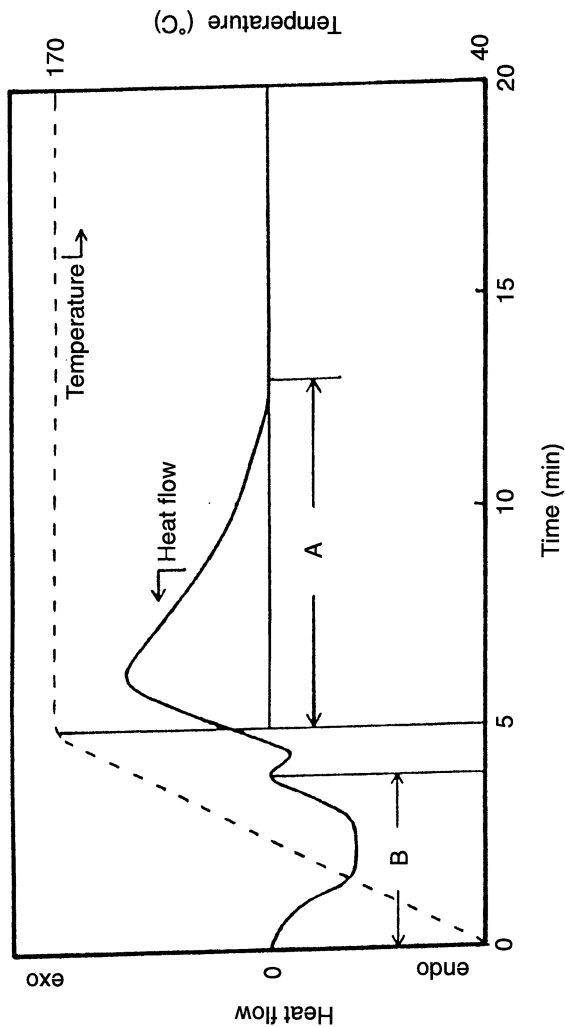


Figure 1. Preparation of IPN varnish.



A: Time to complete reaction after reaching 170°C
B: Time to peak 1

Figure 2. DSC thermogram for a typical IPN varnish.

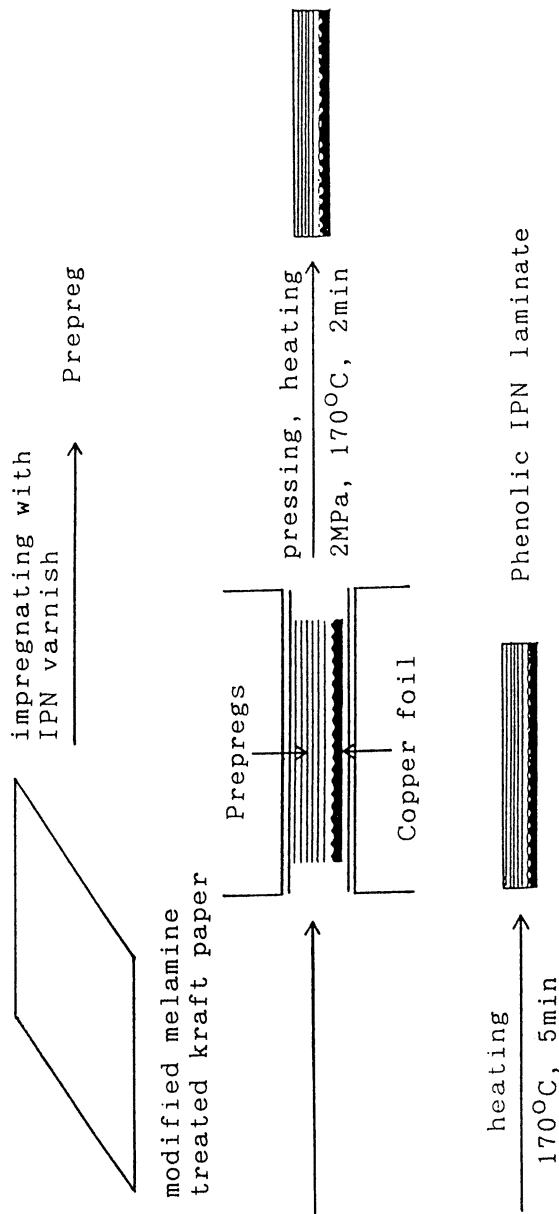


Figure 3. Preparation of laminate.

Table II. Measurement of the General Properties of the Laminate

<i>Test</i>	<i>Conditioning of Specimen</i>
Water absorption	Immersed in water at 23 °C for 24 h
Solvent resistance	Immersed in boiling 1,1,1-trichloroethylene for 10 min
Inflammability	As received (according to UL94-vertical)
Insulation resistance	As received
Dielectric constant	Immersed in water at 50 °C for 48 h
Tracking resistance	As received (according to IEC, comparative tracking index)
Solder resistance	As received (measured at 260 °C)
Peel strength	As received
Punchability	As received
Flexural strength	As received

optimization of the phenolic–epoxy equivalent ratio (P:E), addition of curing catalysts or initiators, and combinations of the two methods. In these systems, acrylate components were cured first; then phenolic and epoxy components were cured. Therefore, the time to complete the reaction (time *A*) is the most significant parameter for estimation of the time required to manufacture laminates.

Table III presents the results of DSC measurements of IPN varnishes with various kinds of initiators. The influence of initiator on curing speed was thus determined. Runs 3, 5, and 6 show a short time *A*. These results indicate that the curing time of a varnish depends strongly on the species of initiator and that 3M is a good initiator for rapid curing of IPN varnishes.

The data in Table IV show the influence of phenolic–epoxy equivalent ratio (P:E) on curing speed. The curing rate increased, to a lesser extent, with decreased P:E. P:E = 1:1 and 1:2 IPN varnishes are preferable for rapid curing. The results listed in Table V show the influence of the amount of curing catalyst. To avoid heterogeneity of initiator concentration in IPN varnish, sample varnishes that used PO instead of PL were prepared. This step was taken because PL is only partially soluble in these varnishes. The half-life period of PO is similar to that of PL initiator. The difference between the two initiators is their state at room temperature: PO is liquid, whereas PL is solid. The amount of 2E4MZ curing catalyst had little effect on the curing speed; BDMA catalyst was inferior to 2E4MZ.

From the viewpoint of laminate manufacture, the time to peak 1 (time *B*) is also significant. This time period is the time to the gelation point of the acrylate component. However, in some systems, no time *B* was observed, and this time was seen to be insensitive to the initiator, the P:E, and the curing catalyst.

Varnishes that contain both PL and 3M initiators generated some gelation (run 6 in Table III and runs 13 and 14 in Table V), which made them

Table III. Results of DSC Measurement: Influence of Initiator

Run No.	Initiator (phr)	Curing Catalyst	P:E (equivalent ratio)	Time (min)		Gelation	Pot Life ^a
				A	B		
1	$\frac{\text{AIBN}}{\text{DCP}} = \frac{0.2}{0.8}$	0.5	1:1	5.8	4.1	No	Long
2	DCP = 1.0	0.5	1:1	6.5	—	No	Long
3	3M = 1.0	0.5	1:1	3.9	—	No	Long
4	$\frac{\text{PL}}{\text{DCP}} = \frac{0.2}{0.8}$	0.5	1:1	8.9	3.5	No	Long
5	$\frac{3\text{M}}{\text{PH}} = \frac{0.2}{0.8}$	0.5	1:1	3.9	4.6	No	Long
6	$\frac{\text{PL}}{3\text{M}} = \frac{0.2}{0.8}$	0.5	1:1	4.4	—	No	Long
7	None	0.5	2:1	6.1	—	No	Long

^a Long means 7 days or more.

Table IV. Results of DSC Measurement: Influence of P:E

Run No.	P:E (equivalent ratio)	Initiator (phr)	Curing Catalyst	Time	Time	Gelation	Pot Life ^a
				A (min)	B (min)		
8	2:1	3M = 1.0	0.5	5.1	—	No	Long
3	1:1	3M = 1.0	0.5	3.9	—	No	Long
9	1:2	3M = 1.0	0.5	4.0	—	No	Short
10	2:1	$\frac{3\text{M}}{\text{PH}} = \frac{0.2}{0.8}$	0.5	6.1	4.2	No	Long
5	1:1	$\frac{3\text{M}}{\text{PH}} = \frac{0.2}{0.8}$	0.5	3.9	4.6	No	Long
11	1:2	$\frac{3\text{M}}{\text{PH}} = \frac{0.2}{0.8}$	0.5	3.2	4.4	No	Short
7	2:1	None	0.5	6.1	—	No	Long

^a Long means 7 days or more; short means less than 3 days.

unsuitable for impregnating kraft paper in preparation for laminate manufacture. In addition, varnishes that contained a large amount of curing catalyst and low P:E had short pot life (runs 9 and 11 in Table IV and run 15 in Table V), which is undesirable because special preservation equipment is necessary.

The foregoing results indicated that the varnishes used in runs 3, 5, and 15 had the desired property for rapid curing. Therefore, further tests on laminates that used these IPN varnishes were conducted.

Table V. Results of DSC Measurement: Influence of Curing Catalyst

Run No.	Curing Catalyst		Initiator (phr)	P:E (equivalent ratio)	Time (min)		Gelation	Pot Life ^a
	2E4MZ	BDMA			A	B		
5	0.5	0	$\frac{3M}{PH} = \frac{0.2}{0.8}$	1:1	3.9	4.6	No	Long
12	1.0	0	$\frac{3M}{PH} = \frac{0.2}{0.8}$	1:1	4.3	—	No	Long
6	0.5	0	$\frac{PL}{3M} = \frac{0.2}{0.8}$	1:1	4.4	—	Yes	Long
13	1.0	0	$\frac{PL}{3M} = \frac{0.2}{0.8}$	1:1	4.0	3.6	Yes	Long
14	0	1.0	$\frac{PL}{3M} = \frac{0.2}{0.8}$	1:1	5.8	3.4	Yes	Long
15	1.0	0	$\frac{PO}{3M} = \frac{0.2}{0.8}$	1:1	4.0	4.3	No	Long
16	2.0	0	$\frac{PO}{3M} = \frac{0.2}{0.8}$	1:1	3.8	4.4	No	Short
7	0.5	0	None	2:1	6.1	—	No	Long
17	1.0	0	None	2:1	5.1	—	No	Long

^a Long means 7 days or more; short means less than 3 days.

Evaluation of Laminates. Table VI lists the gelation times of the selected IPN varnishes and the appearance of the test IPN laminates. The varnish made with laminate IPN 2 showed the shortest gelation time (17 s) at 160 °C. However, blow holes were observed inside the laminate and the appearance of the laminate was not acceptable. The gelation time of IPN 1 was also short enough (34 s), but its appearance was also unacceptable because blow holes were observed at the surface of the laminate. Laminate IPN 3 had a satisfactory appearance and a varnish gelation time of 37 s. Tung-oil-modified phenolic varnish has a long gelation time—more than 5 times that of the IPN varnish (200–300 s).

These results indicate that the gelation times of the varnishes of laminates IPN 1 and 2 are too short for preparation of laminates by the process conducted in this work.

Table VII lists the general properties of laminate IPN 3 compared with a conventional commercial product. Laminate IPN 3 showed superior properties, including lower water absorption, lower dielectric constant, higher resistance to tracking, and better punchability. This laminate passed the Japanese Industrial Standard (JIS) (PP7F grade), American Society for Testing and Materials (ASTM) (FR1 grade), and National Electrical Manufactur-

Table VI. Gelation Time of Selected IPN Varnishes and Appearance of Laminates

<i>Laminate Code No.</i>	<i>Run No.</i>	<i>Curing Catalyst^a (phr)</i>	<i>Initiator (phr)</i>	<i>Gelation time at 160 °C (s)</i>	<i>Appearance of Laminate</i>
IPN 1	4	0.5	3M = 1.0	34	NG (blow holes at surface of laminate)
IPN 2	5	0.5	$\frac{3M}{PH} = \frac{0.2}{0.8}$	17	NG (blow holes inside laminates)
IPN 3	15	1.0	$\frac{PO}{3M} = \frac{0.2}{0.8}$	37	satisfactory
Tung-oil-modified phenolic varnish		—	—	200–300	—

^a 2-Ethyl-4-methylimidazole.

Table VII. General Properties of Laminates

<i>Properties</i>	<i>Unit</i>	<i>Laminate</i>	
		<i>IPN3</i>	<i>Conventional</i>
Physical			
Water absorption	%	0.63	0.78
Solvent resistance	—	Good	Good
Inflammability	s	2.5	2.0
Electrical			
Insulation resistance	$\times 10^{12} \Omega$	17.0	2.7
Dielectric constant at 1 MHz	—	4.27	4.58
Tracking resistance CTI	V	465	310
Mechanical			
Solder resistance	s	32	35
Peel strength	kN/m	1.9	1.8
Punchability at 20 °C	—	Better	Good
Flexural strength at 20 °C	MPa	120	140
Manufacturing time	min	10	120

ers Association (NEMA) (XPCFR grade) standards. In addition, less than 10 min was required to obtain the laminate from prepregs. From an engineering viewpoint, the short manufacturing time is an obvious advantage when compared with the time for a conventional commercial laminating process (more than 120 min).

Summary and Conclusions

DSC measurements were used to estimate the curing properties of IPN varnishes. Then, formulations of varnish for laminate were determined based on the results, and the properties of the IPN laminates, prepared on a laboratory scale, were compared with a conventional commercial product.

The most important determinants of curing speed were the species of radical polymerization initiator, followed by phenolic-epoxy equivalent ratio.

The IPN varnish identified as IPN 3 gave good results in both curing time and appearance. The resulting IPN laminate had the advantages of low water absorption, low dielectric constant, high resistance to tracking, and good punchability, and offers the promise of higher speed of laminate manufacture compared with a conventional commercial product.

References

1. Itou, K. *Electron. Parts Mater.* **1991**, *30(10)*, 32-40.
2. Aoki, M. *Surf. Mount Technol.* **1992**, *12(6)*, 1-11.
3. Takahashi, Y. *J. Appl. Polym. Sci.* **1961**, *5*, 468-477.
4. Hsu, E. T.; Pascavage, D. *Abstracts of Papers*, TAPPI Annual Meetings Proceedings; Technical Association of the Pulp and Paper Industry: Atlanta, GA, 1980; pp 277-290.
5. Jayabalan, M.; Balakrishnan, T. *Angew. Makromol. Chem.* **1983**, *118*, 65-80.
6. Noguchi, K.; Matsuda, Y.; Yasui, S.; Saai, S. Japanese Patent 5,970, 1980.
7. Matsumura, M.; Sakamoto, K.; Sakamoto, T. Japanese Patent 43,147, 1980.
8. Nakazato, I.; Tsurumi, Y. Japanese Patent 73,721, 1980.
9. Hara H.; Orii, S.; Araki, Y. Japanese Patent 154,153, 1980.
10. Tajima, Y.; Yokoo, T.; Ema, K.; Ikado, S. Japanese Patent 133,354, 1981.
11. Yamamoto, K.; Kumakura, T.; Yoshimura, Y. *Polym. Prepr. Jpn.* **1986**, *35*, 802.
12. Yamamoto, K.; Yasuzawa, K.; Nomoto, M.; Takahashi, A.; Yoshimura, Y.; Nanaumi, K. *Abstracts of Papers*, Proceedings of the Thermosetting Plastics Symposium, Japan; Japan Thermosetting Plastics Industry Association: Tokyo, Japan, 1988; pp 23-26.
13. Yamamoto, K.; Takahashi, A. In *Sound and Vibration Damping with Polymers*; Corsaro, R. D.; Sperling, L. H., Eds.; ACS Symposium Series 424; American Chemical Society: Washington, DC, 1990; pp 431-444.
14. Yamamoto, K.; Yasuzawa, K.; Nomoto, M.; Kumakura, T. Japanese Patent 225,551, 1987.
15. Yamamoto, K.; Yasuzawa, K.; Nomoto, M.; Kumakura, T. Japanese Patent 225,552, 1987.

RECEIVED for review October 9, 1991. ACCEPTED revised manuscript September 10, 1992.

Rodlike, Cross-Linked, Flexible Polyimide Semi-interpenetrating Polymer Network Composites

Miscibility and Properties

Moonhor Ree^{1*} and Do Y. Yoon²

¹IBM Technology Products, Hopewell Junction, NY 12533

²IBM Almaden Research Center, San Jose, CA 95120

Rodlike (or semirigid), flexible polyimide semi-interpenetrating polymer network composites were prepared by solution mixing of flexible precursors of rodlike poly(p-phenylene pyromellitimide) (PMDA-PDA) or semirigid poly(4,4'-oxydiphenylene pyromellitimide) (PMDA-ODA) with cross-linkable, oligomeric, acetylene-terminated isoimide of 3,3',4,4'-benzophenonetetracarboxylic dianhydride-1,3-bis(3-aminophenoxy)benzene (BTDA-APB) or imide of 2,2'-bis(3,4-dicarboxyphenyl)hexafluoropropane dianhydride-1,3-bis(3-aminophenoxy)benzene (6FDA-APB), followed by solvent drying and thermal curing. A homogeneous ternary solution with a relatively high concentration of 20–30 wt% was easily achieved in N-methyl-2-pyrrolidone for various compositions of the polyimide precursor blends. The diethyl ester precursors of PMDA-PDA and PMDA-ODA were more miscible than the corresponding poly(amic acid) precursors with BTDA-APB and 6FDA-APB. Optically transparent films were obtained for some compositions of PMDA-PDA composites with 6FDA-APB and BTDA-APB. The PMDA-ODA composite films showed relatively larger phase separation than the PMDA-ODA composites. The glass-transition temperature of the 6FDA-APB or BTDA-APB component did not vary with the composition of the

* Corresponding author.

composites, which is indicative of molecular demixing of the components. Phase separation took place primarily during drying cast films. The domain size set during the drying was not changed significantly by thermal imidization. The mechanical properties of 6FDA-APB and BTDA-APB were significantly improved by composite formation with PMDA-ODA or PMDA-PDA. The self-adhesion property of both PMDA-ODA and PMDA-PDA was significantly improved by the composite formation with 6FDA-APB, but the composite formation with BTDA-APB showed no enhancement. In addition, the residual stress behavior was measured in situ on Si wafers during curing and cooling, whereas the stress relaxation due to moisture uptake was investigated in 50% relative humidity at room temperature.

HIGH-TEMPERATURE AROMATIC POLYIMIDES are widely used as high-performance specialty polymers, because of excellent thermal stability and mechanical properties (1, 2). In particular, applications in advanced microelectronic devices require good physical properties, such as high glass-transition temperature, high thermal stability, good toughness, low dielectric constant, low thermal expansivity, high chemical resistance, and good adhesion (3). Some of the desired properties can be achieved by using a rodlike or semirigid polymer; some other properties are characteristic of a flexible chain polymer. However, all the property requirements cannot easily be met by a single homopolymer.

To meet the property requirements, one approach is to blend a rodlike polymer with a flexible polymer to combine their beneficial properties. However, it is difficult to achieve a rodlike-flexible polymer blend with a desired level of molecular mixing through direct mixing in a mutual solvent, because the polymers are inherently immiscible and usually lead to large-scale phase separation. Another difficulty is finding a mutual solvent that is sufficient to make a homogeneous solution with an appreciable concentration of the polymer mixture. These difficult problems can be avoided in the case of polyimides because we use more random coillike soluble polyimide precursors instead of insoluble polyimides.

Recently, Ree et al. (4-7) reported several rodlike-flexible polyimide composites via in situ rod formation by thermal imidization. In the studies, a polyamic dialkyl ester precursor of one component was mixed with a polyamic acid or polyamic dialkyl ester precursor of another component in a common solvent, *N*-methyl-2-pyrrolidone (NMP). This mixture prevents the formation of segmented blocky copolymer of both components due to transamidation exchange reactions in a mixture of polyamic acid precursors, as reported previously by Ree et al. (8, 9). The polyimide precursor components that were used were always phase separated due to their immiscibility during film drying when cast from the homogeneous solution in NMP. The dried precursor blend films were followed by thermal imidization to convert the

rodlike-flexible polyimide composites. Once phase separation took place in the precursor mixtures through the drying process, the size of the phase domains was not changed further by subsequent thermal imidization. Rodlike-flexible polyimide composites on a submicrometer scale were easily achieved through the conventional polyimide fabrication process (that is, spin-cast, drying, and thermal curing).

In the present study, the concept of rodlike-flexible composites via in situ rod formation is extended to an interpenetrating polymer network (IPN) or semi-interpenetrating polymer network (SIPN) system to make IPN- or SIPN-based polyimide composites. A cross-linked flexible polymer has some advantageous properties that cannot be obtained from a rodlike or semirigid polymer. A potential candidate material for cross-linkable flexible components is an acetylene-terminated oligomeric imide or isoimide that is known to exhibit excellent solubility and good interfacial adhesion to itself, ceramic substrates, and metals (Ree, M., unpublished results; Lee, K.-W., unpublished results): acetylene-terminated 2,2'-bis(3,4-dicarboxyphenyl)hexafluoropropane dianhydride-1,3-bis(3-aminophenoxy)benzene (6FDA-APB) imide and 3,3',4,4'-benzophenonetetracarboxylic dianhydride-1,3-bis(3-aminophenoxy)benzene (BTDA-APB) isoimide oligomers (*see* Chart I). In this study, the cross-linkable oligomers were blended in NMP with the flexible

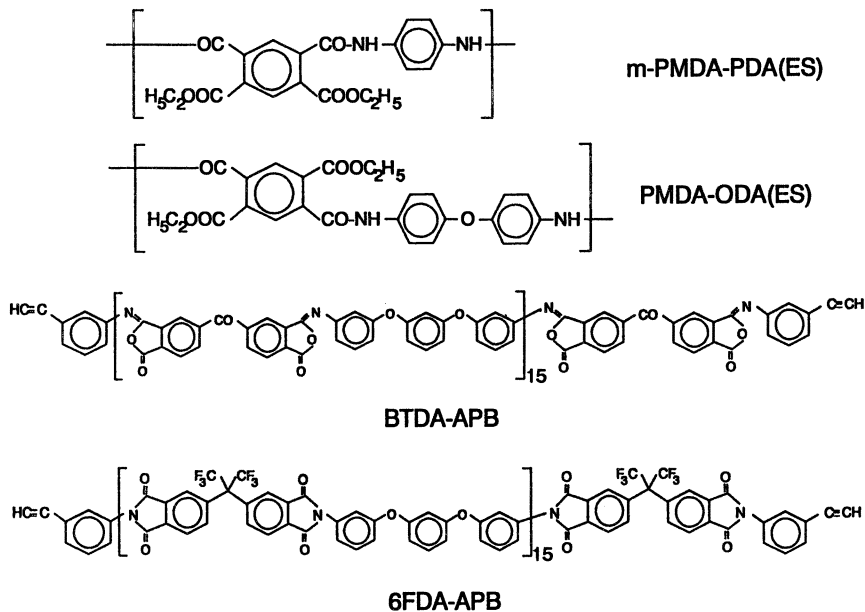


Chart I. Chemical structures of acetylene-terminated oligomers (BTDA-APB and 6FDA-APB) and precursors of rodlike PMDA-PDA and semirigid PMDA-ODA polyimides.

polyamic diethyl ester precursor of rodlike poly(*p*-phenylene pyromellitimide) (PMDA–PDA) or semirigid poly(4,4'-oxydiphenylene pyromellitimide) (PMDA–ODA) polyimide.

From homogeneous ternary solutions of the blends, the resultant rodlike (or semirigid)–cross-linked polyimide composites were prepared through conventional solution casting and drying and a subsequent thermal curing process that is widely used in the microelectronics industry. Here, the question that arises is “How much molecular demixing can be achieved in the composites?” The degree of phase demixing in the resultant composites may be dependent upon the history of molecular demixing in the cross-linkable oligomer–polyamic diethyl ester precursor mixtures after solvent drying.

As schematically presented in Figure 1, when the precursor components are well mixed at the molecular level, it is possible to obtain IPN-type molecular composites by minimizing further phase separation via thermal curing. Otherwise, through phase separation in the precursor mixtures and the resultant polyimide blends, a SIPN type of polyimide composites may be obtained. The miscibility of the mixtures was investigated in NMP solution, in the condensed state, and in the thermally cured solid state using an optical microscope or dynamic mechanical thermal analyzer. Properties of the resul-

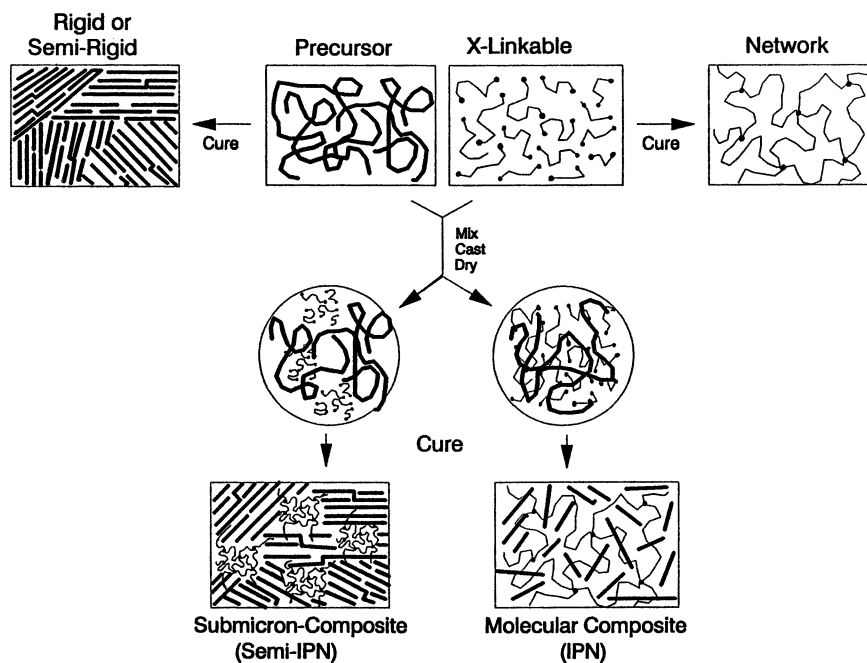


Figure 1. Schematic representation of IPN and SIPN types of rodlike-flexible polyimide composites via *in situ* rod and cross-link formations.

tant composites were investigated by dynamic mechanical thermal analysis, stress-strain analysis, residual stress analysis, and self-adhesion measurement. In addition, the surface composition characteristic was examined, in particular for the (PMDA-ODA-6FDA-APB) composite.

Experimental Details

Materials and Sample Preparation. Poly(4,4'-oxydiphenylene pyromellitic acid) [PMDA-ODA (PAA)] [ca. 30,000 weight-average molecular weight (\bar{M}_w); 16.0 wt%] and its diethyl ester [PMDA-ODA(ES)] (ca. 35K \bar{M}_w ; 16.7 wt%) solutions in NMP were used in the present study as the flexible precursors of semirigid PMDA-ODA polyimide, whereas poly(*p*-phenylene *meta*-pyromellitic diethyl ester) [*m*-PMDA-PDA(ES)] (ca. 30K \bar{M}_w ; 27.5 wt%) solution in NMP was used as the flexible precursor of fully rodlike PMDA-PDA polyimide. Cross-linkable oligomers were acetylene-terminated imide of 2,2'-bis(3,4-dicarboxyphenyl)hexafluoropropane dianhydride-1,3-bis(3-aminophenoxy)benzene (6FDA-APB; degree of polymerization, DP, of 15) and isoimide of 3,3',4,4'-benzophenonetetracarboxylic dianhydride-1,3-bis(3-aminophenoxy)benzene (BTDA-BAPB; DP = 15), which were supplied (from National Starch & Chemical Company) as powders. These powders were dissolved in NMP and filtered with 1.0- μm filter membranes (Fluoropore): 34.5-wt% 6FDA-APB and 35.0-wt% BTDA-APB solutions. Several binary blends, such as (PMDA-ODA(PAA))-(6FDA-APB), (PMDA-ODA(ES))-(6FDA-APB), (*m*-PMDA-PDA(ES))-(6FDA-APB), (PMDA-ODA(ES))-(BTDA-APB), and (*m*-PMDA-PDA(ES))-(BTDA-APB), were prepared from these materials. The ternary homogeneous solutions of these blends were obtained with various compositions in NMP through solution mixing on a roller mixer at room temperature for 1 day. The homogeneous ternary solutions were cast on glass slides or Si wafers by doctor-blading or spin-coating and were subsequently soft-baked at 80 °C for 30 min or 1 h on a hotplate or in a convection oven. Then thermal curing was performed in an oven with nitrogen flow with the following cure process: 150 °C for 30 min, 230 °C for 30 min, 300 °C for 30 min, and 400 °C for 1 h. For both peel test and residual stress measurement, the film samples were prepared on Al(100) (0.1% γ -aminopropyltriethoxysilane in 90-vol% EtOH-10-vol% deionized (DI) water or in DI water) primed Si(100) wafers of 82.5-mm diameter. The thickness of the fully cured films was 10–20 μm .

Characterization. Phase-separated domains in both dried and cured blend films were examined with the aid of a microscope (Jena or Polyvar-Met) under crossed polarization and a photographic light-scattering apparatus with a He-Ne laser source under parallel polarization. Dynamic mechanical thermal properties were measured at a heating rate of 10 °C/min and a frequency of 10 Hz in ambient nitrogen over the range of 25–500 °C using a dynamic mechanical thermal analyzer (DMTA; Polymer Laboratories) with a tensile head. Mechanical properties were measured at room temperature, using a tensile tester (Instron model 1122). In tensile testing, the grip gauge length was ca. 50 mm and the strain rate was $1.6 \times 10^{-2} \text{ s}^{-1}$. The width of the film strips was 3.175 mm. Peel tests for self-adhesion were performed in a 90° peeling mode with the aid of a tensile tester (Instron) equipped with a 90° peel test fixture. The crosshead speed was 0.2–2.0 mm/min and the width of the peel strips was 2.0–5.0 mm. All the film strips were prepared with the aid of a dicer equipped with a circular blade.

Residual stress measurements were dynamically performed in ambient nitrogen during thermal curing of the dried films on Si(100) wafers through the cure process and subsequent cooling at the rate of 1.0 °C/min using a double He-Ne laser-beam-based stress analyzer (Flexus Company, model 2-300) equipped with a hot stage and controlled by a computer (IBM PC/AT). In addition, the analysis of surface composition was done for the 6FDA-APB composites with PMDA-ODA polyimide, using an ESCA (electron spectroscopy for chemical analysis) spectrometer (Surface Science Instruments, SSX-100 model 05).

Results and Discussion

Miscibility Behavior. For the (PMDA-ODA(ES))-(6FDA-APB) system, ternary homogeneous solutions with various compositions were obtained in NMP over the total polymer concentration of ≤ 30 wt%. The homogeneous solutions of 10-wt% solid content were cast on glass slides and subsequently dried at 80 °C for 1 h. Then, optically clear films were obtained for all the various compositions. The optical transparency of these blend films, (except the 30:70 (w/w) and 50:50 compositions) was retained even after thermal imidization at 400 °C through the cure process (see Table I). However, the optical clarity of the (PMDA-ODA)-(6FDA-APB) films of some compositions does not mean that the two components are miscible. The phase separation in the optically clear films might be on a scale less than submicrometer. In contrast, the (PMDA-ODA(PAA))-(6FDA-APB) blend showed quite different miscibility behavior. For this blend system, the ternary solution was homogeneous for 10-wt% solid content and various compositions, but was turbid for > 20 -wt% solid content. Even the films prepared from the homogeneous solutions of 10-wt% solid content exhibited a large phase separation. The domain size was on the order of tens of micrometers. These results indicate that the miscibility between PMDA-ODA precursor and 6FDA-APB depends on the functionality (acid or ethyl ester) of the PMDA-ODA precursor. The PMDA-ODA(ES) precursor is more miscible than the PMDA-ODA(PAA) with 6FDA-APB.

The BTDA-APB blends with PMDA-ODA precursors were limited to the PMDA-ODA(ES) precursor, because of gel formation via the reaction of carboxylic acid groups of the PMDA-ODA(PAA) precursor with isoimide groups of the BTDA-APB. For the (PMDA-ODA(ES))-(BTDA-APB) blend system, homogeneous ternary solutions with ≤ 30 -wt% solid content were obtained in NMP for various compositions, as observed in the (PMDA-ODA(ES))-(6FDA-APB) blend system. The dried films prepared from the miscible solutions of 10-wt% solids were optically clear for various compositions, except the 30:70 composition, which contained phase-separated domains of several micrometers (see Table I). After curing, phase domains of submicrometer size were observed for the 50:50, 70:30 and 90:10 compositions under the enhanced contrast of the cured films. However, the 10:90 blend was still optically clear after curing. Overall, the miscibility behavior of

Table I. Apparent Miscibility Behavior of PMDA-ODA Blends with 6FDA-APB and BTDA-APB as Observed by Optical Microscopy and Light Scattering

Composition (w/w)	(PMDA-ODA(ES))-(6FDA-APB)			(PMDA-ODA(ES))-(BTDA-APB)		
	Solution (10 wt% in NMP)	Dried at 80 °C for 1 h	Cured at 400 °C for 1 h	Solution (10 wt% in NMP)	Dried at 80 °C for 1 h	Cured at 400 °C for 1 h
90:10	Clear	Clear	Clear	Clear	Clear	< 1 μm
70:30	Clear	Clear	Clear	Clear	Clear	< 1 μm
50:50	Clear	Clear	≤ 1 μm	Clear	Clear	< 1 μm
30:70	Clear	Clear	< 1 μm	Clear	≥ 1 μm	≥ 1 μm
10:90	Clear	Clear	Clear	Clear	Clear	Clear

NOTE: Clear means optically clear.

(PMDA-ODA(ES))-(BTDA-APB) blends was similar to that of (PMDA-ODA(ES))-(6FDA-APB) blends, but their phase-separated domain size was relatively larger than that of (PMDA-ODA(ES))-(6FDA-APB) blends.

The *m*-PMDA-PDA(ES) blends with 6FDA-APB or BTDA-APB were also investigated in the present study. Miscible solutions with ≤ 20 -wt% solid content were obtained in NMP for both blend systems. During drying, all the compositions except 30:70 blends exhibited phase separation in ≤ 1.5 - μm domain size as shown in Table II. The 30:70 blends showed very large phase-separated domains of > 20 μm . For 6FDA-APB blends, domain size was slightly smaller than for BTDA-APB blends. However, for the (PMDA-PDA(ES))-(6FDA-APB) blends, the size of phase domains was still larger than in the PMDA-ODA(ES) blends with 6FDA-APB or BTDA-APB.

Overall, for the polyimide precursor blends considered here, miscible ternary solutions in NMP were easily achieved up to 20–30-wt% solid content. In the case of commercial polyimide precursor solutions for micro-electronic applications, the solid content is generally less than 20 wt%. Therefore, in the practical sense, the high concentration of 20–30 wt% is very useful for the fabrication of microelectronic devices. For the blend systems, phase separation takes place during solvent evaporation from the homogeneous ternary solutions in NMP. In the phase separation, the resultant demixing level is controlled by a compositional quenching process that results from the removal of NMP solvent. During evaporation of NMP solvent, the ternary solution may be instantaneously plunged into the spinodal decomposition region. Then, the spinodal decomposition, which causes phase separation, competes with the compositional quenching process that is driven by solvent evaporation. Of course, when the evaporation of solvent is slow, the nucleation and growth mechanism may be involved and, consequently, the ternary solution reaches into the binodal region. However, this process is slow compared to the spinodal decomposition process. In fact, solvent evaporation is a continuous process, so that the nucleation and growth process

Table II. Apparent Miscibility Behavior of (PMDA-PDA)-(6FDA-APB) Blends as Observed by Optical Microscopy and Light Scattering

<i>Composition</i> (<i>w/w</i>)	<i>Solution</i> ^a (10 wt% in NMP)	<i>Dried at</i> 80 °C for 1 h (μm)	<i>Cured at</i> 400 °C for 1 h (μm)
90:10	Clear	≤ 1.5	≤ 1.5
70:30	Clear	≤ 1.5	≤ 1.5
50:50	Clear	≤ 1.5	≤ 1.5
30:70	Clear	> 20	> 20
10:90	Clear	≤ 1.5	≤ 1.5

^a Clear means optically clear.

should not have enough time to occur. Therefore, for the precursor blend films obtained from homogeneous ternary solutions through the conventional spin-coating-thermal drying process, the level of demixing is believed to be controlled predominantly by the competition of the spinodal decomposition and the compositional quenching by continuous solvent evaporation.

For the PMDA-PDA(ES) blends with 6FDA-APB and BTDA-APB, observations indicate that the phase-separated domains, which were set primarily during solvent drying, were preserved in size without any further significant phase separation during thermal curing. Similar behavior for rodlike PMDA-PDA microcomposites with flexible linear polyimides was reported previously by Ree et al. (4, 6, 7). This behavior may be the result of the continuous freezing of the mixture systems by elevation of the glass-transition temperature (T_g) due to imidization and cross-link formation, as well as the result of residual solvent removal during thermal curing. For this particular situation in the present precursor mixtures, the domains made during the drying process are preserved in size and are not affected significantly by the subsequent imidizing-curing process. Therefore, the level of demixing in the resulting rodlike (or semirigid)-cross-linked flexible polyimide composites studied here is predominantly dependent on the history of molecular demixing in the condensed state of the precursor mixtures created by the competition of the compositional quenching process with the spinodal decomposition that occurs during the drying process. Based on this particular phase-demixing situation, an IPN-type molecular polyimide composite can be achieved only through a faster compositional quenching process, such as freeze-drying, and subsequent curing capable of phase separation prevention.

Properties. The properties of blend films cured at 400 °C were investigated by means of DMTA, stress-strain analysis, and residual stress analysis. The glass transition behavior and dynamic mechanical properties (storage and loss moduli, E' and E'') were investigated over the temperature range of 25–500 °C. The DMTA results of (PMDA-ODA)-(6FDA-APB) composite films are shown in Figure 2. The PMDA-ODA polyimide showed a gradual decrease in storage modulus E' up to ca. 380 °C and a relatively large drop above 380 °C. The T_g of the PMDA-ODA was estimated to be ca. 410 °C. The thermally cross-linked 6FDA-APB exhibited E' versus temperature behavior up to ca. 240 °C similar to the behavior observed for PMDA-ODA. However, the 6FDA-APB polyimide showed a very sharp glass transition at ca. 245 °C, which is much lower than the PMDA-ODA. Composite samples of 6FDA-APB and PMDA-ODA showed two transitions: one at ca. 245 °C and the other in the range of 330–410 °C. The softening point at 245 °C, which corresponds to the T_g of the 6FDA-APB component, changed little with composition, which indicates that the PMDA-ODA and 6FDA-APB components demixed. The other softening behavior in the higher temperature region is due to the glass transition of the

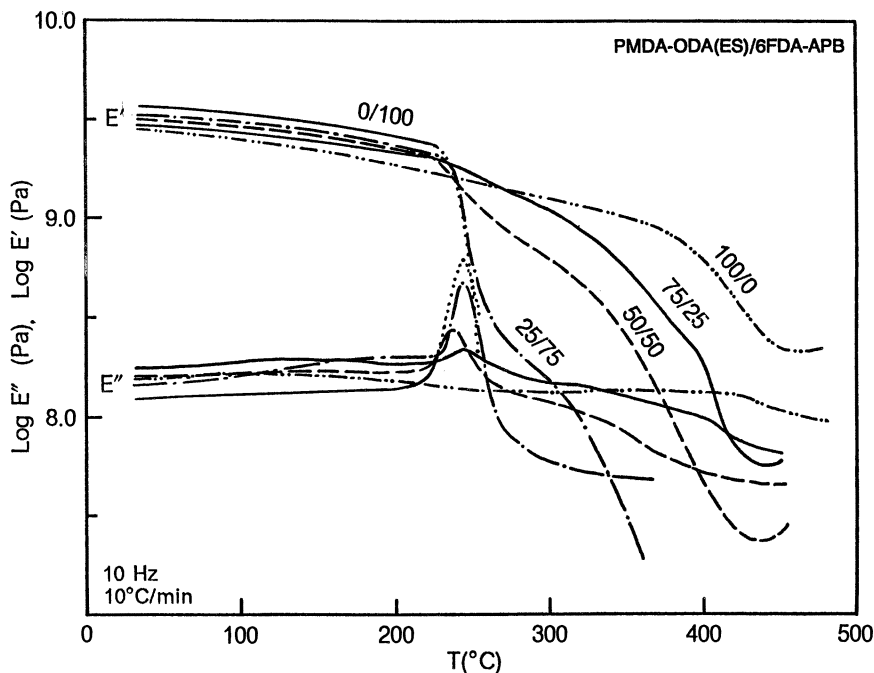


Figure 2. Dynamic mechanical relaxation behavior (storage and loss moduli, E' and E'') of the composite films cured from the (PMDA-ODA(ES))-(6FDA-APB) blends at 400 °C. The heating rate and frequency were 10 °C/min and 10 Hz, respectively.

PMDA-ODA component. This softening temperature decreased as the content of PMDA-ODA component in the composite decreased. This decrease might be due to the characteristic of the tensile mode near the glass transition of the higher T_g component (PMDA-ODA) in DMTA measurements, rather than its miscibility with 6FDA-APB. That is, above the T_g of the 6FDA-APB component, the dimensional stability of the composite film decreases with decreasing content of the PMDA-ODA component. Variation of this dimensional stability of the composite film might be directly reflected in the E' versus temperature behavior measured in the tensile mode. Similar DMTA behavior was observed for the other blend systems. However, in contrast to the semirigid PMDA-ODA, the fully rodlike PMDA-PDA polyimide did not show any phase transition over the temperature range of 25–500 °C. Blends of PMDA-PDA with 6FDA-APB or BTDA-APB showed only a single softening behavior at about the T_g of the 6FDA-APB or BTDA-APB component, and the dimensional stability of the blends was relatively higher than the dimensional stability of the PMDA-ODA composites (see Figure 3).

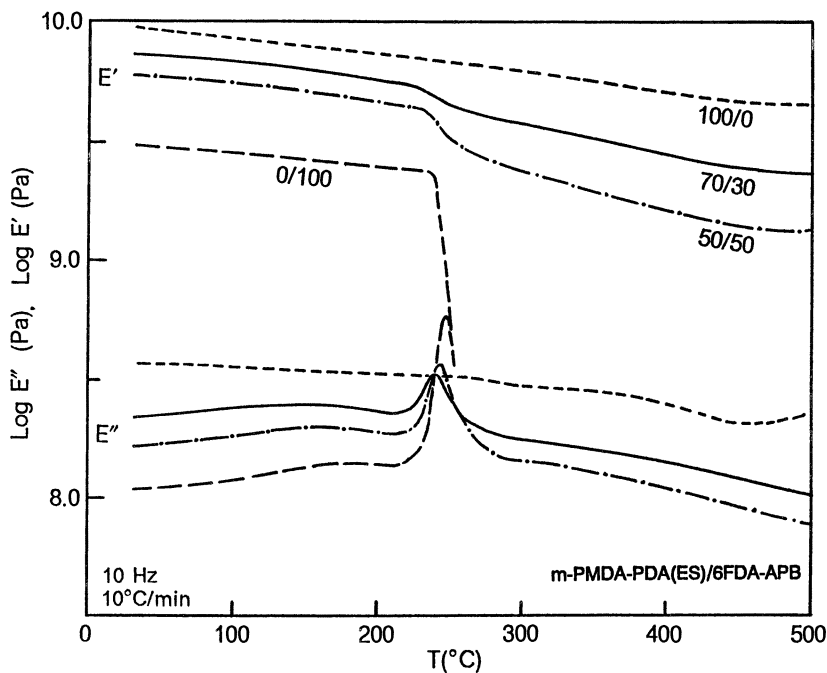


Figure 3. Dynamic mechanical relaxation behavior of the 400 °C cured (PMDA-PDA)-(6FDA-APB) composite films measured at 10 °C/min heating rate and 10-Hz frequency as a function of temperature over the range of 25–500 °C.

The mechanical properties of cured blend films were investigated at room temperature. The Young's modulus (E) was 9.8 GPa for PMDA-PDA, 2.9 GPa for PMDA-ODA, and 3.7 GPa for 6FDA-APB and BTDA-APB polyimides. The strain at break (ϵ_b) was 6% for PMDA-PDA, 106% for PMDA-ODA, and 5% for 6FDA-APB and BTDA-APB. Blends of these components exhibited mechanical properties intermediate between those of the blend components. For the (PMDA-ODA)-(6FDA-APB) composite, the strain at break (ϵ_b) was 33% for the 25:75 composition and 107–109% for both 50:50 and 75:25 compositions, as presented in Table III. In particular, the 25:75 composite exhibited highly improved strain behavior, even though the matrix component was 6FDA-APB. That is, the toughness of 6FDA-APB polyimide was significantly improved through its composite formation with PMDA-ODA. Both 25:75 and 50:50 composite films showed yielding behavior on the stress-strain curves typically observed for most flexible polymers. The yield stress and strain (σ_y and ϵ_y) were 145.4 MPa and 6% for the 25:75 composite and 126.9 MPa and 6% for the 50:50 composite, respectively. This yielding behavior results from the 6FDA-APB

component and indicates that the yield strain of 6FDA-APB is 6%, which could not be measured for 6FDA-APB polyimide because its elongation at break was lower than the yield strain. In addition to the yielding behavior, these composite films showed a multiple necking behavior on the stress-strain curve. However, the yielding and multiple necking behavior was not observed for the 75:25 composite and the PMDA-ODA polyimide film. The mechanical properties of (PMDA-PDA)-(6FDA-APB) composite are summarized in Table IV. The rodlike PMDA-PDA polyimide is a high modulus polymer, but shows very poor (only 6%) elongation at break. Therefore, composites of PMDA-PDA with 6FDA-APB did not show a high elongation at break. In fact, the mechanical toughness of 6FDA-APB polyimide was slightly improved by its composite formation with PMDA-PDA, owing to the high modulus properties, but still poor in comparison with that of (PMDA-ODA)-(6FDA-APB) composites.

The residual stress behavior of precursor blends and their resulting polyimide composite films was measured on Si(100) wafers with the aid of a stress analyzer (Flexus) equipped with a hot stage. Here, the residual stress

Table III. Mechanical Properties of (PMDA-ODA)-(6FDA-APB) Composite Films Thermally Cured at 400 °C

<i>Mechanical Properties</i>	<i>100:0</i>	<i>75:25</i>	<i>50:50</i>	<i>25:75</i>	<i>0:100</i>
Modulus (GPa)	2.9	3.2	3.3	3.5	3.7
Stress at break (MPa)	221.1	215.8	186.9	139.4	133.5
Strain at break (%)	106	107	109	33	5
Stress at yield (MPa)	—	—	126.9	145.5	—
Strain at yield (%)	—	—	6	6	—

NOTE: The column headings are the ratios of PMDA-ODA(ES) precursor to 6FDA-APB (weight:weight).

Table IV. Mechanical Properties of (PMDA-PDA)-(6FDA-APB) Composite Films Thermally Cured at 400 °C

<i>Mechanical Properties</i>	<i>100:0</i>	<i>70:30</i>	<i>50:50</i>	<i>30:70</i>	<i>0:100</i>
Modulus (GPa)	9.8	7.6	5.8	4.3	3.7
Stress at break (MPa)	248.9	174.3	156.7	143.5	133.5
Strain at break (%)	6	5	5	6	5

NOTE: The column headings are the ratios of PMDA-PDA(ES) precursor to 6FDA-APB (weight:weight).

(σ_F) was calculated from radii of wafer curvatures measured before and after polyimide film deposition (10). During thermal curing and subsequent cooling, the stress of precursor blend films on Si wafers was monitored in situ as a function of temperature over the range of 25–400 °C. As a representative example, the stress versus temperature behavior of PMDA–ODA(ES) precursor is presented in Figure 4. During thermal imidization, the stress level of PMDA–ODA(ES) precursor film soft-baked at 80 °C was less than 5 MPa over the range of 25–400 °C and reflects the variation of intrinsic stress of the soft-baked precursor film system due to its continuous imidization and volume change through the evaporation of residual NMP and ethyl alcohol byproduct. After the completion of imidization at 400 °C, the stress increased with decreasing temperature on cooling and finally reached 29 MPa at room temperature.

Similar stress–temperature behavior was observed for the other polyimides studied here, but the stress level was dependent on backbone chemistry. For the films dried at 80 °C for 30 min, the residual stress at room temperature was 27 MPa for the *m*-PMDA–PDA(ES), 5 MPa for the PMDA–ODA(ES), and 12 MPa for both BTDA–APB and 6FDA–APB. The stress of a dried precursor film depends on the degree of drying in addition to the chemical backbone. The high residual solvent in the film gives the lower stress. After thermal curing at 400 °C, the stress at room temperature was 19 MPa for the PMDA–PDA [from *m*-PMDA–PDA(ES)], 29 MPa for the PMDA–ODA [from PMDA–ODA(ES)], 35 MPa for the BTDA–APB, and 38 MPa for the 6FDA–APB. Composite films of these materials exhibited stress behavior intermediate between those of the components. However, the stress of the composite films was significantly influenced by high-stress component, BTDA–APB or 6FDA–APB. As an example, the stress behavior of the (PMDA–ODA)–(6FDA–APB) composite films cured at 400 °C is illustrated in Figure 5. Cooling 6FDA–APB polyimide from 400 °C rapidly increased the stress from ca. 210 °C, due to its relatively low T_g (245 °C), whereas for the PMDA–ODA polyimide the stress increased gradually from 400 °C. In the stress–temperature curve, the slope of 6FDA–APB is relatively steeper than for the PMDA–ODA polyimide. The slope is primarily proportional to the degree of mismatch between the thermal expansion coefficients (TECs) of polyimide film and Si wafer (11). The TEC of Si(100) wafer is ca. 3.0 ppm/°C over the temperature range of 25–400 °C. Therefore, the TEC of 6FDA–APB is much higher than the TEC (30 ppm/°C) of PMDA–ODA polyimide (12). As shown in Figure 5, over the temperature range of 90–400 °C, the stress level of PMDA–ODA polyimide that exhibits higher T_g is higher than the stress level of 6FDA–APB, even though it has a relatively shallow slope in the stress–temperature curve. For this temperature range, the composite films show stress behavior intermediate between that of both components. However, below ca. 90 °C, the stress level of the PMDA–ODA polyimide is lower than that of the 6FDA–APB because of its

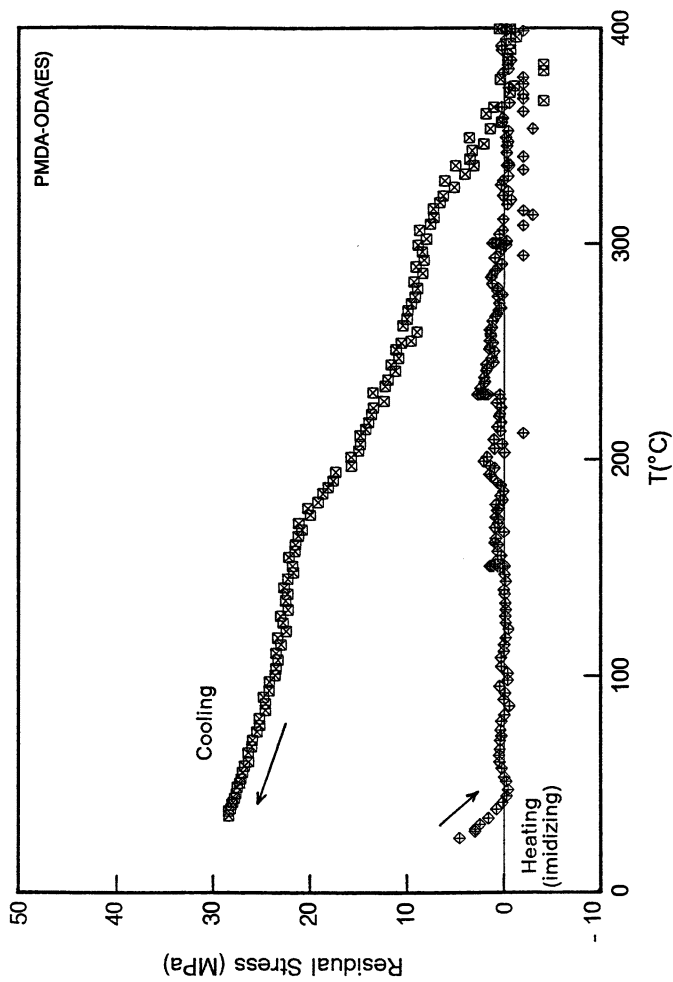


Figure 4. Residual stress versus temperature of the PMDA-ODA(ES) film soft-baked at 80 °C for 30 min dynamically monitored on a Si wafer during thermal curing and subsequent cooling.

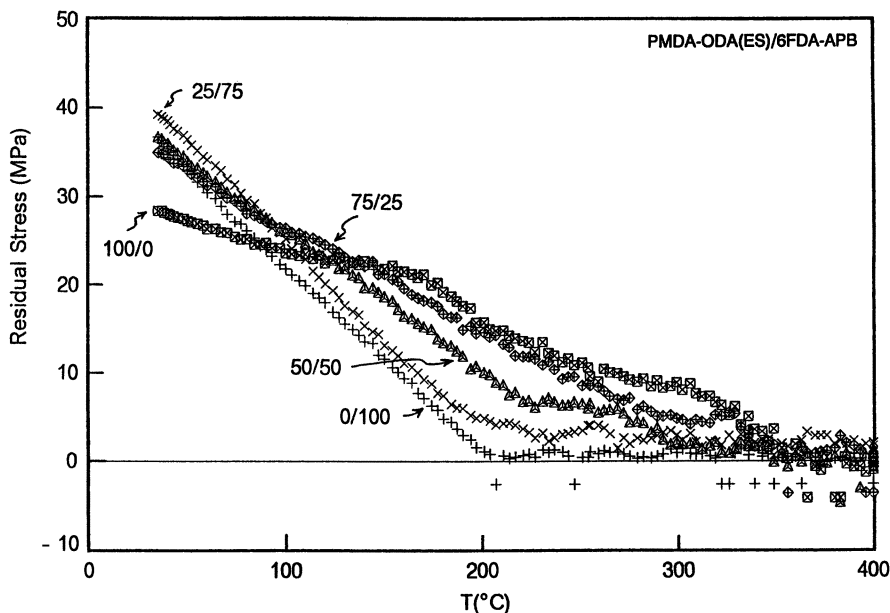


Figure 5. Residual stress versus temperature of the (PMDA-ODA)-(6FDA-APB) composite films dynamically measured on Si wafers during subsequent cooling with 1.0 °C/min rate after curing at 400 °C.

relatively shallow slope of stress-temperature variation. Below ca. 90 °C, the composite films no longer exhibit intermediate stress behavior, but rather show the same or slightly higher than stress level of the 6FDA-APB polyimide. Consequently, at room temperature the stress of the composite films cured at 400 °C was significantly increased by addition of 6FDA-APB component. This result indicates that the TEC of (PMDA-ODA)-(6FDA-APB) composite film, which is primarily responsible for generating thermal stress (10, 12) is highly influenced by the flexible, high stress (i.e., high TEC) 6FDA-APB component.

The stress relaxation of (PMDA-ODA)-(6FDA-APB) composite films was also studied in air with 50% RH (relative humidity) at room temperature. In general, the residual stress in a polymer film relaxes in two different modes: creep- and moisture-induced (14). For high T_g polymers, such as PMDA-ODA and 6FDA-APB polyimides, the creep-induced stress relaxation at room temperature may be small, because of very restricted molecular chain mobility in the highly supercooled state (14). For this reason, the stress relaxation of composite films measured in 50% RH at room temperature is believed to be mainly due to moisture-induced relaxation. The stress relaxation results of the composite films are illustrated in Figure 6. When the composite films on Si wafers were exposed to air with 50% RH, stress rapidly

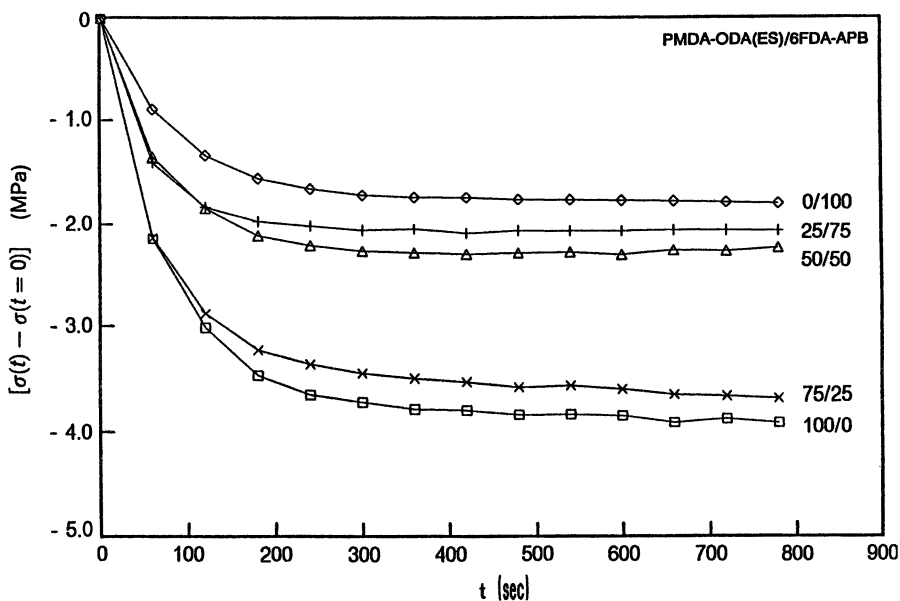


Figure 6. Moisture-induced residual stress relaxation behavior of the (PMDA-ODA)-(6FDA-APB) composite films on Si wafers measured in air with 50% relative humidity at 25 °C as a function of time.

relaxed with time at the initial stage, thereafter gradually decreased, and finally leveled off. The stress difference between the initial and relaxed states [$\Delta\sigma = \sigma(t = \infty) - \sigma(t = 0)$] reflects the degree of moisture uptake in the composite films. The stress difference $\Delta\sigma$ was 1.8 MPa for the 6FDA-APB, 2.1 MPa for the 25:75 composite, 2.3 MPa for the 50:50 composite, 3.7 MPa for the 75:25 composite, and 3.9 MPa for the PMDA-ODA polyimide. The initial slope in the $\Delta\sigma$ versus time plots is dependent on the diffusion coefficient of moisture in the composite films. The results in Figure 6 indicate that the diffusion of moisture is faster in PMDA-ODA polyimide than in 6FDA-APB, which leads to the conclusion that the PMDA-ODA polyimide film has absorbed relatively more water than the 6FDA-APB polyimide. Their composite films showed water uptake intermediate between those of the component polyimides. In addition, water uptake in the composite films was further dependent on the matrix component.

Adhesion Properties and Surface Composition. Several bilayer samples were prepared to investigate the self-adhesion behavior of polyimides and their composites. In this study, each layer was thermally cured at 400 °C as described in the experimental details section. The thickness of each layer was ca. 20 μm . The peel tests were performed at room temperature in the

90° peel mode. For both PMDA-PDA and PMDA-ODA, the peel strength was ca. 1 g/mm at a peeling rate of 2 mm/min, regardless of the precursor origin: polyamic acid or polyamic diethyl ester; that is, their self-adhesion was very poor. On the other hand, both 6FDA-APB and BTDA-APB samples could not be peeled apart, which indicates that enough molecular interdiffusion occurred between film layers to result in good adhesion. For all the composite systems [i.e., (PMDA-PDA)-(6FDA-APB), (PMDA-PDA)-(BTDA-APB), (PMDA-ODA)-(6FDA-APB), and (PMDA-ODA)-(BTDA-APB)], the 30:70 composition showed excellent self-adhesion (cannot peel) as expected on the basis of their matrix component, 6FDA-APB or BTDA-APB. However, for the 70:30 composition, the peel strength was strongly dependent on the cross-linkable oligomer component, 6FDA-APB or BTDA-APB. The 6FDA-APB composites with PMDA-ODA or PMDA-PDA showed high peel strength (ca. 80 g/mm) regardless of their high T_g polyimide matrices, whereas the corresponding BTDA-APB composites exhibited very poor self-adhesion (ca. 1 g/mm; *see* Table V). These results suggest that the self-adhesion of the composites with PMDA-PDA and PMDA-ODA matrices strongly depends on the flexible polyimide dispersant (BTDA-APB or 6FDA-APB). Furthermore, the surface composition of the 6FDA-APB composites is different from the surface composition of the BTDA-APB composites.

For the 6FDA-APB composites that exhibited excellent self-adhesion, the surface composition was analyzed by means of X-ray photoelectron spectroscopy (XPS). In XPS measurements, the penetration depth into the film surface was 50 Å. The content of 6FDA-APB at the surface region was estimated from the surface atomic concentration of fluorine. The results are shown in Table VI. The film surface of the (PMDA-ODA)-(6FDA-APB)

Table V. Self-Adhesion Properties of Polyimides and Their Composites

<i>Polyimide or Composite (w/w)</i>	<i>Peel Strength^a (g/mm)</i>
PMDA-PDA	ca. 1
PMDA-ODA	ca. 1
(PMDA-PDA)-(6FDA-APB) (70:30)	Cannot peel
(PMDA-ODA)-(6FDA-APB) (70:30)	80
(PMDA-PDA)-(BTDA-APB) (70:30)	ca. 1
(PMDA-ODA)-(BTDA-APB) (70:30)	ca. 1
6FDA-APB	Cannot peel
BTDA-APB	Cannot peel

^a $T_1 = T_2 = 400$ °C.

Table VI. Surface Composition and Self-Adhesion Strength of (PMDA-ODA)-(6FDA-APB) Composites

6FDA-APB		
Bulk (wt%)	Surface (wt%) ^a (top 50 Å)	Peak Strength ^b (g / mm)
0	0	ca. 1
25	90.2	80
50	98.4	(≥ 80)
75	97.6	(≥ 80)
100	100	Cannot peel

^a X-ray photoelectron spectroscopy data.

^b $T_1 = T_2 = 400$ °C.

(75:25) composite at a depth of 50 Å is composed of 90.2% 6FDA-APB. This high concentration of 6FDA-APB component at the film surface increased slightly with increasing concentration in the bulk: 98.4% 6FDA-APB for the 50:50 composite and 97.6% for the 25:75 composite. The results indicate that the 6FDA-APB component has been highly segregated on the surface of its composite films even with the PMDA-ODA matrix. This surface segregation might have taken place during solvent drying and subsequent thermal curing, due to the relatively lower surface energy of 6FDA-APB accompanied by phase separation because of its immiscibility with PMDA-ODA. Therefore, when the second layer film is cast on the 6FDA-APB-rich surface of the first film layer, enough molecular interdiffusion takes place between the layers to result in high adhesion strength. This molecular interdiffusion in 6FDA-APB is due to its flexible conformation characteristic with lower T_g and high swelling in NMP.

Such surface segregation may not be favorable in the BTDA-APB composites because the surface energy is similar to PMDA-ODA or PMDA-PDA, even under the circumstance of phase separation due to their immiscibility. In this case, there is still the question about the surface composition of the BTDA-APB composites. There are two possibilities:

1. The surface is composed of the open type of phase-separated domains of the flexible BTDA-APB component and its composition is equivalent to the bulk composition.
2. The surface composition is dominated by the matrix component.

If the BTDA-APB composites are like the first case, their self-adhesion is dependent on the amount of BTDA-APB component added into the PMDA-PDA or PMDA-ODA matrix, as well as the degree of phase separation. Consequently, in the first case, the self-adhesion of both

PMDA-PDA and PMDA-ODA composites can be improved by adding the BTDA-APB component, which exhibits excellent adhesion. However, if the second type of surface composition occurs in the BTDA-APB composites, the adhesion of the BTDA-APB composites with PMDA-ODA or PMDA-PDA matrix may be as poor as the adhesion of the PMDA-ODA or PMDA-PDA alone. In peel tests, neither PMDA-PDA nor PMDA-ODA composites with the BTDA-APB dispersant showed any improvement in self-adhesion. This result suggests that the surface composition of the BTDA-APB composites with the PMDA-ODA or PMDA-PDA matrix is dominated by the matrix component. In conclusion, the adhesion of the polyimide composites studied here is dependent on the nature of the flexible component and the surface composition characteristic, which includes phase separation and surface segregation.

Summary

SIPN-type rodlike (or semirigid) polyimide-flexible polyimide composites were prepared from acetylene-terminated oligomers (6FDA-APB and BTDA-APB) and soluble precursors of fully rigid PMDA-PDA and semirigid PMDA-ODA polyimides through solution blending and conventional solution casting-thermal curing processes to meld all advantageous properties of rigid or semirigid and cross-linked polyimides into one system. A homogeneous ternary solution with a relatively high concentration of ≤ 30 wt% was easily obtained in NMP for various compositions of the blend systems studied here. For all the blends, phase separation occurred during solvent drying before thermal curing. The domain size, which was set primarily during solvent removal, was preserved through subsequent thermal curing. The size of phase-separated domains was dependent on the blend system, composition, and functional group of polyimide precursors. For both fully rodlike PMDA-PDA and semirigid PMDA-ODA polyimides, the polyamic diethyl ester precursors exhibited better miscibility than the polyamic acid precursors with 6FDA-APB in NMP. The fluorinated preimidized 6FDA-APB was more miscible than the non-fluorinated BTDA-APB isoimide with these precursors in NMP. In particular, for the (PMDA-ODA(ES))-(6FDA-APB) blends, except the 30:70 and 50:50 compositions, optically transparent polyimide composite films were obtained. A transparent composite film was also obtained for the 10:90 (PMDA-ODA(ES))-(BTDA-APB) blend. However, the DMTA results indicate that the T_g s of both 6FDA-APB and BTDA-APB components do not vary with composition in their composites, which indicates the molecular demixing of the components.

The mechanical properties of cross-linked 6FDA-APB and BTDA-APB polyimides were significantly improved by the SIPN type of composite formation with PMDA-ODA polyimide owing to the good mechanical prop-

erties, in particular, good mechanical toughness. On the other hand, their composites with fully rodlike PMDA-PDA exhibited a significant improvement in the Young's modulus due to the high modulus characteristics of PMDA-PDA, but did not show any great improvement in the toughness, due to the poor elongation properties of both components. The residual stress behavior of the polyimides and their composite films was investigated in situ on Si wafers during curing and subsequent cooling, and was primarily dependent on the rigidity of the polyimide backbone. The stress level increased in the order of PMDA-PDA, PMDA-ODA, BTDA-APB, and 6FDA-APB. In particular, for the (PMDA-ODA)-(6FDA-APB) composites, stress at room temperature was equivalent to or slightly higher than the stress at room temperature of 6FDA-APB, which indicates that the stress of the PMDA-ODA composite film was influenced significantly by the 6FDA-APB component. This observation suggests that the TEC of the PMDA-ODA composites is significantly increased by the 6FDA-APB component. Similar stress behavior is expected for the polyimide composite systems considered here. The stress relaxation results due to moisture uptake indicate that the PMDA-ODA polyimide has absorbed more water than 6FDA-APB and their composites show water absorption intermediate between those of both components.

The self-adhesion of the polyimide composites has been strongly dependent on the surface composition characteristic, which is generally controlled by bulk composition as well as surface segregation and phase separation due to the surface energy difference and degree of immiscibility. The 6FDA-APB composites with PMDA-ODA and PMDA-PDA matrices exhibited excellent self-adhesion that results from the formation of a 6FDA-APB rich surface, due to its favorable surface segregation. In contrast, the BTDA-APB composites with PMDA-ODA or PMDA-PDA matrices showed no improved self-adhesion, which indicates that their surfaces are dominated by the matrix components.

Acknowledgments

The authors thank W. Volksen for providing *m*-PMDA-PDA(ES) polyimide precursor and D. Miller for XPS measurements.

References

1. Sroog, C. E. *J. Polym. Sci., Macromol. Rev.* **1976**, *11*, 161.
2. Mittal, K. L., Ed. *Polyimides: Synthesis, Characterization, and Applications*; Plenum: New York, 1984.
3. *Microelectronics Packaging Handbook*; Tummala, R. R.; Rymaszewski, E. J., Eds.; Van Nostrand Reinhold: New York, 1989.
4. Ree, M.; Yoon, D. Y.; Volksen, W. *Polym. Prepr. (Am. Chem. Soc., Div. Polym. Chem.)* **1990**, *31(1)*, 613.

5. Ree, M.; Swanson, S. A.; Volksen, W.; Yoon, D. Y. U.S. Patent 4,954,578, 1990.
6. Ree, M.; Yoon, D. Y.; Volksen, W. *Proc. Ultralloy '90*; Williams, D. J., Ed.; Schotland Research: Princeton, NJ, 1990; p 50.
7. Rojstaczer, S.; Ree, M.; Yoon, D. Y.; Volksen, W. *J. Polym. Sci., Polym. Phys. Ed.* **1991**, *30*, 133.
8. Ree, M.; Yoon, D. Y., Volksen, W. *J. Polym. Sci., Polym. Phys. Ed.* **1991**, *29*, 1203.
9. Ree, M.; Yoon, D. Y., Volksen, W. *Polym. Mat. Sci. Eng.* **1989**, *60*, 179.
10. Ree, M.; Swanson, S.; Volksen, W. *Polym. Prepr. (Am. Chem. Soc., Div. Polym. Chem.)* **1991**, *32(3)*, 308 and references therein.
11. Hoffman, W. R. In *Physics of Thin Film*; Hass, G.; Thun, R. E., Eds; Academic: New York, 1966; Vol. 3, p 211.
12. Ree, M.; Nunes, T. L.; Volksen, W.; Czornyj, G. *Polymer* **1992**, *33*, 1228 and references therein.
13. Timoshenko, S. *J. Opt. Soc. Am.* **1925**, *11*, 233.
14. Ree, M.; Nunes, T. L.; Chen, K.-J. R.; Czornyj, G. In *Materials Science of High Temperature Polymers for Microelectronics*; Grubb, D. T.; Mita, I.; Yoon, D. Y., Eds.; Materials Research Society Symposium Proceedings; Materials Research Society; Pittsburgh, PA, 1991; Vol. 227, p 211.

RECEIVED for review October 9, 1991. ACCEPTED revised manuscript August 24, 1992.

Phase Morphology of Simultaneous Interpenetrating Polymer Networks

Effect of Differences of Component Solubility Parameters and Glass-Transition Temperatures

H. L. Frisch and Peiguang Zhou

Department of Chemistry, State University of New York at Albany,
Albany, NY 12222

Recently we prepared two classes of simultaneous interpenetrating polymer networks (IPNs): the members of the first class always contained cross-linked poly(2,6-dimethyl-1,4-phenylene oxide) (PPO), a glassy material, as one network; the second class members always contained cross-linked aliphatic polycarbonate-urethane, a rubbery material, as one network. Except for polystyrene-PPO, the linear polymers that correspond to these IPNs were wholly immiscible. On the other hand, many but not all of the IPNs were fully miscible or showed large ranges of single-phase morphology (as seen from thermal, mechanical, or transmission electron microscopy studies). We approximately correlate the phase morphologies of these IPNs with differences in the solubility parameter and glass-transition temperatures of the linear homologs of the IPN components. All of the IPNs show an intermediate composition (or an intermediate composition in the single-phase region) in which the tensile stress to break exhibits a maximum. All the IPNs show superior physical properties to the corresponding physical blends of the linear polymers.

SIMULTANEOUS INTERPENETRATING POLYMER NETWORKS (1, 2) and related topological macromolecular isomers, such as the polymeric catenanes (3), involve at least two chemically different polymers predominantly held to-

gether by permanent entanglements (catenation) rather than direct grafting bonds between the different polymers. Simultaneous interpenetrating polymer network (SIN) phase morphology has been reviewed in a number of references (4, 5). Binder and Frisch (6) pointed out the theoretical possibility that fully miscible binary interpenetrating polymer networks (IPNs) could be formed (at all compositions of the two different component cross-linked networks) from polymers that have completely immiscible linear chains. As yet no rigorous, complete statistical dynamical theory of IPN formation and stability has been established.

Nonetheless, among the many factors on which such a theory may depend, there are two factors that certainly will play an important role. The first factor is the sign and magnitude of the excess Gibbs free energy of mixing of the linear polymer chains. Although this function is not directly available, a rough guide to its magnitude is provided by the following considerations: The order of magnitude of the entropy of mixing as given by the usual Flory expression for polymer mixtures is so small that the critical entity for van der Waals polymer mixtures with no strong H bonding, donor-acceptor, or acid-base interaction is played by the Van Laar-Hildebrand-Scatchard-type enthalpy. A rough guide to the magnitude of the excess Gibbs free energy is provided by the square of the difference of the solubility parameters of the polymers in the mixture. The larger this quantity is, the larger will be the tendency to phase separate. We will utilize the overall solubility parameter value, δ , or, more significantly (if available), the dispersive, δ_d , the polar δ_p , and the hydrogen bonding, δ_h , contributions (2). Even when δ has not been reported in the literature, we can crudely compute its value from group contributions as listed in reference 2. The better the match is (i.e., the smaller the difference) in δ or δ_d , δ_p , and δ_h of the component linear chains, the less positive is the excess Gibbs free energy of their mixing and, thus, we expect a smaller "thermodynamic" demixing tendency in the IPNs that produces either complete or microphase separation.

The second factor is the magnitude of the chain mobilities of the IPN polymers and their differences. In the preparation of miscible simultaneous IPNs (SINs), one attempts to approximately match the kinetic rates of cross-linking of the individual networks (1). Phase separation would tend to be suppressed if the rate of "uphill" diffusion were small compared to the effective rate of network cross-link formation. Suppressed phase separation topologically prevents the separation of the networks through permanent entanglements. Chains in "glassy" polymers move more sluggishly than chains of polymers with very low glass-transition temperatures, T_g . Therefore, polymer chains with well matched T_g s ("rough match of chain mobilities"), particularly if both T_g s are glassy, should show a smaller "dynamical" demixing tendency.

We investigated two series of IPNs and our conclusions bear only on these investigations. References in the literature indicate that there are fewer

miscible IPNs than the corresponding blends of linear polymers (12). In the first G (for glass) series, one network was always composed of poly(2,6-dimethyl-1,4-phenylene oxide) (PPO), a glassy material at room temperature. The PPO was cross-linked by methyl bromination of PPO and condensation of the resultant bromide of PPO with a diamine such as ethylene diamine (ED) or hexamethylene diamine (HMD). This condensation cross-linking of PPO did not interfere with (or was interfered with) the simultaneous free radical cross-linking employed to make the other network component of this G series of IPNs. The other free radical cross-linked networks were made from polystyrene (7) (PS), poly(methyl methacrylate) (8) (PMMA), polybutadiene (9) (PB), polyurethane–polyacrylate (10) (PUA), and poly(dimethylsiloxane) (11) (PDMS) chains. PPO was chosen because (1) the linear and cross-linked PPO is glassy, (2) linear PPO and PS chains are miscible, and (3) polymers of other architectures of PPO and, say, PDMS (e.g., graft, block, and fully anionically mutually grafted material) can be easily made (11).

In the second series, the R (for rubber) series, one network was always a polycarbonate–polyurethane (PCU). The PCU was prepared by cross-linking poly(1,6-hexanediol carbonate) with the biuret triisocyanate derived from hexamethylene diisocyanate via an addition reaction. This addition cross-linking reaction does not interfere with (or is interfered with) the simultaneous free radical cross-linking reaction employed to make the other network component of the SIN. The other free radical cross-linked components of this R series of IPNs we made from PMMA (13), PB (14), poly(4-vinylpyridine) (15) (PVP), and PS (16). PCU was chosen for its low T_g and because it can produce polymers with other architectures (e.g., graft copolymers with PMMA).

Experimental Details

Experimental details of the synthesis and characterization of these IPNs can be found in references 7–11 and 13–16. Both the G and R SINs are made by simultaneously mixing and cross-linking the prepolymers and cross-linking agent (possibly with catalysts) of the first network in homogeneous toluene solution with the difunctional monomer, polyfunctional cross-linker, and initiator of the second network. The molar masses between cross-links in these networks were typically of the order of 2×10^3 g/mol or a few multiples thereof. The materials were considered to be single-phased if they exhibited a single T_g from differential scanning calorimetry (DSC) or dynamic mechanical analysis (DMA) studies, exhibited no resolvable domains in high-magnification transmission electron microscopy (TEM) with appropriate staining (mercury stains for PPO, osmium tetroxide for PB, etc.), and had solid films (1 mm thick or thereabouts) that were transparent to visible light. Materials that exhibited two distinct T_g s (generally shifted inward from the T_g values of the pure cross-linked networks) were generally optically opaque and exhibited resolvable TEM domains and were thus classified as phase-separated (usually into two phases). Tensile strength and

elongation to break tests were carried out on a tensile tester (Instron) as a function of network composition. Essentially all IPNs exhibited an intermediate composition, y_c (in weight percent of one network component), at which a maximum tensile strength to break was observed (7–11, 13–17).

Ultimate Properties. The tensile strength and elongation to break were measured at room temperature on a tensile tester (Instron) at a crosshead speed of 5 in./min (ASTM D638).

Differential Scanning Calorimetry and Dynamic Mechanical Analysis.

The glass-transition temperatures (T_g 's) were determined by both DSC (DuPont 2910) and DMA (DuPont 983 DMA). DSC was calibrated using a 10-mg indium standard. DSC measurements were carried out on 10-mg samples from -100 to 200 °C at various scanning rates (e.g., 20 °C/min) under a nitrogen atmosphere. DMA testing was carried out from -100 to 200 °C (using a heating rate of 5 °C/min).

Transmission Electron Microscopy. TEM micrographs were taken on a transmission electron microscope (Philips 300). The preparation of specimens for electron microscopy was as follows: All samples were slivered and the shavings were stained for 3 days in 4% aqueous osmium tetroxide. The samples were then rinsed briefly and dried, after which they were embedded in Spurr resin. Sections were cut with glass knives on an L.K.B. Ultratome III, were stained with uranyl acetate and lead citrate, and were then viewed. For the G series, we also stained the PPO with mercuric trifluoroacetate (17).

Results and Discussion

The phase morphology of the G and R series of IPNs is summarized and compared to the corresponding blends of the linear polymers in Table I. All linear blends in Table I were immiscible except for the PPO–PS blend. The y_c is given for the PPO cross-linked with ED. Five of the IPNs made from completely immiscible blends (PPO–PMMA, PPO–PUA, PPO–PB, PCU–PMMA, and PCU–PB) are completely miscible over the complete composition range, whereas two (PCU–PS and PCU–PVP) are fully miscible over half the PCU composition range. Only the PPO–PDMS system is microphase separated over essentially the whole composition range (with domain sizes ranging (18) from 0.01 to 0.2 μm).

We suggest that this behavior correlates well with the difference in solubility parameters (19) and glass-transition temperatures (20) of the linear chains that compose the networks. The values of these parameters are shown in Table II. As Table II suggests, the complete match in solubility parameters of PPO and PS is sufficient to produce fully miscible linear blends. The

Table I. Phase Morphology of the G and R Series of IPNs and that of the Corresponding Blend of Linear Polymers

IPN	Composition Range (wt%)	Number of Distinct T_g s	y_c (wt%)	Number of Phases	
				In IPN	In Blends ^a
PPO-PS	Whole	1	75 (PPO)	1	1
PPO-PMMA	Whole	1	80 (PPO)	1	2
PPO-PUA	Whole	1	80 (PPO)	1	2
PPO-PB	Whole	1	90 (PPO)	1	2
PPO-PDMS	Whole	2	90 (PPO)	2	2
PCU-PMMA	Whole	1	30 (PCU)	1	2
PCU-PB	Whole	1	50 (PCU)	1	2
PCU-PS	100-60 PCU	1	30 (PCU)	1	2
50 PCU or less		2		2	2
PCU-PVP	100-60 PCU	1	70 (PCU)	1	2
50 PCU or less		2		2	2

^a The composition of the linear blends is the same as the IPN.

Table II. T_g and Solubility Parameters of the Linear Polymer Chains Found in the IPNs

Polymer	Solubility Parameters [(cal / cm ³) ^{1/2}]				T_g (°C)
	δ	δ_d	δ_p	δ_h	
PPO		8.6	3.0	2.0	211
PVP		9.6	5.1		142
PMMA	9.1-12.8	9.2	5.0	4.2	105
PS	8.5-9.3	8.6	3.0	2.0	100
PUA	9.1 ^a				
PCU	8.8 ^a				-40
PB	8.1-8.6	8.8	2.5	1.2	-95
PDMS	7.3-7.6				-127

^a δ computed from group contributions (2).

perturbation produced by the cross-linking system is sufficiently small and both chain T_g s are significantly above room temperature so that the IPNs are completely miscible. The small mismatch in solubility parameters in the PPO-PMMA system prevents miscibility of the linear blends but still allows full miscibility in the IPNs (which, among other factors, are held together by long-range permanent topological entanglements). Clearly there is also an approximate "match" (i.e., small enough difference) in the solubility parameters and T_g s in this system. The large mismatch in solubility parameters and T_g s of the PPO-PDMS system is where phase separation is found in both the blends and the IPNs over the whole composition range. The approximate

match in the solubility parameters and the relatively small differences in T_g s are in accord with the full miscibility of the PCU–PB IPNs, even though the difference in solubility parameters prevents any miscibility of the linear blends of the somewhat polar PCU and nonpolar PB. PCU and PMMA are both somewhat polar and the solubility parameter mismatch is sufficiently small that the IPNs are fully miscible even though there is a significant mismatch in the T_g s; see Figure 1. It is not unreasonable to suppose the larger difference in T_g s of the PCU–PS and PCU–PVP results in miscibility over only a part of the full composition range. The phase morphology of the pseudo (or semi) IPNs is summarized in Table III. As expected the pseudo IPNs are generally phase separated as are the polymeric catenanes of PPO and PDMS.

Figure 1 illustrates the difference in the DSC behavior of the (linear polymer) blend (two T_g s; phase separated) and the IPN (one T_g ; single phase) composed of 50-wt% PCU and 50-wt% PMMA as well as illustrates the fully transparent samples typically remain single phase with one T_g two and one-half years after preparation. The T_g of the IPN has decreased by about 15 °C. The original T_g s and tensile strength, τ , for IPN samples of PCU and PMMA are shown in Figure 2. Most samples exhibit such a decrease in the single T_g they possess. Almost all the pseudo (or semi) IPNs of PCU and PMMA as well as their linear blends are phase separated and exhibit two T_g s, as do the recently synthesized graft copolymer PMMA-*graft*-PCU and the fully gelled mutually grafted (cross-linked) PCU–PMMA network (21).

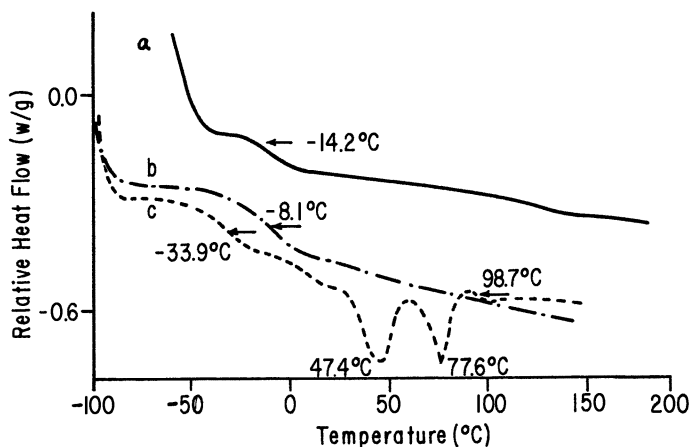


Figure 1. DSC spectra of the full IPN of PMMA–PCU [50-wt% PCU; run date, 1 October 1992 (DSC V₄.OB Dupont 2000)] (a); the same full IPN of PMMA–PCU [50-wt% PCU; run date, 17 April 1990 (DSC V₄.OB Dupont 2100)] (b); and a linear blend of PMMA and PCU (50-wt% PCU) (c).

Table III. Phase Morphology of the Pseudo (or Semi) IPNs of R and G Series and the PPO-PDMS Polymeric Catenanes

<i>Pseudo IPNs</i> ^a	Number of T_g s	Phase Domains	Number of Phases
C-PPO-L-PMMA and L-PPO-C-PMMA	2	Present	2
C-PPO-L-PB and L-PPO-C-PB	2	Present	2
C-PPO-L-PDMS and L-PPO-C-PDMS	2	Present	2
Polymeric catenanes of PPO-PDMS	1 ^b	Present	2
L-PCU-C-PMMA	2 ^c	Present	2
C-PCU-L-PB and L-PCU-C-PB	2	Present	2
C-PCU-L-PVP and L-PCU-C-PVP	2	Present	2

^a C is cross-linked and L is linear.

^b The melting point of pure cyclic PDMS.

^c Also two T_m s.

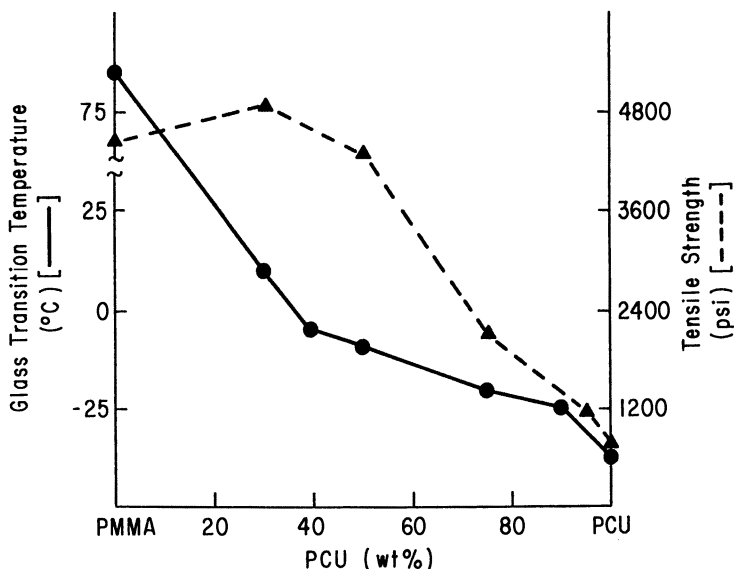


Figure 2. The glass-transition temperatures (solid line) and tensile strength (dashed line) of the full IPNs of PCU-PMMA.

In contrast, the PCU-PVP IPNs are only single phase if the weight percentage of PCU is larger than 50%; Figure 3 shows the T_g s and the τ of this system. Figure 4 shows the transmission electron micrographs of the pure cross-linked PCU and PVP, the single-phase IPN (of 70-wt% PCU), the phase-separated IPN (of 50-wt% PCU), and the phase-separated blend of the linear polymers.

Figure 2 illustrates the existence of a (absolute) maximum in τ with composition, y_c , expressed as weight percent (in this case) of PCU. We

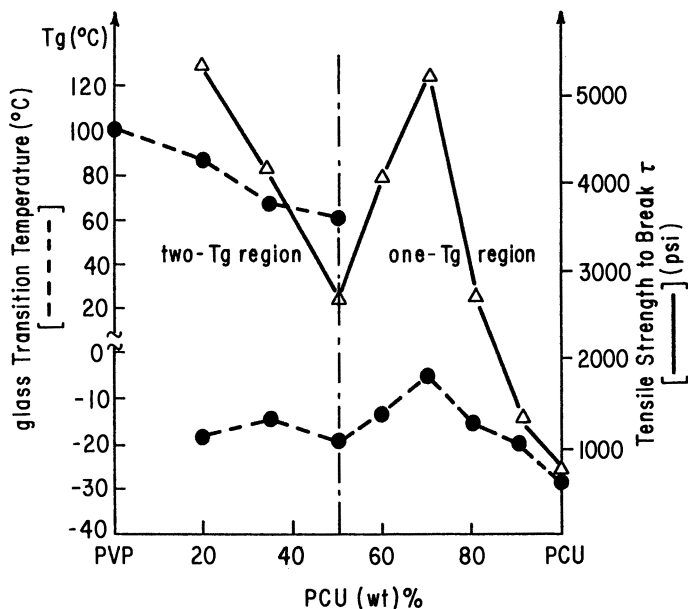


Figure 3. The glass-transition temperatures (dotted lines) and tensile strength (solid line) of the full IPNs of PCU–PVP.

previously proposed a simple plausibility argument to explain why such maxima in τ can be observed (18); this argument will be discussed next.

Theoretical Details

A mean field plausibility argument explains why a maximum in tensile strength can sometimes be observed. The cohesive component of the tensile stress to break, τ_{coh} , of a one-phase system of two components that are not permanently entangled with each other is generally a monotone function of composition, say, the weight fraction of the first component, w . For initial mathematical simplicity we take this monotone relation as linear and write

$$\tau_{\text{coh}} = a + bw; \quad a, a + b > 0 \quad (1)$$

with a the τ_{coh} of the second network and $a + b$ the τ_{coh} of the first network. In an IPN there is another source of ultimate “strength” due to the permanent mutual entanglement of the component networks, τ_{ent} .

We take the total tensile strength to break τ to be additive; that is,

$$\tau = \tau_{\text{coh}} + \tau_{\text{ent}} \quad (2)$$

Little is gained by taking a more general linear combination for τ because it can be assumed that the proportionality factors of this combination are already factors in the constants that appear in τ_{coh} and τ_{ent} . To obtain a crude, mean field estimate of τ_{ent} , we consider first a special IPN composed of chains of two isotopic species, all of identical molar mass between cross-links, that meet at the vertices of a cubic lattice (six chains of each separate network are cross-linked there). We further assume that end effects and effects due to the thickness of the chains are negligible. Clearly the only effective mechanism by which such chains can interpenetrate extensively to form an IPN of two coherent, connected networks is if the species consist of two interpenetrating cubic lattices. w is the weight fraction of the first isotopic species and $1 - w$ is the weight fraction of the second species. The center of the unit cell of the second network can be displaced anywhere within the unit cell of the first network in this (cesium chloride) structure network. The probability of effective entanglements in this IPN is $P(w) = w(1 - w)$, by symmetry and neglecting higher order terms in w . $P(w)$ has a maximum value at $w_c = 1/2$ when $dP(w)/dw$ vanishes. We expect that in this case we can take

$$\tau_{\text{ent}} = AP(w) = Aw(1 - w); \quad A > 0 \quad (3)$$

with A the maximum contribution to the tensile strength that can come from entanglements. This entanglement contribution to the stress must be positive (hence $A > 0$). In the general case of an IPN formed from nonequivalent chains with different molar masses between cross-links of possibly different functionality, we introduce in roughly the same approximation an effective entanglement weight fraction of network 1, ϕ , by defining two entanglement efficiencies, e_1 and e_2 , that take into account the different abilities of the two chains to encounter one another in such a way that loops of the two networks are permanently entangled. We set

$$\begin{aligned} \phi &= e_1 w / [e_1 w + e_2(1 - w)]; \\ 1 - \phi &= e_2(1 - w) / [e_1 w + e_2(1 - w)] \end{aligned} \quad (4)$$

and take now, in sufficient approximation,

$$P(w) = \phi(1 - \phi) \quad (5)$$

and

$$\tau_{\text{ent}} = AP(w) = A\phi(1 - \phi) \quad (6)$$

Note that this choice correctly makes $P(w)$ vanish for $w = 0$ or $w = 1$ and reduces eq 5 correctly to $P(w) = w(1 - w)$ for the isotopic IPN for which

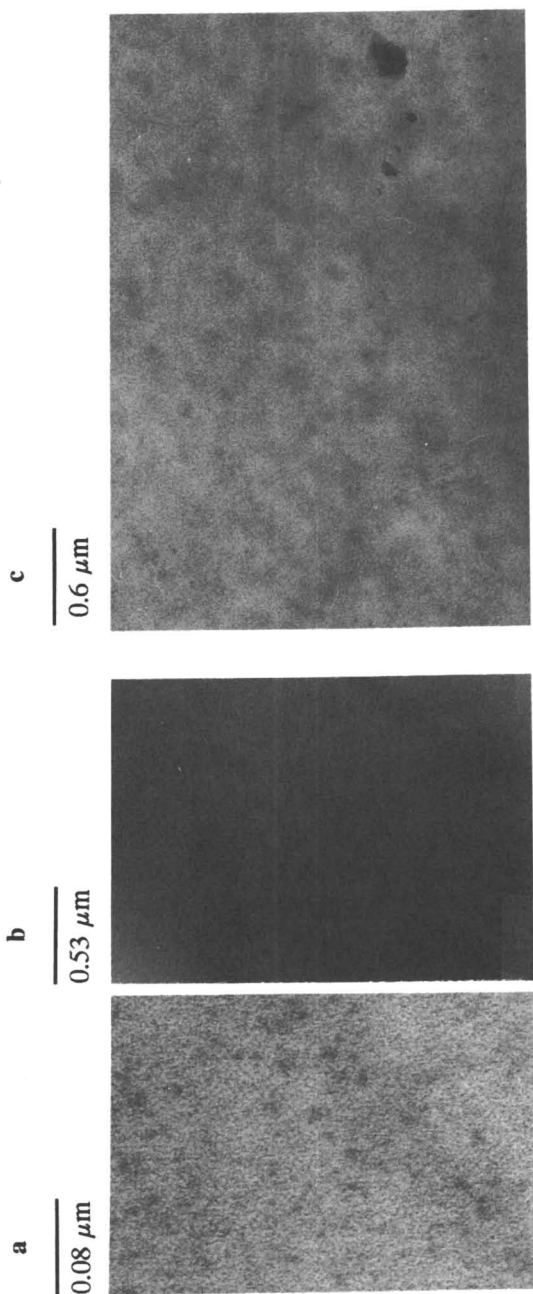


Figure 4. Transmission electron micrographs of the full IPNs, linear blend, and pure cross-linked components of PCU and PVP: Pure cross-linked poly(vinylpyridine) ($\times 221,000$) (a); pure cross-linked polycarbonate-polyurethane ($\times 38,000$) (b); the full IPN of PCU-PVP (70-wt% PCU; $\times 31,200$) (c).

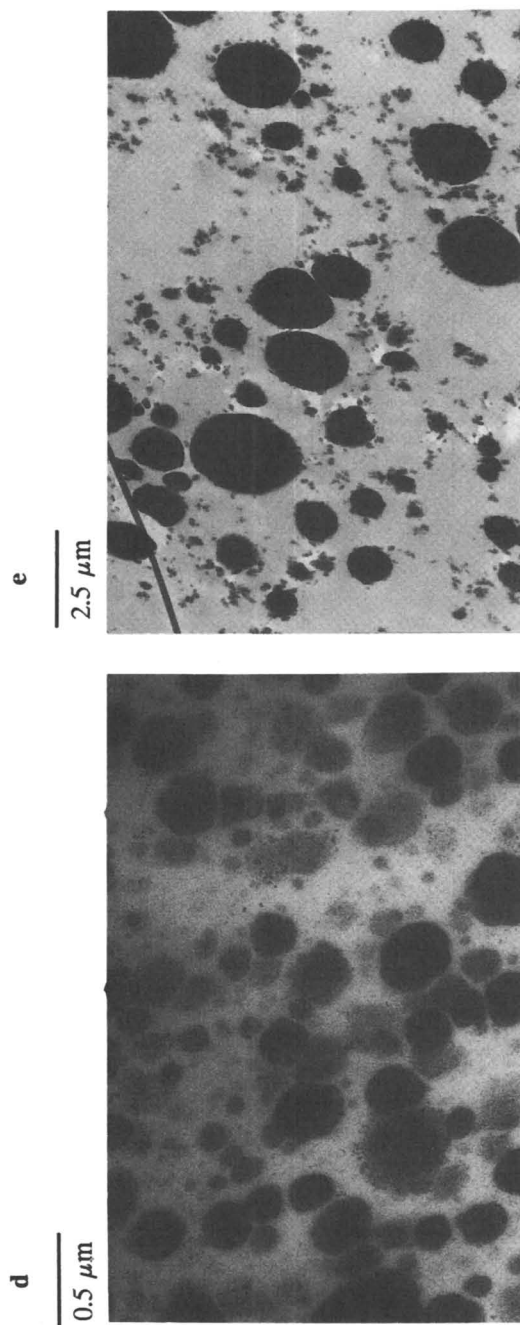


Figure 4. Continued. The full IPN of PCU-PVP (50-wt% PCU; $\times 40,000$) (d); the linear blend of PCU-PVP (50-wt% PCU; $\times 7,000$) (e).

$e_1 = e_2$. Substituting eqs 5 and 1 into eq 2 yields

$$\tau = a + bw + A\phi(1 - \phi) \quad (7)$$

To find a possible maximum value of τ for $0 \leq w \leq 1$, we equate the first derivative of τ with respect to w (given by eq 7) to zero. Setting $\Delta = e_1 - e_2$, $\sigma = e_1 + e_2$, and $\kappa = A/b$, we find that the composition $w = y$ for which τ reaches maximum, y_c , must satisfy the cubic relation in y :

$$\Delta^3 y^3 + 3e_2 \Delta^2 y^2 + (3e_2^2 \Delta - \kappa e_1 e_2 \sigma) y + e_2 (e_2^2 + \kappa e_1 e_2) = 0 \quad (8)$$

For sufficiently small Δ and large κ , so that terms of order Δ^2 and Δ^2/κ^3 can be neglected,

$$\begin{aligned} y_c &= \frac{1}{2} \left[(1 + 1/\kappa) - \frac{1}{2} (1 - 3/\kappa^2) (\Delta/e_2) \right] \\ &\approx w_c + (2\kappa)^{-1} \end{aligned} \quad (9)$$

where w_c is the w value that maximizes $P(w)$.

Finally, a somewhat better engineering approximation to the monotone τ_{coh} than the linear relation given by eq 1 is

$$\tau_{\text{coh}} = a + bw^\alpha; \quad a, a + b > 0, \quad (10)$$

with α an empirical parameter, where $\alpha > 0$. Introducing this relation into eq 2, we have

$$\tau = a + bw^\alpha + A\phi(1 - \phi) \quad (11)$$

where ϕ still is given by eq 4. The only parameters involved are the tensile stress to break of the pure network components, $\tau(w = 0) = a$ and $\tau(w = 1) = a + b$, and three previously defined dimensionless parameters α , κ , and $r = e_2/e_1$. Without loss of generality, we assume $b > 0$ and rearrange eq 11:

$$\tau/b - a/b = w^\alpha + \kappa r w(1 - w)/[w + r(1 - w)]^2 \quad (12)$$

where

$$r = e_2/e_1 \quad (13)$$

Figure 5 shows plot of $(\tau/b - a/b)$ versus w for various values of α , κ , and r that exhibit maxima or no maxima. Figure 6 shows the maxima in τ with PPO composition for the G series of IPNs (7-11) that resemble roughly the theoretical dependence. Figure 6 also represents the behavior of the R series

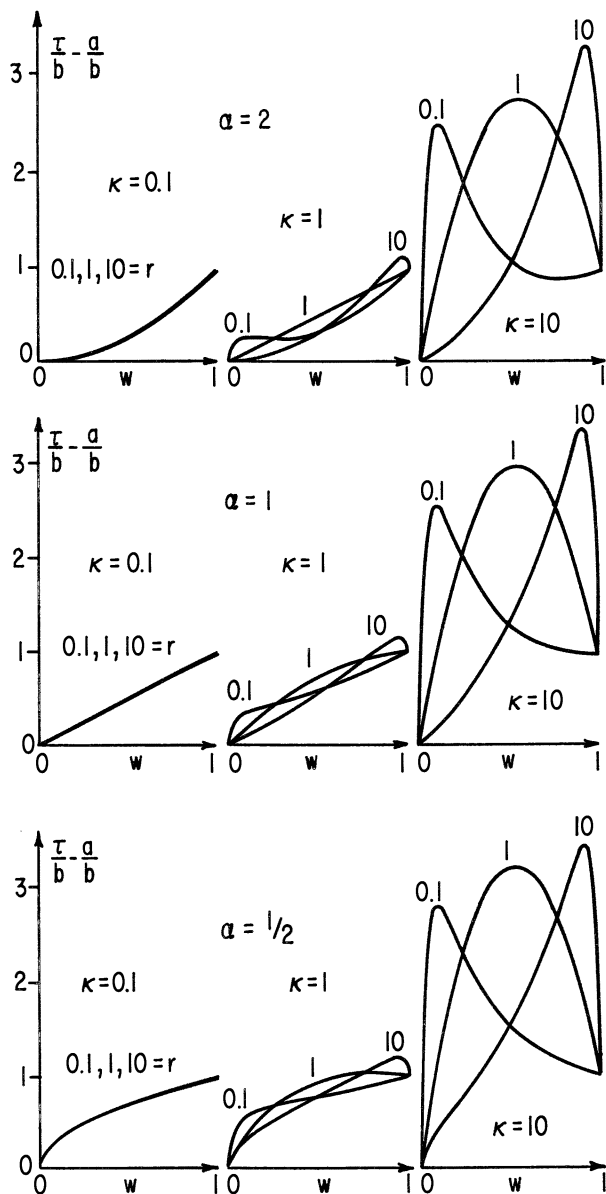


Figure 5. Plot of $\tau_b/b - a/b$ versus w given by eq 1, $b > 0$, for the dimensionless parameter values $\alpha = 1/2, 1, 2$, $r = 0.2, 1, 10$, and $\kappa = 0.1, 1, 10$.

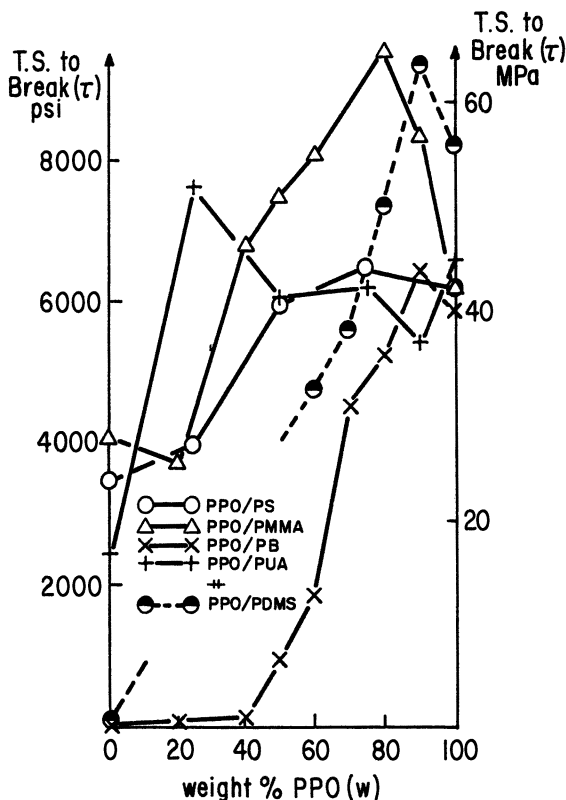


Figure 6. The tensile strength to break, τ , versus weight percent PPO for the G series of IPNs.

(cf. Figure 2). The PPO-PUA curve shown in Figure 6 is for a sample that has a PPO network cross-linked with HMD.

Summary and Conclusions

Completely miscible, one-phase IPNs can be made from components whose linear polymers are wholly immiscible (e.g., PPO-PMMA, PPO-PUA, PPO-PB, PCU-PMMA, and PCU-PB). In some cases, one-phase IPNs that are miscible only over a portion of the composition range result (e.g., PCU-natural rubber, PCU-PS, and PCU-PVP), whereas other IPNs are two-phased in the whole composition range (e.g., PPO-PDMS). As previously suggested (19, 20), the differences in solubility parameter and T_g s roughly correlate with the phase morphology of fully or partially miscible IPNs even in compositions of polymers that form immiscible linear blends. These IPNs can have superior properties (e.g., ultimate mechanical strength) compared to the

pure cross-linked networks or any blend of the corresponding linear polymers.

Acknowledgment

This work was supported by the National Science Foundation under Grant DMR-90-23541.

References

1. Sperling, L. H. *Interpenetrating Polymer Networks and Related Materials*; Plenum: New York, 1981.
2. Olabisi, O.; Robeson, L. M.; Shaw, M. T. *Polymer-Polymer Miscibility*; Academic: New York, 1976.
3. Huang, W.; Frisch, H. L.; Hua, Y. H.; Semlyen, J. Z. *J. Polym. Sci., Polym. Chem. Ed.* **1990**, *28*, 1807.
4. *Recent Developments in Polymethanes and Interpenetrating Polymer Networks*; Frisch, K. C., Jr., Ed.; Technomic: Lancaster, PA, 1988.
5. *Polymer Alloys*; Klempner, D.; Frisch, K. C., Eds.; Plenum: New York, 1977.
6. Binder, K.; Frisch, H. L. *J. Chem. Phys.* **1984**, *81*, 2126.
7. Frisch, H. L.; Klempner, D.; Yoon, H. K.; Frisch, K. C. *Macromolecules* **1980**, *13*, 1016.
8. Singh, S.; Chiradella, H.; Frisch, H. L. *Macromolecules* **1990**, *23*, 375.
9. Frisch, H. L.; Hua, Y. H. *Macromolecules* **1989**, *22*, 91.
10. Mengnjoh, P. C.; Frisch, H. L. *J. Polym. Sci., Polym. Chem. Ed.* **1989**, *27*, 3363; Frisch, H. L.; Mengnjoh, P. C. *J. Polym. Sci., Polym. Lett. Ed.* **1989**, *27*, 285.
11. Frisch, H. L.; Gebreyes, K.; Frisch, K. C. *J. Polym. Sci., Polym. Chem. Ed.* **1988**, *26*, 2589; Gebreyes, K.; Frisch, H. L. *J. Polym. Sci., Polym. Chem. Ed.* **1988**, *26*, 3391; Huang, W.; Frisch, H. L. *Macromol. Chem. Phys. Suppl.* **1989**, *15*, 137.
12. Briber, R. M.; Bauer, B. J. *Macromolecules* **1991**, *24*, 1899.
13. Frisch, H. L.; Zhou, P.; Frisch, K. C.; Xiao, X. H.; Huang, W.; Chiradella, H. J. *Polym. Sci., Polym. Chem. Ed.* **1991**, *29*, 1031-1038.
14. Frisch, H. L.; Zhou, P. *J. Polym. Sci., Polym. Chem. Ed.* **1992**, *30*, 2794.
15. Zhou, P.; Frisch, H. L. *J. Polym. Sci., Polym. Chem. Ed.* **1992**, *30*, 835.
16. Zhou, P.; Frisch, H. L. *J. Polym. Sci., Polym. Chem. Ed.* **1992**, *30*, 887.
17. Hobbs, S. Y.; Watkins, V. H.; Russell R. R. *J. Polym. Sci., Polym. Phys. Ed.* **1980**, *18*, 393.
18. Frisch, H. L.; Huang, M. W. In *Siloxane Polymers*; Semlyen, J. A.; Clarkson, S., Eds.; Prentice-Hall, Englewood Cliffs, NJ, 1993.
19. Frisch, H. L. *Mater. Res. Soc. Symp. Proc.* **1990**, *171*, 231.
20. de Barros, G. G.; Huang, M. W.; Frisch, H. L. *J. Appl. Polym. Sci.* **1992**, *44*, 255.
21. Zhou, P.; Frisch, H. L. *J. Polym. Sci., Polym. Chem. Ed.* **1992**, *30*, 2577.

RECEIVED for review September 20, 1991. ACCEPTED revised manuscript October 15, 1992.

Microstructural Aspects of Interpenetrating Polymer Networks Based on Block Copolymers

R. P. Burford¹, J. J. Jones¹, and Y.-W. Mai²

¹Department of Polymer Science, University of New South Wales, P.O. Box 1, Kensington, NSW 2033, Australia

²Department of Mechanical Engineering, Sydney University, Sydney, NSW 2066, Australia

The morphologies of block copolymers used in the preparation of interpenetrating polymer networks (IPNs) are examined by high-resolution transmission electron microscopy (TEM) to allow changes in microstructure during IPN production to be followed. For both the di- and triblock styrene butadiene copolymers used, thin films cast from toluene give different images from cryosectioned bulk samples. The IPNs are made by the in situ thermal polymerization of styrene absorbed in chemically cross-linked copolymer sheets. The morphology of the IPN at each stage of preparation together with the morphology of the associated copolymer at a similar stage of processing is given. Image analysis is used to obtain additional characterization.

THE MAJOR CHARACTERISTICS OF INTERPENETRATING POLYMER NETWORKS (IPNs) have been reported extensively over the past two decades. In addition to symposium series monographs (for example, references 1 and 2), a series of specialized books (3) and a journal (4) have appeared. As indicated by Klempner and Frisch in the introduction of the *Advances in Interpenetrating Polymer Networks* series (3), the scope of IPN research now includes systems where little cross-linking and sometimes substantial grafting exist.

IPNs based on synthetic elastomers and polystyrene are direct extensions from existing high-impact polystyrene (HIPS) analogs. Such IPNs were

described thoroughly in the 1970s by Donatelli et al. (5, 6) and Fernandez et al. (7). The same authors also reported (8, 9) on IPNs based on styrene-based block copolymers and presented important contributions to the thermodynamics of mixing and associated changes in domain dimensions. However, only limited high-resolution transmission electron microscopy (TEM) (for example, Figure 1) was included. In contrast to the present chapter, little attempt was made to compare changes in morphology of the constituent block copolymer as it was transformed to the final product.

Block Copolymer Morphology

Thermoplastic elastomers generally comprise block copolymers with hard and soft segments, which aggregate to give regions that are resolvable by transmission electron microscopy and other techniques. For example, highly regular structures of stained styrene-butadiene copolymers have been known since the 1970s (10). Block copolymer morphology has been reviewed comprehensively for over two decades (11–13). As more sophisticated instruments and data analysis systems have appeared, higher resolution studies of

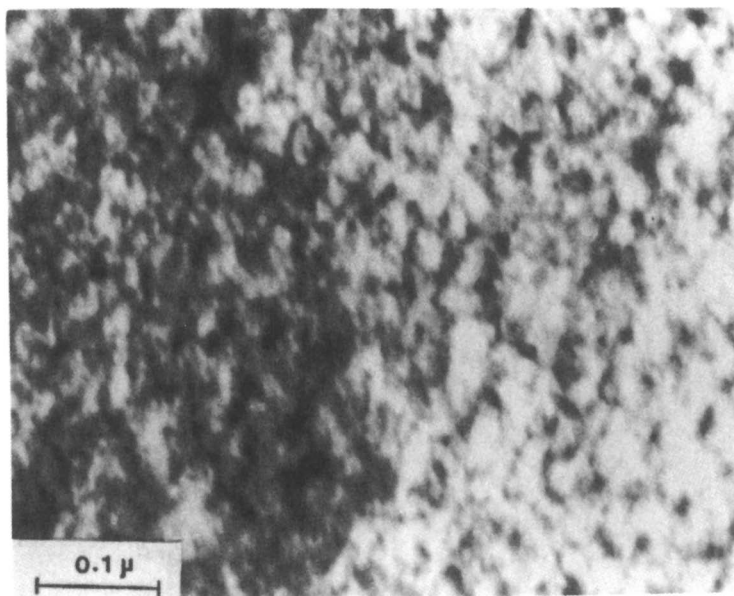


Figure 1. Fully polymerized PB-PS IPN. The PB phase is stained dark with OsO₄ (9).

the domain morphology and the interfacial bonding characteristics of the hard and soft segments have evolved (14, 15).

The domain structures formed by microphase separation in block copolymers that comprise two immiscible block chains have dimensions and shapes that are directly related to molecular dimensions and to the thermodynamic interactions of the block components. Meier (16) concluded that the predominant factor that controls domain size is the need of chain segments to uniformly fill space.

Well-established thermodynamic theories show the effect of equilibrium domain structure on component relative weights and explain the change from spherical to cylindrical to lamella morphology as second monomer content increases. For example, Spontak et al. (17) showed that the morphology of a styrene-butadiene-styrene (SBS) block copolymer will vary with increasing polystyrene (PS) weight fraction.

Equilibrium domain structure is also influenced by the segment molecular weight, which affects the location of the boundary that defines the transition from homogenous to microphase-separated states. The role of processing history on domain morphology is also important (18, 19): morphologies range from semicontinuous to aggregates.

Blends Incorporating Block Copolymers

Block copolymers have been used widely as interfacial agents typically between two immiscible thermoplastics (20). In many cases suitable compatibilizers can be predicted by matching hard and soft segments of the block copolymer with the major blend constituents. Thus styrene-butadiene block copolymers can be used successfully where hard and soft nonpolar polymers are present, but in practice this use limits the range of possible blends. More recently, hydrogenated copolymers [e.g., styrene-ethylene-butylene-styrene block copolymers (SEBS)] have been used for polyethylene-polystyrene blends (21) and functionalized SEBS is used widely for blends of polar engineering polymers including polyamides and polyesters (22).

Transparent modified grades of polystyrene have been formed using SBS block copolymers when a continuous lamellar microstructure exists. Examples of these materials are reviewed by Eehte (23), who designates these polymers as "transparent HIPS."

The morphology of polystyrene and styrene-butadiene block copolymers has been shown (24) extensively, but in these polymers fracture toughness is mediocre. In summary, binary mixtures of polystyrene and butadiene-styrene block copolymer achieve a wide range of morphologies, dependent on composition and block architecture, that leads to a wide range of optical and

physical properties. However, very stiff and tough products comparable with, for example, acrylonitrile–butadiene–styrene (ABS), have not been reported.

IPNs Based on Polystyrene and Block Copolymers

IPNs based on polystyrene and block copolymers have been reported (9, 25) and the morphology of associated products has been revealed. In particular, it was shown that the phase structure of the original SBS was retained, but that dimensions changed.

Theories that relate to changes in polymer dimensions exist. Yeo et al. (26) developed a series of theoretical equations to predict the domain size (D_2) in IPNs and related materials. The equations are based on a domain formation process and comprise the cross-linking density of each polymer, mixing and demixing thermodynamics, network swelling, and the elastic deformation of each polymer network.

Thus, equation 1 provides D_2 in terms of the experimental variables for polymer 1 and polymer 2 of volume fraction (ϕ_1, ϕ_2), cross-link level (ν_1, ν_2), molecular weight (M_1, M_2), density (ρ_1, ρ_2), interfacial tension (γ), and temperature (T), where R is the gas constant:

$$D_2 = 4\gamma [RT(A\nu_1 + B\nu_2 - C)]^{-1} \quad (1)$$

$$A = \frac{1}{2}(1/\phi_2)(3\phi_1^{1/3} - 3\phi_1^{4/3} - \phi_1 \ln \phi_1) \quad (2)$$

$$B = \frac{1}{2}(\ln \phi_2 - 3\phi_2^{2/3} + 3) \quad (3)$$

$$C = (\phi_1/\phi_2)(\rho_1/M_1)\ln \phi_1 + (\rho_2/M_2)\ln \phi_2 \quad (4)$$

Specific forms of equation 1 for individual cases were derived by Yeo et al. (26).

Burford et al. (27, 28) formed sequential semi-IPNs and full-IPNs based on two block copolymers and showed that tough transparent polymers can form when the block copolymer is highly chemically cross-linked. Strain energy release rates are up to 10 times greater than corresponding cross-linked polybutadiene or random styrene–butadiene rubber IPNs. Further, Burford et al. provided some description of the microstructure of resulting IPNs and emphasized changes in domain size and anisotropy (29, 30). How morphology develops from the constituent block copolymers to the final IPN is shown in this chapter.

Experimental Details

Materials Preparation. Solprene 1205 and 416 block copolymers from the Phillips Chemical Company were used throughout. Solprene 1205 is stated by the manufacturer (31) to be a styrene–butadiene linear diblock that contains

25-wt% PS and has a molecular weight of 83,000. Solprene 416 is a radial SBS triblock with 30-wt% PS and a molecular weight of 140,000.

Both semi-IPNs and true IPNs were prepared by sequential polymerization where the first polymer was cross-linked and the second polymer was synthesized or cross-linked in situ. The synthesis of IPNs based on these block copolymers has been given in detail elsewhere (29, 30), but a summary is given. The block copolymer granules are premixed with dicumyl peroxide (DICUP) cross-linker (up to 1% DICUP) in an internal mixer (Haake 600) for 5 min at 75 °C. The block copolymers with cross-linker are then cured in a steam-heated press with molds that conform to ASTM D3182 at 145 °C for 60 min. The pads are then swollen in styrene containing 1% benzoyl peroxide with and without 5% divinylbenzene (DVB; a cross-linker for the PS). Thermal curing in metal frames leads to transparent or translucent samples with 70% additional polystyrene weight increase.

Transmission Electron Microscopy. A major challenge in polymer analysis by TEM is to obtain specimens with adequate transparency and contrast when exposed to a 75–125-kV electron beam. Generally samples less than 100 nm thick are required from bulk substrate. The sections are prepared by ultramicrotome techniques commonly used for biological materials. SBS–PS IPNs that are relatively stiff can be satisfactorily sectioned at 25 °C with an ultramicrotome (Reichert–Jung Ultracut E) and a glass knife (32, 33).

Because of their softness at ambient temperatures, constituent block copolymers were cryosectioned at –100 °C with an ultramicrotome (Reichert–Jung Ultracut FC4E) in liquid nitrogen facilities.

In addition to the ultramicrotomed samples, the constituent block copolymers were solvent-cast. The SBS was evaporated from 0.01-wt% toluene solutions onto formvar (polyvinyl formar) supported grids (34).

In the TEM, image contrast between phases is generally poor in unstained polymers because the low atomic number elements that comprise the polymers produce little electron scattering. This problem is dealt with by staining with heavy metal compounds that react selectively with certain structural features and produce contrast by local scattering of the electron beam. Osmium tetroxide reacts with carbon–carbon double bonds and therefore produces excellent image contrast in polymers that contain one unsaturated phase, like these SBS systems. The OsO₄ not only stains, but hardens the rubber phase, which renders softer samples sectionable. The bulk block copolymers were thus stained before cryosectioning.

Sections typically 80 nm thick were obtained and subsequently stained in 5% aqueous OsO₄ for 30 min. Then the samples were viewed with a TEM (Hitachi 7000) at 75–125 kV.

Results and Discussion

Morphology of Block Copolymers. The Solprene 416 and 1205 elastomers have comparable morphologies, although some slight differences can be found. Furthermore, the trends that are found at each processing stage, and also the more intensive three-dimensional examinations, give similar results for each elastomer; therefore, only one type will be illustrated.

Because these polymers are generally employed with no chemical cross-linkers but after some significant thermal history, an appropriate reference point is examination of their morphologies after compression molding. Thus the Solprene morphologies are shown (Figures 2 and 3) after premixing in an internal mixer unit for 5 min at 75 °C and molding at 145 °C for 30 min.

The morphologies comprise cylindrical domains that are consistent with other styrene-butadiene copolymers such as, for example, the morphologies reported by Aggarwal (35). There is some modest difference in the polystyrene-rich (i.e., unstained) domain width that might be attributed to differences in polymer segment length. The micrograph for Solprene 1205 suggests a more aligned structure compared with the semicontinuous nodes and isolated spheres evident in Solprene 416. However, as will be shown,

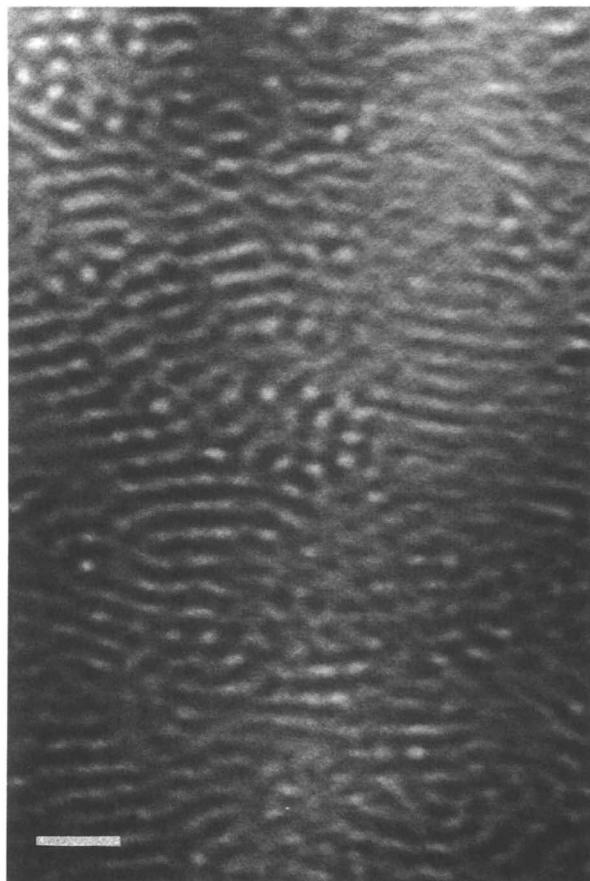


Figure 2. TEM of Solprene 1205 (bar = 100 nm).

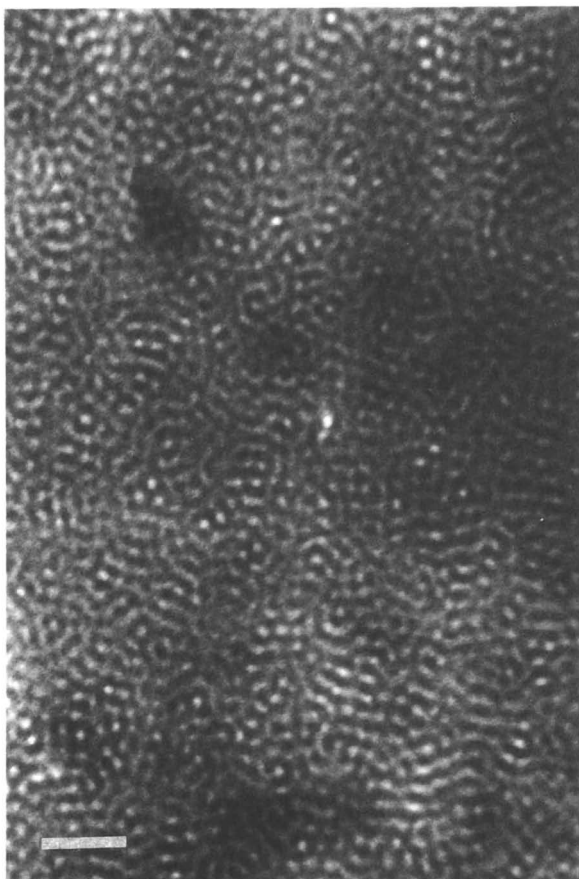


Figure 3. TEM of Solprene 416 (bar = 100 nm).

both polymers are anisotropic and these differences can be attributed to small changes in sectioning direction.

Note that, as previously indicated (36), the morphologies differ from solvent-cast thin films. For example, Solprene 1205 cast from 0.01-wt% toluene solution has the morphology shown in Figure 4a. Scattered styrene-rich domains are ~ 50 -nm diameter, but the primary feature is a diffuse mosaic of less-stained 10–15-nm domains in the butadiene-rich continuous phase. Although there is some evidence for the aggregation of spheres, the pattern is quite diffuse and the contrast between stained and less-stained regions is low. The corresponding solvent-cast Solprene 416 (Figure 4b) film is similar but with smaller (< 10 -nm) domains. This observation indicates the care needed in phase transition studies of block copolymers because solvents

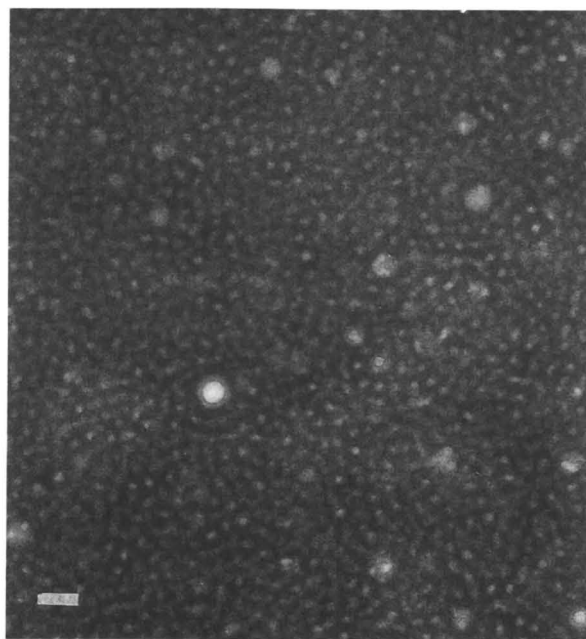
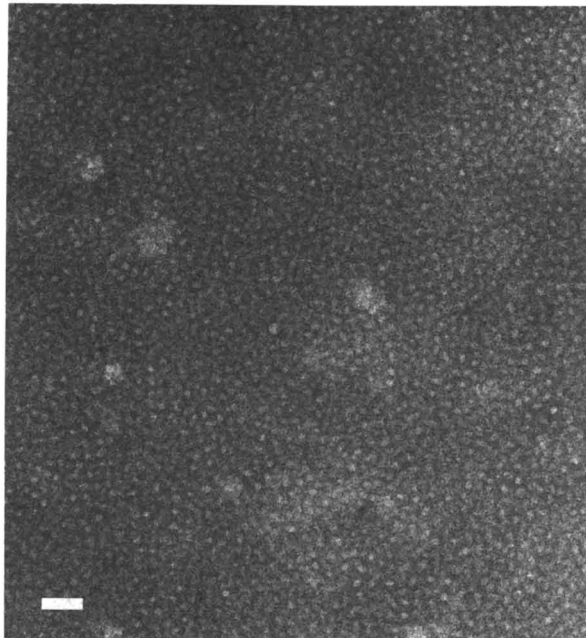
**a****b**

Figure 4. TEM of solvent cast Solprene 1205 (a) and Solprene 416 (b) (bars = 100 nm).

will increase the complexity of interactions that take place. Therefore, the cryosectioned samples provide a more realistic indication of these block copolymers, and are the more appropriate controls to compare with the IPN morphology.

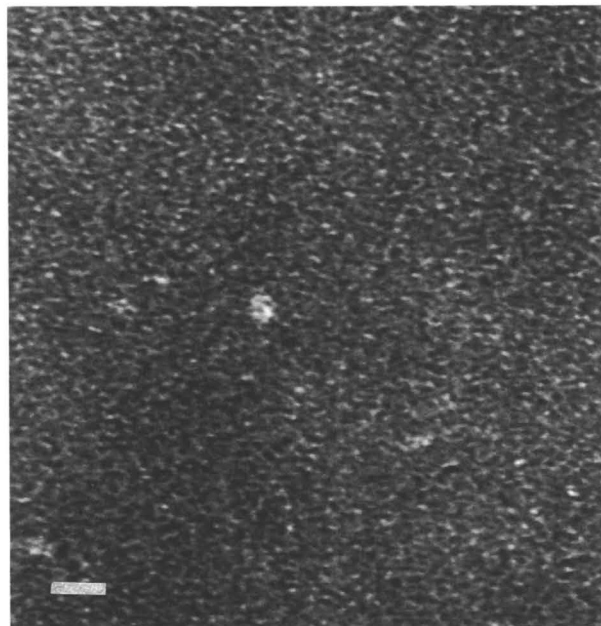
Morphological Changes Coincident with IPN Formation.

Morphological changes that occur coincident with the formation of an IPN based on Solprene 416 block copolymer are now described. The morphology of the SBS triblock taken directly from the internal mixer (Figure 5a) seems to be amorphous and granular, although higher resolution microscopy using higher voltages (Figure 5b) reveals some ordered domains of finer dimensions (10-nm). After annealing (compression molding), cylindrical domains develop with domains of the order of 10 nm (Figure 3). The more amorphous morphology of the block copolymer after internal mixing results because the mixing temperature of 75 °C is below the softening point of the polystyrene. This low mixing temperature leads to fragmentation of the glassy domains and breakdown of short-range ordered structures. When the samples are subsequently annealed at 145 °C, both styrene and butadiene phases can flow to give the typical domain morphology. The same trends in morphologies are seen with the cross-linked (1.0-wt% DICUP) block copolymer sample taken from the internal mixer (Figure 6a) and the corresponding compression-molded sample (Figure 6b).

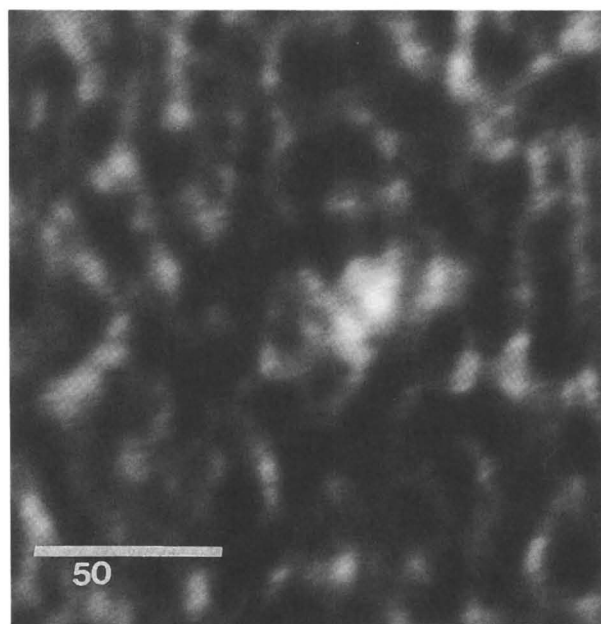
The next step of IPN formation is to swell the cross-linked block copolymer with styrene. Cryogenically ultramicrotomed sections of styrene-monomer-swollen cross-linked SBS samples, with no thermal polymerization of the styrene, were prepared. However, because no cold stage was available on the TEM, micrographs were impossible to obtain without distortion of the sections (Figure 7).

Conceptually, semi-IPNs and true IPNs comprise two independent polymer networks. However, structurally there are further complexities due to at least two factors: (1) numerous grafting reactions between the rubber and the polystyrene, even in the absence of the DVB cross-linkers and (2) structure comprised of well-ordered soft and hard domains. During SBS swelling, preferential migration of styrene monomer into styrene-rich segments of the polymers is expected because the solubility of polybutadiene in styrene is relatively low, despite similar solubility parameters.

The final step of IPN formation is the polymerization (together with intended cross-linking and concomitant grafting) of the styrene. The morphology of a typical IPN based on Solprene 416 is shown in Figure 8a. As expected both semi-IPNs and true IPNs show distinct microphase separation. The IPNs have larger domain sizes (30–40 nm) than the bulk block copolymer. This expansion from the original bulk dimensions shown in Figure 3 is in broad agreement with the equation by Yeo et al. (26). Therefore, if the

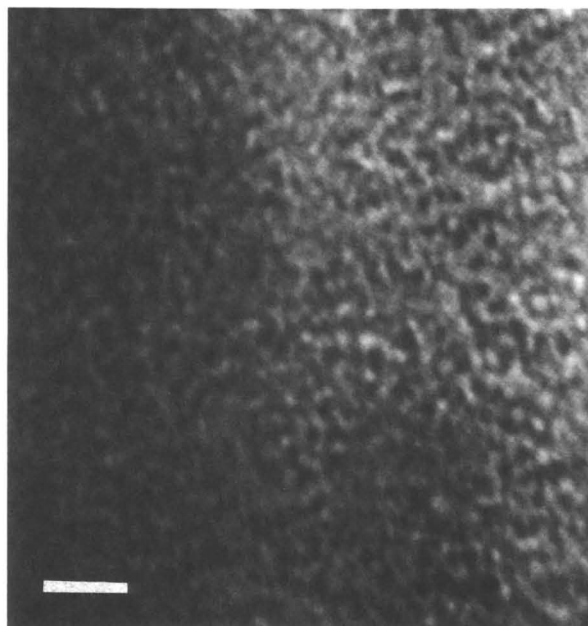


a

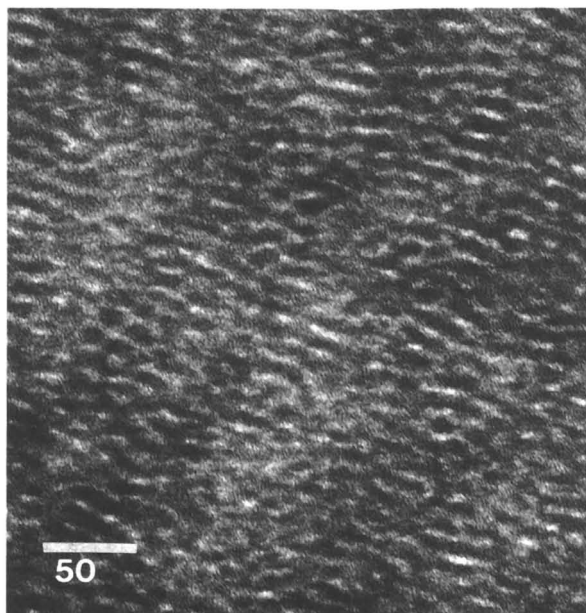


b

Figure 5. Ultrathin section of Solprene 416 taken directly from internal mixer at 75°C (a) (bar = 100 nm) and a higher magnification of the same section (b) (bar = 50 nm).



a



b

Figure 6. Ultrathin section of cross-linked Solprene 416 from internal mixer at 75 °C (a) (bar = 800 nm) and from compression molding at 145 °C (b) (bar = 50 nm).



Figure 7. Distorted ultrathin section of styrene-swollen Solprene 416 (bar = 800 nm).

solvent-cast film is used as a basis, the erroneous conclusion of domain contraction may be reached. As previously noted (34), care is needed in phase transition studies of block copolymers because solvents will increase the complexity of interactions that take place. Therefore, the cryosectioned bulk samples provide a more realistic indication of the microstructure of these block copolymers and are the more appropriate controls to compare with the IPN morphology.

The anisotropic domain morphology of these IPNs was explored by sectioning in three directions. The series in Figure 8 shows that a reasonably symmetric mosaic is found in the x direction and more elongated rodlike domains are found in the y and z directions. The z direction was orientated parallel to the surfaces of the samples and deviates slightly throughout the sample. The domains appear as irregular spheres; hence, the system exhibits nonequilibrium characteristics.

The corresponding anisotropic domain morphology is also revealed with IPNs based on Solprene 1205, although a larger domain size (40 nm) was found. This observation correlates with the relative dimensions of the bulk precursor block copolymers and is due to differences in the molecular weight of the chain segments between the 416 and 1205 and the differing chain geometry. In the case of the radial Solprene 416, spiderlike filaments of

stained polybutadiene-rich segments intrude into the polystyrene domains. Greater interpenetration of the hard and soft segments has occurred, which gives a more complex morphology.

Micrographs also indicate that an increase in the level of polymer I cross-link density leads to smaller polystyrene domains. This effect is well documented and reflects the tighter initial network that limits the size of the regions in which polymer II can phase-separate. It can also be rationalized by a semiempirical thermodynamic model with the equation of Yeo et al. (26), which predicts that the phase domain size of polymer II will decrease with increases in the cross-linking level of polymer I. The equation predicts domain sizes of around 30–60 nm for IPNs such as these. This prediction agrees well with results.

Elastomeric block copolymers, which have two multiphase solid-state structures with glassy domains in a matrix of an elastomer, show strain-induced plastic-to-rubber transitions. The plastic-to-rubber transition in these block copolymers has been interpreted (35) as a consequence of the fragmentation of the lamellar and interconnected glassy domains on stretching. Similar conclusions can be drawn with our IPNs based on block copolymers. Figure 9a is a micrograph of a cross-linked IPN based on the Solprene 416 block copolymer. Figure 9b is the corresponding microstructure after stretching (~150%). The spherical domains in the original sample are deformed to more elliptical domains. This structural re-formation in block copolymers has been attributed (35) to orientation of the elastomer segments and an increase in the interfacial energy that results from fragmentation of the glassy domains and breakdown of the short-range order.

Image Analysis of Microstructure. Quantitative and statistically meaningful data from these micrographs must be acquired for a more rigorous picture of the structures of these block copolymers and IPNs to emerge. Image analysis has been used previously with TEM micrographs of block copolymers (36). A major problem with this procedure is that the stained regions in these micrographs are rather broad and diffuse, especially for full IPNs. Some of the ill-defined elastomer-rich areas are of similar dimensions to the polystyrene domains. This problem is probably caused by osmium tetroxide overstaining. Hence the main challenge in the use of this technique is to select valid “grey levels.”

Image analysis was conducted on selected micrographs with a pulse-shape analyzer (Optomax V PSA 3.06). The particle size distribution (Figure 10) is for a lightly cross-linked (0.2-wt% DICUP) true IPN based on Solprene 1205. The mean spherical domain diameter is 20 nm with a standard deviation of 7 nm. Other micrographs tested by image analysis displayed similar domain sizes that agree well with values for related materials given by Donatelli et al. (5).

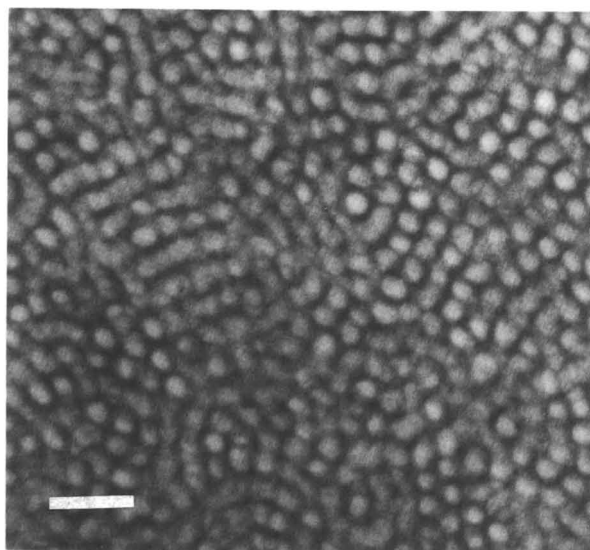
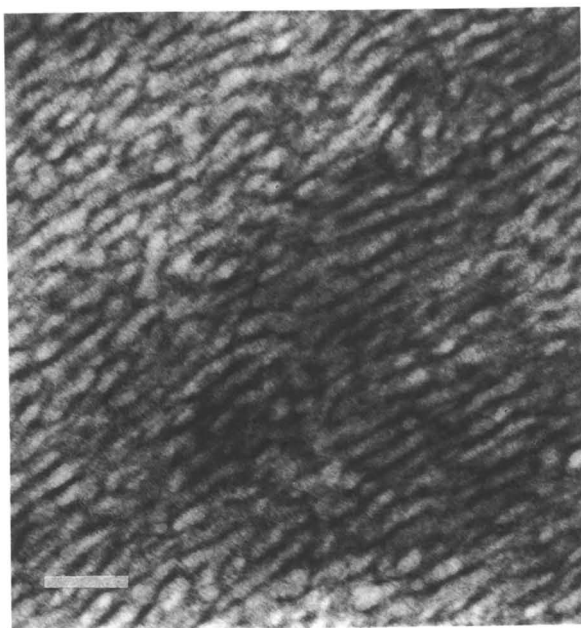
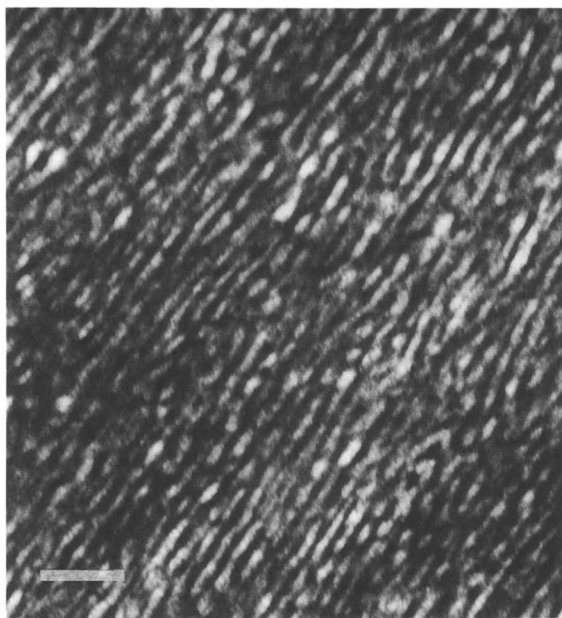
**a****b**

Figure 8. Ultrathin sections of semi-IPN (highly cross-linked based on 416) (bar = 100 nm): (a) direction x; (b) direction y.



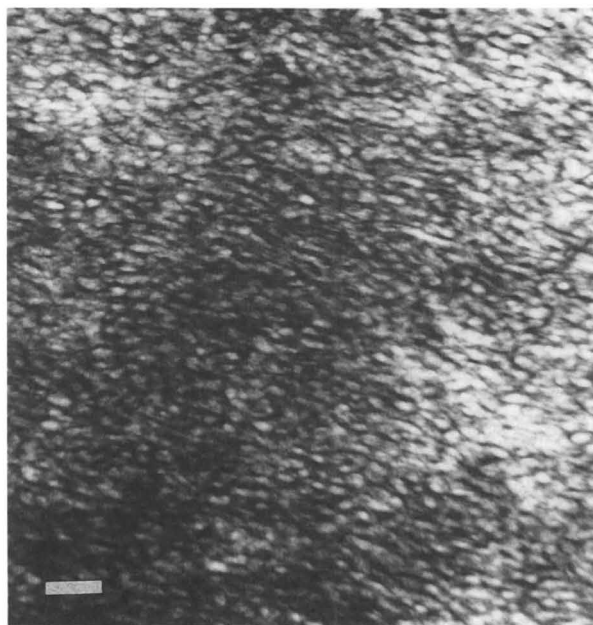
c

Figure 8. Continued. (c) direction z .

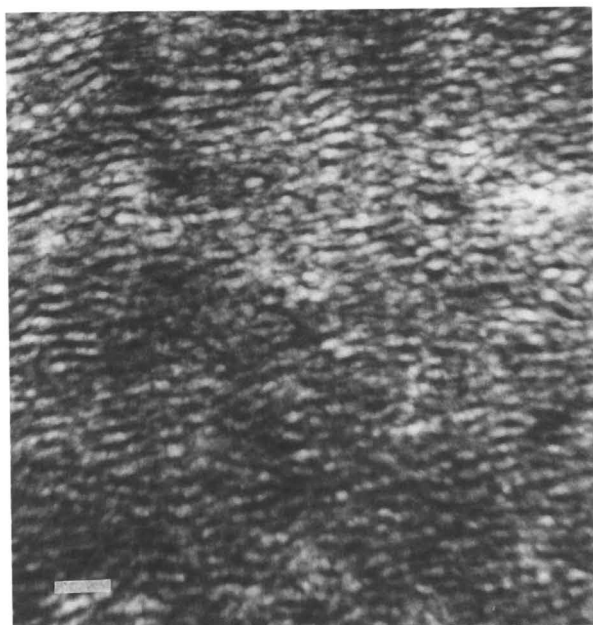
Another main problem with this technique is selection of the point where a domain starts and an interfacial region ends. This point is shown more clearly by computerized image enhancement (IE) (Figure 11) of the micrograph used in Figure 10. The IE can be used to deduce additional information. The white line across the IE corresponds to the distance measurement on the horizontal of Figure 12. The trace of intensity versus distance shows that the intensity of the domains does not drop off quickly, but instead decreases gradually. Image analysis with these morphologies requires an arbitrary decision be made regarding where the domains meet the interfacial region. However, IE has the advantage that it makes the diffuse interface much more clearly visible and allows more precise measurement of the interfacial region. With this method, the best estimate for this sample is 4 nm.

Summary

TEM micrographs indicate that the block copolymers and the IPNs display distinct microphase separation. The elastomeric phase is continuous whereas



a



b

Figure 9. Ultrathin section of nonstretched (a) and stretched (b) lightly cross-linked IPN based on Solprene 416 (bar = 100 nm).

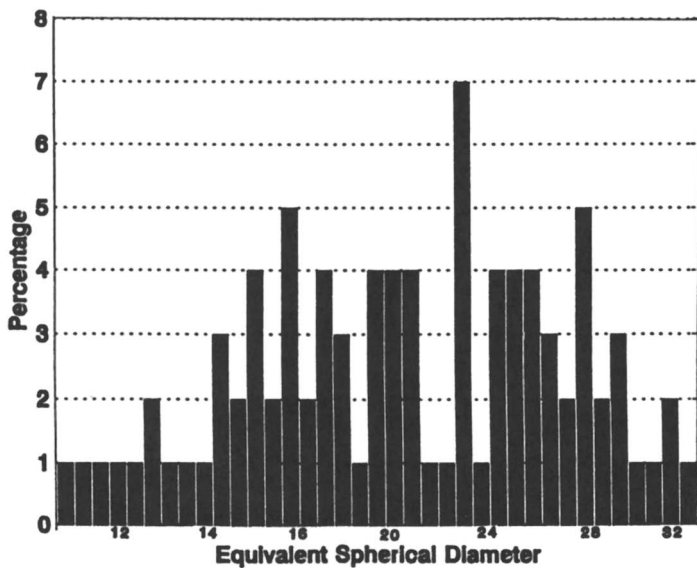


Figure 10. Particle size distribution of full IPN 1205 (lightly cross-linked).

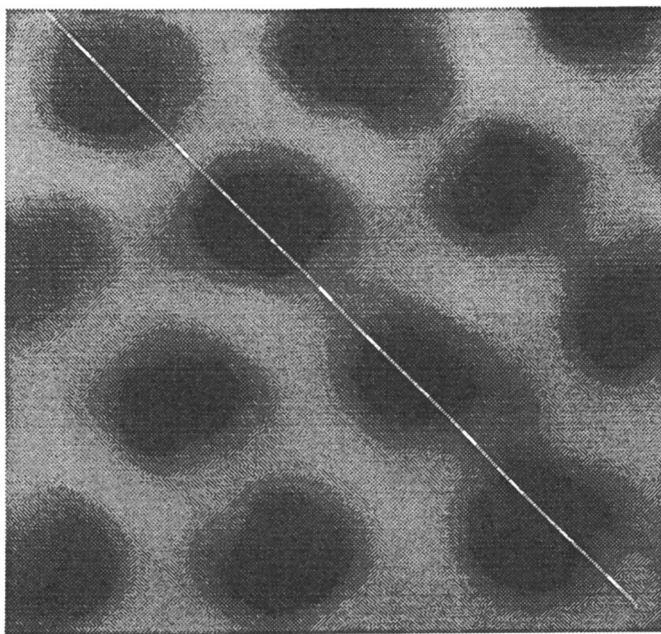


Figure 11. Computerized image enhancement of the full IPN 1205 micrograph.

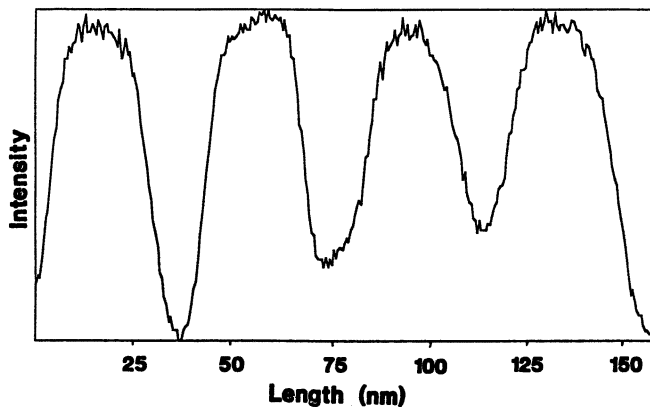


Figure 12. Distance (nanometers) versus intensity of IE shown in Figure 11.

the PS-rich phase exists in domains. Both the semi-IPNs and full IPNs show anisotropic domain morphology. The morphology of the IPN at each stage of preparation was seen. A suitable synthetic mechanism remains to be identified: further labeling of polymer segments so that migration during IPN formation can be monitored is required.

Image analysis of the IPN microstructure was complicated due to rather broad and diffuse stained regions. To eliminate the problem of osmium tetroxide overstaining, techniques such as electron energy filter TEM and laser light scattering are currently being used on unstained sections of IPNs.

References

1. *Interpenetrating Polymer Networks and Related Materials*; Sperling, L. H., Ed.; Plenum: New York, 1981.
2. *Multicomponent Polymer Materials*; Paul, D. R.; Sperling, L. H., Eds.; Advances in Chemistry 211; American Chemical Society: Washington, DC, 1986.
3. *Advances in Interpenetrating Polymer Networks*; Klempner, D.; Frisch, K. C., Eds.; Technomic: Lancaster, PA, 1989; Vols. I–III.
4. *Polymer Networks and Blends*; ChemTec Publishing: Toronto, Canada, 1991.
5. Donatelli, A. A.; Sperling, L. H.; Thomas, D. A. *Macromolecules* **1976**, *9*, 671.
6. Donatelli, A. A.; Sperling, L. H.; Thomas, D. A. *Macromolecules* **1976**, *9*, 676.
7. Fernandez, A. M.; Wignall, G. A.; Sperling, L. H. In *Multicomponent Polymer Materials*; Paul, D. R.; Sperling, L. H., Eds.; Advances in Chemistry 211; American Chemical Society: Washington, DC, 1986, p 153.
8. Donatelli, A. A.; Sperling, L. H.; Thomas, D. A. *J. Appl. Polym. Sci.* **1977**, *21*, 1189.
9. An, J. H.; Fernandez, A. M.; Sperling, L. H.; *Macromolecules* **1987**, *20*, 191.
10. *Block and Graft Polymerisation*; Ceresa, R. J., Ed.; Wiley: New York, 1972.
11. Meier, D. J. In *Thermoplastic Elastomers*; Legge, N. R.; Holden, G.; Schroeder, H. E., Eds.; Hanser: New York, 1987; p 269.

12. *Handbook of Thermoplastic Elastomers*, 2nd ed.; Rader, C. P.; Walker, B. M., Eds.; Van Nostrand Reinhold, New York, 1988.
13. Morton, M. J. *Polym. Sci., Polym. Symp.* **1977**, *60*, 1.
14. Miller, J. A.; Cooper, S. L. In *Thermoplastic Elastomers*; Legge, N. R.; Holden, G.; Schroeder, H. E., Eds.; Hanser: New York, 1987; p 385.
15. Riess, G. In *Thermoplastic Elastomers*; Legge, N. R.; Holden, G.; Schroeder, H. E., Eds.; Hanser: New York, 1987, p 325.
16. Meier, D. J. In *Polymer Blends and Mixtures*; Walsh, D. J.; Higgins, J. S.; Maconnachie, A., Eds.; ASI E89; Nijhoff: The Hague, Netherlands, 1985; p 173.
17. Spontak, R. J.; Williams, N. C.; Agard, D. A. *Polymer* **1988**, *29*, 387.
18. Arnold, K. R.; Meier, D. J. *J. Appl. Polym. Sci.* **1970**, *14*, 427.
19. Arridge, R. G. C.; Folkes, M. J. In *Processing Structure and Properties of Block Copolymers*; Folkes, M. J., Ed.; Elsevier: London, 1985.
20. Cho, K.; Brown, H. R.; Miller, D. C. *J. Polym. Sci., Polym. Phys. Ed.* **1990**, *28*, 1699.
21. Paul, D. R. In *Thermoplastic Elastomers*; Legge, N. R.; Holden, G.; Schroeder, H. E., Eds.; Hanser: New York, 1987, p 431.
22. Gergen, W. P.; Lutz, R. G.; Davidson, S. In *Thermoplastic Elastomers*; Legge, N. R.; Holden, G.; Schroeder, H. E., Eds.; Hanser: New York, 1987; p 507.
23. Eehte, A. In *Rubber-Toughened Plastics*; Riew, C. K., Ed.; Advances in Chemistry 222; American Chemical Society: Washington, DC, 1987, p 15.
24. Folkes, M. J. *Processing Structure and Properties of Block Copolymers*; Elsevier: London, 1985.
25. Siegfried, D. L.; Thomas, D. A.; Sperling, L. H. *J. Appl. Polym. Sci.* **1981**, *26*, 177.
26. Yeo, J. K.; Sperling, L. H.; Thomas, D. A. *Polymer* **1983**, *24*, 307.
27. Burford, R. P.; Chaplin, R.; Mai, Y.-W. *Contemporary Topics in Polymer Science*; Plenum: New York, 1989 Vol. 6, p 699.
28. Burford, R. P.; Mai, Y.-W. In *Advances in Interpenetrating Polymer Networks*; Klempner, D.; Frisch, K. C., Eds.; Technomic: Lancaster, PA, 1991; Vol. III, p 75.
29. Jones, J. J.; Burford, R. P. *Polym. Int.* **1991**, *26*, 163.
30. Byun, H. S.; Burford, R. P.; Mai, Y.-W. *Mater. Forum*, **1989**, *13*, 26.
31. "Solprene-Elastomers and Plastomers." Information Sheet from the Phillips Petroleum Company.
32. Sayer, L. C.; Grubb, D. T. *Polymer Microscopy*; Chapman and Hall: New York, 1987, p 76.
33. Thomas, D. A. *J. Polym. Sci., Polymer Symp.* **1977**, *60*, 189.
34. Spontak, R. J. *Abstracts of Papers*, 44th annual meeting of the Electron Microscopy Society of America: Albuquerque, NM, 1986; p 788.
35. Aggarwal, S. L. In *Processing Structure and Properties of Block Copolymers*; Folkes, M. J., Ed.; Elsevier: London, 1985.
36. Spontak, R. J.; Williams, M. C.; Schooley, J. J. *Mater. Sci.* **1986**, *21*, 3173.

RECEIVED for review November 26, 1991. ACCEPTED revised manuscript May 19, 1992.

Kinetic, Rheological, and Morphological Changes of Polyurethane–Unsaturated Polyester Interpenetrating Polymer Networks

Y. C. Chou and L. J. Lee*

Department of Chemical Engineering, The Ohio State University, Columbus,
OH 43210

Interpenetrating polymer networks (IPNs) based on a polyurethane and three unsaturated polyester resins with different functional end groups were prepared. The interactions between components of the polyurethane and unsaturated polyester phases were examined by a comparison of rheological and reaction kinetic changes. The reaction between end groups of unsaturated polyester molecules and isocyanate was found to lead to more reactive vinyl polymers. The formation of polyurethane networks was also accelerated by the presence of carboxyl groups on the unsaturated polyester molecules. Phase morphologies of the molded IPNs analyzed by electron microscopy, dynamic mechanical analysis, and mechanical models were found to depend on the extent of chemical grafting.

INTERPENETRATING POLYMER NETWORKS (IPNs) are blends of two cross-linked polymers in which at least one network is synthesized in the presence of the other (1). This method of IPN synthesis has been used to improve the material properties of many widely used polymers (2–12). For example, polyurethanes, the first materials applied to reaction injection molding (RIM), are generally inappropriate for structural applications due to their low rigidity and high thermal expansion coefficient. To improve the physical properties of

* Corresponding author.

polyurethanes, there has been much work to develop new RIM resins such as nylon, epoxy, and unsaturated polyester, or to reinforce existing materials externally by compounding with various reinforcement agents. Another approach is internal reinforcement by the introduction of a second reactive polymer, which forms an IPN, to overcome the inherent deficiencies of polyurethanes. Many polyurethane-based IPNs have been developed successfully. Usually polyurethane-based IPNs consist of polyurethanes and a glassy polymer such as poly(methyl methacrylate) (4–6), polystyrene (7, 13, 14), epoxy (10), or unsaturated polyester (15–25).

Most IPNs are developed for slow processes such as casting and coating. For instance, Frisch et al. (15, 26) prepared IPNs by casting and curing films from mixtures of prepolymers, catalysts, and cross-linkers. These binary systems consist of two cross-linked networks: one is a polyurethane and the other is an epoxy, polyacrylate, and unsaturated polyester. For fast processes such as in RIM applications, there are only a few commercially available IPN compounds. For example, a series of materials based on isophthalic unsaturated polyester–urethane hybrids has been introduced by Amoco Chemical Company in sheet molding compound and foam formulation (27). These materials resulted from the reaction of unsaturated polyester glycols with diisocyanates to produce high molecular weight linear polyurethanes that are also cross-linkable because of unsaturation on the polyester chains. The formation of urethane and unsaturated polyester in one material results in hybrids that often have properties superior to either of the constituent polymers. Ashland Chemical also developed an acrylamate polymer (28, 29). Instead of using unsaturated polyester diols, monofunctional unsaturated alcohols were reacted with diisocyanates to form an unsaturated ester–urethane hybrid. An added advantage of these two hybrid systems is that the heat generated by the mixing-activated polyurethanes can internally trigger the thermally activated free radical polymerization of the unsaturated polyester resin. A similar polyurethane–unsaturated polyester IPN was studied by Nguyen and Suh (17, 18), Kim and Kim (24, 25), Hsu and Lee (20–22), and Yang and Lee (23). These researchers found that the processing conditions in the RIM process, such as impingement pressure, stream Reynolds number, temperature, compound composition, and reaction kinetics, can all affect the morphology and, subsequently, the physical properties of the IPNs. The reason that IPNs are more sensitive to the processing conditions than the constituent polymers is probably due to the strong interaction between the two polymerizations (21).

In many cases interactions between the two reactive systems may give rise to a synergistic effect on the properties of IPNs. The interactions have been attributed to an increase in cross-link density due to the formation of a mutual interpenetration of network chains (30, 33). Other specific interactions such as grafting (34, 35) and opposite charged group interaction (36) between two networks also have been considered as possible reasons for property enhancement. The introduction of grafting monomers or opposite

charged groups changes the IPN morphology from a two-phase structure to a single-phase structure. Improved tensile strength and higher adhesive strength were found in ionomer polyurethane–vinyl chloride copolymer IPN coatings (36). On the other hand, increasing grafting level in the epoxy–poly(*n*-butyl acrylate) IPNs enhanced the toughness of the materials slightly, but lowered tensile strength (34). To date, most research has concentrated on the influence of these specific interactions on the morphology and mechanical properties of the IPNs. However, little is known about the effect of these specific interactions on the rheology and reaction kinetics during the polymerization of IPNs.

In typical reactive polymer processing, physical properties of the final products depend not only on the raw materials, but also on the operating conditions during mixing, mold filling, and curing. These manufacturing processes are governed by reaction kinetics, rheology, and morphology of the materials. Rheological changes can affect the flow pattern in the mixing and mold-filling stage. The reaction kinetics determine the curing profile of the resins and the final conversion of the products. The morphological changes determine physical properties of the products. Furthermore, each governing phenomenon may be affected by the changes in other phenomena. For example, a rheological change of the reactive resins from a liquid to a gel may alter the reaction mechanism of the resins from kinetic control to diffusion control. A morphological change that results from phase separation or crystallization may induce viscosity changes and heterogeneous reaction. Consequently, the reaction kinetics become more complicated due to these physical changes. To investigate the effect of processing variables on the ultimate mechanical properties, a kinetic, rheological, and morphological study on the reactive system is of great importance.

Hsu and Lee (20, 21) studied the kinetics of polyurethane–unsaturated polyester (PU–UPE) IPNs. By comparison of reaction rate profiles measured by differential scanning calorimetry (DSC), Hsu and Lee found that interaction exists between the two competing reactions. For PU–UPE IPNs, the hydroxyl and carboxyl end groups of the UPE molecules may form the urethane and amide linkages with isocyanates. Such grafting between the PU and the UPE phases may affect the network formation of both components. Therefore, these two reaction systems cannot be considered independently. In this chapter, the interactions between the two reactive systems in several PU–UPE systems are investigated and their influence on reaction kinetics, rheological changes, and morphology are studied.

Experimental Details

Materials. The materials used in this study are listed in Table I. The PU consists of a poly(ϵ -caprolactonetriol) (TONE-310, Union Carbide) with a number-average molecular weight of 900 and a liquid form of 4,4'-diphenylmethane diisocyanate (MDI-143 L, Dow Chemical). The MDI contains a mixture

Table I. Materials Used for Polyurethane–Unsaturated Polyester IPNs

<i>Material</i>	<i>Description</i>
Polyol	TONE-310, $f = 3$, MW = 900
Diisocyanate	MDI-143 L, $f = 2.3$, MW = 287
Catalyst	dibutyltin dilaurate (T-12)
Unsaturated polyester (UPE)	acid value = 35, OH value = 35, MW = 1580
OH-free unsaturated polyester	acid value = 26
Capped unsaturated polyester	phenylurethane and phenylamide derivative of unsaturated polyester
Styrene ^a	reagent grade
Initiator	2,5-dimethyl-2,5 bis(2-ethyl- hexanoylperoxy)hexane

^a The ratio of styrene C=C bonds to UPE C=C bonds is 2:1.

of diphenylmethane diisocyanate, carbodiimide, and trisocyanate adduct. The polyol was degassed under vacuum at 50 °C to remove moisture. In most cases, PU was prepared by mixing polyol TONE-310 and MDI together at room temperature without catalyst. In some cases, however, dibutyltin dilaurate (T-12, Aldrich Chemical) was used as a catalyst for the PU reaction. The polyol that contained the catalyst was mixed with MDI at room temperature for preparation of the catalyzed PU.

An uncapped UPE resin and an OH-free experimental UPE resin (partially capped) with a number-average molecular weight of 1580 were received from Ashland Chemical. Both resins consist of maleic anhydride and propylene glycol with an average of 10.3 C=C bonds per molecule. The acid value and hydroxyl value of the uncapped UPE are the same (about 35). The OH-free UPE has no hydroxyl groups, but has an acid value of 26. An OH- and COOH-free UPE (totally capped) was prepared in our laboratory. The styrene-free uncapped UPE was reacted with a stoichiometric amount of phenyl isocyanate in a reactor under mechanical stirring and nitrogen flow at 80 °C. The reaction was followed to completion by IR spectroscopy (disappearance of the isocyanate absorption peak at 2300 cm⁻¹).

Styrene was added to all UPE resins to adjust the molar ratio of styrene to unsaturated polyester molecules to 2:1 (about 43 wt% of UPEs in styrene). The initiator, 2,5-dimethyl-2,5 bis(2-ethyl-hexanoylperoxy)hexane (DMB; Lucidol) was used as received. The amount of DMB was 2% by weight of the UPE resin. The UPE resins were dried overnight using 4-Å molecular sieves.

The weight ratio of PU to the three UPEs was fixed at 50:50 for most of the IPNs prepared. In addition to the —OH groups in the polyol, the end groups of —OH and —COOH in the UPE resins were taken into account for the calculation of NCO—OH stoichiometry. Except for the case of totally capped UPE, extra amounts of isocyanate were added to keep the stoichiometric ratio of NCO to OH at 1.05. The polyol [with or without dibutyltin dilaurate (T-12)], UPE–styrene, and initiator were blended in a flask under strong stirring at room temperature before MDI addition. A small quantity of the mixture was quickly removed from the flask for measurement of reaction kinetics and rheology; the remainder of the mixture was poured into a mold. The resin in the mold was then cured in an oven at 60 °C for 10 h and postcured at 120 °C for 6 h and at 150 °C for 1 h. The IPN based on the uncapped UPE is denoted as a fully grafted IPN,

which means that the UPE molecules could be chemically linked onto the PU phase by their end groups of —OH and —COOH. The IPN based on the OH-free UPE is denoted as a semigrafted IPN in which only one end group (—COOH) of the UPE molecule was able to graft onto the PU molecule. The capped UPE resin had no reactive end groups, and the prepared IPN is denoted as a nongrafted IPN.

Methods of Analysis. A differential scanning calorimeter (DSC; TA-Instruments TA-2000) was employed to follow the reaction kinetics. The sample weight was 10–15 mg with an empty pan as a reference. A nitrogen supply was used to purge air in the sample cell. The reaction exothermic rate versus time was measured in the isothermal mode at 60 °C.

A rheometrics dynamic analyzer (RDA, Rheometrics RDA-700) in the oscillatory mode was used to follow the rheological changes and gelation at isothermal conditions. Alternatively, gel time can be measured by use of the steady shear method. However, the steady shear method has two distinct disadvantages. First, gel time is defined as the point at which the viscosity reaches an infinite value, which is a very ambiguous term. Second, the microstructure of the reacting system is very fragile near the gel point and hence shear may cause it to break and thereby delay gelation. Consequently the gel time measured by this method is often longer than that measured by RDA (37, 38).

Several researchers (39, 41) have suggested that the crossover of shear storage modulus, G' , and shear loss modulus, G'' , could be an indication of the liquid–solid transition for cross-linking polymers when the stress relaxation at the gel point follows a power law [i.e., $G'(\omega) = G''(\omega) = A\omega^{1/2}$, where ω is frequency and A is a constant]. However, for many cross-linking systems, the relaxation exponent at the gel point may not be equal to 1/2 (37, 41). In such cases, gel time can be determined by carrying out a frequency sweep. Gel time occurs when G' is parallel to G'' . However, because of our equipment limitations, the method of frequency sweep cannot be used for a fast reaction. Hence, in this study we assume gel time to be the point at which G' and G'' cross over.

The sample cell used in the RDA for the gel time measurement consists of a set of serrated aluminum parallel plates. The gap between the two plates was fixed at 1.1 mm and the frequency used was 10 rad/s. The strain ratio was set at 10%.

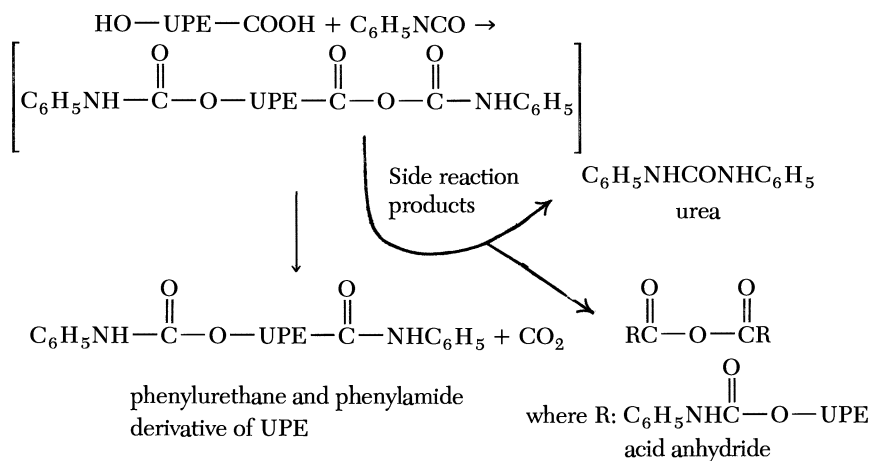
In addition to the gel time measurement, the RDA was used to carry out the dynamic mechanic analysis for cured samples. The molded IPN samples were cut into rectangular shapes with dimensions of 50 × 7.5 × 1.7 mm. The rectangular samples were held between two fixtures and the frequency used was 10 rad/s. The strain ratio was set at 1%. The temperature dependence of the loss tangent ($\tan \delta$), G' , and G'' was measured.

An electron spin resonance (ESR) spectrometer (Bruker Instrument ESP 300) was employed to measure the radical concentrations and radical spectra in the UPE phase of the IPN. 2-2'-diphenyl-1-picrylhydrazyl hydrate (DPPH) was used as a standard solution for the radical concentration calibration (42). Benzene was used as a solvent for dilution. The spectrometer was operated at X band (9.51 GHz) with a TE mode cavity.

The morphology of IPN samples was observed using a transmission electron microscope (TEM; Phillips EM-300). The samples were prepared by an ultramicrotome (LKB HT-2B) and stained with 1% osmium tetroxide solution. Samples were examined at a power of 60 kV at various magnifications.

Results and Discussion

Reactivity of Three UPE Resins. To identify the influence of end capping on the reactivity of the UPE resins, the capped and uncapped resins were compared. Figure 1 shows the DSC isothermal runs for the three UPEs. The onset of reaction occurred earlier for capped UPE as compared to either OH-free UPE or uncapped UPE. A comparison of $G' = G''$ time in Table II also shows that the capped UPE gelled fastest among the three UPEs. Thus, the capped UPE molecules were more reactive than the uncapped UPE or OH-free UPE molecules. In the end-capping reaction of UPE resin with phenyl isocyanate, the hydroxyl groups of UPE molecules reacted with isocyanates to form urethane linkage. On the other hand, the reaction of carboxyl groups of UPE with phenyl isocyanate led to amide linkage and some other side reaction products such as acid anhydrides and urea (43). The end-capping reaction may be pictured as follows:



Rheological Study. PU reaction is a step growth polymerization, whereas UPE reaction is a free radical copolymerization. The formation of PU-UPE IPN is shown schematically in Figure 2. Due to the complexity of the competing reactions, examination of the influence of PU components on the UPE reaction and the UPE components on the PU polymerization was essential.

Effect of PU Components on UPE Gelation. Different amounts of MDI were mixed with each of the three UPE resins and the $G' = G''$ times were measured. The amount of MDI had a pronounced effect on the gelation

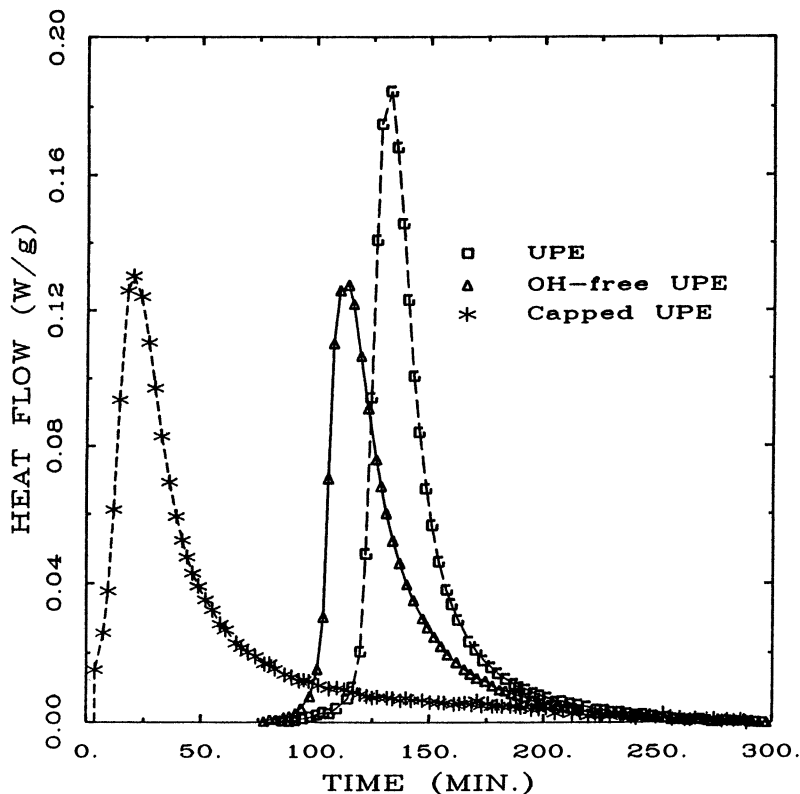


Figure 1. DSC isothermal runs for three UPE resins at 60 °C.

Table II. Effect of MDI on UPE Gelation
($G' = G''$ Time at 60 °C)

Description	Time (min)
2% DMB initiator	
UPE	30.2
UPE-MDI = 1:0.01 by weight (stoichiometry)	26.9
UPE-MDI = 1:0.382 by weight (same ratio as in IPN)	10.8
OH-free UPE	22.1
OH-free UPE-MDI = 1:0.348 by weight	5.9
Capped UPE	3.8
Capped UPE-MDI = 1:0.328 by weight	1.8
Divinylbenzene ^a	10.5
Divinylbenzene-MDI = 1:0.382 ^a	7.7
No DMB	
UPE	> 180
UPE-MDI = 1:0.382	58.2

^a $G' = G''$ at 80 °C.

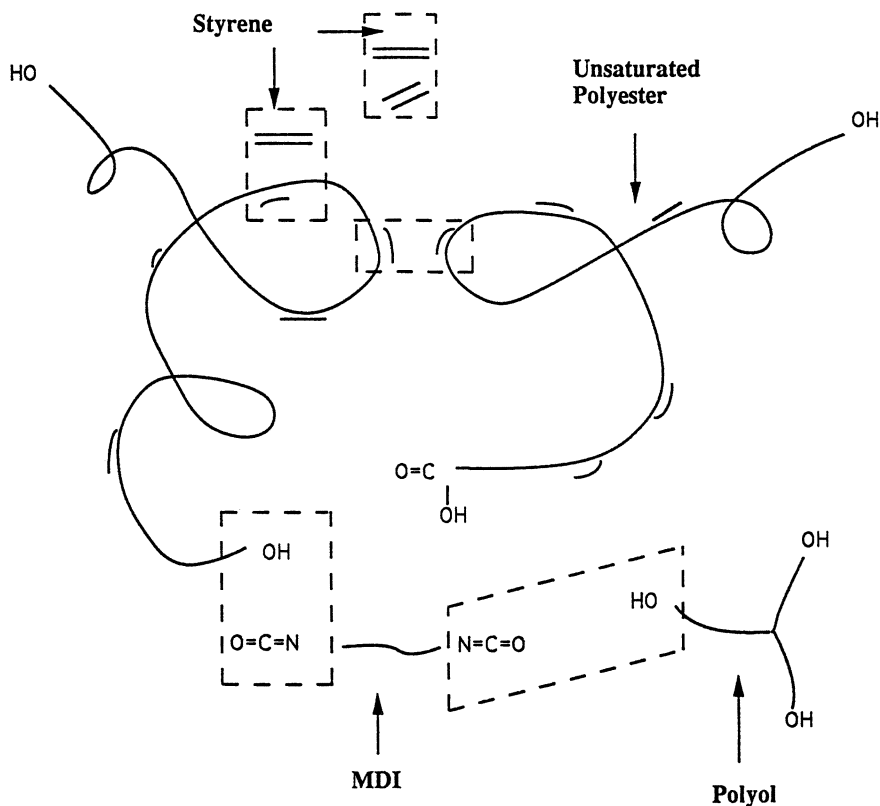


Figure 2. Schematic diagram of the reaction mechanism and structure of PU-UPE IPN.

as shown in Table II. With 2% DMB initiator, the $G' = G''$ time of the three UPEs decreased with the increase of the amount of MDI. The decrease of $G' = G''$ time was more significant for the uncapped and OH-free UPEs than for the capped UPE. The catalytic effect of MDI on UPE gelation was also true without the presence of any initiator. In addition to the UPE resins, the reaction of divinylbenzene and a stoichiometric amount of styrene (55.5% by weight in styrene) was carried out with and without the presence of MDI. Divinylbenzene has C=C bonds different from those of UPE and has no end functional groups that can react with MDI. Table II shows that the gelation of divinylbenzene and styrene reaction was slightly accelerated from 10.5 to 7.7 min at 80 °C. Apparently, MDI has a weak catalytic effect on the C=C bonds. The strong effect of MDI on the gelation of the uncapped UPE and OH-free UPE resins may be a result of urethane and amide formation between MDI and the end groups of UPE. This may have enhanced the reactivity of UPE C=C bonds. The acceleration of vinyl polymer gelation by

isocyanates was also observed by Avella et al. (44) for blends of unsaturated polyesters with isocyanate-terminated polybutadiene rubbers.

Effect of UPE Components on PU Gelation. Styrene and UPE (styrene-free) were mixed separately with PU and their influence on PU gelation was investigated. To convert the solid UPE into the liquid phase, the styrene-free UPE was dissolved in 57% by weight of ethylbenzene. As can be seen in Table III, with the addition of styrene, the $G' = G''$ time of PU increased with or without the presence of catalyst T-12. Thus, the styrene had a dilution effect on PU gelation. This effect was more significant when the catalyst T-12 was present.

The $G' = G''$ time of uncatalyzed PU greatly decreased from 37 to 10 min with the presence of styrene-free UPE. The formation of amide, urea, and anhydrides from the reaction between the carboxyl groups of UPE and isocyanates probably accounts for the strong catalytic effect on PU gelation.

Gelation of IPNs. Table IV compares the $G' = G''$ time for PU, UPEs, fully grafted IPN, semigrafted IPN, and nongrafted IPN. As mentioned before, for UPE gelation, the capped UPE has the shortest $G' = G''$ time, whereas the uncapped UPE had the longest $G' = G''$ time. For the PU reaction, the uncatalyzed system gelled at 37.8 min; adding 12.7 ppm of T-12 accelerated the gelation to 2.5 min. The gelation times for all IPNs were very close but far different from that of either PU or UPE. The gelation of the three IPNs based on the uncatalyzed PU occurred at about 10 min. On the other hand, the gelation of the three IPNs based on catalyzed PU all occurred around 9 min.

To understand the gelation sequence of the preceding IPNs, the gelation of an IPN prepared from a linear PU and UPE was measured. Here, the triol (TONE-310) in the PU formulation was replaced by a diol (TONE-210).

**Table III. Effect of Styrene or UPE on PU Gelation
($G' = G''$ Time at 60°C)**

<i>Description</i>	<i>Time (min)</i>
No T-12	
PU	37.8
PU–styrene = 1:1 by weight	39.1
PU–UPE (in 57 wt.% of ethylbenzene) = 1:1 by weight	10.5
12.7-ppm T-12	
PU	2.5
PU–styrene = 1:1 by weight	20.1

Table IV. Gelation of Fully Grafted, Semigrafted, and Nongrafted IPNs ($G' = G''$ Time at 60 °C)

<i>Description</i>	<i>Time (min)</i>
UPE	30.2
OH-free UPE	22.1
Capped UPE	3.8
No T-12	
PU	37.8
PU-UPE (fully grafted)	10.7
PU-OH-free UPE (semigrafted)	10.6
PU-capped UPE (nongrafted)	9.4
Linear PU-UPE (fully grafted)	45.3
12.7-ppm T-12	
PU	2.5
PU-UPE (fully grafted)	9.5
PU-OH-free UPE (semigrafted)	9.6
PU-capped UPE (nongrafted)	8.6

Table IV shows that the gelation of this linear PU-UPE (i.e., the network formation due to UPE reaction) occurred around 45 min. Therefore, the gelation of cross-linked PU-UPE IPNs must be a result of the formation of PU networks.

For cross-linked PU-UPE, both PU and UPE can form the networks. Gelation measured by a rheometer (RDA) in this study can only determine the first network formation (PU gelation in this study). It is important to identify the second network formation (i.e., UPE gelation) and how the formation of the second network was affected by the first network. ESR is a useful tool to study the radical chain growth polymerizations because it can directly measure the radical concentration and radical behavior. For the UPE cross-linking reaction, many researchers have pointed out that the long chain molecules tend to form locally dense areas called microgels (45, 46), and the polymeric radicals are likely to be buried in the microgels. Thus, ESR is able to measure the spectra and concentrations of those "trapped" radicals. The ESR radical spectra can reflect the environmental status of the radical. Tollens and Lee (42) have related ESR radical spectra to gelation measured by a rheometer for the same UPE resin used in this study.

Figure 3 presents the ESR results (42) of Tollens and Lee that show the radical concentration profile and the radical spectra of the UPE polymerization initiated with 1% DMB at 75 °C. The radical concentration profile shows that the radical concentration initially remained in a steady state region between points A and B. The radicals were in a liquid-like state. After this region the radical concentration started to increase and reached point E, which was the gel point measured by a rheometer. After the gel point E, the

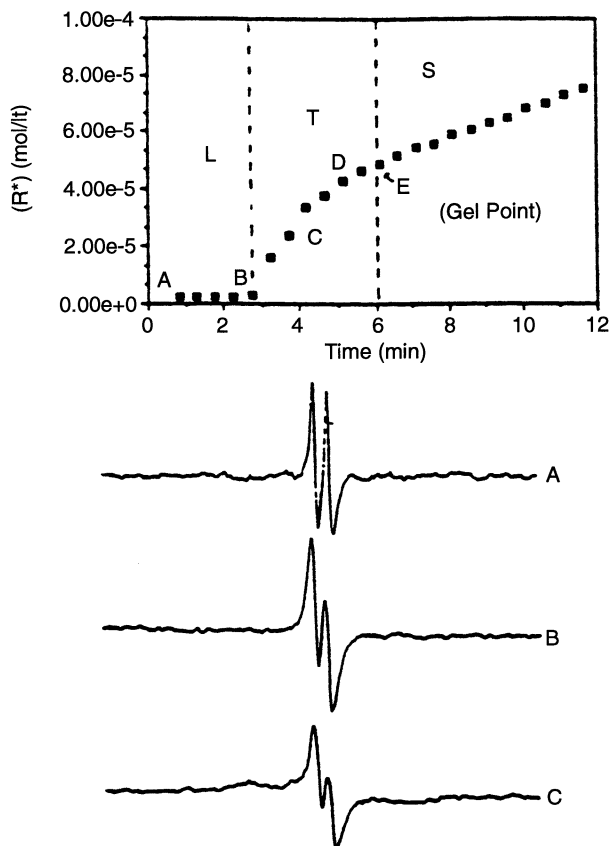


Figure 3. Radical concentration profile for UPE with 1% DMB at 75 °C. (Reproduced with permission from reference 42. Copyright 1993.) Continued on next page.

radical concentration continued to increase and finally leveled off. The radicals were in a solid-like environment after point E. The region between points B and E, was a transition region. The spectra of radicals confined in various environments showed different shapes. In the liquid state region (points A and B), the spectrum showed sharp triple peaks, whereas, in the solid state region (after point E), the peaks became broader and the original middle peak of the triple peaks disappeared. The spectrum (points C and D) in the transition region was mainly a superposition of liquidlike and solidlike spectra. Thus, the UPE phase gelation could be determined by the appearance of a solidlike spectrum in the study of IPNs.

The radical spectra measured by ESR for the cross-linked PU–UPE are shown in Figure 4. As can be seen, the radical spectra of UPE reaction in

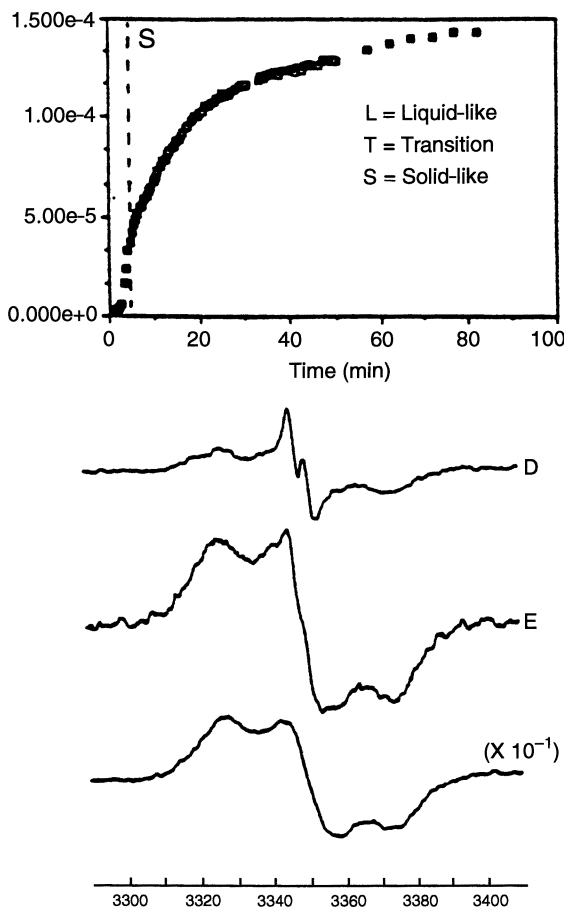


Figure 3. Continued. Radical spectra for UPE with 1% DMB at 75 °C.

IPN were similar to those of pure UPE reaction. At points A and B, the UPE radicals were in the liquid and the transition regions, respectively. When the system was gelled by PU phase at the time of point B (measured by the rheometer), the UPE radicals were still in the transition region. The UPE cross-linking did not occur until point C. After the UPE gelation was formed, the shape of the radical spectra showed no further change except the peak size.

Figure 5 compares the radical concentrations of the cross-linked PU-UPE and the linear PU-UPE measured by ESR. Initially, there was a steady state region and after some time the radical concentration began to increase. For the linear PU-UPE the gelation caused by the network formation of UPE and measured by RDA agreed very well with that determined by ESR. On

the other hand, for the cross-linked PU–UPE the gelation measured by RDA, which indicates the network formation of the PU phase was far ahead of the gelation determined by ESR, which represents the network formation of the UPE phase. Compared to pure PU and UPE reactions under the same conditions, the PU gelation is accelerated due to the presence of carboxyl groups on the UPE molecules, whereas the UPE gelation is retarded, probably due to the solidification effect of the gelled PU phase.

Kinetic Study

Figure 6 shows the DSC isothermal runs for UPE–MDI blends. As stated previously, the capped UPE resin was the most reactive, whereas the uncapped UPE resin was the least reactive among the three UPE resins. With the addition of MDI the three UPE reactions responded differently. The reaction peak of the uncapped UPE shifted greatly from 130 min in Figure 1 to about 35 min in Figure 6. The reaction peak of OH-free UPE only shifted slightly from 110 min in Figure 1 to about 80 min in Figure 6. On the other hand, the reaction peak of the capped UPE did not shift noticeably. Because the quantity of MDI added to the three UPEs was about the same, the catalytic effect of MDI could not be the reason for this discrepancy. As can be seen in Figure 6, the initial reaction exotherm represents the reaction between the functional end groups of UPEs and isocyanates. Such a reaction leads to more reactive vinyl polymers. Consequently, the uncapped UPE molecules were affected more by the presence of MDI than the OH-free UPE molecules because they had more functional end groups. On the other hand, the capped UPE could not react with MDI; thus the reaction peak did not shift.

When polyol (TONE-310) was added to the mixture, the PU network was formed, and the formation of the PU network on the reaction kinetics of UPE was investigated. The comparison of DSC isothermal runs for the three UPE–MDI mixtures and the three UPE–PU IPNs at 60 °C is shown in Figure 7. For the three IPNs, the PU reaction occurred at the very beginning and was followed by the UPE reaction after an induction period. As shown in Figure 7a, due to the formation of PU network, the reaction peak of the uncapped UPE shifted drastically from 35 to 480 min. On the other hand, for the nongrafted IPN, the UPE peak only shifted from 50 to 100 min as shown in Figure 7c. This may be explained by the stronger solidification effect of PU in the fully grafted IPN through its extensive grafting to the uncapped UPE phase, where the diffusion of a UPE molecule to form a polymer chain is greatly retarded by the gelled PU phase. However, for the semigrafted IPN shown in Figure 7b, the PU network formation slightly accelerated, instead of delaying, the UPE reaction. The reason for this behavior is still unknown.

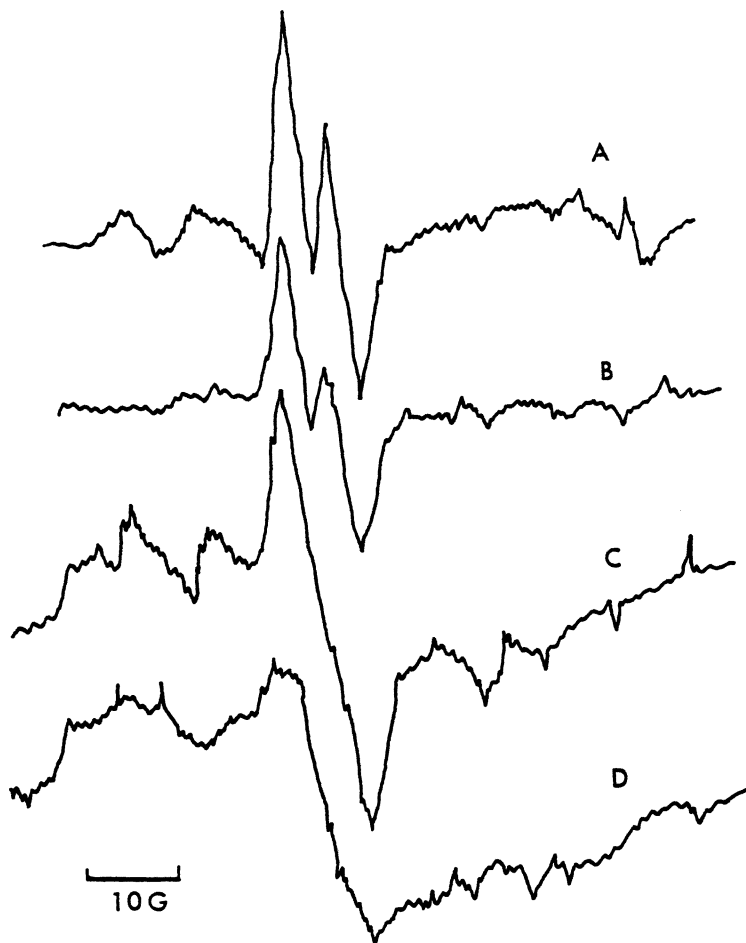


Figure 4. Radical spectra for cross-linked PU-UPE IPN at 60°C: (A) initial stage; (B) PU gelation; (C) UPE gelation; and (D) final stage.

Morphological Study

The transmission electron micrographs for the three IPNs are shown in Figure 8. In general, the black areas represent the PU-rich phase and the bright areas represent the UPE-rich phase (47). For the fully grafted IPN, the small inclusions (0.2 μm in diameter) consisted of mainly PU-rich phase. For the semigrafted IPN the inclusions were solely large PU-rich phase and were 5 μm in diameter. For the nongrafted IPN both PU- and UPE-rich phases formed inclusions of $\sim 0.5\text{--}1$ μm in size.

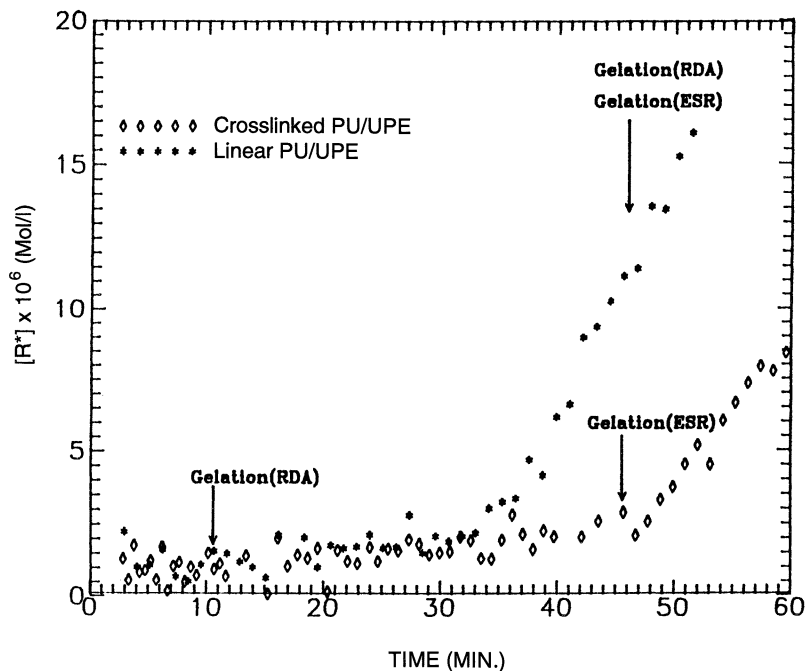


Figure 5. Radical concentration profile at 60 °C that compares the network formation of the UPE phase for cross-linked and linear PU–UPE IPNs.

Dynamic mechanical analysis (DMA) is expressed in terms of complex moduli or compliances. The complex moduli are defined by

$$G^* = G' + G'' \quad (1)$$

where G^* is the complex shear modulus, G' is the real part of the modulus, and G'' is the imaginary part of the modulus. The loss modulus (G'') is a damping or energy dissipation term. The angle that reflects the time lag between the applied stress and strain is δ , and it is defined by a ratio called the dissipation factor:

$$\tan \delta = G''/G' \quad (2)$$

The $\tan \delta$ is a damping term and is a measure of the ratio of energy dissipated as heat to the maximum energy stored in the material during one cycle of oscillation. With DMA spectroscopy, the frequency may be varied at constant temperature or, more conveniently, the temperature may be varied at constant frequency. The glass transition temperature (T_g) of a polymer is

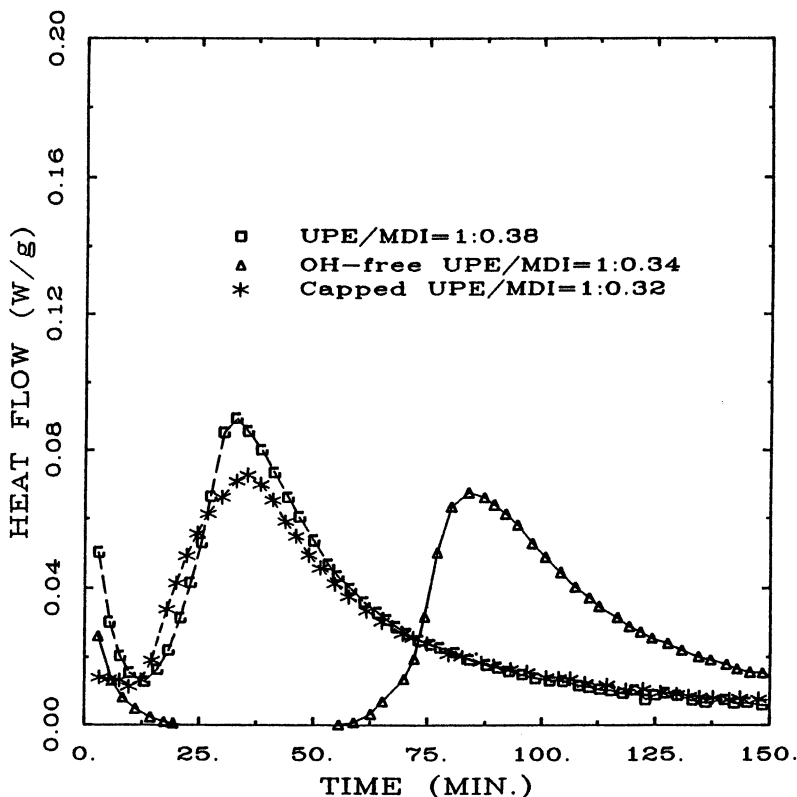


Figure 6. DSC isothermal runs for UPE-MDI blends at 60 °C.

defined as the temperature that corresponds to the maximum G'' or $\tan \delta$ in the DMA curves.

The dynamic mechanical analysis may reveal the degree of phase mixing in multiphase polymers. A comparison of the temperature dependence of storage modulus, G' , for UPE, PU, and the three IPNs is given in Figure 9a. As can be seen, the G' curves of all the IPNs lie in between those of pure UPE and PU. The level of G' depends on the extent of chemical grafting. The temperature dependence of $\tan \delta$ for the three IPNs and the pure UPE is shown in Figure 9b. The pure UPE shows a single T_g around 120 °C. For the fully grafted IPN the $\tan \delta$ curve shows a broad transition from 50 to 110 °C, which suggests extensive phase mixing. On the other hand, the $\tan \delta$ curves of the semigrafted IPN and nongrafted IPN show multiple distinct peaks that indicate stronger phase separation. These peaks, however, do not overlap with either the UPE peak or the PU peak (below room temperature, not shown in the figure), which indicates that both the continuous and the dispersed phases are mixtures of PU and UPE.

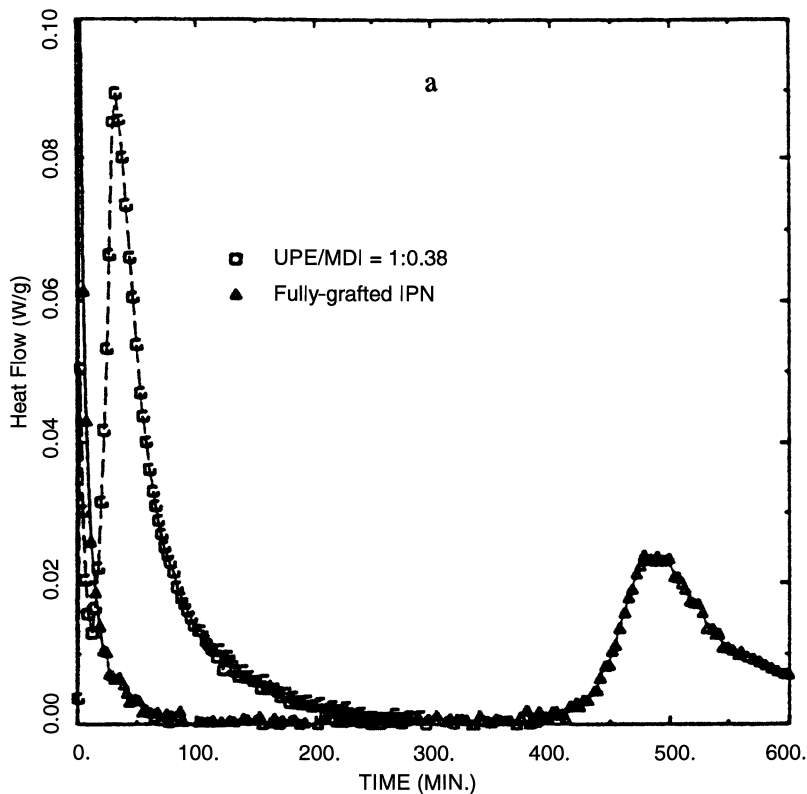


Figure 7. DSC isothermal runs at 60 °C for UPE–MDI blend and UPE–PU IPN (a). Continued on next page.

From the TEM micrographs and dynamic mechanical analysis it is difficult to interpret the phase structure of the polymer. Many theoretical models are available for predicting the modulus behavior of polymer blends. They are helpful for evaluating the features of phase continuity and phase inversion. However, when these theories are used to interpret experimental data, the limitations of theories should be realized. Most models were derived for solid particle reinforcement; that is, under the assumption that neither the shape of the reinforcing particles nor their orientation changes with composition. In general, these assumptions are invalid for IPNs. Thus, model predictions presented here can only serve as guidelines when compared with the experimental data. If the glassy component, UPE, is the continuous phase, the Takayanagi parallel model (48) can be used as a upper bound:

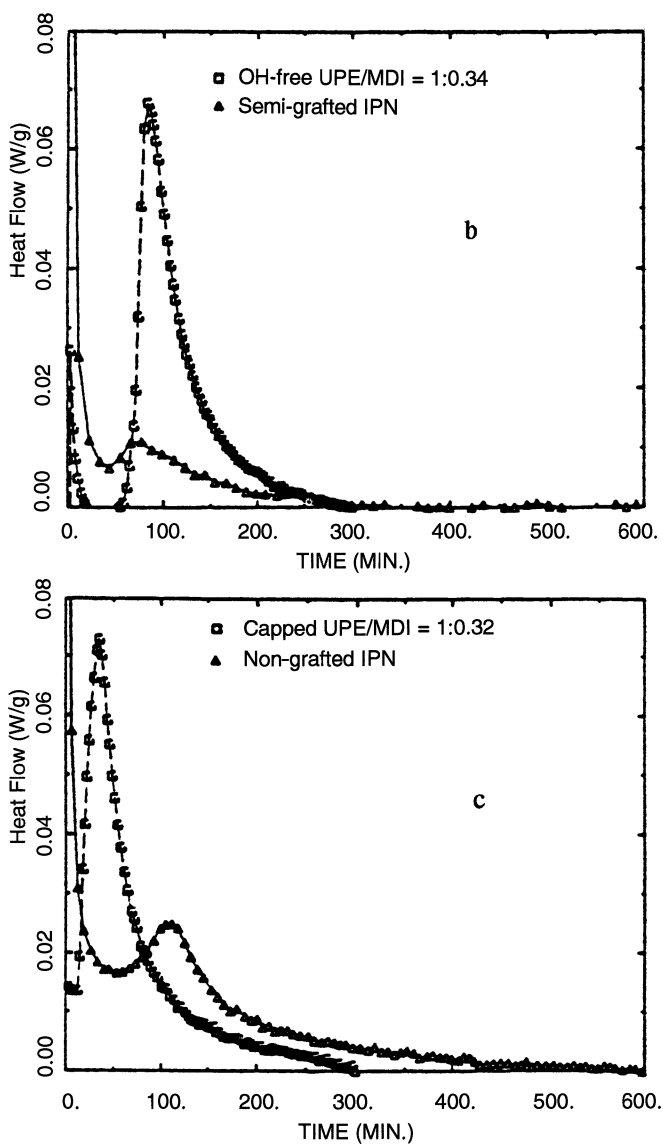
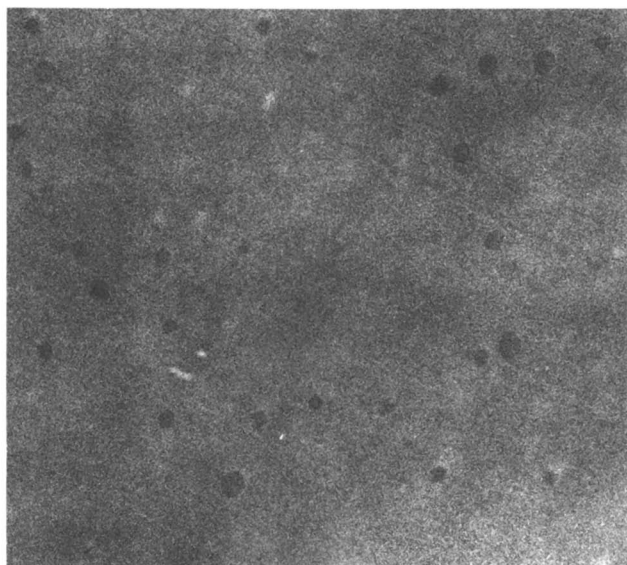


Figure 7. Continued. OH-free UPE-MDI blend and OH-free UPE-PU IPN (b); and capped UPE-MDI blend and capped UPE-PU IPN (c).



a

Figure 8. Transmission electron micrographs for fully grafted (a). Continued on next page.

$$G^* = \phi_A G_A^* + \phi_B G_B^* \quad (3)$$

where ϕ_i and G_i^* are the volume fraction and the complex modulus for the component i respectively, and G^* is the complex modulus of the polymer blend.

If the rubbery polymer, PU, forms the continuous phase, the Takayanagi series model (48) can be used as a lower bound:

$$G^* = \left[\frac{\phi_A}{G_A^*} + \frac{\phi_B}{G_B^*} \right]^{-1} \quad (4)$$

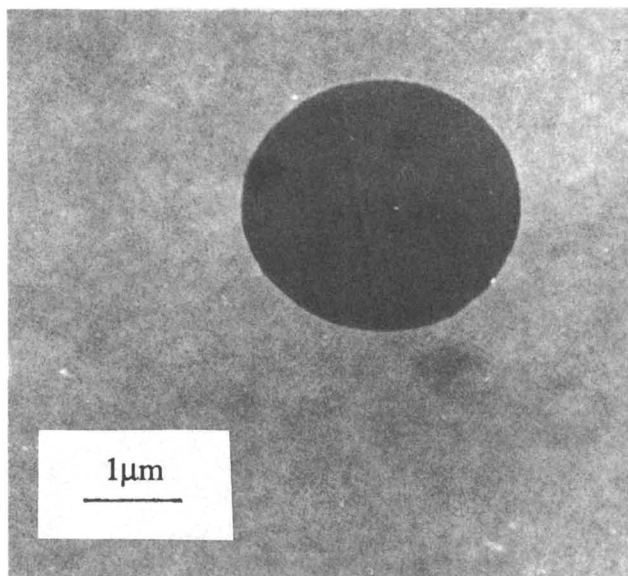
For the real (G') component of the modulus of the composite, the Takayanagi parallel and series models give the relationships

$$G' = (1 - \lambda)G'_A + \lambda X / (X^2 + Y^2) \quad (5)$$

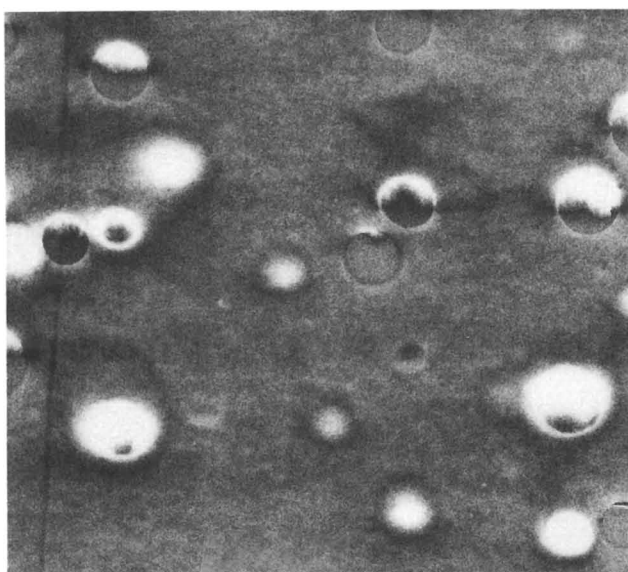
where $\lambda = \phi_B$, $\zeta = 1$ for parallel model and $\lambda = 1$, $\zeta = \phi_B$ for series model, and

$$X = (1 - \zeta)G'_A / (G_A'^2 + G_A''^2) + \left[\zeta G'_B / (G_B'^2 + G_B''^2) \right]$$

$$Y = (1 - \zeta)G''_A / (G_A'^2 + G_A''^2) + \left[\zeta G''_B / (G_B'^2 + G_B''^2) \right]$$



b



c

Figure 8—Continued. Transmission electron micrographs for semigrafted (b), and nongrafted (c) IPNs.

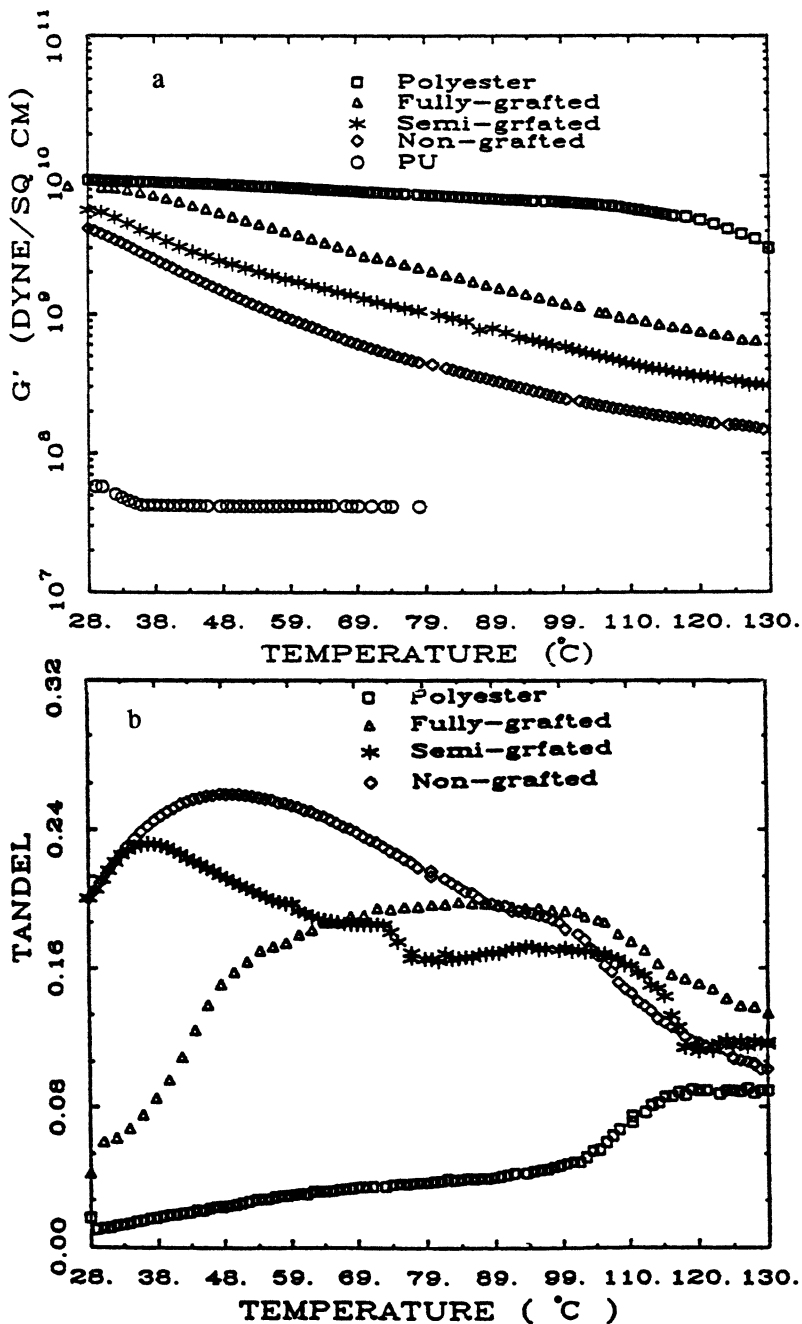


Figure 9. Temperature dependence of G' (a) and $\tan \delta$ (b) for UPE, PU, and three IPNs.

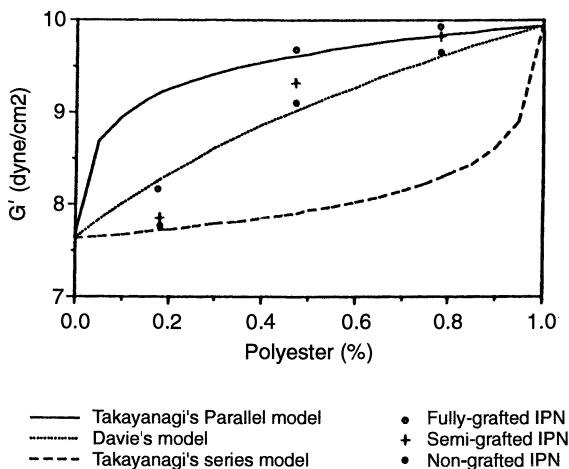


Figure 10. G' versus UPE composition plot at 50 °C of IPNs.

A dual-phase continuity model was derived by Davies (49, 50):

$$G^{1/5} = \phi_A G_A^{1/5} + \phi_B G_B^{1/5} \quad (6)$$

The G' versus UPE composition at 50 °C of such a plot is shown in Figure 10. A comparison between models and the experimental data for fully grafted IPN shows that even at 20% of UPE content, the PU phase does not comprise most of the matrix; the matrix is predominantly a co-continuous phase. When the UPE content is increased to 50% or higher, the UPE dominates the matrix. Apparently, the fully grafted IPN tends to form a more UPE-dominated matrix because of strong chemical grafting. On the other hand, the nongrafted IPN seems to have a PU-dominated phase around 20% of UPE. At 50% and higher UPE composition, the matrices of nongrafted IPNs are co-continuous phase. The matrix morphology of the semigrafted IPNs lies in between the other two IPNs. Many researchers have found that the sequence of network formation was the major factor of phase morphology in IPNs. Generally, the network formed first tends to dominate the continuous phase (51). This, however, was not the case in our IPN system. Because the cross-linking density of UPE was theoretically about seven times that of PU, it might have played an important role in determining the phase morphology of IPNs.

Summary

In this study, interactions between PU and UPE phases in IPN formation were investigated. For the rheological study, the effects of PU components

on UPE gelation and UPE components on PU gelation were identified. Some effects (e.g., formation of amide linkage and catalytic effects) accelerated gel formation, whereas other effects delayed gel formation (e.g., dilution and solidification effects). The experimental results show that for the 50:50 PU–UPE IPNs used in this study, the PU gelation is accelerated mainly due to the presence of carboxyl groups on the UPE molecules. On the other hand, the UPE gelation is retarded because of the strong solidification effect of the PU phase.

For the kinetic study, the formation of urethane and amide linkages between the functional end groups of UPE molecules and isocyanates resulted in more reactive resins. During the IPN formation, the solidification effect of the gelled PU phase affected the reactions of the three UPEs in different ways. The maximum reaction rate of the uncapped UPE was significantly delayed as compared to the reaction rate of the capped UPE due to the extensive grafting between the PU and the UPE phases in the uncapped UPE.

The morphological study of the cured IPNs showed that grafting played an important role in reduction of the extent of phase separation between PU and UPE networks. Chemical grafting also played a role in determination of the matrix composition of the IPNs.

Outlook

Reaction-induced phase separation in IPNs resembles phase separation in thermoplastic polymer blends except that the driving force in thermoplastic polymer blends is temperature change, whereas chemical reaction is the driving force in IPNs. The phase separation rate interacts with the chemical reaction rate. Both rates are dependent on temperature and amount of catalyst. The three IPNs prepared in this study underwent phase separation during polymerization. TEM and dynamic mechanical analysis revealed the morphologies of the three IPNs only after structure formation. To better control the morphology and properties of the IPN products, the dynamics of the phase separation process need to be understood.

For the PU–UPE IPNs, the reaction kinetics of UPE are strongly affected by the formation of PU phase. Unlike the fully grafted and non-grafted IPNs, the UPE reaction was accelerated instead of being retarded by the formation of the PU phase in the semigrafted IPN. The difference of phase separation in each IPN may have affected the kinetics differently. During the phase demixing process, the amount of initiator in the UPE phase and even the composition of the UPE phase (ratio of styrene to UPE resin) may redistribute in the newly formed phases. These factors may affect the reaction kinetics of the UPE phase. To understand the influence of phase

demixing on resin reaction kinetics, further study on the partition of catalyst and resins should be conducted.

Modeling of dynamic mechanical properties using Takayanagi's models was limited by the model assumptions. These models are derived for solid particle reinforcement under the assumption that neither the shape of the reinforcing particles nor their orientation changes with composition. In general, these assumptions are invalid for IPNs. More detailed models based on the actual morphology of IPNs should be developed.

PU-UPE and other types of IPNs have been used in many applications such as coating (15, 26), RIM and composite resins (52, 53), membranes (54, 55), acoustical materials (56, 57), and biomedical materials (58). Because of their unique properties, IPNs have a great potential to grow further. However, the presence of dual reactions and the strong interactions among morphology, kinetics, and rheology make manufacture of these materials very complicated.

For example, in liquid composite molding, the use of PU-UPE IPNs as matrix resins provides better composites than use of PU resins only (52, 53). This phenomenon is explained by the fact that PU-UPE IPNs are more compatible to the sizing of glass fiber reinforcement than PU resins. Better fiber wetting and interface bonding contributes to the better mechanical properties of the molded composites. IPN-based matrix resins, however, are more sensitive to molding conditions than PU resins. A better understanding of the relationship between resin moldability (i.e., rheological and kinetic changes), processing conditions, and properties is necessary.

Thermoplastic-based microporous membranes can be produced by a thermally-induced phase separation method (59, 60). In this method, a homogeneous polymer-solvent mixture is converted to a two-phase structure by temperature jump or drop. The membrane structure is then fixed by freeze drying. A drawback of the resulting membrane is that around the glass transition temperature of the thermoplastic polymer, the membrane morphology changes. Similar membranes also can be prepared by reaction-induced phase separation of IPNs. Here, a semi-IPN (one linear and one cross-linked polymer) with specific morphology (e.g., co-continuous structure) can be obtained by controlling the phase separation process during polymerization. The linear phase can then be removed by a proper solvent and a thermally stable and microporous thermosetting membrane remains. However, reaction-induced phase separation is much more complicated than thermally induced phase separation. More effort must be spent in this area.

Some IPNs are effective acoustical absorbing materials because of broad transitions that result from microstructures (56, 57). Microstructure formation (61) strongly affects the area under loss modulus (G'') versus temperature curves; that is, the damping ability. However, the detailed correlation between microstructure and damping ability has not been established. A

thorough study in this area can provide guidelines to better design of acoustical materials.

Acknowledgment

The authors would like to acknowledge Ashland Chemical, Dow Chemical, and Union Carbide companies for material donation. Technical help from C. P. Hsu of The Ohio State University and Jack Tsai of Ashland Chemical Company is greatly appreciated.

References

1. Thomas, D. A.; Sperling, L. H. In *Polymer Blends*; Paul, D. R.; Newman, S., Eds.; Plenum: New York, 1976; Vol. II, Chapter 11.
2. Sperling, L. H. In *Multicomponent Polymeric Materials*; Sperling, L. H., Paul, D. R.; Eds.; Advances in Chemistry Series 211. American Chemical Society: Washington, DC, 1986.
3. Frisch, K. C.; Klempner, D.; Migdal, S.; Frisch, H. L. *J. Polym. Sci., Polym. Chem. Ed.* **1974**, *12*, 885.
4. Kim, S. C.; Klempner, D.; Frisch, K. C.; Radigan, W.; Frisch, H. L. *Macromolecules* **1976**, *9*, 258.
5. Allen, G.; Bowden, M. J.; Blundell, D. J.; Jeffs, G. M.; Vyvoda, J.; White, T. *Polymer* **1973**, *14*, 604.
6. Djomo, H.; Morin, A.; Damyanidu, M.; Meyer, G. C. *Polymer* **1983**, *24*, 65.
7. Kim, S. C.; Klempner, D.; Frisch, K. C.; Frisch, H. L.; Ghiradella, H. *Polym. Eng. Sci.* **1975**, *15*, 339.
8. Yeo, J. K.; Sperling, L. H.; Thomas, D. A. *Polym. Eng. Sci.* **1981**, *21*, 696.
9. Sperling, L. H. *Interpenetrating Polymer Networks and Related Materials*; Plenum: New York, 1981.
10. Frisch, H. L.; Foreman, R.; Schwartz, R.; Yoon, H.; Klempner, D.; Frisch, K. C. *Polym. Eng. Sci.* **1979**, *19*, 284.
11. Hourston, D. J.; Zia, Y. *J. Appl. Polym. Sci.* **1984**, *29*, 2951.
12. Natchimuthu, N.; Pajalingam, P.; Radhakrishnan, G.; Francis, D. J. *J. Appl. Polym. Sci.* **1990**, *41*, 3059.
13. Lipatov, Y. S.; Karabanova, L. V.; Sergeyeva, L. H. *Polym. Sci. USSR* **1977**, *19*, 1237.
14. Kaplan, K.; Tschoegl, N. W. *Polym. Eng. Sci.* **1975**, *15*, 343.
15. Frisch, H. L.; Frisch, K. C.; Klempner, D. *Polym. Eng. Sci.* **1974**, *14*, 646.
16. Meyer, G. C.; Mehrenberger, P. Y. *Eur. Polym. J.* **1977**, *13*, 383.
17. Nguyen, L. T.; Suh, N. P. *Polym. Eng. Sci.* **1986**, *26*, 799.
18. Nguyen, L. T.; Suh, N. P. *Polym. Eng. Sci.* **1986**, *26*, 843.
19. Lee, S. S.; Kim, S. C. *Polym. Eng. Sci.* **1991**, *31*, 1182.
20. Hsu, T. J.; Lee, L. J. *J. Appl. Polym. Sci.* **1988**, *36*, 1157.
21. Hsu, T. J.; Lee, L. J. *Polym. Eng. Sci.* **1985**, *25*, 951.
22. Hsu, T. J.; Lee, L. J. *Polym. Eng. Sci.* **1988**, *28*, 956.

23. Yang, Y. S.; Lee, L. J. *Macromolecules* **1987**, *20*, 1490.
24. Kim, J. H.; Kim, S. C. *Polym. Eng. Sci.* **1987**, *27*, 1243.
25. Kim, J. H.; Kim, S. C. *Polym. Eng. Sci.* **1987**, *27*, 1252.
26. Frisch, K. C.; Klemmner, D.; Frisch, H. L.; Chiradella, H. In *Recent Advances in Polymer Blends, Grafts, and Blocks*; Sperling, L. H., Ed.; Plenum: New York, 1974; p 395.
27. Edwards, H. R. *Annu. Tech. Conf. Soc. Plast. Eng.* **1986**, *32*, 1326.
28. Wilkinson, T. C.; Borgnaes, D.; Chappel, S. F.; Kelly, W. L. *Polym. Mater. Sci. Eng.* **1983**, *49*, 469.
29. Kelly, W. L. *Plast. Eng.* **1986**, *9* (February).
30. Frisch, H. L.; Klemmner, D.; Frisch, K. C. *J. Polym. Sci., Polym. Phys. Ed.* **1969**, *7*, 775.
31. Matsuo, M.; Kwei, T. K.; Klemmner, D.; Frisch, H. L. *Polym. Eng. Sci.* **1970**, *10*, 921.
32. Frisch, K. C.; Klemmner, D.; Antczak, T. J. *Appl. Polym. Sci.* **1974**, *18*, 683.
33. Frisch, K. C.; Klemmner, D.; Mukherjee, S. K. *J. Appl. Polym. Sci.* **1974**, *18*, 689.
34. Scarito, P. R.; Sperling, L. H. *Polym. Eng. Sci.* **1979**, *19*, 297.
35. Yeo, J. K.; Sperling, L. H.; Thomas, D. A. *J. Appl. Polym. Sci.* **1981**, *26*, 3283.
36. Xiao, H. X.; Frisch, K. C.; Al-Khatib, S. In *Cross-linked Polymers, Chemistry, Properties, and Applications*; Dickie, R. A.; Labana, S. S.; Bauer, R. S., Eds.; ACS Symposium Series 367; American Chemical Society: Washington, DC, 1988; Chapter 21.
37. Winter, H. H. *Polym. Eng. Sci.* **1988**, *27*, 1698.
38. Hsu, C. P.; Lee, L. J. *Polymer* **1991**, *32*, 2263.
39. Muthukumar, M.; Winter, H. H. *Macromolecules* **1986**, *19*, 1284.
40. Winter, H. H.; Chambon, F. *J. Rheol.* **1987**, *30*, 367.
41. Chambon, F.; Winter, H. H. *J. Rheol.* **1987**, *31*, 683.
42. Tollens, F. R.; Lee, L. J. *Polymer* **1993**, *34*, 29.
43. Saunders, J. H.; Frisch, K. C. *Polyurethanes Chemistry and Technology*; Krieger: Melbourne, FL, 1978; Part I, p 79.
44. Avella, M.; Martuscelli, E.; Volpe, M. G. *J. Thermal Anal.* **1988**, *34*, 441.
45. Yang, Y. S.; Lee, L. J. *Polymer* **1988**, *29*, 1793.
46. Dusek, K. In *Network Formation by Chain Crosslinking Copolymerization*; Haward, R. N., Ed.; Developments in Polymerization 3; Applied Science Publishers: London, 1982; Chapter 4.
47. Wang, K. J.; Hsu, T. J.; Lee, L. J. *Polym. Eng. Sci.* **1989**, *29*, 397.
48. Takayanagi, M.; Vermura, S.; Minami, S. *J. Polym. Sci., Polym. Lett. Ed.* **1963**, *5*, 113.
49. Davies, W. E. A. *J. Phys. D* **1971**, *4*, 318.
50. Davies, W. E. A. *J. Phys. D* **1971**, *4*, 1325.
51. Huelck, V.; Thomas, D. A.; Sperling, L. H. *Macromolecules* **1972**, *5*, 340.
52. Patel, N.; Rohatgi, V.; Lee, L. J. *Polym. Composites*, in press.
53. Damani, S. G.; Lee, L. J. *Polym. Composites* **1990**, *11*, 174.
54. Lee, Y. K.; Sohn, I. S.; Jeon, E. J.; Kim, S. C. *Polym. Mater. Sci. Eng.* **1991**, *65*, 125.
55. Mizutani, Y. J. *Membrane Sci.* **1990**, *49*, 121.
56. Klemmner, D.; Sophiea, D.; Suthar, B.; Frisch, K. C.; Sendjarevic, V. *Polym. Mater. Sci. Eng.* **1991**, *65*, 82.

57. Klempner, D.; Wang, C. L.; Ashtiani, M.; Frisch, K. C. *J. Appl. Polym. Sci.* **1986**, *32*, 4197.
58. Feldman, J. A.; Huang, S. J. S. In *Cross-linked Polymers, Chemistry, Properties, and Applications*; Dickie, R. A.; Labana, S. S.; Bauer, R. S., Eds.; ACS Symposium Series 367; American Chemical Society: Washington, DC, 1988; Chapter 18.
59. Castro, A. J. U.S. Patent 4,247,498, January 27, 1981.
60. Kinzer, K. E.; Lloyd, D. R. *Polym. Mater. Sci. Eng.* **1989**, *63*, 82.
61. Fay, J. J.; Thomas, D. A.; Murphy, C. J.; Sperling, L. H. *Polym. Mater. Sci. Eng.* **1990**, *63*, 493.

RECEIVED for review October 9, 1991. ACCEPTED revised manuscript August 26, 1992.

Morphology–Processing Relationship in Interpenetrating Polymer Blends

Styrene-Ethylene / Butylene-Styrene Block Copolymer and Poly(ether ester)

H. Verhoogt, J. van Dam, and A. Posthuma de Boer

Faculty of Chemical Engineering and Materials Science, Department of Polymer Technology, Delft University of Technology, P.O. Box 5045, 2600 GA Delft, The Netherlands

Interpenetrating polymer blends, which show properties of their constituents as well as new properties, usually are formed in limited ranges of compositions. Blends of a styrene-ethylene/butylene-styrene (SEBS) block copolymer and a poly(ether ester) were studied as an example of systems that show co-continuity over a broader range of compositions. The blends were prepared on a two-roll mill. The morphology of the blends was studied by extraction experiments, scanning electron microscopy, and confocal laser scanning microscopy. Complete dual-phase continuity existed over a wide range of compositions (20–60-vol% SEBS) in blends quenched after blending. Compression molding or annealing at 200 °C narrowed the range of fully co-continuous compositions to 30–60 vol%. Extrusion of the annealed blends resulted in recovery of the broader range of full dual-phase continuity. The viscosity of the blends as measured by capillary rheometry showed a minimum in the intermediate composition range, possibly caused by interfacial slip.

WHEN TWO POLYMERS ARE MECHANICALLY BLENDED the result usually is a heterogeneous system because of the positive free energy of mixing (1). The resulting morphology is most likely the dispersed-phase matrix type in which the minority phase can be spherical, fibrous, or lamella-like. In the intermedi-

ate composition range blends with dual-phase continuity may be formed. Such blends are frequently called thermoplastic interpenetrating polymer networks (IPNs) (2–7), in accordance with the definition given by Gergen (8, 9): “a combination of two dissimilar polymers in which each polymer is topologically independent and has three-dimensional continuity”. The term “network” in this definition is not restricted to networks on a molecular scale or on a phase-domain scale, and a distinction is sometimes difficult to make (3, 9). In the case of the co-continuous blend morphologies, the term “interpenetrating polymer blend” (IPB) (10) seems preferable, because any reference to molecular cross-links is avoided.

The earliest examples of IPBs were mechanically blended combinations of polypropylene (PP) and ethylene-propylene-diene-monomer rubber (EPDM) (11). Since then there has been a lot of interest in this kind of blend because of the large variety of applications for PP-EPDM blends (12–14). The properties of IPBs are combinations of the properties of the components, which retain their individual identities, and thus the properties of both components are fully expressed. The advantage of an IPB structure versus a dispersed structure is that the properties can generally be described by additive relationship (9, 15, 16). Additive behavior is reported for the dynamic modulus (8, 9) and for the tensile strength (17, 18) of IPBs. However, synergistic and antagonistic behavior with respect to the tensile strength is found as well (17–19).

Two main routes can be employed to prepare IPBs:

- *Physical blending* of two existing polymers, either in the molten state or in solution. The most common method is mechanical blending in the molten state. With this method various IPBs were obtained that consisted, for example, of a styrene-ethylene/butylene-styrene (SEBS) block copolymer and several thermoplastics like PP, nylon, and saturated polyesters, (8, 9, 15, 16); of polystyrene (PS) and *cis*-polybutadiene (PBD), of PS and poly(methyl methacrylate) (PMMA), and of PMMA and ethylene-propylene rubber (EPR) (10); of sulfonated EPDM ionomers and several thermoplastics (PP, high-density polyethylene (HDPE), SBS) (17, 18); of PP and EPR, and of PS and styrene-butadiene rubber (SBR) (20); and of styrene-isoprene-styrene (SIS) block copolymer and a polyethylene phase consisting of 75% linear low-density polyethylene (LLDPE) and 25% low-density polyethylene (LDPE) (21). Solution blending (reference 1, Chapter 2) was used by Hsu et al. (19) to prepare IPBs that consisted of polyurethanes and poly(vinyl alcohol).

- *Chemical blending*, for example, by swelling monomer 2 into polymer 1 and polymerization in situ. Phase separation during or after polymerization may result in a co-continuous morphology. This method was used to synthesize IPBs that consisted of SEBS and a neutralized ionomer prepared from a random copolymer of styrene, methacrylic acid, and isoprene (SMAAI) (4-6). Nishiyama and Sperling (7) synthesized an IPB by combination of poly(*n*-butyl acrylate) and polystyrene; both polymers were cross-linked independently with acrylic acid anhydride. De-cross-linking of both polymers was carried out by hydrolysis, after which neutralization formed the ionomers. The chemically blended IPBs (4-7) were compared with their mechanically blended equivalents. For all IPBs it was found that the chemically prepared blends had better mechanical properties than the mechanically prepared blends.

According to Gergen et al. (9) the most efficient mixing of two components into an interpenetrating structure can be obtained when the viscosities and volume fractions of the two polymers are equal. Avgeropoulos et al. (22) reported that the critical volume fraction for the formation of dual-phase continuous structures was primarily determined by the viscosity ratio of the blend components. Paul and Barlow (23, 24) gave an empirical relation for the condition for the point of phase inversion (where dual-phase continuity exists) that was confirmed by Jordhamo et al. (25) and by Gergen et al. (9). This relation was generalized by Miles and Zurek (10) to

$$\frac{\eta_1(\dot{\gamma})}{\eta_2(\dot{\gamma})} = \frac{\phi_1}{\phi_2} \quad (1a)$$

or

$$\phi_2 = 1/[1 + \lambda] \quad (1b)$$

where $\eta_i(\dot{\gamma})$ is the viscosity of polymer *i* at the shear rate $\dot{\gamma}$ that prevails in the mixing equipment during preparation of the blend, $\dot{\gamma}$ is the shear rate, ϕ_i is the volume fraction of polymer *i*, and $\lambda = \eta_1/\eta_2$ is the viscosity ratio. From filament instability considerations Metelkin and Blekht (26) derived for the point of phase inversion

$$\phi_2 = 1/[1 + \lambda F(\lambda)] \quad (2)$$

where $F(\lambda) = 1 + 2.25 \log \lambda + 1.81(\log \lambda)^2$.

According to Utracki (27), eqs 1 and 2 are reasonably close. By equating expressions for the viscosity of (hypothetical) systems of one component

dispersed in the other and vice versa, Utracki (28) derived the condition for phase inversion:

$$\lambda = [(\phi_m - \phi_{2I}) / (\phi_m - \phi_{1I})]^{[\eta]\phi_m} \quad (3)$$

where ϕ_m is the maximum packing volume fraction, ϕ_{1I} is the phase inversion concentration ($= 1 - \phi_{2I}$), and $[\eta]$ is the intrinsic viscosity. Especially for values of λ away from unity, eq 3 gives improvement over eq 1 (28).

Although it is possible to predict the point of phase inversion with eqs 1–3, the equations do not give information about the range of compositions that allow dual-phase continuity. Schematic expectations of this range as a function of viscosity ratio are given by Sperling (3) and by Gergen et al. (9). In a figure, Nelson et al. (29) presented morphological changes as a function of viscosity ratio and composition for EPDM–PBD blends. The figure shows that a broad range of EPDM–PBD compositions was formed that possessed co-continuity. Similar figures were presented by Siegfried et al. (4) for IPBs of SEBS and SMAAI and by Jordhamo et al. (25) for IPBs of PS and PBD. Recently, Lyngaae-Jørgensen and Utracki (30) showed that the critical volume fraction for formation of infinite structures, $\phi_{cr} = 0.156$, as predicted from percolation theory for monodisperse spherical domains, is in reasonable accordance with experimental data from various authors.

Experimental determination of blend morphology, and of co-continuity in particular, is not straightforward. Electronic and optical microscopy methods are primarily used, but determination of three-dimensional structures from two-dimensional pictures is notoriously difficult. However, three-dimensional pictures of the internal structure of unprepared blend samples can be made by computer-aided reconstruction of video images obtained by confocal laser scanning microscopy (CLSM). Selective extraction of one of the polymer phases can be a reliable method provided that the soluble polymer is selectively and quantitatively dissolved and that the remaining structure still has the shape and continuity of the sample and is intact structurally without any crumbling or delamination (16). The percentage of extracted polymer gives a direct measure of the degree of continuity of this polymer, which cannot be determined directly from methods such as electron microscopy (30, 31). Other methods, such as measurements of electrical conductivity and mechanical properties, depend on model descriptions for interpretation of results (30, 32). A critical discussion of various methods that can be used for estimation of co-continuous structures in two phase blends was given by Lyngaae-Jørgensen and Utracki (30). Because ambiguities may be the result of reliance on a single technique, a combination of the results of at least two techniques is strongly recommended.

Morphological changes can occur at elevated temperatures due to post-mixing relaxation and microrheological processes driven by the interfacial

energy (reference 1, Chapter 8). Quintens et al. (33, 34) showed that phase coarsening occurred upon annealing of co-continuous polycarbonate-styrene-acrylonitrile copolymer (PC-SAN) blends, but that the co-continuity was preserved. The phenomenon was also reported by Gergen et al. (9) for a 70:30 PP-PBD IPB. These results indicate that IPBs with co-continuous phases can possess some stability against morphological changes that usually occur during annealing and further processing of polymer blends.

One of the differences between an IPB and a chemically cross-linked IPN is that an IPB can flow at elevated temperatures. The consequences of the morphology for the flow behavior and the stability of the co-continuous morphology against disruption by the flow field are not yet fully understood. Han (35) reported that an "interlocked" morphology should give a maximum in the viscosity-composition curve of polymer blends. This interlocked morphology indicates that the viscosity of IPBs should be higher than the viscosity of the components. However, IPBs of SEBS and SMAAI (4), PP and EPDM, and PS and SBR (20) showed lower viscosities than the components. Nishiyama and Sperling (7) found that the torques of the IPBs that consisted of poly(*n*-butyl acrylate) and PS were almost equal to the torques of the components. Lyngaae-Jørgensen et al. (36) suggested that the lower viscosity of the blends compared to the viscosity of the components might be caused by interfacial slip. Recently, Utracki and Sammut (37) reported that due to the shearing forces, the structure of a blend is destroyed during steady shear viscosity measurements. Thus, the results obtained do not give information on the viscosity of the starting structure of the blend.

Here we report investigations of blends of two thermoplastic elastomers that, because of their rheological properties, were expected to form IPBs over a wide range of compositions. The two polymers used were a SEBS block copolymer and a semicrystalline poly(ether ester) that have almost equal viscosities in a wide range of shear rates. The objectives of this research were to study the formation of IPBs in a wide range of compositions, to study the stability of the formed morphologies during subsequent annealing and extrusion, and to study the viscosity of the IPBs.

Experimental Details

Materials and Methods. The two materials used were Kraton G1657X and Arnitel EM400. Kraton G1657X (Shell Co.) is a SEBS thermoplastic elastomer that consists of an ethylene/butylene matrix with glassy styrenic domains. The percentage of styrene is 13% (38). Arnitel EM400 (Akzo Co.) is a semicrystalline copoly(ether ester) that consists of 40% poly(butylene terephthalate) (PBT) as the hard crystalline segments and 60% poly(oxytetramethylene terephthalate) (POTMT) as the soft amorphous segments (39). Dynamic mechanical thermal analysis (DMTA) and differential scanning calorimetry (DSC) were used to determine if (some) miscibility between the polymers existed.

Blends of SEBS and the poly(ether ester) were prepared in steps of 10 vol% over the entire composition range on a two-roll mill at a temperature of 200 °C. The maximal apparent shear rate $\dot{\gamma}$ at the roll surface was 266 s⁻¹. After blending for 7 min the blend was scraped off the mill and either quenched in room temperature water or pressed into a sheet (thickness 3.5 mm) with a platen press at 200 °C and, after compressing times of 0.5–1 min (estimated range of effective heating time due to variations in contact of the milled material with the hot platens), subsequently quenched in room temperature water. Variations in effective compression times are inevitable, but did not influence the results according to the reproducibility of various samples of various positions of three sheets at each composition.

The pressed blends were granulated to study their rheological and morphological behavior during further processing.

Rheological Tests. Flow curves of the blend components and the pressed blends were determined with a twin-bore capillary rheometer (Rosand RH 7/8-2) at a temperature of 200 °C in the shear rate region $\dot{\gamma} = 16\text{--}1024$ s⁻¹. The capillaries had a diameter of 1 mm and length-to-diameter ratios (L/D) of 4 and 20. The reported values are Bagley and Rabinowitsch corrected. A resonance mass spectrometer (Rheometrics RMS 800) was used to determine the rheological behavior at lower shear rates at 200 °C. Measurements were performed in the cone-plate configuration.

The capillary rheometer also was used to extrude granulate of the pressed sheets at 200 °C to study the change in morphology as a result of processing. The pressed blends with SEBS–poly(ether ester) compositions of 20:80, 30:70, 50:50, and 80:20 were extruded three times at $\dot{\gamma} = 400$ s⁻¹ and at $\dot{\gamma} = 1000$ s⁻¹. After the first and the third extrusion some material was collected for morphological experiments.

Determination of Morphology. Extraction experiments were performed on samples of the directly quenched, the pressed, and the annealed blends. Diethyl ether was used to extract the SEBS polymer out of the blends at room temperature. Extraction time was 18 days. Reported values are the averages of three samples. No reliable extraction data for Arnitel could be obtained due to its limited solubility. The pressed blends with the compositions of 20:80, 30:70, 50:50, and 80:20 were kept for 5 and 10 min at 200 °C to study a possible change in the morphology due to annealing. These time intervals were comparable with the time the blends were held in the rheometer before the viscosity measurements and the extrusion of the materials started.

A scanning electron microscope (Jeol JSM 35) was used to obtain images of the morphology of the blends. The morphologies of the directly quenched, the pressed, the annealed, and the extruded blends were examined. Samples were prepared from the fracture surfaces of the blends, broken in liquid nitrogen, and from the remainder of the blends after extraction of the SEBS polymer. The samples were coated with a thin layer of gold using a sputter-coater (Edwards 150 B).

Experiments with a confocal laser scanning microscope (CLSM), developed by the Netherlands Organization for Applied Scientific Research (TNO) (40–42) were performed on the directly quenched and the pressed blends. With this method it is possible to obtain micrographs at a very large number of different levels in the sample, starting from the surface to a depth of 40–60 μm (for the blends described here). By recording the images of the morphology with a video recorder while moving from the surface to a depth of 50 μm, a three-dimensional

image of the morphology of the blend was obtained. Playing back these tapes gives an excellent view of the morphology of the blends. With the aid of a software-based visualization system (Application Visualization System 3.0; Student Computers Inc.), it was possible to reconstruct the phase boundaries in a form more suitable for reproduction. A more detailed discussion of the CLSM experiments is described elsewhere (43).

Results

The rheological measurements at 200 °C indicate that both the SEBS polymer and the poly(ether ester) show non-Newtonian behavior in the shear rate range of 30–2000 s^{-1} (see Figure 1). The viscosity ratio of the polymers is constant in this range of shear rates, which includes the shear rate of blending (266 s^{-1}): $\eta_{\text{Kraton}}/\eta_{\text{Arnitel}} = 1.2$. This constancy means that according to eq 1 the point of phase inversion is expected to be at the 55:45 SEBS:poly(ether ester) composition. Equations 2 and 3 yield values that are not significantly different from the values obtained with eq 1. Figure 2 shows that blends of the two polymers have a lower apparent shear viscosity than the blend components. A shift of the glass temperatures of the polymers has not been detected in the DMTA and DSC experiments; that is, these polymers are immiscible.

Extraction of SEBS with diethyl ether was performed over the entire composition range for the directly quenched and compression molded blends, and for the annealed blends as indicated in the experimental details section. Extraction of 100% of the SEBS out of the directly quenched blends containing 30 vol% or more of SEBS appeared to be possible always. The Arnitel residue remained as one coherent piece for compositions up to and including 60 vol% SEBS. For larger volume fractions of SEBS, the Arnitel

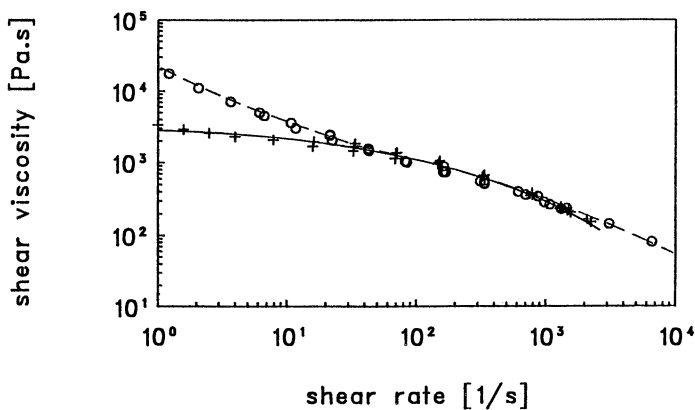


Figure 1. Flow behavior of Kraton G1657X (+) and Arnitel EM400 (O) at 200 °C.

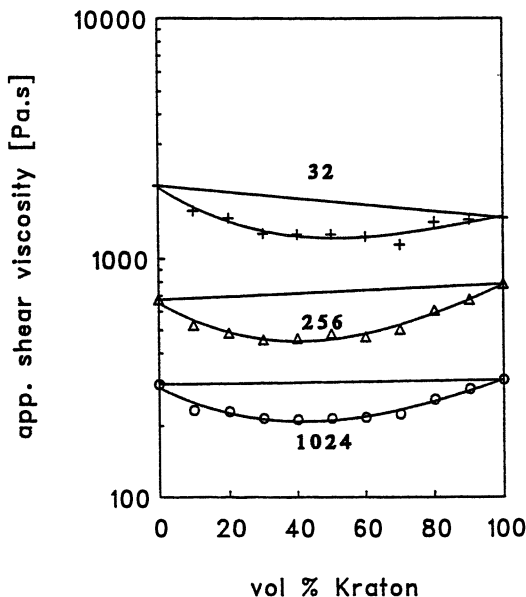


Figure 2. Apparent shear viscosity as a function of volume fraction of Kraton at 200 °C and at several apparent shear rates.

residue fell apart. Compression molding or annealing did not significantly alter the results in this range of compositions. The quenched 20-vol% blend also allowed 100% extraction of the SEBS, whereas the compression molded or annealed samples released only 70 or 20%, respectively, of the SEBS upon extraction. These extraction results are illustrated in Figure 3. Only 25% SEBS could be extracted from the 10-vol% blends. The residues of the 10- and 20-vol% blends were always one coherent piece of Arnitel.

The scanning electron (SE) micrographs indicate that the morphologies of the directly quenched and the pressed blends that contain 10-, 80-, or 90-vol% SEBS were all dispersed phase-matrix morphologies. The 70-vol% blends possessed partly co-continuous structures and partly dispersed phase-matrix structures. The directly quenched and pressed blends that contained 20–60-vol% SEBS possessed full dual-phase continuity with the exception of the pressed blend that contained 20-vol% SEBS, as illustrated in Figures 4 and 5. Annealing of the blends resulted in a decrease of dual-phase continuity in the blend with 20-vol% SEBS and in phase coarsening in the blend with 30-vol% SEBS, as can be seen in Figure 6.

Some photographs obtained from the CLSM experiments at a depth of 10 and 20 μm are depicted in Figure 7 for blends that contain 20- and 50-vol% SEBS. The pressed blends show morphologies a little coarser than the directly quenched blends. In common with SE micrographs, these

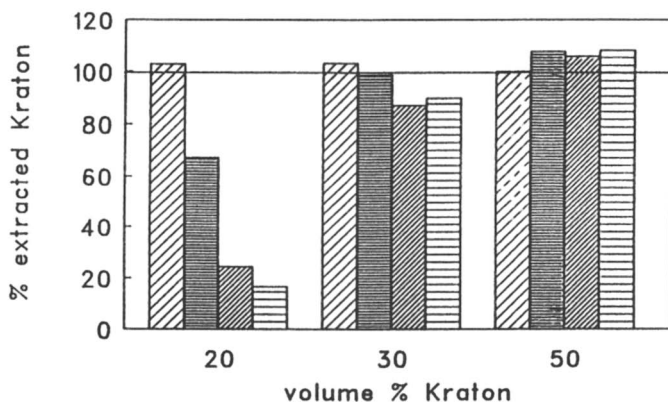


Figure 3. Percentages of Kraton extracted from directly quenched blends (diagonal lines), pressed blends (solid grey), blends annealed for 5 min (diagonal lines, opposite), and blends annealed for 10 min (horizontal lines).

pictures only give an indication of the structure. Clear three-dimensional impressions were obtained from the video recordings of the CLSM pictures. These three-dimensional impressions show Arnitel dispersed in SEBS for 80-vol% blends, a fully co-continuous structure for 50-vol% blends, a fully co-continuous structure for 30-vol% blends, a full co-continuous structure for 20-vol% directly quenched blend, and a partly co-continuous, partly dispersed structure for 20-vol% pressed blend.

The video recordings were converted into three-dimensional pictures using the application visualization system (AVS 3.0) (43). An example of the result of this processing is given in Figure 8, which shows the interface between the Arnitel and the SEBS polymers in a 50:50 pressed blend. The co-continuous morphology is clearly visible.

SE micrographs of blends extruded three times at $\dot{\gamma} = 400$ and 1000 s^{-1} , respectively, are given in Figures 9 and 10, which indicate dual-phase continuity for the 20- and 50-vol% SEBS blends and a dispersed morphology for the 80-vol% blends. Extraction of the extruded blends always resulted in 100% removal of the SEBS, whereas the poly(ether ester) phase remained coherent. Similar results were obtained after only one extrusion.

Discussion

A polymer component in a blend has formed a continuous phase if selective extraction of 100% of the component out of the blend is possible provided that the residue is fully coherent after extraction (16). The results from the extraction experiments show that the quenched blends contain a SEBS phase that is partially continuous in 10-vol% blends and fully continuous for

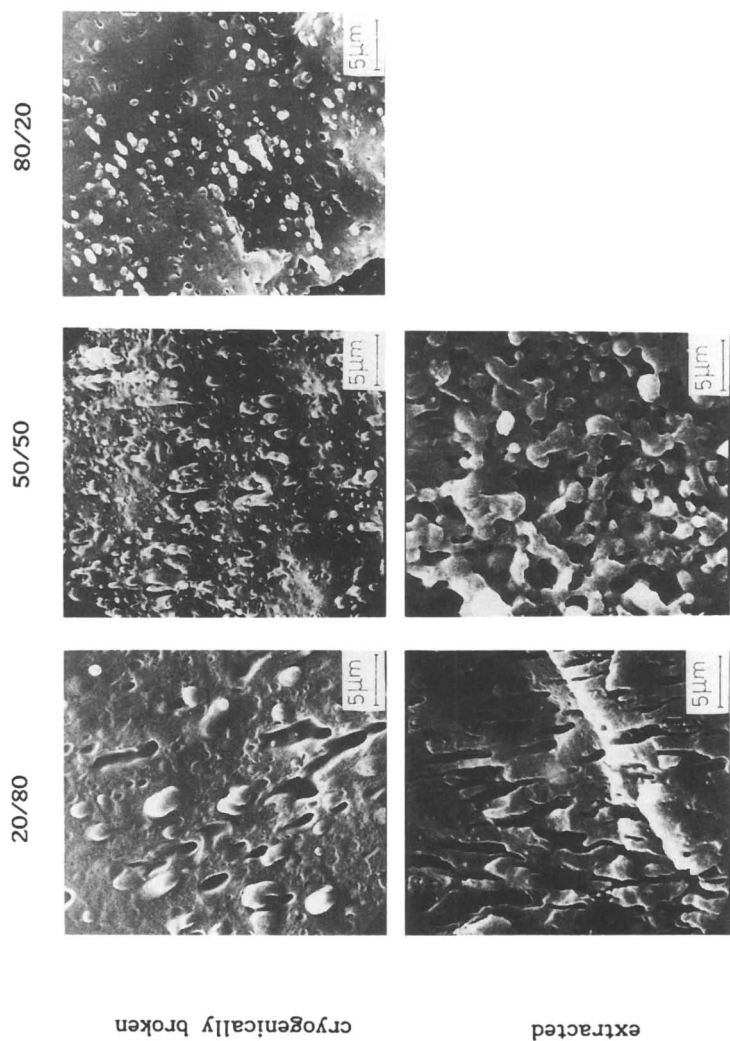


Figure 4. SEM micrographs of the directly quenched SEBS-Armitel blends: 20:80 (left); 50:50 (middle); 80:20 (right). The upper panels are fracture surfaces; the lower panels are after extraction of SEBS. (Reprinted with permission from reference 44. Copyright 1991.)

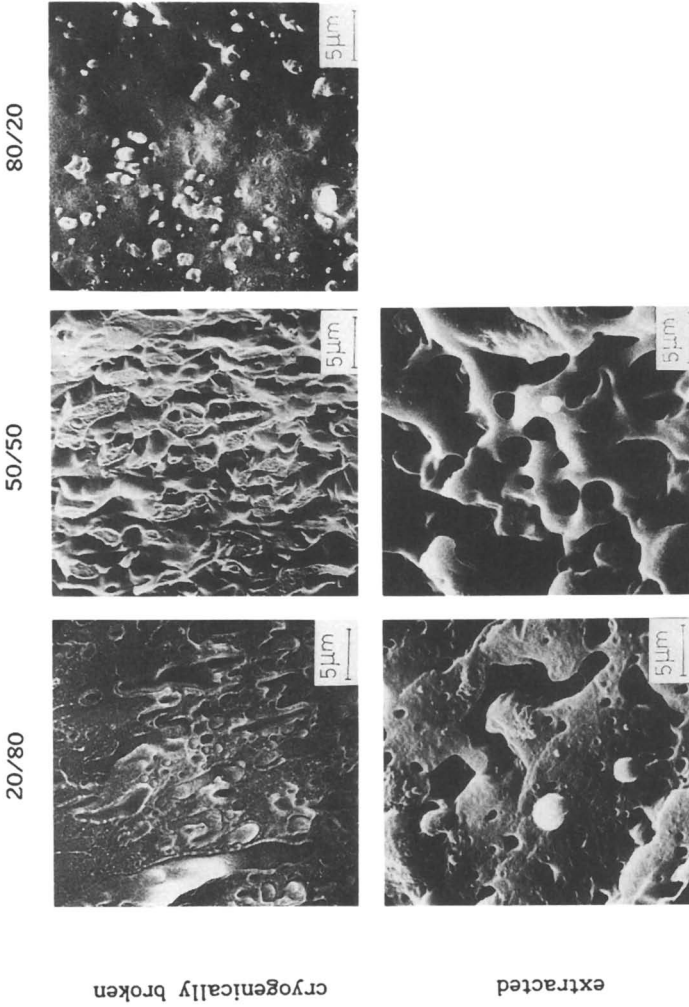


Figure 5. SEM micrographs of the pressed SEBS-Armitel blends: 20:80 (left); 50:50 (middle); 80:20 (right). The upper panels are fracture surfaces; the lower panels are after extraction of SEBS. (Reprinted with permission from reference 44. Copyright 1991 Elsevier Applied Science Publishers Ltd.)

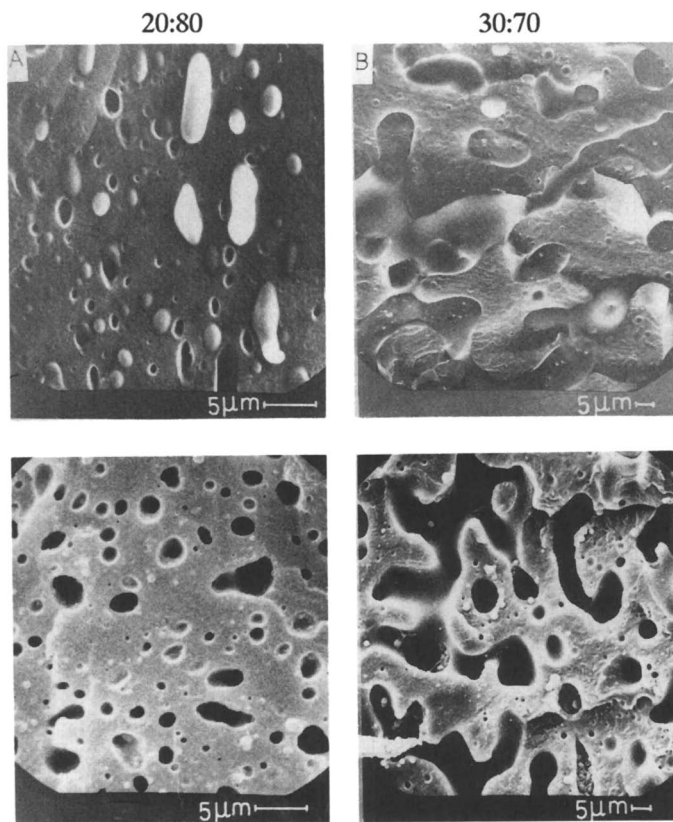


Figure 6. SEM micrographs of the 5-min annealed 20:80 (left) and 30:70 (right) blends. The upper panels are fracture surfaces; the lower panels are after extraction of SEBS.

compositions of 20 vol% and greater. These observations are corroborated by scanning electron microscopy (SEM) and CLSM results. No extraction data are available for the Arnitel phase. However, the SEBS extraction results show that the Arnitel residues retain their shape and coherence for blend compositions of 60-vol% SEBS and lower. Combination of this observation with the SEM and CLSM results indicates partial continuity of the Arnitel in 70-vol% blends and full continuity in 60-vol% blends and lower. We therefore conclude that our blends show co-continuity over the composition range of 10–70 vol%, and show full 100% co-continuity over the composition range of 20–60 vol%.

This result is clearly different from results for various other polymer blends obtained by different investigators as summarized by Lyngaae-Jørgensen and Utracki (30). Note that the composition ranges for co-continuity are asymmetric with respect to the point of phase inversion as calculated with eqs

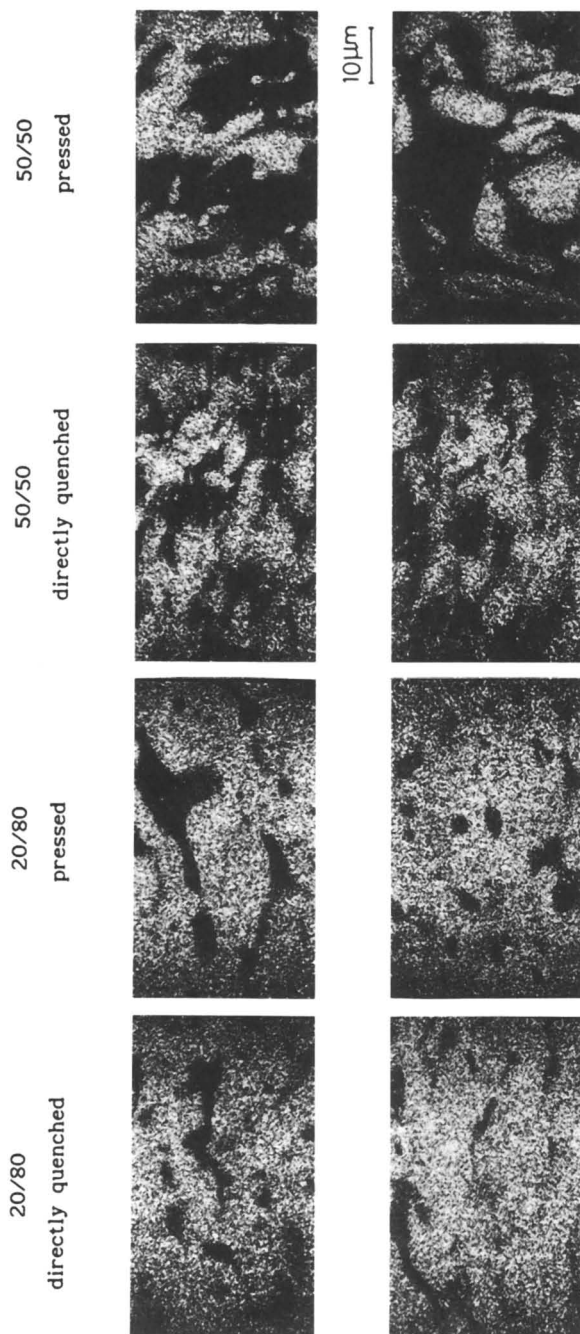


Figure 7. Photographs of morphologies of the 20:80 and 50:50 blends at 10 μm (upper panels) and at 20 μm (lower panels) as obtained with the CLSM. (Reprinted with permission from reference 43. Copyright 1993 Butterworth-Heinemann Ltd.)

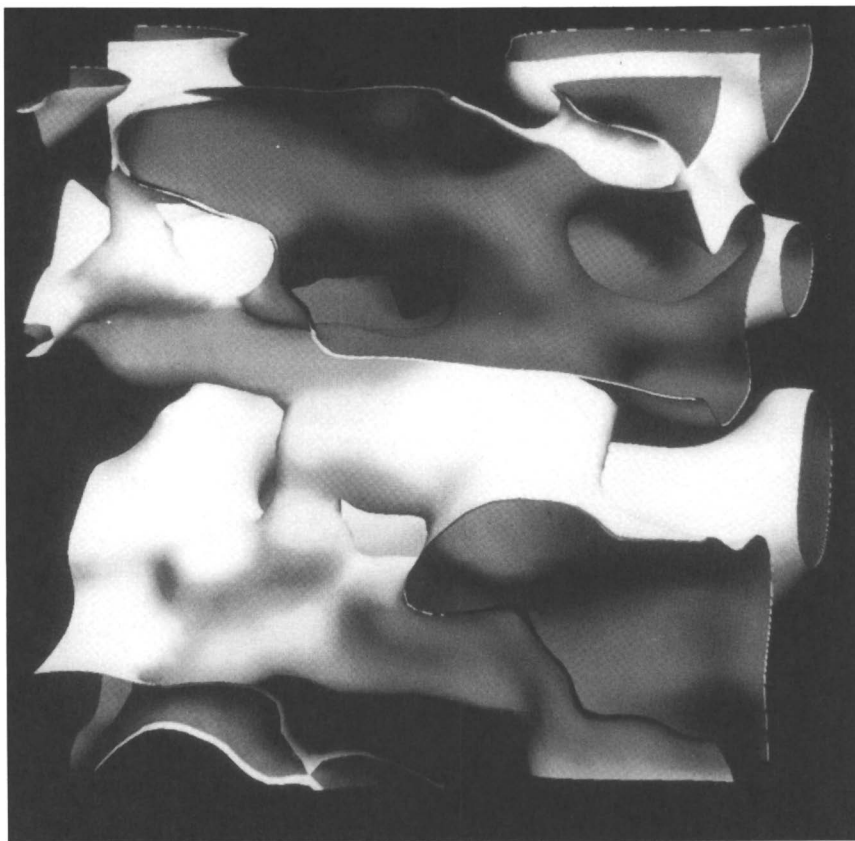


Figure 8. Interface between the poly(ether ester) and the SEBS polymers in the 50:50 pressed blend. (Reprinted with permission from reference 43. Copyright 1993 Butterworth-Heinemann Ltd.)

1–3: 55-vol% SEBS. The very low threshold value (<10 vol%) for onset of co-continuity of the SEBS component indicates percolation of elongated domains as the likely mechanism of formation of these structures.

A second interesting feature of these blends is the wide range of compositions for which full 100% co-continuity exists. This behavior is different from results for PS–PE blends, for example, which are fully co-continuous over a range of approximately 25–50% (30).

To compare our results with the results of other investigators, it is important to take into account details of the preparation methods, in particular whether or not annealing has occurred. Keeping our blends at elevated temperatures (as in the compression molding and annealing treatments) resulted in a narrowing of the composition ranges of partial and full co-con-

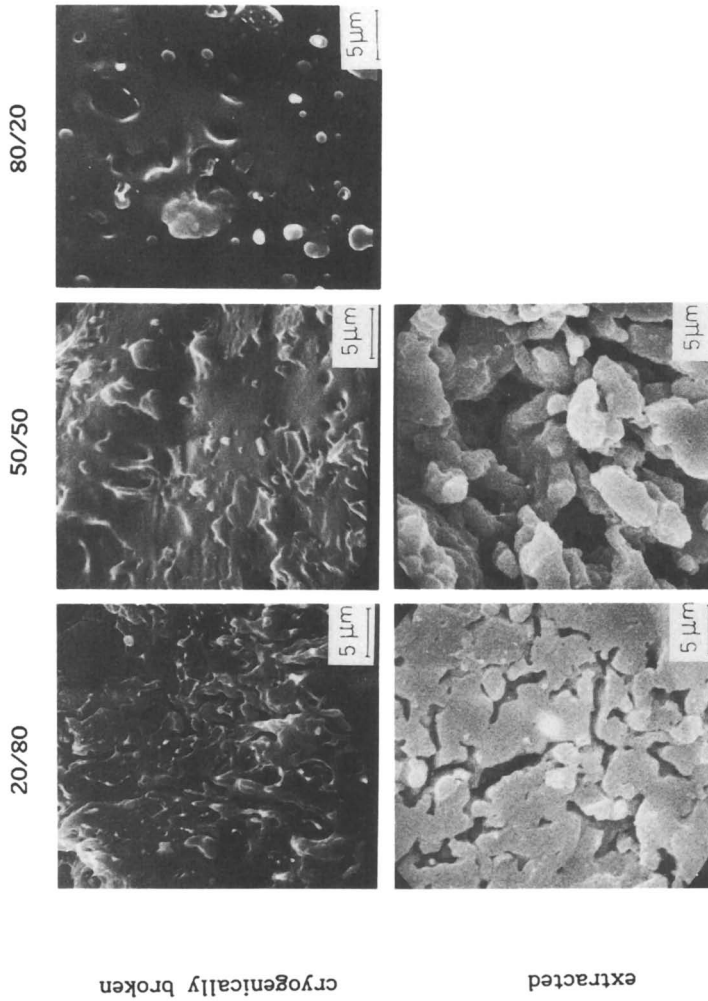


Figure 9. SEM micrographs of some SEBS-Armitel blends after triple extrusion at $\dot{\gamma} = 400 \text{ s}^{-1}$; 20:80 (left); 50:50 (middle); 80:20 (right). The upper panels are fracture surfaces; the lower panels are after extraction of SEBS.

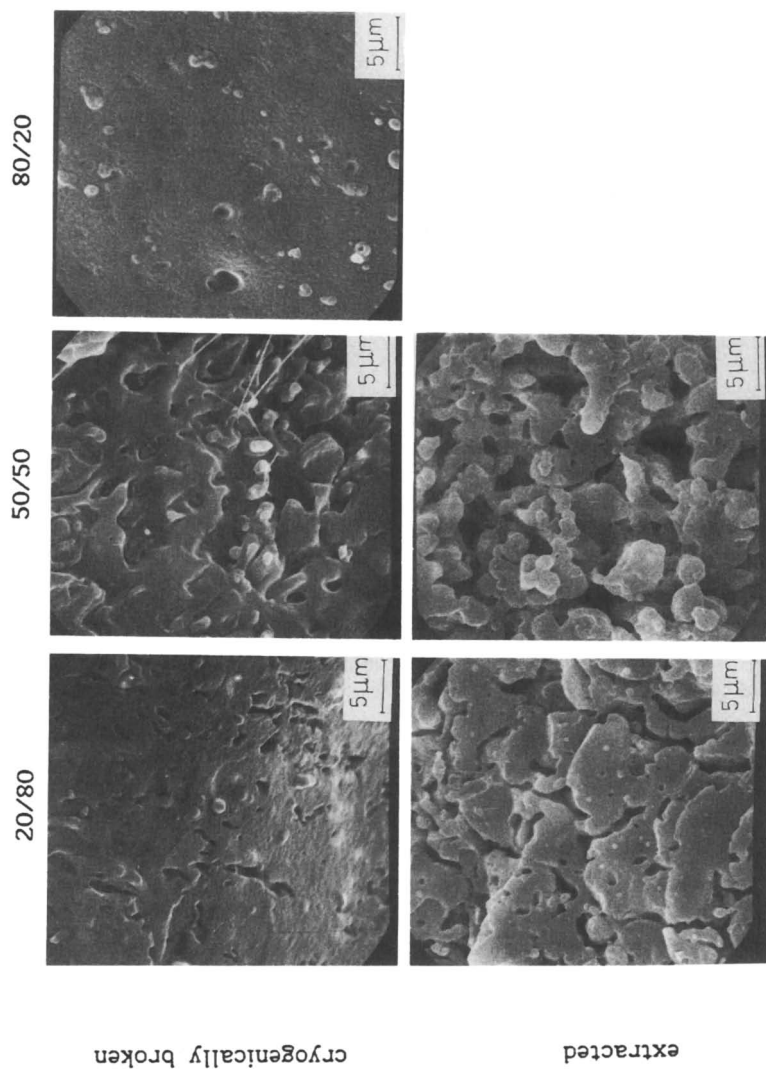


Figure 10. SEM micrographs of some SEBS-Armitel blends after triple extrusion at $\dot{\gamma} = 1000 \text{ s}^{-1}$; 20:80 (left); 50:50 (middle); 80:20 (right). The upper panels are fracture surfaces; the lower panels are after extraction of SEBS.

tinuity by 10 vol%: co-continuity narrowed from 20–70-vol% and full 100% co-continuity narrowed from 30–60-vol% SEBS. Perhaps these last figures should be used for comparison with the results reported for PS–PE blends obtained by Lyngaae-Jørgensen and Utracki (30).

The wide range of co-continuous compositions left after annealing, in particular the lower limit of less than 20 vol% for onset of co-continuity, demonstrates that these blends are stable against morphological changes driven by post-blending relaxation or interfacial energy. This insensitivity to processing conditions, of course, is a desirable property for practical applications. A tentative explanation may be found in the strongly elastic behavior of the SEBS melt (45). This elasticity may also be responsible for the easy formation of continuous SEBS structures.

The rheological measurements show that the blends have lower viscosities than the parent polymers. The blends that contain 30–60-vol% SEBS, which are fully co-continuous, possess the lowest viscosities. This observation is in agreement with the results of Siegfried et al. (4) and Ho et al. (20). A possible explanation may be interfacial slip (28, 36, 46). During flow through the capillary, however, morphological changes occur, as is demonstrated by the morphology of the reextruded 20-vol% blends. These changes in morphology make interpretation of such rheological measurements difficult (37).

Confocal laser scanning microscopy (CLSM) is a valuable new tool for the determination of morphologies of blends. Two advantages are of particular importance:

1. There is no need for sample preparation and, therefore, no risk of creating artifacts as often occurs in electron microscopy.
2. It is possible to make images quickly of a very large number of cross sections of the intact material. In addition, viewing the recorded images gives unambiguous information on the three-dimensional structure.

Computerized reconstruction of the three-dimensional structure not only gives beautiful pictures, but is expected to offer new possibilities in the future for quantitative structure analysis.

References

1. Paul, D. R.; Newman, S. *Polymer Blends*; Academic: New York, 1978; Vols. 1 and 2.
2. Sperling, L. H. *Interpenetrating Polymer Networks and Related Materials*; Plenum: New York, 1981.
3. Sperling, L. H. In *Multicomponent Polymer Materials*; Paul, D. R.; Sperling, L. H., Eds.; Advances in Chemistry 211; American Chemical Society: Washington, DC, 1986.

4. Siegfried, D. L.; Thomas, D. A.; Sperling, L. H. *J. Appl. Polym. Sci.* **1981**, *26*, 177.
5. Siegfried, D. L.; Thomas, D. A.; Sperling, L. H. *Polym. Eng. Sci.* **1981**, *21*, 39.
6. Siegfried, D. L.; Thomas, D. A.; Sperling, L. H. U.S. Patent 4,468,499, 1984.
7. Nishiyama, Y.; Sperling, L. H. *J. Appl. Polym. Sci.* **1986**, *32*, 5903.
8. Gergen, W. P. *Kautsch. Gummi Kunststoffe* **1984**, *37*, 284.
9. Gergen, W. P.; Lutz, R. G.; Davison, S. In *Thermoplastic Elastomers: A Comprehensive Review*; Legge, N. R.; Holden, G.; Davison, S., Eds.; Carl Hanser Publishers: Munich, Germany, 1987; pp 507-540.
10. Miles, I. S.; Zurek, A. *Polym. Eng. Sci.* **1988**, *28*, 796.
11. Fisher, W. K. U.S. Patent 3,806,558, 1974.
12. Kresge, E. N. In *Polymer Blends*; Paul, D. R.; Newman, S., Eds.; Academic: New York, 1978; Vol. 2, Chapter 20.
13. Kresge, E. N. *J. Appl. Polym. Sci., Appl. Polym. Symp.* **1984**, *39*, 37.
14. Kresge, E. N.; Lohse, D. J.; Datta, S. *Macromol. Chem., Makromol. Symp.* **1992**, *53*, 173.
15. Davison, S.; Gergen, W. P. U.S. Patent 4,041,103, 1977.
16. Gergen, W. P.; Davison, S. U.S. Patent 4,101,605, 1978.
17. Xie, H. Q.; Ma, B. Y. *Contemp. Top. Polym. Sci.* **1989**, *6*, 601.
18. Xie, H. Q.; Xu, J.; Zhou, S. *Polymer* **1991**, *32*, 95.
19. Hsu, J. S.; Su, F. H.; Chen, S. A. *Makromol. Chem.* **1992**, *193*, 833.
20. Ho, R. M.; Wu, C. H.; Su, A. C. *Polym. Eng. Sci.* **1990**, *30*, 511.
21. David, C.; Trojan, M.; Jacobs, R.; Piens, M. *Polymer* **1991**, *32*, 510.
22. Avgeropoulos, G. N.; Weissert, F. C.; Biddison, P. H.; Böhm, G. G. A. *Rubber Chem. Technol.* **1976**, *49*, 93.
23. Paul, D. R.; Barlow, J. W. *J. Macromol. Sci., Rev. Macromol. Chem.* **1980**, *C18*, 109.
24. Paul, D. R.; Barlow, J. W. In *Multicomponent Polymer Materials*; Paul, D. R.; Sperling, L. H., Eds.; Advances in Chemistry 211; American Chemical Society: Washington, DC, 1986; p 3.
25. Jordhamo, G. M.; Manson, J. A.; Sperling, L. H. *Polym. Eng. Sci.* **1986**, *26*, 517.
26. Metelkin, V. I.; Blekht, V. S. *Colloid J. USSR (Engl. Transl.)* **1984**, *46*, 425; *Kolloid, Zh.* **1984**, *46*, 476.
27. Utracki, L. A. *Polymer Alloys and Blends*; Hanser Publishers: New York; 1989.
28. Utracki, L. A. *J. Rheol.* **1991**, *35*, 1615.
29. Nelson, C. J.; Avgeropoulos, G. N.; Weissert, F. C.; Böhm, G. G. A. *Angew. Makromol. Chem.* **1977**, *60/61*, 49.
30. Lyngaae-Jørgensen, J.; Utracki, L. A. *Macromol. Chem., Macromol. Symp.* **1991**, *48/49*, 189.
31. Widmaier, J. M.; Sperling, L. H. *Macromolecules* **1982**, *15*, 625.
32. Nielsen, L. E. *Predicting the Properties of Mixtures*; Marcel Dekker: New York, 1978.
33. Quintens, D.; Groeninckx, G.; Guest, M.; Aerts, L. *Polym. Eng. Sci.* **1990**, *30*, 1474.
34. Quintens, D.; Groeninckx, G.; Guest, M.; Aerts, L. *Polym. Eng. Sci.* **1990**, *30*, 1484.
35. Han, C. D. *Multiphase Flow in Polymer Processing*; Academic: New York, 1981.
36. Lyngaae-Jørgensen, J.; Dahl Thomsen, L.; Rasmussen, K.; Søndergaard, K.; Anderson, F. E. *Int. Polym. Proc.* **1988**, *2*, 123.
37. Utracki, L. A.; Sammut, P. *Polym. Network Blends* **1992**, *2*, 23.
38. Brochure, *Kraton Thermoplastic Rubber: Typical Properties*; Shell Chemical Company, 1990.
39. Brochure, *Arnitel Polymers*; Akzo, 1984.

40. Wilson, T.; Sheppard, C. *Theory and Practice of Scanning Optical Microscopy*; Academic: London, 1980.
41. Draaijer, A.; Houpt, P. M. *Scanning* **1988**, *10*, 139.
42. Houpt, P. M., Draaijer, A. *Inst. Phys. Conf. Ser.* **1989**, *98*, 639.
43. Verhoogt, H.; van Dam, J.; Posthuma de Boer, A.; Draaijer, A.; Houpt, P. M. *Polymer*, **1993**, *34*, 1325.
44. Verhoogt, H.; van Dam, J.; Posthuma de Boer, A. In *Integration in Fundamental Polymer Science and Technology*; Lemstra, P. J.; Kleintjens, L. A., Eds.; Elsevier Science Publishers: London, 1991; Vol. 5, p 357.
45. Verhoogt, H. Ph.D. Thesis, Delft University of Technology, Delft, Netherlands, 1992.
46. Lin, C. C. *Polym. J.* 1979, *11*, 185.

RECEIVED for review September 10, 1991. ACCEPTED revised manuscript September 16, 1992.

Polystyrene–Cross-Linked Polystyrene Blends: Latex Semi-interpenetrating Polymer Networks

Naum Nemirovski and Moshe Narkis

Department of Chemical Engineering, Technion–Israel Institute of Technology, Haifa 32000, Israel

Latex polystyrene–cross-linked polystyrene (PS–XPS) systems were generated via a sequential emulsion polymerization method. Three different blend structures were prepared by (1) physical blending of PS and XPS latices [the XPS is lightly cross-linked with divinylbenzene (up to 1% by weight)], (2) styrene polymerization in the presence of XPS seed latex, and (3) styrene and divinylbenzene copolymerization in the presence of PS seed latex. Different rheological and mechanical behaviors were observed. These behaviors are affected by both XPS content and cross-link density. This kind of behavior stems from the unique morphology of each system.

Types of Polymer Systems

Multiphase Polymer Systems. Considerable research and development efforts on new materials with improved properties and performance have focused on multiphase polymer systems. The multiphase structure, which is determined by the synthesis and frequently affected by processing, is critical to tailor-making polymer systems with desired mechanical and rheological properties. Synergistic effects that are sometimes found when different polymers are combined may lead to multiphase structures (1, 2). These multiphase structures encompass a wide spectrum of structures that include

immiscible and partially miscible blends, block and graft copolymers, and interpenetrating polymer networks (IPNs). The ultimate properties of elastomeric and glassy multiphase polymers depend on the size, number, and composition of the dispersed domains. Morphology control in multiphase systems, which results in property tailoring by means of selected components, composition, molecular weight, and cross-linking level, thus becomes advantageous.

Considerable attention has been paid in recent years to improvement of the impact resistance of polymeric materials by increasing fracture toughness. However, as a consequence of increased fracture toughness, the modulus and strength are significantly reduced. The primary requisite for improvement of fracture toughness is phase separation. Thus, the following three major approaches currently are employed to toughen polymers:

1. Rubber modification; that is, the inclusion of a dispersed elastomeric phase in a brittle matrix. Superior toughness is derived from energy dissipation mechanisms (namely crazing and plastic shear yielding in the matrix). Differences of 3–4 orders of magnitude in elastic moduli of glassy polymers and rubber are responsible for this kind of behavior. The changes in properties of a toughened polymer depend on various parameters, such as processing conditions, particle size and volume fraction, and cross-link density of the dispersed rubber phase, glass-transition temperature, T_g , of the rubber (actually the end-use temperature minus the glass-transition temperature, $T_{\text{work}} - T_g$), compatibility of the phases, and interfacial adhesion.
2. Addition of a rigid particulate phase such as inclusions of inorganic fillers can significantly reduce the cost. The coefficient of thermal expansion of the system decreases. Whereas the stiffness increases, the strength decreases with increasing filler content. The fracture energy may show a maximum. However, improvements are relatively modest compared with improvements obtained by rubber modification. The main toughening mechanism is crack pinning.
3. Thermoplastic modification via either polymer blending or addition of a thermoplastic to a thermoset (e.g., epoxy). Ductile drawing-tearing of the thermoplastic phase may be operative.

Latex IPNs. Because phase separation may lead to complex morphologies with useful properties, the design of novel phase-separated systems is of major interest. One method in a two-phase system is to include at least one cross-linked phase, which thus reduces the entropy of mixing. This

mechanism has the effect of reducing component miscibility, whereas structural constraints due to cross-linking may limit the phase separation process.

IPNs, which are characterized by bicontinuous structure, show interpenetrated physical entanglements that may prevent complete phase separation (3). Thus, IPN domain structures that result from incomplete phase separation are usually much finer than domain structures of the parent polymer blends. However, a practical limitation arises from the domain structure thermoset character. Bulk-polymerized IPNs cannot be processed by standard thermoplastic methods and machinery; therefore, IPN-made articles must be shaped, at the latest, by the end of the synthesis.

Latex interpenetrating polymer networks (LIPNs) combine the morphological characteristics of IPNs with the characteristics of polymer latices through the synthesis of IPN structures framed to latex particles (4). Under molding conditions, particle intermingling takes place at the relatively intact surface of the latex particles. The extent of intermingling is process-dependent and restricted mostly to the interface. The individual latex particles retain their identity, even when lightly cross-linked. LIPN particle morphology is the result of swelling, polymerization, cross-linking, grafting, and phase separation that take place simultaneously within submicrometer latex polymerization sites. Among the numerous factors that affect morphology are reaction conditions (method and rate of monomer addition, temperature, initiator type, and, probably, reactor geometry), composition (monomer ratio, cross-link density), relative hydrophilicity of the polymerizing monomer and the seed, compatibility of the polymers, miscibility of polymer I in monomer II (I and II represent the first and second phases in a two-phase IPN, respectively), degree of grafting, and T_g of the polymers (5, 6).

Latex-interpenetrated systems can be synthesized via a sequential emulsion polymerization method, where polymerization or cross-linking of monomer I takes place and subsequently is used as a seed latex for the emulsion polymerization or cross-linking of monomer II.

Two-stage polymerization is effectively used in industry to produce multiphase polymer systems. This technique is also utilized for synthesis of latex with narrow particle size distribution, as calibration standards for particle size determination, and for biomedical applications (e.g., cytometry) where less than 1% standard deviation is required (7).

The polymerization procedure may be varied to control particle size, number, and morphology. The use of batch, semibatch, continuous, and seeded reactions is widespread.

So-called two-stage latex (TSL) polymerization may result in various morphologies (8), which include:

1. A core of more hydrophobic polymer I is surrounded by a shell of polymer II.

2. An inverted core-shell structure: The core is made of polymer II and the shell is made of more hydrophilic, low molecular weight polymer I. Phase separation is governed by the miscibility of the polymers and is usually accompanied by swelling.
3. A domain structure, where the high molecular weight and more hydrophilic polymer I contains domains of polymer II. Domain size is a function of hydrophilicity and phase mobility.
4. Cross-linking of any of the phase leads to altered morphologies. For instance, a more hydrophilic cross-linked polymer I will give an IPN domain structure with restricted phase separation.

Semi-IPNs. Semi-IPNs consist of linear chains threaded through a cross-linked network. The polymerization process is identical to that of IPNs, although one of the monomers is deprived of the cross-linking agent, which yields an uncross-linked phase (9). The extent of phase segregation lies somewhere between the phase segregations of blends and IPNs due to entropic effects (the linear chains have more conformational freedom compared to the network). The uncross-linked phase is susceptible to disentanglement upon annealing, solvent, or stress action. This time-dependent effect is consequential to the resultant morphology. Synergism also exists in semi-IPN properties and is dependent on the extent of mixing (10).

High-impact semi-IPNs, like other high-impact materials, owe their superior properties to the fraction of rubbery component, domain size, cross-linking, grafting, and processing parameters (11). Acrylonitrile-butadiene-styrene terpolymer (ABS) that is synthesized by emulsion polymerization of styrene-acrylonitrile (SAN) on a cross-linked polybutadiene (PB) latex yields a latex semi-IPN morphology with grafted SAN domains and wartlike protrusions from the surface contained in the cross-linked PB rubber at low SAN conversions. At higher SAN content, phase-separated SAN domains on the surface join into a core-shell domain morphology. Factors that affect morphology are the size of rubber domains and cross-link density. Upon molding, the coalescence of the shells forms a SAN continuous matrix and yields a high-impact material. Impact resistance is imparted by the formerly cross-linked particle cores through a combined mechanism of shear yielding and craze formation. Because the semi-IPNs do not have an IPN interlocking network structure that could preserve the particle morphology under the action of heat, stress, and solvents, this structure is influenced by processing conditions.

Latex Blends. The processing properties of raw elastomers are markedly improved by operations that increase the amount of gel or cross-linked material. The observed improvements in properties, such as reduced

swelling on emergence from an extruder die, smoother surface finish, and better shape retention, are in many ways similar to improvements produced by the addition of carbon black or other fillers to the rubber (12). Improvements are primarily in elastic responses. Higher extrusion rates are also amenable.

Commercially, the acceptance of gelled rubbers for superior processing has rapidly increased in recent decades. Most reports indicate that improvements in processing are obtained (at least partially) at the expense of certain physical properties of the finished product. However, a wide variety of vinyl fillers (i.e., cross-linked particles of colloidal size) have proven highly effective as reinforcement in an equally wide variety of rubbers and plastics (13). This reinforcement occurs only with latex blending where the gel is well dispersed and the degree of dispersion is typical of latices. These conditions cannot be achieved by mill blending.

The viscosity of poly(ethyl acrylate) that contains up to 40% gel particles has been measured in a capillary rheometer (14). The addition of gel always increases the shear stress at a given shear rate. This effect was greatest at the lowest shear rates (10^{-3} – 10^{-1} s $^{-1}$).

A butadiene–acrylonitrile latex copolymer that contains 33% acrylonitrile also has been studied (15). The gel content varied from 0 to 100% with cross-link density and particle size held constant. The cross-linked particles were prepared by adding divinylbenzene (DVB) at about one part per hundred based on the total monomer. The viscosities of these materials at shear rates in the range 3–3000 s $^{-1}$ were not affected by the presence of up to 50% gel particles. A supermolecular flow unit was postulated to explain this behavior, after the concept originally suggested by Mooney and Wolstenholme (16) and discussed by Swanson et al. (17). This concept consists of a slip-on–roll-on particle flow mechanism, which represents the supermolecular flow units, and is characterized by a relatively low melt viscosity and reduced extrudate swell. This mechanism is possible because the particle structure that originates during emulsion polymerization is somewhat preserved in molded samples. Such a mechanism has been identified in poly(vinyl chloride) (PVC) polymers that contain cross-linked rubber particles or rigid particles and in IPNs (18). For instance, the identity of latex PVC particles is preserved under 180 °C, but at higher temperatures the apparent viscosity increases due to particle melting. Hence rapid interparticle diffusion occurs across the surface of the particles, the particle flow mechanism thus diminishes and gradually vanishes, and viscous flow takes over until completion.

An amorphous polymer that contains submicrometer cross-linked particles of the same polymer is unique in that the system contains structural units (the cross-linked particles) that are orders of magnitude larger than the size of the coiled polymer molecule that is characteristic of the continuous phase. The particle itself may deform in accordance with its viscoelastic properties, and the specific cohesion forces between gel particles or between gel and

uncross-linked molecules resemble the cohesion forces between the uncross-linked molecules. Therefore, there is no need to ponder specific surface particle–molecule interactions.

A polystyrene–cross-linked polystyrene (PS–XPS) system was studied at low shear rates (19). The matrix that contained 50% polystyrene and 50% poly(divinyl benzene) showed a Newtonian plateau at short relaxation times. This Newtonian plateau reflects the entangled continuous phase behavior. Furthermore, a secondary plateau in the relaxation spectrum appeared at higher relaxation times, which indicates an interparticle interaction. The existence of a particle-based three-dimensional network was suggested. Reportedly this system does not meet the Cox–Merz equation, which is known to hold for polymer melts and polymer solutions (20).

Latex PS–XPS Systems. Latex PS–XPS systems were prepared via a sequential emulsion polymerization method. The idea was to physically blend PS and XPS latices or to proceed by a two-stage polymerization, where the seed is either PS or XPS. Mixture of the two phases was thus pursued by different routes that resulted in three different structures:

1. The PS–b–XPS system, which consisted of a physical *blend* of PS and XPS latices, where the XPS latices were lightly cross-linked with divinylbenzene (DVB < 1%).
2. The (XPS–s)–PS system, which was obtained by styrene polymerization in the presence of XPS *seed* latex.
3. The (PS–s)–XPS system, in which styrene and DVB were copolymerized in the presence of PS *seed* latex.

These procedures are depicted in Figure 1. Different microstructure was expected to result from each of the procedures. Different rheological and mechanical behaviors were observed, along with a rather interesting property dependence on XPS content and cross-link density. This kind of behavior stems from the unique morphology of each system. Various techniques are instrumental to the understanding of structure and structure–property relations.

The main goals of this research on structured PS–XPS systems are (1) latex PS–XPS semi-IPN characterization, including an insight into particle level structure, and a study of particle–matrix interactions; (2) determination of polymerization sites in the two-stage lattices; (3) study of the flow behavior in the molten state; and (4) study of the deformation mechanisms of PS–XPS materials in the solid state.

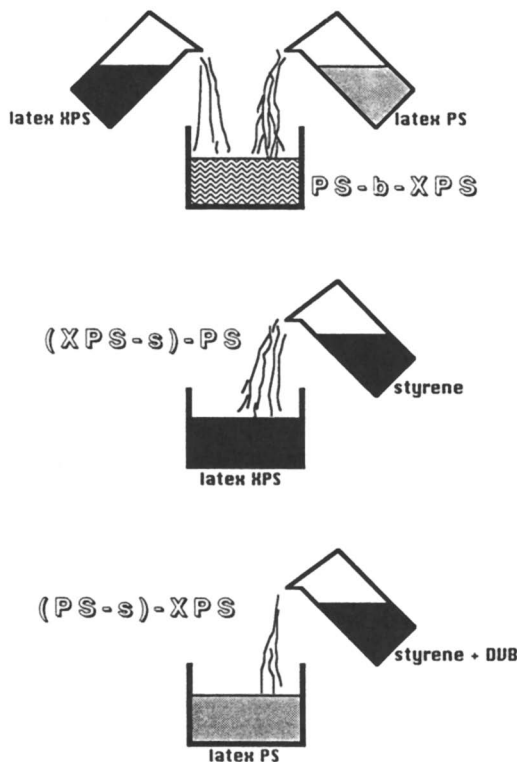


Figure 1. Latex PS-XPS semi-IPN. Mixture of the two phases is pursued by three different routes.

Experimental Details

Synthesis and Characterization. PS and XPS latices were synthesized by conventional emulsion polymerization techniques. A typical formulation is shown in Table I. The reaction was carried out in a stirred resin reaction flask at 80 °C under a nitrogen blanket. Monomers, detergent, and initiator were added dropwise to the semibatch reactor from different vessels. Nearly complete conversion was determined from solid content evaluation (about 35%) at the end of the reaction. Unless indicated, the cross-linker concentration was fixed at 0.25% technical DVB based on the cross-linked phase monomer.

Physical blending of PS and XPS latices at the desired proportions, followed by co-coagulation, filtering, washing with boiling methanol (for low fractions removal), drying, and compression molding (5 min at 100 °C and 10 GPa followed by 5 min at 180 °C and 2 GPa) lead to the formation of PS-b-XPS systems.

The systems (XPS-s)-PS and (PS-s)-XPS were obtained by the previously mentioned seeding procedures. The ratio of soap to total monomers was kept the same for all three systems. The thoroughly washed and dried materials resulted in compression-molded samples with good transparency.

Table I. A Typical Formulation for Latex XPS

<i>Phase</i>	<i>Component</i>	<i>Amount (g)</i>
Reactor	Water	445
	Sodium dodecyl sulfate (1%)	33
	Triton X-100 ^a (18%)	33
	Sodium pyrophosphate (buffer)	0.4
Aqueous	Water	196
	Sodium dodecyl sulfate (1%)	126
	Triton X-100 ^a (18%)	126
	Potassium persulfate (3%)	33
Organic	Styrene	525
	Divinylbenzene	1.32

^a Rohm and Haas.

The molecular weight of PS was determined by solution viscometry, with an Ubbelohde-type viscometer, at 25 °C (21). Commercial polystyrene was checked for control. The values of viscosity average molecular weight, M_v (grams per mole), obtained for latex-type PS and commercial GPPS (a general purpose PS from Israel Petrochemical Enterprises Ltd.) were, respectively, 440,000 and 170,000.

Polymer samples from each composition were extracted in boiling toluene. The gel content was defined by the ratio of undissolved polymer weight to the original weight of the sample. For the XPS sample, gel content amounted to 84%.

Particle size was determined by transmission electron microscopy (TEM) with a transmission electron microscope (Jeol 120CX) operated at 100 kV. A single diluted latex drop was deposited onto a 100-mesh grid previously covered with a 20-nm carbon film. Latex PS and XPS particles showed rather narrow monosized distributions with 0.16- and 0.19- μm average particle diameters, respectively. (XPS-s)-PS consisted of bimodal populations that are indicative of the formation of a second population during the second polymerization stage. (PS-s)-XPS particles were monosized. TEM micrographs that show the latex particles appear in Figure 2.

Solid-State Testing. The mechanical performance was investigated with a universal testing instrument (Instron). Specimens of constant cross section (10×2 mm) were cut from compression-molded plates and tested at both tensile and three-point bend modes.

Specimens were frozen in liquid nitrogen and halved, and the exposed fracture surface was sputter-coated with gold. Scanning electron microscopy (SEM) was then performed with a scanning electron microscope (Jeol 840).

Melt Rheology. Rheological properties of the PS-XPS systems were measured using a capillary rheometer (Instron) with a 50.8×1.27 -mm die at three temperatures (190, 215, and 240 °C). Attainable shear rates lie between 0.3 and 3000 s^{-1} . Extrudate swell was measured with a digital caliper or with a swell tester, and swelling ratios were calculated.

Steady shear viscosity at low shear rates (4×10^{-3} – 14 s^{-1}) was measured at 200 °C with a rheogoniometer (Weissenberg) in a cone and plate geometry.

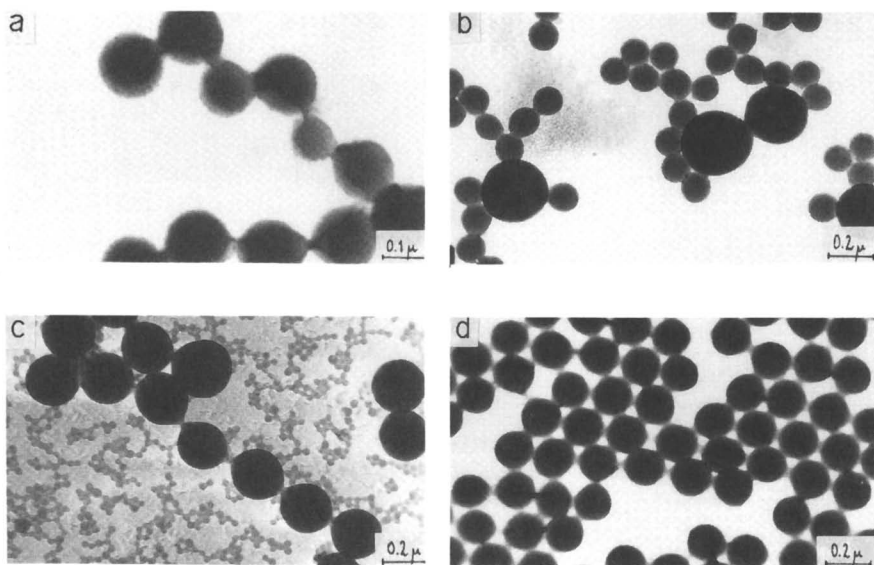


Figure 2. TEM micrographs that show particle size of latex PS (a), (10% XPS-s)-PS (b), (20% XPS-s)-PS (c), and (PS-s)-30% XPS (d).

Results and Discussion

Mechanical Properties. During compression molding of the first PS-b-XPS system, up to about 40% XPS (by weight), PS merges into a continuous thermoplastic matrix in which inclusions of ca. 0.2- μ m XPS particles are dispersed. This degree of dispersion is typical of LIPNs.

At higher XPS content, a continuous PS phase is difficult to obtain. Although PS particles coalesce, XPS particles, which are primary flow units, preserve their identity, although they interact with the continuous matrix and among themselves. In Figure 3, the flexural strength of PS-b-XPS reaches a maximum of 82 MPa at 15% XPS—about 10% strength improvement compared to PS. Note that the standard deviation for these data is 5%. At 100% XPS the strength is reduced to 45 MPa. Upon increasing the XPS content, the continuity of the thermoplastic matrix is gradually lost, and beyond a certain XPS concentration, XPS becomes the “continuous” phase because XPS particles (contrary to ordinary particulate fillers) are able to strongly interact among themselves. Hence, 100% XPS is, in principle, made of only cross-linked particles pressed together and held by particle-particle interaction characterized by interparticle chain penetration formed at the high molding temperature.

Comparison of the strength of the PS-b-XPS and (XPS-s)-PS systems in flexural and tensile mode shows a somewhat different mechanical behavior.

In Figures 3 and 4, the physical blend shows maxima in both modes at about 20% XPS. In comparison, the (XPS-s)-PS system has poorer performance than the blend. Styrene diffuses into the seed XPS particles during second-stage polymerization of (XPS-s)-PS and polymerizes there, which leads to occluded PS in the XPS network. This PS does not contribute practically to the formation of the continuous PS matrix; on the contrary, it remains confined within the cross-linked particles and its deformation is thus restrained. The “effective” XPS content, which takes into account the occluded PS, is higher than the nominal content and, thus, increases the relative contribution of the particle–particle interaction, which causes a decrease in strength. Note that this (XPS-s)-PS system as well as the PS-b-XPS system, consists of cross-linked particles embedded in a thermoplastic matrix. However, both particle structure and particle–matrix interaction are different.

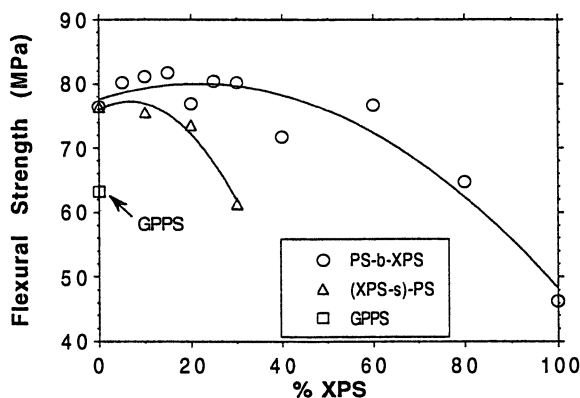


Figure 3. Flexural strength at break of PS-XPS systems.

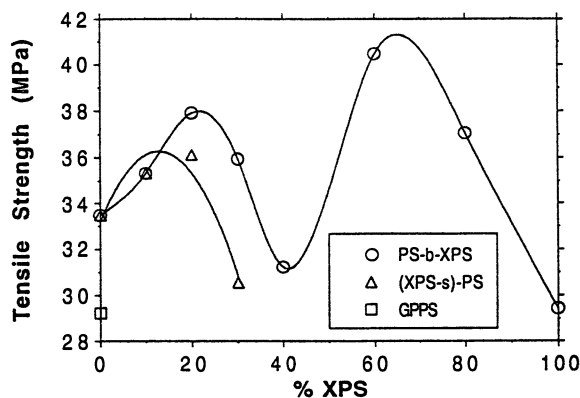


Figure 4. Tensile strength at break of PS-XPS systems.

In Figure 5 the flexural modulus of PS-b-XPS shows a first maximum of 3 GPa at 30% XPS (20% higher modulus than that for PS) and a second higher maximum of about 3.5 GPa, in the range of 60–80% XPS. The “phase-inversion” XPS range (between 40–60% XPS) remains of unknown character. The term “phase inversion” should be taken with precaution because the PS phase probably remains continuous throughout the whole XPS content range, which thus leads to a bicontinuous structure beyond 60% XPS. The measured moduli of molded PS and 100% XPS are 2.5 and 2.9 GPa, respectively. The measured modulus of molded XPS is assumed to be lower than the “true” value given by the modulus of a single XPS bead, apparently due to defects present in the molded 100% XPS structure. Although PS-b-XPS moduli data showed an average standard deviation of only 4%, moduli data for the (XPS-s)-PS system showed a larger scattering (9%). This difference is important because otherwise the moduli results for (XPS-s)-PS in both tensile and flexural modes (Figures 5 and 6) would be uninterpretable. In the present case, the flexural modulus of (XPS-s)-PS seems to be rather independent of XPS content within the content range studied. Note that the flexural properties of PS-b-XPS behave, in general, similarly to the tensile properties (strengths in Figures 3 and 5 and moduli in Figures 4 and 6, respectively).

The tensile moduli are plotted in Figure 6. The tensile modulus of the blend is higher than the modulus of (XPS-s)-PS in most of the XPS content range studied. The tensile modulus of (XPS-s)-PS increases by 12% at 5–10% XPS and then decreases; however, beyond about 40% XPS, there is another steady moderate increase in modulus with XPS content. As before, the irregular modulus data of (XPS-s)-PS are apparently a consequence of the somewhat large limit of error, so that the tensile modulus for this system is likely to be constant between 0 and 30% XPS.

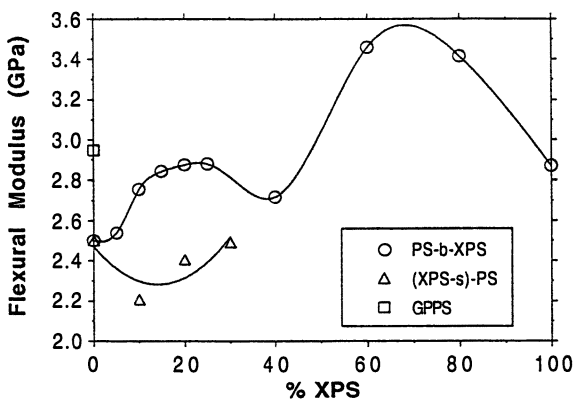


Figure 5. Flexural modulus of PS-XPS systems.

The effect of cross-link density is evident in Figure 7. Up to 0.50% DVB, the flexural strength is rather constant for the system (XPS-s)-PS with constant XPS (20%). Higher DVB concentrations are detrimental to this property. Furthermore, the flexural modulus is raised by 20% for DVB content of 0.50% and greater. This effect is similar to the effect of increasing XPS content in that the stiffness of the system is enhanced, while strength is decreased due to the weaker particle-matrix penetration depth. Tensile results are essentially identical.

The elongation at break of the physical blend showed a bimodal behavior, with two maxima at 20–30% and 60–70% XPS. In Figure 8, elongation

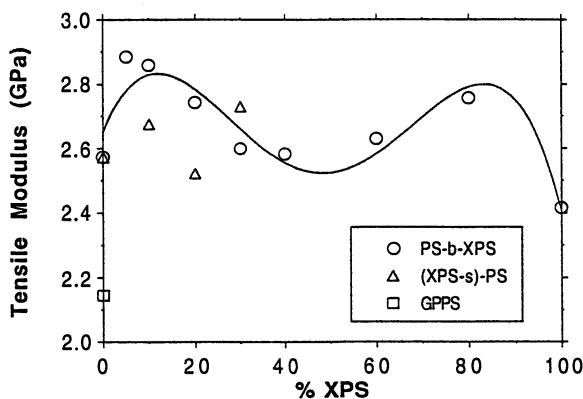


Figure 6. Tensile modulus of PS-XPS systems.

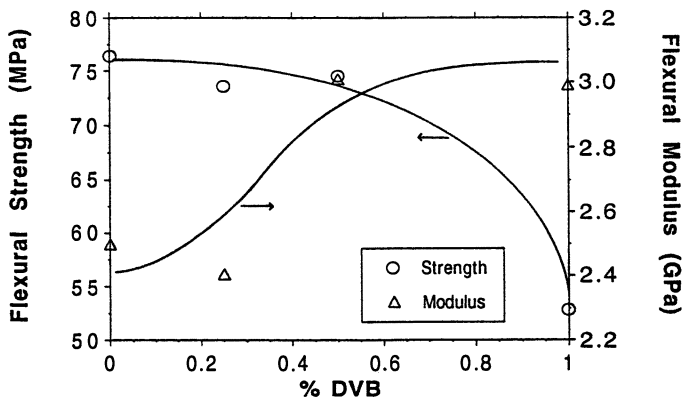


Figure 7. The effect of cross-linking density on the flexural properties of (XPS-s)-PS: Flexural strength at break (\circ); flexural modulus (Δ). DVB concentration was varied in the range 0–1% DVB while XPS content was kept constant at 20% XPS. Tensile results are essentially identical.

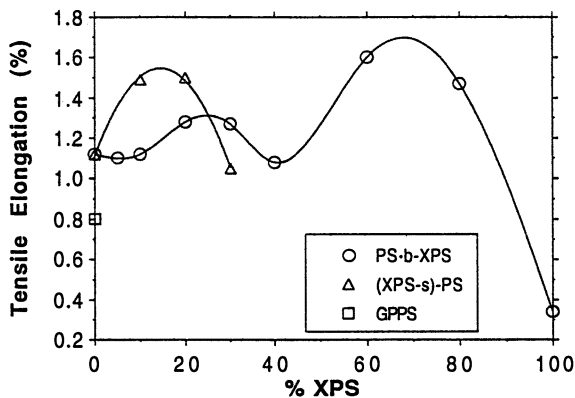


Figure 8. Elongation at break of PS-XPS systems in tension.

at 60% XPS is 1.6%, which is an increase of roughly 50% over the elongation of PS. (XPS-s)-PS develops maximum elongation at about 20% XPS, where almost 40% improvement compared to PS is demonstrated. Careful observation of broken specimens led to the conclusion that the specimens were crazed throughout their volume. The PS-b-XPS physical blends differ from PS in that they contain XPS submicrometer particles that are stiffer than the matrix. Up to 30–40% XPS content, the particles essentially behave as individual embedded inclusions within the thermoplastic matrix and act as fillers due to their reduced deformability. These particles retain their identity upon molding, yet physical entanglements exist between the particles and the matrix that have to be torn apart or loosened by an advancing crack. Crack-tip propagation is affected by the presence of XPS particles and is either disturbed or else deviated from its course (the crack path if the particles were not present). Due to the superior strength and stiffness of the particles, it is less probable that the crack-tip propagation runs through the particles. SEM micrographs of freeze-fractured specimens (Figure 9) show spherical beads 0.2 μm and smaller in size (the XPS particles exposed to the crack surface), as well as spherical concavities of the same sizes. The concavities are attributed to the crack path that is compelled to “swerve” (i.e., surround the particles) so that craters or partially exposed particles are left behind the crack tip. Hence, the fracture surfaces demonstrate that the interactive force between particle and matrix is much weaker than the interactive force of the particle itself. Thus, two mechanisms are postulated for the system PS-b-XPS: a fillerlike strength-reinforcing mechanism and a mechanism of craze formation. The strength reinforcement is operative at 20–30% XPS, whereas the craze formation is most effective around 60%. At XPS content of 60–80%, the contribution of the interparticle interaction is much higher, and a concomitant change in morphology occurs (i.e., the formation of a “continu-

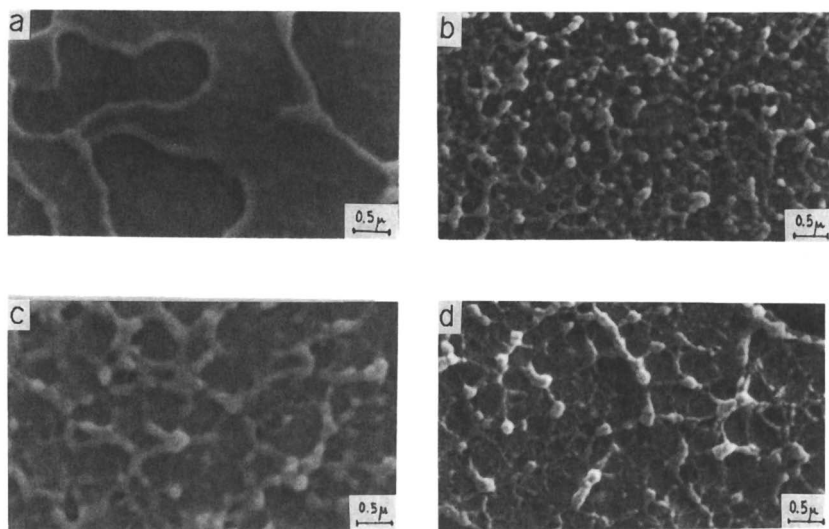


Figure 9. SEM micrographs of freeze-fractured specimens: PS (a); XPS (b); PS-*b*-40% XPS (c); (20% XPS-*s*)-PS (d).

ous" XPS phase). The interparticle chain penetration depth increases during compression molding, and the XPS particles remain of limited deformability as demonstrated by SEM micrographs. These high-XPS-content samples showed the best tensile elongation of all the physical blends due to crazing of the PS matrix. However, the role of the particles has still not been explained; that is, whether the particles induce crazing via stress concentration effects or perhaps due to the presence of defects caused by the introduction of high XPS content.

For the (XPS-*s*)-PS system the tensile elongation is highest at about 20% XPS. Samples with only 10–20% XPS showed significant crazing, which explains the higher elongation that was obtained. However, the role of particle size (the bimodal particle size distribution findings; Figure 2) is not clear and the mechanism of craze formation still remains to be determined. Beyond 20% XPS content, elongation is reduced due to the higher XPS content as well as the inability of the 30% XPS sample to undergo extensive crazing. We conclude that two opposing effects (i.e., craze formation and XPS content increase) result in a maximum elongation for this system at about 20% XPS content. The crazing of (XPS-*s*)-PS at only 10–20% XPS content, as opposed to PS-*b*-XPS for which crazes form at 60–80% XPS, may be caused by the higher "effective" XPS content. This concept might explain such a shift in XPS content in the range where crazes are observed.

For the (PS-*s*)-XPS system, a very high molecular weight was found from gel permeation chromatography measurements, as well as an increasing

gel content with increasing XPS content. At the least, this system stands out because no particles have been identified in the SEM micrographs; rather, these micrographs resemble PS fracture surfaces. Because a second generation of new particles has not formed during the second stage (see Figure 2d), styrene–DVB addition to PS seed particles produces tiny intraparticle cross-linked domains or very high molecular weight branched chains with a consequential increase in overall molecular weight. This change may lead to enhanced mechanical performance. The role of the gelled domains is unclear.

Rheological Properties. The viscosity of PS–b–XPS at 190 °C is plotted against shear rate in Figure 10. The viscosity remains roughly unchanged with varying XPS content up to 80% XPS, although XPS addition slightly raises viscosity in a uniform manner. SEM micrographs of freeze-fractured extrudates prove that XPS particles preserve their identity as primary flow units (Nemirovski, N.; Narkis, M., unpublished). The flow curves follow a power-law relationship that covers almost four shear rate decades.

At lower shear rates (0.1 s^{-1} and lower) the viscosity tends to level off into a Newtonian plateau as obtained by steady shear rheogoniometry (Figure 11). Within the region of low shear rate the viscosity becomes XPS content-dependent: an increasing XPS content leads to higher viscosities and the appearance of the Newtonian plateau is delayed. This kind of behavior has been described elsewhere (22). Rheogoniometry in the dynamic mode is the topic of current research (Nemirovski, N.; Narkis, M.; Salovey, R., unpublished).

Flow curves of the (XPS-s)–PS and (PS-s)–XPS systems are essentially identical to those of the PS–b–XPS system. Here, also, the effect of XPS

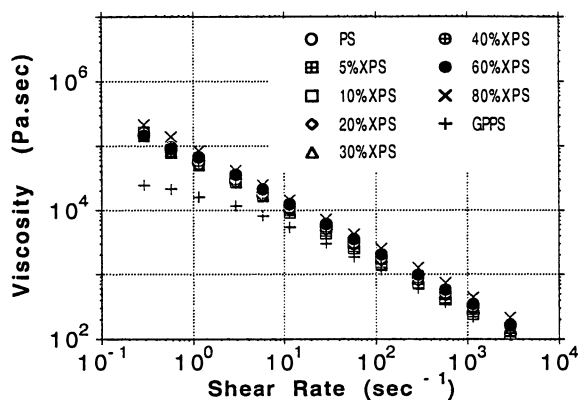


Figure 10. Rheology of PS–b–XPS at 190 °C.

content is rather mild and similar to the effect of fillers in a polymeric matrix at high shear rates (23), although, in general, viscosity tends to slightly increase with increasing XPS content.

Extrudate swell ratios ($B = D/D_0$, where D/D_0 is the extrudate-to-die diameter ratio) of PS-b-XPS are plotted in Figure 12. At 190 and 215 °C, B decreases with increasing XPS content. For instance, at 190 °C, the 20% XPS blend swelling ratio is reduced by 15% compared to PS (for which $B = 1.25$); at 215 °C this reduction is only 6%. Whereas PS chains orient when they enter the die, XPS particles do not, and, thus, the XPS particles do not contribute to the swelling process. Therefore, the swelling ratio decreases with increasing XPS content. At the higher temperature, the relaxation time is

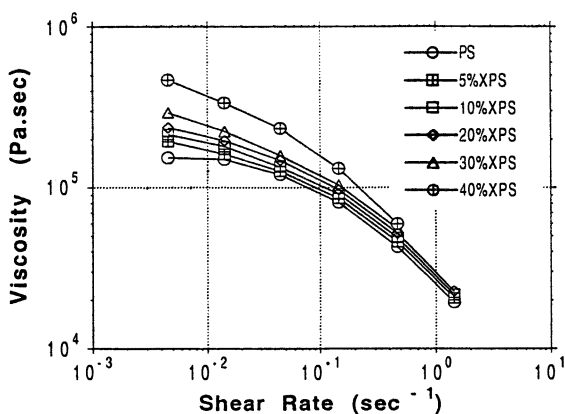


Figure 11. Steady shear rheogoniometry in cone and plate geometry. The effect of XPS content is evident at these low shear levels.

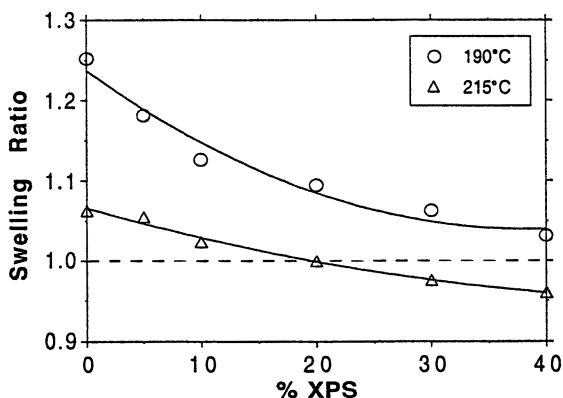


Figure 12. Extrudate swell, B , of PS-b-XPS extrudates at 190 and 215 °C.

shorter; thus, oriented chains are able to relax faster as they flow along the die and swelling is reduced. Above 20% XPS at 215 °C, the swelling ratios are practically unity. In any case, the dependence of extrudate swelling upon XPS content at 215 °C is rather moderate. An anomalous behavior at 240 °C with significant voiding of the extrudate was related to extensive degradation of the polymer. This behavior probably originated at the expense of a few unsaturations in the particles that result from dangling ends that copolymerize but failed to cross-link.

Swelling ratios are reported for the three systems at 190 °C. An interesting unexpected behavior readily can be seen for the two-stage system, as opposed to the expected reduction in extrudate swelling with XPS content for PS-b-XPS. In Figure 13 the swelling ratio of (XPS-s)-PS is maximum at 10% XPS and then decreases with higher XPS content. Note that the second population created during second-stage polymerization of (XPS-s)-PS may have different molecular weights for varying XPS content, in addition to the observed difference in average size (Figure 2). Information concerning the molecular weight of these second crops is not yet available, but no speculations should be made to explain the maximum at 10% XPS unless the issue of molecular weight is considered. The observed reduction in swelling ratio beyond 10% XPS is a result of the increasing XPS content—actually the so-called effective XPS content—after the PS occlusion effect. This reduction is more pronounced than the reduction in the case of PS-b-XPS, possibly because of the magnifying effect of the effective content. The swelling of (PS-s)-XPS is the highest among all the systems. Generally, the swelling of polymers upon extrusion through a die increases with higher molecular weights and molecular weight distributions (23). The very high molecular weight of this system is in agreement with this observation.

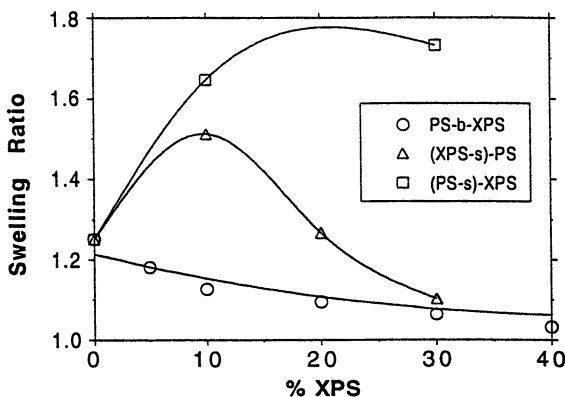


Figure 13. Extrudate swell, *B*, of PS-XPS systems at 190 °C.

Melt fracture of PS-*b*-XPS extrudates is delayed by increasing the temperature and XPS content (i.e., melt fracture onset appears at higher shear rates). In Figure 14 melt fracture of the thermoplastic PS starts at 10 s^{-1} at $190 \text{ }^\circ\text{C}$, but for the 40% XPS blend melt fracture starts only at 60 s^{-1} . In general, values of shear rate for the onset of this elastic phenomenon are in very good agreement with extrudate swell reported previously (an elastic effect as well) because earlier melt fracture should correspond with higher swelling ratios. Correspondingly, the (PS-*s*)-XPS system already showed melt fracture at 0.3 s^{-1} —the lowest attainable shear rate in the capillary rheometer. Values of the critical stress for onset of melt fracture range between 100 and 300 kPa.

Summary and Conclusions

The synthesis of latex polystyrene-cross-linked polystyrene (PS-XPS) blends has been accomplished by three different mixing routes. Generation of these systems either by physically blending PS and XPS lattices or by a two-stage polymerization technique (where the seed is either XPS or PS and the second stage is either styrene or styrene-DVB solution, respectively) led to the formation of distinct microstructures in each of the procedures. The different rheological and mechanical behaviors observed were affected by XPS content and cross-link density. The order of monomer addition appears to be critical to the development of well-characterized, tailor-made latex microstructures because the sequence of addition determines the polymerization sites.

Outlook

Some of the goals of this research on structured PS-XPS systems have been achieved. The flow behavior in the molten state has been studied and some

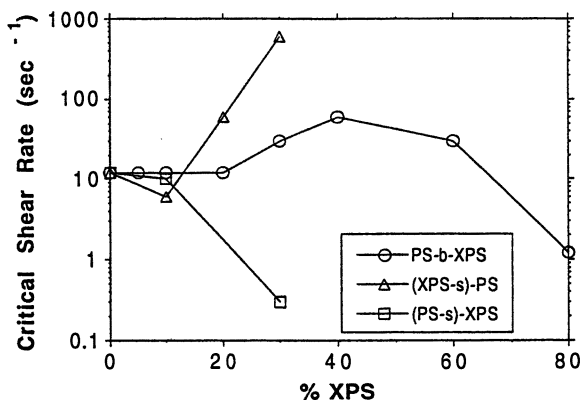


Figure 14. Critical shear rate at the onset of melt fracture.

deformation mechanisms of solid state PS–XPS materials have been detected. The polymerization sites in the two-state latices have been partially determined. However, more work is required to study the occlusion of PS in seed XPS particles further because it is not clear whether all the occluded PS is homogeneously distributed in the particle. A core–shell structure may also exist; that is, a PS shell over a core of XPS within which PS is occluded. This structure may well affect the particle–matrix interaction. It is also important to study the two-stage systems at higher XPS content. Different structures, possibly a monosized particle distribution for (XPS-s)–PS and a bimodal population for (PS-s)–XPS could be obtained in these cases. Finally, we point out that no property balance optimization has been done.

References

1. Manson, J. A.; Sperling, L. H. *Polymer Blends and Composites*; Plenum: New York, 1976.
2. Paul, D. R.; Newman, S. *Polymer Blends*; Academic: New York, 1978.
3. Sperling, L. H. *Interpenetrating Polymer Networks and Related Materials*; Plenum: New York, 1981.
4. Silverstein, M. S.; Narkis, M. In *Advances in Interpenetrating Polymer Networks*; Klemmner, D.; Frisch, K. C., Eds.; Technomic: Lancaster, PA, 1989; Vol. 1, p 117.
5. Okubo, M.; Kanaida, K.; Matsumoto, T. *J. Appl. Polym. Sci.* **1987**, *33*, 1151.
6. Hourston, D. J.; Satgurunathan, R.; Varma, H. C. *J. Appl. Polym. Sci.* **1987**, *34*, 901.
7. Ugelstad, J.; Mørk, P. C.; Nordhuus, I.; Mfutakamba, H.; Soleimany, E. *Makromol. Chem. Suppl.* **1985**, *10/11*, 215.
8. Silverstein, M. S.; Talmon, Y.; Narkis, M. *Polymer* **1989**, *30*, 416.
9. Allen, G.; Bowden, M. J.; Blundell, D. J.; Hutchinson, F. G.; Jeffs, G. M.; Vyvoda, J. *Polymer* **1973**, *14*, 597.
10. Hourston, D. J.; McCluskey, J. A. *J. Appl. Polym. Sci.* **1985**, *30*, 2157.
11. Blundell, D. J.; Longman, G. W.; Wignall, G. D.; Bowden, M. J. *Polymer* **1974**, *15*, 33.
12. Hofman, W. *Rubber Chem. Technol.* **1964**, *37*(2), 85–86.
13. Burke, O. W. Brit. Patent 799043, 1958.
14. Rosen, S. L.; Rodriguez, F. *J. Appl. Polym. Sci.* **1965**, *9*, 1601.
15. Nakajima, N.; Collins, E. A. *J. Rheol.* **1978**, *22*, 547.
16. Mooney, M.; Wolstenholme, W. E. *J. Appl. Phys.* **1954**, *25*, 1098.
17. Swanson, C. L.; Fanta, G. F.; Bagley, E. B. *Polym. Composites* **1984**, *5*, 52.
18. Silverstein, M. S.; Narkis, M. *Polym. Eng. Sci.* **1985**, *25*, 257.
19. Matsumoto, T.; Hitomi, C.; Onogi, S. *Trans. Soc. Rheol.* **1975**, *19*(4), 541.
20. Cox, W. P.; Merz, E. H. *J. Polym. Sci.* **1958**, *28*, 619.
21. Bianchi, U.; Magnasco, V. *J. Polym. Sci.* **1959**, *41*, 177.
22. Park, M.; Gandhi, K.; Sun, L.; Salovey, R.; Aklonis, J. *J. Polym. Eng. Sci.* **1990**, *30*, 1158.
23. Racin, R.; Bogue, D. C. *J. Rheol.* **1979**, *23*(3), 263.

RECEIVED for review November 11, 1991. ACCEPTED revised manuscript July 2, 1992.

Three-Stage Latex Interpenetrating Polymer Networks

Zhang Liucheng, Li Xiucuo, and Liu Tianchang

Department of Chemical Engineering, Hebei Institute of Technology, Tianjin, People's Republic of China 300130

Three-stage latex interpenetrating polymer networks (LIPNs) have been reported in many patents, but reported investigations on the effect of particle diameter, morphology, and dynamic mechanical properties have been limited in the literature. We have prepared a poly(butyl acrylate)–polystyrene–poly(methyl methacrylate) LIPN by three-stage emulsion polymerization. The morphology of this system was studied by transmission electron microscopy using RuO₄ staining. The particle diameters and their distribution, as well as the dynamic mechanical properties of the material, were determined, and the influence of monomer feeding rate and initiator and emulsifier doses on particle diameter and morphology was investigated.

LATEX INTERPENETRATING POLYMER NETWORKS (LIPNs) are a unique type of polymer blend that is prepared by seeded emulsion polymerization (multi-stage emulsion polymerization) (1, 2). The preparation involves creation of a seed latex of cross-linked polymer (polymer 1). Then a second monomer (monomer 2) together with its cross-linking agent is introduced into the reaction vessel and monomer 2 is polymerized. Because no fresh emulsifier is added during the second-stage polymerization, it is assumed that no new nucleation takes place during the monomer 2 polymerization. Hence growth occurs on the established latex particles. Transmission electron microscopy (TEM) and dynamic mechanical analysis (DMA) studies led to the proposal of an essentially core–shell model for the resulting latex particles (1–7). Previous research (4–6, 8–10) has shown that the particle morphology depends on the miscibility of monomer 2 in polymer 1, the mutual compati-

bility of polymers 1 and 2, the cross-link density of the networks, the hydrophilicity of the polymers, the addition method of the second monomer, the type and amount of initiator, and the polymerization temperature. Latex interpenetrating polymer networks based on acrylic polymers have great practical value in adhesives, foams, paints, paper coatings, textile sizings, and polymer modifications (1, 2, 7). Most of the works reported hitherto are limited to two-stage latex interpenetrating polymer networks. Recently, three-stage LIPNs based on acrylic polymers have been reported in many patents (11–15). The apparent kinetics of the polymerization process for three-stage LIPN has been studied by Liucheng et al. (16), but reported investigation on the effect of the particle diameter, morphology, and dynamic mechanical properties has been limited in the literature. We prepared a three-stage LIPN by a three-stage emulsion polymerization of *n*-butyl acrylate, styrene, and methyl methacrylate (LIPN PBA–PS–PMMA [poly(butyl acrylate)–polystyrene–poly(methyl methacrylate)]). The particle diameters and distribution as well as the dynamic mechanical properties and morphology of this material are reported herein.

Experimental Details

The emulsion polymerization was carried out in a 1000-mL tetra-neck bottle (2). The reaction temperature change was no more than ± 0.2 °C and the agitation speeds were 250 rpm. In the first stage of the three-stage emulsion polymerization, deionized and deoxidized water was placed in the tetra-neck bottle. Then emulsifier (sodium dodecyl sulfonate) and P-modifying agent (sodium borate) were added and dissolved while stirring thoroughly. The polymerization and cross-linking of *n*-butyl acrylate (BA) with ethylene glycol dimethacrylate (EGMA) were carried out in a nitrogen atmosphere while $K_2S_2O_8$ water solution was added. After the first-stage polymerization was completed, styrene (ST), cross-linking agent, divinylbenzene (DVB), and initiator $K_2S_2O_8$ were fed into the bottle and the second-stage polymerization was carried out. At the third stage, methyl methacrylate (MMA) and $K_2S_2O_8$ were charged. Three-layer LIPN PBA–PS–PMMA was produced. The composition and the polymerization conditions of the samples are tabulated in Table I.

Determination of Particle Diameter and Distribution. The latex particle diameters and distribution were determined by electron microscopy (Hitachi-600) and the micrographs were analyzed with a photography-analyzing instrument (Ibasi model II). The specimens were prepared by dilution of the LIPN and bromination for 10 min. Then the specimens were coated onto small copper grids with supporting wafers (used for observation and for taking the micrographs). The size and distribution of the latex particle diameters were obtained by analyzing the micrographs. The polydispersity index (distribution width) was defined as

$$\frac{\bar{D}_w}{\bar{D}_n} = \frac{\sum N_p D_w / \sum N_p D_c}{\sum N_p D_n / \sum N_p D_c}$$

Table I. Polymerization Condition and Composition of the Samples

Stage	Components	PBSM -CSS-4	PBSM -CSS-6	PBSN -CSS-8	PBSN -CSS-11	PBSN -CSS-14	PBSN -CSS-20	PBSN -CSS-22
First	Deionized water (mL)	400	400	400	400	400	400	400
	Emulsifier (g)	0.7	0.7	0.7	0.7	0.7	0.7	0.7
	BA (g)	40	40	40	40	40	40	40
	EGDMA (g)	2.5	2.5	2.5	2.5	2.5	2.5	2.5
	K ₂ S ₂ O ₈ (g/L water)	1.0	1.0	1.0	1.0	1.0	1.0	1.0
Second	ST (g)	30	30	30	30	30	30	30
	DVB (g/100 ST)	3.5	3.5	0	0	4.0	3.5	3.5
	Initiator K ₂ S ₂ O ₈ ^a (g/L water)	0.6	1.0	0	0.6	0.6	0.6	0.6
	AIBN ^b (g)	0	0	1.24	0	0	0	0
	Sodium borate (g)	0.3	0.3	0.4	0.3	0.3	0.3	0.3
Third	MMA (g)	55	55	55	55	55	55	55
	Initiator K ₂ S ₂ O ₈ (g/L water)	0.55	0.55	0	0.55	0.55	0.55	0.55
	AIBN ^c (g)	0	0	0.22	0	0	0	0
Polymerization temperature (for all three stages) (°C)		70	70	70	70	70	80	60

NOTE: Dropwise feeding mode.

^a The residual concentration of K₂S₂O₈ from the first-stage reaction is 0.85 g/L of water. Therefore, the K₂S₂O₈ concentration in the second-stage has this additional amount of K₂S₂O₈.

^b Azobis(isobutyronitrile).

where, \bar{D}_w and \bar{D}_n are the weight-average and number-average diameters of the particles, respectively, and N_p is the number of latex particles with diameter within a range of central value D_c .

Determination of Dynamic Mechanical Properties. The emulsion obtained in the three-stage polymerization was coagulated with aluminum sulfate, filtered, washed to neutrality, and stove-dried at 80 °C. The resultant powder was then hot-pressed at 180 °C to form wafers of 0.20–0.30-mm thickness. The dynamic mechanical properties of the wafer were determined in a viscoelastometer (Rheovibron model DDV-II-EA). The measuring frequency was 100 Hz and the heating rate was 2 °C/min.

Characterization of Latex Particle Morphology. The use of osmium tetroxide as a staining agent is limited to polymers that have some level of unsaturation. Hobbs et al. (17) reported that mercuric trifluoroacetate can effectively stain poly(phenylene ether) (PPO) and styrene-butadiene-styrene (SBS) three-block copolymers, but is ineffective for polystyrene. Trent et al. (18) reported that ruthenium tetroxide (RuO₄) is a good staining agent for polymers that contain polystyrene (PS).

The morphology of the three-stage latex particles was observed with a transmission electron microscope (Hitachi EM-H-800) after the specimen was stained with RuO_4 . For PBA-PS-PMMA latex, the dry-staining method was found to be preferable to the wet-staining method. The dry-staining method consisted of mixing powdered NaIO with powdered $\text{RuO}_2 \cdot 2\text{H}_2\text{O}$. Reaction of the mixture with aqueous water vapor in air resulted in the RuO_4 used for staining. Exposure for 14 h was required to achieve adequate staining.

The general procedures for electron microscopy were as follows: The three-stage latex was spread on clean slide glass and dried in air. Because of the high glass-transition temperature of PS and PMMA, the latex formed small flat fragments rather than a film. The fragments were dried overnight at 60 °C under vacuum and then carefully transferred into capsules. Epoxy resin (Epon 812) that contained a curing agent was poured into the capsules to embed the LIPN and the capsules were cured at 38, 45, and 65 °C for 24 h, respectively. The cured blocks were ultramicrotomed into thin sections that were mounted on copper grids, dried in air, and stained with RuO_4 . Then the electron micrographs were taken.

Results and Discussion

Particle Diameters and Distribution. The influence of monomer feeding type and initiator concentration on particle diameter and distribution is tabulated in Tables II–V and shown graphically in Figure 1. The data in Table II demonstrate that the distribution width that corresponds to the batch process is slightly wider than the distribution width of the semibatch

Table II. Number- and Weight-Average Diameters and Distribution (conversion > 97%)

Feeding Type	D_n (μm)	D_w (μm)	D_w/D_n
Batch process	0.0670	0.0722	1.078
Drop feeding for 0.5 h	0.0792	0.831	1.048

Table III. Influence of MMA Feeding Type on LIPN PBA-PS-PMMA Particle Diameters and Distribution (conversion > 97%)

Feeding Type	D_n (μm)	D_w (μm)	D_w/D_n
Batch process	0.0657	0.0848	1.292
Drop feeding for 0.5 h	0.0839	0.0879	1.047

Table IV. Influence of $\text{K}_2\text{S}_2\text{O}_8$ Concentration on LIPN PBA-PS Particle Diameters and Distribution

$\text{K}_2\text{S}_2\text{O}_8 \times 10\text{ M}$	D_n (μm)	D_w (μm)	D_w/D_n
2.13	0.0556	0.0625	1.124
3.94	0.0543	0.0600	1.105

Table V. Influence of $K_2S_2O_8$ Concentration on LIPN PBA-PS-PMMA Particle Diameters and Distribution

$K_2S_2O_8 \times 10 M$	$D_n (\mu m)$	$D_w (\mu m)$	D_w/D_n
1.85	0.0845	0.0892	1.055
2.70	0.0795	0.0831	1.045
3.90	0.0717	0.0762	1.062

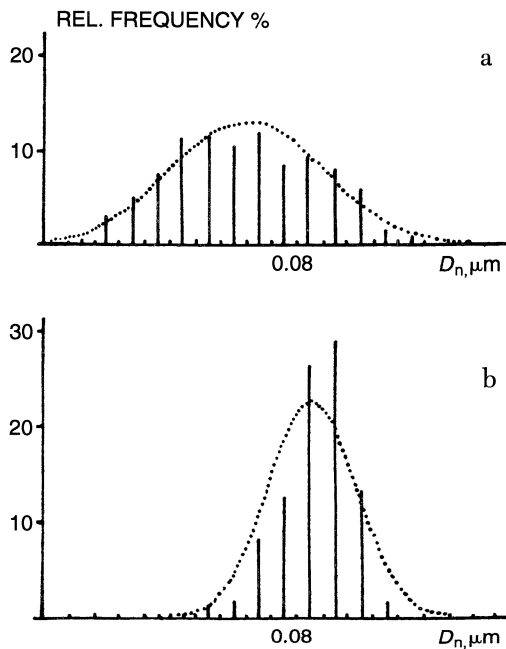


Figure 1. The influence of MMA feeding type on the diameter distribution of LIPN PBA-PS-PMMA latex particles: a, batch addition; b, dropwise addition.

process and the average particle diameter is slightly smaller for LIPN PBA-PS.

Fluid-dynamic chromatography was used to determine the particle diameters and distribution of the product of two-stage emulsion polymerization of PBA-PS (in every stage; no added cross-linking agent). For the semibatch process, Muroi (19) obtained distribution width 1.022 and average particle diameter $D_n = 0.105 \mu m$, whereas for the batch process, the distribution width was 1.037 and the average diameter $D_n = 0.106 \mu m$. These values are similar to the data reported herein. For LIPN PBA-PS-PMMA, the important influence of feeding type is obvious from Table III and Figure 1. The use of drop feeding (semibatch process) for MMA resulted in a large average particle diameter and narrow distribution, which is probably due to the

greater solubility of MMA in water (the homogeneous nucleation cannot be neglected). The probability of homogeneous nucleation is greater for batch processes. Table IV shows no distinct influence of the initiator concentration on the LIPN PBA-PS particle diameters but a small effect on the particle distribution. The data in Table V show that the dose initiator has no distinct influence on the distribution width, but it does have a small effect on the particle diameter of LIPN PBA-PS-PMMA, which again may be related to the greater solubility of MMA in water.

The experimental data on the influence of the dose of emulsifying agent at the first stage of polymerization on particle diameters and distribution indicate that increasing the dose decreases the LIPN PBA-PS particle diameters and widens the distribution. For LIPN PBA-PS-PMMA, the average particle diameter decreases with increasing emulsifier dose, but has no obvious influence on the particle distribution width.

Dynamic Mechanical Properties. Figure 2 presents the dynamic mechanical spectrum of LIPN PBA-PS. Two distinct spectral peaks are shown. The observed glass-transition temperatures (T_g) are higher than values in the literature. This discrepancy may be caused by the higher cross-linking and higher test frequency. Figure 3 shows the dynamic mechanical spectrum of LIPN PBA-PS-PMMA. The two distinct transition peaks correspond to the glass transitions of PBA and PS-PMMA. In addition, there is a wide transition region at about 50 °C that corresponds to the secondary transition of PMMA. Careful comparison of Figures 2 and 3 reveals that the temperature that corresponds to the low-temperature transition peak of LIPN

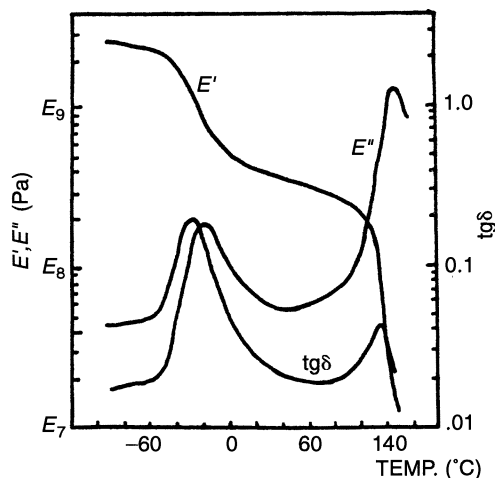


Figure 2. The dynamic mechanical spectra of LIPN PBA-PS.

PBA-PS is higher than the low-temperature transition peak of LIPN PBA-PS-PMMA (see Table VI). This difference may be related to diffusion of MMA into the cross-linked PBA phase during third-stage polymerization. MMA is partially miscible with PBA. Because cross-linked PBA has high viscosity and the protection of PMMA at the outer layer, the small amount of MMA monomer is hard to eliminate from PBA even when the films are stove-dried. Experiments show that the temperature that corresponds to the

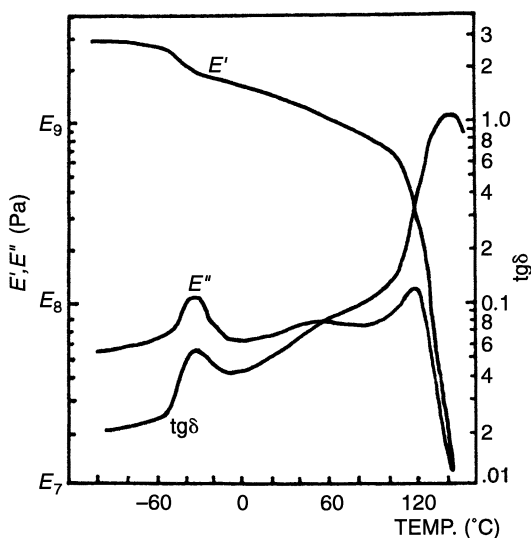


Figure 3. The dynamic mechanical spectra of LIPN PBA-PS-PMMA (PBMS-CSS-14).

Table VI. Dynamic Mechanical Properties of LIPN PBA-PS and LIPN PBA-PS-PMMA

Properties	LIPN PBA-PS	LIPN PBA-PS-PMMA			
		PBMS-CSS-14	PBMS-CSS-11	Batch	Dropwise
E' (Pa)					
Glass transition	1.6×10	1.6×10	1.6×10	1.6×10	1.6×10
Rubber plateau	1.5×10	8.0×10	8.0×10	8.0×10	8.0×10
E'' peak position (°C)					
Glass transition	125	120	120	118	120
Rubber plateau	-20	-38	-30	-25	-30
		~ 50	~ 50	~ 50	~ 50
Value of $\tan \delta$ peak					
Glass transition	0.045	1.01	1.01	1.01	1.01
Rubber plateau	0.20	0.07	0.12	0.11	0.05

transition peak of the cross-linked PBA is lower than the value for non-cross-linked PBA (*see* Figure 4). This difference may stem from the same MMA diffusion. Experimental data show that cross-linking causes the value of T_g to be between the two peaks, which indicates that the miscibility of the two phases is increased.

Morphology. Influence of Initiators. The influence of initiators and their concentration on the morphology of the three-stage latex particles was investigated. For the first-stage of the emulsion polymerization, only the water-soluble initiator ($K_2S_2O_8$) was used. In the second- and third-stage polymerization, both the oil-soluble initiator [azobis(isobutyronitrile) (AIBN)] and the water-soluble initiator ($K_2S_2O_8$) were used to examine the influence of initiator water solubility on the product morphology.

When oil-soluble AIBN was used as the initiator in the second and third stages, the latex particles formed an “inverted” core-shell morphology; that

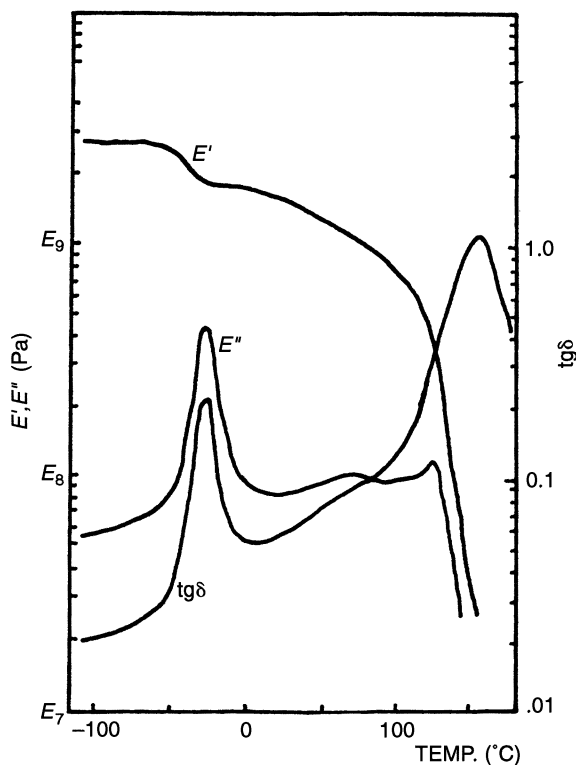


Figure 4. Dynamic mechanical spectra of PBSM-CSS-11. No cross-linking agent was added in the polymerization process.

is, the PS formed a core surrounded by PBA and PMMA (Figure 5). This construction results because both styrene (ST) and AIBN are hydrophobic. The monomer ST with dissolved AIBN migrates into the seed (PBA) particles and polymerizes. This process is consistent with Iwhan's observations (9). When the water-soluble initiator $K_2S_2O_8$ was used in the second and third stages, the particles formed a typical core-shell morphology (Figures 6 and 7). From Figures 6 and 7 it can be seen that the core-shell morphology becomes increasingly distinct with increasing amounts of initiator. The reason this phenomenon occurs is the reduction of interfacial tension between the water phase and the PS domains that is caused by coupling the initiator fragments, $-SO_4$, to PS chains, which enhances the stability of the latex particles. This stability improves with increasing amounts of initiator. On the other hand, increasing $K_2S_2O_8$ concentration increases the polymerization rate and enhances the rate of viscosity increase in polymerization loci; hence, the mobility of monomer and polymer molecules is decreased. Thus, more PS is formed on the surface of the seed latex particles; that is, based on both thermodynamic and kinetic considerations, the core-shell morphology is favored by increasing $K_2S_2O_8$ concentration. This conclusion is consistent with Iwhan's investigation of two-stage latex particles (9).

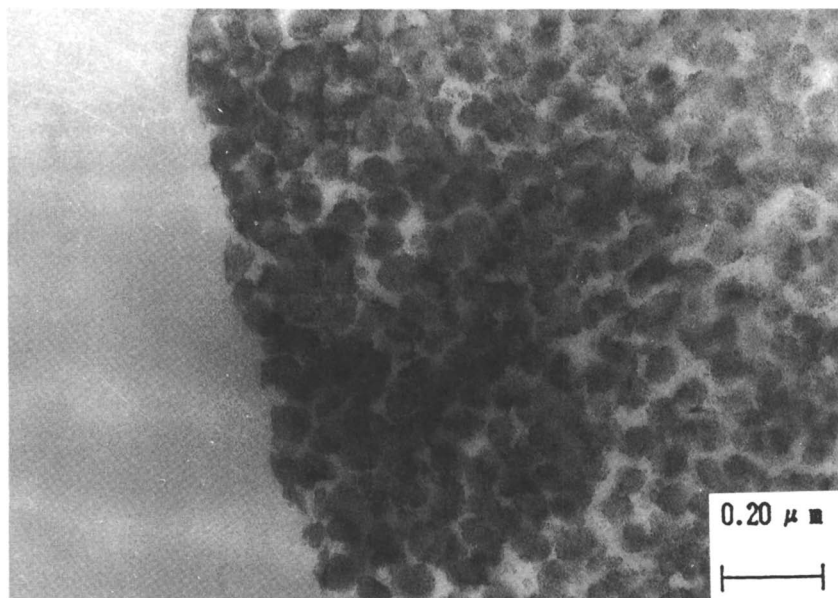


Figure 5. Transmission electron micrograph of PBSM-CSS-8 with AIBN initiator. Magnification 7.5×10^4 .

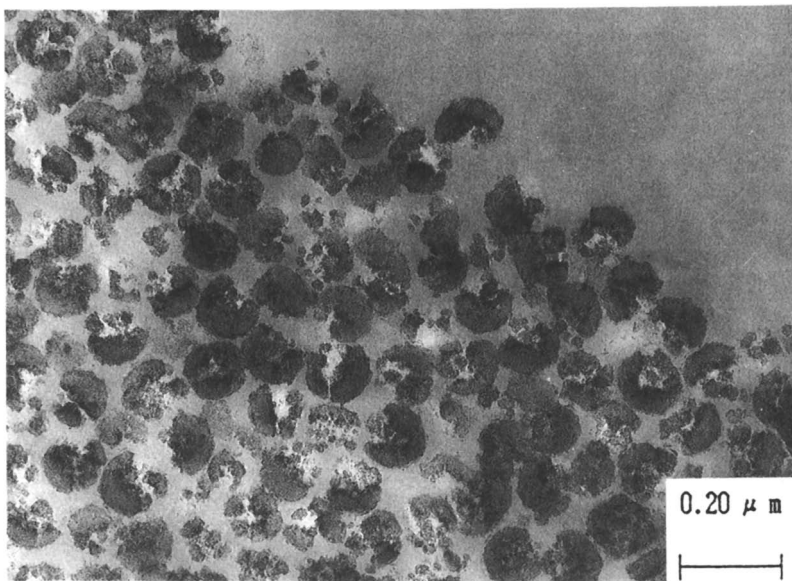


Figure 6. Transmission electron micrograph of PBSM-CSS-4 with $K_2S_2O_8$ initiator in 1.45 g/L of water. Magnification 7.5×10 .

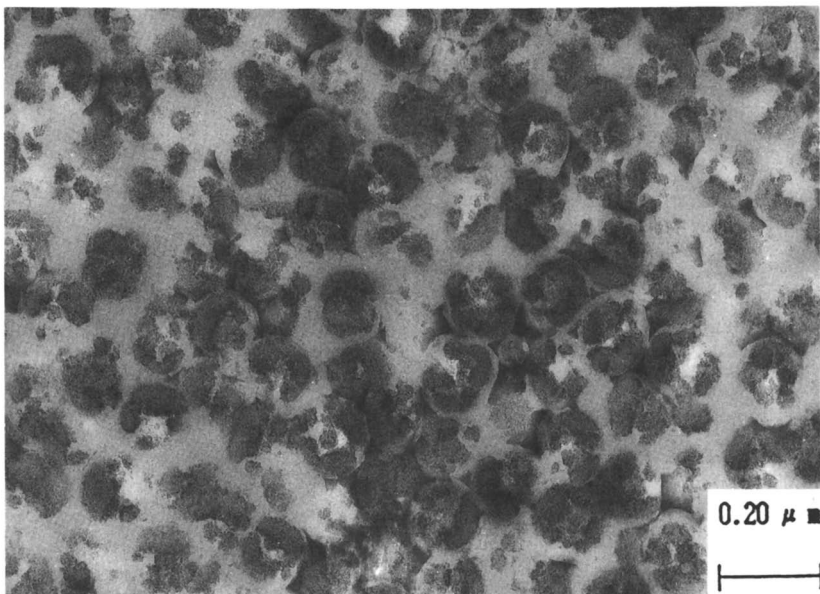


Figure 7. Transmission electron micrograph of PBSM-CSS-6 with $K_2S_2O_8$ initiator in 1.95 g/L of water. Magnification 7.5×10 .

Influence of the Degree of Cross-Linking. In the three-stage emulsion polymerization without cross-linking agent, the “inverted” core–shell morphology of latex particles was observed. The PS formed the core surrounded by the PBA and PMMA. Because neither PBA nor PMMA is stained by RuO_4 , the three-layer structure is not detectable on the electron micrograph (Figure 8). When cross-linking agent is added, the distinct core–shell morphology is visible on the transmission electron micrographs. With increasing amounts of cross-linking agent, more distinct core–shell morphology is formed as shown in Figures 6 and 9.

PBA and PS are inclined to phase separate because of immiscibility, whereas the more hydrophobic PS and ST tend to diffuse into the seed particles; this is the reason for the “inverted” core–shell morphology. The diffusion process is controlled by the viscosity in polymerization loci. When cross-linking agent is used in the polymerization process, the viscosity in polymerization loci increases and the diffusibility of molecules slows down. Thus increasing the cross-linking agent concentration hinders the diffusion and the more distinct core–shell morphology is formed.

Influence of Monomer Feeding Type. In the three-stage emulsion polymerization, monomer 2 (ST) and the monomer 3 (MMA) were added by the following two methods:

1. **Batch or bulk addition.** The total amount of monomers is added to the reaction bottle prior to starting the seeded emulsion polymerization.
2. **Dropwise addition.** The total amount of monomer is slowly drop-fed into the reaction bottle through a microfeeder at a constant rate (ca. 5 mL/min).

The method of monomer addition has a considerable effect on the morphology of the three-stage latex particles. Figure 10 is a transmission electron micrograph of the three-stage latex particles for which the monomer was added in batch. Comparison with Figure 9 (dropwise addition) indicates that when batch addition is used, the regularity of the core–shell morphology is poor and a more diffused boundary interface is formed. This observation was confirmed by DMA analysis (Figure 11). From Figure 11 and Table VI it can be seen that the distance between the two glass-transition peaks is shortened when batch addition is used. The reasons for this decreased distance are as follows. First, when batch addition is used, the degree of grafting is greater as compared with dropwise addition (19). Therefore, the mutual compatibility of the involved polymers is enhanced. Second, as

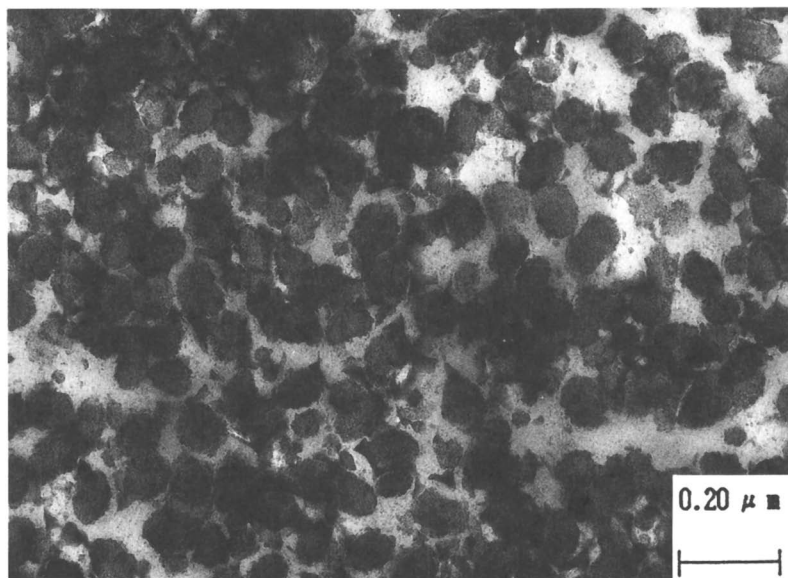


Figure 8. Transmission electron micrograph of PBSM-CSS-11 without cross-linking agent. Magnification 7.5×10 .

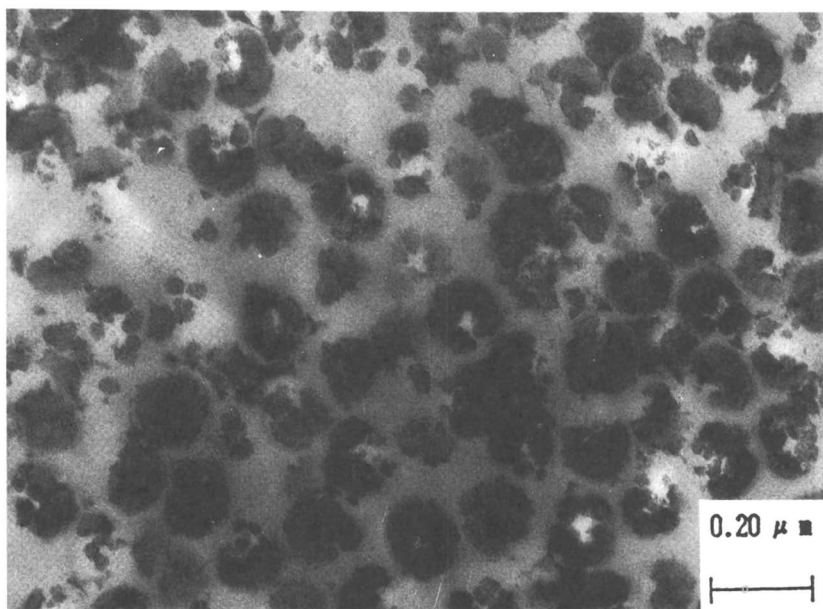


Figure 9. Transmission electron micrograph of PBSM-CSS-14 with 3 and 4% cross-linking agent added in the first and second stages, respectively. Magnification 7.5×10 .

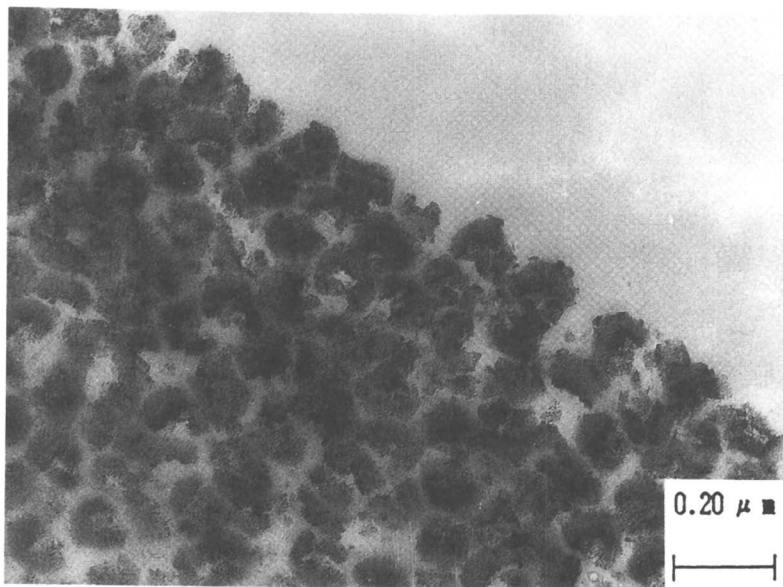


Figure 10. Transmission electron micrograph of the three-stage latex particles. The polymerization condition is equal to PBSM-CSS-14, but monomer was added via the batch addition method. Magnification 7.5×10 .

compared to the dropwise method, more monomer content in polymerization loci is maintained in batch addition. Hence, the viscosity in the polymerization loci that facilitates diffusion of the monomer is lower and the extent of interpenetration among the polymers is increased.

Influence of the Polymerization Temperature. The experimental results (Figure 12) show that the regularity of the core-shell morphology of the latex particles is poor and the boundary between the core and the shell becomes indistinct when the polymerization temperature is increased. This result is inconsistent with Iwhan's work on the study on two-stage PMMA-PS latex particles (10). Because the initiator concentration was greater and no cross-linking agent was used in Iwhan's work, this inconsistency is probably due to differences in concentration of the initiator and the cross-linking agent. In fact, the morphology and structure of the latex particles is controlled by competition between thermodynamic and kinetic factors. The promoting force for phase separation is thermodynamic, the main criterion of which is thermodynamic miscibility of the constituents. All factors that promote miscibility decrease the domain dimension and enhance the extent of interpenetration of the phases. However, the extent of phase separation is controlled by the kinetic factors, where the basic criterion is the rate of

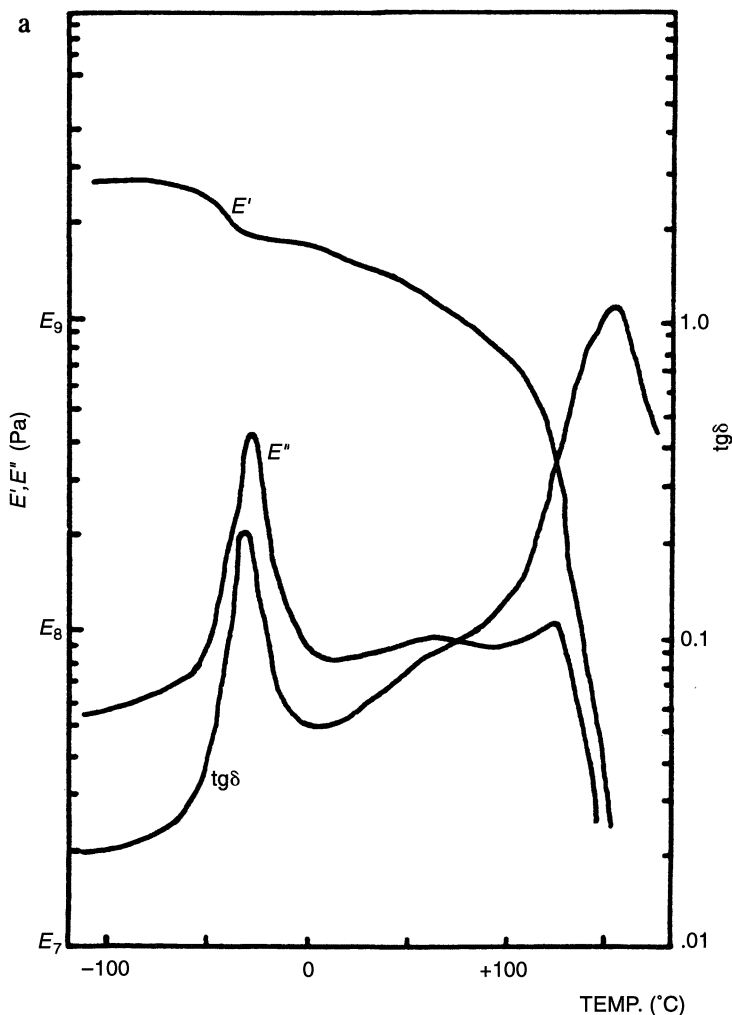


Figure 11. Dynamic mechanical spectra of the LIPN PBA-PS-PMMA: a, batch addition.

viscosity increase relative to the kinetics of phase separation. All factors that enhance the viscosity trend to reduce the rate and extent of phase separation. With increasing temperature, the viscosity in polymerization loci is reduced and the phase separation increases. However, owing to increased polymerization rate with increasing temperature, the speed of viscosity increase in the polymerization loci increases. The final result depends on the competition between these two aspects. In our work, the second aspect made the predominant contribution.

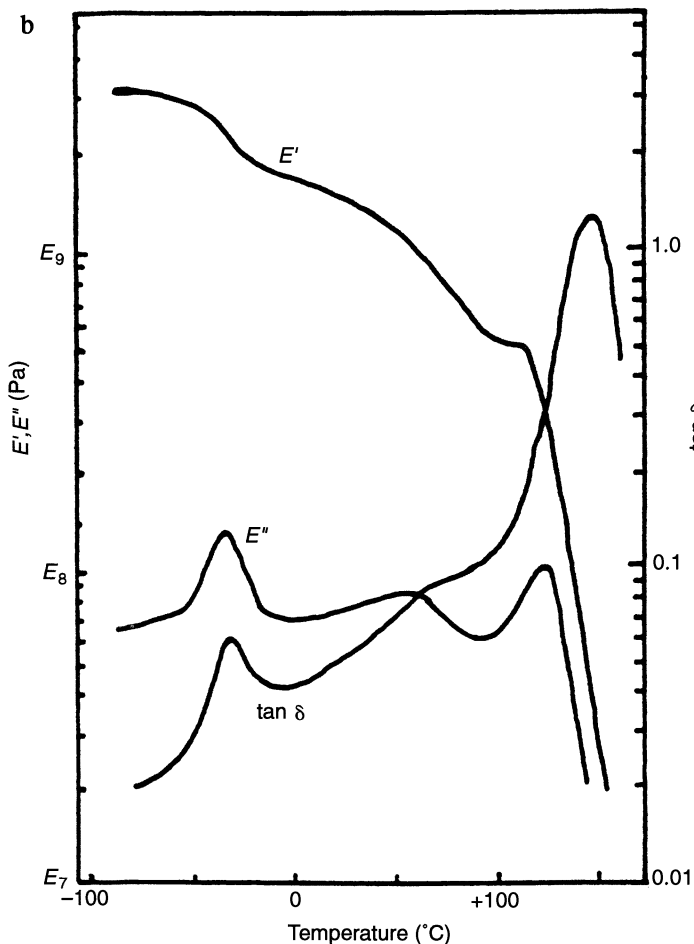
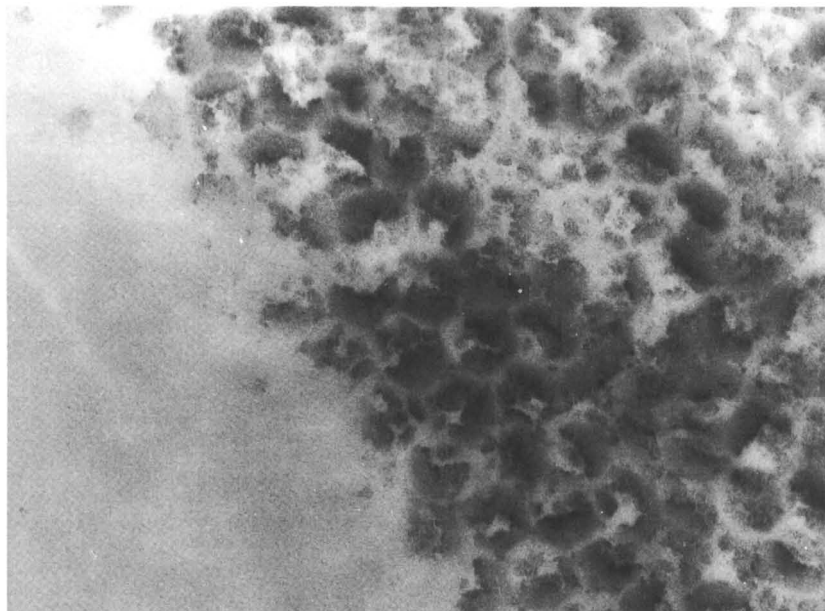


Figure 11.—Continued. Dynamic mechanical spectra of the LIPN PBA-PS-PMMA: b, dropwise addition.

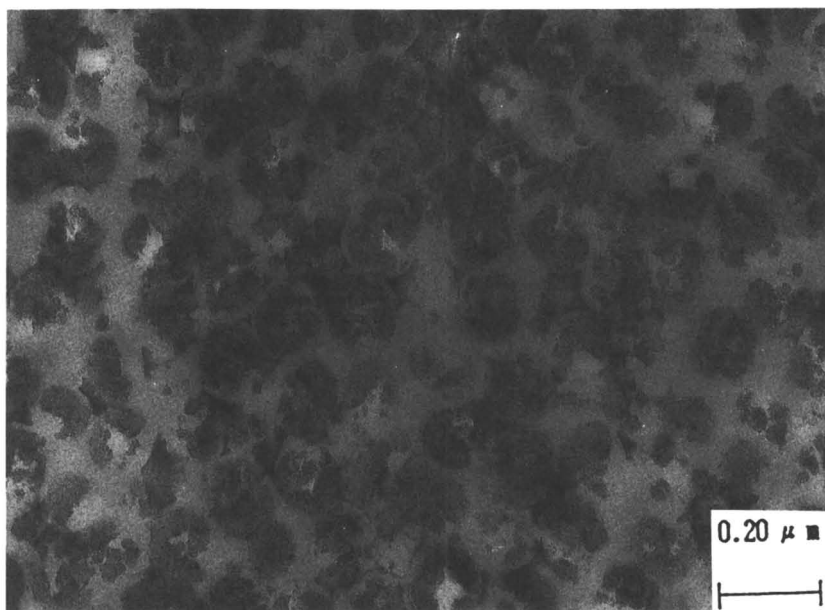
Summary and Conclusions

Three-stage latex interpenetrating polymer networks (LIPN PBA-PS-PMMA) were prepared in three-stage emulsion polymerization of *n*-butyl acrylate, styrene, and methyl methacrylate. The latex particle diameters and distribution were determined by electron microscopy and the dynamic mechanical properties were determined with a viscoelastometer. The morphology of the latex particles was observed via transmission electron microscopy using RuO_4 as a staining agent. The following conclusions were drawn from analysis of the experimental data:

1. The influence of monomer feed type and initiator dose on the particle distribution width is negligible. However, the influence



a



b

Figure 12. The effect of polymerization temperature on the morphology of the three-stage latex particles: a, PBSM-CSS-20, 80 °C; b, PBSM-CSS-20, 60 °C.

of MMA feeding style on the particle distribution of LIPN PBA-PS-PMMA is significant.

2. The investigation of dynamic mechanical properties indicates phase separation in the LIPN PBA-PS-PMMA.
3. The use of oil-soluble AIBN as an initiator promotes the formation of inverted core-shell morphology, whereas use of water-soluble $K_2S_2O_8$ initiator favors the formation of normal core-shell morphology. The formation of normal core-shell morphology is further enhanced by lower polymerization temperature and increased amounts of cross-linking agent.

References

1. Sperling, L. H. *Interpenetrating Polymer Networks and Related Material*; Plenum: New York, 1981.
2. Liucheng, Z. *Interpenetrating Polymer Networks*; Hydrocarbon-Processing Press: Peking, China, 1990; pp 17-88.
3. Hourston, D. J.; Satgurunathan, R. *J. Appl. Polym. Sci.* **1984**, *29*, 2969.
4. Hourston, D. J.; Satgurunathan, R.; Varma, H. C. *J. Appl. Polym. Sci.* **1986**, *31*, 1955.
5. Hourston, D. J.; Satgurunathan, R.; Varma, H. C. *J. Appl. Polym. Sci.* **1987**, *33*, 215; *34*, 901.
6. Merkel, M. P.; Dimonie, V. L.; El-Aasser, M. S.; Vanderhoff, J. W. *J. Polym. Sci., Polym. Chem. Ed.* **1987**, *25*, 1775.
7. Bufkin, B. G. *J. Coatings Technol.* **1978**, *50(5)*, 65.
8. Min, T. I.; Klen, A.; El-Aasser, M. S.; Vanderhoff, J. W. *J. Polym. Sci., Polym. Chem. Ed.* **1983**, *21*, 2845.
9. Iwhan, C.; Kyung-Woo, L. *J. Appl. Polym. Sci.* **1985**, *30*, 1903.
10. Shaffev, O. L.; Dimonie, V. L.; El-Aasser, M. S.; Vanderhoff, J. W. *J. Polym. Sci., Polym. Chem. Ed.* **1987**, *25*, 2595.
11. Morimachi, Y. Japanese Patent 60-155215, 1985.
12. Kamta, K. Japanese Patent 60-51737, 1985.
13. Nakayi, H. Japanese Patent 60-99114, 1985.
14. Tsurumi, T. U.S. Patent 4,515,914, 1986.
15. Kazuo, K. Japanese Patent 61-12739, 1986.
16. Liucheng, Z.; Xiucuo, L.; Tianchang, L. *J. Appl. Polym. Sci.* **1991**, *42*, 891.
17. Hobbs, S. Y.; Watkins, V. H.; Russell, R. R. *J. Polym. Sci., Polym. Phys. Ed.* **1980**, *18*, 393.
18. Trent, J. S.; Scheinbein, J. I.; Couchman, P. R. *J. Polym. Sci., Polym. Lett. Ed.* **1981**, *19*, 315.
19. Muroi, S.; Hashimoto, H.; Hosoi, K. *J. Polym. Sci., Polym. Chem. Ed.* **1984**, *22*, 1365.

RECEIVED for review October 9, 1991. ACCEPTED revised manuscript August 27, 1992.

Silicone and Poly(tetrafluoroethylene) Interpenetrating Polymer Networks

Brief History, Summary of Recent Developments, and Discussion of Applications

Mark E. Dillon

Bio Med Sciences, Inc., 115 Research Drive, Bethlehem, PA 18015

A series of semi-interpenetrating polymer networks based on poly(tetrafluoroethylene) and silicone elastomers was synthesized by extrusion of the polymers into ribbons and then biaxially stretching the material into thin films. The resultant membranes have tensile strengths of 3580–8960 kPa and increasing transparency as the silicone content increases. Although the films are effective liquid water barriers, they exhibit excellent water vapor permeability, which suggests uses as filtration membranes, protective barrier textiles, and wound-care products.

Historical Perspective

Poly(tetrafluoroethylene) [PTFE; commonly known as Teflon (DuPont)] was invented in the late 1930s. Initial applications were as inert coatings for valve and pipe systems for the Manhattan Project, as well as other military uses. For example, it was found that the velocity of ballistic objects could be increased by coating PTFE onto the projectile or the barrel from which it was fired. Later, consumer applications such as nonstick coatings on cookery became routine. PTFE has a great potential for applications in the biomedical field: it is among the most biocompatible materials because its inert nature elicits no toxic or thrombogenic reactions (1).

In the early 1960s the production of microporous materials made of expanded PTFE was demonstrated. However, although microporous PTFE sheets proved to have numerous applications in medical and nonmedical fields, processing conditions and cost effectiveness were problematic (2).

Silicones were first developed by Kipping (3) in the early 1900s, and were named because they were thought to be silicon-containing analogues of ketones. By the 1950s silicone oils and elastomers were being used in many industrial and medical applications.

In 1983 Arkles (4) described thermoplastic interpenetrating polymer network (IPN) compositions based on silicone and polyurethane. These melt-processable compositions possessed improved physical properties and biocompatibility. Principle applications of these silicon-based IPNs were in the field of biomedical devices. This work represented a significant advancement in the field because the poor physical properties of unfilled silicones often limited their usefulness. Fillers, such as fumed silica, are often used to improve certain physical properties, but toughness and biocompatibility are usually compromised.

In the mid 1980s Dillon et al. (5, 6) formed PTFE and silicones into semi-IPNs to produce semipermeable membranes for filtration, protective clothing, and certain medical applications such as burn dressings. The material is called a semi or pseudo IPN because only one phase of the system is cross-linked; the other phase is linear (7). The semi-IPNs exhibit physical and chemical properties that combine many of the unique characteristics of the two ingredients. The product is strong and durable, and when it is made from medical grade silicone, it is highly biocompatible. This chapter will describe semi-IPN synthesis as well as the physical, mechanical, and biomedical behavior of the products.

Physical Characterization

PTFE. Poly(tetrafluoroethylene) has a low glass-transition temperature of approximately 20 °C, so some stages of PTFE processing are performed below room temperature and others are performed above. PTFE resin is highly crystalline (> 95%) in the virgin or unsintered state. In this context, sintering refers to heating the polymer above its crystalline melting point (327 °C) and then allowing it to cool. Because of an exceptionally high melt viscosity, the molten PTFE retains some of its amorphous structure after recrystallization (8). In theory, the increase in amorphous content tends to inhibit slippage along the crystalline axis, thereby providing a more dimensionally stable structure. Sintering can be done in either a loose powder or finished shaped form. However, if the PTFE is sintered as a powder, further processing into shaped forms is greatly limited.

Although PTFE is technically a thermoplastic polymer, it is not melt-processable by conventional thermal processing methods. PTFE particles do,

however, have the unusual ability to fuse and coalesce at room temperature upon exposure to even slight shear stress. Under flow conditions small regions of polymer chains are irreversibly formed in directions that are oriented according to the flow parameters and rheology of the system. Exposure of PTFE powder to pressure and shear forces bonds the particles together to form a coherent bulk. For the production of shaped articles such as sheets or blocks, PTFE is often molded or oriented, and then sintered to provide a finished article.

Microporous PTFE Sheets. PTFE can be processed into microporous structures for a variety of applications. The well known process of biaxially stretching (or expanding) PTFE ribbon into breathable waterproof microporous sheets is used for barrier clothing, filtration media, and various medical applications (2). The production of such sheets begins with the extrusion of PTFE in the form of ribbon. PTFE cannot be extruded with a conventional screw-style extruder because the PTFE inevitably fibrillates in a random fashion under the chaotic shear stresses created in the screw barrel. Instead, the process is accomplished by first dampening PTFE resin with an organic lubricant such as kerosene and then ram extruding cylindrical preforms through a slit orifice die at room temperature. The lubricant aids the orientation process much as elevated temperatures aid other extrusion systems.

The extrudate is then calendared to a thickness of several hundred micrometers and the organic lubricant is volatilized at slightly elevated temperatures. The resultant product is stretched and fibrillated in a tenter frame apparatus under controlled thermal conditions. A tenter frame is a device that consists of two sets of gripping conveyors that grab the ribbon by its edges. The conveyors move further away from one another as they move forward into a tunnel oven. The extrudate is thereby stretched in the traverse direction in a continuous fashion. Orientation in the longitudinal direction can be accomplished by use of differential speed rollers before entrance into the tenter frame. When both stretching processes are performed on the same material, the resultant product is said to be biaxially expanded. This stretching stage is carried out at elevated temperatures below 327 °C, and the heating profile is critical to achievement of a uniform product.

The fibrillated PTFE does not become thinner by stretching; rather, the material undergoes an internal fracture process or expansion phenomenon that results in a microporous structure. The morphology of the material is characterized by particulate nodes connected by fibrils, which gives the appearance of “spiders holding hands” as shown in Figure 1. While the material is retained in the extended position, it is passed through a final zone in the oven that sinters the film above 327 °C and results in a thermosetting effect that fixes the microporous material into a dimensionally stable form. These membranes are always opaque.

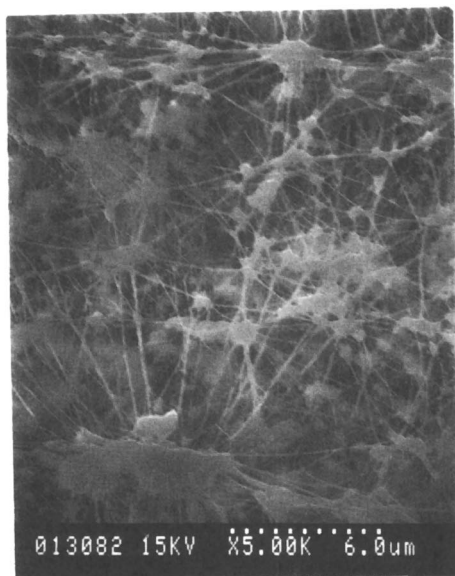


Figure 1. Scanning electron micrograph ($\times 5000$) of a microporous expanded PTFE membrane.

Silicone Elastomers. Silicone polymers consist of a backbone of alternating oxygen and silicon atoms with selected organic branches connected to the silicon atoms. Thermoset silicone elastomer compositions typically contain a cross-linking agent, a catalyst to accelerate vulcanization, and an inhibitor to prevent premature reaction. Cross-linking is initiated in heat vulcanized systems when a peroxide curing agent thermally decomposes and releases a free radical. The radicals react with hydrogen atoms on the organic branches of the siloxane molecule and cause the hydrogen atoms to break loose and provide sites for cross-linking between the polymer chains (9). Room temperature vulcanization systems (RTVs) are usually activated either by a catalyst that contains trace levels of metal or by ambient moisture. A typical silicone elastomer composition is given in Table I. Such silicone compositions are usually supplied as a two-part system: poly(dimethylsiloxane) and catalyst components comprise part A and dimethylvinylsiloxane and trimethoxysilylpropyl components comprise part B.

Numerous silicone systems are used in many industrial applications; however, for toxicological reasons, medical siloxane compositions are exclusively limited to poly(dimethylsiloxane) (PDMS) systems.

Silicone thermoset polymers can be processed in liquid or paste form at room temperature and then vulcanized into the elastomeric end products. The physical properties of the polymer, such as modulus of elasticity and

Table I. Curable Silicone Composition

<i>Component</i>	<i>Weight Percent</i>
Vinyl N-stopped poly(dimethylsiloxane)	68.2
MDQ silicone resin blend	22.7
Dimethyl vinylsiloxane resin blend	8.2
Bis(trimethoxysilylpropyl) maleate	0.9
Lamoreaux platinum catalyst	10 ppm

tensile strength, are determined by the prepolymer molecular weight, silica filler content, and the cross-link density of the final elastomer.

Theory

Due to the nature of composite structures, IPNs provide extended capabilities in comparison to the capabilities of their basic ingredients. The properties of the final products are a function of both the overall chemistry of the system and the morphological characteristics of the particular IPN structure. In theory, an IPN could be designed to use a fibrillated PTFE matrix as a supporting scaffold for a silicone network. If the IPN is structured so that the surface of the PTFE is largely masked by the silicone, a system where physical strength is governed by the fibrillated PTFE matrix and the surface characteristics are controlled by the silicone composition would be expected. PTFE behaves plastically and silicone behaves elastically, so the final material would further be expected to exhibit elastic properties in proportion to the amount of silicone present. In addition, different silicone compositions could be used to achieve different surface characteristics and to provide varying elastic properties.

Experimental Details

A blend of approximately 3 kg of PTFE (dispersion grade Fluon CD123 resin; ICI Americas), 220 g of the curable silicone composition outlined in Table I, and 590 g of kerosene was prepared. The silicone was dispersed in the kerosene and then blended with PTFE powder. This process effectively coats the PTFE particles with silicone prepolymer. The PTFE-silicone-kerosene mix was then extruded through a slit-orifice die, linearly stretched 84%, transversely stretched 1278% in a tenter frame, and sintered at above 327 °C. The biaxial stretching process was performed the same as for ordinary PTFE, except that a number of process parameters had to be altered to compensate for the effect of the silicone. To achieve the highest amounts of silicone studied, some samples were further enriched with silicone during proprietary stages of the process.

Physical properties, such as tensile strength and elongation, optical trans-

parency, moisture vapor permeability, and resistance to water penetration, were evaluated via established methods.

Scanning electron microscopy was used to examine the morphology of the material. To confirm the existence of an IPN structure, extraction experiments were conducted on the final product to determine if all of the silicone could be removed from the PTFE network. This removal determines if trapped "islands" of silicone exist within the PTFE matrix. The absence of such islands indicates a continuous network of silicone. To extract the silicone, the extrusion and stretching process was performed with several silicone compositions that did not contain a cross-linking agent. These silicone compositions would not vulcanize into an elastomer upon exposure to heat and could, therefore, be removed with an appropriate solvent.

Additional samples were produced using a medical grade poly(dimethylsiloxane) composition (Silastic MDX4-4210; Dow Corning) so that biological characteristics could be assessed. Because the samples were made of a network of two of the most well-established biomaterials, PTFE-PDMS semi-IPNs were expected to be highly biocompatible. In fact, PTFE and PDMS are often used (separately) as negative control specimens in biocompatibility studies.

Results

The end product was similar to expanded PTFE sheeting, although there were a few key differences. The product was stronger, more uniform in general appearance and microstructure, and could be expanded at significantly lower temperatures than pure PTFE (6).

Extraction of Silicone. Extraction studies with hexane were carried out on the noncurable specimens. In each case, 100% of the silicone could be removed, which indicates a continuous silicone network. The remainder of the microporous PTFE sheets were coherent and did not shed lint or dust when mechanically agitated, which indicates that the PTFE also formed a continuous network.

Physical Properties. With increasing amounts of silicone, the final product exhibited increasing elasticity. Table II gives a brief list of the physical properties for the PTFE-silicone sheets synthesized with the silicone composition shown in Table I. The tensile strength of the semi-IPNs varied from about 3450 to 8960 kPa. Although these values are quite low for engineering plastics, they are in the useful range for applications that do not require high strength. Elongations at break ranged from about 50 to 250%, which is extremely useful for wound and burn dressings, where patient movement requires significant elastic behavior.

To investigate breathability, the moisture vapor transmission rates (MVTRs) of the membranes were determined using ASTM method E96-80B. The samples exhibited a moisture vapor transmission of about 600–750 g/m² per day. Using the Mullen water entry test for hydrostatic resistance (Federal Test 191A, Method B), the samples were each evaluated for water barrier

Table II. Physical Properties of PTFE–Silicone Semi-IPN Membranes (25 μm Thick)

Property	Volume Fraction PDMS (%)					
	15	30	35	40	55	100
Moisture vapor transmission (22 °C, 50% relative humidity) (ASTM E96-80) (g/m^2 per day)	736	755	764	720	638	202
Hydrostatic resistance (Federal Test 191A, Method 5512) (kPa)	550	565	580	630	860	> 1380
Tensile strength (kPa)	8960	6890	5510	4825	3580	< 3790 ^a
Elongation at break (percent)	45	95	125	200	250	< 350 ^a
Porosity (percent)	53	43	38	34	27	–0
Percent transparency (TAPPI ^b digital opacometer)	50	51	63	65	83	–95

^a Tensile and elongation properties are given for Silastic MDX4-4210 as published in Dow Corning Technical Bulletin “Silicones for Medical Devices”, form number 51-779A.

^b Technical Association of the Pulp and Paper Industries.

effectiveness. Although the samples are substantially breathable to moisture vapor, they are simultaneously impermeable to liquid water (550–860-kPa resistance). The moisture vapor transmission correlates with the overall porosity, which ranges from about 25–50% as determined by density measurements.

Optical Properties. Beyond a certain threshold of silicone content, the semi-IPN composition becomes quite translucent or transparent. Table II indicates that as the silicone content increases, the transparency increases considerably (digital opacometer; Thwing Albert). Although the transparency results from significant loss in porosity (as indicated in Table II and by scanning electron microscopy), surprisingly the membranes maintained their high MVTR.

Electron Microscopy. Scanning electron micrographs were taken of two specimens. Figure 2 represents a specimen that contained approximately 15-vol% PDMS. An electron micrograph of a semi-IPN that contained approximately 55-vol% PDMS is shown in Figure 3.

Surface Chemistry. Liquid–solid contact angle measurements were made on two samples as shown in Table III. The two samples represent the two extremes of the semi-IPN composition: approximately 15- and 55-vol% PDMS (shown in Figures 2 and 3 respectively).

Table III indicates that as the volume fraction of PDMS increases, the liquid–solid contact angle for liquids of various surface tensions decreases.

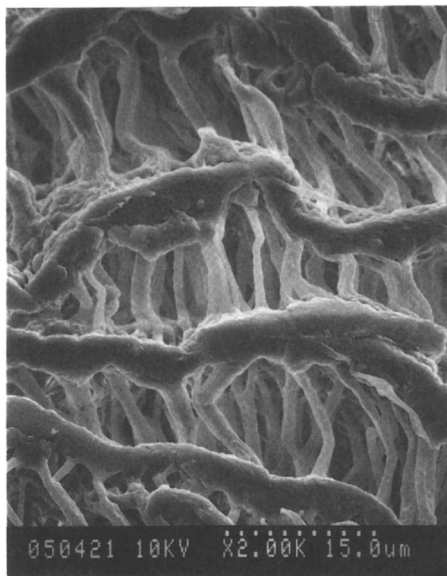


Figure 2. Scanning electron micrograph ($\times 2000$) of a microporous expanded semi-IPN of PTFE and silicone (15 vol% silicone).

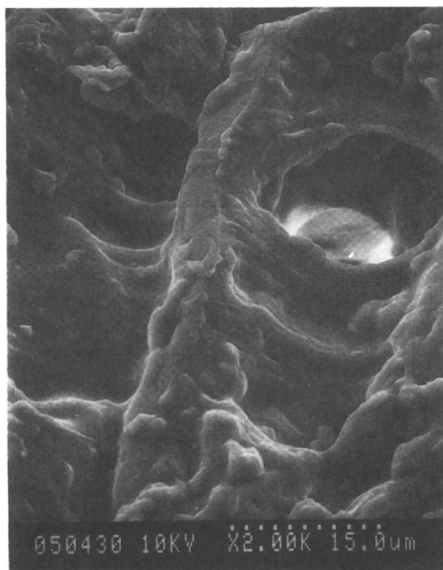


Figure 3. Scanning electron micrograph ($\times 2000$) of a microporous expanded semi-IPN of PTFE and silicone (55 vol% silicone).

Table III. Liquid–Solid Contact Angles for the Two Extremes of PTFE–PDMS Semi-IPN Compositions

<i>Liquid Surface Tension (N/m)</i>	<i>15 vol% PDMS</i>	<i>55 vol% PDMS</i>
0.0650	140	103
0.0580	124	96
0.0535	136	87
0.0490	122	74
0.0450	119	63
0.0390	105	56
0.0330	42	47
0.0275	Penetrated	32
0.0260	Penetrated	35
0.0240	Penetrated	35

NOTE: All values are contact angles in degrees.

This situation is indicative of a trend away from the extremely low surface energy of PTFE (0.018 N/m) and toward the more hydrophilic nature of silicone. Semi-IPN compositions with high volume fractions of PTFE are more hydrophobic, yet are more readily penetrable by fluids than semi-IPNs with high volume fractions of PDMS. Semi-IPNs with high volume fractions of PDMS are more hydrophilic in nature, but are only permeable to liquids with very low surface tensions. This phenomenon is atypical because hydrophobic compositions are expected to be more resistant to the penetration of high surface tension or aqueous liquids.

Biocompatibility. In both direct contact and liquid extract studies using L929 mouse fibroblast cells, the medical grade PTFE–PDMS semi-IPNs exhibited no cytotoxic effects (10). In fact, the test results were identical to results for the negative control specimens. Studies of hemolytic activity using rabbit blood indicated that the semi-IPN samples were nonhemolytic and, therefore, will not cause a breakdown of blood when exposed *in vivo* (11). In addition, the PDMS–PTFE semi-IPN membranes did not cause complement activation (the initial event that ultimately results in a cascade of undesired immunological responses). Skin contact studies indicated that the semi-IPN samples were nonsensitizing and nonirritating (12, 13).

Discussion

The tensile strength of the semi-IPNs increased with higher amounts of PTFE. This response is consistent with the concept that the PTFE matrix provides the bulk of the strength for the system. Increasing amounts of silicone increased the elongation properties of the system, which is also consistent with the theory that the elastic nature of the semi-IPN increases with silicone content. The surface chemistry of the system was also strongly

influenced by the silicone content. Contact angle measurements indicate that as the amount of silicone was increased, the system became less hydrophobic.

The penetration of a liquid into the capillary structure of a solid is referred to as wicking and is a function of both the pore geometry and the liquid–solid contact angle. Accordingly, the permeability characteristics of PTFE–silicone semi-IPNs are a function of microstructure and composition. The novel permeability characteristics of the PTFE–silicone semi-IPNs arise from the ability to change pore size and critical surface energy independently of one another. For example, by a change in biaxial stretching parameters, the same porosity characteristics can be achieved with low or high amounts of PTFE (giving low or high liquid contact angles, respectively). Alternatively, from a single blend of PTFE and silicone, semi-IPNs can be produced with different porosity characteristics and identical surface energies but different wicking properties.

Applications

Wound-Care Systems. One immediate application of the PTFE–silicone semi-IPN technology is in the field of advanced wound care. A wound dressing should be soft and flexible to eliminate dead air space around the wound bed, but also should be lint-free to eliminate contamination of the wound with particulate matter; it must be an effective bacteria barrier, and the components of the device must be nontoxic and biocompatible. Furthermore, wound dressing should be moisture vapor and gas permeable to reduce exudate (wound fluid) accumulation, yet simultaneously must maintain a moist layer over the wound bed to aid healing and epidermal cell migration (14, 15).

Conventional wound dressings (i.e., absorbent gauze) that are commonly used are not the optimum choice of treatment in most cases. Such dressings allow drying and scab formation, and often cause tissue inflammation and desiccation (16).

PTFE–PDMS semi-IPNs have many skinlike qualities that are ideal for such applications. Wound dressings made from the semi-IPN composition (Silon Non-Adherent Dressings, Bio Med Sciences, Inc.) have been cleared by the U.S. Food and Drug Administration for commercial marketing and distribution for advanced wound-care systems (17). These dressings drastically reduce pain, increase healing rates, and provide improved cosmetic results in comparison to conventional wound-care products (18). The dressings are used as a covering over skin graft sites, for the closure of partial thickness wounds such as second degree burns and skin graft donor sites, and as a treatment for chronic wounds such as decubitus and venous stasis ulcers.

Drug Delivery Systems. In addition to wound care, another application is in the area of pharmacology. Steady release systems are desired for many drugs. Uniform delivery avoids the peaks and valleys associated with

doses, and is similar to the way biochemicals are naturally released from within the body (19). Membrane-moderated transdermal drug delivery systems (such as nitroglycerine and scopolamine) require a selectively permeable matrix to release the medicament in a controlled fashion, while also preventing unwanted diffusion or seepage of the active ingredient (20). Other sustained release devices also use semipermeable materials as the rate controlling mechanism, such as the recently introduced implantable birth control system (Norplant, Norwich Eaton).

In experiments conducted beyond the scope of this discussion, semi-IPN material displayed the ability to be loaded with antibiotics. Controlled release of the drug over a period of as long as four days was achieved. Although the release of antibiotics is most relevant to topical wound-care products, it is anticipated that other drugs could be loaded into the semi-IPN system for use as transdermal drug delivery devices.

Other Medical Applications. Other potential medical applications include vascular grafts for prosthetic or bypass applications and perfusion membranes for blood oxygenation devices. Vascular grafts have been produced by the biaxial expansion method except with tubes instead of sheets. In this case the product is extruded through a tubular die and primarily stretched in the longitudinal direction. Microporous semi-IPNs of PTFE and PDMS also have been produced in the form of tubes. Blood oxygenation devices require a semipermeable membrane that is biocompatible. In particular, the material must be nonhemolytic and non-complement-activating. Although detailed experimental evaluations for this application have not been conducted yet, it is anticipated that semi-IPN material will be useful in this capacity.

Barrier Textile. As a laminate to fabrics, semi-IPNs have a potential nonmedical application in the field of chemical barrier textiles. Improved protective clothing that can shield individuals from chemical contamination and allow breathability is needed. Breathable chemical barriers are additionally required for chemical-biological defense systems. Although evaluation of semi-IPN technology for this application is only beginning, semi-IPNs have already shown promise. The material can be tailored for a high resistance to liquid penetration while also having a high breathability factor.

Filtration Systems. Because the pore size, pore volume, and wettability properties of the semi-IPN can be tailored, it is likely that there are many filtration applications for the material as well. For example, if low-pressure differentials and high flow rates are required for a particulate filtration process, semi-IPNs with a low amount of silicone and high amount of open porosity would be most appropriate. Conversely, if an osmotic membrane is required for a "molecular sieve" type of application, a dense membrane with a low volume fraction of PTFE would be best.

Summary and Conclusions

The biaxial orientation process used for the production of microporous PTFE was used to produce microporous semi-IPNs of PTFE and silicones. Scanning electron microscopy and extraction studies confirmed the IPN nature of the structure. The semi-IPN materials have semipermeable qualities that allow unique applications. The surface energy and morphology of the semi-IPNs are a function of composition. The PTFE component contributes physical strength and the silicone component contributes increased elasticity and transparency. Medical grade semi-IPNs are biocompatible, which led to initial commercial applications in the field of advanced wound-care technology. Numerous other medical and nonmedical applications are contemplated, such as drug delivery systems, filtration media, and barrier textiles. Further investigation is required to determine the effect of various silicone compositions. Lower modulus silicones and permutations on porosity and composition should be studied for usefulness.

References

1. Lee, H. *Handbook of Biomedical Plastics*; Pasadena Technology Press: Pasadena, CA, 1971.
2. Gore, W. L. U.S. Patent 3,315,020, 1967.
3. Kipping, F. S. *J. Chem. Soc.* **1907**, 91, 209–240.
4. Arkles, B. C. *Medical Device and Diagnostic Industry*, **1983**, Nov.
5. Dillon, M. E. U.S. Patent 4,832,009, 1989.
6. Dillon, J. A.; Dillon, M. E. U.S. Patent 4,945,125, 1990.
7. Sperling, L. H. *Interpenetrating Polymer Networks and Related Materials*; Plenum: New York, 1981; pp 1–5.
8. Fifoot, R. E. *Modern Plastics Encyclopedia*; McGraw-Hill: New York, 1988.
9. Park, J. B. *Biomaterials Sciences and Engineering*; Plenum: New York, 1984; pp 291–293.
10. *U.S. Pharmacopeia*; 1990; Vol. XXII, pp 1495–1499.
11. ASTM F756-87; American Society for Testing and Materials: Philadelphia, PA, 1989; pp 243–245.
12. Marzulli, I. N.; Maiback, H. I. *Dermatotoxicology*, 3rd ed.; Hemisphere Publishing: New York, 1987.
13. *U.S. Pharmacopeia*; 1990; Vol. XXII; pp 1497–1499.
14. Shires, G. T.; Black, E. A. *J. Trauma* **1979**, 19, 855.
15. Cuzzell, J. Z. *Am. J. Nursing* **1990**, October, 53–63.
16. Hansbrough, J. F. *J. Trauma* **1990**, 30(12), S155–S160.
17. U.S. Food and Drug Administration 510(k), K912032, August 20, 1991.
18. Dillon, M. E.; Okunski, W. J. *Wounds: A Compendium of Clinical Research and Practice* **1992**, 4(5), 203–207.
19. 3M Health Care Specialties Department, Technical Bulletin 70-2008-2572-0 (57.5) II, 1987.
20. Komerska, J. F. *J. Plastic Film Sheeting* **1987**, 3.

RECEIVED for review December 9, 1991. ACCEPTED revised November 18, 1992.

Morphology of Acrylic–Epoxy Bichain Simultaneous Interpenetrating Polymer Networks

Song Ma¹ and Xinyi Tang²

¹Department of Pure and Applied Chemistry, University of Strathclyde, 295 Cathedral Street, Glasgow, G1 1XL, United Kingdom

²Department of Chemistry, Jilin University, Changchun, People's Republic of China

Simultaneous interpenetrating polymer networks (SINs) were synthesized by two chain reactions of poly(n-butyl acrylate-co-ethyl dimethacrylate) (PnBA) and epoxy network. Degree of swelling, density, dynamic mechanical properties, and morphology of the SINs were measured. Theoretical analysis suggests a greater probability of interpenetration and entanglement between two networks for SINs from two chain reactions than for SINs from a chain reaction–step reaction combination. Comparison of the results of the glass-transition temperature of the bichain SINS with PNBA–epoxy SINs from the chain reaction–step reaction combination agrees with this conclusion. The PnBA–epoxy SINs are partially miscible systems. The presence of a third phase in a number of SINs is believed to represent the real interpenetration between two networks. Both composition and cross-linking density of PnBA affect the miscibility of SINs. The system is miscible at a supermolecular level for 2% cross-linked PnBA:epoxy = 10:90 SINs. The swelling property of SINs is affected by both phase continuity and interpenetration between two networks. The density measurements clearly show the presence of additional interactions. The interpenetration degree estimated from the density difference after the formation of SINs agrees with dynamic mechanical results. The transmission electron micrographs show a fine microstructure.

SEVERAL BASIC SYNTHETIC METHODS TO PREPARE INTERPENETRATING polymer networks (IPNs) have been developed since the initial studies in the 1960s and 1970s (1–5). These methods include materials now known as sequential IPNs (SIPN), where the networks are created sequentially; simultaneous interpenetrating polymer networks (SINs), where both monomers are mixed together and polymerized by independent and noninterfering routes; latex interpenetrating polymer networks (LIPN), where both networks are on each latex particle; and interpenetrating elastomeric networks (IENs), where two types of latex are mixed and subsequently cross-linked. Among these methods, SIN received more attention because it had advantages over the other methods: ease of synthesis, better miscibility, more interpenetration, and, more importantly, the ability to enhance the physical properties of polymer materials. Most recent work has been based on SIN methodology.

Because the morphology of multiphase materials affects their properties significantly, it is very important to control the morphology of the SIN system to achieve desired properties.

Three different routes are available for the formation of a SIN after the two monomers or prepolymers have been mixed: Monomer I may be polymerized first, monomer II may be polymerized first, or the two might be truly simultaneously polymerized. A systematic study of the effects of each of these three approaches with an acrylate and an epoxy system showed that the normal SIN, with the acrylate polymerized first, was heterogeneous, whereas SINs based on the other two routes behaved much more homogeneously (6).

In addition to the synthetic routes, Park et al. (7) outlined several other factors that control the extent of miscibility in SINs:

1. Miscibility of each of the component polymers.
2. Relative rates of reaction and network formation.
3. Average molecular weight per cross-link.
4. Weight fraction of each polymer network component.
5. Degree of polymerization at the time of gelation.
6. Mobility of the polymer chains, especially to phase separate.

The first four points will be examined in detail; the last two points are, more or less, decided by the polymer itself.

The miscibility of each of the component polymers plays a decisive role in controlling the extent of miscibility in SINs, although the interpenetration and entanglements between the two networks can increase the miscibility in SINs. The thermodynamic forces that lead to phase separation in highly immiscible polymers are so powerful that phase separation occurs substantially before the kinetic ramification can prevent it. In such cases only small gains in phase mixing occur. In cases where the polymers are more miscible, the phase behavior of SINs may vary dependent on other factors. However, fully miscible SINs can only come from miscible polymers. Poly(2,6-di-

methyl-1,4-phenylene oxide) (PPO) and polystyrene (PS) are miscible in all proportions: Truly interpenetrating polymer networks have been produced from this polymer pair (8, 9).

The lower average molecular weight per cross-link means higher cross-link density. The internetwork interlocks and entanglements depend on the cross-link densities of each component network. The higher the cross-link densities of each component networks are, the greater the chances for formation of internetwork interlocks and entanglements. Experiments indicate that the glass-transition temperature (T_g) shifts are relatively large when M_c (the molecular weight between cross-links) is small (7).

Observations from theoretical analysis and polymer-polymer phase diagrams imply that the polymer pair will have better miscibility when one component content is in the high rather than in the intermediate range (10). The same conditions hold for SIN systems, although there is some deviation, which depends on different situations.

In early studies, the network that reacts the fastest (gels and cures first) was found to have a more continuous structure and to make a larger contribution to the properties of SINs than the other network. The gelation time of the two networks has a large effect on structure, morphology, and properties (11, 12). Touhsaent et al. (13) pointed out that the smallest domain size of epoxy-acrylic SINs occurred when the respective reactions were closest to simultaneity. Frisch et al. (14) concluded from the study on polyurethane-methacrylate (PU-MA) SINs that as the rate of the respective polymerizations increases and approach simultaneity, the T_g s of these SINs shift inward, which indicates less phase separation. Results of a study (15) of the kinetic effects in polyurethane-epoxide episulfide resin (PU-ES) SINs showed that the extent of inward glass-transition shift increases and the phase domains that were observed by transmission electron microscopy (TEM) become smaller as the gelation time difference of the two networks decreases.

However, until now, all SINs have been synthesized by the combination of step reaction-chain reaction mechanisms. It is well known that the molecular weight distributions of polymers from chain reactions and step reactions are quite different. The molecular weight distribution of polymers before gelation will affect the miscibility because only long polymer chains can form interlocks and interpenetrations between two networks.

Theoretical Approach

The miscibility for a given system depends on the mixing free energy, δG :

$$\delta G = \delta H - T \delta S \quad (1)$$

where δH is the mixing enthalpy, δS is the mixing entropy, and T is the temperature in kelvins.

If δG is positive, the system will tend to phase separate; if δG is negative, the system will be miscible. The entropy of mixing for two polymeric species is very small because of the very long chains involved. Coupled with the usually positive heat of mixing, the resultant free energy of mixing is positive and causes these materials to phase separate.

For the formation of SINs when the two monomers are mixed together, the mixing entropy can be expressed as

$$\delta S = k \ln \Omega = k \ln [(N!)/(N_1!)(N_2!)] \quad (2)$$

where Ω is the total number of ways to arrange N_1 and N_2 molecules on a regular lattice that comprises $N = N_1 + N_2$ cells. N_1 is the number of monomer I molecules, N_2 is the number of monomer II molecules, and N is total number of molecules. Thus for the mixing of low molecular weight monomers, generally a large entropy can be obtained. Thus the mixing free energy will be negative except when the system has extremely large positive enthalpy of mixing.

When polymerization begins, the monomers are polymerized into polymers; the monomers are connected together by chemical bonds. Thus the system becomes more ordered and Ω will decrease accordingly because the connection of monomers decreases the total number of possible molecular arrangements. As the conversion rate of monomers to polymers increases, Ω will become smaller and smaller. At the point where $T \delta S$ is smaller than positive δH , the mixing free energy will become positive and phase separation will occur. The foregoing analysis demonstrates that a given polymeric pair will begin to phase separate at a certain conversion rate (or average degree of polymerization).

One feature to consider here is molecular weight distribution. Molecular weight distributions of polymers from chain reactions and step reactions are quite different. In a step reaction system monomers tend to convert to polymers very quickly; for example, monomers form dimers, dimers form polymers with four monomers, and so forth. At a fixed conversion rate (average degree of polymerization), most molecules have a degree of polymerization (DP) near the average degree of polymerization; fewer molecules will have very large or very small DP. For a chain reaction system, polymers tend to increase in DP, whereas other monomers are still not converted to polymers. Thus, under a fixed average DP (say, the average DP where phase separation will occur) there will be more high-DP molecules in a chain reaction system than in a step reaction system.

Another known fact is that the longer the molecules are, the easier intermolecular locks and entanglements form.

A combination of the foregoing analyses enables us to conclude that there should be a greater probability for interpenetration and internetwork entanglements in SINS from chain reaction-chain reaction mechanisms than in SINS from a chain reaction-step reaction mechanism.

Poly(*n*-butyl acrylate-*co*-ethylene dimethacrylate)-epoxy (PnBA-epoxy) SINS were selected for the following reasons. PnBA polymerized by 2,2'-azobis(isobutyronitrile) (AIBN) is a free radical reaction, and epoxy resin cured by tertiary amine, *N,N'*-dimethylbenzylamine (DMBA), may be taken as an oxygen anionic chain reaction (16). Thus, this SIN system has been synthesized by the combination of an anionic chain reaction and a free radical chain reaction. Some experiments on PnBA-epoxy SINS (13, 17, 18) used epoxy resin cured with acid anhydride. Thus, the SINS were formed from a step reaction-chain reaction combination. The availability of this experimental data makes it easier to compare SINS from different synthetic methods.

Experimental Details

Materials. All materials and descriptions are listed in Table I. *n*-Butyl acrylate (nBA) and ethylene dimethacrylate (EDMA) were distilled to remove the inhibitor before use. AIBN was recrystallized before use. Epoxy and DMBA were used as supplied. All the solvents were the highest purity available.

Procedure. Preparation of Epoxy Network. After the epoxy resin was melted, the DMBA (3% by weight) was added. After a thorough mixing, the mixture was agitated under vacuum for 30 s and placed in a poly(tetrafluoroethylene) (PTFE) mold for curing.

Preparation of PnBA Network. The nBA mixture [nBA, cross-linking agent (EDMA), and initiator (AIBN; 0.2% of nBA)] was placed in a reaction kettle equipped with heating, stirring, condensing, and N₂ inlet apparatuses and prepolymerized under nitrogen with stirring at 90–95 °C until near gelation. Then the prepolymer was placed in a PTFE mold for curing.

Table I. Materials

<i>Code</i>	<i>Description</i>
Epoxy	Glycidyl ether of bisphenol A molecular weight: 400
nBA	<i>n</i> -Butyl acrylate
AIBN	2,2'-Azobis(isobutyronitrile)
EDMA	Ethylene dimethacrylate
HEMA	β-Hydroxyethyl methacrylate
DMBA	<i>N,N</i> -Dimethylbenzylamine

Preparation of SINs. In the reaction kettle, epoxy resin and nBA mixture (nBA, cross-linking agent (EDMA), initiator (AIBN; 0.2% of nBA), and inter-cross-linking agent [β -hydroxyethyl methacrylate (HEMA)], where applicable) were blended and then 3% (by weight of the whole system) DMBA was added. After prepolymerizing at 90–95 °C under nitrogen with stirring until one component neared gelation, the prepolymer was placed in a PTFE mold for curing.

All samples were cured at 100 °C for 24 h and post-cured at 120 °C for 4 h. The compositions of all samples are shown in Table II.

Measurements. Swelling Properties. Samples were placed in flasks filled with acetone at 25 °C to swell. Swollen samples were weighed daily until no weight change was detected for 3 continuous days (most samples require about 14 days). This weight was taken as the weight at equilibrium swelling. Then the samples were dried at 80 °C for 24 h under vacuum and weighted again. This weight was taken as the weight of the dry sample. The swelling degree (S) is defined as

$$S = \frac{\text{weight of equilibrium swelling}}{\text{weight of dry sample}}$$

Dynamic Mechanical Properties by Torsion Braid Analysis. Braids coated with prepolymer and cured under the previously described condition were measured with an automatic torsion braid analysis (TBA) system (QNP-1 type produced by No. 8200 Instrumental Factory, Jilin City, China). The sample was initially subjected to a torsion angle and then was allowed to vibrate freely. The damping of free vibration was measured to calculate the loss tangent, $\tan \delta$. The operating frequency was 0.2–10 Hz, the temperature range was 150–400 K, and the heating rate was 3 K/min. The precision of temperature control was ± 1 K. The glass-transition temperature was defined as the maximum peak temperature on the $\tan \delta$ versus temperature (T) curve.

Density Measurement. A density bottle was used to measure the densities of all samples at 20 °C. The density of distilled water at 20 °C ($d^{20} = 1$) was taken as the reference. A density bottle is a bottle with a fixed volume and a capillary tube on its cap to ensure that the bottle can be filled fully with distilled water for every measurement. The weight of the empty bottle is designated by W_0 ; the weight of the bottle filled with distilled water is designated by W_1 . Approximately 8 g of sample was weighed into the bottle; the weight of the bottle plus the sample is designated by W_2 . The bottle that contains the sample is filled with distilled water; the weight of the bottle plus the sample plus the distilled water is designated by W_3 . If the density of distilled water is assumed to be 1.0000 at 20 °C, the density of the sample at 20 °C (d) can be derived:

$$d = \frac{W_2 - W_0}{(W_1 - W_0) - (W_3 - W_2)} \quad (3)$$

Five measurements were carried out for each sample. The data listed in Table III represent the average of the five measurements. The standard error for all samples is ± 3 kg/m³.

Table II. Compositions and Glass-Transition Temperatures

Composition (PnBA:Epoxy)	Cross-Link (%PnBA)	Intercross (%PnBA)	T_g (K)		
			PnBA	Interface ^a	Epoxy
0:100	N/A	N/A	N/A	N/A	361
10:90	0	0	262	—	347
25:75	0	0	258	—	310
50:50	0	0	218	(288)	325
75:25	0	0	221	262	305
100:0	0	0	215	—	—
10:90	0.25	0	282	—	353
25:75	0.25	0	265	288	315
50:50	0.25	0	224	(288)	324
75:25	0.25	0	218	254	307
90:10	0.25	0	217	283	335
100:0	0.25	0	216	—	—
10:90	0.5	0	290	—	346
25:75	0.5	0	230	275	314
50:50	0.5	0	225	(289)	314
75:25	0.5	0	224	—	282
90:10	0.5	0	218	252	290
100:0	0.5	0	217	—	—
10:90	1	0	322	—	356
25:75	1	0	235	275	308
50:50	1	0	234	(290)	317
75:25	1	0	232	284	343
90:10	1	0	223	—	295
100:0	1	0	219	—	—
10:90	2	0	—	346	—
25:75	2	0	280	—	326
50:50	2	0	229	(291)	314
75:25	2	0	225	—	330
90:10	2	0	222	—	330
100:0	2	0	220	—	—
25:75	0.5	0.8	247	—	311
25:75	0.5	1.6	—	302	—

NOTE: Cross-link is the cross-linking density of PnBA; intercross is the intercross-linking density. The initiator of PnBA is 0.3%. The curing agent of epoxy is 3% of the whole system.

^a T_g in parantheses is calculated for 50:50 miscible SINs.

Transmission Electron Microscopy. Transmission electron micrographs were obtained with an electron microscope (Hitachi model H-600). The samples were microtomed and stained with hydrazine and osmium tetroxide vapor, prior to examination.

Results and Discussion

Swelling Behavior. The equilibrium swelling degree of SINs is characteristically smaller than the degree that can be calculated under the assumption of additivity. This discrepancy is caused by the interpenetrations

Table III. Density and Interpenetration

<i>Composition (PnBA:Epoxy)</i>	<i>Cross-Link (%)</i>	d_{exp} (kg/m^3)	d_{th} (kg/m^3)	<i>Epoxy Inter</i>	<i>PnBA Inter</i>
0:100	N/A	1177	1177	N/A	N/A
10:90	0	1192	1168	1.13	10.19
25:75	0	1217	1158	3.23	9.70
50:50	0	1143	1131	1.04	1.04
75:25	0	1126	1107	3.33	1.11
100:0	0	1084	1084	N/A	N/A
10:90	0.25	1204	1169	1.60	14.41
25:75	0.25	1218	1158	3.30	9.89
50:50	0.25	1176	1139	3.15	3.15
75:25	0.25	1139	1119	3.46	1.16
100:0	0.25	1100	1100	N/A	N/A
10:90	0.5	1198	1170	1.31	11.77
25:75	0.5	1213	1159	2.97	8.90
50:50	0.5	1180	1141	3.31	3.31
75:25	0.5	1134	1123	1.94	0.65
100:0	0.5	1105	1105	N/A	N/A
10:90	1	1221	1169	2.38	21.42
25:75	1	1193	1156	2.05	6.16
50:50	1	1210	1136	6.12	6.12
75:25	1	1138	1115	4.04	1.35
100:0	1	1094	1094	N/A	N/A
10:90	2	1226	1169	2.58	23.25
25:75	2	1225	1156	3.76	11.27
50:50	2	1175	1138	3.15	3.15
75:25	2	1123	1118	0.89	0.30
100:0	2	1098	1098	N/A	N/A

NOTE: Inter is the interpenetration degree; cross-link is the cross-linking density of PnBA.

and entanglements between the two networks that increase the cross-linking densities of SINs. Curves of the degree of swelling versus composition for PnBA–epoxy SINs are shown in Figure 1 for different degrees of cross-linking.

From the data in Figure 1, it is obvious that the degrees of swelling in SINs are smaller than the degrees of swelling of the component arithmetic mean at all compositions with all cross-linking densities of PnBA. Another important factor is that for SINs with low PnBA content, S is almost constant and independent of the cross-linking density, whereas S in PnBA changes very sharply with changing cross-linking density.

Because the interpenetrations and entanglements between two networks cannot decrease the swelling degrees so much, we may suppose two reasons for the decrease of swelling degree in SINs.

1. The epoxy network limits the swelling of the PnBA network.
2. The interpenetration and entanglements between the two networks increases the cross-linking densities.

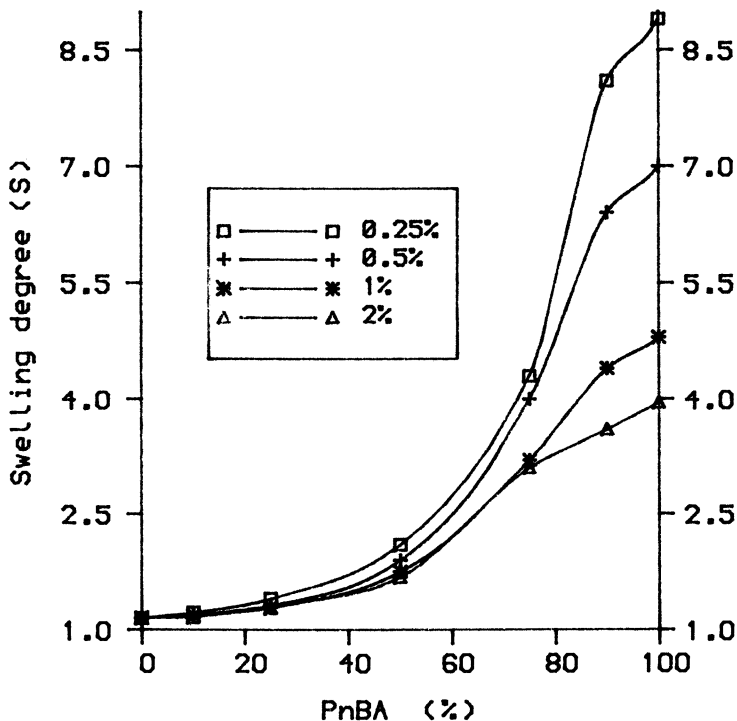
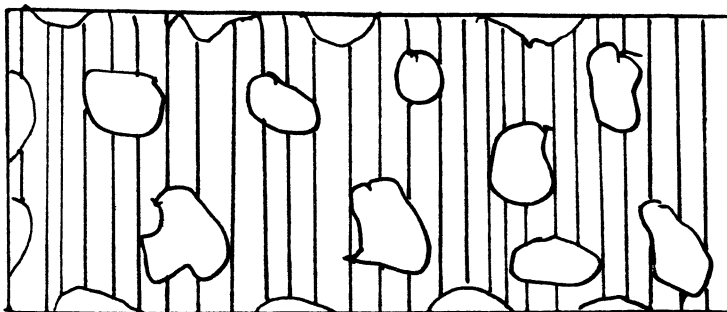


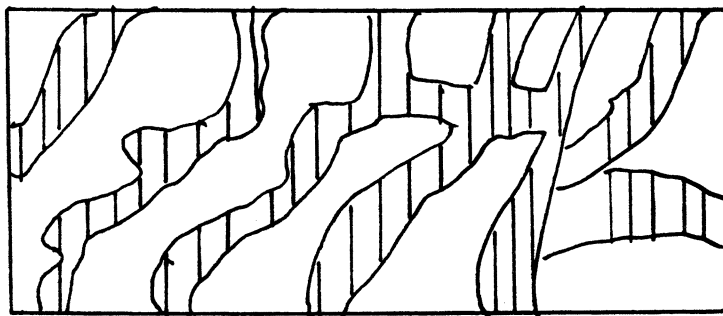
Figure 1. S vs. composition for PnBA-epoxy SINs with different cross-linking density.

These proposals may be described by the models in Figure 2. In SINs with high epoxy content, the epoxy forms the continuous phase and the PnBA is dispersed. Under such conditions, the epoxy network limits the swelling of the PnBA phase domains. PnBA can only swell within the space allowed by the epoxy phase. For these compositions, the swelling degree of the SINs mainly depends on the phase continuity. Thus the swelling degree of SINs must be lower than the degrees calculated as the component arithmetic mean and they change little with cross-linking density of PnBA. An increase in the PnBA content changes the phase continuity of the SINs little by little and the limitation of the epoxy network on the swelling of PnBA decreases.

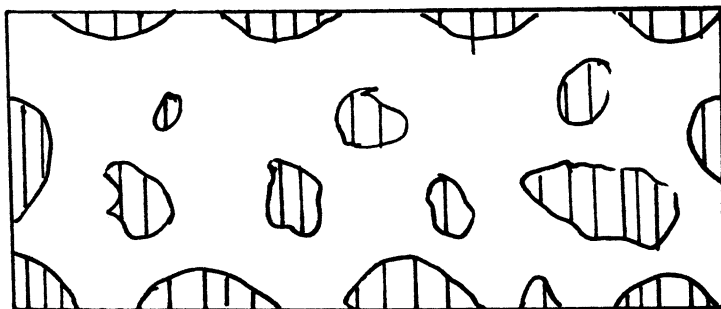
When the PnBA content is 50–75% in SINs, the change of continuity of PnBA in SINs with changing cross-linking density can be seen clearly from Figure 1. In this region, phase reversion occurs; for example, PnBA becomes the continuous phase whereas the epoxy become dispersed. When the cross-linking density of PnBA is 0.25%, the continuity of the PnBA network is poor and the degree of swelling, S , of the PnBA is still largely limited by the epoxy network. With an increase of cross-linking densities, the continuity of



High Epoxy Content



Intermediate Epoxy Content



Low Epoxy Content

Figure 2. Phase models for PnBA-epoxy SINs.

the PnBA network increases and the restraints of the epoxy on the swelling decreases. As the cross-linking density reaches 2%, S is nearly equal to the S of the component arithmetic mean. This near equality indicates that PnBA forms a continuous phase and the epoxy has dispersed. At this point, the swelling degrees of SINs are still lower than the swelling degrees of the component arithmetic mean, which indicates additional physical interaction in the SIN system.

When the PnBA content is 90%, the swelling degree of all SINs is slightly lower than the S of the component arithmetic mean. These results imply that PnBA forms the continuous phase and there are additional interactions between the two networks.

A comparison of these results with the early studies on the swelling of polystyrene-polystyrene IPNs (1, 19, 20) suggests that there are additional interactions between the two networks in PnBA-epoxy systems. The additional interactions may occur because the SINs were synthesized simultaneously via the chain reaction-chain reaction mechanism, whereas the IPNs were synthesized sequentially.

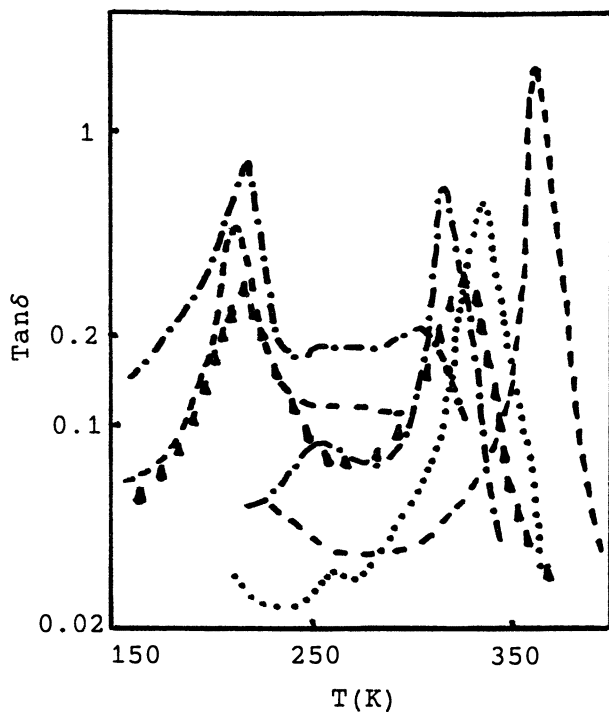
Glass-Transition Behavior. The dynamic mechanical properties of PnBA-epoxy SINs that were measured by TBA are shown in Figures 3-6 (due to the similarity, only part of spectra are shown). The glass-transition temperature, T_g , was taken as the temperature at which the loss tangent, $\tan \delta$, reached maximum. The T_g s are listed in Table II.

The composition of the SINs affects the interaction of the two networks in the system. Like other polymer alloys, the SINs with either high epoxy content or high PnBA content show good miscibility whereas the SINs with intermediate compositions have poor miscibility.

The change of cross-linking density has several effects on these SINs:

1. The increase of cross-linking density decreases the gelation time of PnBA; thus, the relative reaction rate of the two networks changes. As previously mentioned, the relative reaction rate significantly affects interpenetration and entanglements between the two networks.
2. The increase of cross-linking density of PnBA increases the interpenetration and entanglement between the two networks.

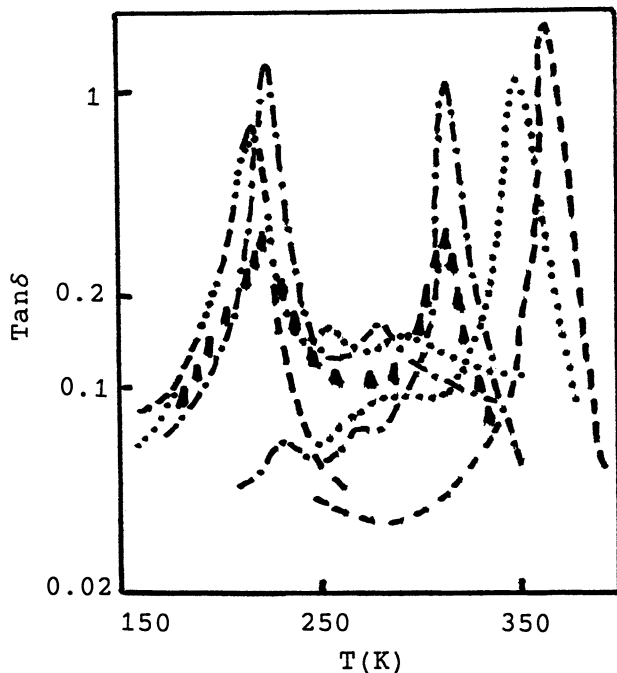
The combination of the preceding two effects leads to the complicated results. Under fixed composition and at high PnBA content, the miscibility between the two networks increases first and then decreases with the increasing cross-linking density of PnBA. At high PnBA content, the epoxy is



PnBA/Epoxy	Line
100/0	-----
90/10
75/25	-.-.-.-
50/50	▲ ▲ ▲
25/75	-.-.-.-
10/90
0/100	-----

Figure 3. TBA curves of PnBA-epoxy semi-SINs.

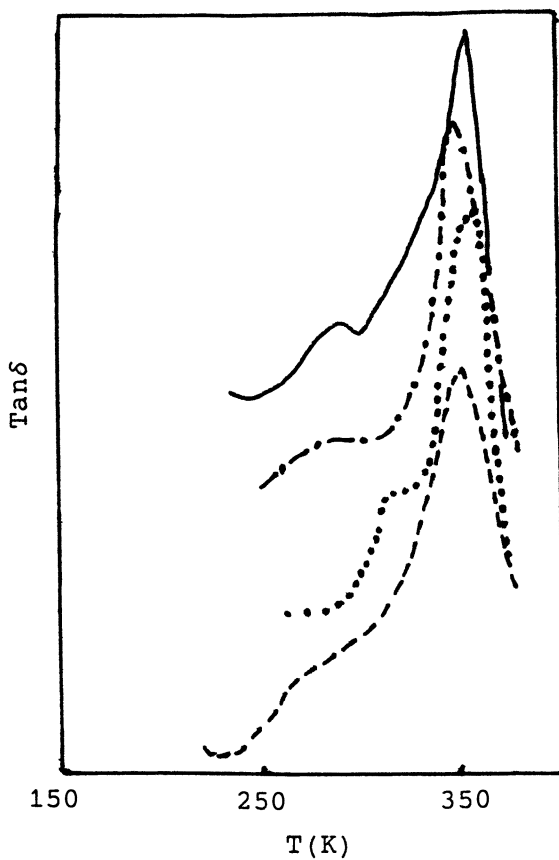
diluted; thus, its gelation time will decrease. With the increase of cross-linking density, PnBA gels quickly. The gelation time difference becomes large and the miscibility in the SINs decreases. Combined with the effect of the corresponding increase of miscibility and cross-linking density, the foregoing result is obtained.



PnBAc/Epoxy	Line
100/0	-----
90/10
75/25	-.-.-.-
50/50	▲ ▲ ▲
25/75	-.-.-.-
10/90
0/100	-----

Figure 4. TBA curves of 0.5% cross-linked PnBA-epoxy SINs.

At higher epoxy content, PnBA is diluted and gels slowly. With the increase of cross-linking density, the gelation time of PnBA decreases; thus, the gelation time difference of the two networks decreases. Therefore, the miscibility in SINs continuously improves with the increase in cross-link density of PnBA. Figure 5 shows the TBA curves of PnBA:epoxy = 10:90



Crosslinking density (%)	Line
0.25	—————
0.5
1	-----
2	- . - . - .

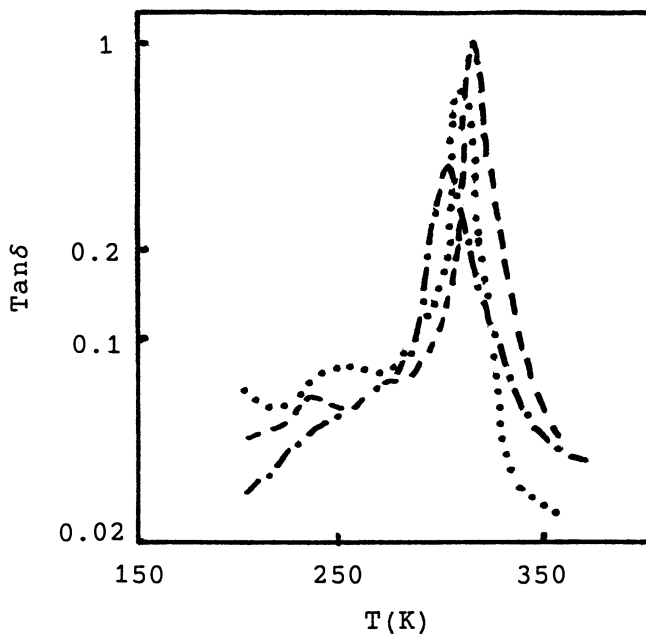
Figure 5. TBA curves of PnBA:epoxy = 10:90 SINs with different cross-linking density of PnBA.

SINs with different cross-linking density of PnBA. Clearly the two transition peaks become closer with the increase of cross-linking density of PnBA. The two peaks finally merge when the cross-linking density of PnBA is 2%.

In all cases the full SIN systems have better miscibility than semi-SIN systems.

Generally SINs are partially miscible systems, but for 2% cross-linked PnBA:epoxy = 10:90 SINs, there is a single glass-transition peak, which indicates that the SIN system has become miscible on a supermolecular scale due to the large amount of interpenetration and entanglements between the two networks.

Figure 6 shows TBA curves of 0.25% cross-linked PnBA-epoxy SINs with different degrees of intercross-linking. The miscibility in SINs increases



Intercross linking Density (%)	Line
0	-----
0.8
1.6	-.-.-.-

Figure 6. TBA curves of 0.25% cross-linked PnBA:epoxy = 25:75 SINs with different degrees of intercross-linking density.

with increasing intercross-linking levels, and at high levels of intercross-linking, the SIN systems become miscible on a supermolecular scale. A comparison of the preceding two cases easily reveals the similarity of the mechanisms by which chemical intercross-linking and physical interpenetration and entanglements increase the miscibility in SIN systems.

A very special characteristic of these SINs is the existence of a third transition peak for 25:75 and 75:25 compositions PnBA–epoxy. Studies on polyurethane–polystyrene IPNs by Lipatov et al. (21) used the inverse gas chromatography method to obtain an intermediate transition peak. The transition is believed to be the true interpenetrating or intermediate region at the interface between the two networks.

The T_g s of miscible PnBA:epoxy = 50:50 SINs that are calculated from the following equation are listed in Table II in parentheses:

$$T_g = T_{g1} \times \Phi_1 + T_{g2} \times \Phi_2 \quad (4)$$

where T_{g1} is the glass-transition temperature of PnBA, Φ_1 is the volume fraction of PnBA, T_{g2} is the glass-transition temperature of epoxy, and Φ_2 is the volume fraction of epoxy.

Note that the glass-transition temperatures of the third peak are very near the temperatures calculated from composition 50:50, and it is reasonable to believe that the third glass-transition peak comes from the real interpenetration interface between the two networks. Therefore, the SINs made from two chain reactions tend to produce an interphase region.

To facilitate a comparison of the SINs from different combinations (either chain reaction–chain reaction or chain reaction–step reaction), the glass-transition temperatures of PnBA–epoxy SINs for different mechanism combinations are listed in Table IV.

The data in Table IV clearly show that SINs from bichain reactions have better miscibility than SINs from chain reaction–step reaction combinations in two respects:

1. The glass-transition temperature of SINs from the bichain reaction move inward more than SINs from the chain reaction–step reaction combination.
2. There is a third transition peak for some SINs from the bichain reactions; that is, the real interpenetration between the two networks has formed.

Density and Interpenetration. The densities of PnBA–epoxy SINs are listed in Table III. Figure 7 is a plot of density versus composition of 0.5% cross-linked PnBA–epoxy SINs (with error bar). The densities of SINs clearly are higher than densities calculated from the component arithmetic mean.

Table IV. Comparison of T_g s of PnBA-Epoxy SINs from Different Reaction Combinations

Composition (PnBA:Epoxy)	C_1 (%)	I (%)	C_2 (%)	T_g (K)		
				PnBA	Interface	Epoxy
25:75 ^a	0	0.2	3 ^b	258	—	310
25:75 ^a	0.25	0.2	3 ^b	265	288	315
25:75 ^a	0.5	0.2	3 ^b	230	275	314
50:50 ^a	1	0.2	3 ^b	235	275	308
75:25 ^a	2	0.2	3 ^b	280	—	326
100:0 ^c	1.6	0.16	31.1 ^d	219	—	358
10:90 ^c	1.6	0.24	31.1 ^d	219	—	348
25:75 ^c	1.6	0.4	31.1 ^d	219	—	362

NOTE: C_1 is the cross-linking density of PnBA, I is the initiator level of PnBA, and C_2 is the curing agent level of epoxy.

^a Results from this work. Epoxy resin was cured by chain reaction.

^b Percentage of the whole system.

^c From Figure 9 in reference 13. Epoxy resin was cured by step reaction.

^d Percentage of the epoxy.

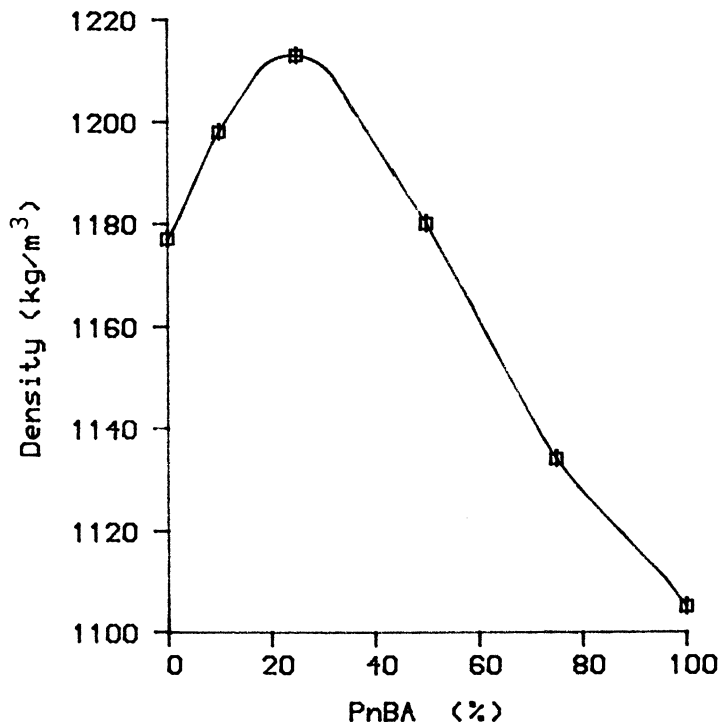


Figure 7. The density of 0.5% cross-linked PnBA-epoxy SINs.

Studies conducted by Millar (1) and Kim et al. (22) revealed a density increase after the formation of IPNs but studies by Shibayama and Suzuki (20), Klemmner et al. (23), and Lipatov et al. (24) reported no density difference before or after the IPN formation. Because of the relationship between increasing density and the interpenetration and entanglements between the two networks in the IPN system, extensive interpenetration and entanglements would lead to increased density after formation of the SINS. Several factors, such as chemical miscibility, synthetic method, and reaction kinetics, effect the interpenetration and entanglements. Thus it is natural that different results are obtained for different systems. For our work, where the SINS were simultaneously synthesized from two chain reactions, significant amounts of interpenetration and entanglements have occurred, and there are clear density increases in the SINS.

Based on the concept that density increase results from the interpenetration and entanglements between two networks, the degree of interpenetration and entanglements can be estimated from the density difference.

Suppose that interpenetration and entanglements are the same for both networks; for example, both networks have the same number of chains interpenetrated and entangled with each other. Then suppose that interpenetration chains and entanglements chains have no volume. Thus

$$\text{inter} = \delta d / (2Cd_{\text{exp}})$$

where inter is the degree of interpenetration and entanglements, $\delta d = d_{\text{exp}} - d_{\text{th}}$, $d_{\text{th}} = C_1d_1 + C_2d_2$, and C is the composition. d_1 and d_2 are densities of two separate components.

The results are shown in Table III. To confirm the results, the values have been compared with dynamic mechanical results. In a previous paper (15), M , the degree of inward shift of the glass-transition temperature, was used to characterize the miscibility of SINS:

$$M = \frac{(T_{g2\text{pure}} - T_{g1\text{pure}}) - (T_{g2\text{insin}} - T_{g1\text{insin}})}{T_{g2\text{pure}} - T_{g1\text{pure}}}$$

where $T_{g1\text{insin}}$ denotes the T_g of SIN that reflects the contribution of that component.

Figure 8 shows $(1 - M)$ versus inter-PnBA curve for PnBA:epoxy = 10:90 SINS. With increasing degree of interpenetration and entanglements, the miscibility of the two networks increases. Thus the inward shift of the glass-transition temperature (M) increases. When the degree of interpenetration and entanglements is high enough, the system is miscible on a supermolecular level and the degree of inward shift of the glass transition temperature reaches 1. Results from two methods agree very well and lead us

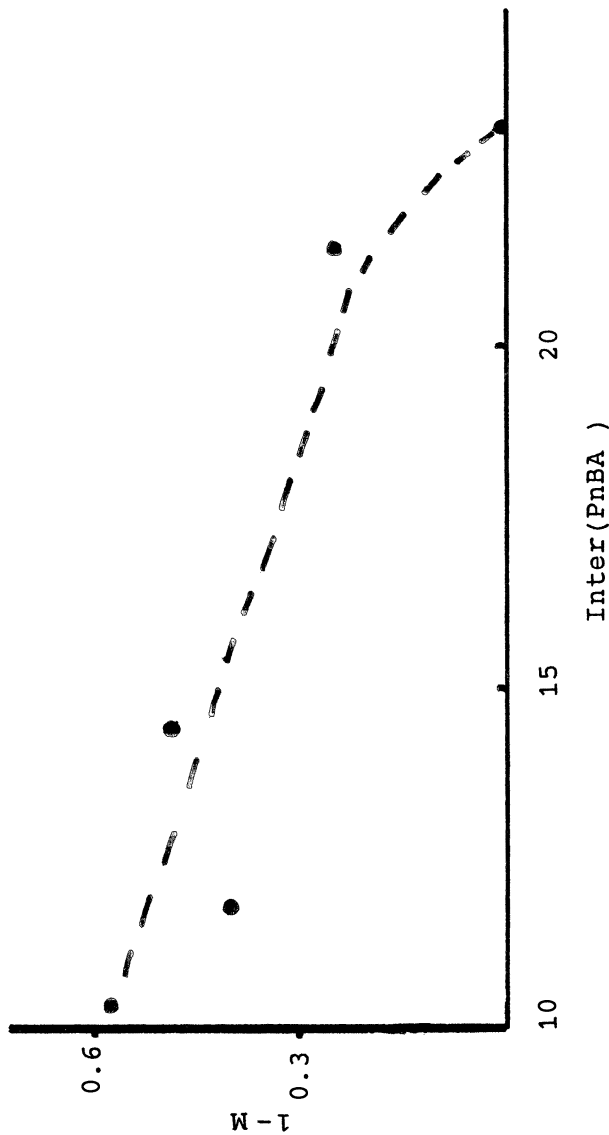


Figure 8. Coordination of TBA and density results for PnBA-epoxy SINs.

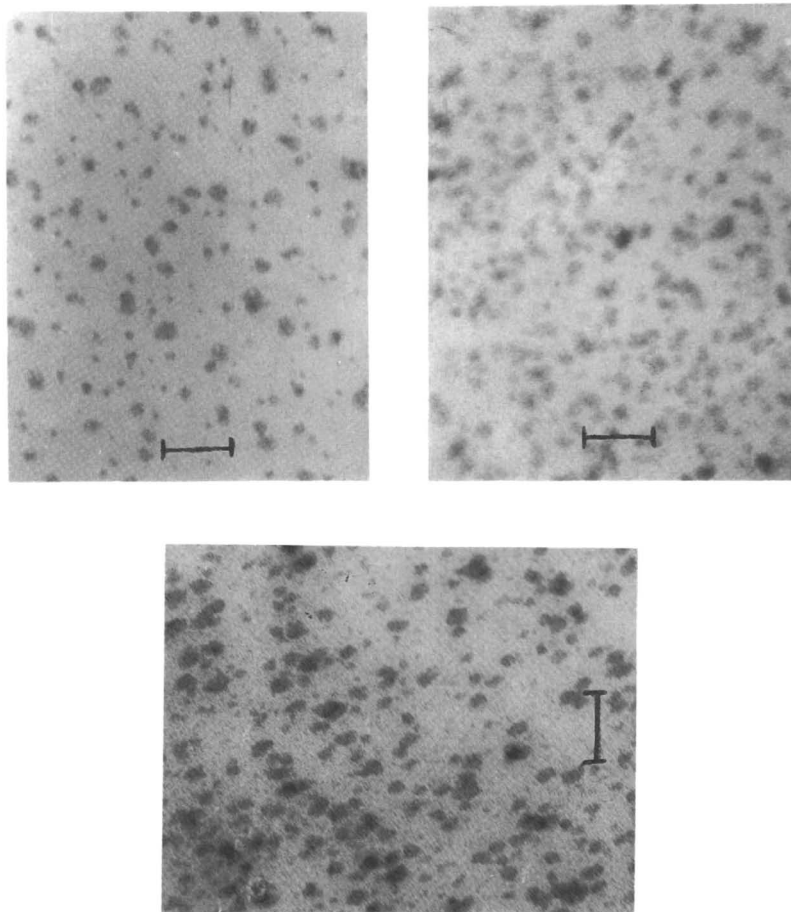


Figure 9. Transmission electron micrographs of PnBA-epoxy semi-SINs: 1, 25:75; 2, 50:50; 3, 75:25. The bar represents 100 nm.

to conclude that estimation of the degree of interpenetration and entanglements from the density increase is reasonable here.

TEM Morphology. TEM photographs (see Figure 9) show that PnBA-epoxy SINs have two-phase structure, but the phase domains are very fine and the phase boundary is not clear. With high epoxy content, the epoxy forms the continuous phase and PnBA forms phase domains which ~ 25 nm in size. At intermediate composition, the epoxy is still more continuous. When PnBA content reaches 75%, it forms the continuous phase. These results agree with results from the swelling degree experiment.

Summary

SINs synthesized from the bichain reaction combination tend to produce more interpenetration and entanglements between the two networks compared with SINs synthesized from the chain reaction-step reaction combination.

The PnBA-epoxy SIN is a partially miscible system. Composition and cross-linking density of PnBA both affect the miscibility of the SINs. A third phase occurs for some SINs and this third phase is believed to be the real interpenetration between the two networks. The system is miscible on a supermolecular level for 2% cross-linked PnBA:epoxy = 10:90 SINs.

Both morphology (phase behavior) and interpenetration and entanglement between the two networks affect the swelling behavior of PnBA-epoxy SINs.

The density of SINs increases after formation. The degree of interpenetration estimated from the density difference agrees with TBA results.

Chain reaction-chain reaction (bichain) combination SINs would be useful to increase the miscibility in partially miscible system.

References

1. Millar, J. R. J. *Am. Chem. Soc.* **1960**, *82*, 1311.
2. Sperling, L. H.; Friedman, D. W. *J. Polym. Sci., Polym. Chem. Ed.* **1969**, *1*, 425.
3. Frisch, H. L.; Klempner, D.; Frisch, K. C. *Polym. Lett.* **1969**, *7*, 775.
4. Sperling, L. H.; Arnts, R. R. *J. Appl. Polym. Sci.* **1971**, *15*, 2317.
5. Huelck, V.; Thomas, D. A.; Sperling, L. H. *Macromolecules* **1976**, *9*, 671.
6. Suzuki, Y.; Frijimoto, T.; Tsunoda, S.; Shibayama, K. *J. Macromol. Sci., Phys.* **1980**, *B17*, 787.
7. Park, I. H.; Lee, J. H.; Kim, S. C. *Polym. Bull.* **1983**, *10*, 126.
8. Frisch, H. L.; Klempner, D.; Yoon, H. K.; Frisch, K. C. In *Polymer Alloys II*; Klempner, D.; Frisch, K. C., Eds.; Plenum: New York, 1980.
9. Frisch, H. L.; Klempner, D.; Yoon, H. K.; Frisch, K. C. *Macromolecules* **1980**, *13*, 1016.
10. Olabisi, O.; Roberson, L. M.; Shaw, M. T. *Polymer-Polymer Miscibility*; Academic: New York, 1979.
11. Sperling, L. H. *Interpenetrating Polymer Networks and Related Materials*; Plenum: New York, 1981.
12. Sperling, L. H. *J. Polym. Sci., Macromol. Rev.* **1977**, *12*, 141.
13. Touhsaent, R. E.; Thomas, D. A.; Sperling, L. H. *J. Polym. Sci., Polym. Lett. Ed.* **1974**, *46*, 175.
14. Frisch, K. C.; Klempner, D.; Frisch, H. L. *Polym. Eng. Sci.* **1982**, *22*, 1143.
15. Ma, S.; Zhang, J.; Li, Y.; Zhang, D.; Tang, X. In *Advances in Interpenetrating Polymer Networks*; Klempner, D.; Frisch, K. C., Eds.; Technomic: Lancaster, PA, 1988; Vol. 1, p 21.
16. Potter, W. G. *Epoxide Resin*; The Plastics Institute: London, 1970.
17. Touhsaent, R. E.; Thomas, D. A.; Sperling, L. H. In *Toughness and Brittleness of Plastics*; Deanin, R. D.; Crugnola, A. M., Eds.; Advances in Chemistry 154; American Chemical Society: Washington, DC, 1976.

18. Ma, R. T.; Ma, S. *Gaodeng Xiuxiao Huaxiu Xiubao* **1985**, 6, 1036.
19. Siegfired, D. L.; Manson, J. A.; Sperling, L. H. *J. Polym. Sci., Polym. Phys. Ed.* **1978**, 16, 583.
20. Shibayama, K.; Suzuki, K. *Kobunshi Kagaku* **1966**, 23, 24.
21. Lipatov, Yu. S.; Chramova, T. S.; Sergeva, L. M. *J. Polym. Sci., Polym. Chem. Ed.* **1977**, 15, 427.
22. Kim, S. C.; Klempner, D.; Frisch, K. C.; Frisch, H. L. *Macromolecules* **1976**, 9, 263.
23. Klempner, D.; Frisch, K. C.; Frisch, H. L. *J. Polym. Sci., Polym. Chem. Ed.* **1970**, 8, 921.
24. Lipatov, Yu. S.; Sergeva, L. M.; Mozzukhina, L. M.; Apukhtina, N. P. *Vysokomol. Soedin., Ser. A* **1974**, 16, 2290.

RECEIVED for review November 11, 1991. ACCEPTED revised manuscript November 2, 1992.

Glass-Fiber Composites from Polyurethane and Epoxy Interpenetrating Polymer Networks

K. H. Hsieh¹, S. T. Lee¹, D. C. Liao¹, D. W. Wu¹, and C. C. M. Ma²

¹ Department of Chemical Engineering, National Taiwan University, Taipei 106, Taiwan

² Department of Chemical Engineering, National Tsing Hua University, Hsin-Chu 300, Taiwan

Unidirectional glass-fiber-reinforced composites of polyurethane-cross-linked epoxy and polyurethane-epoxy interpenetrating polymer network with polyurethane (PU) grafted on epoxy (graft-IPN) were prepared and their mechanical properties were investigated. The tensile strength of the PU-cross-linked epoxy or the PU-epoxy graft-IPN was significantly increased in the longitudinal direction but decreased in the transverse direction. The effect of PU content in the matrix on the tensile strength of the composites is not significant. The Izod impact strength of these composites was greatly improved by the addition of glass fiber in either the transverse or longitudinal direction. The values of impact strength strongly increased with increasing PU content, especially for transverse direction properties.

THE USE OF FIBER-REINFORCED POLYMERIC COMPOSITES for engineering applications has grown rapidly over the past few decades. Many signs indicate that this trend will continue. The elements that influence the mechanical properties of composites are the fibers and their orientation, the resin, and the interface adhesion between the fibers and the resin. Epoxy resins, which are associated with high modulus and strength, have been employed in

high-performance structural composites. However, such resins suffer from low fracture strength and brittle behavior (1); therefore, applications are often limited by the low mechanical properties.

To meet required end-use performance, the epoxy resin must be modified with either thermoplastics (2, 3) or conventional rubber or elastomers. Only recently, interpenetrating polymer networks (IPNs) have been considered for such application. The IPN structure is generally a network form with both polymer components cross-linked (4–6). The permanent entanglements and interlocking between the networks reduces the phase separation (for two incompatible polymers) and enhances the mechanical properties and compatibility (7). In material technology, the term “compatibility” often is used to describe whether desirable or beneficial properties occur when polymer mixtures are blended (8). The two glass transition temperatures of two polymers shift to the intermediate range if the mixture polymers are compatible (9).

In our previous work (10–13), polyurethane–cross-linked epoxy resin based on diglycidyl ether of bisphenol A with epoxy equivalent weight (EEW) of 186 (epoxy) and graft–interpenetrating polymer networks of various types of polyurethane (PU) and epoxy were synthesized and their characteristics were investigated. The results showed that epoxy was significantly toughened and exhibits maximum values of tensile strength. The intensity of the loss modulus (E'') peaks of PU–cross-linked epoxy increased when the polyester-type PU(PU(PBA)) [where PBA is poly(butylene adipate) glycol] was employed. Single-phase morphology was formed in the PU(PBA)–cross-linked epoxy, whereas the epoxy cross-linked with the polyether-type PU(PU(PPG)) [where PPG is poly(propylene oxide) glycol] exhibited a two-phase morphology with the PU particles dispersed in the epoxy matrix. Two distinct E'' peaks were observed: one at a high temperature of 107 °C (alpha transition) and the other at a low temperature of –73 °C (beta transition) for the pure epoxy. For the graft–IPNs based on PU (PBA), the alpha transition peaks shifted to lower temperatures and the intensity of the beta transition peaks decreased. Furthermore, the PU (PBA)-based graft–IPNs showed lower alpha transition temperatures as compared with the PU (PPG)-based graft–IPNs. This difference suggests that the PU(PBA) has better compatibility with the alpha transition domain of the epoxy than does the PU(PPG). The morphological micrographs of the PU(PBA)–epoxy graft–IPNs showed a homogeneous system (one phase), whereas the PU(PPG)–epoxy showed a heterogeneous morphology (phase separation) with rubber particles dispersed in the matrix. Interpenetrating polymer networks now are considered for use in composites because of their outstanding matrix toughness.

In the present work, the polyurethane-modified epoxy system is employed as the composite matrix. The polyurethane–cross-linked (PU–cross-linked) epoxy and PU–grafted epoxy IPN (graft–IPN) were prepared and

used as the matrix for the unidirectional glass-fiber composite. The effect of various matrix properties on the mechanical properties of the composites will be investigated and discussed.

Experimental Details

Materials. The materials required and their designations are listed in Table I. Poly(propylene oxide) glycol with molecular weights 400 (PPG400) and 1000 (PPG1000), and poly(butylene adipate) glycol with molecular weight 1000 (PBA1000) were used as polyols; trimethylolpropane (TMP) and 1,4-butanediol (1,4-BD) were used as the cross-linking agent and chain extender, respectively. 4,4'-Diphenylmethane diisocyanate (MDI) was used as the isocyanate for PU preparation. Diglycidyl ether of bisphenol A with epoxy equivalent weight (EEW) of 186 (epoxy) was employed for this study, and 2,4,6-tris(dimethylaminomethyl)-phenol (TDMP) was used as catalyst for the epoxy. Polyols, TMP, 1,4-BD, and epoxy were continuously stirred and degassed overnight at 60 °C in a flask before use. MDI and catalyst TDMP were employed as received.

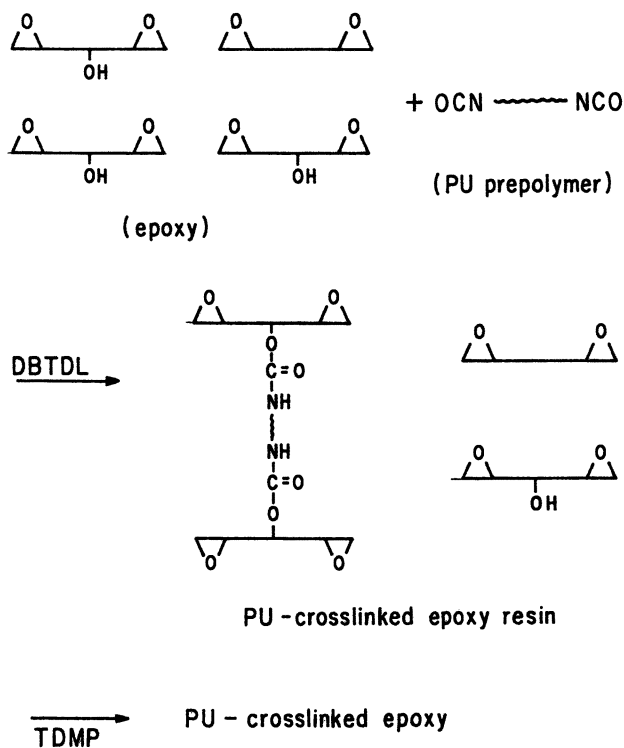
Preparation of Polyurethane Prepolymers. To prepare PU prepolymers, two equivalents of MDI were charged into a reaction kettle and heated until molten at ~55 °C. Then one equivalent of polyol was added and mixed with the molten MDI. The mixture was vigorously agitated by a mechanical stirrer. The reaction took place under dry nitrogen atmosphere at a temperature of 68 °C. When the —NCO content, which was determined by the di-*n*-butylamine titration method (14), reached the theoretical value, the reaction was stopped.

Table I. Materials

<i>Designation</i>	<i>Description</i>	<i>Source</i>
PPG400	Poly(propylene oxide) glycol; MW = 400	Chiun Glong Co.
PPG1000	Poly(propylene oxide) glycol; MW = 1000	Chiun Glong Co.
PBA1000	Poly(butylene adipate) glycol; MW = 400	Tai Chin Chem. Industry Co. Ltd.
MDI	4,4'-Diphenylmethane diisocyanate	Bayer Chemical Co.
1,4-BD	1,4-Butanediol	Hayashi Pure Chem.
TMP	Trimethylolpropane	Hayashi Pure Chem.
Epoxy	Diglycidyl ether of bisphenol A; EEW = 186	Dow Chemical Co.
TDMP	2,4,6-Tris(dimethylaminomethyl)-phenol	Merck Chemical Co.
Glass fiber	Unidirectional E-glass fiber	Kyntex Inc.
DBTDL	Dibutyltin dilaurate	Merck Chemical Co.

Preparation of PU-Cross-Linked Epoxy. Epoxy was put into a reaction kettle. Dried nitrogen gas was blown into the reaction kettle to remove both the air and the moisture present in the kettle. A suitable amount of PU prepolymer was then poured into the kettle to mix with epoxy. The temperature was maintained at 68 °C. Several drops of dibutyltin dilaurate (DBTDL), approximately 0.02 wt% based on the weight of the PU prepolymer, was added and vigorously agitated with the mixture to accelerate the reaction for several hours. Afterward, a sample was taken to detect the —NCO group at 2270 cm^{-1} in the infrared (IR) spectrum until the —NCO absorption peak disappeared.

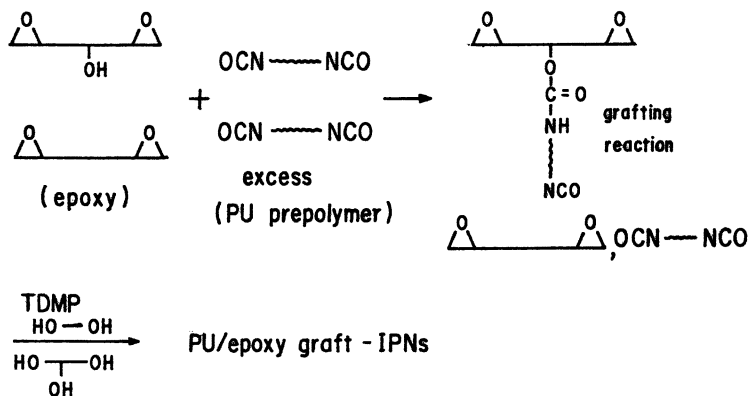
The PU-cross-linked epoxy has the following reaction:



To cure the PU-cross-linked epoxy, a suitable amount of PU-cross-linked epoxy was placed in a cup into which 3 phr (parts per hundred parts of resin by weight) of curing agent (TDMP) was added, vigorously stirred, and drafted for several minutes to eliminate all the bubbles produced in the course of agitation. After the bubbles were removed, the reaction mixture was poured into a mold for the preparation of composites.

Preparation of PU-Epoxy Graft IPNs. The preparation of PU-epoxy graft-IPNs was carried out in two steps. The first step involved the reaction of an excess of PU prepolymer with epoxy resin in the reaction kettle. Because the concentration of the —NCO groups exceeds the equivalent —OH groups in the

epoxy resin, the grafting reaction took place at 68 °C as follows:



A sample of the reacting mixture was taken every hour for IR analysis. The ratio of the absorption peak of the —NCO group (2270 cm^{-1}) to that of the epoxide group (920 cm^{-1}) decreased during the reaction course and eventually became a constant value. This stabilization indicates that the pendant secondary hydroxyl groups in the epoxy completely reacted with the —NCO group of the PU prepolymer. The use of excess PU prepolymer resulted in unreacted —NCO groups in the mixture. Thereafter, 2 wt% of TDMP based on the epoxy resin and a stoichiometric amount of 1,4-BD-TMP mixture at an equivalent ratio of 4:1 were added to the mixture. After mechanical agitation and degassing for 30 s, the reaction mixture was poured into a mold for the preparation of composites.

Preparation of PU-Epoxy Composites. The composites reinforced by glass fiber were prepared by a hand lay-up fabrication technique in a mold. Eight layers of unidirectional glass fiber were placed in the mold; then the resin mixture was poured uniformly over the reinforcement. After degassing for 5 min, the resin mixture was pressed and cured at 80 °C and the molding pressure was increased to approximately 14 MPa for 2 h. Finally, the samples were postcured at 120 °C for 6 h.

Testing Methods. Stress-strain and flexural strength were measured using a tensile tester (Tensilon mode TCF-RC, Yashima Works Ltd., Japan). The test procedure for stress-strain followed ASTM D-638 with a crosshead speed of 10 mm/min, and at least five specimens were taken for the test. Flexural strength was measured by following ASTM D-790 with a crosshead speed of 1.3 mm/min and a sample size of $80 \times 25 \times 32$ mm.

The Izod impact strength of the composites was measured according to ASTM D-256.

Dynamic mechanical analysis (DMA) was performed on a DMA unit (DuPont 983) with an operating temperature range from -100 °C to 250 °C. The heating rate was set as 5 K/min. The sample size was approximately $60 \times 10 \times 2$ mm.

The mechanical properties measured for all the composite samples in the longitudinal and transverse directions are listed in Tables II through VI.

Table II. Tensile Strength of PU–Cross-Linked Epoxy Composites

Sample	(NCO:OH) Equivalent Ratio	PU (wt%)	Tensile Strength (MPa)		
			Neat Resin	Transverse Direction	Longitudinal Direction
PU(PPG400)–epoxy	0:100	0	55	26	412
	30:100	4	74	17	340
	50:100	6	61	29	337
	80:100	10	66	27	331
	100:100	12	61	47	414
PU(PPG1000)–epoxy	0:100	0	55	26	412
	30:100	6	58	34	323
	50:100	10	76	27	409
	80:100	15	79	25	313
	100:100	19	70	27	305
PU(PBA1000)–epoxy	0:100	0	55	26	412
	30:100	6	53	27	394
	50:100	10	70	31	414
	80:100	15	54	35	441
	100:100	19	40	40	443

Table III. Izod Impact Strength of PU–Cross-Linked Epoxy Composites

Sample	(NCO:OH) Equivalent Ratio	PU (wt%)	Impact Strength (k_j/m)		
			Neat Resin	Transverse Direction	Longitudinal Direction
PU(PPG400)–epoxy	0:100	0	0.92	236	8
	30:100	4	1	297	7.85
	50:100	6	0.86	426	8.18
	80:100	10	0.87	313	8.99
	100:100	12	0.9	360	8.32
PU(PPG1000)–epoxy	0:100	0	0.92	236	8
	30:100	6	0.96	339	6.26
	50:100	10	0.92	452	8.2
	80:100	15	0.88	343	11.7
	100:100	19	0.85	391	8.57
PU(PBA1000)–epoxy	0:100	0	0.92	236	8
	30:100	6	1.47	360	10
	50:100	10	1.61	421	10.1
	80:100	15	1.54	489	10.2
	100:100	19	1.51	349	8.1

Results and Discussion

Stress–Strain Properties. As shown in Figures 1 and 2, the tensile strength changes along with increasing PU content in the PU–epoxy matrix. The broken marks on the curves are the PU–epoxy compositions where the pendant hydroxyl group of the epoxy is stoichiometrically equivalent to the

Table IV. Flexural Strength of PU–Cross-Linked Epoxy Composites

Sample	(NCO:OH) Equivalent Ratio	PU (wt%)	Flexural Strength (MPa)	
			Transverse Direction	Longitudinal Direction
PU(PPG400)–epoxy	0:100	0	513	52
	30:100	4	642	54
	50:100	6	658	53
	80:100	10	564	48
	100:100	12	750	51
PU(PPG1000)–epoxy	0:100	0	513	52
	30:100	6	481	48
	50:100	10	611	66
	80:100	15	519	57
	100:100	19	526	58
PU(PBA1000)–epoxy	0:100	0	513	52
	30:100	6	513	51
	50:100	10	731	56
	80:100	15	705	62
	100:100	19	794	52

Table V. Tensile Strength and Izod Impact Strength of PU–Epoxy Graft–IPN Composites

Sample	PU		Tensile Strength (MPa)			Impact Strength (k_j/m)		
	Content prh	wt%	Neat Resin	Transverse Direction	Longitudinal Direction	Neat Resin	Transverse Direction	Longitudinal Direction
PPG400- based	—	0	42	26	412	0.84	236	8
	5	16	72	37	336	1.02	420	8.6
	10	19	80	44	341	1.09	418	8.6
	15	22	80	38	380	1.18	409	7.1
PPG1000- based	—	0	42	26	412	0.84	236	8
	5	22	53	38	315	0.92	426	8.2
	10	25	54	28	316	0.93	360	9
	15	27	65	27	301	0.96	344	8.1
PBA1000- based	—	0	42	26	412	0.84	235	8
	5	22	76	41	287	1.23	400	8.2
	10	25	80	40	329	1.23	400	8.3
	15	27	78	34	428	1.26	380	11

Table VI. Flexural Strength of PU-Epoxy Graft-IPN Composites

Sample	PU Content phr wt%		Flexural Strength (MPa)	
			Transverse Direction	Longitudinal Direction
PPG400-based	—	0	513	52
	5	16	702	49
	10	19	717	59
	15	22	721	57
PPG1000-based	—	0	513	52
	5	22	549	50
	10	25	458	40
	15	27	444	39
PBA1000-based	—	0	513	52
	5	22	747	60
	10	25	639	56
	15	27	641	48

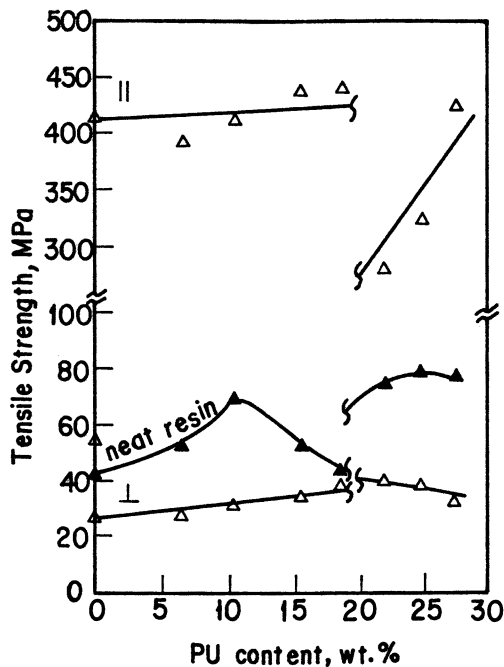


Figure 1. Effect of PU(PBA1000) content in PU-epoxy matrix on the tensile strength of composites. Key: Δ , PU(PBA1000)-epoxy composites; \blacktriangle , PU(PBA1000)-epoxy neat resin.

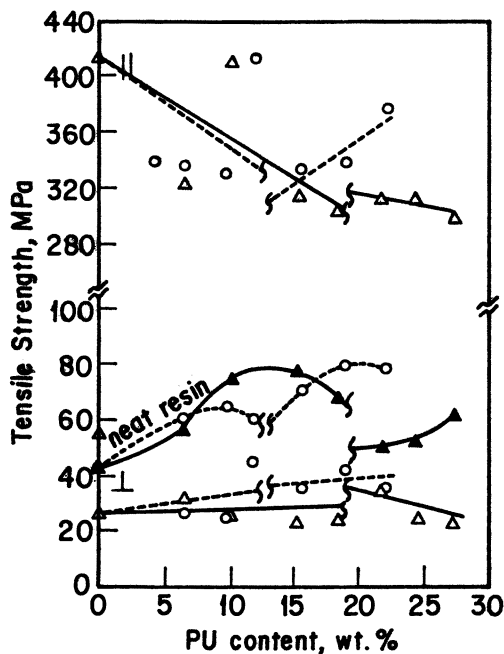


Figure 2. Effect of PU(PPG) content in PU-epoxy matrix on the tensile strength of composites. Key: ○, PU(PPG400)-epoxy composite; △, PU(PPG1000)-epoxy composites; ▲, PU(PPG1000)-epoxy neat resin.

isocyanate group of the PU prepolymer. If a sufficiently strong fiber-matrix bonding exists for the unidirectional composites, the modulus equation of the composite from the rule of mixture can be derived. However, the fiber should possess a much higher modulus than the matrix and the fiber content is generally controlled at about 60–65% (9). Therefore, when a longitudinal stress is applied to a fiber-reinforced composite, the fibers bear the major part of the stress. Thus, the resin matrix transfers the stress and binding between the fiber and the matrix. This transference is well illustrated in Figures 1 and 2, where the longitudinal tensile strength of the composites is much higher than the tensile strength of the neat resin.

The longitudinal tensile strength of the PU(PBA1000)-epoxy composites increases rapidly with an increase of PU content in the matrix for the PU-cross-linked epoxy composites and increases significantly for the PU-epoxy graft-IPN composites. This increase indicates that the contribution of matrix modification should not be neglected. The cross-linking and interpenetrating structure in the resin matrix result in an increase of tensile strength of PU-cross-linked epoxy and PU-epoxy graft-IPN matrix as in the previous study (10–13). The cross-linking reaction between the PU prepolymer and the pendant hydroxyl group in the epoxy actually contributes to the

soft characteristics of the PU as well as to the cross-linking structure of the epoxy. The tensile strength can be increased by the cross-linking structure (cross-linking effect) and decreased by the introduction of more or longer soft segments of the PU (softening effect). Compared to the tensile strength of the neat resin with its corresponding composites, the longitudinal tensile strength of the PU(PBA1000)–epoxy composite jumps to a high value of 400 MPa when the glass fiber is introduced and then gradually increases, similar to the neat resin, with an increase of PU content in the matrix for the PU–cross-linked epoxy (PU content below the broken mark) composite as shown in Figure 1.

For the PU(PBA)–epoxy matrix, the cross-linking effect of the epoxy matrix cross-linked by the PU(PBA) on the longitudinal tensile strength of the composite plays a more important role than the softening effect of the PU(PBA) soft segment. The higher cross-linking density of the matrix provides a stronger tensile strength and adhesion property with the glass fiber of the PU(PBA)–epoxy composite. On the other hand, as shown in Figure 2, the longitudinal tensile strength decreases with an increase of PU(PPG) content in the matrix for the PU(PPG)–cross-linked epoxy composite, although the higher cross-linking density of the PU(PPG400)–cross-linked epoxy was in the matrix. The morphology from scanning electronic microscopy (SEM) in previous work (13) showed that the PU(PPG)–epoxy is a two-phase system with PU(PPG) particles dispersed in the epoxy matrix. This observation implies that the morphology of the matrix can significantly change the longitudinal tensile strength of the corresponding glass-fiber composite. Although the two-phase morphologies are toughened for the neat resin, they tend to decrease the longitudinal tensile strength of the resultant composites. As discussed before, the PU(PBA)–epoxy matrix is a one-phase morphology in SEM (13) and, therefore, results in a great increase of composite strength as expected.

The irregular changes in the longitudinal tensile strength of the composites as shown in Figure 2 for the PU(PPG)–cross-linked epoxy composites are probably a result of the phase-separated matrix, which might easily interfere with the fibers during preparation. Furthermore, the longitudinal tensile strength of the PU(PPG1000)–epoxy graft–IPN composite is lower than that of the PU(PPG400)–epoxy graft–IPN composite. The longitudinal tensile strength of the PU(PPG1000)–epoxy graft–IPN composites decreases, but that of the PU(PPG400)–epoxy graft–IPN composites increases as the PU content increases. This observation points out that the long soft segment of the PU in the polymeric networks will reduce the longitudinal tensile strength of the composite; that is to say, the softened matrix has a lower ability to transfer stress from one fiber to another. The foregoing observation also shows that the lower the molecular weight of polyol in PU, the higher the compatibility between the PU and epoxy.

The observed tensile strength in the transverse direction of the PU–cross-linked epoxy or the PU–epoxy graft–IPN composites was lower

than the tensile strength of the neat resin. Unlike the longitudinal tensile strength, there is no simple relation such as the rule of mixture for predicting the transverse strength of the composites. Generally speaking, many factors affect the transverse tensile strength of composites: the presence and distribution of voids, the interfacial bonding strength, and the properties of the matrix and the fiber. Reduction of the transverse tensile strength of the composites is probably due to the lesser content of resin in the sample as well as the foregoing factors. As a result, the changing curves of the transverse tensile strength of the composites are dissimilar to the curves of the neat resin as PU content increases in the system. There is no significant change in the transverse tensile strength of the composite as the PU content increases in the matrix for both PU(PBA) and PU(PPG)-epoxy composites (Figures 1 and 2, respectively).

Izod Impact Strength. The impact strength of the PU(PBA)-epoxy composites is shown in Figure 3. The longitudinal impact strength of the composites increases by about 1 order of magnitude, reaches a maximum value in the PU(PBA)-cross-linked region, and increases with increasing PU(PBA) content in the PU(PBA)-epoxy graft-IPN region. The increase of impact strength with increasing PU content is similar to that of the neat resin for the PU content below the break mark. Therefore, the longitudinal impact strength of the composites might result mainly from the bridging effects of the fibers and partially from the resin itself. In the PU(PBA1000)-epoxy

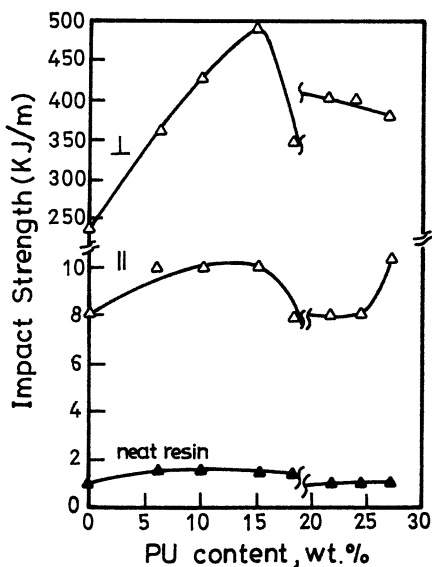


Figure 3. Effect of PU(PBA1000) content in PU-epoxy matrix on the impact strength of composites. Key: Δ , PU(PBA1000)-epoxy composites; \blacktriangle , PU(PBA1000)-epoxy neat resin.

graft-IPN region, the longitudinal impact strength increases with increasing PU(PBA) content, especially when the PU content is at 27 wt%. This increase indicates that an interpenetrating network structure with a one-phase matrix actually does improve the longitudinal impact strength of the composite. As shown in Figure 4, the longitudinal impact strength of the PU(PPG)-epoxy composites also reaches a maximum value in the PU-cross-linked epoxy region. For the PU content beyond the break mark in PU-epoxy graft-IPN composites, the longitudinal impact strength also increases to a maximum value along with the increase of PU content. This increase might be caused by a better interpenetration network with the soft PU in the matrix as shown in Figures 9 and 12. On the other hand, for the PU(PPG)-epoxy composites, the short soft segments of PU(PPG) in the networks make a more positive contribution than the long soft segments do.

As expected, the impact strength in the transverse direction increases with increasing PU content in the matrix and reaches a maximum value for either PU(PBA)-cross-linked epoxy or PU(PPG)-cross-linked epoxy composites. Thus, the toughened matrix resin also evidently leads to composite toughening in the transverse direction. Moreover, the toughening effect on composites from either the one-phase PU(PBA)-epoxy or the less-compatible PU(PPG)-epoxy matrix is more significant than on the neat resin. The transverse Izod impact strength decreases, in some cases, with increasing PU content in the PU(PBA)-epoxy graft-IPN and PU(PPG)-epoxy graft-IPN

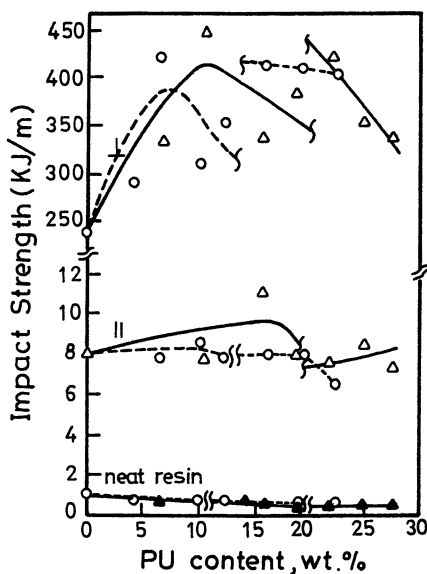


Figure 4. Effect of PU(PPG) content in PU-epoxy matrix on the impact strength of composites. Key: \circ , PU(PPG400)-epoxy composite; Δ , PU(PPG1000)-epoxy composites; \blacktriangle , PU(PPG1000)-epoxy neat resin.

systems. This decrease is probably the result of the dominance of the softening effect over the interpenetrating effect as more PU is introduced into the matrix. Some irregular changes in transverse impact strength of the PU(PPG)-epoxy composites observed in Figure 4 are probably due to the imperfect structure formed from the interference of fibers with the less-compatible PU(PPG)-epoxy matrix during the preparation.

Flexural Strength. When flexural strength is measured, the inner surface of the sample is loaded with a compression force and a tension force is placed on the outer surface of the sample. The compression force loaded on the inner surface of the sample results in buckling of the fibers and local enrichment of the resin. Therefore, the flexural strength of the composites is affected by many complicated factors. As shown in Figures 5 and 6, the flexural strength of the composites greatly improved for both the PU(PBA)-cross-linked epoxy and PU(PPG)-cross-linked epoxy systems with the increase of PU content in the matrix. The improvement in the flexural strength of the composite is more effective for the one-phase PU(PBA)-cross-linked epoxy composite as can be seen in Figure 5. The transverse flexural strength increases significantly with an increase of the PU content in the PU(PBA)-cross-linked epoxy composite. As shown in Figure 6,

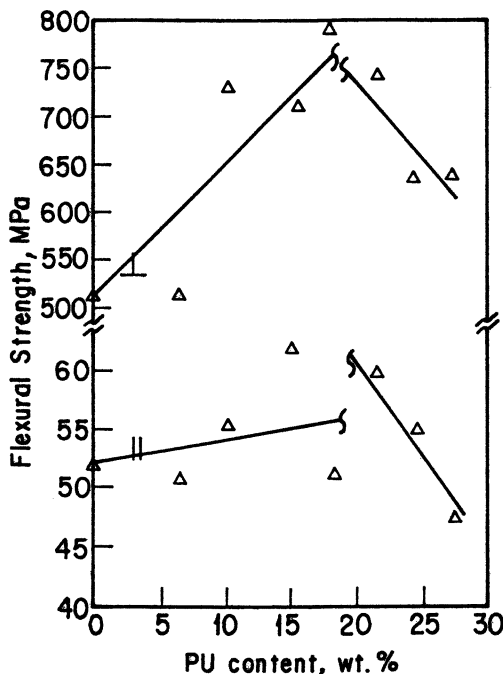


Figure 5. Effect of PU(PBA1000) content in PU-epoxy matrix on the flexural strength of composites.

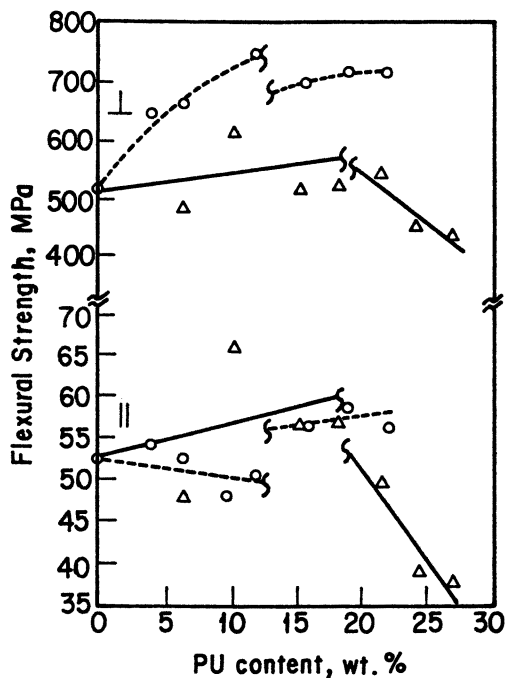


Figure 6. Effect of PU(PPG) content in PU-epoxy matrix on the flexural strength of composites. Key: \circ , PU(PPG400)-epoxy composites; \triangle , PU(PPG1000)-epoxy composites.

enhancement of the strength by the long chain segments of the PU(PPG1000) is not as significant as enhancement by the short chain segments of the PU(PPG400) in the PU(PPG)-epoxy composite. The flexural strength of the composites based on the PU(PBA1000)-epoxy graft-IPNs and the PU(PPG1000)-epoxy graft-IPNs decreases significantly as the PU content increases in the matrix as shown in Figures 5 and 6. For the composites based on PU(PPG400)-epoxy graft-IPNs, the flexural strength of the composite increases with an increase of PU(PPG400) content in the matrix. This behavior in the flexural strength shows that the softness of the matrix has a dominant effect on the flexural strength of the composites. The two-phase and softened PU(PPG)-epoxy matrix causes a small improvement in flexural strength of the composites. The changes of longitudinal flexural strength with increasing PU content are irregular and probably due to the interference of fibers with the PU-epoxy morphology during preparation.

Dynamic Mechanical Properties. The effect of PU(PBA) content in the PU(PBA)-epoxy matrix on the dynamic mechanical properties of the composites is shown in Figures 7 and 8. As shown in Figure 7, the epoxy has transition peaks at 130 °C (alpha transition) and -73 °C (beta transition).

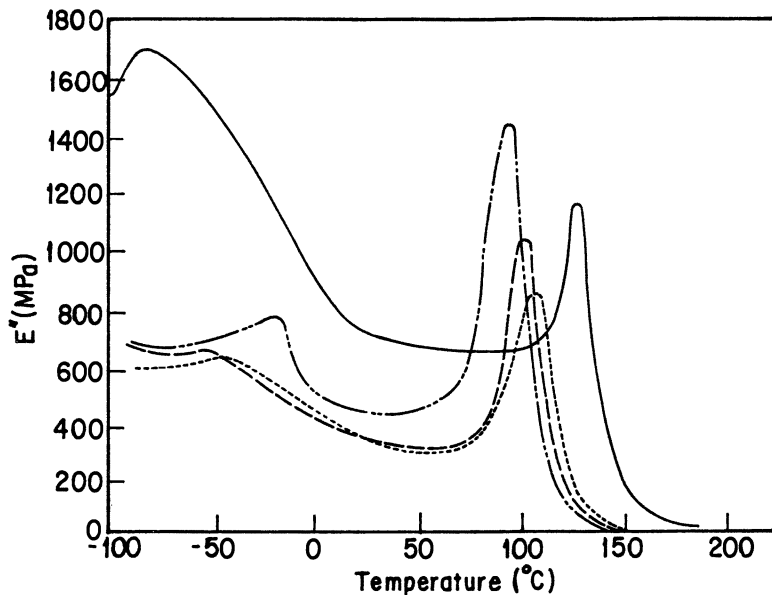


Figure 7. Temperature dependence of loss modulus (E'') for the PU(PBA1000)-cross-linked epoxy composites with various PU(PBA) content (wt%) in the matrix: —, 0; ---, 6 wt%; - · - ·, 10 wt%; - - - -, 19 wt%.

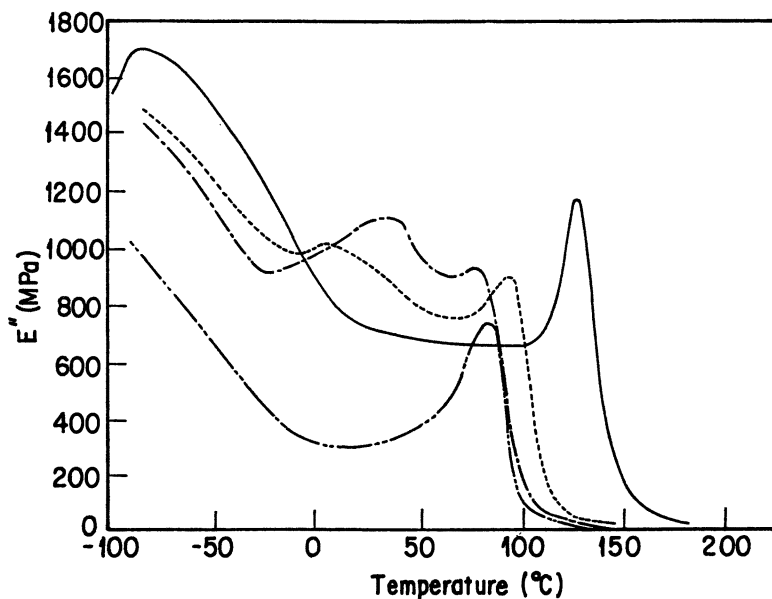


Figure 8. Temperature dependence of loss modulus (E'') for the PU(PBA1000)-epoxy graft-IPN composites with various PU(PBA) content (wt%) in the matrix: —, 0; ---, 22 wt%; - · - ·, 25 wt%; - - - -, 27 wt%.

Because PU(PBA1000) is employed as a cross-linking agent to cross-link the epoxy, the alpha-transition peak shifts to a lower temperature and increases its intensity of loss modulus (E'') when the PU(PBA1000) content increases. On the other hand, the beta transition peak shifts to a higher temperature and rapidly reduces its E'' intensity as the PU(PBA1000) cross-links the epoxy. This reaction indicates that the epoxy matrix (alpha-transition domain) is toughened and compatible with the cross-linked PU(PBA1000). Furthermore, the intensity of the beta-transition domain of the epoxy rapidly reduces as the pendant hydroxyl group of the epoxy is cross-linked by PU(PBA1000). This response indicates that the beta-transition domain is associated with the motion of the linear epoxy structure, which contains hydroxyl group. For the PU(PBA1000)-epoxy graft-IPNs as shown in Figure 8, the alpha-transition peak and the PU(PBA1000) transition peak (at $-35\text{ }^\circ\text{C}$) gradually merge when the PU(PBA1000) content increases up to 27 wt%. This merger indicates that the structure of the interpenetration, in addition to the grafting, can enhance the compatibility of the two polymers. However, for the PU(PPG)-epoxy system as shown in Figures 9 and 10, the short PU(PPG-

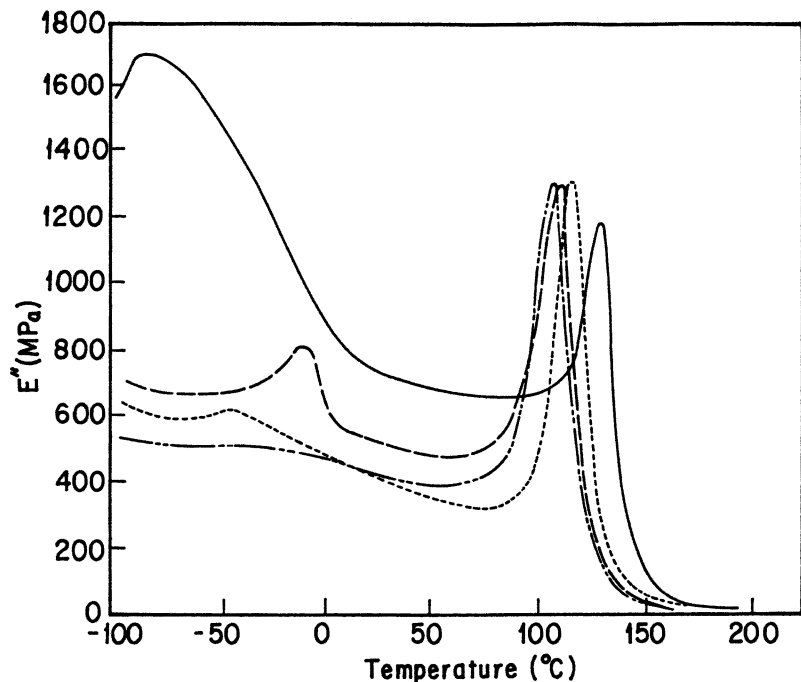


Figure 9. Temperature dependence of loss modulus (E'') for the PU(PPG400)-cross-linked epoxy composites with various PU(PPG400) content (wt%) in the matrix: —, 0; ---, 4 wt%; - · - ·, 10 wt%; - - - -, 12 wt%.

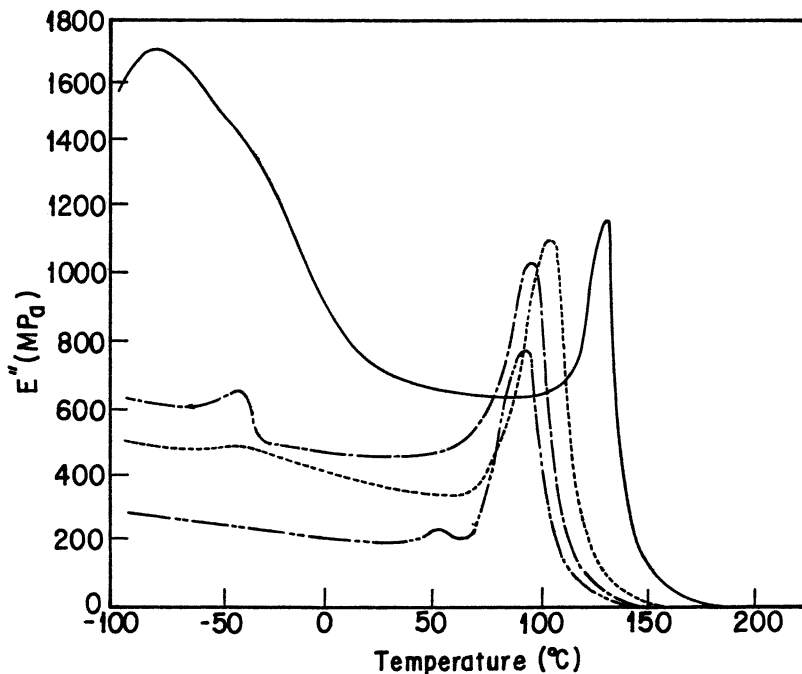


Figure 10. Temperature dependence of loss modulus (E'') for the PU(PPG400)-epoxy graft-IPN composites with various PU(PPG400) content (wt%) in the matrix: —, 0; ---, 16 wt%; - · - ·, 19 wt%; - - - -, 22 wt%.

400) soft segment, which acts as a cross-linking agent in the PU(PPG400)-epoxy matrix, is miscible with the epoxy matrix. Smaller shifts in the alpha-transition peak, compared with those in Figure 7, indicate that the PU(PPG400)-cross-linked epoxy matrix is toughened less but has higher cross-linking than the PU(PBA1000)-cross-linked epoxy matrix. For the PU(PPG400)-epoxy graft-IPN system (Figure 10), the alpha-transition peak of the epoxy shifts to a much lower temperature than the peak in the PU(PPG400)-cross-linked epoxy system. The peak broadens and reduces in intensity as the PU(PPG400) content increases. This phenomenon results from the matrix being grafted and interpenetrated by the cross-linked PU(PPG400) structure that has less compatibility with the epoxy. However, the compatibility is enhanced by the grafting and interpenetration network of the short PPG400 segments in the PU. For the longer PU(PPG1000) soft segment in the PU-epoxy matrix, two distinct transition peaks (alpha and beta) are observed as shown in Figures 11 and 12. The behavior is similar to the behavior of the neat resin in previous work (13). Thus, we believe that a

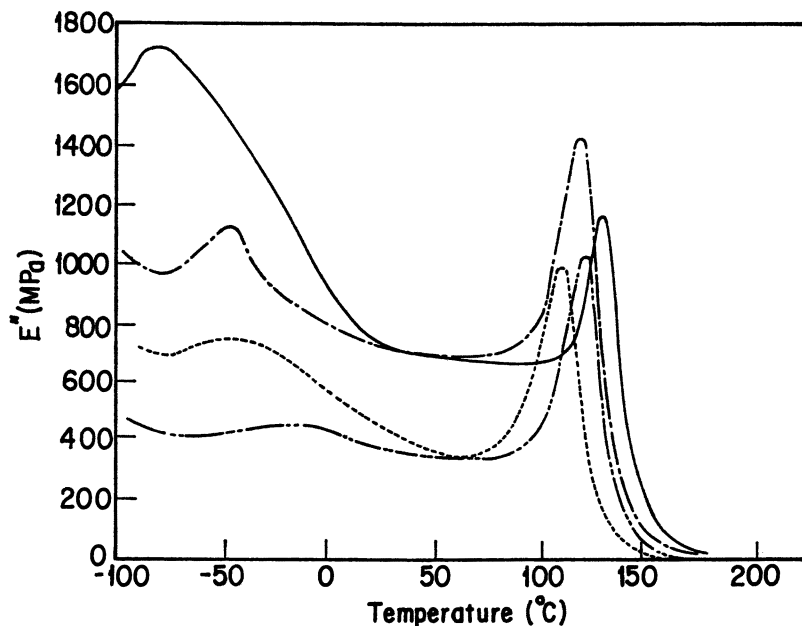


Figure 11. Temperature dependence of loss modulus (E'') for the PU(PPG1000)-cross-linked epoxy composites with various PU(PPG1000) content (wt%) in the matrix: —, 0; ---, 6 wt%; — · —, 15 wt%; - - - - -, 19 wt%.

two-phase matrix is formed in the composite. The increase of PU(PPG1000) content in this composite system partially results in an increase in the number of dispersed PU particles in the matrix as found in the previous study by SEM. Therefore, the small shift of the alpha-transition peak to low temperatures is observed for the longer PU(PPG1000) soft segment introduced into the system (Figures 11 and 12). The foregoing observation implies that the shifts in alpha-transition peak are merely contributed to the epoxy matrix by the grafted structure. This contribution indicates enhanced compatibility between the two polymers.

Conclusions

The mechanical properties of fiber-reinforced composites can be significantly enhanced through modification of the matrix resin. Moreover, the effect of matrix resin modification on the toughness of the composites is more significant than the effect of the neat resin.

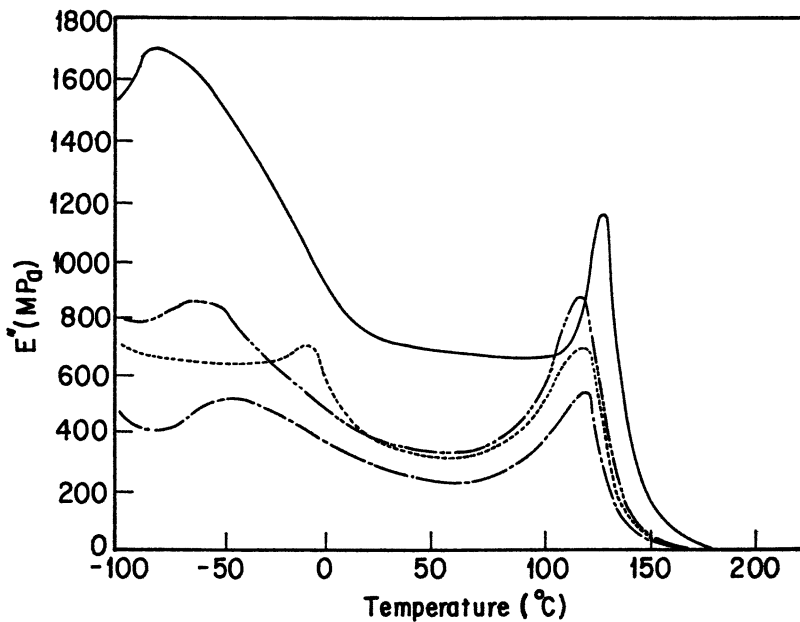


Figure 12. Temperature dependence of loss modulus (E'') for the PU(PPG1000)-epoxy graft-IPN composites with various PU(PPG1000) content (wt%) in the matrix: —, 0; ---, 22 wt%; — · — ·, 25 wt%; — — — —, 27 wt%.

Acknowledgment

The authors acknowledge with gratitude the financial support of the National Science Council, Taipei, Taiwan, Republic of China, through Grant NSC78-0405-E002-07.

References

1. Lee, H.; Neville, K. *Handbook of Epoxy Resin*; McGraw-Hill: New York, 1978.
2. Ibrahim A. M.; Quinlivan, T. J.; Seferis, J. C. *Polym. Prepr. (Am. Chem. Soc., Div. Polym. Chem.)* **1985**, 26, 277.
3. Bucknall, C. B.; Partridge, I. K. *Polymer* **1983**, 24, 639.
4. Ika, P. V.; Frisch, H. L.; Frisch, K. C. *J. Polym. Sci., Polym Chem. Ed.* **1985**, 23, 1163.
5. Kim, S. C.; Klempner, D.; Frisch, K. C.; Radigan, W.; Frisch, H. L. *Macromolecules* **1976**, 9, 258.
6. Klempner, D. *Angew. Chem.* **1978**, 17, 97.
7. Klempner, D.; Frisch, K. C. *Advances in Interpenetrating Polymer Network*; Technomic: Lancaster, PA, 1989; Vol. 1.
8. Paul, D. R.; Newman, S. *Polymer Blends*; Academic: New York, 1978; Vol. 1, pp 17-18.

9. Paul, D. R.; Newman, S. *Polymer Blends*; Academic: New York, 1978; Vol. 2, pp 21–22.
10. Hsieh, K. H.; Han, J. L. *J. Polym. Sci., Polym. Phys. Ed.* **1990**, 28, 623.
11. Hsieh, K. H.; Han, J. L. *J. Polym. Sci., Polym. Phys. Ed.* **1990**, 28, 783.
12. Han, J. L.; Tseng, S. M.; Mai, J. H.; Hsieh, K. H. *Angew. Makromol. Chem.* **1990**, 182, 193.
13. Han, J. L.; Tseng, S. M.; Mai, J. H.; Hsieh, K. H. *Angew. Makromol. Chem.* **1990**, 184, 89.
14. Kadurind, T. I.; Prokopenko, V. A.; Omelchenko, S. I. *Eur. Polym. J.* **1986**, 22, 865.

RECEIVED for review November 11, 1991. ACCEPTED revised manuscript September 3, 1992.

Gas Permeability of Latex Interpenetrating Polymer Network Films

A. K. Holdsworth and D. J. Hourston

The Polymer Centre, Lancaster University, Lancaster LA1 4YA, United Kingdom

The study of the transport of gases through membranes based on polymer blends is increasingly prevalent. These investigations are generally designed either to assess the ability of such membranes to separate gas mixtures or to use the gas molecules as morphology probes. This field is briefly reviewed. The polymers involved in this study are poly(ethyl acrylate) and poly(ethyl methacrylate) combined in three distinct ways: as a latex blend, as a poly(ethyl acrylate)-poly(ethyl methacrylate) latex interpenetrating polymer network, and as a poly(ethyl methacrylate)-poly(ethyl acrylate) latex interpenetrating polymer network. Carbon dioxide acted as a plasticizer for both homopolymers. The measured permeabilities were modeled using the relations proposed by Robeson, Maxwell, and Bottcher that attempt to relate permeability to morphology. The Robeson approach worked well for the latex blends, whereas the Bottcher equation was the most appropriate for interpenetrating polymer networks.

THE SORPTION AND TRANSPORT OF GASES IN POLYMER BLENDS has been increasingly studied over the last 15 years because it is possible to use the penetrant as a probe to investigate the phase morphology of blends (1). The majority of the work has been done in the area of miscible polymer blends with respect to the effect of blend composition on permeability, diffusivity, and solubility coefficients of these blends. For miscible blends, a simple logarithmic relationship has been postulated (2) between permeability (P)

and blend composition:

$$\ln P = \phi_1 \ln P_1 + \phi_2 \ln P_2 \quad (1)$$

P_1 and P_2 are the permeability coefficients of components 1 and 2, respectively, and ϕ_1 and ϕ_2 are the volume fractions of the components in the blend. This relationship, however, is a special case of more general mixing rules and is applicable (3) only under certain conditions. It has been shown (4) that gas transport in polymer films follows an Arrhenius-type relation, which describes the temperature dependence of the diffusion coefficient. In general, the activation energy of diffusion (E_D) may be written (3) as in eq 2, where ΔE_{12} is a deviation term:

$$E_D = \phi_1 E_{D1} + \phi_2 E_{D2} + \Delta E_{12} \quad (2)$$

Empirical observations (5) indicate that E_D and D (the diffusion coefficient) are related in the following way:

$$\ln D = aE_D + b \quad (3)$$

where a and b are constants.

From eqs 2 and 3,

$$\ln D = \phi_1 \ln D_1 + \phi_2 \ln D_2 + \frac{(aRT - 1) \Delta E_{12}}{RT} \quad (4)$$

where R is the gas constant and T is the absolute temperature. Similarly, the solubility coefficient (K_D) for the blend may be related to the components by

$$\ln K_D = \phi_1 \ln K_1 + \phi_2 \ln K_2 + \frac{BV_3\phi_1\phi_2}{RT} \quad (5)$$

B is the binary interaction parameter for components 1 and 2 and V_3 is the molar volume of the small molecule penetrant (component 3). Combining the preceding two equations and remembering that $P = K_D D$, it follows that

$$\ln P = \phi_1 \ln P_1 + \phi_2 \ln P_2 + \frac{(aRT - 1) \Delta E_{12}}{RT} + \frac{BV_3\phi_1\phi_2}{RT} \quad (6)$$

For weakly interacting components, the thermodynamic term B is zero, and when the transport interaction energy term, ΔE_{12} , is also zero, eq 6 reduces to the special case, eq 1.

Sorption and transport of small molecules in miscible blends are often complicated by several factors.

1. The experimental temperature may be below the glass-transition temperature of one component of a blend and above the glass-transition temperature for the other component. The result for a miscible blend is that the mixture is glassy over a portion of the composition range and rubbery over the remainder. Of course, rubbers and glasses behave rather differently with respect to sorption and diffusion of gases.
2. One or both of the blend components may be partially crystalline with the result that the fraction of the mixture that is amorphous varies with blend composition.
3. The permeability may depend on concentration in a variety of ways, and care must be exercised to select a common basis for comparison of one blend composition with another.

In the case of immiscible blends, as S-shaped relationship between P and ϕ is usually observed (6–12). This contrast readily allows a miscible blend system to be distinguished from an immiscible blend system. Shur and Ranby were early investigators (8–12). The early work was centered on the study of mechanical blends of poly(vinyl chloride) (PVC) with ethylene–vinyl acetate copolymers (EVA) (13) and with PVC–acrylonitrile–butadiene copolymers (NBR) blends (14). The EVA copolymers contained 45 and 65% vinyl acetate, respectively. The effect of variation of vinyl acetate content on miscibility and, hence, on transport behavior of the blends was the focus of the study. Higher vinyl acetate content in the EVA and a higher milling temperature was found to coincide with decreased rate of permeation, decreased rate of diffusion, and increased activation energy, E_D . The data were interpreted as the result of denser packing of polymer molecules because of increased PVC–EVA interaction at the higher vinyl acetate content and with higher milling temperature. An S-shaped plot obtained from P versus EVA weight percent for the blends containing 45% vinyl acetate is indicative of a two-phase system because of phase inversion. Blends milled at lower temperatures gave curves concave toward the composition axis, which indicates the possibility of poor mixing. Similar results were obtained (14) with PVC–NBR blends: increased acrylonitrile content in the NBR gave rise to lower values of P and D , but an increase in E_D was

observed. The blends also showed increased volume contraction with increased acrylonitrile content. These effects were caused by an increased degree of polymer–polymer interaction that resulted in reduced segmental mobility and increased compatibility of the two polymers.

Work by Kim and co-workers (15) using poly(methyl methacrylate)–poly(vinylidene fluoride) (PMMA–PVF₂) membranes and some hydrolyzed PMMA–PVF₂ films showed interesting results. At 30% PVF₂ composition the blend was completely amorphous and homogeneous. However, a blend that underwent hydrolysis with sulfuric acid for 30 min showed a crystalline melting point and became cloudy—indications that phase separation had occurred. These phenomena were reflected in permeability experiments where it was shown that unmodified PMMA–PVF₂ membranes gave a convex shape when plotted against composition, whereas the partially hydrolyzed materials gave S-shaped curves.

The blend of poly(2,6-dimethyl-1,4-phenylene ether) (PPE) and polystyrene (PS) has been studied (16) extensively in terms of its sorption and transport behavior with gaseous molecules. The authors studied the transport behavior of neon, argon, and krypton in solution-cast, annealed, glassy PPE–PS blends and observed that the permeabilities of argon and krypton increased monotonically with respect to increasing PPE content. The permeability of neon was not monotonic and, hence, could not be explained in terms of a homogeneous system. The authors also observed that a plot of diffusivity versus composition was nonadditive and there was a minimum at the 50:50 composition whose magnitude decreased with increasing penetrant size. It was concluded that the nonadditivity behavior was the result of a change in the relative contribution of the two sorption mechanisms (16) operative in glasses that was not taken into account when the diffusion coefficients were calculated.

Paul and co-workers also studied (17, 18) this blend system and deduced that the results could be described by the dual sorption model (17) for glassy polymers. An interaction parameter that quantified the exothermic heat of mixing for the system was also obtained. Transport properties of the blends were found to lie well below predictions based on simple additivity; this finding is consistent with the strong interaction between the two polymers.

Paul and co-workers investigated (19, 20) several other miscible, glassy blends that include blends based on copolyesters and polycarbonates. The results were again described well by the dual sorption model and the fact that negative deviations of permeability and diffusion coefficients from simple additivity relations could be explained as a result of decrease in volume on mixing for the blends. The effect of crystallinity was also studied, and, although the relative rates of permeation of one gas with respect to another varied greatly with blend composition, it was shown that the effect of crystallinity was not large.

Two papers by Chiou and Paul (21, 22) on the gas permeation of homopolymer-copolymer blends compared the differences between blends containing PMMA and styrene-*co*-acrylonitrile (SAN) copolymer and tetramethyl bisphenol A polycarbonate (TMPC) and SAN copolymer. The study of the PMMA-SAN system showed that gas transport was different from many other miscible blends in several aspects. The gas permeability and diffusion coefficients for the miscible blends were somewhat higher than the values calculated from the semilogarithmic additivity rule (2), whereas most other miscible blends show either a negative deviation or no deviation at all. On the other hand, the ideal gas separation factors for PMMA-SAN blends followed this rule well, whereas the other miscible TMPC-SAN blend gave higher separation factors than predicted. The observed behavior of the PMMA-SAN blend was attributed to the very weak interactions between PMMA and SAN, whereas the negative deviations in the TMPC-SAN materials were indicative of strong polymer-polymer interactions. This behavior also has been observed in other blends (23-25). The gas transport behavior of phase-separated PMMA-SAN blends was described well by a two-phase interconnected model proposed by Kraus and Rollmann (26).

Chiou and Paul (27, 28) also investigated gas permeation and sorption in PVF₂-PMMA blends and found that CO₂ caused significant plasticization for all blends; in some blends, further crystallization of PVF₂ was induced. Also, permeabilities increased with increased upstream pressure for all blend compositions and high separation factors were achieved for the CO₂-CH₄ gas pair.

Kang et al. (29) studied polymer blend membranes of PS and poly[1,1,1-tris(trimethylsiloxy)methacrylate propylsilane] (PTMPS) and showed that the permeability for an immiscible polymer blend could be represented by

$$P = (1 - \alpha)P_1 + \alpha P_2 + P_h \quad (7)$$

P_1 and P_2 are the permeation coefficients of PS and PTMPS, α is the fraction of the discontinuous phase (PTMPS in this case), and P_h represents the permeation through the interstices at phase boundaries. A dramatic decrease in P was observed if a graft copolymer that was miscible with both PS and PTMPS was incorporated. The explanation for this was an increase in the miscibility in the two components that gave rise to better mixing and a reduction in the number of phase boundaries and interstices. Because these interstices are the major pathway for gaseous flux, a reduction in their number led to a decrease in permeability. When 10% of graft copolymer (that contained 30% by weight of PTMPS) was added to the blend, no visible interstices were observed using light microscopy.

A study by El-Hibri and Paul (30) reported on the gas sorption and transport properties of a multiphase acrylic polymer before and after subjection to mechanical drawing operations. A number of previously published reports have demonstrated (31–34) that molecular orientation of amorphous polymer films by mechanical drawing causes significant improvements in the gas barrier properties.

In this chapter, permeation and dynamic mechanical analysis data are reported for latex interpenetrating polymer networks (IPNs) and a latex blend based on poly(ethyl acrylate) (PEA) and poly(ethyl methacrylate) (PEMA). The permeation data are modeled using the equations of Maxwell (35), Robeson et al. (36), and Bottcher (37):

Maxwell equation:

$$P = P_m \frac{P_d + 2P_m - 2\phi_d(P_m - P_d)}{P_d + 2P_m + \phi_d(P_m - P_d)} \quad (8)$$

P_d is the permeability of the domains, P_m is the matrix permeability, and ϕ_d is the volume fraction of polymer in the domains.

Equations used by Robeson et al. (36) are as follows:

$$P = P_m P_d / (\phi_m P_d + \phi_d P_m) \quad \text{series model}$$

$$P = \phi_m P_m + \phi_d P_d \quad \text{parallel model} \quad (9)$$

The Bottcher equation is:

$$P = \frac{1}{2} \left[3(\phi_m P_m + \phi_d P_d) - (P_d + P_m) + \frac{P_m P_d}{P} \right] \quad (10)$$

Experimental Details

Synthesis. The latex IPNs (38, 39) and the linear homopolymers for the latex blends were prepared at 80 °C by emulsion polymerization using $\text{NH}_4\text{S}_2\text{O}_8$ as initiator and sodium dodecyl sulfate as stabilizer. The first monomer and, if required, cross-linker (tetraethylene glycol dimethacrylate) (TEGDM) at 0.4 wt% were introduced to the reaction vessel over a period of 30 min. The temperature was maintained at 80 °C for a further 2 h to ensure complete conversion. For IPN

synthesis, the second monomer and the TEGDM (at the same level) were then added, again over a 30-min period, after the addition of more initiator, but no further surfactant. Conversion in all cases was virtually 100% and the solids contents of the final lattices were 50% by weight.

Dynamic Mechanical Analysis. Samples were obtained by casting the latex followed by careful drying at 20 °C, under vacuum, for a period of at least 2 weeks. A Polymer Laboratories instrument was used in the dual cantilever mode. The impressed frequency was 10 Hz and the heating rate was 2 °C/min.

Permeation Experiments. The instrument used was constructed locally and is a pressure-rise apparatus based very loosely on a design by Koros and Paul (40). Membranes were prepared by casting latex onto carefully degreased glass plates and then spreading it using a K-bar. The resultant membranes were dried (20 °C) under vacuum for at least a week prior to use.

Permeation experiments were conducted over the 30–50 °C temperature range using a standard up-stream pressure of 14.5 psi. The gases used were CO₂, N₂, O₂, Ar, and He and were all ultrahigh purity.

Results and Discussion

The three systems of interest are a PEA–PEMA latex IPN, the inverse PEMA–PEA latex IPN, and an uncross-linked PEA–PEMA latex blend prepared by carefully mixing the separate lattices. In all three cases the composition was 50:50 by weight. These materials were characterized (*see* Table I) by dynamic mechanical analysis.

Clearly, all three modes of blending result in phase separation. However, some level of mixing is observed in all three cases, but this level is slight (*see* Figure 1) in the latex blend. The extent of mixing is greatest in the PEMA–PEA IPN. Numerous factors are known to influence the morphologies of composite latex particles such as these IPNs. One of the principal factors is the relative hydrophilicities of the two polymers. The foregoing evidence on the resultant morphologies could suggest that PEA is more hydrophobic than PEMA.

Table I. Dynamic Mechanical Data

<i>Material</i>	<i>Lower T_g</i> (°C)	<i>Upper T_g</i> (°C)
PEA	6	—
PEMA	—	106
PEA–PEMA blend	6	102
PEA–PEMA IPN	10	100
PEMA–PEA IPN	12	96

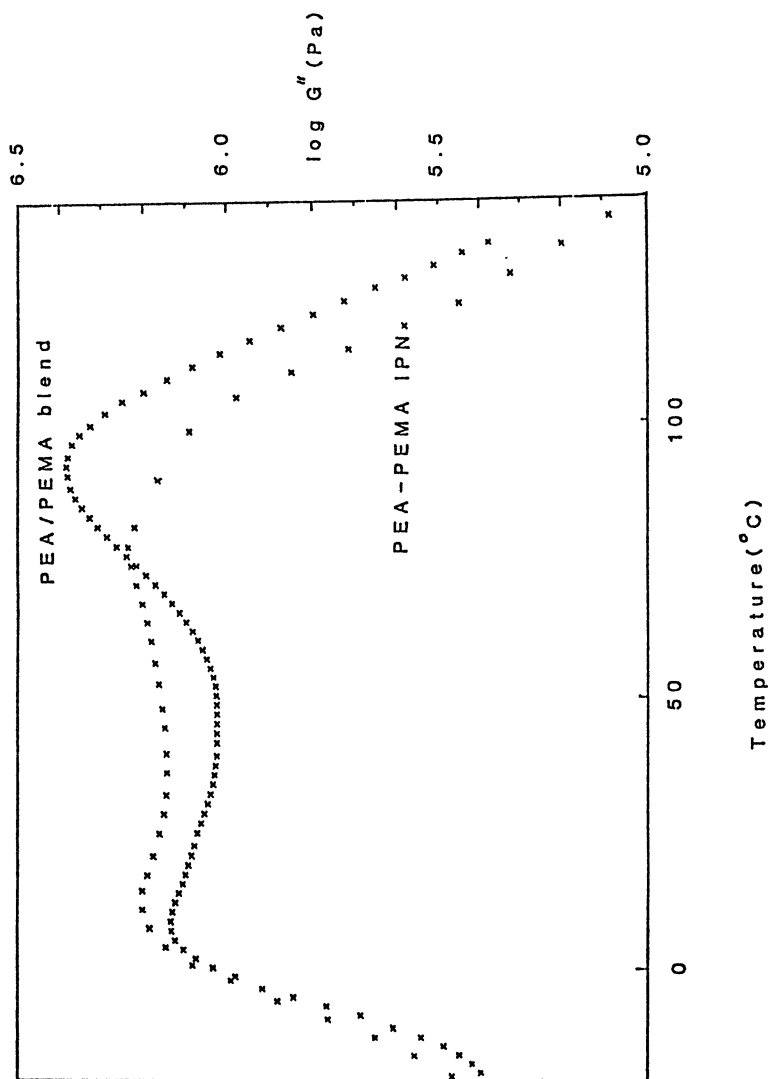


Figure 1. Plot of $\log G''$ vs. temperature (10 Hz) for both the PEA-PHEMA latex blend and the PEA-PHEMA IPN.

Table II presents the permeability coefficients for both of the cross-linked homopolymer membranes and for the membranes prepared from the latex blend and from the two IPNs. Despite the fact that helium is significantly the smallest permeant, CO₂ has the highest *P* value (70.0 Barrer units) for the PEA membrane, which is the result of the high solubility of CO₂ in PEA. This high solubility is commonly found (27, 28) for acrylate and methacrylate polymers. As would be expected, plots (Figure 2) of $-\ln P$ versus $1/T$ are linear for this rubbery polymer.

PEMA, however, is glassy at 30 °C and the equivalent type of plot (Figure 3) shows a marked slope change at the glass-transition temperature, T_g . Consequently, below the T_g the dual sorption mode (41) is believed to be in operation. In this case only, helium permeates faster than does CO₂.

It is clear from Table II that the permeabilities for all gases are lowest in the latex blend membranes and highest in the PEMA-PEA IPN membranes. For the larger permeants, argon and nitrogen, the differences between the three membranes are, however, increasingly less obvious.

For the latex blend membranes, eq 9 was found (Table III) to satisfactorily predict the permeability coefficients except in the helium case. It seems entirely reasonable that a membrane prepared from a mixed latex should be able to be modeled by the parallel relation. In Table II the *P* for CO₂ in the latex blend membrane was greater than for He. Considering the values of *P* for the homopolymer membranes, this might indicate that PEA at least is present as a continuous phase.

Both the Maxwell (35) and the Bottcher (37) theories also have been applied to model the permeation behavior of the IPNs; see Table IV. Both the Maxwell and the Bottcher equations (eqs 8 and 10) are based on spheres embedded in a matrix model. This model seems entirely reasonable for latex IPN materials where a core-shell-type of morphology is quite probable.

With the Maxwell approach a decision must be made as to which component constitutes the matrix phase. If the latex IPN particles have a core-shell morphology, then the matrix will consist of the shell material. Table IV shows that both PEA and PEMA have been considered as the matrix component. With the exception of the CO₂ case, it makes little

Table II. Permeability Data (in Barrer Units) at 30 °C

<i>Gas</i>	<i>PEA</i>	<i>PEMA</i>	<i>Latex Blend</i>	<i>PEA-PEMA IPN</i>	<i>PEMA-PEA IPN</i>
CO ₂	70.0	13.9	42.0	44.0	46.0
He	21.0	41.0	26.0	31.0	36.0
O ₂	8.0	3.5	5.8	6.1	7.1
Ar	6.5	1.6	4.2	4.4	4.8
N ₂	2.8	0.7	1.6	1.8	1.8

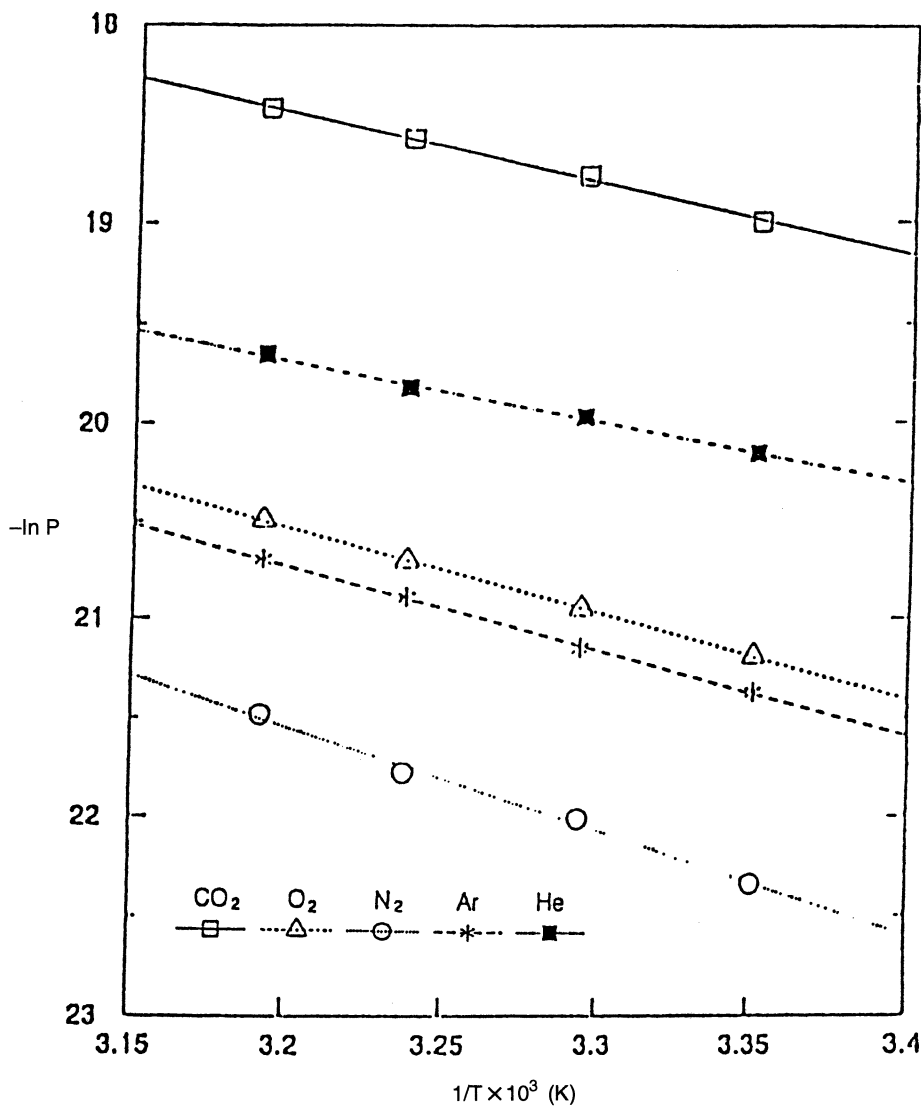


Figure 2. A plot of $-\ln P$ vs. $1/T$ for all five gases with the cross-linked PEA membrane.

difference which network is regarded as the matrix. Neither situation leads to a satisfactory modeling of the data shown in Table II.

Alternatively, the Bottcher equation gives a reasonable prediction, especially for the PEA-PEMA IPN. As mentioned earlier, the PEA component can be the more hydrophobic of the two network polymers, in which case it

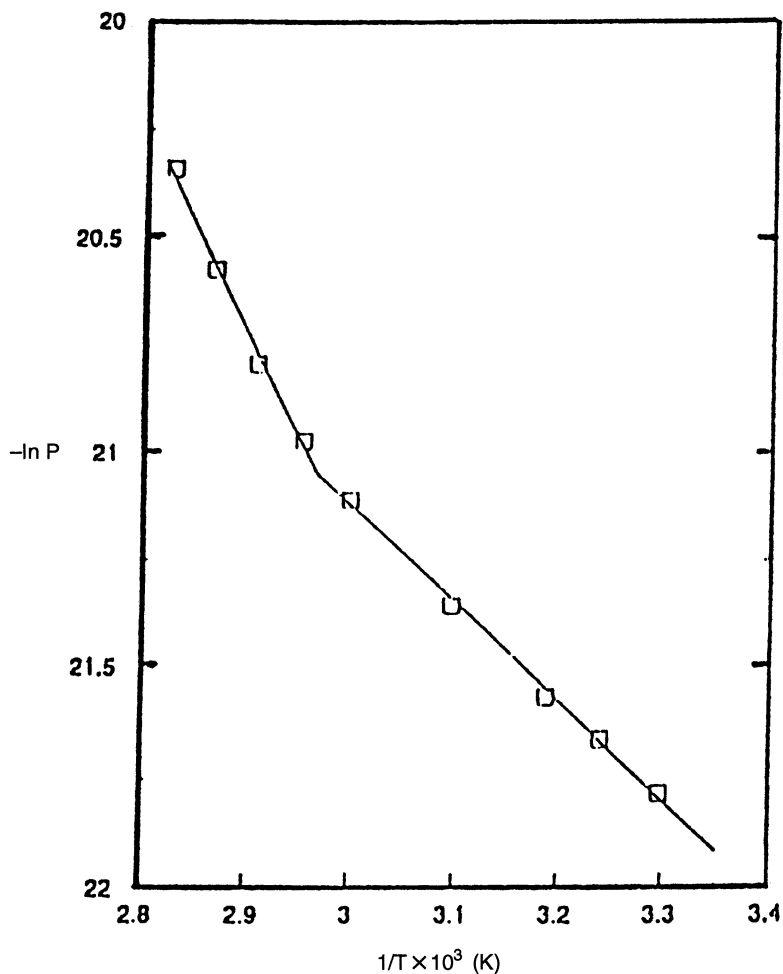


Figure 3. A plot of $-\ln P$ vs. $1/T$ for oxygen with the cross-linked PEA membrane.

Table III. Experimental and Predicted Permeability Coefficients (in Barrer Units) at 30°C for the Latex Blend Membranes

Gas	P (Experimental)	P (Robeson: Parallel Relation)
CO ₂	42.0	42.0
He	26.0	31.0
O ₂	5.8	5.7
Ar	4.2	4.0
N ₂	1.6	1.7

Table IV. Predicted Values of Permeability Coefficients (in Barrer Units) at 30°C for the IPN-Based Membranes

Gas	<i>Maxwell Model</i>		<i>Bottcher Model</i>
	<i>PEA as Matrix</i>	<i>PEMA as Matrix</i>	
CO ₂	38.0	31.0	42.2
He	30.0	30.0	31.1
O ₂	5.5	5.3	5.7
Ar	3.6	3.2	4.1
N ₂	1.6	1.3	1.7

would be reasonable to propose that the PEA-PEMA IPN would have a definite PEMA shell, and, consequently, would be better modeled by the Bottcher equation.

References

1. Kwei, T. K.; Nishi, T.; Roberts, R. F. *Macromolecules* **1974**, *7*, 667.
2. Hopfenberg, H. B.; Paul, D. R. In *Polymer Blends*; Paul, D. R.; Newman, S., Eds.; Academic: New York, 1978; Vol. I.
3. Paul, D. R. *J. Membrane Sci.* **1984**, *18*, 75.
4. Kummins, C. A.; Kwei, T. K. In *Diffusion in Polymers*; Crank, J.; Park, G. S., Eds.; Academic: London, 1968.
5. McGregor, R. In *Permeability of Plastic Films and Coatings to Gases, Liquids and Vapours*; Hopfenberg, H., Ed.; Plenum: New York, 1974.
6. Robeson, L. M.; Noshay, A.; Matzner, M.; Merriam, C. N. *Angew. Makromol. Chem.* **1973**, *29/30*, 47.
7. Barnabeo, A. E.; Creasy, W. S.; Robeson, L. M. *J. Polym. Sci., Polym. Chem. Ed.* **1975**, *13*, 1979.
8. Shur, Y. J.; Ranby, B. *J. Appl. Polym. Sci.* **1975**, *19*, 1337.
9. Shur, Y. J.; Ranby, B. *J. Appl. Polym. Sci.* **1975**, *19*, 2143.
10. Shur, Y. J.; Ranby, B. *J. Appl. Polym. Sci.* **1976**, *20*, 3105.
11. Shur, Y. J.; Ranby, B. *J. Appl. Polym. Sci.* **1976**, *20*, 3121.
12. Shur, Y. J.; Ranby, B. *Macromol. Sci. Phys.* **1977**, *B14*, 565.
13. Olabisi, O.; Robeson, L. M.; Shaw, M. T. *Polymer-Polymer Miscibility*; Academic: New York, 1979.
14. Nishi, T.; Wang, T. T. *Macromolecules* **1975**, *8*, 909.
15. Kim, L. H.; Duran, R. S.; Rogers, D. E. *Polym. Prepr. (Am. Chem. Soc., Div. Polym. Chem.)* **1986**, *27*, 387.
16. Stallings, R. L.; Hopfenberg, H. B.; Stannett, V. J. *Polym. Sci., Polym. Lett. Ed.* **1973**, *41*, 23.
17. Morel, G.; Paul, D. R. *J. Membrane Sci.* **1982**, *10*, 273.
18. Maeda, Y.; Paul, D. R. *Polymer* **1985**, *26*, 2055.
19. Masi, P.; Paul, D. R.; Barlow, J. W. *J. Polym. Sci., Polym. Phys. Ed.* **1982**, *20*, 15.
20. Preston, W. E.; Barlow, J. W.; Paul, D. R. *J. Appl. Polym. Sci.* **1984**, *29*, 845.
21. Chiou, J. S.; Paul, D. R. *J. Appl. Polym. Sci.* **1987**, *34*, 1037.
22. Chiou, J. S.; Paul, D. R. *J. Appl. Polym. Sci.* **1987**, *34*, 1503.
23. Chiou, J. S.; Barlow, J. W.; Paul, D. R. *J. Appl. Polym. Sci.* **1985**, *30*, 1173.

24. Chiou, J. S.; Paul, D. R. *J. Appl. Polym. Sci.* **1987**, *33*, 2935.
25. Barbari, T. A.; Koros, J. W.; Paul, D. R. *J. Polym. Sci., Polym. Phys. Ed.* **1988**, *26*, 709.
26. Kraus, G.; Rollmann, K. W. In *Multicomponent Polymer Systems*; Gould, R. F., Ed.; Advances in Chemistry 99; American Chemical Society: Washington, DC, 1971; p 189.
27. Chiou, J. S.; Paul, D. R. *J. Appl. Polym. Sci.* **1986**, *32*, 4793.
28. Chiou, J. S.; Paul, D. R. *J. Appl. Polym. Sci.* **1986**, *32*, 2897.
29. Kang, Y.; Iwamoto, A. K.; Seno, M. *J. Appl. Polym. Sci.* **1982**, *27*, 2025.
30. El-Hibri, M. J.; Paul, D. R. *J. Appl. Polym. Sci.* **1986**, *31*, 2583.
31. Wang, L. H.; Porter, R. S. *J. Polym. Sci., Polym. Phys. Ed.* **1984**, *22*, 1645.
32. Brady, T. E.; Jabarin, S. A.; Miller, G. W. In *Permeability of Plastic Films and Coatings to Gases, Vapours and Liquids*; Hopfenberg, H. B., Ed.; Plenum: New York, 1974; pp 301.
33. Ito, Y. *Kobunshi Kagaku* **1962**, *19*, 412.
34. Barker, R. E.; Tsai, R. C.; Willency, R. A. *J. Polym. Sci., Polym. Symp.* **1978**, *63*, 109.
35. Maxwell, J. C. *Electricity and Magnetism*; Dover: New York, 1904.
36. Robeson, L. M.; Noshay, A.; Matzner, M.; Merriam, C. M. *Angew, Makromol. Chem.* **1973**, *29/30*, 47.
37. Bottcher, C. J. F. Ph.D. Thesis, University of Leiden, Netherlands, 1940.
38. Klempner, D.; Frisch, H. L.; Frisch, K. C. *J. Polym. Sci., Polym. Chem. Ed.* **1970**, *8*, 921.
39. Sperling, L. H.; Chiu, T. W.; Hartman, C.; Thomas, D. A. *Int. J. Polym. Mater.* **1972**, *1*, 331.
40. Koros, W. J.; Paul, D. R. *J. Polym. Sci., Polym. Phys. Ed.* **1976**, *14*, 1903.
41. Vieth, W. R.; Sladek, K. J. *J. Colloid Sci.* **1965**, *20*, 1014.

RECEIVED for review December 5, 1991. ACCEPTED revised manuscript August 12, 1992.

Gas Transport in Polyurethane–Polystyrene Interpenetrating Polymer Network Membranes

Effect of Cross-Linked State and Annealing

Doo Sung Lee^{1*}, Jeong Ho An², and Sung Chul Kim³

¹Department of Polymer Science and Engineering, Sung Kyun Kwan University, Suwon, Kyungki 440-746, Republic of Korea

²Department of Chemical Engineering, Pohang Institute of Science and Technology, P.O. Box 125, Pohang, Kyungbuk 790-600, Republic of Korea

³Department of Chemical Engineering, Korea Advanced Institute of Science and Technology, P.O. Box 131, Cheongryangri, Seoul 130-650, Republic of Korea

A series of polyurethane–polystyrene (PU–PS) interpenetrating polymer networks (IPN), semi-IPNs (only the PU component is cross-linked), and linear blend membranes were prepared while synthesis temperature and composition were varied. Due to the homogeneity increase of PU and PS, the permeability coefficient decreased and the separation factor increased for preparations made at the lower temperature. The permeability coefficient increased in the sequence IPN, semi-IPN, and linear blends. Annealing increased the permeability coefficients and caused a decrease in selectivity and the extent of synergistic behavior. The annealing effect on the permeation characteristics was dependent on the cross-linked nature of the membrane (IPN < semi-IPN < linear blends). The change of homogeneity, which was modulated by the change of composition, cross-linked state, synthesis temperature, and annealing temperature, could play an important role to control the gas transport characteristics.

* Corresponding author.

SEVERAL FACTORS DETERMINE THE DEGREE OF MIXING IN interpenetrating polymer networks (IPNs): the onset point of phase separation, the rate of phase separation, and the time of physical interlocking (2, 3). The onset point of phase separation is the time when the Gibbs free energy of mixing becomes positive. The Gibbs free energy of mixing is determined by the conversion (or molecular weight), synthesis pressure, and synthesis temperature. The rate of phase separation is related to the mobility of the polymer chain and the medium viscosity of the reaction mixture. Thus, the rate of phase separation is indirectly related to the synthesis pressure and temperature. The time of physical interlock or network formation is the time when both component polymers reach the gel point, and thus the phase domain size cannot increase much further beyond this point.

These three factors depend directly or indirectly on the reaction conditions (such as initiator concentration, catalyst type and amount, cross-link density, synthesis temperature, and synthesis pressure) and thermodynamic values such as interaction parameter ($I-6$). Among these factors, the relative rate of the two competing kinetic processes of phase separation and network formation is the major factor of importance that is responsible for the morphology of the final product for given polymer pairs. When the rate of chemical reaction is very fast compared to the rate of phase separation, the interlocking of the two component polymers occurs in the early stage (i.e., at low conversion), the medium viscosity increases, and the rate of phase separation is reduced. The resulting IPNs show a highly homogeneous state. When the rate of chemical reaction is slow compared to that of phase separation, the opposite process occurs and IPNs with heterogeneous morphology are obtained where only partial interpenetration exists around the phase boundaries of the dispersed phases. Therefore, we conclude that the domain size and the degree of partial interpenetration are dependent on the relative ratio of the rate of phase separation to that of network formation. In the thermodynamic point of view, the morphology and homogeneity of the IPN is in a nonequilibrium state after finishing the synthesis. The extent of accomplishment of thermodynamic equilibrium can be controlled by the kinetic parameters such as cross-linking, fast reaction, and high medium viscosity.

During the past several years, we have tried to enhance the homogeneity of IPNs by application of reaction conditions, such as synthesis pressure and temperature, to control the relative ratio of the rate of phase separation to the rate of chemical reaction. The application of high pressure (up to 20,000 atm) during the simultaneous polymerization process of polyurethane-poly(methyl methacrylate) (PU-PMMA) (2) and polyurethane-polystyrene (PU-PS) IPNs (3-5) enabled the degree of interpenetration and the homogeneity between constituents to increase. These IPNs synthesized under high pressure appeared transparent, which is indicative of very small domain size or formation of a near molecular level mixture. The synthesis temperature also has direct

and indirect effects on the onset point of phase separation, the rate of phase separation, and the time of interlocking. When we synthesized the IPNs at low temperature (0 °C), we were able to increase the homogeneity because the medium viscosity increased at low temperature and thus the rate of phase separation (diffusion-controlled) decreased (6–8).

Many recent studies have reported the gas-transport phenomena in heterogeneous and homogeneous polymer blends (9–16). In these reports, the gas-transport characteristics were correlated with the chemical structure and the morphology of the polymer blends. The IPNs have been studied for their unusual physical properties, especially enhancement in mechanical strength, and the IPN can maintain its morphological structure and physical properties for a long period due to its cross-linked nature. The enhancement of durability, mechanical properties, and homogeneity of IPN are good features for membrane application.

Frisch et al. (17) measured the water-vapor permeability coefficient for a polyurethane–polyepoxide IPN and found no occurrence of maxima and minima in the composition plot. Chen and Ju (18) studied the oxygen permeability of polyurethane–polyepoxide IPNs and observed that the permeability coefficient decreased and showed minimum values due to their interpenetration.

Our recent studies of the IPNs suggest the possibility of changing the degree of intermixing and the morphology with little change in chemical structure. Therefore, IPNs prepared under various synthetic conditions (pressure and temperature) provide a useful system to study the effects of homogeneity and phase morphology on the permeability and selectivity of the multicomponent polymeric membrane (19–21).

In previous studies (19), when the PU–PS IPN membranes were synthesized at low temperature, the permeability coefficient decreased and the separation factor increased due to the homogeneity increase. The oxygen permeability coefficient $P(O_2)$ and nitrogen permeability coefficient $P(N_2)$ ranged in the 10^{-9} and 10^{-10} orders of magnitude, respectively. The permeability coefficient showed a minimum value and the separation factor showed a maximum value at about 25% PU content. At this composition, the separation factor showed a higher value than the separation factor of the PS homopolymer. This synergistic effect resulted from the free volume change due to the homogeneity change. The logarithmic permeability coefficient of the IPN increased linearly with increasing free volume, so that the free volume model (22) could be applied to the PU–PS IPN membranes, which means that there is no interaction effect other than the free volume effect in the PU and PS membrane system.

In addition, the effect of testing pressure and temperature, molecular weight of polyol, and aromatic content (MDI, 4,4'-diphenylmethane diisocyanate; TDI, tolylene diisocyanate; and HDI, hexamethylene diisocyanate) of the PU component on the gas permeability were studied (20). The

permeability of PU, PS, and IPN membranes shows nearly constant value regardless of the pressure difference. The permeability coefficient increases linearly with increasing testing temperature. The permeability coefficient decreased and the separation factor increased with increasing aromatic content in the polyurethane component. The morphology, the dynamic mechanical behavior, and the density behavior of the IPN membranes supported the permeability characteristics. The tensile strength of the membrane increased with decreasing synthesis temperature and with increasing cross-link density and polystyrene content.

In this chapter, IPN, semi-IPN, and linear blend membranes composed of PU-PS were synthesized at low temperature and the gas permeability characteristics through the membranes were investigated. The present work deals with evaluation of the effect of the cross-linked state and annealing on the gas (oxygen and nitrogen) permeability and selectivity. We were able to obtain a highly homogeneous state via low-temperature synthesis, and the homogeneity of the membrane could be gradually changed by annealing at the appropriate temperature. Because our experimental scheme can affect only the morphology with no change in chemical structure of the constituents, the effect of homogeneity could be investigated exclusively.

Experimental Details

Materials. Poly(tetramethylene ether) glycol (PTMG; molecular weight 1000), 1,4-butanediol (1,4-BD), and trimethylolpropane (TMP) were degassed at 60 °C for about 6 h under vacuum. Styrene monomer was purified before use (23). 4,4'-Diphenylmethane diisocyanate (MDI), divinylbenzene (DVB), and benzoin (photoinitiator) were used without further purification.

Membrane Preparation. The isocyanate-terminated polyurethane prepolymer was prepared by reacting 1 equivalent of PTMG with 2 equivalents of MDI at 65 °C. The reaction was carried out until the theoretical isocyanate (NCO) content was reached. This theoretical content was determined by the di-*n*-butylamine titration method (24). A mixture of 1,4-BD-TMP in 1:4 equivalent ratio was used as the cross-linking and chain-extending agent for the polyurethane (PU) network. DVB (5.05 wt% in styrene monomer) was used as the cross-linking agent for the PS network. The thoroughly mixed and degassed mixture of PU prepolymer, TMP-1,4-BD mixture (the amount is adjusted to give a total NCO:OH ratio of 1), polyurethane catalyst dibutyltin dilaurate (T-12; 0.001 wt% for PU prepolymer), styrene monomer, DVB, and benzoin photoinitiator (0.5 wt% to PS component) was charged between two glass plates sealed with a polyester [poly(ethylene terephthalate) (PET)] film spacer 50 μm thick. The sample was kept at 40 °C for about 6 h to polymerize the PU component in the presence of styrene monomer mixture. Then, the sample was photopolymerized by exposure to UV light. The photopolymerization of the styrene monomer mixture was carried out in a temperature-controlled chamber for 24 h with temperatures ranging from 0 to 40 °C. The wavelength of UV light was 3500 Å. The PU component (which forms the network) was allowed to react first to allow observation of the effect of temperature on the mobility of the polystyrene

component (which phase separates during the photopolymerization). The resulting theoretical molecular weight between cross-links (\bar{M}_c) of the IPN membrane was 2000.

Semi-IPNs and linear blend membranes also were prepared at varying reaction temperatures and compositions. In the semi-IPN, the PU component was cross-linked while the linear PS component was employed. Semi-IPNs and linear blends (both components are linear) were formed by exclusion of the appropriate cross-linking agents (TMP and DVB) in both component formulations. Samples were dried under vacuum at room temperature for 3 days before testing.

The membranes were annealed at 80 and 110 °C for 12 h to study the effect of the degree of mixing on the permeation characteristics. Phase separation of the specimen is induced by annealing at high temperature due to the increase of chain mobility and the thermodynamic driving force.

Determination of Gas Permeability. Permeability coefficients were obtained from steady-state rates of gas permeation through the PU-PS membranes. The permeation rates were measured by means of a permeability apparatus designed by Stern et al. (25). The permeation cell consists of two horizontal stainless steel flanges. The membrane is supported by a filter paper on the top of a metal screen. Two different sizes of synthetic rubber gaskets ensures a pressure-tight seal between the membrane and the flanges. The effective area of the membrane is $1.965 \times 10^{-3} \text{ m}^2$. The penetrant gas is supplied to the permeation cell via stainless steel tubing. The rate of gas permeation through the membrane is measured by a bubble flowmeter. The assembled apparatus is immersed in a constant-temperature bath. The permeability coefficients of the membranes for O_2 and N_2 [$P(\text{O}_2)$ and $P(\text{N}_2)$] were measured under 800 kPa (N/m^2) pressure difference at 30 °C. After the permeability coefficients for each penetrant gas (O_2 and N_2) were measured, the permeability ratio [$P(\text{O}_2):P(\text{N}_2)$] was used to determine the separation factor, α . The membrane thickness was about 100 μm .

Density. The density was measured with a density gradient column with sodium bromide aqueous solution. All measurements were carried out at 25 °C.

Results and Discussion

Gas Permeation and Selectivity Characteristics. The gas permeability of the IPN membranes can be characterized by a mean permeability coefficient, or mass transfer coefficient, P , that is defined by the relation (26)

$$P = \frac{J_s \cdot l}{\mathcal{P}_H - \mathcal{P}_L} \quad (1)$$

where J_s is the steady-state gas permeation rate through the unit membrane area when the constant gas pressures \mathcal{P}_H and \mathcal{P}_L are maintained at the membrane interfaces ($\mathcal{P}_H > \mathcal{P}_L$) and l is the membrane thickness. The gas permeability can be expressed by means of diffusivity and solubility. Diffu-

sivities are regarded as kinetic in nature and associated with the gas activity through the membranes. The diffusivities are dependent on the size of gas molecules, the size of the free volume, mobility, and chain length of the polymers, and so forth. Solubilities also can be regarded as thermodynamic in nature because they are determined by the interactions between the polymers and the gases.

We also can define a separation factor, α , as a measure of the membrane selectivity for one component of a mixture over another. This separation factor becomes equal to the ratio of the permeabilities of the two components in the mixture. The separation factor can be resolved into two factors: the so-called mobility selectivity and solubility selectivity terms,

$$\alpha = P_A/P_B = [D_A/D_B][S_A/S_B] \quad (2)$$

where the subscripts denote the penetrant, and $[D_A/D_B]$ and $[S_A/S_B]$ are the mobility and solubility terms of permeability and separation factors, respectively.

Because rubbery polymers have better chain mobility overall, the deviations of the diffusion coefficient between various penetrant gas molecules is small regardless of their sizes. The activation energy for diffusion in rubbery polymers is higher than for glassy polymers. Consequently, the permeation of rubbery polymer is dependent on the difference of the solubility (in polymer) of the penetrant gas rather than the diffusivity difference, so the rubbery polymers retain high permeability coefficients and low separation factor.

On the other hand, glassy polymers have very stiff chain structures caused by the restriction of the molecular motion in the polymers. Therefore, the penetrant gas can only diffuse through the voids in the stiff polymer, which results in lower activation energy of diffusion in the glassy polymer compared with the rubbery polymers. Consequently, the diffusion rates vary remarkably and depend on the size of the penetrant gases.

As previously indicated, the permeability and selectivity in the glassy polymers is more dependent on the distance between the chain length rather than the gas-polymer interaction. The glassy polymer has relatively higher selectivity instead of reduced gas permeability relative to the rubbery polymer.

The simple mixture rules for gas permeation do work for miscible blends for weakly interacting components, and the permeability of a particular gas through a blend is related to the permeabilities of that gas in the component polymers by

$$\ln P = \phi_1 \ln P_1 + \phi_2 \ln P_2 \quad (3)$$

where ϕ_i is the volume fraction of component i (27). For more strongly interacting components, the permeability is expected to fall below this

additivity value to an extent related to the degree of interaction. The separation factor for gas O₂ related to gas N₂ may follow a similar mixing rule:

$$\ln \alpha = \phi_1 \ln \alpha_1 + \phi_2 \ln \alpha_2 \quad (4)$$

The permeability of incompatible two-component systems can be predicted by a parallel flux model (28):

$$P = \phi_1 P_1 + \phi_2 P_2 \quad (5)$$

$$\alpha = \phi_1 \alpha_1 + \phi_2 \alpha_2 \quad (6)$$

In these cases (eqs 4 and 6), α for blends lies on a simple monotonic curve that connects the values of the separation factor for the pure component polymers. In our system, little difference in calculated values for the IPN membranes is observed when either of the two models is employed because of the small difference in density (1.1019 and 1.0564 g/cm³ for PU and PS, respectively) and experimental permeation data for the pure components.

The poly(phenylene oxide)–polystyrene miscible blend (28) and polyurethane–polyepoxide IPN (18) show similar results with this system and show negative volume change on mixing. The separation factor shows a synergistic effect at more than 50% PS content. Note that the separation factor of the IPN membrane is higher than the separation factor of the component polymers of PU and PS. A similar effect was observed by Maeda et al. (29) in the study of He–CH₄ and CO₂–CH₄ gas permeability in a polystyrene–poly(phenylene oxide) miscible system.

We reported the free volume–permeability coefficient relationship of the IPN membrane in a previous article (19). The permeability coefficient versus the reciprocal of the free volume of the IPN is shown to allow comparison with the free volume model that was reported by Lee (22). Lee showed correlations for a wide range of polymers using the equations

$$P = A \exp\{-B/(V - V_0)\} \quad (7)$$

$$V_f = V - V_0 \quad (8)$$

where A and B are constants for a particular gas, V_f and V are the specific free volume and the specific volume of the polymer, respectively, and V₀ is the volume occupied by the polymer chain (specific volume at 0 K) that is calculated by the simplistic definition (30)

$$V_0 = 1.3V_w \quad (9)$$

$$V_r(298)/V_w = 1.6 \quad (10)$$

$$V_g(298)/V_w = 1.55 \quad (11)$$

where V_w is the van der Waals specific volume and $V_r(298)$ and $V_g(298)$ are the observed specific volume of the rubbery (PU) and glassy (PS) polymer at 298 K, respectively. The linear thermal expansion coefficient of PU–PS IPNs are decreased exponentially with increasing PS content. These data were used to calculate the specific free volume at different temperature.

The logarithmic permeability coefficient of the IPN increases linearly with increasing free volume, so that the free volume model can be applied to the PU–PS IPN membranes. This application means that there is no interaction effect other than the free volume effect in the MDI-based PU and PS membrane system. The corresponding equation of the permeability coefficient of the PU–PS IPN membranes at 30 °C and 4 atm can be expressed in the form

$$P(\text{O}_2) = 1.14 \times 10^{-7} \exp\{-1.03/(V - V_0)\} \quad (12)$$

$$P(\text{N}_2) = 3.17 \times 10^{-5} \exp\{-2.23/(V - V_0)\} \quad (13)$$

Effect of Synthesis Temperature and Cross-Linked State.

The mean permeability coefficient, P , and separation factor, α , for the oxygen and nitrogen as a function of the composition in the IPN, semi-IPN, and linear blend membranes are displayed in Figures 1, 2, and 3, respectively. Each sample was synthesized at two different temperatures, 0 °C and 40 °C, to allow investigation of the effect of synthesis temperature.

The three different samples, IPN, semi-IPN, and linear blend, showed similar overall behavior and had permeability coefficients of oxygen and nitrogen on the order of 10^{-9} and 10^{-10} , respectively. However, a lower permeability was observed for samples prepared at lower temperature at every experimental point.

To explain why low-temperature synthesis caused the reduced permeability, it is relevant to discuss the IPN formation process. When the membranes were synthesized at the lower temperature (0 °C), the rate of phase separation was reduced due to the higher medium viscosity of the mixture at low temperature, whereas the relative rate of network formation is only marginally affected by the change of synthesis temperature. Such a reduced rate of phase separation at low temperature results in a decrease in free volume as well as improved homogeneity. These features are substantiated by the experimental data such as density that showed the increased differences from the values calculated from the additivity rule in the case of low-temperature synthesis (19, 20). Therefore, the origin of the reduced permeability in the samples synthesized at low temperature could be considered a consequence of the reduced free volume.

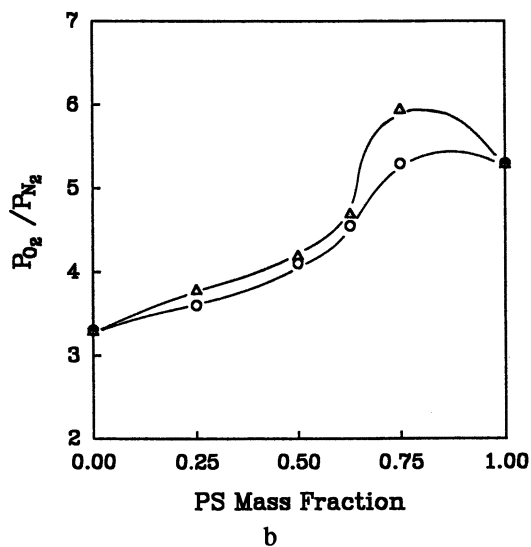
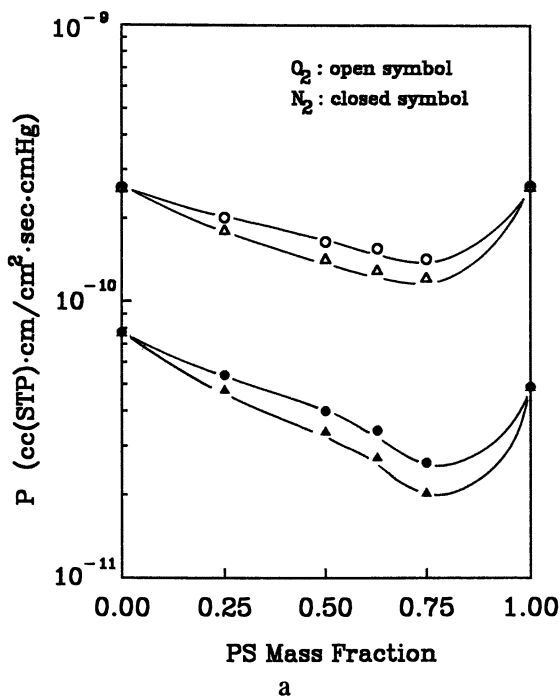


Figure 1. Permeability coefficient (a) and separation factor (b) vs. PS content of IPN membranes synthesized at 0°C (Δ) and 40°C (\circ).

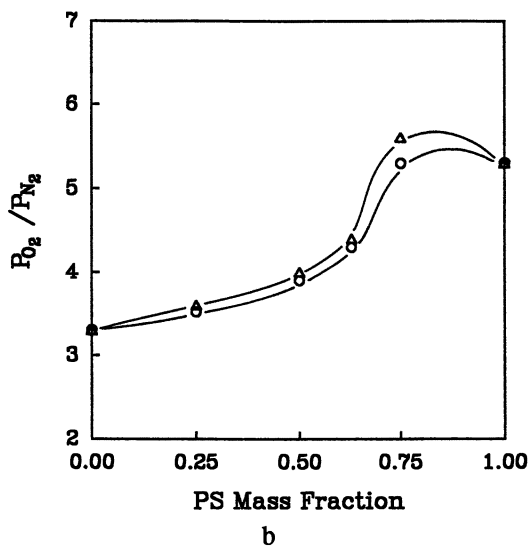
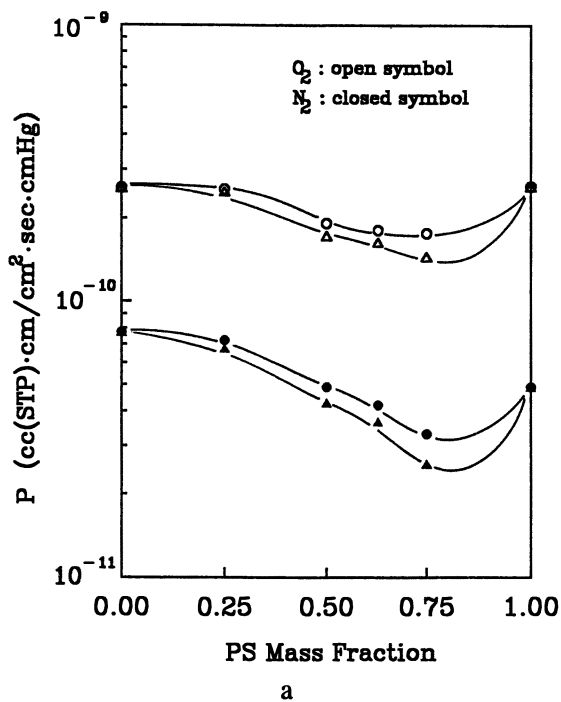


Figure 2. Permeability coefficient (a) and separation factor (b) vs. PS content of semi-IPN membranes synthesized at 0 (Δ) and 40 $^{\circ}\text{C}$ (\circ).

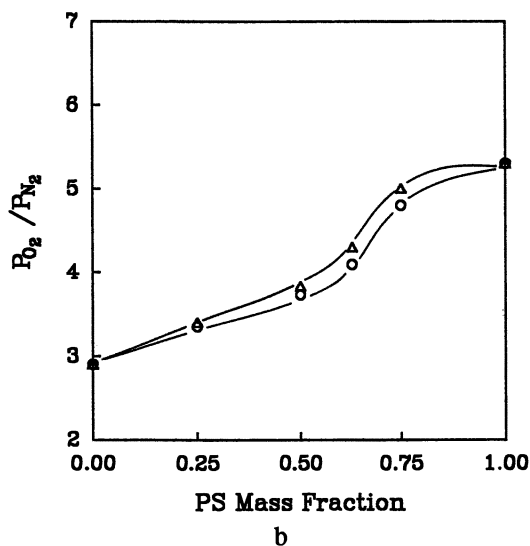
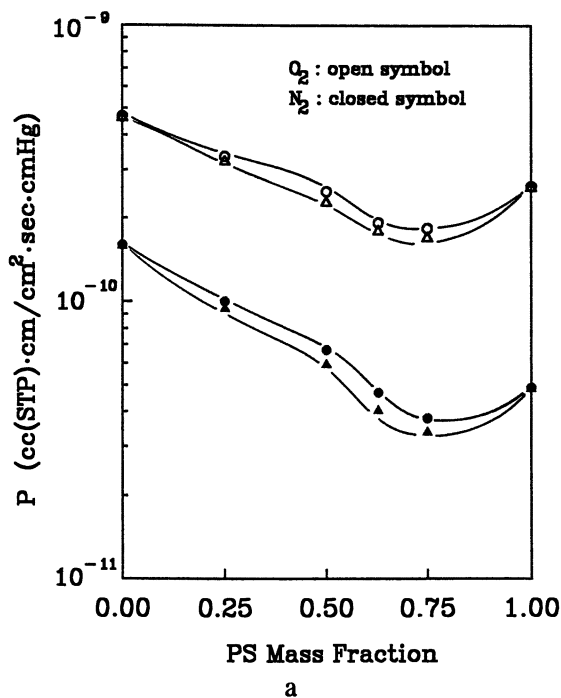


Figure 3. Permeability coefficient (a) and separation factor (b) vs. PS content of linear blend membranes synthesized at 0 (Δ) and 40 $^{\circ}\text{C}$ (\circ).

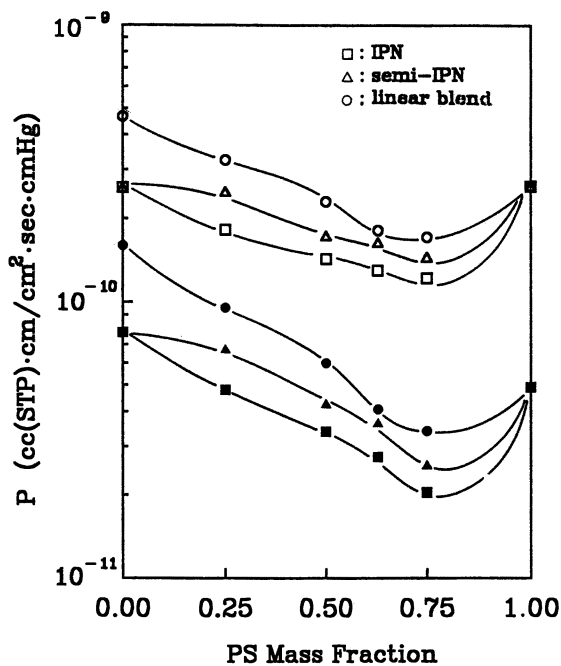
The permeability coefficient becomes lower as the content of the PS component increases. Similar trends have recently been reported in the poly(phenylene oxide)–PS miscible system (28) and PU–polyepoxide IPN system (18). In addition, at about 75% by weight of PS component, the permeability coefficient shows a minimum.

The separation factors of the specimen are within 3–6 [ratio of $P(O_2)/P(N_2)$]. The separation factor of the specimens increased as the permeability coefficient decreased. The separation factor showed a maximum value, which indicates a synergistic effect at about 75-wt% PS composition, where the permeability coefficient showed a minimum value. This relationship is probably because the degree of mixing in the IPN membrane is highest and the free volume is lowest at this point, as evidenced by the morphology and the density behavior that will be discussed later, and seems to be the result of an optimum morphology and structural packing. Thus, the selectivity difference between IPNs prepared at 0 and 40 °C is much larger at this specific composition than in any other regions. In particular, specimens synthesized at 0 °C have improved synergistic effects as compared with the high-temperature case. Such synergistic effects generally cannot be expected in the case of single-component polymeric membranes.

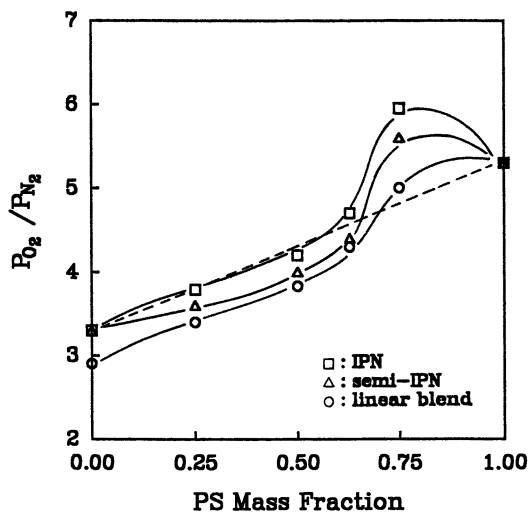
We now turn our attention to comparison of the permeability characteristics between IPNs, semi-IPNs, and linear blends. The introduction of cross-links into both or either polymer(s) is generally believed to restrict the phase separation due to physical interlocking (interpenetration) that, thus, results in enhanced homogeneity between constituents (1, 31).

Such interpenetration effects become most significant when both components are cross-linked (IPN) and decrease in the order of semi-IPN and linear blend. Therefore, the influence of homogeneity variation caused by change in the synthesis temperature on the permeability characteristics could be expected to be most significant in IPNs and to be least significant in linear blends. This expectation can be confirmed by comparison of the selectivity and permeability data of each class of sample as summarized in Figure 4. First of all, the maximum separation factors observed at 75-wt% PS content decrease in the order of IPN, semi-IPN, and linear blend. The selectivity difference between 0 and 40 °C samples at this maximum point is also decreasing in the same order (Figures 1, 2, and 3). At the same time, the maximum gradually disappears in the case of the semi-IPN and linear blend whereas a distinct maximum could be observed in the IPN sample. These differences among the three types of alloys are also supported by the density data. The permeability increases in the relative order of IPN < semi-IPN < linear blend membranes whereas the separation factor shows the opposite behavior.

Figure 5 represents the densities of the IPNs synthesized at two different temperatures (0 and 40 °C). Specimens synthesized at the lower temperature (0 °C) showed higher values than corresponding samples synthesized at 40



a



b

Figure 4. Comparison of permeability coefficient (a) and separation factor (b) vs. PS content with varying cross-linked state of the membranes synthesized at 0 °C. Closed symbol, N_2 ; open symbol, O_2 ; dashed line, calculated value from a parallel flux model (20, 32).

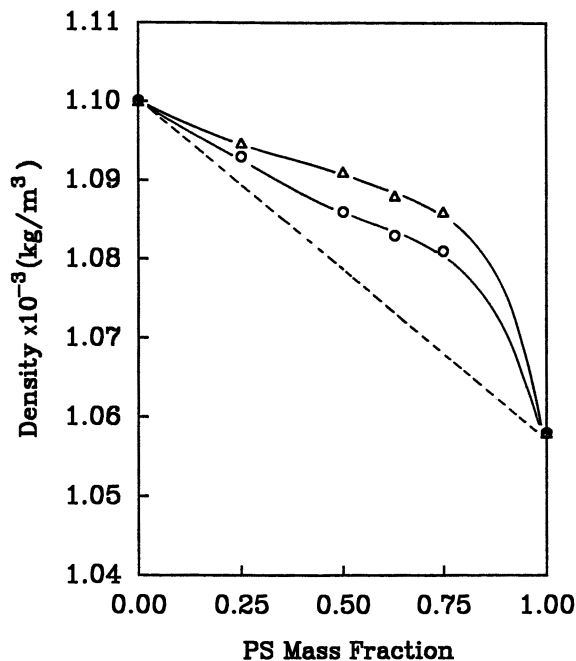


Figure 5. Density vs. PS content in IPN membranes synthesized at 0 (Δ) and 40 $^{\circ}$ C (\circ). Dashed line, calculated values based on volume additivity rule.

$^{\circ}$ C. This difference indicates that specimens synthesized at 0 $^{\circ}$ C have less free volume due to the improved degree of mixing and supports the earlier observation of better selectivity in low-temperature synthesized samples.

Generally an abrupt decrease of density was observed about 75-wt% PS content in all three types of samples, which implies that a significant morphological change might occur. The morphological change as studied by transmission electron microscopy of IPNs with varying PS content was shown in previous articles (19, 20). In those papers, the homogeneity of the IPN membrane was nearly equal at 25 and 50% PS content, but the morphology of the IPN membrane that had 75% PS content showed a more highly homogeneous state than the other two PS compositions. This homogeneity increase reduces the free volume of the membrane and the permeability coefficient while it increases the separation factor.

Figures 6 and 7 compare the densities of each class of samples at 0 and 40 $^{\circ}$ C, respectively. When we compare the deviation of experimental density values with values from the simple rule of mixture in the three types of alloys, the difference is decreasing in the order of IPN, semi-IPN, and linear blends. The absolute densities follow the sequence IPN > semi-IPN > linear blend, and this density behavior supports the earlier results.

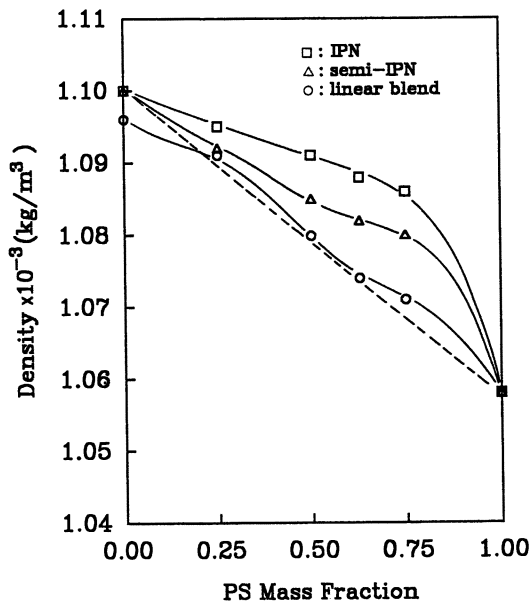


Figure 6. Density vs. PS content with varying cross-linked state of the membranes synthesized at 0 °C. Dashed line, calculated values based on volume additivity rule for the IPN.

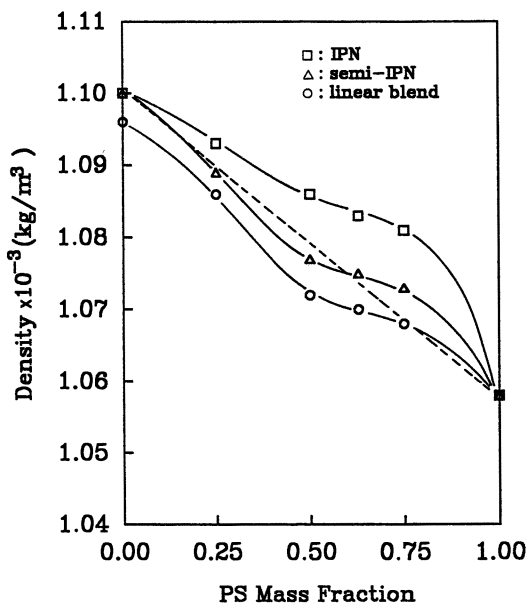


Figure 7. Density vs. PS content with varying cross-linked state of the membranes synthesized at 40 °C. Dashed line, calculated values based on volume additivity rule for the IPN.

Effect of Thermal Annealing. To confirm the effect of degree of mixing on the permeability coefficient and selectivity, an annealing experiment was carried out. Figures 8, 9, and 10 show the permeability coefficient and the separation factor of the specimens synthesized at 0 °C and their changes after 12 h annealing at 80 (below the glass-transition temperature (T_g) of PS) and 110 °C (above the T_g of PS).

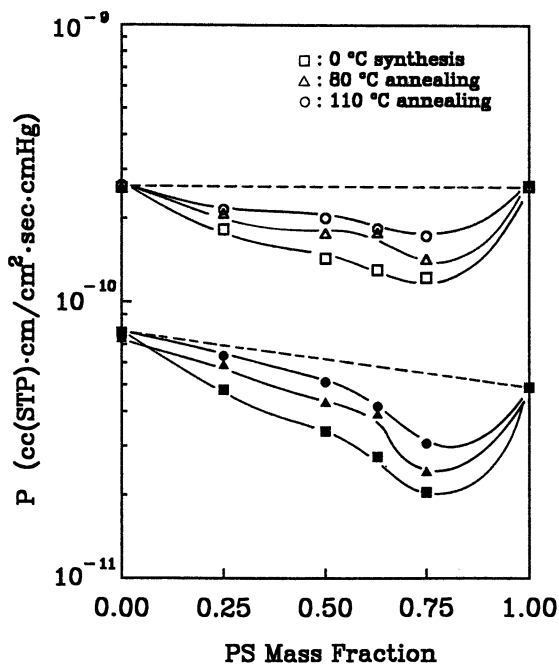
After the annealing of the membranes, the permeability increases and the separation factor decreases because the free volume increases due to further phase separation caused by annealing. Also, a positive deviation from the simple additivity rule could be observed, dependent on composition and cross-link state. Annealing effects become more significant at 110 °C than at 80 °C.

When the effects of annealing in the three types of samples are compared, the linear blends experience the most significant change in both permeability and selectivity, whereas the IPN and semi-IPN are relatively less sensitive to annealing. This difference is probably due to the fact that the polymer chains in linear blends are more mobile due to the lack of physical interlocking.

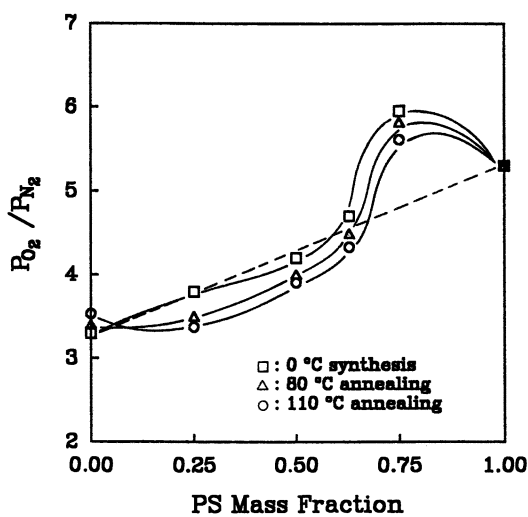
The foregoing observation can be explained on the basis of the free volume change estimated from the density behavior shown in Figures 11, 12, and 13. In a certain range of composition of semi-IPN and linear blend, the positive volume change of mixing was observed after annealing. This change explains the permeability increases above the value calculated from the additivity rule. The large positive deviation from the additive rule is observed in annealed samples (*see* Figures 9 and 10). Such positive deviation is more readily accomplished by annealing in linear blends than in semi-IPN. Note that the difference of permeability between pure PU and PS tends to diminish after annealing, which may result from the post-reaction or the reaction of a few unreacted parts within the pure PU component, which can be retained at low temperature synthesis.

In the case of selectivity, the maximum selectivity at 75% PS composition decreased gradually with annealing in all three types of samples, but the selectivity of IPN remained the best even after annealing. From the foregoing annealing experiment, it can be concluded that, for the gas separation blend membrane that shows a negative volume change of mixing, the homogeneity of the membrane is a very important parameter for determination of the gas permeation characteristics.

From Figures 8–10, the effect of the cross-linked state in the annealed sample on the permeation characteristics can be summarized as follows. The IPN membrane maintains a high separation factor at high PS composition even after annealing at 110 °C for 12 h, but the linear blend membrane shows a low separation factor after annealing due to phase separation. IPN formation is a good route to maintain long-term membrane properties [e.g., permeability, selectivity, and mechanical properties (20)] owing to the cross-

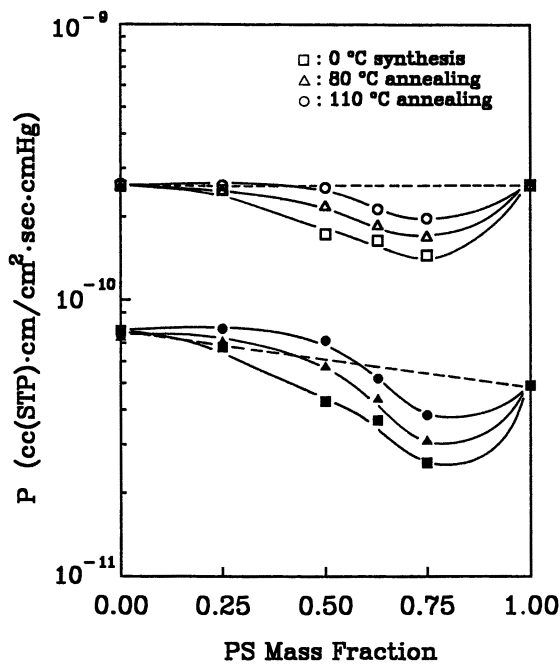


a

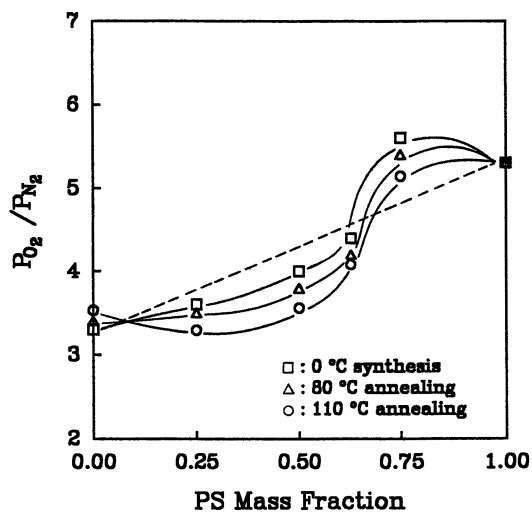


b

Figure 8. Permeability coefficient (a) and separation factor (b) vs. PS content of IPN membranes synthesized at 0 °C and of their annealed samples at 80 and 110 °C for 12 h. Closed symbol, N_2 ; open symbol, O_2 ; dashed line, calculated values from a parallel flux model (20, 32).



a



b

Figure 9. Permeability coefficient (a) and separation factor (b) vs. PS content of semi-IPN membranes synthesized at 0 °C and of their annealed samples at 80 and 110 °C for 12 h. Closed symbol, N_2 ; open symbol, O_2 ; dashed line, calculated values from a parallel flux model (20, 32).

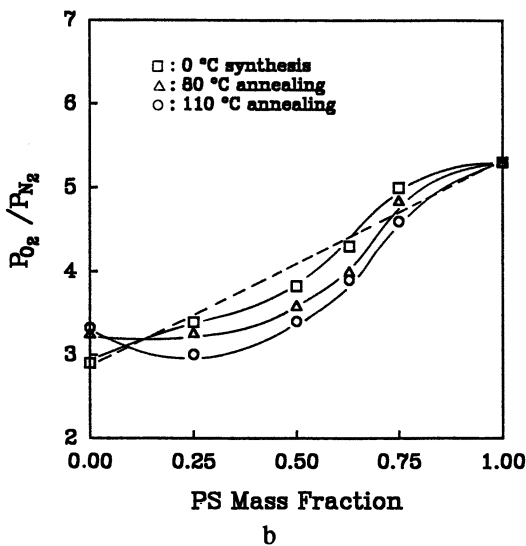
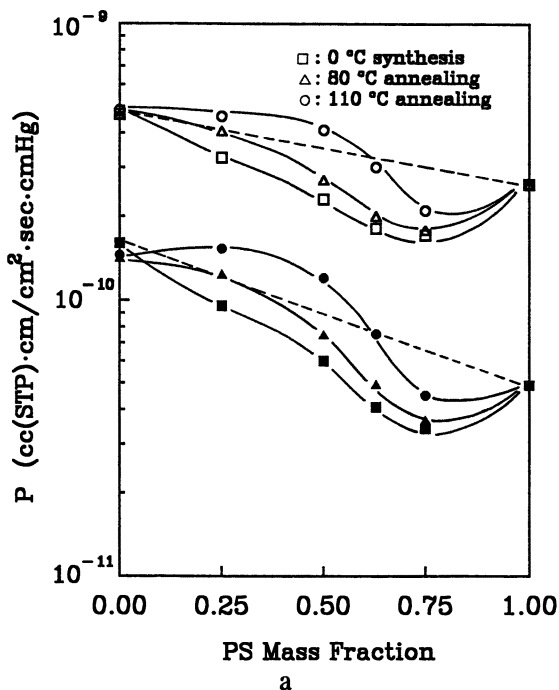


Figure 10. Permeability coefficient (a) and separation factor (b) vs. PS content of linear blend membranes synthesized at 0 °C and of their annealed samples at 80 and 110 °C for 12 h. Closed symbol, N_2 ; open symbol, O_2 ; dashed line, calculated values from a parallel flux model (20, 32).

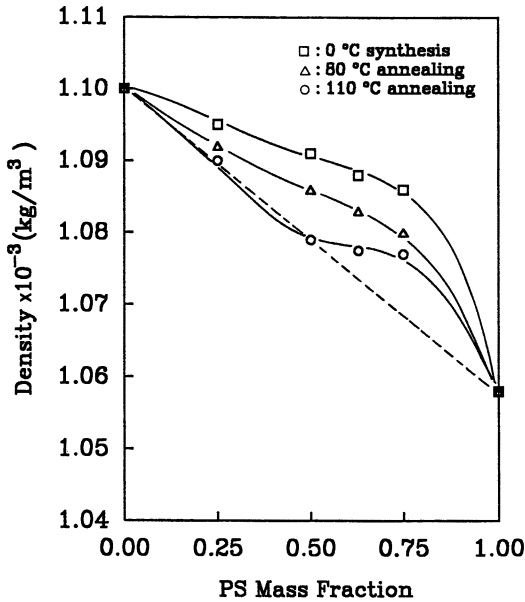


Figure 11. Density vs. PS content in IPN membranes synthesized at 0 °C and their annealed samples at 80 and 110 °C for 12 h. Dashed line, calculated values based on volume additivity rule.

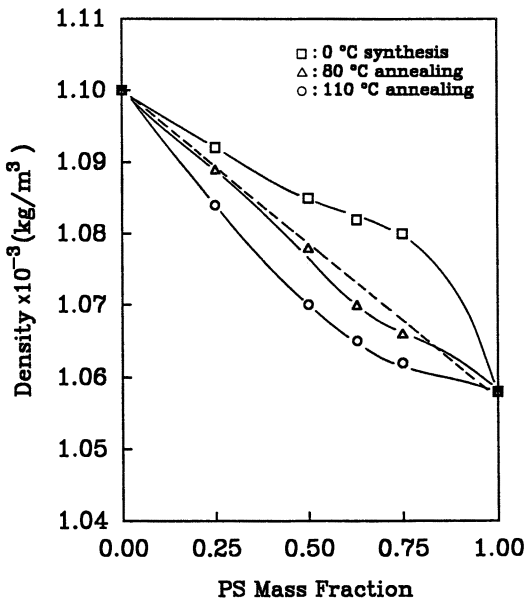


Figure 12. Density vs. PS content in semi-IPN membranes synthesized at 0 °C and their annealed samples at 80 and 110 °C for 12 h. Dashed line, calculated values based on volume additivity rule.

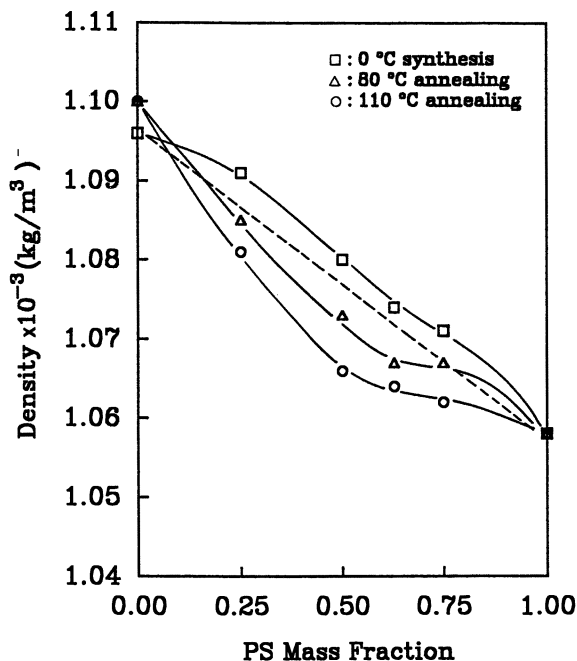


Figure 13. Density vs. PS content in linear blend membranes synthesized at 0 °C and their annealed samples at 80 and 110 °C for 12 h. Dashed line, calculated values based on volume additivity rule.

linked structure. In addition, good membrane properties resulted from the enhanced homogeneity during membrane formation.

Conclusion

In this study, a series of polyurethane–polystyrene (PU–PS) interpenetrating polymer network (IPN), semi-IPN (only the PU component is cross-linked), and linear blend membranes were prepared while the synthesis temperature and composition were varied. The permeability coefficient decreased and the separation factor increased when the membranes were prepared at lower temperature rather than at high temperature due to the homogeneity increase of PU and PS. The permeability coefficient was varied with varying cross-linked state and increased in the sequence IPN, semi-IPN, and linear blends. Annealing increased the permeability coefficients due to further phase separation and caused a decrease in selectivity and the extent of synergistic behavior. The annealing effect on the permeation characteristics was dependent on the cross-linked nature of the membrane (IPN < semi-IPN < linear blends). The change of homogeneity, which was modulated by

change of composition, cross-linked state, synthesis temperature, and annealing temperature, could play an important role in controlling the gas-transport characteristics. The cross-linked nature of IPN can make the membrane highly homogeneous during the synthesis process and can maintain the morphological structure and the membrane properties for a long time. The mechanical properties of IPN show the synergistic value. In conclusion, the IPN is a novel route for preparation of the gas separation membrane.

Acknowledgment

This research was supported by the Korea Science and Engineering Foundation, through grant 90-03-00-29.

References

1. Sperling, L. H. *Interpenetrating Polymer Networks and Related Materials*; Plenum: New York, 1981; p 11.
2. Lee, D. S.; Kim, S. C. *Macromolecules* **1984**, *17*, 268.
3. Lee, D. S.; Kim, S. C. *Macromolecules* **1984**, *17*, 2193.
4. Lee, D. S.; Kim, S. C. *Macromolecules* **1984**, *17*, 2222.
5. Lee, D. S.; Kim, S. C. *Macromolecules* **1985**, *18*, 2173.
6. Kim, B. S.; Lee, D. S.; Kim, S. C. *Macromolecules* **1986**, *19*, 2589.
7. Lee, D. S.; Park, T. S. *Polym. J.* **1991**, *23*, 241.
8. Lee, D. S.; Park, T. S. *J. Appl. Polym. Sci.* **1991**, *43*, 481.
9. Ranby, B. G. *J. Polym. Sci. Symp. Ed.* **1975**, *51*, 89.
10. Shur, Y. J.; Ranby, B. J. *J. Appl. Polym. Sci.* **1975**, *19*, 1337, 2143.
11. Shur, Y. J.; Ranby, B. J. *J. Appl. Polym. Sci.* **1976**, *20*, 3105.
12. Shur, Y. J.; Ranby, B. J. *J. Appl. Polym. Sci.* **1976**, *20*, 3121.
13. Barrie, J. A.; Munday, K. J. *J. Membr. Sci.* **1983**, *13*, 175.
14. Barrie, J. A.; Williams, M. J. L. *J. Membr. Sci.* **1984**, *21*, 185.
15. Chiou, J. S.; Paul, D. R. *J. Appl. Polym. Sci.* **1986**, *32*, 4793.
16. Paul, D. R. *J. Membr. Sci.* **1984**, *18*, 75.
17. Frisch, H. L.; Frisch, K. C.; Klempner, D. *Mod. Plast.* **1977**, *54*(5), 84.
18. Chen, S. A.; Ju, H. L. *J. Appl. Polym. Sci.* **1980**, *25*, 1105.
19. Lee, D. S.; Tak, T. M.; Kim, G. S.; Kim, S. C. *Polym. Adv. Tech.* **1990**, *1*, 231.
20. Lee, D. S.; Jung, D. S.; Kim, T. H.; Kim, S. C. *J. Membr. Sci.* **1991**, *60*, 233.
21. Lee, J. H.; Kim, S. C. *Macromolecules* **1986**, *19*, 644.
22. Lee, W. M. *Polym. Eng. Sci.* **1980**, *20*, 65.
23. Perrin, D. D.; Armarego, W. L. F.; Perrin, D. R. *Purification of Laboratory Chemicals*; Pergamon: Oxford, England, 1988; p 276.
24. Malec, E. J.; David, D. J. *Analytical Chemistry of Polyurethane*; Wiley: New York, 1966; p 87.
25. Stern, S. A.; Shah, V. M.; Hardy, B. J. *J. Polym. Sci., Polym. Phys. Ed.* **1987**, *25*, 1263.
26. Crank, J. *The Mathematics of Diffusion*, 2nd ed.; Clarendon: Oxford, England, 1975; p 45.

27. Barrie, J. A.; Ismail, J. B. *J. Membr. Sci.* **1983**, *13*, 197.
28. Stalling, R. L.; Hopfenberg, H. B.; Stannett, V. *J. Polym. Sci. Symp. Ed.* **1973**, *41*, 23.
29. Maeda, Y.; Paul, D. R. *Polymer* **1985**, *26*, 2055.
30. Van Krevelan, D. W. *Properties of Polymers*; Elsevier: Amsterdam, Netherlands, 1976; p 64.
31. Kim, S. C.; Klempner, D.; Frisch, K. C.; Frisch, H. L.; Ghiradella, H. *Polym. Eng. Sci.* **1975**, *15*, 339.
32. Hopfenberg, H. B.; Paul, D. R. In *Polymer Blends*; Paul, D. R.; Newman, S., Eds.; Academic: New York, 1978; Vol 1, p 445.

RECEIVED for review October 9, 1991. ACCEPTED revised manuscript June 19, 1992.

Semi-interpenetrating Polymer Networks Composed of Poly(ethylene terephthalate) and Castor Oil

Synthesis, Structure, Physical Properties, and Crystallization

L. W. Barrett¹, L. H. Sperling¹, J. W. Gilmer², and S. G. Mylonakis²

¹Center for Polymer Science and Engineering, Materials Research Center, Whitaker Laboratory 5, Lehigh University, Bethlehem, PA 18015

²EniChem America, Inc., Research & Development Center, 2000 Cornwall Road, Monmouth Junction, NJ 08852

Semi-interpenetrating networks (semi-IPNs) have been produced from castor oil and poly(ethylene terephthalate) (PET) by a synthetic method that involves bond interchange reactions that form partial miscible copolymers. Based on the energy absorbed during tensile fracture, the composition that contains 50 wt% PET has over 10 times greater toughness than the constituent PET. The crystallization kinetics of PET were enhanced by the presence of castor oil, both in cooling from the melt state and heating from the quenched glassy state. In conjunction with the chemical nucleating agent (sodium benzoate), PET compositions were even further enhanced in terms of their crystallization characteristics. Semi-IPNs with up to 30 wt% castor oil polyurethane displayed a higher fraction of PET crystallinity than neat PET, but had a lower melting temperature. Greater amounts of castor oil in these semi-IPNs significantly disrupted PET crystallinity and resulted in lower and broader melting and crystallization transitions and overall loss in crystallinity.

INTERPENETRATING POLYMER NETWORK RESEARCH THAT INVOLVES naturally functionalized triglyceride oils has been a topic of great interest at Lehigh University (1–9). These oils are prepared by nature with multiple chemical functionality, and are thus a renewable resource that provides an alternative to petroleum as a chemical feedstock. The oils may be cross-linked to form an elastomeric material, usually by step-growth reactions, which has prompted their use in interpenetrating polymer networks (IPNs) along with chain-growth polymerized plastics. Castor oil in particular has received much attention, primarily because of its status as a large-scale commercial product (1, 2). Other functionalized triglyceride oils are numerous, but none is produced in the same quantities as castor oil. Some of these oils, however, are promising for the future because of their high functionality and the ability to cultivate the precursor oil-seed plants in arid climates at economical yields (10, 11).

Barrett and Sperling (12a, 12b) studied semi-IPNs made from castor oil and poly(ethylene terephthalate) (PET). In the prior IPN literature, primarily amorphous plastics were used. PET is a departure from that norm in that it is a semicrystalline thermoplastic. Castor and other triglyceride oils with other polymers have mostly been limited to use as a plasticizer or stabilizer (11, 13–16). Because PET is semicrystalline, the morphology of the semi-IPN becomes more complicated, which introduces crystallinity as a factor to be considered. Semicrystalline PET has outstanding material properties that are required for an engineering plastic. However, the crystallization rate of PET is slow, which forces long cycle times in injection molding applications. Crystalline PET injection molding grades tend to have lower molecular weight, which increases the crystallization rate and improves melt flow, but the resulting material can be quite brittle and is nearly always sold as a composite with up to 40-vol% chopped glass fiber for increased toughness (17). To address these drawbacks of PET, it was thought that by making semi-IPNs with functionalized triglyceride oils, toughness as well as crystallization rate could be improved. The present chapter reviews and extends the research of Barrett and Sperling (12a, 12b), with an emphasis on the entire composition range: basic characterization, mechanical behavior, and crystallization behavior.

Description of Components

Naturally Functionalized Triglyceride Oil IPNs. The extensive use of castor oil in IPN research began in 1977 with sulfur-cross-linked castor oil that was swelled with styrene and divinylbenzene (8) or methyl methacrylate and glycol dimethacrylate (9) and then polymerized. This form of cross-linked triglyceride, known as factice, makes use of the unsaturated bonds in the triglyceride oil, and can be made with any unsaturated oil (18). The uniqueness of castor oil does not lie in its ability to form factice,

however, and subsequent to this early work, the hydroxyl functionality was exploited to form polyester or polyurethane networks. Castor oil polyester and polyurethane IPNs with polystyrene were studied at Lehigh University during the late 1970s and early 1980s (4–9), and today, research on castor oil polyurethane IPNs with acrylic as well as other polymers is active worldwide (19–22).

Commercial castor oil consists of triglycerides that contain 90% ricinoleic acid residues and 10% nonfunctional acid residues, so that castor oil has an effective hydroxyl functionality of 2.7 (23–25). By reaction of the hydroxyls with a difunctional reactant, castor oil may be cross-linked to form a soft elastomer, with a glass transition temperature, T_g , as low as $-50\text{ }^\circ\text{C}$ (4, 5), dependent on the cross-linker used. Utilizing a dibasic acid, a polyester network can be formed; however, this reaction releases a condensation product: water. Sebacic acid ($\text{HOOC}[\text{CH}_2]_8\text{COOH}$) has often been used as the dibasic acid because it is derived from castor oil (26). If instead a diisocyanate is used, a polyurethane network can be made without the release of any byproduct. Because of the difficulty involved in making a void-free material when water is released during cross-linking, hybrid polyester-urethane networks have been made, where the castor oil polyester is polymerized to just below the gel point, all the water is driven off, and then the material is cross-linked with a diisocyanate.

The formation of polyester or polyurethane networks has two distinct advantages over factice. Because the step growth reaction does not interfere with radical chain polymerizations, simultaneous polymerization with monomers such as styrene and acrylics is possible. The other advantage is that the triglyceride oil double bonds remain intact in the polyester or polyurethane networks, which allows staining for electron microscopy imaging of the phase structure in the IPNs formed. These characteristics of triglyceride oils have made them invaluable in the study of morphology development in IPNs.

Many other functionalized triglyceride oils, such as vernonia, lesquerella, crambe, and linseed, as well as their epoxidized analogs, also have been used in the past to form IPNs with chain-polymerizable monomers, such as styrene and acrylics (2, 3, 5, 23, 27, 28a, 28b). Vernonia oil, a naturally epoxidized oil, was combined with PET to make semi-IPNs in research (28b) parallel to that described in this paper. These functionalized triglyceride oils, although not yet commercially available, offer different characteristics than castor oil, both in terms of the chemistry involved and the physical properties and morphology development of the IPNs.

IPNs may, in general, be formed by two methods (29). In the sequential method, a cross-linked network is formed, then swelled with the monomer and cross-linker of the second component and polymerized to create the interpenetrating network. If the two components polymerize by noninterfering routes, then the IPN may be formed by the simultaneous method, where monomers and cross-linkers of both materials may be mixed and polymerized

simultaneously. Prior triglyceride oil IPN research has proceeded by polymerizing both components from their monomeric state. In this way, the components are initially miscible either as monomers (simultaneous method) or as a swollen network (sequential method) and then phase separate as polymerization and cross-linking occur. It is the relationship between cross-linking and phase separation kinetics that controls the final IPN morphology (30a).

In the present research, fully polymerized PET is the starting material, which puts some constraints on the IPN formation process. PET may be considered as the condensation product of terephthalic acid and ethylene glycol. Because the castor oil would polymerize with terephthalic acid in competition with ethylene glycol, simultaneous semi-IPN formation from monomers is not possible, because noninterfering polymerization routes are required. Although PET and castor oil polyester network are both polyesters, PET is aromatic and castor oil is aliphatic, and the two are immiscible. Thus, castor oil will not dissolve in PET nor will polymerized PET swell a castor oil network. These factors make sequential IPN formation impossible. To control the IPN morphology of PET and castor oil network, the two components must first be either miscible or well mixed, and then be allowed to phase separate as the castor oil cross-linking occurs.

The discovery that continued heating of castor oil and PET results in a miscible mixture—a consequence of bond interchange reactions that form a compatibilizing copolymer (12a)—solved the problem of initial immiscibility. Because PET contains ester groups and castor oil contains both ester and hydroxyl groups, either ester–ester or hydroxyl–ester interchange (or both) take place (12a, 30b). In either case, the resultant semi-IPN is a hybrid structure in which the cross-linked or uncross-linked materials may be copolymers rather than pure components. Thus, the extent to which the bond interchange reactions take place affects many aspects of the resulting semi-IPN. This method, wherein miscibility between the two components is affected by bond interchange copolymer formation, is potentially applicable to many other systems where bond interchange takes place and should make interesting new IPNs and semi-IPNs.

Crystallization of Poly(ethylene terephthalate). PET is a widely utilized polymer because of its high strength, thermal stability, good barrier properties, low price, and good solvent resistance. PET is established as a primary material in bottles, textiles, recording tape, and packaging film. Injection molding is, however, one area in which, until recently, PET has not been extensively utilized due to a slow crystallization rate that results in poor dimensional stability of molded parts. The crystallization rate of PET on cooling from the melt to the glass is considerably slower than the rate of poly(butylene terephthalate) (PBT) possibly due to difficulty in chain fold formation (Runt, J. P., private communication). The maximum crystallization rate of PET occurs at about 180 °C, which is halfway between its glass-transi-

tion temperature (approximately 70 °C) and its equilibrium melting point (about 285 °C). At 90 °C, a typical mold temperature used in injection molding polyesters, the rate of crystallization for PET is virtually zero. Although one method to improve the moldability of PET is to raise the temperature of the mold, at temperatures greater than 110 °C it is no longer possible to use water to heat the mold, so oil must be utilized instead. Because most molders do not wish to switch to oil heating to mold PET, nucleation agents and mobility enhancers have been developed that allow molding at temperatures of 100 °C or lower. Thus, much of the prior art that had been developed in the area of PET molding concerns the development of nucleating agents that are effective to induce rapid PET crystallization at high temperatures when cooling from the melt temperature to the mold temperature (31).

Developments in the 1970s and early 1980s in PET nucleation (32–35) involved the use of aliphatic and aromatic sodium carboxylates to nucleate reinforced PET. Unlike the traditional inert solid physical nucleation agents such as talc, which work by an epitaxial mechanism, these chemical nucleation agents work by dissolving in PET. Extensive nucleation technology that has been developed for PET involves the use of low molecular weight alkali metal carboxylates (36–42) as well as polymeric nucleants that contain pendant alkali metal carboxylates (43–45). Technology developed by Deyrup (33) describes the combined use of a nucleant, “a sodium or potassium salt of a hydrocarbon acid containing between about 7 and 25 carbon atoms, or with the sodium or potassium salt of an organic polymer which contains pendant carboxyl groups...”, and a mobility enhancer—a low molecular weight organic plasticizer (for example, ketones, esters, or sulfones). A filler is also added for the purpose of reinforcement of the resin. The presence of a chopped glass fiber in injection moldable PETs markedly increases both the tensile strength and modulus of the PET and results in improved toughness. The use of carbonyl-containing plasticizers, such as esters and ketone, in reinforced PET in conjunction with selected sodium or potassium carboxylates enhances the rate of crystallization as the molded part has nearly cooled to the mold temperature (33, 44). Additional mobility enhancers that have been developed include mixtures of oligoethers and oligoether segments that are employed jointly to synergistically increase the mobility of the PET (46, 47). The addition of small amounts of polyolefins such as polyethylene also enhances the mobility of PET in the melt, as well as improves its toughness (48, 49).

Research by Biebuyck et al. (50) details the nucleation of PET by a variety of different basic salts of the alkali metals including carboxylic, phenolic, phosphonic, phosphinic, and sulfonic salts. This study describes the use of a range of ionizable metal salts that are able to activate the PET chain end and thus are useful in the nucleation of PET. The alkali metal salts of various metal oxides also nucleate PET (51). The mechanism by which alkali

metal salts function to nucleate PET was best addressed by the spectroscopic study undertaken by Dekoninck et al. (52), who were able to demonstrate by Fourier transform infrared (FTIR) spectroscopy that a basic sodium salt reacts with the ester to cleave the PET chain and to form a sodium carboxylate chain end. The presence of sodium on the end of the PET chain then facilitates nucleation. If the PET is annealed in the melt for extended periods of time, it gradually loses its nucleating ability. This loss occurs by the reaction of two neighboring sodium carboxylate chain ends to form disodium terephthalate—a very poor nucleating agent for PET.

Most group I carboxylates are effective as nucleants for PET along with many other group I salts. Two examples of group I carboxylates that were found to be totally ineffective as PET nucleants are disodium terephthalate and sodium parahydroxybenzoate. The precise reason that some salts are more effective than others is not understood, but is believed to depend, at least in part, on the ability of the salt to react with PET and transfer the group I metal to the chain end. This capability could involve such factors as solubility of the salt in molten PET, the heat of fusion of the salt crystal, and the relative basicity of the salt.

Finally, chemical nucleation with ionic groups on chain ends is transferable to polymers other than PET. Legras et al. (53, 54) have shown how polycarbonate and poly(ether ether ketone) (PEEK) can be nucleated by the presence of ionic groups on the chain end. This mechanism presumably would be extendible as well to other high-performance condensation polymers, such as polyimides, poly(phenylene ether), and high-temperature polyesters.

Summary. Until now, triglyceride oil IPN research has concentrated on morphology and physical properties of amorphous compositions. The large amount of work that has been done in this field has expanded the knowledge base regarding how to control phase continuity and domain size and how to correlate morphology and physical properties. To a large extent, however, the use of semicrystalline polymers in IPNs has been ignored. Because PET is a semi-crystalline polymer, the effect of crystallinity on IPN morphology and physical properties becomes a significant new variable to be considered. In this chapter, the effectiveness of castor oil to improve the crystallization characteristics of PET is considered, as is the crystallinity of PET–castor oil network semi-IPNs. In the present research, only a small number of the questions related to crystallizable IPNs have been addressed, and perhaps more questions have been raised by the work than have been answered. It is hoped that interest in the area of semicrystalline IPNs may be stimulated by this work.

Prior IPN systems were primarily based on miscible monomers that polymerize to form immiscible networks and were produced by either

simultaneous or sequential methods of IPN synthesis. In the present research, castor oil semi-IPNs have been produced with fully polymerized PET by taking advantage of bond interchange reactions to create an initially miscible mixture prior to cross-linking and subsequent phase separation. The resultant structure contains a significant fraction of copolymer, both in the network as well as in the uncross-linked portion. Although in this chapter just enough copolymer to create a miscible mixture was utilized, the extent of copolymerization becomes another synthetic variable that may be controlled to tailor structure, morphology, and physical properties. Creation of IPN materials from fully polymerized immiscible polymers through a bond interchange copolymerization process, followed by cross-linking, is a concept applicable to many other systems. This concept opens the possibility to create novel IPN compositions and microstructures.

Experimental Details

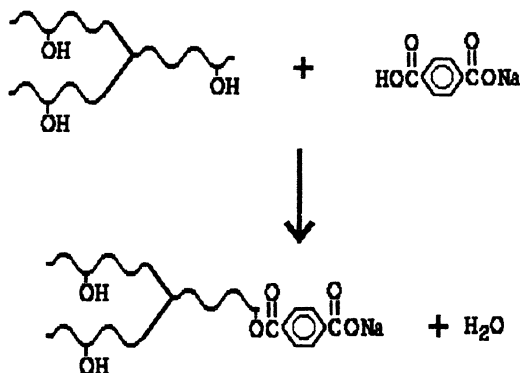
Materials and Syntheses. Poly(ethylene terephthalate) was supplied by EniChem America, Inc. with intrinsic viscosity of 0.60 dL/g, as measured in 60:40 by weight tetrachloroethane:phenol. This viscosity corresponds to viscosity average molecular weight of ~ 13 kg/mol (55). The PET was dried at 120 °C in a vacuum oven for at least 48 h prior to use. PET may be polymerized further in the solid state at temperatures just below the melting point under vacuum (56–58). High molecular weight PET of ~ 40 kg/mol (viscosity average) was produced in this manner by annealing fully dried PET pellets for 72 h at 240 °C under vacuum.

Castor oil was supplied by CasChem, Inc., and contains triglycerides in which some 90% of the acid residues are the hydroxyl-bearing ricinoleic acid. Toluene 2,4-diisocyanate (TDI) was purchased from Aldrich. Hydrogenated methylene diphenyl diisocyanate (HMDI) or 1,1'-methylene-bis(4-isocyanatocyclohexane), commercially available as Desmodur-W, was supplied by Mobay Corp.

Monosodium terephthalic acid (MSTA) was prepared by dissolving terephthalic acid in dimethyl sulfoxide (DMSO) and stirring in the presence of insoluble sodium hydroxide pellets at room temperature. In this heterogeneous reaction, when a sodium hydroxide molecule is able to neutralize one of the carboxylic acids on terephthalic acid, the monosodium terephthalic acid precipitates from DMSO. Monosodium terephthalic acid is insoluble in both DMSO and water, and is therefore easily purified from the water-soluble sodium hydroxide and terephthalic acid, which is DMSO-soluble and water insoluble. Elemental analysis, performed by Galbraith Laboratories, Inc. (Knoxville, TN) yielded 50.7-wt% carbon, 4.0-wt% hydrogen, 29.9-wt% oxygen, 3.6% sulfur, and, by difference, 11.8-wt% sodium, as compared to calculated values of 51.1-wt% carbon, 2.7-wt% hydrogen, 34.0-wt% oxygen, and 12.2-wt% sodium. The sulfur detected in the MSTA material was apparently due to incomplete separation from the DMSO solvent.

Castor oil monosodium terephthalate (COMSTA) was prepared by direct esterification by heating castor oil with monosodium terephthalic acid at 180 °C

for 10 h. The reaction scheme is



This reaction was not carried to completion, and the product had to be filtered from the remaining MSTA. Fourier transform infrared spectroscopy of the resulting COMSTA mixture showed new absorbance peaks at 1100 and 1240 cm^{-1} , where the benzoate functionality absorbs strongly. Elemental analysis gave 73.1-wt% carbon, 9.8-wt% hydrogen, 15.2-wt% oxygen, and 1.0-wt% sodium; calculated values were 70.8-wt% carbon, 9.7-wt% hydrogen, 17.4-wt% oxygen, and 2.1-wt% sodium. Based on the sodium analysis, the mixture as used contained about 50% COMSTA; the remainder was castor oil.

Two methods of mixing and reacting PET and castor oil were used. The first method used a Brabender batch melt mixer; a flask with magnetic stirring was used in the second method. The Brabender mixtures of PET with the castor oil or prepolymers were made at 290 °C in a 50-mL torque rheometer batch mixer (Brabender Plasticorder) equipped with sigma blades. The PET is first added and allowed to melt, after which the oil is added by syringe. The compositions made by this method all contain 90-wt% PET and 10-wt% castor oil product. The mixing was carried out for approximately 8 min with nitrogen purging. Samples of the material were removed from the mixer at specific times and quenched in ice water, but the bulk of the PET compositions were allowed to cool slowly at room temperature, which resulted in highly crystalline materials. Semi-IPNs were also made in the Brabender mixer by first melting the PET, and then adding the premixed castor oil and TDI prepolymer. The isocyanate-hydroxyl reaction takes place almost instantly at the mixing temperature and forms the castor oil network in the presence of PET. Due to the viscosity mismatch between molten PET and castor oil, blends that contain more than 10-wt% oil were made by a different method, which shall be described next.

A wide range of compositions were made by the second method, which utilizes a flask and magnetic stirring. A time-temperature schematic that summarizes this synthesis procedure is shown in Figure 1. First, the requisite amount of PET was melted in castor oil in a flask at 280 °C under nitrogen atmosphere and with stirring; then the temperature was raised to 300 °C. With continued stirring at 300 °C, the initially immiscible mixture becomes miscible to the point of optical clarity. At this stage, the heat source is removed and the miscible mixture is allowed to cool to 240 °C (cooling below this temperature results in crystallization and precipitation of the PET from solution). The required amount of diisocyanate cross-linker (HMDI) is then rapidly added by syringe and the

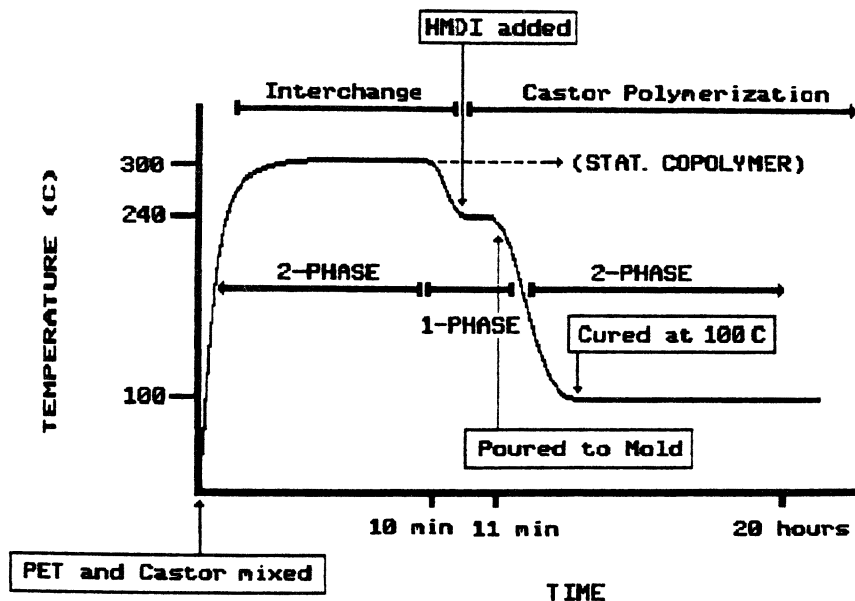


Figure 1. Schematic diagram that depicts the synthetic procedure used in production of PET-castor oil-HMDI urethane network semi-IPNs. Axes are not drawn to scale.

solution is mixed quickly and poured into molds. The hydroxyl-isocyanate reaction occurs rapidly at 240 °C, so the mixture must be poured into the mold within less than 1 min, before the castor oil gel point has been reached. After pouring, the molds are placed in an air oven at 100 °C for 18 h, where the cross-linking reaction is brought to completion.

Measurement Techniques. Differential scanning calorimetry (DSC) was done using a differential scanning calorimeter (Mettler TA-3000) in scanning (20 °C/min) and isothermal modes. The sample size was kept close to 15 mg. Quenched samples were first melted in the DSC for 3 min at 300 °C, then quickly taken out and submerged in liquid nitrogen. The samples were then reheated at 20 °C/min to measure the glass transition, crystallization, and melting temperatures.

Mechanical testing was done using a material test system (Instron) interfaced to a microcomputer (IBM PS/2). The general test procedure and sample preparation is described in the ASTM D-1708 microtensile test method. The strain rate was 112%/min, which was calculated from 25-mm/min displacement for specimens of gauge length 22.25 mm. Load versus displacement data was converted directly to stress versus strain without making any corrections, because it is assumed that strain outside the gauge section was minimal. The tensile strength, Young's modulus, and percent elongation were calculated in a straightforward manner per the ASTM standard, and the energy to break was calculated from the area under the stress-strain curve.

Fourier transform infrared (FTIR) spectroscopy was carried out using a spectrometer (Mattson Polaris) interfaced to a microcomputer (Zenith-386). Sample preparation was generally performed by making a 1-wt% solution of the material to be analyzed in trifluoroacetic acid (TFA), followed by dropwise addition of the solution onto silver chloride (AgCl) plates and evaporation of the TFA. In general, 64 scans from 800–4000 cm^{-1} were taken at 2- cm^{-1} resolution and averaged. Because the thickness of the film on the AgCl plates was unknown, quantitative methods required determination of the ratio of peak heights to a standard of known composition.

Results

The flask mixture method was used to prepare the entire range of castor oil–PET compositions in increments of 10 wt% by weight. In these materials, the PET and castor oil were mixed and heated to the point of miscibility; then the castor oil was cross-linked with HMDI to form a polyurethane network. The resultant materials were yellow–white in appearance and ranged in properties from elastomeric to plastic, dependent on composition.

Mechanical Properties. Selected stress–strain curves of these materials are shown in Figure 2, and calculated values given in Table I. The initial PET material has a low molecular weight ($M_v = 12.9$ kg/mol), at or just slightly below the critical entanglement molecular weight (59), so that

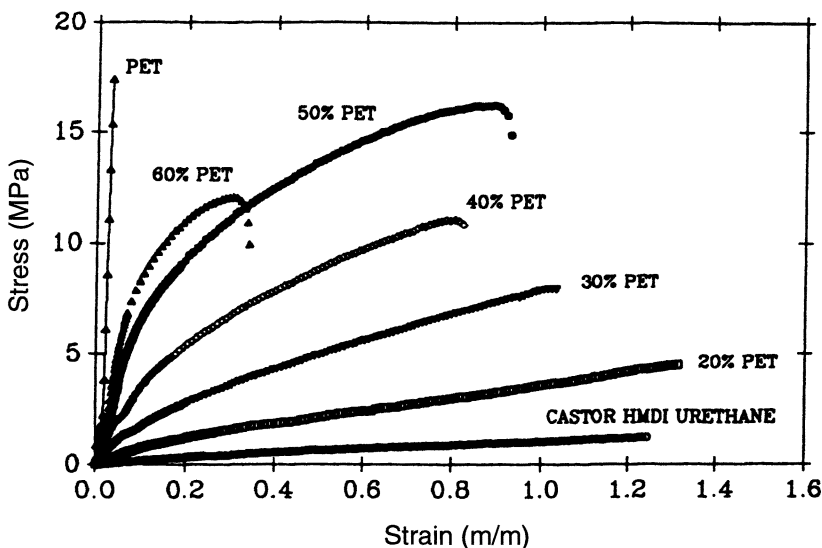


Figure 2. Stress–strain curves for a range of PET–castor oil–HMDI polyurethane network semi-IPN compositions. (Reproduced with permission from reference 12b. Copyright 1993.)

Table I. Calculated Values from Tensile Stress-Strain Data

<i>PET</i> (%)	<i>Tensile</i> (MPa)	<i>Modulus</i> (MPa)	<i>Elongation</i> (%)	<i>Energy</i> (J/m ³)
0	1.2	4.1	116.3	850
10	1.6	5.7	139.1	1,216
20	4.3	14.7	132.7	3,410
30	8.4	27.7	116.9	6,121
40	10.6	53.3	85.3	6,589
50	13.5	68.5	93.6	10,867
60	10.9	192.8	31.0	3,251
100	16.4	1269.0	1.1	114
100 (HMW)	55.0	1700.0	39.0	12,500
50 (HMW)	18.2	116.7	119.8	16,000

NOTE: Standard deviation in measured values was 15% (of the mean) for tensile strength, 25% for modulus, 17% for elongation, and 22% for energy density.

SOURCE: Data are taken from reference 12a.

this PET became brittle when crystallized. Added to this problem is the bond interchange with castor oil that would further reduce the average molecular weight. As a result, compositions with over 60-wt% PET were too brittle to be tested. Despite these effects, the intermediate composition semi-IPNs have much better toughness than the materials from which they were made. The 50-wt% PET semi-IPN clearly stands out with elongation close to that of the castor oil elastomer and tensile strength almost as high as the neat PET.

When a similar 50-wt% semi-IPN was made with higher molecular weight PET ($M_v = 40$ kg/mol), the mechanical properties were improved, but not nearly as much as the improvement in the neat PET by the molecular weight increase (Figure 3). Here the reduction in molecular weight of PET caused by bond interchange reactions with castor oil must be considered. Starting with PET of $M_v = 12.9$ kg/mol, after reaction with castor oil, the viscosity average molecular weight dropped to 1450 g/mol. This drop represents nearly a ninefold decrease in molecular weight. Although this drop may be overestimated due to the dilute solution viscosity method of molecular weight measurement (the PET-castor copolymer may have tighter coils and lower solution viscosity than neat PET at equal molecular weight), the evidence suggests that PET chains are severed. Thus, although at 40 kg/mol, the neat PET is well above the critical entanglement molecular weight and quite strong and tough, the castor-PET semi-IPN may contain PET with molecular weight below the critical entanglement molecular weight, and is thus only slightly improved over a semi-IPN made with low molecular weight PET.

Values calculated from the stress-strain curves are tabulated in Table I, in which only the materials denoted by HMW were made with the high molecular weight PET. Although the modulus surely increases with PET

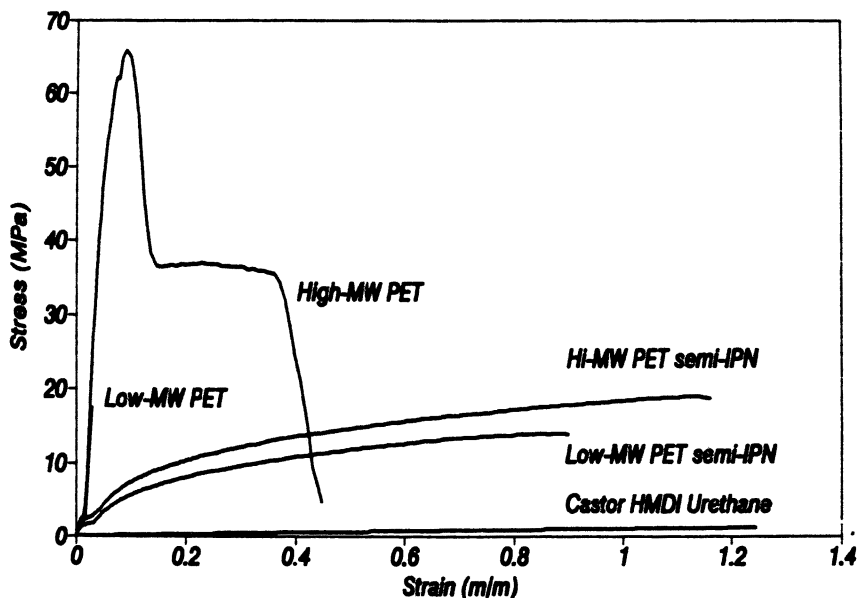


Figure 3. Stress-strain curves that compare 50:50 PET:castor oil-HMDI polyurethane network semi-IPNs made with high ($M_v = 40$ kg/mol) and low ($M_v = 13$ kg/mol) molecular weight PET.

content, it takes a large jump between 40- and 60-wt% PET, which is indicative of a change in the continuous phase from castor oil-HMDI polyurethane (low modulus) to PET (high modulus). The energy to break for the samples is greater for the semi-IPNs than for either of the constituent materials, even in the case where the tough high molecular weight PET was used. The energy required to break the 50-wt% low molecular weight PET composition is over 10 times that for the neat PET used, and is comparable to that for castor oil-polystyrene IPNs (60).

Glass-Transition Behavior. Although the modulus versus composition data indicate which component predominantly constitutes the continuous phase, a more detailed picture of phase structure may be obtained by studying the glass transition. In Figure 4, the glass transitions as measured by DSC for the components and their mixtures are shown, both in conventional heat flow versus temperature and derivative of heat flow formats. In the 50:50 castor oil:PET mixture, which was sampled just before the diisocyanate cross-linker was added but after the solution became clear at 300 °C, two phases were present: one with a glass-transition temperature that matches that of castor oil and the other with a transition temperature near that of

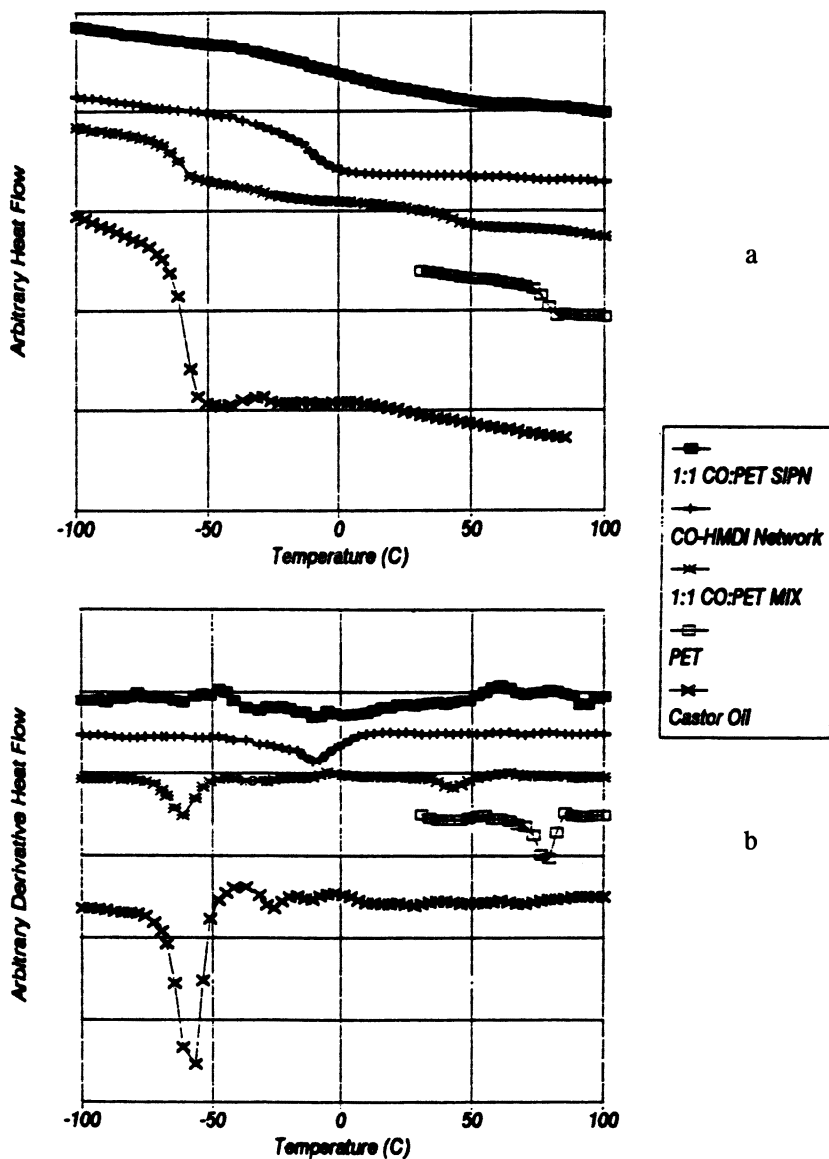


Figure 4. DSC glass-transition curves for the 50:50 PET:castor oil-HMDI polyurethane network composition and its components. Conventional DSC scans, with heat flow versus temperature (A), as well as derivative heat flows (B) are shown. (Reproduced with permission from reference 12b. Copyright 1993.)

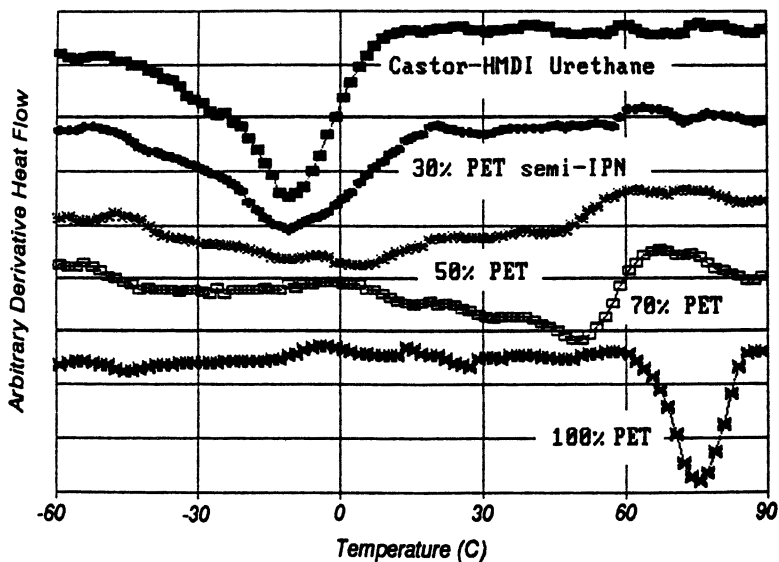


Figure 5. DSC derivative heat flow plots that show the glass transition for a range of PET-castor oil-HMDI polyurethane network semi-IPN materials.

PET, but shifted downward from 75 to 45 °C. When the diisocyanate was added to this mixture, which created cross-links between the hydroxyls present, the resultant glass transition was broadened to a range roughly from the start of the castor oil polyurethane transition to the end of the PET-rich phase transition observed in the mixture before cross-linking. This behavior is common to microheterogeneous phase morphology, where a single broad glass transition is observed over the range that covers the transitions of the constituent materials (29). It should be emphasized that the glass transition reveals information about only the noncrystalline portion of the mixture. In these semi-IPNs, PET is able to crystallize, so that a single glass transition could be observed when the PET is highly crystalline. However, as the PET content is reduced in the semi-IPN, so is its ability to crystallize to large extents. Thus, when a single glass transition is encountered in these semi-IPNs, it is most likely due to microheterogeneous morphology, not high crystallinity of the PET fraction.

Derivative heat flow DSC plots that show a range of PET-castor oil-HMDI polyurethane compositions are depicted in Figure 5. These curves reveal the transition from two-phase morphology (30-wt% PET) to microheterogeneous morphology (50-wt% PET) and back again to two phases (70-wt% PET) as a function of composition. This behavior is the result of the effects of bond interchange on miscibility and the rates of cross-linking and phase separation, which determine the morphology.

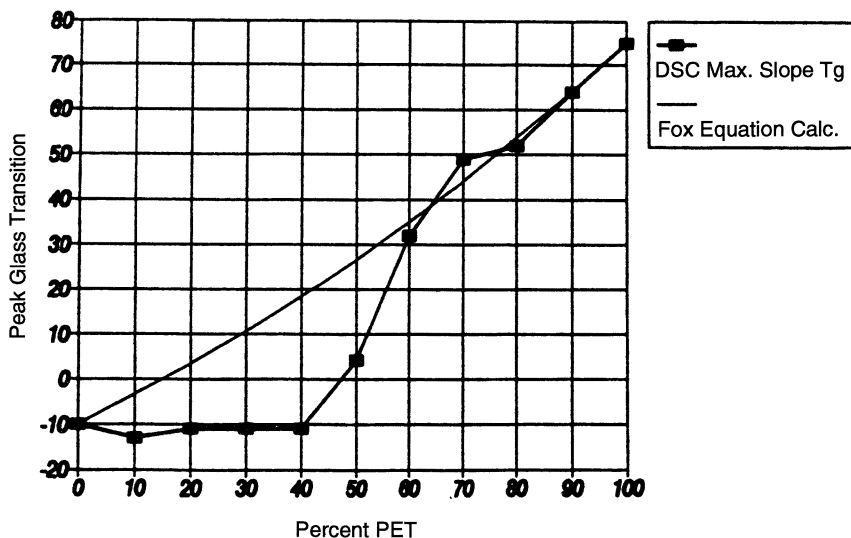


Figure 6. Peak glass-transition temperature versus weight percentage PET for the range of PET-castor oil-HMDI polyurethane network semi-IPN compositions. The straight line represents the glass-transition temperature calculated through use of the Fox equation. (Reproduced with permission from reference 12a. Copyright 1991.)

Further analysis of the glass-transition behavior of the series of semi-IPNs reveals some interesting characteristics. Determining of the peak glass-transition temperature (the temperature corresponding to the minimum in derivative heat flow) of a wider range of compositions and plotting of these temperatures versus weight percent PET revealed the values shown in Figure 6. The straight line depicted in Figure 6 shows the value of glass-transition temperature calculated by the Fox equation (61), which correctly predicts the data for the high-PET end of the composition. Because the Fox equation was derived for prediction of the glass-transition temperature of miscible blends or random copolymers, this agreement suggests that the PET-containing phase is a miscible mixture, or copolymer, formed between PET and castor oil. At the low-PET end, the peak glass-transition temperature is virtually constant and equal to that for castor oil-HMDI polyurethane, which suggests that the pure polyurethane is the predominant phase in that case.

Crystallization Behavior. Castor oil is compared with common nucleating agents in PET compositions in Figure 7, where the normalized extent of crystallization is plotted versus temperature. In crystallization from the melt, 1 wt% of the chemical nucleating agent sodium benzoate effectively

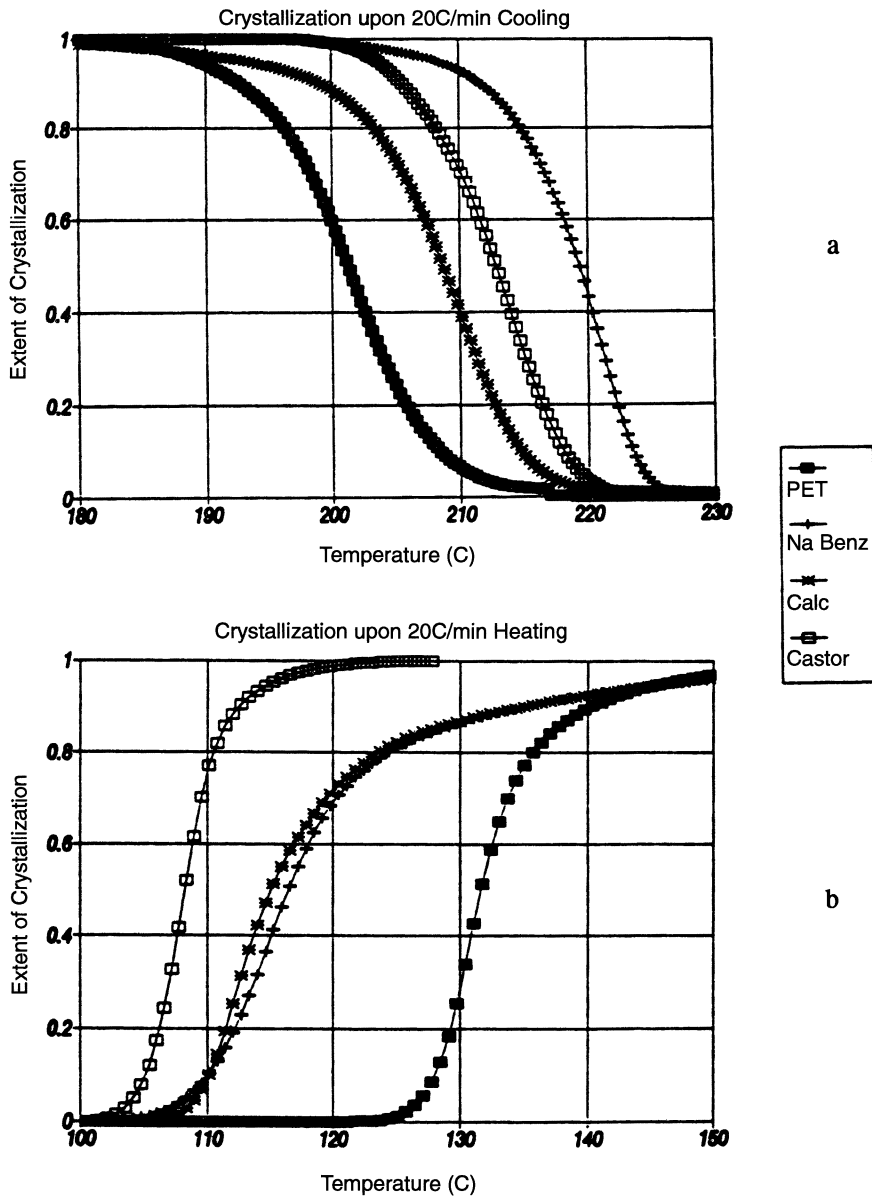
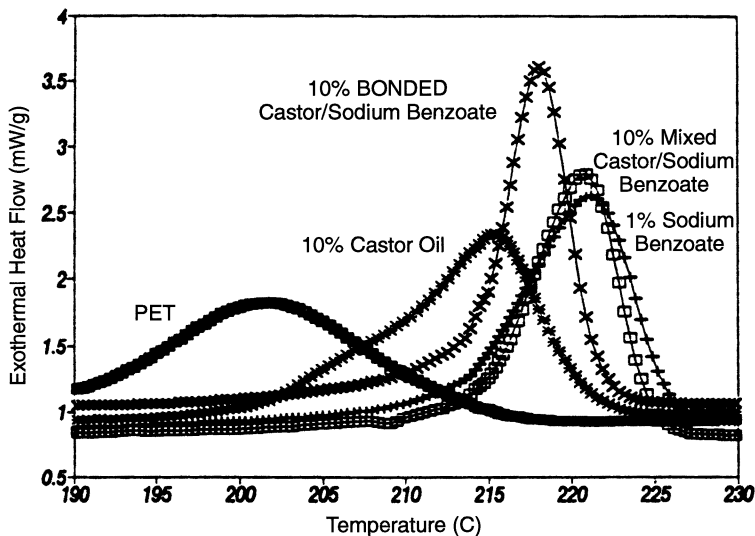


Figure 7. Extent of crystallinity versus temperature calculated from DSC data during cooling from the melt state (A) and heating from the glassy state (B) for PET and PET compositions that contain either 1-wt% sodium benzoate, 1-wt% calcium acetate, or 10-wt% castor oil.

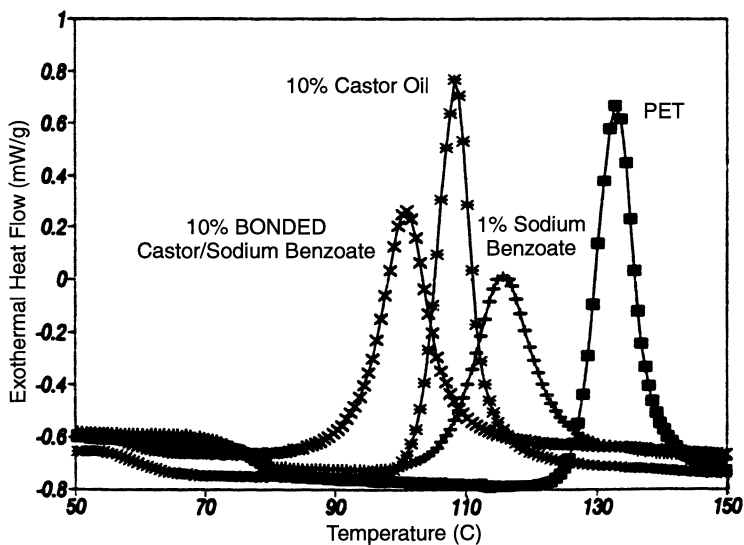
improves the onset and peak crystallization temperature of PET; however, the effectiveness of castor oil is close behind and is, in fact, better than 1 wt% of the physical nucleation agent, calcium acetate. In crystallization from the glass, castor oil is significantly better than sodium benzoate, which in this case is no more effective than calcium acetate.

Combinations of sodium benzoate and castor oil were investigated next. The castor oil and sodium benzoate may simply be mixed together with PET, or else a new molecule can be created in which the sodium benzoate functionality is bonded to a castor oil molecule. The reaction scheme used to form such a hybrid molecule, castor oil monosodium terephthalate (COMSTA) was shown earlier in eq 1. In Figure 8, DSC crystallization scans of PET compositions that contain the bonded castor-sodium benzoate are compared with similar compositions wherein the castor oil and sodium benzoate are simply mixed. In crystallization from the melt, the simple mixture has a higher onset and peak crystallization temperature, whereas the COMSTA composition has a much sharper crystallization peak. Table II gives some of the numerical crystallization data for these compositions, both in cooling from the melt and as heating from the quenched glassy state. The COMSTA composition has a greater heat of fusion (ΔH) than the simple mixture in cooling and neat PET in both heating from the glass and cooling from the melt. The theoretical heat of fusion for 100% crystalline PET is 130 J/g (59), so the materials in Table II range in crystallinity from ~ 25 wt% up to 45 wt%. In crystallization from the glass, the simply mixed castor oil-sodium benzoate composition could not be adequately quenched to yield comparable data, due to rapid crystallization during cooling, and therefore is not included. Although the COMSTA composition could be quenched in liquid nitrogen, it had a crystallization temperature 8 °C lower than the castor oil composition, which has a crystallization temperature ~ 20 °C lower than PET.

The enthalpy of fusion measured for the synthesized series of semi-IPNs is plotted versus the amount of PET in Figure 9. These materials have relatively high crystallinity as a result of the semi-IPN synthesis procedure, wherein they were held at 100 °C for 18 h, which effectively annealed the PET. The semi-IPNs with 80-wt% and 90-wt% PET actually have greater crystallinity per gram of PET than similarly annealed neat PET; however, the crystallinity of semi-IPNs with less than 60-wt% PET falls off rapidly. Figure 10 shows the peak melting temperature upon heating and the onset and peak crystallization temperature upon cooling as a function of weight percent PET for the semi-IPN series. The addition of 60-wt% castor oil-HMDI polyurethane network depresses the PET melting point by over 50 °C. The difference between crystallization onset and peak temperatures also becomes greater because there is less PET in the semi-IPN; thus, the transition is broadened by the addition of the castor oil polyurethane.



A



B

Figure 8. DSC heating scans that show crystallization from the melt (A) and glass transition and crystallization from the glassy state (B) for PET and compositions that contain castor oil or sodium benzoate. (Reproduced with permission from reference 12b. Copyright 1993 Society of Plastics Engineers.)

Table II. PET Crystallization Data for Castor Oil or Sodium Benzoate Compositions

<i>Composition</i>	ΔH_m	T_{cm}	ΔH_g	T_{cg}
PET	45.9	202.2	36.5	133.6
10% Castor oil	58.1	215.0	40.6	109.7
1% Sodium benzoate	52.4	222.5	33.3	117.2
10% Castor + 1% sodium benzoate	49.4	221.8	— ^a	— ^a
10% COMSTA	55.9	219.5	38.7	102.1

NOTE: ΔH_m is the heat of crystallization as measured in cooling from the melt state; T_{cm} is the peak crystallization temperature as measured in cooling from the melt state; ΔH_g is the heat of crystallization as measured in heating from the glassy state; T_{cg} is the peak crystallization temperature as measured in heating from the glassy state.

^a This sample could not be quenched effectively enough for comparable data.

SOURCE: Data are taken from reference 12a.

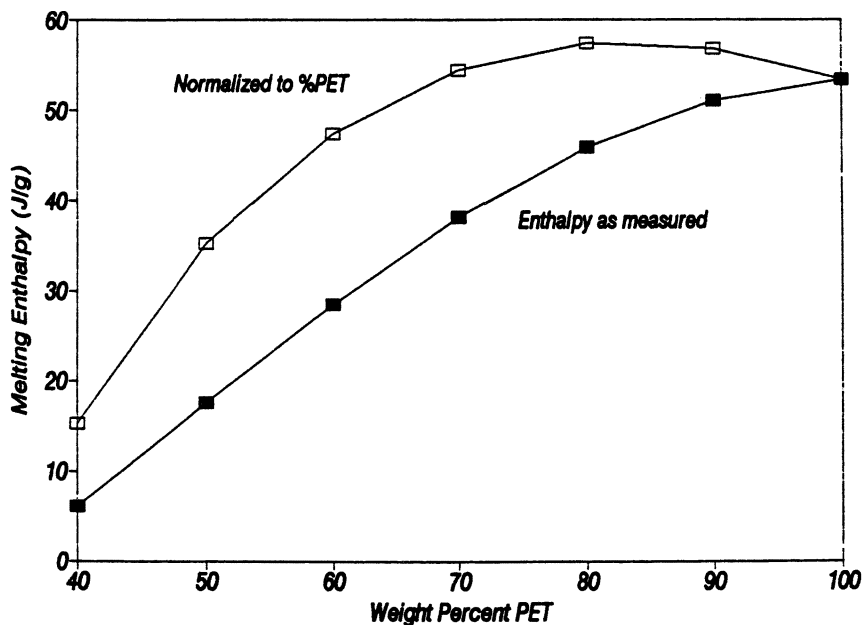


Figure 9. Enthalpy of fusion (ΔH) recorded in DSC experiments for the PET-castor oil semi-IPNs, plotted as a function of PET content. "Normalized to %PET" is the enthalpy value divided by the weight fraction of PET in the semi-IPN.

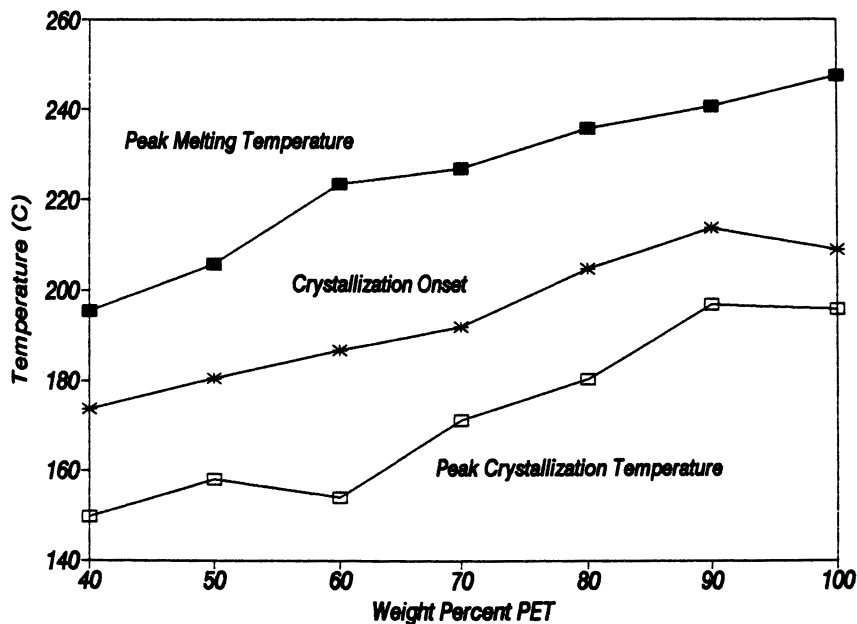


Figure 10. Peak melting temperature upon heating, and onset and peak crystallization temperature upon cooling the PET-castor oil-HMDI polyurethane network semi-IPNs as a function of PET content.

Discussion

Semi-IPN Structure. Castor oil and PET are initially immiscible; however, if the mixture is given time at elevated temperature to react, it eventually becomes miscible. The addition of diisocyanate HMDI to the mixture causes the castor oil to become cross-linked in the presence of the linear PET. The resultant materials are then semi-IPNs, wherein two materials are combined: one material is cross-linked and the other material is linear. Typically in such a system where rubbery and plastic materials are combined, mechanical properties, particularly toughness and impact resistance, may be enhanced (29). In fact, the 50-wt% semi-IPN composition has much greater toughness than either PET or castor oil-HMDI polyurethane (Figure 2 and Table I), and has glass-transition behavior indicative of microheterogeneous morphology (Figure 5).

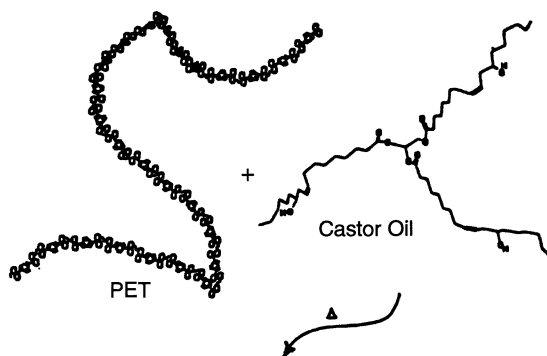
To elucidate the structure of the created materials, a more intense study of the 50:50 PET:castor oil-HMDI polyurethane composition was undertaken. As seen in Figure 5, the glass transition of PET in the material before cross-linking has been depressed from 75 to 45 °C. This decrease occurs as a result of the method where the mixture is maintained at 300 °C until a single phase mixture is obtained. During this extended heating, which typically takes

about 10 min, the castor oil could simply be slowly dissolving the PET or a bond interchange reaction could be taking place between the castor oil and PET, which results in copolymer that eventually compatibilizes the two materials to the point of optical clarity. Examples of such a "miscibility window" for blends of homopolymers with copolymers composed of similar monomer units are numerous (62).

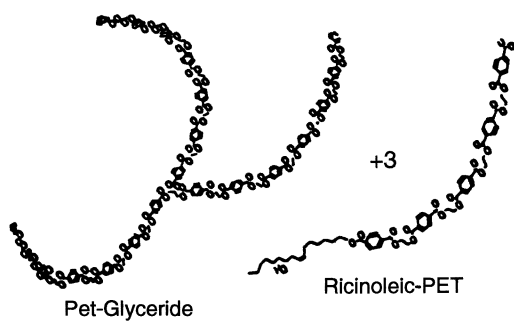
When the solution is cooled to room temperature, the pure castor oil phase separates from the PET-castor oil mixed phase. This separation apparently exhibits an upper critical solution temperature. A determination should be made as to whether the PET-castor oil phase is a miscible mixture, contains some compatibilizing copolymer, or is entirely a copolymer. If the phase is simply a miscible blend of castor oil and PET, then the material formed upon cross-linking with HMDI will be a true PET-castor oil semi-IPN. If the PET has been completely converted to PET-castor oil copolymer, then the material that results from addition of HMDI may not be a semi-IPN. Instead, the material structure could resemble a castor oil network with PET chains bonded to the network as dangling ends or segments. If ester-ester interchange proceeds to its fullest extent, a "PET-triglyceride" molecule and PET chains with ricinoleic acid residues ("ricinoleic-PET") would be formed, as illustrated in Chart I. Hydroxyl-ester interchange is also a possibility wherein the castor oil molecule is left essentially intact, except with PET segments attached where hydroxyls had existed (also illustrated in Chart I). In either case, a hybrid semi-IPN structure would result with cross-linking through the hydroxyl groups, where a predominantly castor oil network would form, but with PET segments bonded into the network and with PET-castor oil copolymer forming the uncross-linked phase. In practice, interchange reactions were carried out only to the extent where the mixture became optically clear at 300 °C, not to the ultimate statistical copolymer.

To determine whether the PET-castor oil phase is a miscible blend or a copolymer, an extraction procedure was developed. The uncross-linked 50:50 PET:castor oil (heated to the point of optical clarity at 300 °C) was first ground to a powder and then mixed with methylene chloride for about 1 h. The methylene chloride should dissolve most of the free castor oil in the mixture. The solvent mixture was filtered and the solid that contained the undissolved PET fraction was retained. DSC analysis of the heat capacity change in this solid showed that approximately 20-wt% free castor oil remained in the material. Next, the material was mixed in a similar manner with liquefied phenol to dissolve the PET fraction. The solution was then filtered and the filtered solution was poured into ethyl alcohol, which causes the PET to precipitate and leaves free castor oil in solution. The ethyl alcohol mixture was then filtered to leave the solid PET extraction product, which was examined by DSC analysis and showed no evidence of any free castor oil.

The extract was then analyzed by FTIR spectroscopy in an attempt to determine its composition. Neat PET, castor oil, the uncross-linked 50:50



Ester-Ester Interchange



Hydroxyl-Ester Interchange

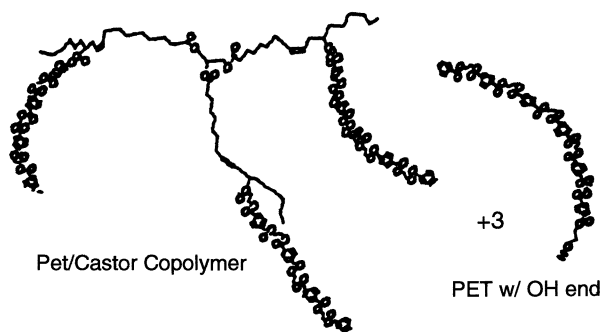


Chart I. Schematic of possible bond interchange reactions between castor oil and PET for complete ester-ester interchange and hydroxyl-ester interchange.

mixture, and the extract were dissolved in trifluoroacetic acid and the solutions were allowed to evaporate onto silver chloride infrared windows. Absorption peaks that are unique to PET and castor oil were chosen at 1270 and 1165 cm^{-1} , respectively. Because the film thicknesses were unknown, a ratio method (63) that used the uncross-linked 50:50 mixture as the standard of known composition to calculate the extract composition. The resultant extract composition was about 85-wt% PET and 15-wt% castor oil. Because of the extraction process, the 15-wt% castor oil found in the extract must be bonded to the PET as a copolymer—the result of bond interchange.

The composition of the extracted copolymer as determined by FTIR (85-wt% PET and 15-wt% castor oil) coincides closely with the drop in PET glass transition observed in the uncross-linked 50:50 mixture DSC scan (Figure 5). A drop in the PET glass-transition temperature from 75 to 45 °C is consistent with the Fox equation calculation for a 85:15 copolymer that uses 75 °C and -60 °C as the glass transitions for PET and castor oil, respectively. Calculations based on the heat capacity change associated with the glass transition for the semi-IPN and pure castor elastomer yielded the same result for the PET phase composition. In the case of the FTIR absorption method, the extract was analyzed, but in the DSC glass transitions, the unextracted PET-rich phase was measured. Thus it was concluded that the extract and the PET-rich phase in the uncross-linked material were identical (each contained 15-wt% castor oil) and that all the castor oil in that phase is copolymerized with PET.

With this understanding of the chemical structure of the phases in the uncross-linked mixture comes an understanding of the structure of the semi-IPN. At the mixing temperature of 300 °C, the two phases of the foregoing 50:50 mixture are apparently miscible. Only when the mixture is cooled does phase separation occur, which is indicative of an upper critical solution temperature. When HMDI is added to this miscible mixture at 240 °C, bonds form between the hydroxyl groups of ricinoleic segments that cross-link the free castor oil and connect the hydroxyl-bearing copolymer molecules into the polyurethane network. The resulting network structure is thus itself a copolymer of PET and castor oil segments. With the cross-linking, the two phases observed in the mixture at room temperature can no longer phase separate into large domains; instead, they adopt a microheterogeneous morphology, as evidenced by the broadened glass transition (Figures 4 and 5).

Uncross-linked material that still remains in the semi-IPN must be formed by molecules without hydroxyl functionality. The uncross-linked material was able to be extracted by a PET solvent, but not by a castor oil polyurethane solvent. This material may have one of the copolymer structures depicted in Chart I. Infrared spectra of the uncross-linked extracted material revealed absorbance peaks associated with both PET and castor oil, but with very little hydroxyl absorbance. This observation indicates that the material

extracted (the uncross-linked portion of the semi-IPN) contains copolymer composed of PET and castor oil, in addition to uncross-linked PET.

Crystallinity in Blends and Semi-IPNs. As previously discussed, in injection molding crystalline PET, the molds are typically heated to less than 100 °C. In such a cool mold, the PET can become quenched to the amorphous state as it contacts the mold surfaces. This effect can cause poor surface quality of the molded article. To be a useful engineering plastics material for injection molding applications, PET must have the ability to crystallize rapidly both as it is cooled from the melt and as it is heated from a quenched amorphous glassy state. Rapid crystallization from the melt allows short cycle times, whereas rapid crystallization from the glassy state alleviates the quenched mold surface crystallinity problem. Thus both a nucleation agent and a mobility enhancer are required for optimal performance.

Sodium benzoate effectively creates nucleation sites for crystallization and so effectively enhances crystallization from the melt, where PET mobility is adequate, but nucleation sites are few. On the other hand, in crystallization from the glassy state, mobility is more important than nucleation sites; this is where castor oil excels and sodium benzoate or calcium acetate are fairly ineffective (Figure 7). In both the mixed and bonded castor oil–sodium benzoate compositions, a synergism develops between the mobility-enhancing castor oil and the nucleation-providing sodium benzoate, which yields a PET material with crystallization enhanced from both the melt and glassy states (Figure 8).

The fact that PET may crystallize significantly complicates the morphology of the semi-IPN. Because, in this case, crystallization may be considered to be a phase-separation process, which can be more rapid than amorphous phase separation, the cross-linking step in the IPN formation process should be carried out above the melting temperature of the crystallizable component(s), or at least be achieved at a comparable rate simultaneous with crystallization, if a microheterogeneous material is to be obtained. In the synthesis method utilized here, diisocyanate is added to the mixture above the temperature where PET crystallizes, so that the castor oil polyurethane gels before the PET can crystallize.

In the compositions that contain up to 30-wt% castor oil-HMDI polyurethane, the normalized extent of crystallization was greater than neat PET (Figure 9). This may be due to the formation of PET–castor oil copolymer. In the 85-wt% PET–15-wt% castor oil copolymer extracted from the uncross-linked 50:50 PET:castor mixture, the enthalpy of fusion of the PET was 41.0 J/g, as compared to 37.7 J/g for the neat PET in a parallel experiment carried out without annealing. Because the molecular weight of the PET is reduced by interchange, this too can lead to greater extent of crystallization as well as greater crystallization rate, so that the copolymer itself cannot be given full credit for improvement in the PET crystallinity. In

compositions with more than 30-wt% castor oil-HMDI polyurethane, the total extent of crystallization, as well as the peak crystallization temperature, falls off rapidly as more castor is added. This falloff is presumably due to the restraining effect of the network. The melting and crystallization transitions are also lowered and broadened as more castor oil-HMDI polyurethane is included in the semi-IPN (Figure 10).

The type and extent of crystallinity, and thus the rate of crystallization developed in the semi-IPNs, can be quite different from that of neat PET because of the effect of copolymerization, the restraining effect of the network, and the amorphous phase interactions created as a result of the microheterogeneous phase structure. In general, the presence of a network reduces the PET crystallization rate; however, in the presence of oil, the crystallization rate increases (12*b*). With the semi-IPNs described herein, the objective was to create a microheterogeneous material, so that cross-linking and crystallization were carried out nearly simultaneously. If instead, a rapidly crystallizing PET semi-IPN is desired, crystallization would have to be accomplished prior to network formation and take advantage of the ability of the oil to improve PET crystallization. In this case, however, greater phase separation takes place, which leads to less desirable physical properties.

Summary

Semi-interpenetrating polymer networks were formed between a castor oil polyurethane network and linear semicrystalline poly(ethylene terephthalate). The mechanism of formation of the semi-IPN was different in that the initial miscibility needed to form an IPN was achieved through a bond interchange reaction between the castor oil ester and hydroxyl and PET ester groups. As a result of the interchange, a hybrid semi-IPN structure was formed, wherein both of the separated phases may contain PET-castor oil copolymer. A microheterogeneous morphology was developed at intermediate compositions as evidenced by the broadened glass-transition behavior observed by DSC. The microheterogeneous semi-IPNs display much better mechanical properties than the component materials.

Crystallization of the PET in the presence of small amounts of castor oil was accelerated in both cooling from the melt state and heating from the glassy state. In conjunction with the chemical nucleating agent sodium benzoate, either chemically bonded to castor oil or as a simple mixture, even greater enhancements in crystallization were observed. The PET crystallinity in semi-IPNs of intermediate castor oil-HMDI polyurethane content can be higher than the crystallinity of neat PET (on a per gram of PET basis). Crystallinity in compositions with high castor oil-HMDI polyurethane content was greatly affected by the presence of the network: large melting point depression and loss in overall crystallinity were observed.

Outlook

Research on semi-crystalline IPNs has only just begun. The wide variety of means available to control the microstructure of such materials requires exploration in greater detail. Similarly, IPNs made from copolymerized materials is another area of research that could yield useful results in the future. These areas of research can only grow as the need for more versatile materials and for a basic understanding of IPN microstructure increases.

Acknowledgments

Financial support for this work was generously provided by EniChem America, Inc. L. W. Barrett is also partially funded by, and thankful for, a supplemental fellowship grant from the Plastics Institute of America.

References

1. Sperling, L. H.; Carraher, C. E.; Qureshi, S. P.; Manson, J. A.; Barrett, L. W. In *Polymers from Biotechnology*; Gebelein, C. G., Ed.; Plenum: New York, 1991.
2. Sperling, L. H.; Manson, J. A.; Linne, M. A. *J. Polym. Mater.* **1984**, *1*, 54.
3. Linne, M. A.; Sperling, L. H.; Fernandez, A. M.; Qureshi, S.; Manson, J. A. In *Rubber Modified Thermoset Resins*; Riew, C. K.; Gillham, J. K., Eds.; Advances in Chemistry 208; American Chemical Society: Washington, DC, 1984.
4. Sperling, L. H.; Manson, J. A. *J. Am. Oil Chem. Soc.* **1983**, *60*, 1887.
5. Sperling, L. H.; Manson, J. A.; Qureshi, S. A.; Fernandez, A. M. *Ind. Eng. Chem. Prod. Res. Dev.* **1981**, *20*, 163.
6. Sperling, L. H.; Devia, N. A.; Manson, J. A.; Conde, A. In *Modification of Polymers*; Carraher, C. E., Jr.; Tsuda, M., Eds.; ACS Symposium Series 121; American Chemical Society: Washington, DC, 1980.
7. Devia, N.; Manson, J. A.; Sperling, L. H.; Conde, A. *Macromolecules* **1979**, *12*, 360.
8. Devia-Manjarres, N.; Conde, A.; Yenwo, G. M.; Pulido, J. E.; Manson, J. A.; Sperling, L. H. *Polym. Eng. Sci.* **1977**, *17*, 294.
9. Yenwo, G. M.; Manson, J. A.; Pulido, J.; Sperling, L. H.; Conde, A.; Devia, N. *J. Appl. Polym. Sci.* **1977**, *21*, 1531.
10. Perdue, R. E., Jr. *Agric. Eng.* **1989**, May/June.
11. Carlson, K. D.; Chang, S. P. *J. Am. Oil Chem. Soc.* **1985**, *62*, 934.
- 12a. Barrett, L. W.; Sperling, L. H. *Polym. Eng. Sci.* **1991**, *3*.
- 12b. Barrett, L. W.; Sperling, L. H.; Gilmer, J. W.; Mylonakis, S. G. *J. Appl. Polym. Sci.* **1993**, *48*, 1035.
13. Sears, J. K.; Darby, J. R. *The Technology of Plastisizers*; Wiley: New York, 1982.
14. Chung, J. Y. J.; Jones, J. D.; Li, H. M. U.S. Patent 4,539,352, 1985.
15. Wypych, J. In *Polyvinyl Chloride Stabilization*, Elsevier: Amsterdam, Netherlands, 1986.
16. Cuadrado, T. R.; Williams, R. J. *J. Poly. Commun.* **1989**, *30*, 239.
17. Rigby, P. J. *Mod. Plast.* **1990**, *67(11)*, 50.
18. Erhan, S. M.; Kleiman, R. J. *Am. Oil Chem. Soc.* **1990**, *67*, 670.
19. Suthar, B.; Parikh, N.; Patel, N. *Polym. Int.* **1991**, *25(3)*, 173.

20. Rajalingam, P.; Radhakrishnan, G. *Polym. Int.* **1991**, 25(2), 87.
21. Patel, N.; Suthar, B. *Polym. Plast. Technol. Eng.* **1990**, 29(5,6), 535.
22. Tan, P. *Polym. Mater. Sci. Eng. Prepr.* **1991**, 65, 182.
23. Fernandez, A. M.; Manson, J. A.; Sperling, L. H. In *Renewable Resource Materials: New Polymer Sources*; Carraher, C. E., Jr.; Sperling, L. H., Eds.; Plenum: New York, 1983.
24. Ramos, L. C. D.; Tango, J. S.; Savi, A.; Leal, N. R. *J. Am. Oil Chem. Soc.* **1984**, 61, 1841.
25. Princen, L. H. *J. Am. Oil Chem. Soc.* **1979**, 56(9), 845.
26. Vasishtha, A. K.; Trivedi, R. K.; Das, G. *J. Am. Oil Chem. Soc.* **1990**, 67, 333.
27. Afolabi, O. A.; Aluko, M. E.; Wang, G. C.; Anderson, W. A.; Ayorinde, F. O. *J. Am. Oil Chem. Soc.* **1989**, 66, 983.
- 28a. Qureshi, S. A.; Manson, J. A.; Sperling, L. H.; Murphy, C. J. In *Polymer Applications of Renewable Resource Materials*; Carraher, C. E., Jr.; Sperling, L. H., Eds.; Plenum: New York, 1983.
- 28b. Barrett, L. W.; Shaffer, O. L.; Sperling, L. H. *J. Appl. Polym. Sci.* **1993**, 48, 953.
29. Sperling, L. H. In *Interpenetrating Polymer Networks and Related Materials*; Plenum: New York, 1981.
- 30a. Utracki, L. A. Chapter 3 in this volume.
- 30b. Barrett, L. W.; Ferguson, G. S.; Sperling, L. H. *J. Polym. Sci. A, Polym. Chem.* **1993**, 31, 1287.
31. Deyrup, E. J. *Abstracts of Papers*, High Performance Polymers Processing Symposium, 1986.
32. Barenburg, S. A. U.S. Patent 4,429,067, 1984.
33. Deyrup, E. J. U.S. Patent 4,352,904, 1979.
34. Hoeschele, G. K. U.S. Patent 4,351,757, 1982.
35. Hoechst, A. G., United Kingdom Patent Application 1,282,679, 1972.
36. Dunkel, S. R.; Haylock, J. C. European Patent Application 185,981, 1986.
37. Vanderkooi, N., Jr.; Haylock, J. C.; Schulze, S. R.; Tuller, H. W. European Patent Application 55,687, 1982.
38. Aharoni, S. M. U.S. Patent 4,349,503, 1982.
39. Aharoni, S. M. U.S. Patent 4,336,343, 1982.
40. Vanderkooi, N., Jr. U.S. Patent 4,753,975, 1988.
41. Christians, J.; Lu, S. Z. European Patent Application 46,052, 1984.
42. Christians, J.; Lu, S. Z. U.S. Patent 4,483,955, 1984.
43. Deyrup, E. J. U.S. Patent 4,486,564, 1984.
44. Hoeschele, G. K. U.S. Patent 4,351,757, 1982.
45. Dolce, T. J.; Vijayendran, B. R. European Patent Application 112,167, 1984.
46. Garrison, W. E., Jr. U.S. Patent 4,548,978, 1985.
47. Garrison, W. E., Jr. International Patent Application 8,503,717, 1985.
48. Garrison, W. E., Jr. International Patent Application 8,503,718, 1985.
49. Ostapchenk, G. J. U.S. Patent 4,303,573, 1981.
50. Biebuyck, J. J.; Mercier, J. P.; Nield, E.; Legras, R. M. H.; Griffin, B. P. European Patent Application 21,648, 1981.
51. Christians, J.; Lu, S. Z. U.S. Patent 4,425,457, 1984.
52. Dekoninck, J. M.; Legras, R.; Mercier, J. P. *Polymer* **1989**, 30, 910.
53. Legras, R.; Leblanc, D.; Daoust, D.; Devaux, J.; Nield, E. *Polymer* **1990**, 31, 1429.
54. Legras, R.; Dekoninck, J. M.; Vanzieleghem, A.; Mercier, J. P.; Nield, E. *Polymer* **1986**, 27, 109.
55. Moore, W. R.; Sanderson, D. *Polymer* **1968**, 9, 153.

56. Chen, S.; Chen, F. J. *Polym. Sci., Polym. Chem. Ed.* **1987**, *25*, 533.
57. Chang, S.; Sheu, M.; Chen, S. J. *Appl. Polym. Sci.* **1983**, *28*, 3289.
58. Droscher, M.; Wegner, G. *Polymer* **1978**, *19*, 43.
59. Lawton, E. L.; Ringwald, E. L. In *Polymer Handbook*; 3rd ed.; Brandup, J.; Immergut, E. H., Eds.; Wiley: New York, 1989; Section V, p 102.
60. Devia-Manjarres, N. *Polym. Eng. Sci.* **1979**, *19*, 878.
61. Sperling, L. H. In *Introduction to Physical Polymer Science*, 2nd ed.; Wiley-Interscience: New York, 1992.
62. Paul, D. R.; Barlow, J. W. *Polymer* **1984**, *25*, 487.
63. Zichy, V. J. I. In *Laboratory Methods in Infra-red Spectroscopy*, 2nd ed.; Miller, R. G. J.; Stace, B. C., Eds.; Heyden: London, 1979; p 56.

RECEIVED for review December 5, 1991. ACCEPTED revised manuscript June 16, 1992.

Two-Phase Interpenetrating Epoxy Thermosets That Contain Epoxidized Triglyceride Oils

Part I. Phase Separation

Isabelle Frischinger and Stoil Dirlikov

Eastern Michigan University, Coatings Research Institute, 122 Sill Hall,
Ypsilanti, MI 48197

Homogeneous formulations of diglycidyl ether of bisphenol A (DGEBA) epoxy resin and a commercial diamine that contain liquid rubber, based on an epoxidized vegetable oil and diamine, form two-phase interpenetrating epoxy thermosets. At lower rubber content, the formulations consist of a rigid DGEBA matrix and randomly distributed small “vegetable” rubbery particles. At higher rubber content, the thermosets are characterized by a continuous “vegetable” rubbery phase and small rigid DGEBA particles. Phase inversion is observed at intermediate rubber content. Particle size and phase inversion depend on the miscibility of the two (rubbery and DGEBA) phases and can be regulated in a broad range by the nature of the epoxidized “vegetable” rubber and the diamine used for thermoset preparation.

TWO-PHASE INTERPENETRATING EPOXY THERMOSETS are formed, under certain conditions, from homogeneous mixtures of diglycidyl ether of bisphenol A (DGEBA) epoxy resins and commercial diamines that contain epoxidized vegetable oils. These thermosets consist of a rigid DGEBA epoxy matrix and randomly distributed small “vegetable” rubbery particles (1, 2). In the present study, the effect of the nature of the epoxidized vegetable oil and the diamine on the phase separation (morphology, particle size, and phase inversion) of DGEBA epoxy thermosets has been evaluated.

Experimental Details

Materials. Epoxidized soybean oil (Flexol Plasticizer EPO) with average epoxy functionality of 4.5 is a product of Union Carbide Co. Vernonia oil with average epoxy functionality of 2.4 was kindly supplied by J. Elmore (Rhône Poulenc). Diglycidyl ether of bisphenol A is solid epoxy resin (Epon 825) from Shell Company. 4,4'-Diaminodiphenylmethane (DDM) and 4,4'-diaminodiphenylsulfone (DDS) were obtained from Aldrich Chemicals.

Epoxidized Soybean and Vernonia Liquid Rubbers. Epoxidized soybean liquid rubber (ESR) was obtained by prepolymerization of a mixture of 100 g of epoxidized soybean oil and 22.8 g (stoichiometric amount) of DDM, at 135 °C under nitrogen for 37–40 h. Similarly, vernonia liquid rubber (VR) was obtained by prepolymerization of 100 g of vernonia oil and 25.63 g (twice the stoichiometric amount) of DDM under nitrogen at 180 °C for 37–40 h. The time of prepolymerization varied slightly from batch to batch dependent on the quality of the oil. The exact conversion of the rubbers is not known, but further heating for several hours leads to gelation.

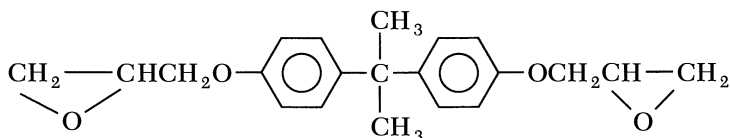
Preparation of Two-Phase Epoxy Thermosets. Two-phase epoxy thermosets were prepared from homogeneous stoichiometric mixtures of DGEBA and diamine (DDM or DDS), which contained varying amounts of liquid rubber (ESR or VR). The rubber was dissolved first in DGEBA at 70 °C. Then, the diamine (DDM or DDS) was added and the mixture was stirred (at 70 °C) until the diamine was dissolved (about 15 min). The homogeneous (one-phase) transparent mixture was then degassed before reaching its cloud point (phase separation). The formulations cross-linked with DDS were cured at 150 °C for 2 h, whereas the formulations cross-linked with DDM were cured first at 75 °C for 4 h and then at 150 °C for 2 h.

Morphology. The morphology of the fracture surface of neat and rubber-modified epoxy resins was examined by scanning electron microscopy (SEM) using an electron microscope (Amray model 1000B). The fracture of single-edge-notched specimens was carried out with a three-point bending assembly at room temperature according to the conventional test for fracture toughness (3). SEM specimens were sputter-coated with a thin film of gold. Some specimens that contained vernonia liquid rubber were stained with an aqueous solution of osmium tetroxide (OsO_4) and then evaporation-coated with a layer of carbon. A backscattered electron imaging technique also was used, especially to visualize the phase inversion phenomena.

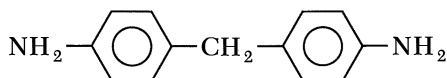
Dynamic Mechanical Analysis. A thermal analyzer (DuPont 2100, model 983) based on a flexural bending deformation measurement and rectangular bar specimens with approximate dimensions of $45 \times 7.8 \times 3.5$ mm were used to study the dynamic mechanical properties over the temperature range from -130 to $+200$ °C at a heating rate of 2 °C/min. Specimen preparation was described previously (3).

Results and Discussion

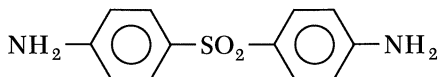
Selection of Epoxy Resin, Epoxidized Vegetable Oil, and Diamine Curing Agent. The epoxy resin (Shell Epon 825) used in this study is practically neat DGEBA:



Two commercial diamines, which have similar molecular structures but are different in polarity, were used to cure DGEBA. DDM is the less polar diamine:

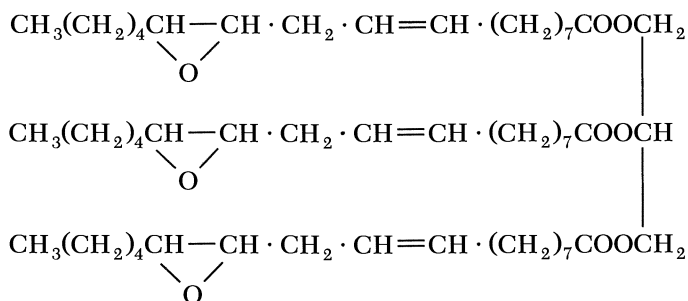


whereas DDS is the more polar diamine:



The effect of two types of epoxidized vegetable oils—vernonia and epoxidized soybean oil—on the phase separation process of DGEBA–DDM and DGEBA–DDS epoxy thermosets has been studied.

Vernonia oil, a naturally epoxidized vegetable oil, consists mainly of a mixture of similar triglycerides (1). The structure of vernonia oil is schematically illustrated below:



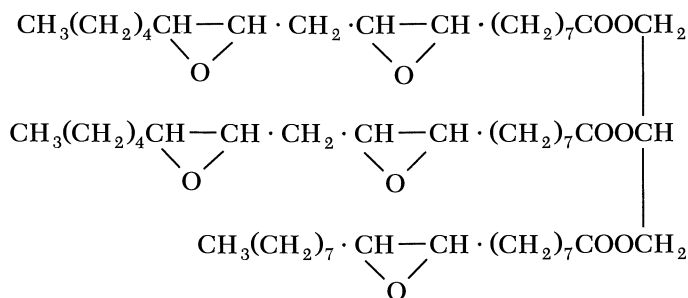
Vernonia oil was selected in this study because it stains with osmium tetroxide. The selective reaction of the electron-dense OsO_4 with vernonia carbon–carbon double bonds provides a contrast in SEM between the rubbery phase (a lighter appearance) and the DGEBA epoxy phase (a darker

shade). This contrast enabled us to identify easily the vernonia phase in the final two-phase thermosets.

Vernonia oil has relative low average epoxy functionality of 2.4. Rubbers of vernonia oil with diamines, therefore, have lower cross-linked density and polarity.

Vernonia galamensis, the plant that produces vernonia oil, is a potential industrial crop presently in the developmental stage.

Epoxidized soybean oil is industrially produced in large volume; it is available at a low price (about \$0.50 per pound) and is very attractive for industrial application in two-phase epoxy thermosets. Epoxidized soybean oil consists of a mixture of different triglycerides. The average molecular structure of epoxidized soybean oil is



Epoxidized soybean oil does not contain carbon-carbon double bonds and does not stain with osmium tetroxide; it has higher average epoxy functionality (4.5) than vernonia oil and its rubbers with diamines, therefore, are characterized with higher cross-link density and polarity.

Preparation of Two-phase Interpenetrating Epoxy Thermosets. The initial attempts to toughen epoxy resins were carried out directly with epoxidized vegetable oil. For this purpose, homogeneous mixtures of DGEBA, a diamine, and epoxidized vegetable oil were cured initially at 70 °C. Because the diamines have a much higher reactivity with DGEBA than with the epoxidized vegetable oils, they react first with DGEBA and form the rigid epoxy phase at 70 °C. The epoxidized vegetable oil separates at this stage as a second phase of small randomly distributed liquid vegetable oil droplets with diameters in the range of 1 μm (3).

Unfortunately, at a higher temperature (in the range from 120 to 220 °C) these liquid droplets do not cure with the unreacted diamine fast enough to form rubbery particles and two-phase thermosets. Instead, the vegetable oil dissolves and plasticizes the rigid DGEBA matrix, and one-phase homogeneous final thermosets are obtained; that is, interpenetrating epoxy networks without phase separation.

Two-phase interpenetrating thermosets were obtained under the same curing conditions by use of epoxidized vegetable liquid rubbers instead of the initial pure epoxidized vegetable oils. The epoxidized soybean liquid rubber was prepared by B-staging (prepolymerization) below the gel point of a stoichiometric mixture of epoxidized soybean oil and DDM at 135 °C under nitrogen for 37–40 h. Vernonia oil has lower epoxy functionality and requires higher temperature and a twice larger amount of DDM to reach the same advanced degree of prepolymerization for the same cure time. Vernonia oil rubber was obtained by prepolymerization at 180 °C for 37–40 h. Both rubbers consist of soluble oligomers with a broad molecular weight distribution in addition to a small amount of the unreacted initial epoxidized vegetable oil (3).

The epoxidized vegetable rubber has lower reactivity than DGEBA. Therefore, the “vegetable” liquid rubber droplets again separated at 70 °C from the initial homogeneous mixture of DGEBA, diamine, and vegetable liquid rubber. In contrast to the neat oils, the liquid rubbers have higher molecular weight and lower miscibility with the epoxy DGEBA phase. The liquid rubbers also have an advanced degree of prepolymerization close to the gel point, and they rapidly cure and cross-link at higher temperature (150 °C) with the remaining unreacted amino groups. As a result, the final interpenetrating thermosets, after being cured at 150 °C, consist of two phases: a continuous phase (matrix) with randomly distributed small spherical particles (for instance, Figure 1). DGEBA forms the rigid phase, whereas the epoxidized vegetable oil forms the rubber. The diamine molecules on the interface probably react with both the epoxy groups of the DGEBA and the unreacted epoxy groups of the epoxidized vegetable rubber to form chemical bonds between the continuous phase and the particles.

Selection of Formulations. The effect of the diamine and epoxidized vegetable oil on the phase separation of DGEBA epoxy thermosets was studied by evaluation of four formulations:

DGEBA-DDM-VR(x)

DGEBA-DDS-VR(x)

DGEBA-DDM-ESR(x)

DGEBA-DDS-ESR(x)

The DGEBA-DDM-VR(x) thermosets were obtained from an initial homogeneous stoichiometric mixture of DGEBA and DDM modified by vernonia rubber. The content of the liquid rubber (x) was varied between 0 and 100 wt%: $x = 0$ corresponds to neat DGEBA-DDM thermoset, whereas $x = 100$ corresponds to a pure vernonia rubber. Analogous abbreviations are used for the remaining three formulations.

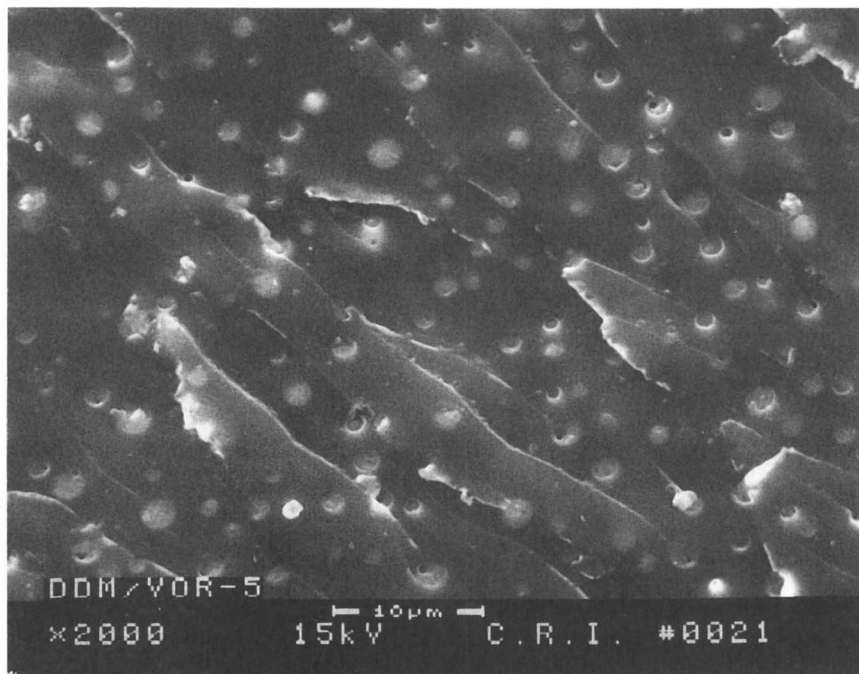


Figure 1. SEM micrograph of the fracture surface of a DGEBA-DDM-VR(5) specimen stained with osmium tetroxide.

DGEBA-DDM-VR Formulations. The fracture surfaces of DGEBA-DDM-VR thermosets with increasing content of vernonia rubber were studied by SEM. The results on the morphology and particle size distribution of these two-phase thermosets are summarized in Table I.

The initial neat DGEBA-DDM formulation forms homogeneous one-phase epoxy thermosets. The introduction of 5% vernonia liquid rubber results in two-phase epoxy thermosets (Figure 1). DGEBA-DDM-VR(5) consists of a rigid DGEBA-DDM matrix and randomly distributed small vernonia spherical rubbery particles (0.5–2.0 μm) with unimodal distribution. The particles can be observed clearly because of their lighter appearance which is due to staining with OsO_4 .

Similar two-phase thermosets are observed for the formulations with 10 and 15% vernonia rubber. The particle size, however, gradually increases with the rubber content and ranges from 1 to 4 μm in DGEBA-DDM-VR(10) and from 1 to 5 μm in DGEBA-DDM-VR(15). The rubber particles at the DGEBA-DDM-VR(15) fracture surface and their internal structure are especially clearly observed by a backscattered electron imaging technique on specimens stained with OsO_4 (Figure 2). The high electron density of

Table I. Morphology and Particle Size Distribution for DGEBA–DDM–VR Formulations

<i>Thermoset Formulation</i>	<i>Morphology</i>	<i>Dispersed Phase</i>	<i>Particle Size (μm)</i>
DGEBA–DDM	homogeneous		
DGEBA–DDM–VR(5)	two phase	vernonia	0.5–2
DGEBA–DDM–VR(10)	two phase	vernonia	1–4
DGEBA–DDM–VR(15)	two phase	vernonia	1–5
DGEBA–DDM–VR(20)	two phase	vernonia PI ^a start	0.5–2, 20–100
DGEBA–DDM–VR(30)	two phase	DGEBA PI ^a end	2–4, 20–250
DGEBA–DDM–VR(50)	two phase	DGEBA	0.5–2
DGEBA–DDM–VR(60)	two phase	DGEBA	— ^b
DGEBA–DDM–VR(70)	two phase	DGEBA	— ^b
VR ^c	homogeneous		

^a PI, phase inversion.^b Data not available.^c Neat cross-linked vernonia rubber.

osmium produces a higher intensity of backscattered electrons from vernonia particles and increases the contrast.

Most of the rubbery particles at the fracture surface of these three formulations have undergone internal (partial or complete) cavitation. The formation of voids is observed as dark circles within the particles or at the particle–matrix interface (Figure 2). Once formed, the voids grow upon stress and dissipate energy. The remaining cavitated rubber is observed distinctly as a lining on the void walls. The cavitation phenomenon increases with increasing rubber content. Cavitation can greatly enhance the shear yielding process (4, 5) and is the main epoxy toughening mechanism.

The matrix surrounding the particles is characterized by a rippled fracture surface with striations (Figure 1) and exhibits plastic shear deformation.

Ejection or debonding of rubbery particles is not observed under the shear deformation during fracture. This result indicates a good adhesion between the DGEBA matrix and rubbery particles. As mentioned earlier, the diamine molecules on the interface probably react with the epoxy groups of both DGEBA and rubber to form chemical bonds between the two phases. Although some debonding is observed as craters at higher rubber content (Figure 3), debonding is not a major toughening mechanism.

A different morphology is observed at 20% vernonia rubber. The DGEBA–DDM–VR(20) thermosets contain two types of particles—large and small (Figures 3–9; Table I)—and are characterized by bimodal particle size distribution that indicates the beginning of a phase inversion phenomenon.

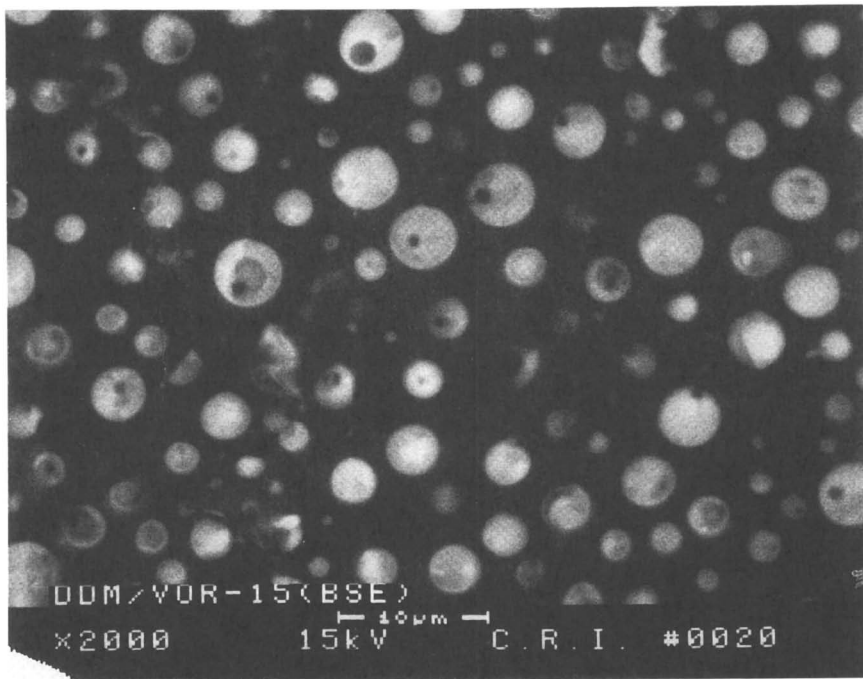


Figure 2. SEM micrograph using a backscattered electron imaging technique of the fracture surface of a DGEBA-DDM-VR(15) specimen stained with osmium tetroxide.

The smaller rubbery particles (0.5–2 μm) correspond to the rubbery particles observed in the thermosets with lower rubber content (below 20%). Figures 3–6 show the same section of the fracture surface with gradually increasing magnification. Cavitation and shear banding as well as the voids formed by debonding of the smaller particles from the DGEBA matrix are clearly observed.

The larger particles have a very broad particle size distribution (20–100 μm). Some of the particles are characterized by the so-called salami-type morphology (5). Figure 7 is a conventional SEM micrograph of the initial unstained specimen. Figure 8 shows the same section of the fracture surface after staining with OsO_4 and using a backscattered electron imaging technique. A single salami-type particle is shown in Figure 9 at higher magnification. Obviously, the larger particles are formed predominantly by the veronia rubbery phase (lighter shade). The smaller spherical DGEBA-DDM particles (1–8 μm ; darker shade) that are dispersed within the larger veronia domains are a result of a local phase inversion phenomenon.

Dynamic mechanical analysis (DMA) of DGEBA-DDM-VR(20) confirmed its bimodal particle size distribution (Figure 10). Two distinct glass-

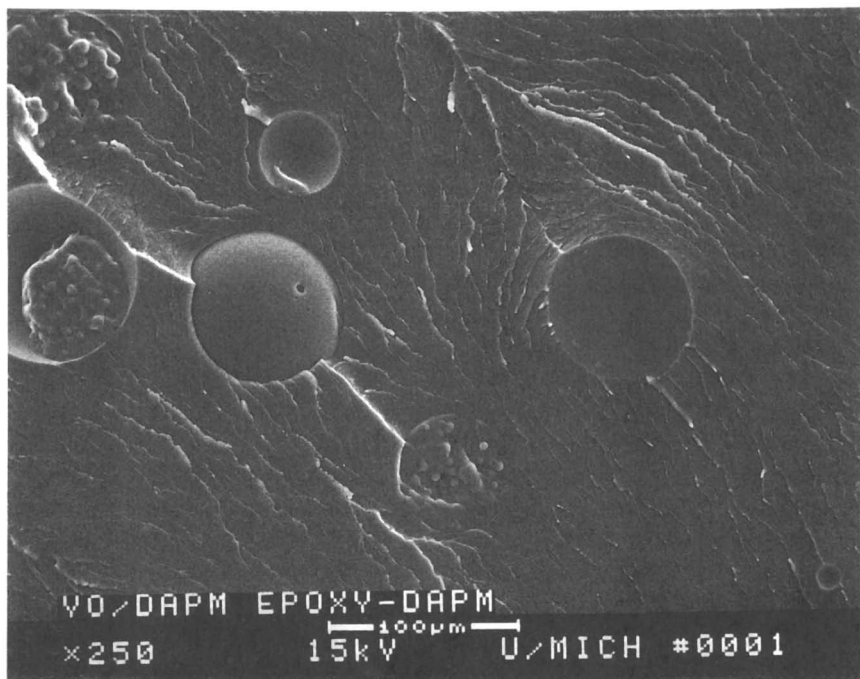


Figure 3. SEM micrograph of the fracture surface of a DGEBA-DDM-VR(20) specimen.

transition temperatures for the rubbery phase are observed and tentatively assigned to the glass-transition temperatures (T_g) of the two types of rubbery particles. The lower glass-transition temperature ($T_g = -35\text{ }^\circ\text{C}$) is assigned to the small particles of neat vernonia rubber because it corresponds to the T_g of the small neat vernonia particles observed in the formulations with lower rubber content and unimodal particle size distribution (1). The larger particles are believed to have glass transition at higher temperature ($+10\text{ }^\circ\text{C}$) due to DGEBA occlusion (probably co-reacting and mixing). The glass-transition temperature of the DGEBA matrix of DGEBA-DDM-VR(20) is observed at $172\text{ }^\circ\text{C}$, which is slightly depressed by $18\text{ }^\circ\text{C}$ below that of a neat DGEBA-DDM thermoset ($190\text{ }^\circ\text{C}$) (3). This observation indicates that the DGEBA-DDM matrix of DGEBA-DDM-VR thermosets is plasticized by a small amount of vernonia rubber. These results are in agreement with a mass-balance calculation based on the rubber content.

Larger particles ($100\text{--}200\text{ }\mu\text{m}$) act as bridging particles and induce the cavitation and shear banding of the small particles in their vicinity (6). Upon stress, a large deformation zone is created, with the formation of very sharp and wide ridges between neighboring large particles. Figure 3 shows two large vernonia particles fractured across their equator, part of a third particle

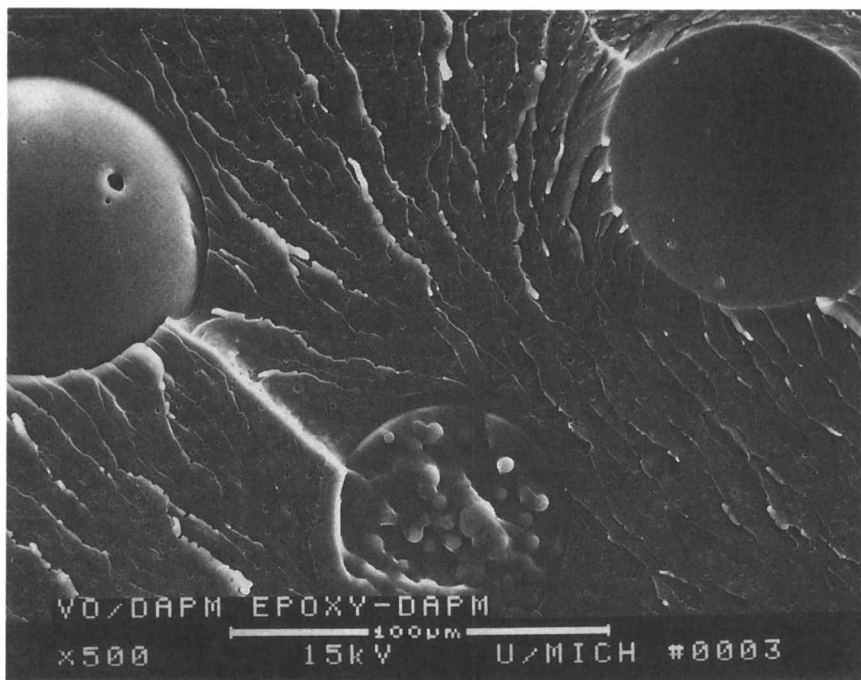


Figure 4. SEM micrograph of the fracture surface of a DGEBA-DDM-VR(20) specimen.

incorporated into the matrix, and two craters left by particles debonded from the matrix.

In summary, the DGEBA-DDM-VR(20) thermosets display two different types of toughening mechanisms that depend on particle size. Internal cavitation and shear banding are observed for the small particles and bridging, fracture, and debonding are exhibited mainly by the larger particles. The bimodal particle size distribution could lead to a synergistic toughening effect (7). This point, however, was recently disputed by Pearson and Yee (6).

In addition, an extensive plastic deformation of the matrix is evidenced by the appearance of numerous striations. In general, the fracture surface of DGEBA-DDM-VR(20) is rougher than the fracture surfaces of the thermosets with lower vernonia content. At higher rubber content, the higher concentration of particles leads to a smaller distance between particles. This closer proximity is probably the reason the plastic deformation becomes a more prominent toughening mechanism in DGEBA-DDM-VR(20).

At higher rubber content, the DGEBA epoxy progressively becomes the dispersed phase. DGEBA-DDM-VR(30) thermosets still are characterized by a bimodal particle size distribution. Further studies (8) show that the

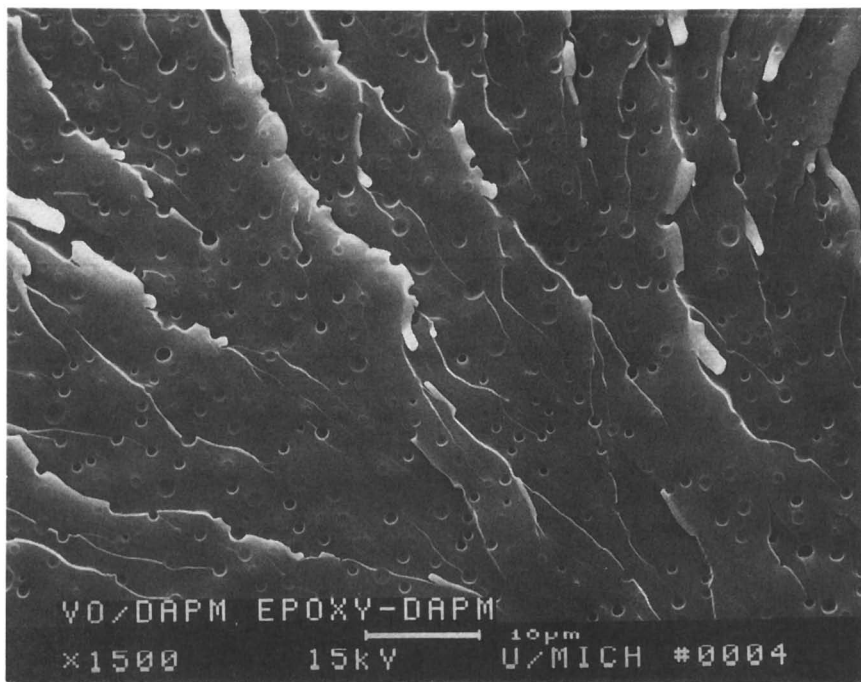


Figure 5. SEM micrograph of the fracture surface of a DGEBA-DDM-VR(20) specimen.

morphology of DGEBA-DDM-VR(30) is exactly the reverse of the morphology of DGEBA-DDM-VR(20): a continuous rubbery phase that contains both small (2–4 μm ; Figure 11) and large (20–250 μm ; Figure 12) DGEBA particles. The large particles are expected to contain rubber (within the particle). These rigid particles, however, do not undergo fracture when surrounded by a continuous rubbery phase and do not reveal their interior. DGEBA-DDM-VR(30) morphology reflects the end of the phase inversion phenomenon.

Further increase of the rubber content leads to a complete phase inversion. DGEBA-DDM-VR(50) thermoset consists of continuous rubbery phase in which small spherical rigid DGEBA particles (0.5–2 μm) are randomly distributed (Figure 13).

As expected, the neat veronia liquid rubber, cured under the same condition, forms a homogeneous cross-linked rubber (Table I).

DGEBA-DDS-VR, DGEBA-DDM-ESR, and DGEBA-DDS-ESR Formulations. Tables II, III, and IV summarize the results on the morphology are particle size distribution in DGEBA-DDS-VR, DGEBA-DDM-ESR, and DGEBA-DDS-ESR thermosets, respectively.

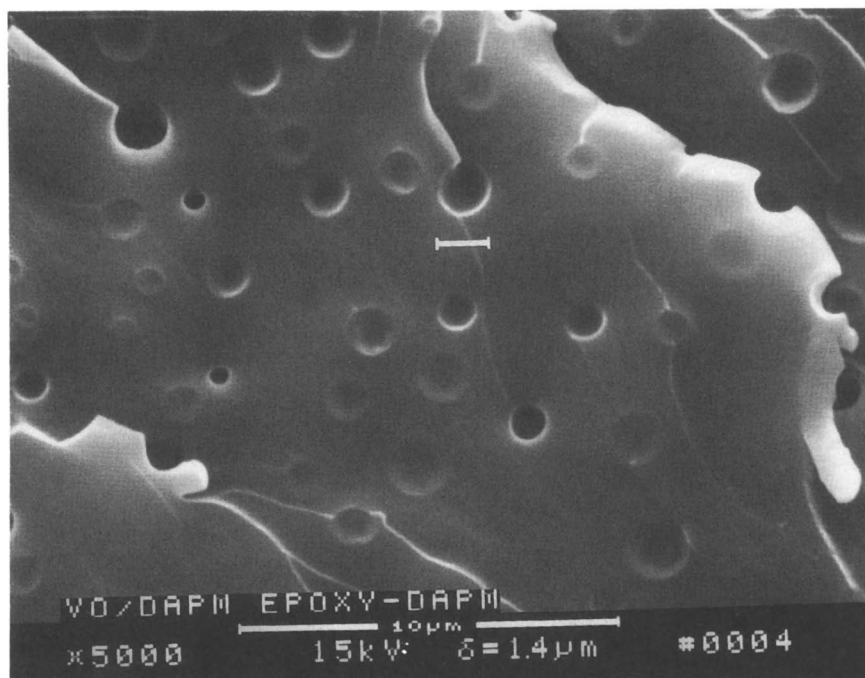


Figure 6. SEM micrograph of the fracture surface of a DGEBA-DDM-VR(20) specimen.

Phase separation in these three formulations follows the patterns of DGEBA-DDM-VR.

At low rubber content, the three formulations form two-phase thermosets with a continuous rigid DGEBA phase (matrix) and randomly distributed small (several micrometers diameter) spherical (vegetable) rubbery particles.

At a certain level of rubber, which is different for each of the four types of formulations, the formulations undergo phase inversion that, with the exception of DGEBA-DDM-ESR, is characterized by the formation of small (several micrometers) and large (several hundred micrometers) rubbery particles dispersed in the DGEBA matrix. The small particles are formed by neat cross-linked vegetable rubber. The large rubbery particles contain many small occlusions (several micrometers) of rigid DGEBA resin.

DMA confirmed this result; it showed two glass-transition temperatures for the small and the large rubbery particles, respectively. DGEBA-DDM-ESR formulations form only small particles and exhibit one glass-transition temperature. In good agreement with our previous results (3), DMA shows that a certain amount of rubber has plasticized the rigid DGEBA matrix in all

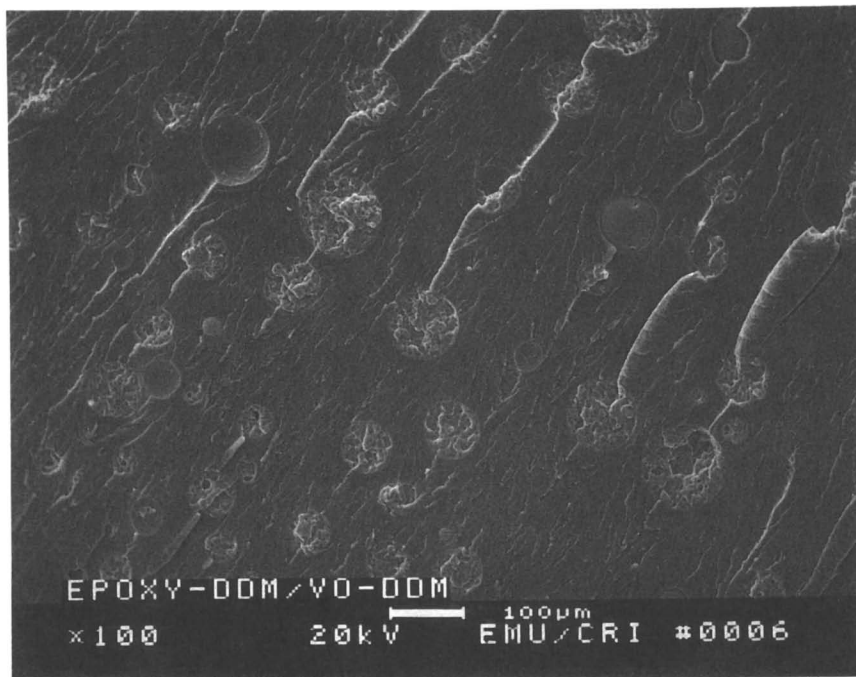


Figure 7. SEM micrograph of the fracture surface of a DGEBA-DDM-VR(20) specimen.

four types of formulations and decreased their glass-transition temperatures by 13–25 °C at 20% rubber content.

At the end of the phase inversion, small (several micrometers) and large (several hundred micrometers) DGEBA particles are dispersed in the continuous rubbery vegetable phase. The large particles probably contain occlusions of much smaller rubbery particles.

Further increase of the rubber content leads to a complete phase inversion with the formation of two-phase thermosets with continuous rubbery phase and randomly distributed small DGEBA rigid particles.

The four formulations, however, also show a pronounced dependence of the phase separation process on the nature of the diamine and the epoxidized vegetable rubber used for their preparation. As mentioned earlier, the DGEBA-DDS matrix is more polar than the DGEBA-DDM matrix because DDS is more polar than DDM diamine. The epoxidized soybean rubber is more polar than vernonia rubber because the epoxy functionality of the initial epoxidized soybean oil is twice as large as the epoxy functionality of vernonia oil. Both the particle size distribution and the rubber content at which phase

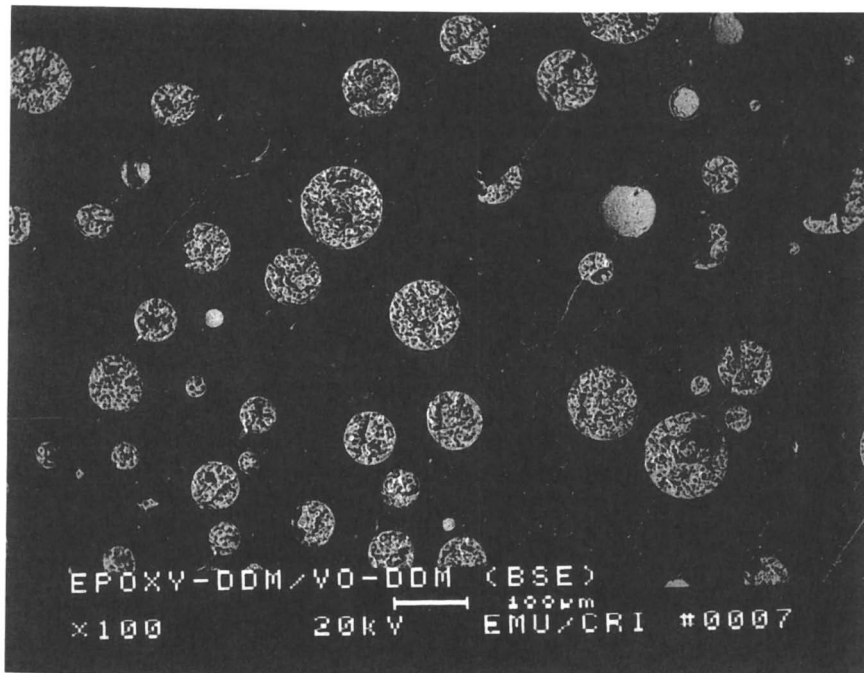


Figure 8. SEM micrograph using a backscattered electron imaging technique of the fracture surface of a DGEBA-DDM-VR(20) specimen stained with osmium tetroxide.

inversion occurs are determined by the miscibility of the two phases of the four types of formulations discussed.

Particle Size Distribution. The dependence of particle size distribution on the composition was elucidated by comparison of all four different types of formulations at 10% rubber content (Tables I-IV).

The two phases—highly polar DGEBA-DDS matrix and highly nonpolar vernonia rubber—in the DGEBA-DDS-VR thermosets are characterized by the lowest miscibility. As a result, the vernonia rubber has the lowest solubility in the matrix; it undergoes phase separation at the lowest rubber content and forms the largest particles (3–25 μm) in DGEBA-DDS-VR(10).

Vernonia rubber has better miscibility and solubility in DGEBA-DDM than in the DGEBA-DDS matrix and forms smaller particles (1–4 μm) in DGEBA-DDM-VR(10).

The epoxidized soybean rubber is more polar than vernonia rubber and has better miscibility with both DGEBA matrixes. The DGEBA-DDS-ESR(10), therefore, undergoes phase separation at a later stage of curing and forms smaller particles (1–2 μm) than both types of vernonia formulations.

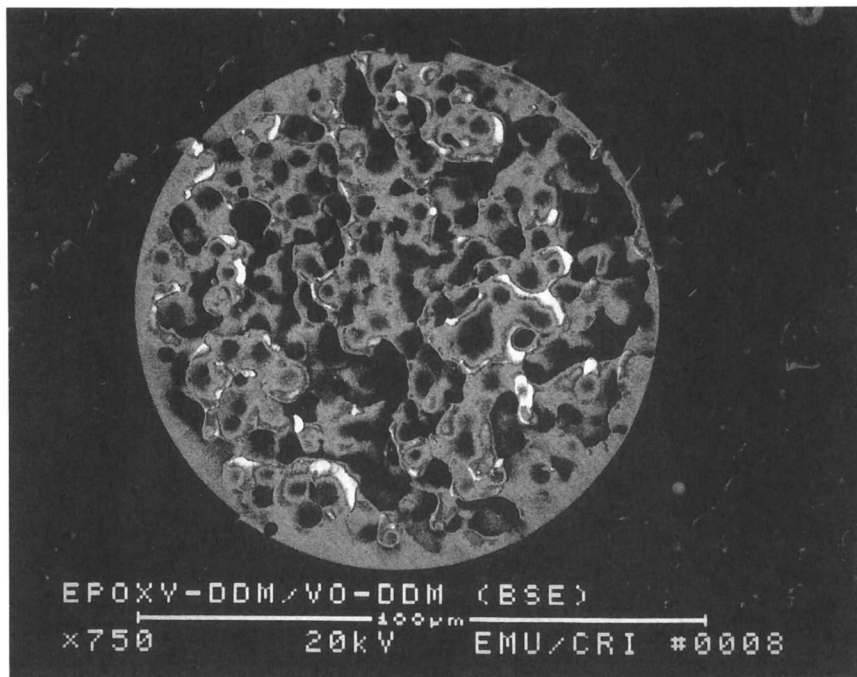


Figure 9. SEM micrograph using a backscattered electron imaging technique of the fracture surface of a DGEBA-DDM-VR(20) specimen stained with osmium tetroxide.

The epoxidized soybean rubber has better solubility in the less polar DGEBA-DDM than in the DGEBA-DDS matrix. As a matter of fact, the two phases of the DGEBA-DDM-ESR are characterized by the highest miscibility from all four types of formulations. As a result, DGEBA-DDM-ESR(10) does not phase separate at all. DGEBA-DDM-ESR thermosets undergo phase separation only at higher content of soybean rubber.

Similar observations can be made by comparison of all four types of formulations with 20% rubber.

In summary, the results on particle size distribution lead to four conclusions:

1. The miscibility of the two phases of the formulations decreases in the order of DGEBA-DDM-ESR, DGEBA-DDS-ESR, DGEBA-DDM-VR, and DGEBA-DDS-VR. A lower miscibility results in the formation of larger particles and vice versa.
2. The particle size of all four types of formulations increases gradually with increasing rubber content (below phase inver-

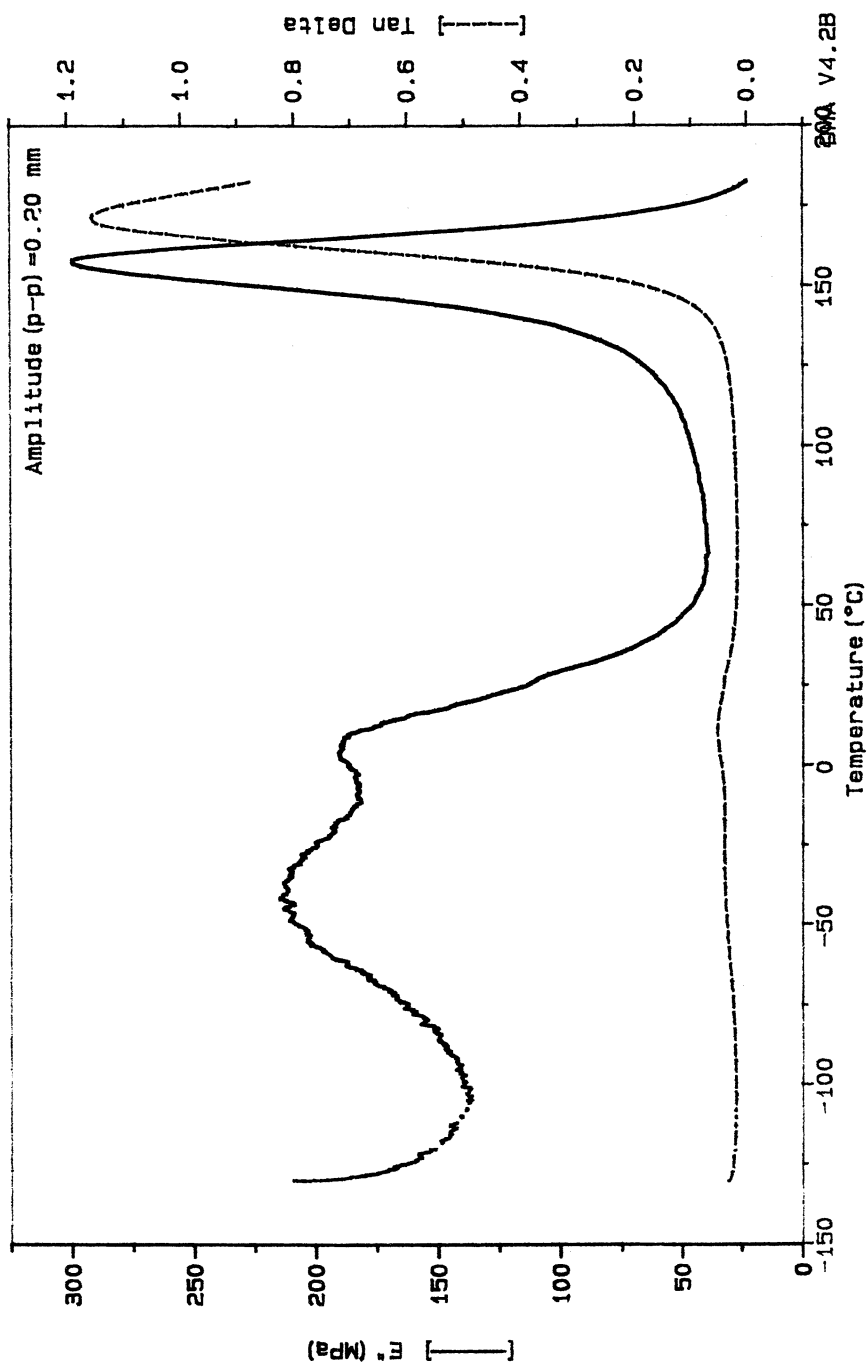


Figure 10. DMA temperature dependence of the dynamic loss (flexure) modulus, E'' (solid line) and $\tan \delta$ (dashed line) of a DGEBA-DDM-VR(20) specimen.

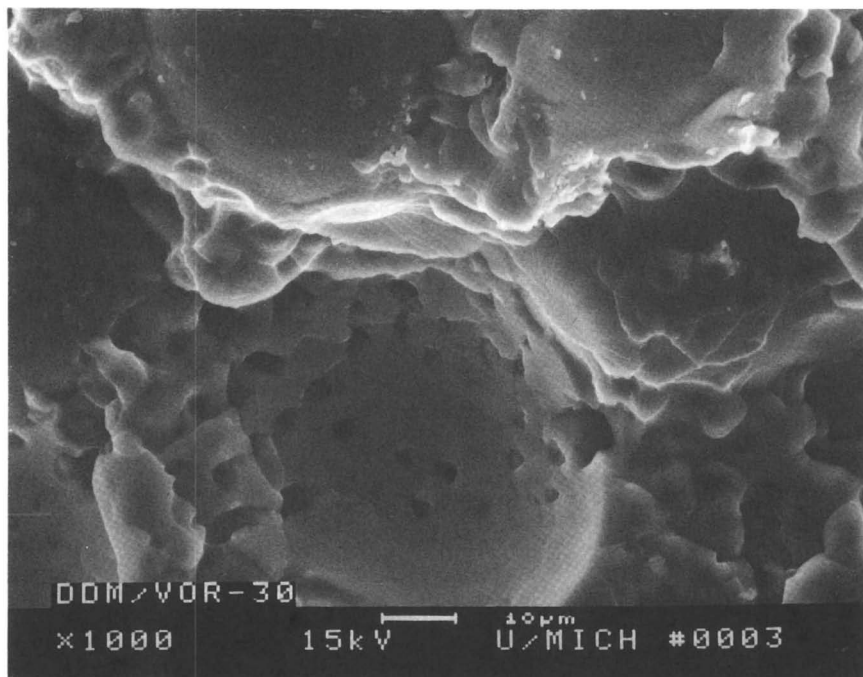


Figure 11. SEM micrograph of the fracture surface of a DGEBA-DDM-VR(30) specimen.

sion). Obviously, at higher rubber content the formulations reach their saturation point at an earlier curing stage. An “early” phase separation results in the formation of larger rubbery particles.

3. An analogous situation is observed for thermosets with high rubber content (above 50%). The highly polar DGEBA-DDS phase easily undergoes phase separation from the nonpolar vernonia rubber and small rigid particles (1–2 μm) are formed even at very high rubber content in DGEBA-DDS-VR(70). The less polar DGEBA-DDM phase has better solubility in the more polar epoxidized soybean rubber and phase separation does not occur in DGEBA-DDM-ESR(70) or even in DGEBA-DDM-ESR(60). The two phases of the remaining two types of formulations (DGEBA-DDM-VR and DGEBA-DDS-ESR) have miscibility characteristics that are intermediate between the two extreme formulations and show intermediate types of morphology.

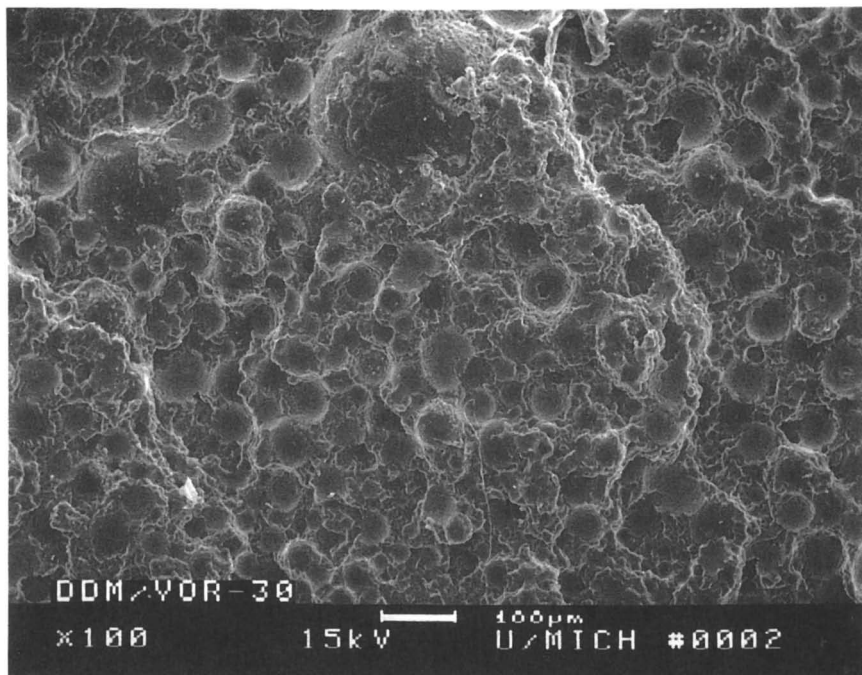


Figure 12. SEM micrograph of the fracture surface of a DGEBA-DDM-VR(30) specimen.

4. DGEBA particle size for all four formulations decreases with increasing rubber content (above 50%). The formulations that contain smaller amounts of DGEBA resin reach their saturation point at a later curing stage. A “late” phase separation results in the formation of smaller DGEBA particles.

Phase Inversion. The percentage of rubber content required for phase inversion increases gradually for the formulations with increasing miscibility of their two phases (Tables I–IV). In this regard, the four types of formulations follow exactly the same order as discussed previously for particle size distribution. This relationship between rubber content and phase inversion miscibility is probably due to different DGEBA partition in the two phases of the formulations. A tentative mechanism for the phase inversion process follows.

DGEBA-DDS-VR formulations start phase inversion at the lowest rubber content (15%). Under the curing conditions, the initial homogeneous formulations form a highly polar DGEBA-DDS epoxy resin, and its polarity increases gradually with progressing cure time due to the formation of additional hydroxyl groups by the reaction of DGEBA epoxy groups with

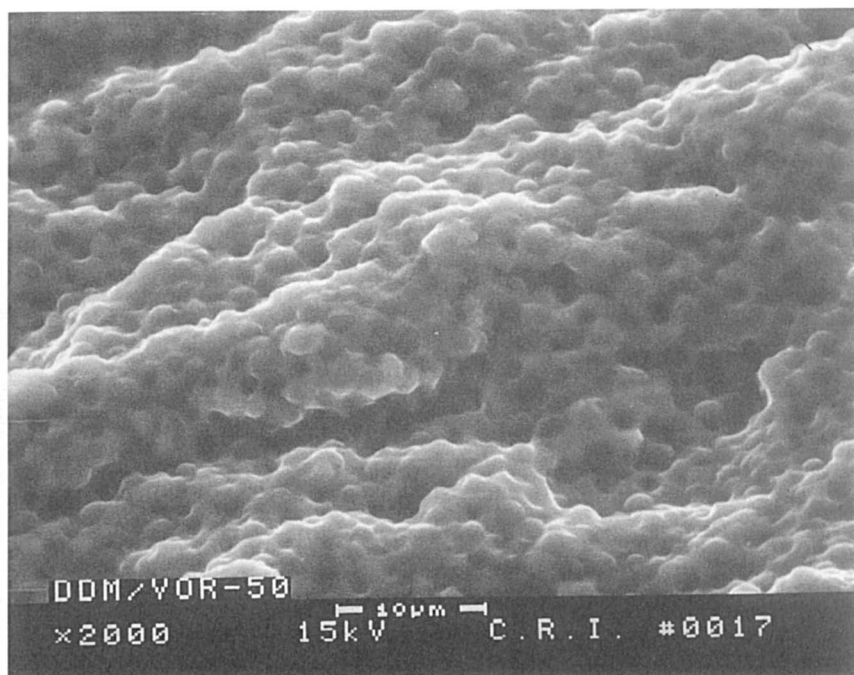


Figure 13. SEM micrograph of the fracture surface of a DGEBA-DDM-VR(50) specimen.

Table II. Morphology and Particle Size Distribution for DGEBA-DDS-VR Formulations

<i>Thermoset Formulation</i>	<i>Morphology</i>	<i>Dispersed Phase</i>	<i>Particle Size (μm)</i>
DGEBA-DDS	homogeneous		
DGEBA-DDS-VR(5)	two phase	vernonia	3-10
DGEBA-DDS-VR(10)	two phase	vernonia	3-25
DGEBA-DDS-VR(15)	two phase	vernonia	3-25, 25-100
DGEBA-DDS-VR(20)	two phase	PI ^a start vernonia	3-25, 25-350
DGEBA-DDS-VR(30)	two phase	DGEBA PI ^a end	2-5, 20-400
DGEBA-DDS-VR(50)	two phase	DGEBA	0.5-4
DGEBA-DDS-VR(60)	two phase	DGEBA	— ^b
DGEBA-DDS-VR(70)	two phase	DGEBA	— ^b
VR ^c	homogeneous		

^a PI, phase inversion.

^b Data not available.

^c Neat cross-linked vernonia rubber.

Table III. Morphology and Particle Size Distribution for DGEBA-DDM-ESR Formulations

<i>Thermoset Formulation</i>	<i>Morphology</i>	<i>Dispersed Phase</i>	<i>Particle Size (μm)</i>
DGEBA-DDM	homogeneous		
DGEBA-DDM-ESR(10)	homogeneous		
DGEBA-DDM-ESR(15)	two phase	soybean	0.1-0.5
DGEBA-DDM-ESR(20)	two phase	soybean	0.1-0.4
DGEBA-DDM-ESR(30) ^a	two phase	soybean	0.1-0.8
DGEBA-DDM-ESR(35) ^a	two phase	DGEBA	3-5
DGEBA-DDM-ESR(50)	two phase	DGEBA	1-2
DGEBA-DDM-ESR(60)	two phase	DGEBA	0.5-1
DGEBA-DDM-ESR(70)	homogeneous		
ESR ^b	homogeneous		

^a Phase inversion occurs between 30 and 35% ESR.

^b Neat cross-linked soybean rubber.

Table IV. Morphology and Particle Size Distribution for DGEBA-DDS-ESR Formulations

<i>Thermoset Formulation</i>	<i>Morphology</i>	<i>Dispersed Phase</i>	<i>Particle Size (Mm)</i>
DGEBA-DDS	homogeneous		
DGEBA-DDS-ESR(10)	two phase	soybean	1-2
DGEBA-DDS-ESR(20)	two phase	soybean	1-5
DGEBA-DDS-ESR(25)	two phase	soybean	2-10
DGEBA-DDS-ESR(30)	two phase	soybean	2-10, 10-100
DGEBA-DDS-ESR(35)	two phase	PI ^a start DGEBA	3-5, 10-100
DGEBA-DDS-ESR(50)	two phase	PI ^a end DGEBA	1-3
DGEBA-DDS-ESR(60)	two phase	DGEBA	— ^b
DGEBA-DDS-ESR(70)	homogeneous		
ESR ^c	homogeneous		

^a PI, phase inversion.

^b Data not available.

^c Neat cross-linked soybean rubber.

DDS. Even more important for phase separation, the molecular weight of the DGEBA-DDS resin increases, which lowers the entropy of mixing. At a certain point, the formulations reach their saturation point and phase separation of the nonpolar vernonia rubber starts. At this point, the unreacted DGEBA monomer has a different partition in the two phases. DGEBA is a nonpolar compound and has relative high partition in the nonpolar vernonia rubber and low partition in the highly polar DGEBA-DDS phase. Thus, vernonia particles contain a relatively large amount of dissolved unreacted DGEBA. This DGEBA is believed to cure at a later stage and form the very

small rigid occlusions (several micrometers) observed within the large rubbery particles (100–200 micrometers). The polarity of the DGEBA–DDS phase gradually increases further with curing time as the solubility of the vernonia rubber decreases in the matrix. This mechanism leads to phase separation of an additional amount of rubber at a later stage of curing and the formation of small neat vernonia rubbery particles (several micrometers) because most of the DGEBA has been already consumed. A bimodal particle size distribution with the formation of small and large vernonia particles is observed for DGEBA–DDS–VR formulations at phase inversion. The apparent volume fraction of the rubbery phase is much larger than the actual vernonia volume fraction as a result of DGEBA occlusion in the large vernonia particles, which triggers phase inversion in DGEBA–DDS–VR formulations at lower rubber content.

The partition of DGEBA monomer in the less polar DGEBA–DDM matrix of the DGEBA–DDM–VR formulations is significantly higher than in the highly polar DGEBA–DDS matrix of DGEBA–DDS–VR. As a result, DGEBA partition in the vernonia phase of DGEBA–DDM–VR formulations and their apparent rubbery volume fraction (at the same rubber content) is lower than in DGEBA–DDS–VR. Phase inversion in DGEBA–DDM–VR, therefore, requires higher rubber content (20%).

Epoxidized soybean rubber is more polar than vernonia rubber. DGEBA partition in soybean particles, therefore, is lower than in vernonia particles, and phase inversion requires much higher rubber content. Phase inversion in DGEBA–DDS–ESR formulations, indeed, starts at 30% of rubber content.

The unreacted DGEBA of the DGEBA–DDM–ESR formulations is expected to have the highest partition in the (DGEBA–DDM) matrix and the lowest partition in the (soybean) rubber from all four types of formulations, which would reduce the formation of large soybean particles with DGEBA occlusions. As a matter of fact, DGEBA–DDM–ESR formulations are the only formulations for which formation of larger particles and transitional states with bimodal particle size distribution are not observed at all during phase inversion. Phase inversion in these formulations is completed in a very narrow range of rubber content (between 30 and 35%). The morphology of continuous rigid DGEBA matrix and rubbery particles at 30% rubber changes into continuous rubbery phase with rigid DGEBA particles at 35% rubber content. The intermediate stages of phase inversion found in the other three formulations have not been observed here. Obviously, the phase inversion in DGEBA–DDM–ESR follows a different mechanism than the other three types of formulations. The phase inversion proceeds practically without DGEBA partition in the rubbery particles.

Phase inversion in all four types of formulations occurs at about 35% rubber volume fraction. This volume fraction is achieved in the DGEBA–DDS–VR formulations at about 15 wt% vernonia rubber by DGEBA occlusion in the large rubbery particles. DGEBA partition in the rubbery phase

gradually decreases in the order of DGEBA-DDM-VR, DGEBA-DDS-ESR, and DGEBA-DDM-ESR. The phase inversion in these formulations, therefore, requires gradually higher rubber content.

All formulations with rubber content below that required for phase inversion form only small rubbery particles. The initial homogeneous formulations reach their saturation point at a later (advanced) curing stage when most of the DGEBA monomer has been consumed. The phase separation process, therefore, proceeds practically without DGEBA partition in the rubbery phase. At higher rubber content (above phase inversion), the phase separation process follows a similar mechanism, but only small DGEBA particles are formed.

Summary and Conclusions

Phase inversion and particle size of the two-phase interpenetrating DGEBA thermosets depend on the miscibility of their two phases and can be regulated in a broad range by the nature of the liquid rubber and the diamine used for preparation.

Epoxidized vegetable oils and especially the epoxidized soybean oil, which is commercially available at a low price, are very attractive for preparation of two-phase epoxy thermosets. Two potential industrial applications for toughening commercial epoxy resins and for preparation of crack resistant epoxy coatings are described in the next chapter (8).

Acknowledgment

The authors thank South Coast Air Quality Management District and the U.S. Agency for International Development for financial support.

References

1. Dirlikov, S. K.; Frischinger, I.; Islam, M. S.; Lepkowski, T. J. In *Biotechnology and Polymers*; Gebelein, C. G., Ed.; Plenum Press: New York, 1991; pp 79-94.
2. Frischinger, I.; Dirlikov, S. *Polym. Mater. Sci. Eng.* **1991**, *65*, 178-179.
3. Frischinger, I.; Dirlikov, S. In *Toughened Plastics: Science and Engineering*; Riew, K. C.; Kinloch, A. J., Eds.; Advances in Chemistry 233; American Chemical Society: Washington, DC, 1992; pp 451-489.
4. Kinloch, A. J. In *Rubber-Toughened Plastics*; Riew, K. C., Ed.; Advances in Chemistry 222; American Chemical Society: Washington, DC, 1989; pp 67-91.
5. Pearson, R. A.; Yee, A. F. *J. Mater. Sci.* **1986**, *21*, 2475.
6. Pearson, R. A.; Yee, A. F. *J. Mater. Sci.* **1991**, *26*, 3828.
7. Riew, C. K.; Rowe, C. H.; Siebert, A. R. In *Toughness and Brittleness of Plastics*; Deanin, D. R.; Crugnola, A. M., Eds.; Advances in Chemistry 154; American Chemical Society: Washington, DC, 1976; p 326.
8. Frischinger, I.; Muturi, P.; Dirlikov, S. This volume, Chapter 26.

RECEIVED for review February 11, 1992. ACCEPTED revised manuscript December 16, 1992.

Two-Phase Interpenetrating Epoxy Thermosets That Contain Epoxidized Triglyceride Oils

Part II. Applications

Isabelle Frischinger¹, Patrick Muturi², and Stoil Dirlikov¹

¹Eastern Michigan University, Coatings Research Institute, 122 Sill Hall, Ypsilanti, MI 48197

²Kenya Industrial Research and Development Institute, Nairobi, Kenya

Two potential applications of two-phase interpenetrating epoxy thermosets based on diglycidyl ether of bisphenol A (DGEBA) epoxy resin, commercial diamine, and epoxidized vegetable oils are described. The applications are toughening commercial epoxy thermosets and preparation of crack-resistant coatings. Thermosets with DGEBA matrix and small "vegetable" rubbery particles have excellent toughness and other physicomechanical properties. Two-phase epoxies, especially those with continuous "vegetable" rubbery phase and small rigid DGEBA particles, form stress- and crack-resistant coatings. This in situ approach for preparation of two-phase coatings is an attractive alternative to the hard core-soft shell and soft core-hard shell reactive latex technology. Epoxidized soybean oil, which is commercially available at a low price, is especially suitable for these applications.

TWO-PHASE INTERPENETRATING EPOXY THERMOSETS are formed, under certain conditions, from homogeneous mixtures of diglycidyl ether of bisphenol A (DGEBA) epoxy resins and commercial diamines that contain epoxidized vegetable oils (1). Morphology, particle size, and phase inversion depend on the nature of the epoxidized vegetable oil and the diamine used for preparation. The two-phase epoxy thermosets, especially those based on the commercially available inexpensive epoxidized soybean oil (\$0.53 per pound), are very

attractive for different industrial applications. In the present chapter, two potential applications—toughening commercial epoxy thermosets and preparation of crack-resistant epoxy coatings—are described.

Experimental Details

The initial materials as well as the preparation of liquid rubbers, based on epoxidized vegetable oils and final two-phase interpenetrating thermosets, have been described in detail in the previous chapter (1). The epoxy morphology and transition temperatures were determined by scanning electron microscopy (SEM) and dynamic mechanical analysis (DMA), respectively, as also described in the previous chapter (1).

Fracture Toughness. Single-edge-notched (SEN) specimens with approximate dimensions of $100 \times 12.7 \times 6.7$ mm were machined from castings (2). A sharp crack was introduced into the specimen by the strike of a razor blade (previously chilled in liquid nitrogen) with a rubber mallet. The tests were carried out with a three-point bending assembly, which was monitored by a servohydraulic materials testing machine (Instron 1331) with a span of 50.8 mm and a piston rate of 2.54 mm/s. A computer interface controlled the machine and recorded the data. A computer (Hewlett-Packard model 310) was programmed to calculate the critical stress intensity factor, K_{Ic} , using the relation (3)

$$K_{Ic} = Y \frac{2PS\sqrt{a}}{3tw^2}$$

where P is the critical load for crack propagation (newtons), S is the length of the span (millimeters), a is the crack length (millimeters), w is the width (millimeters), t is the thickness (millimeters), and Y is the nondimensional shape factor given by

$$Y = 1.9 - 3.07(a/w) + 14.53(a/w)^2 - 25.11(a/w)^3 + 25.80(a/w)^4$$

The following relationship, which holds in case of linear-elastic-fracture mechanics (LEFM) under plane strain conditions, was used for determination of the fracture energy, G_{Ic} :

$$G_{Ic} = \frac{(1 - \nu^2)(K_{Ic})^2}{E}$$

where ν is the Poisson ratio and E is the elastic or Young's modulus. At least eight specimens of each formulation were used for determination of average fracture energy G_{Ic} .

Uniaxial Tensile Test. Dog bone bars with dimensions of $6 \times 0.5 \times 1/8$ in. ($152 \times 12.7 \times 3.5$ mm) were cut with a high speed router and their external surface was polished with very fine (220 grit) aluminum oxide sandpaper (3M). A

screw-driven tensile instrument (Instron model 1185), equipped with an extensometer for determination of the longitudinal strain and a computer interface type 4500 series, was used at a stroke of 60 mm/min. At least 10 specimens of each formulation were used for determination of their average tensile properties at room temperature.

Differential Scanning Calorimetry. Differential scanning calorimetry (DSC) measurements were carried out on a thermal analyzer (DuPont 2100 instrument with DSC model 2910) over the temperature range from -130 to $+200$ °C at a heating rate of 2 °C/min.

Water Absorption. Maximum water absorption was determined on rectangular specimens with approximate dimensions of $45 \times 7.8 \times 3.5$ mm that were predried in a vacuum oven at 60 °C to constant weight and then kept in boiling water for 3 to 4 weeks until saturation (i.e., to constant weight).

Dielectric Properties. Dielectric constant and dissipation factor were measured at 1 MHz and room temperature on specimens with $3 \times 3 \times 1/8$ in. dimensions on an instrument for electrical measurements (Genrad Digibridge model 1687 B) equipped with an LD-3 cell and by using the two-fluid method [air and DC-200, 1 cS (centistoke)].

Sodium and Chlorine Content. Sodium and chlorine content were determined by Galbraith Analytical Laboratories, Inc. (Knoxville, TN). Paint Research Associates (Ypsilanti, MI) confirmed sodium content by analysis with an atomic absorption spectrophotometer (Perkin-Elmer 2380).

Coatings Preparation and Characterization. The coatings were applied as 3-mil-thick wet films on cold rolled steel panels and baked in an oven, first at 75 °C for 4 h and then at 150 °C for 2 h. Coatings properties were characterized at room temperature by ASTM testing methods as follows: adhesion (D3359-87), pencil hardness (D3363-74), rocker hardness (D2134-66), flexibility (D4145-83), and impact strength (D2794-84). Coatings that failed in reverse impact strength tests were used as SEM specimens. Broken pieces of these coatings were mounted on a holder and the fracture surface of their cross-sections was observed via scanning electron microscopy (SEM).

Procedures and Formulations

The initial materials—DGEBA, 4,4'-diaminodiphenylmethane (DDM), 4,4'-diaminodiphenylsulfone (DDS), vernonia oil, and epoxidized soybean oil—were described in detail in the previous chapter (1), together with the procedures for preparation of liquid rubbers and the final cure of two-phase thermosets.

Three types of formulations have been evaluated in the present study: DGEBA-DDM-VR(α), DGEBA-DDM-ESR(α), and DGEBA-DDS-ESR(α). Vernonia (VR) and epoxidized soybean (ESR) liquid rubbers were prepared from DDM and the corresponding oils. The DGEBA-DDM-VR(α) thermosets were obtained from initial homogeneous stoichiometric mixtures

of DGEBA and DDM modified by vernonia rubber. The content of the liquid rubber (x) was varied between 0 and 100 wt%: $x = 0$ corresponds to the neat DGEBA–DDM thermoset, whereas $x = 100$ is pure vernonia rubber. Analogous abbreviations are used for the other two types of formulations.

Toughening Commercial Epoxy Resins

A small amount of discrete rubbery particles with an average size of several micrometers and randomly distributed in a glassy, brittle epoxy thermoset is known to dissipate a part of the impact energy. This energy dissipation improves crack and impact resistance without significant deterioration of other properties (4, 5).

Epoxy toughness is usually achieved by separation of a rubbery phase with a unimodal particle size distribution from the matrix during the curing process. Different reactive liquid rubbers, based on low molecular weight carboxy- or amino-terminated oligomers of butadiene and acrylonitrile (CTBN and ATBN), are usually used for the formation of the rubbery phase. Low molecular weight amino-terminated (methyl) siloxanes offer other alternatives. However, some of these oligomers are quite expensive.

Epoxidized vegetable oils, such as vernonia, epoxidized soybean, and linseed oils, provide new opportunities. Epoxidized vegetable oils react with commercial diamines to form epoxy resins that are elastomers at room temperature with low glass-transition temperatures in the range of -70 to 0 °C, dependent on the nature of the amine used for curing. Epoxidized soybean rubber, therefore, was evaluated for toughening commercial epoxy resins. For this purpose, DGEBA–DDM and DGEBA–DDS formulations were toughened by the addition of 10, 15, 20, and 30% epoxidized soybean liquid rubber. The resulting thermosets consist of a rigid DGEBA matrix and small “soybean” rubbery particles (Table I). The morphology of these thermosets was discussed in detail in the previous chapter (1).

Glass-Transition Temperature. The glass-transition temperatures (T_g) were determined by dynamic mechanical analysis (DMA) from the temperature dependence (maximum) of their tan delta values (Table II).

The glass-transition temperatures of the neat DGEBA–DDM and DGEBA–DDS thermosets are observed at 190 and 185 °C, respectively. Both thermosets also exhibit beta relaxations at lower temperatures of -30 and -35 °C, respectively. The pure epoxidized soybean rubber (ESR), cured under the same conditions in the absence of DGEBA–diamine component, shows a glass-transition temperature of -25 °C by DSC.

The two-phase DGEBA–DDM–ESR and DGEBA–DDS–ESR formulations exhibit two transitions at higher and lower temperatures. The higher temperature transitions in the range of 145–190 °C have been assigned to the T_g of their DGEBA matrices. T_g gradually decreases with an increasing

Table I. Average Range of “Soybean” Particle Size Distribution of the Rubber-Modified DGEBA-DDM-ESR and DGEBA-DDS-ESR Thermosets

<i>Thermoset Formulation</i>	<i>Particle Size (μm)</i>
DGEBA-DDM-ESR(10)	no phase separation
DGEBA-DDM-ESR(15)	0.1–0.5
DGEBA-DDM-ESR(20)	0.1–0.4
DGEBA-DDM-ESR(30)	0.1–0.8
DGEBA-DDS-ESR(10)	1–2
DGEBA-DDS-ESR(20)	1–5
DGEBA-DDS-ESR(30) ^a	1–17
DGEBA-DDS-ESR(30) ^b	5–10, 100–200

^a Tensile specimens.

^b Fracture toughness specimens.

Table II. DMA Lower and Higher Temperature Transitions of Pure DGEBA-DDM and DGEBA-DDS Thermosets and Their Rubber-Modified DGEBA-DDM-ESR and DGEBA-DDS-ESR Formulations

<i>Thermoset Formulation</i>	<i>Transition ($^{\circ}\text{C}$)</i>	
	<i>Overlap^a</i>	<i>DGEBA^b</i>
DGEBA-DDM	–30	190
DGEBA-DDM-ESR(15)	–35	161
DGEBA-DDM-ESR(20)	–33	165
DGEBA-DDM-ESR(30)	–39	145
DGEBA-DDS	–35	185
DGEBA-DDS-ESR(10)	–45	168
DGEBA-DDS-ESR(20)	–43	166
DGEBA-DDS-ESR(30)	–30	161
ESR ^c	–25	

^a The lower transition temperature corresponds to an overlap in the glass-transition temperature of the rubbery particles and the beta transition of the DGEBA matrix.

^b Glass-transition temperature of the DGEBA matrix.

^c Determined by DSC.

amount of soybean liquid rubber due to plasticization of the DGEBA rigid matrix. As previously discussed (1, 2), the nonpolar soybean rubber has higher solubility in less polar DGEBA-DDM than in the more polar DGEBA-DDS matrix. The plasticization phenomenon, therefore, is more pronounced for the DGEBA-DDM-ESR formulations. The depression of the glass-transition temperature of their matrices is about 25 $^{\circ}\text{C}$ at 15–20% soybean rubber content, and almost 45 $^{\circ}\text{C}$ at 30% loading. The less miscible DGEBA-DDS-ESR formulations exhibit smaller depressions: 15 $^{\circ}\text{C}$ at 10% soybean liquid rubber to approximately 25 $^{\circ}\text{C}$ at 30% loading.

The lower temperature transitions of the DGEBA-DDM-ESR and DGEBA-DDS-ESR formulations, observed in the range of -30 to -45 °C, are assigned to an overlap of the glass-transition temperatures of the ESR rubbery particles and the beta transition of their matrix (2). In general, the glass-transition temperature of the rubbery particles in the two-phase thermosets corresponds to the glass-transition temperature of the pure ESR rubber. This result indicates that the rubber phase in these two-phase thermosets does not contain a significant amount of the DGEBA component and is formed by practically pure soybean rubber.

Fracture Toughness. The fracture toughness, in terms of stress intensity factor, K_{Ic} , and fracture energy, G_{Ic} , is given in Table III. The fracture surfaces of both formulations DGEBA-DDM-ESR and DGEBA-DDS-ESR show extensive particle cavitation (1), which is the main toughening mechanism.

A better toughening effect, which gradually increases at a higher soybean rubber content, is observed for the DGEBA-DDM-ESR formulations. This effect is probably due to the plasticization phenomenon that occurs on a larger scale for these formulations (1). The soybean rubber, which acts as a matrix plasticizer, improves toughness.

A smaller improvement of the fracture toughness and an optimum toughening effect at 20% soybean rubber is observed for the DGEBA-DDS-ESR formulations. The DGEBA-DDS-ESR(30) specimens at 30% soybean liquid rubber, which were used here for determination of

Table III. Stress Intensity Factor, K_{Ic} , and Fracture Energy, G_{Ic} , of Pure DGEBA-DDM and DGEBA-DDS Thermosets and Their Rubber-Modified DGEBA-DDM-ESR and DGEBA-DDS-ESR Formulations

<i>Thermoset Formulation</i>	K_{Ic} (MPa · m ^{1/2})	G_{Ic} (J/m ²)
DGEBA-DDM	0.75	175
DGEBA-DDM-ESR(10) ^a		
DGEBA-DDM-ESR(15)	1.24	564
DGEBA-DDM-ESR(20)	1.33	802
DGEBA-DDM-ESR(30)	1.40	1008
DGEBA-DDS	0.75	145
DGEBA-DDS-ESR(10)	1.09	374
DGEBA-DDS-ESR(20)	1.19	596
DGEBA-DDS-ESR(30)	0.54	145
DGEBA-DDS ^b		162
DGEBA-DDS-CTBN(10) ^b		242

^a This formulation does not phase separate due to better miscibility to its two phases (1). Its fracture toughness has not been determined.

^b Reference 6.

fracture toughness, have a bimodal particle size distribution that is characteristic for the beginning of phase inversion phenomena (1). At this point the physicomaterial properties start to deteriorate rapidly and lower fracture toughness is observed.

In summary, the soybean liquid rubber significantly improves the fracture toughness of commercial highly cross-linked, brittle DGEBA-DDS and DGEBA-DDM epoxy thermosets. This toughening effect is due to both rubber toughening as a result of particle formation and enhanced ductility of the matrix through plasticization (1).

Tensile Properties. Young's moduli were determined from the corresponding tensile stress-strain curves as an average value of several independent measurements (Table IV). In contrast to fracture toughness, where DGEBA-DDS-ESR(30) specimens with a bimodal particle size distribution were used, all tensile specimens used in this study had a unimodal distribution (Table I). Reproduction of the exact morphology of DGEBA-DDS-ESR(30) is difficult because this formulation is very close to its phase inversion point and small deviation of the experimental conditions leads to different morphologies.

As expected, the elastic moduli gradually decreased with increasing soybean fraction. Linear relationships can approximately fit for both types of DGEBA-DDM-ESR and DGEBA-DDS-ESR formulations, and a slight deviation is observed only at a higher content of soybean rubber. The tensile properties of the DGEBA-DDS-ESR formulations, however, decrease faster with increasing soybean rubber content than do the tensile properties of DGEBA-DDM-ESR.

Table IV. Young's Modulus, E , of Pure DGEBA-DDM and DGEBA-DDS Thermosets and Their Rubber-Modified DGEBA-DDM-ESR and DGEBA-DDS-ESR Formulations

<i>Thermoset Formulation</i>	<i>E (MPa)</i>
DGEBA-DDM	2840
DGEBA-DDM-ESR(10) ^a	
DGEBA-DDM-ESR(15)	2410
DGEBA-DDM-ESR(20)	1950
DGEBA-DDM-ESR(30)	1720
DGEBA-DDS	3420
DGEBA-DDS-ESR(10)	2810
DGEBA-DDS-ESR(20)	2100
DGEBA-DDS-ESR(30)	1780
DGEBA-DDS ^b	3360
DGEBA-DDS-CTBN(10) ^b	3000

^a This formulation does not phase separate and its tensile properties have not been determined.

^b Reference 6.

Water Absorption. High water absorption is another major disadvantage of commercial epoxy resins in addition to their poor fracture toughness. Maximum water absorption was determined by placing predried samples in boiling water until constant weight was achieved. Although the results are somewhat lower than expected, the water absorption of both formulations decreases gradually and linearly with increasing soybean content (Table V). Obviously, the highly hydrophobic long fatty chains of the epoxidized soybean oil reduce the water absorption of its epoxy thermosets. As expected, the DGEBA–DDS–ESR formulations at different soybean liquid rubber contents have a higher water absorption than the corresponding DGEBA–DDM–ESR formulations, due to the more polar character of DDS in comparison to DDM.

Dielectric Properties. The introduction of epoxidized soybean oil, with its long aliphatic chains, was expected to lower simultaneously the dielectric constant and dissipation factor of the commercial epoxy resins, despite the formation of free hydroxyl groups by the opening of its epoxy rings. Surprisingly, the dielectric properties of both types of formulations do not change with increasing content of soybean liquid rubber (Table VI).

Sodium and Chlorine Content. A requirement for the application of epoxy resins in the electronics industry is low ionic content (often below 10 ppm), especially for sodium and chlorine ions. Electronics-grade epoxy resins are more expensive due to the additional purification procedure needed to lower their ionic content.

The epoxidized soybean oil without any purification has a very low (below 5 ppm) content of sodium and chlorine (Table VII) due to its hydrophobic nonpolar molecular structure that lacks free hydroxyl or carboxyl groups.

Table V. Maximum Water Absorption of Pure DGEBA–DDM and DGEBA–DDS Thermosets and Their Rubber-Modified DGEBA–DDM–ESR and DGEBA–DDS–ESR Formulations

<i>Thermoset Formulation</i>	<i>Water Absorption (%)</i>
DGEBA–DDM	2.42
DGEBA–DDM–ESR(15)	2.22
DGEBA–DDM–ESR(20)	2.00
DGEBA–DDM–ESR(30)	1.62
DGEBA–DDS	3.61
DGEBA–DDS–ESR(10)	3.33
DGEBA–DDS–ESR(20)	3.13
DGEBA–DDS–ESR(30)	2.80

Table VI. Dielectrical Properties of Pure DGEBA-DDM and DGEBA-DDS Thermosets and Their Rubber-Modified DGEBA-DDM-ESR and DGEBA-DDS-ESR Formulations

<i>Thermoset Formulation</i>	<i>Dissipation Factor</i>	<i>Dielectrical Constant</i>
DGEBA-DDM	0.033	3.78
DGEBA-DDM-ESR(15)	0.035	3.78
DGEBA-DDM-ESR(20)	0.036	3.77
DGEBA-DDM-ESR(30)	0.037	3.77
DGEBA-DDS	0.025	3.95
DGEBA-DDS-ESR(20)	0.033	3.88

Table VII. Ionic Content and Bulk Price of Epoxidized Soybean Oil (ESO), Vernonia Oil (VO), and CTBN

	<i>ESO</i>	<i>VO</i>	<i>CTBN^a</i>
Sodium (ppm)	4.2	4.3	380
Chlorine (ppm)	< 5.0	906	952
Price (\$/lb)	0.53	— ^b	2–2.50

^a Hycar (CTBN) 1300 × 16 (BFGoodrich Chemical Co.).

^b Not industrially produced.

Thus, epoxidized soybean rubber is especially suitable for toughening epoxy resins for electronics applications.

Epoxidized Soybean Liquid Rubber versus CTBN. The effect of the epoxidized soybean liquid rubber was compared with the effect of CTBN, which is commonly used for epoxy toughening in commercial-scale applications. The introduction of 10% CTBN liquid rubber into a DGEBA-DDS epoxy resin produced similar two-phase thermosets with CTBN rubbery particles (about 5 μm). The fracture energy of the unmodified DGEBA-DDS thermoset increased from $G_{\text{Ic}} = 162 \text{ J/m}^2$ to $G_{\text{Ic}} = 242 \text{ J/m}^2$ in the presence of 10% CTBN with $\Delta G_{\text{Ic}} = 80 \text{ J/m}^2$, whereas the Young's modulus simultaneously decreased from $E = 3360 \text{ MPa}$ to $E = 3000 \text{ MPa}$ (6). Our unmodified DGEBA-DDS thermoset exhibited similar fracture toughness ($G_{\text{Ic}} = 145 \text{ J/m}^2$) and Young's modulus ($E = 3420 \text{ MPa}$) (Tables III and IV). The introduction of 10% soybean liquid rubber, however, more than doubled the fracture energy from $G_{\text{Ic}} = 145 \text{ J/m}^2$ to $G_{\text{Ic}} = 374 \text{ J/m}^2$ (Table III) with $\Delta G_{\text{Ic}} = 229 \text{ J/m}^2$, whereas the Young's modulus decreased from $E = 3420 \text{ MPa}$ to a slightly lower value of $E = 2810 \text{ MPa}$ (Table IV). The soybean liquid rubber appears to have a better toughening effect than CTBN.

Another advantage of the epoxidized soybean rubber is its low sodium and chlorine content (an important characteristic for electronics applications) in contrast to the carboxy-terminated CTBN (Table VII).

The epoxidized soybean oil does not have carbon-carbon double bonds, and IR epoxy thermosets are expected to have better weatherability and thermal stability than CTBN-modified epoxies. Each CTBN butadiene unit has one carbon-carbon double bond that spontaneously cross-links after prolonged storage and UV radiation or exposure to higher temperatures.

Finally, epoxidized soybean oil is industrially produced and available at about \$0.50 per pound, a price below that of CTBN (in the range of \$2.00–2.50 per pound). The price difference makes the toughening of commercial epoxy resins by epoxidized soybean oil very attractive for commercial applications on a large scale.

Stress-Resistant Two-Phase Epoxy Coatings

Two-phase epoxy thermosets are attractive for preparation of stress-resistant coatings as well. To evaluate the morphology and physicochemical properties of two-phase thermosets, model two-phase interpenetrating epoxy coatings based on a model DGEBA-DDM stoichiometric formulation modified by the addition of 5-, 10-, 15-, 20-, 30-, and 50-wt% vernonia liquid rubber were studied (Table VIII). Vernonia rubber was selected in this research because it contains carbon-carbon double bonds and stains with osmium tetroxide. This stainability enabled us to easily identify the vernonia phase in the final two-phase coatings. In contrast, soybean rubber does not have carbon-carbon double bonds and does not stain with OsO_4 .

The addition of 10 or 15% vernonia rubber [DGEBA-DDM-VR(10) and DGEBA-DDM-VR(15)] results in two-phase coatings that consist of a rigid DGEBA matrix and randomly distributed small vernonia rubber particles with a diameter ranging from 0.2 to 1.2 μm . The small particles are barely observed in the coatings cross section at low magnification (Figure 1), but are distinguished clearly at higher magnification (Figure 2), especially after staining with OsO_4 (Figure 3). As expected these coatings exhibit improved impact strength and flexibility without significant deterioration of hardness and adhesion in comparison to the unmodified DGEBA-DDM coatings. At higher magnification, most of the rubbery particles of the DGEBA-DDM-VR(10) coatings have cavitated (black holes in the particles, Figures 2 and 3), which is a major epoxy toughening mechanism.

In a way, these in situ two-phase epoxy coatings with lower content of vernonia rubber (< 20%) resemble coatings obtained by hard shell-soft core reactive latex technology. In both cases, the coatings consist of a continuous hard rigid phase (matrix) and small soft rubbery particles.

Table VIII. Morphology and Physicomechanical Properties of DGEBA-DDM-VR Coatings

Coating Formulation	Particle Size (μm)	Impact Resistance ^a		Hardness			Adhesion ^b	Flexibility
		Direct	Reverse	Rocker	Pencil			
DGEBA-DDM	Homogeneous	70	50	50	> 8H	5B	— ^c	
DGEBA-DDM-VR(5)	— ^d	70	40	46	> 8H	5B	— ^c	
DGEBA-DDM-VR(10)	0.3–1.2	90	80	45	5H	5B	— ^c	
DGEBA-DDM-VR(15)	0.2–1.0	150	150	50	5H	5B	— ^e	
DGEBA-DDM-VR(20)	0.5–47 ^f	150	160	38	3H	5B	— ^e	
DGEBA-DDM-VR(30)	1–27 ^f	> 160	> 160	41	H	5B	— ^e	
DGEBA-DDM-VR(50)	0.4–1.0	≈ 160	≈ 160	21	H	5B	— ^e	
VR	Homogeneous	> 160	> 160	8	6B	5B	— ^e	

^a In inch-pounds (1 in.-lb = 0.01152 kg · m).

^b 5B corresponds to 100% adhesion.

^c Passed maximum but failed minimum diameter.

^d Not studied by SEM.

^e Passed maximum and minimum diameter.

^f Phase inversion.

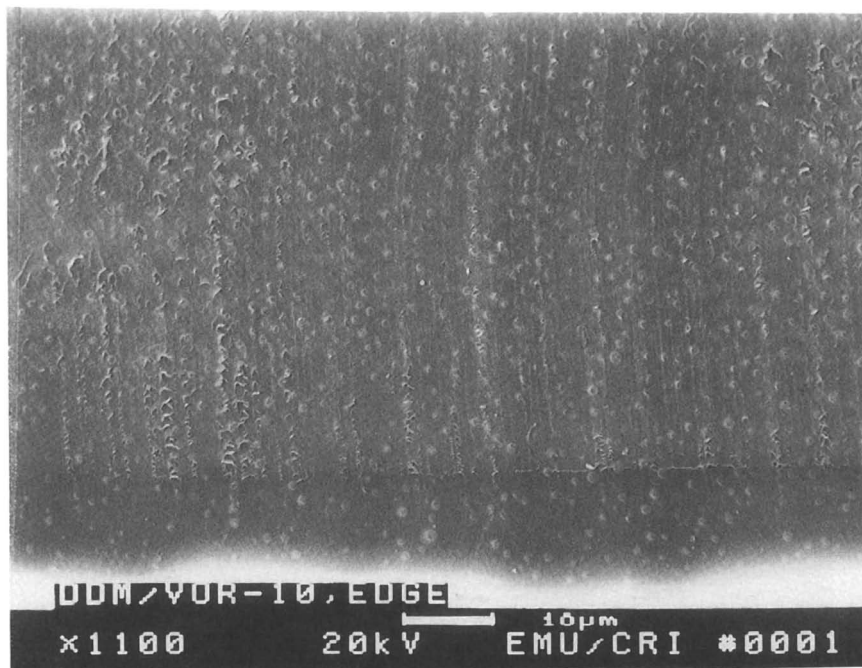


Figure 1. SEM micrograph of the fracture surface of a DGEBA-DDM-VR(10) coating cross-section with lower and upper edges ($\times 1100$).

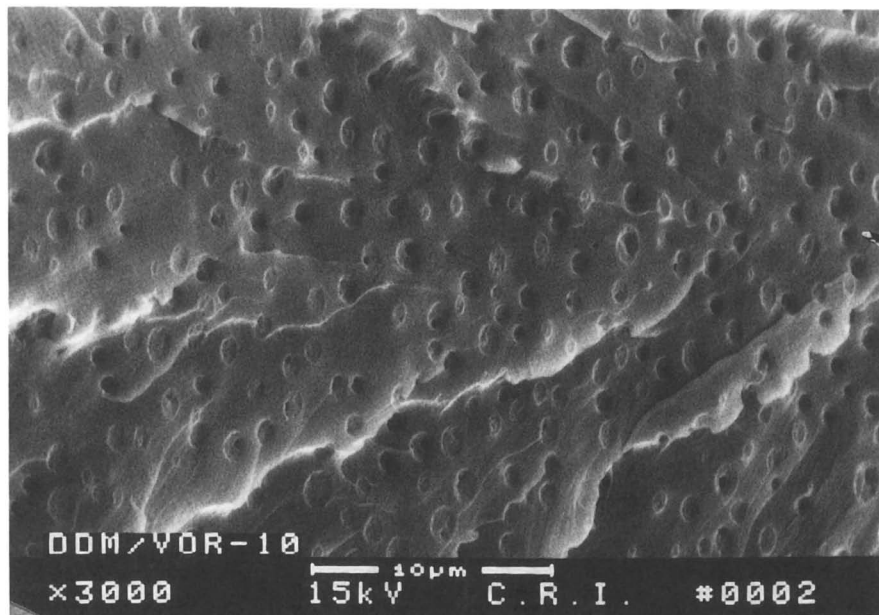


Figure 2. SEM micrograph of the fracture surface of a DGEBA-DDM-VR(10) coating cross-section ($\times 3000$).

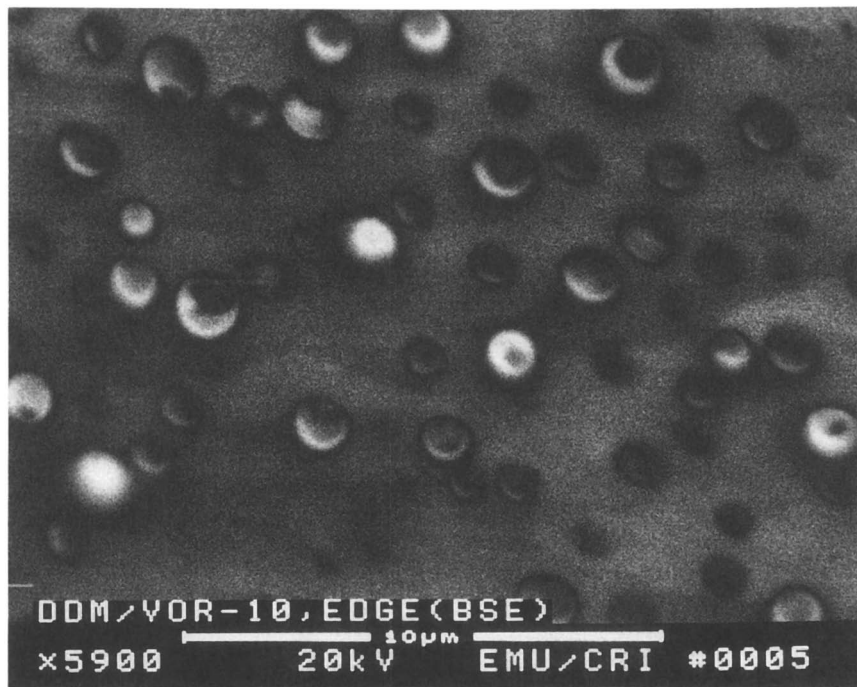


Figure 3. SEM micrograph using a backscattered electron imaging technique of the fracture surface of a DGEBA-DDM-VR(10) coating cross-section stained with osmium tetroxide ($\times 5900$).

The addition of 20% vernonia rubber leads to the beginning of phase inversion observed in DGEBA-DDM-VR(20). Figure 4 shows very large vernonia rubbery particles with diameters from 10 to 50 μm , which is comparable to the coating thickness (about 50 μm). These particles have a lighter shade after staining with OsO_4 (Figure 5), and they contain smaller and darker rigid DGEBA particles with average diameters from 0.5 to 1.0 μm .

Further increase of rubber results in complete phase inversion, and coatings that contain more than 30% vernonia rubber consist of a continuous vernonia rubbery phase that contains small rigid DGEBA particles. The particle diameters of the DGEBA-DDM-VR(50) coatings vary from 0.4 to 1.0 μm and it is difficult to distinguish them in the coatings cross section at low magnification (Figure 6). Coatings morphology is observed better at higher magnification (Figure 7). Coating failure occurs in the continuous rubbery phase and the rigid particles are not well distinguished; obviously, they are covered with vernonia rubber. The rigid particles, however, are clearly observed after staining with OsO_4 using a back scattered electron imaging technique (Figure 8). These coatings have excellent flexibility, impact

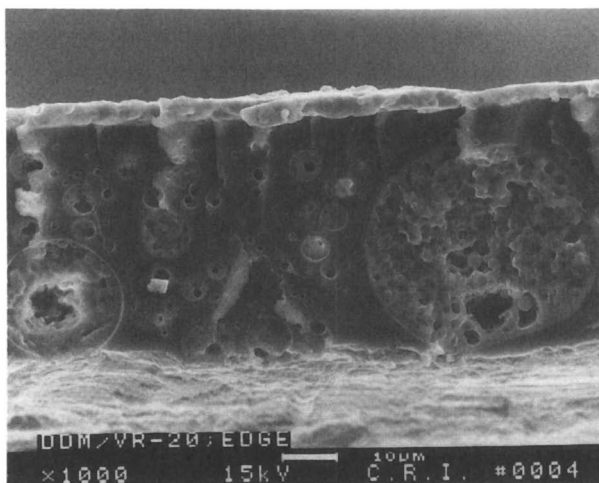


Figure 4. SEM micrograph of the fracture surface of a DGEBA-DDM-VR(20) coating cross-section with lower and upper edges.

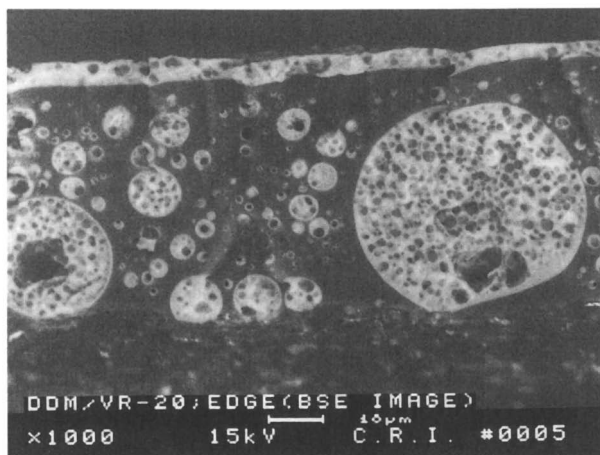


Figure 5. SEM micrograph using a backscattered electron imaging technique of the fracture surface of a DGEBA-DDM-VR(20) coating cross-section with lower and upper edges stained with osmium tetroxide.

strength, and adhesion due to the continuous rubbery phase (Table VIII), and they also have much better hardness, due to the rigid particles, in comparison to the homogeneous one-phase coatings with the same composition prepared directly from vernonia oil (unpublished results). Remember that the introduction of vernonia oil to DGEBA-DDM formulations leads to homogeneous

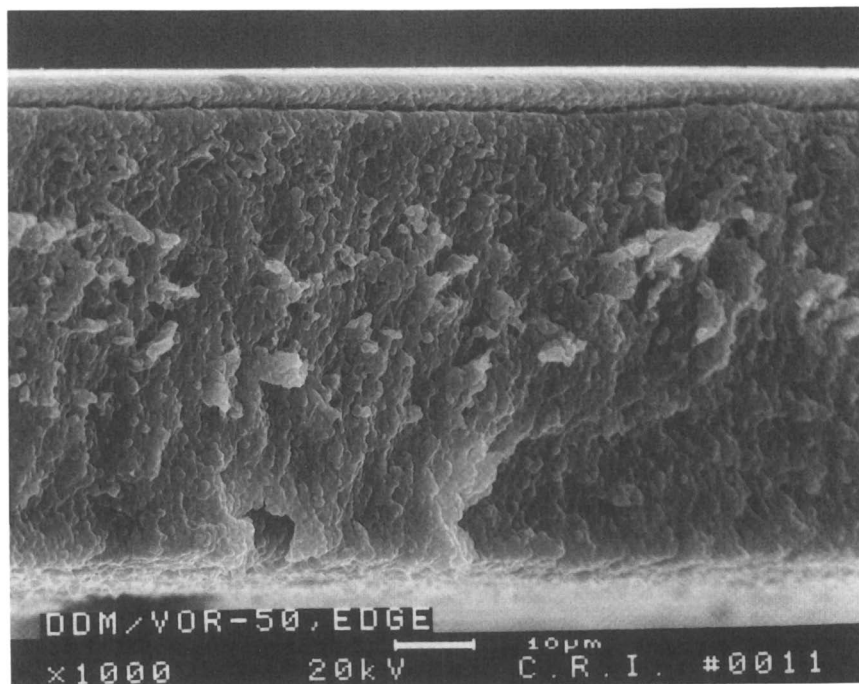


Figure 6. SEM micrograph of the fracture surface of a DGEBA-DDM-VR(50) coating cross-section with lower and upper edges ($\times 1000$).

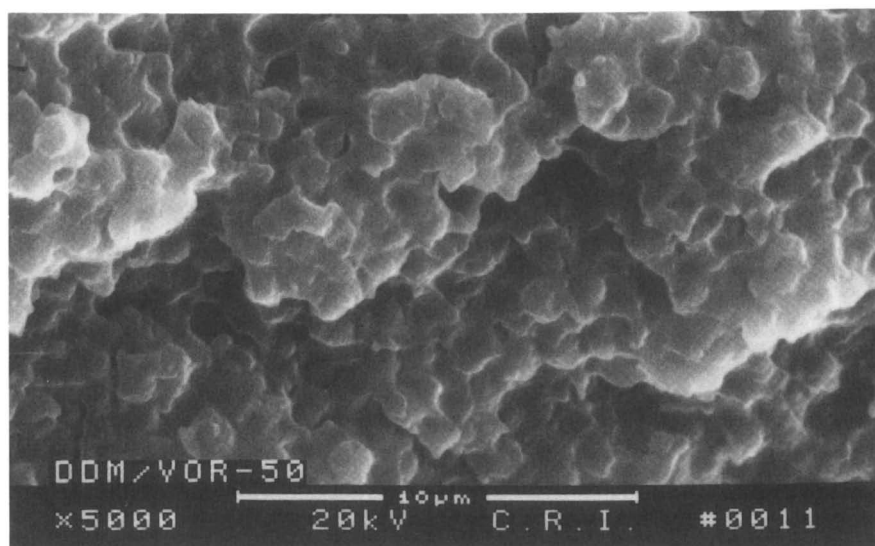


Figure 7. SEM micrograph of the fracture surface of a DGEBA-DDM-VR(50) coating cross-section ($\times 5000$).

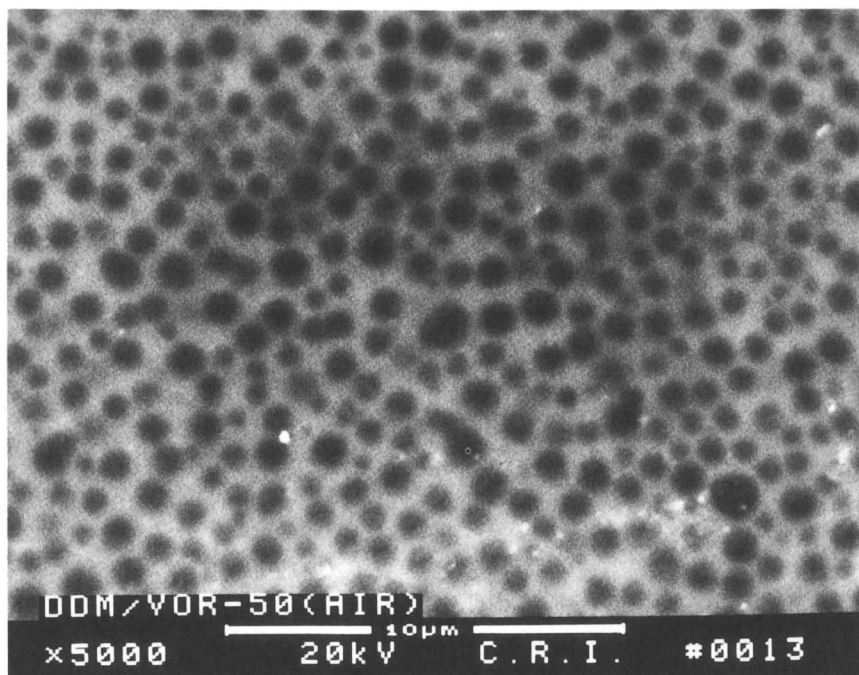


Figure 8. SEM micrograph using a backscattered electron imaging technique of the fracture surface of a DGEBA-DDM-VR(50) coating cross-section stained with osmium tetroxide ($\times 5000$).

one-phase thermosets and coatings in contrast to vernonia rubber that produces two-phase materials (1).

These stress- and crack-resistant two-phase coatings with a continuous rubbery phase are suitable for coil and especially can (container) coatings that undergo deformations after the coating application.

The coatings with higher content of vernonia rubber ($> 30\%$) resemble coatings obtained by hard core-soft shell reactive latex technology. In both cases, the coatings consist of a continuous soft rubbery phase (matrix) and small hard particles.

The neat DGEBA-DDM formulation and the neat vernonia rubber form homogeneous one-phase coatings. The properties of these one-phase coatings are given in Table VIII for comparison.

Discussion

Initial results show that two-phase interpenetrating epoxy coatings based on epoxidized soybean rubber can be obtained. Further research indicates that the introduction of vernonia oil in other formulations such as urethanes (a

mixture of methylenediphenylene diisocyanate and 1,10-decanediol) also results in two-phase thermosets under similar conditions (Dirlikov, S.; Muturi, P., unpublished results).

In general, initial homogeneous formulations based on two components with different polarity and different reactivity and a suitable curing agent are expected to undergo phase separation by two-stage (condensation) polymerization. In the foregoing formulations, the commercial epoxies (and urethanes) are polar components with very fast cure rates. As these materials cure at lower temperature (first stage), they form the rigid phase. At this stage, the hydrophobic epoxidized vegetable oil (or rubber), which is the nonpolar component and has a slow cure rate, phase separates and forms a liquid phase. The liquid phase cures later at a higher temperature (second stage) with the unreacted curing agent (diamine, etc.) to form the rubbery phase.

Similar two-phase thermosets have been prepared via two-stage addition polymerization as reported recently by Derrough et al. (7) for two-component formulations based on methyl methacrylate (or butyl acrylate) and diallyl carbonate of bisphenol A.

Summary and Conclusions

Epoxidized vegetable oils and especially epoxidized soybean oil, which is commercially available at a low price (\$0.50 per pound), are very attractive for preparation of two-phase interpenetrating epoxy thermosets. Two potential industrial applications have been evaluated: toughening commercial epoxy resins and preparation of stress-resistant coatings.

Thermosets with DGEBA matrix and "soybean" rubbery particles have excellent toughness without deterioration of other physicomechanical properties. Epoxidized soybean liquid rubber has a better toughening effect, lower ionic content, and lower price than CTBNs.

Stress- and crack-resistant two-phase epoxy coatings, especially those with a continuous rubbery phase and rigid DGEBA particles, are suitable for coil and container coatings. This in situ approach for preparation of coatings with two-phase morphology is an attractive alternative to hard core-soft shell and soft core-hard shell reactive latex technology.

Acknowledgment

The authors thank South Coast Air Quality Management District and the U.S. Agency for International Development for financial support. Dielectric properties were studied by D. Shimp at Hi-Tek Polymers, Inc.

References

1. Frischinger, I.; Dirlikov, S. This volume, Chapter 25.
2. Frischinger, I.; Dirlikov, S. In *Toughened Plastics: Science and Engineering*; Riew, K. C.; Kinloch, A. J., Eds.; Advances in Chemistry 233; American Chemical Society: Washington, DC, 1992; pp 451–489.
3. Brown, W. F.; Srawley, J. E. *ASTM STP* **1965**, 381, 13.
4. Riew, K. C.; Gillham, J. K., Eds.; *Rubber-Modified Thermoset Resins*; Advances in Chemistry 208; American Chemical Society: Washington, DC, 1984.
5. Riew, K. C., Ed.; *Rubber-Toughened Plastics*; Advances in Chemistry 222; American Chemical Society: Washington, DC, 1989.
6. Pearson, R. A.; Yee, A. F. *J. Mater. Sci.* **1989**, 24, 2571.
7. Derrough, S. N.; Rouf, C.; Widmaier, J. M.; Meyer, G. C. *Polym. Mater. Sci. Eng.* **1991**, 65, 1–2.

RECEIVED for review February 11, 1992. ACCEPTED revised manuscript December 16, 1992.

Castor Oil Polyurethane–Acrylic or Vinyl Polymer Interpenetrating Polymer Networks Cured at Room Temperature

H. Q. Xie, C. X. Zhang, and J. S. Guo

Department of Chemistry, Huazhong University of Science and Technology, Wuhan, 430074, People's Republic of China

During the formation of simultaneously grafted interpenetrating polymer networks (IPNs), the relative formation rates of castor oil polyurethane and poly(methyl methacrylate) are compared by IR spectrophotometry. The formation rate of the polyurethane network is higher than the graft polymerization rate of methyl methacrylate. The time of gelation decreases with increasing polyurethane content. The rate of gel formation in the IPN that contains poly(methyl acrylate) is higher than in the IPN that contains polystyrene. A maximum tensile strength of the IPNs occurs when the polyurethane content is about 50%. Transmission electron micrographs indicate that the polyurethane exists as domains in the continuous phase of polyacrylate. A broad glass-transition temperature occurs in the dynamic mechanical spectrum of the IPN.

AN INTERPENETRATING POLYMER NETWORK (IPN) is a combination of two polymer networks that interpenetrate each other (1, 2). The study of IPNs has aroused great interest because most IPNs exhibit better mechanical properties than their individual networks due to a synergistic effect induced by forced compatibility of the components.

Castor oil is a fine candidate for making IPNs because it is a triglyceride of ricinoleic acid, which contains three hydroxyl groups and three double bonds.

Yenwo et al. (3) were first to utilize castor oil to synthesize IPNs. To obtain sequential IPNs, Yenwo et al. first reacted the castor oil with sulfur or diisocyanate to cross-link it. Cross-linking was followed by swelling with a plastic-forming monomer, such as styrene plus cross-linker, and in situ polymerization. Electron microscopy shows that the polystyrene phase size of the castor oil urethane–polystyrene IPN decreases with increased cross-linking of the castor oil component and increases with increasing polystyrene content.

Dynamic mechanical spectroscopy studies show extensive but incomplete molecular mixing of the two networks (4). The glass-transition temperature of the IPNs gradually merges from two distinct transitions into one broad transition at an intermediate temperature as the cross-link level of the castor oil component is increased. The stress–strain results indicate that at low polystyrene content the IPNs behave like reinforced elastomers, whereas at high polystyrene content the IPNs exhibit decreased elongation and behave like toughened plastics. Toughened plastics materials show well developed yield points, stress whitening, and necking. The tensile strength and Young's modulus are enhanced as the polystyrene content or cross-link level of the polyurethane is increased. The impact strength of the materials is approximately two or three times that of polystyrene. The best materials are materials with compositions in the range of 40–60% castor oil urethane. The materials prepared at an NCO–OH ratio of 0.95 have the best impact properties.

Instead of sequential IPNs, Devia et al. (5) studied the synthesis of simultaneous interpenetrating networks based on elastomeric polymers derived from castor oil and cross-linked polystyrene. The elastomers included the cross-linked polyester of castor oil and sebacic acid, cross-linked polyurethane with 2,4-toluene diisocyanate (TDI), and cross-linked polyester–polyurethane from castor oil, sebacic acid, and TDI. The polystyrene phase was cross-linked with 1% divinylbenzene, and 0.4% benzoyl peroxide was used as the initiator for the styrene polymerization at 80 °C. Experimental data on the extent of the reaction at the gel point agreed remarkably well with prediction based on the Flory–Stockmayer equation for the castor oil–sebacic acid system as a function of COOH–OH ratio in the mixture. Two kinds of materials with elastomer component compositions of 10 and 40% behaved as toughened plastics and reinforced elastomers, respectively.

Devia et al. later reported the morphology and glass-transition behavior of the preceding simultaneous IPNs based on electron microscopy and dynamic mechanical spectroscopy techniques (6). A two-phase morphology was revealed. With 10% elastomer composition, the use of vigorous stirring during the early stages of the reaction resulted in materials that had cross-linked polystyrene in the continuous phase and elastomer domains as the dispersed phase. The elastomer domains contained a polystyrene cellular structure. Materials that had 40% elastomer showed a continuous castor oil

elastomer phase and the polystyrene displayed a bimodal size cellular structure. A 40:60 castor oil polyurethane:polystyrene sequential IPN exhibited greater dual network continuity and smaller, less well-defined phases than the simultaneous IPN counterpart.

The higher formation rate of the elastomer network relative to the plastic network could lead to a morphology where the elastomer is the continuous phase. The bimodal distribution of domain sizes in these systems suggests that phase separation occurs at several different stages.

Dynamic mechanical spectroscopy studies showed two well-defined glass-transition temperatures near respective homopolymer glass transitions, but shifted inward to greater or lesser extent. This shift indicates some molecular mixing between the two polymers.

Devia et al. (7) also investigated the stress–strain and impact loading behavior of the simultaneous IPNs. These materials proved to be tougher than their corresponding homopolymer networks. The castor oil polyester elastomer-toughened plastics yielded the greatest improvement in impact resistance.

In a succeeding paper, these authors (8) also indicated that the toughness of the simultaneous IPNs increased with decreasing domain size of the polystyrene dispersed phase. The use of a prepolymer for elastomer network synthesis promoted the formation of larger polystyrene domains. The impact resistance of the simultaneous IPNs increased with total elastomer content. Properly cross-linked and post-cured compositions developed impact energy of $\sim 60\text{--}70$ J/m. The simultaneous IPNs based on castor-oil-derived elastomers and cross-linked polystyrene formed engineering materials that compared satisfactorily to commercial polymers in terms of mechanical behavior.

Jordhamo et al. (9) studied phase continuity and inversion in the simultaneous IPNs of castor-oil-based polyester–polyurethane elastomers and divinylbenzene cross-linked polystyrene by optical microscopy. The simultaneous IPNs were prepared by adding a proper amount of the oil prepolymer and styrene to the reactor and then adding TDI to react with the remaining OH groups. Early in the reaction all the components formed a clear solution, but at a critical concentration, phase separation occurred. Eventually, the polystyrene phase reached a critical volume fraction and phase inversion occurred when polystyrene became the continuous phase. The phase inversion process was bordered on one side by phase separation and on the other by polystyrene gelation.

Xie and Tan (10) synthesized simultaneous IPNs at room temperature from castor oil polyurethane and copolymers of vinyl monomers (including styrene, methyl methacrylate, and acrylonitrile) using redox initiator without cross-linking agent. These studies differed from the former studies by Devia et al. (5), where the authors used benzoyl peroxide as an initiator, higher polymerization temperature, and divinylbenzene as a cross-linking agent. Xie and Tan showed that benzoyl peroxide–dimethylaniline acted as a better

redox initiator at room temperature than cyclohexanone peroxide-cobalt naphthenate. The simultaneous IPNs exhibited high tensile strength, good resilience, high abrasion resistance, and good chemical resistance to hydrolysis, acid, base, and oil.

Kumar et al. (11) prepared several simultaneous IPNs of castor-oil-based polyurethane and divinylbenzene-styrene copolymer under conditions where the free radical polymerization of styrene and divinylbenzene and the cross-linking reaction of castor oil and TDI progressed at comparable rates. Comparison of the mechanical properties and cross-link density of the IPN and individual networks indicated a marginal increase in tensile strength and cross-link density from polyurethane to 60:40 polyurethane:polystyrene IPN. IPN samples prepared with higher polystyrene content showed a steady decrease in the foregoing properties. This reversal of the expected trend was attributed to the possibility of greater molecular interpenetration achieved due to similar gelation times and the resultant extension of chains and increase in free volume between cross-links. This hypothesis was further confirmed by thermogravimetric data on the initial stage of decomposition of the IPN.

Patel and co-workers (12) investigated simultaneous IPNs prepared from radical copolymerization of liquid prepolyesters that were obtained from castor oil and dibasic acids, such as oxalic acid, malonic acid, and succinic acid, with acrylamide initiated with benzoyl peroxide. When the polyester content was greater than 45 wt%, IPN formation was impossible due to the fact that acrylamide exclusively homopolymerized. Differential scanning calorimetry (DSC) results showed that the IPNs had two glass-transition temperatures and thermograms revealed that the IPN was more stable than the individual components. The IPN was insoluble in acetone, dimethylformamide, dimethylsulfone, and dimethylacetamide.

Patel and Suthar (13) also reported simultaneous IPNs from castor oil polyurethane and cross-linked poly(methyl methacrylate). Isocyanate terminated prepolymers obtained from castor oil and TDI with NCO-OH ratios of 1.6:2.0 were reacted with a mixture of methyl methacrylate, 1% ethylene glycol dimethacrylate, and 0.5% benzoyl peroxide at 60 °C for 24 h and then at 120 °C for 4 h to form the IPNs. The results indicated that, due to experimental difficulties, IPNs with more than 45 wt% prepolymer are not possible. The thermal study revealed that the IPNs were stable up to 300 °C and then started losing weight. An increased chance for physical interaction was postulated to occur between networks containing urethane groups in the polyurethane and the ester groups of poly(methyl methacrylate).

Recently Patel and Suthar published a series of papers concerning the synthesis of sequential IPNs composed of castor-oil-based polyurethane and various polyacrylates. The polyurethane was first prepared from castor oil and methyl diisocyanate, hydroxymethyl diisocyanate TDI, or isophorone diisocyanate with a varying NCO-OH ratio and then swollen in methyl methacry-

late (14), methyl acrylate (15), butyl acrylate (16), or ethyl acrylate (17) that contained ethylene glycol dimethacrylate as cross-linking agent. The mixtures were subsequently polymerized by radical polymerization initiated with benzoyl peroxide to give IPN films via the transfer molding technique. These IPNs were characterized by chemical resistance, mechanical properties, and thermal behavior. The morphology was shown by scanning electron microscopy (SEM) and dielectric properties were measured at different temperatures.

Liu et al. (18) synthesized simultaneous IPNs and AB-cross-linked polymers based on castor oil polyurethane and poly(butyl methacrylate–divinylbenzene). Studies of the dynamic mechanical properties showed that the IPN exhibited a broader loss tangent ($\tan \delta$) peak with two glass-transition relaxations than did the AB-cross-linked polymer, which showed only a single glass-transition relaxation.

Natchimuthu and co-workers (19) reported that semi-IPNs (SIPNs) made by castor oil polyurethane and cellulose nitrate showed some degree of miscibility at 30% cellulose nitrate content. Enhanced miscibility was observed by partial replacement of cellulose nitrate with vinyl chloride–vinyl acetate copolymer. The ternary IPNs of cellulose nitrate, vinyl chloride–vinyl acetate copolymer, and polyurethane based on castor oil showed increased tensile strength and decreased flammability as compared to polyurethane–cellulose nitrate IPNs alone.

Xie et al. (20) studied the formation kinetics of simultaneous interpenetrating polymer networks obtained from castor oil, TDI, and vinyl or acrylic monomer without cross-linking agent at room temperature using redox initiator. Each component of the redox initiator, either benzoyl peroxide or dimethyl aniline, can accelerate formation of the polyurethane network. Castor oil not only reacted with toluene diisocyanate in the formation of the polyurethane network, but also took part in the formation of vinyl copolymer grafts via unsaturation. Heat evolved during the formation of the polyurethane favored the copolymerization of vinyl monomers with castor oil. The final IPN did not dissolve in any solvent, which indicates that the IPN was a grafted SIPN. Had the vinyl monomer not taken part in the formation of grafts with the double bonds of castor oil in the polyurethane network, a SIPN would have been obtained and the resultant vinyl polymer chains would dissolve in solvent. Dynamic mechanical studies of the grafted SIPNs showed two glass-transition temperatures for the IPN that contained polystyrene or poly(methyl methacrylate), but only one glass-transition temperature for the IPN that contained polyacrylonitrile. This observation indicates more molecular mixing in the polyacrylonitrile IPN. The grafted SIPN with vinyl or acrylic terpolymer exhibited two glass-transition temperatures. The second or higher glass-transition temperature was lowered when more acrylonitrile and less styrene were present in the IPN. This result again indicates more interpenetration.

The room temperature cured castor oil polyurethane–acrylic or vinyl polymer grafted SIPNs exhibited good properties, including high strength, good resilience, anticorrosion, oil and solvent resistance, and high abrasion resistance (10, 20). These features make them candidates for room temperature cured coating materials or adhesives on iron or steel without rust removal and also for reinforced rubber, toughened plastics, or damping materials cast at room temperature. Further study of these grafted SIPNs is warranted.

The present work compares the formation rates of polyurethane network and poly(methyl methacrylate) grafts via infrared spectrophotometry (IR), the relationship between gel point and gel content of IPNs with different compositions, and the mechanical properties and dynamic mechanical properties of the IPNs as well as the morphology generated under different conditions. These comparisons will further our understanding of the reaction kinetics of the parallel reactions and the gelation during grafted IPN formation as well as the specific morphologies of the grafted IPNs. This knowledge will allow us to improve the mechanical properties and damping properties of the grafted IPNs by variation of the compositional components.

Experimental Details

Materials. Chemically pure castor oil was dried by azeotropic distillation with chemically pure toluene. Dimethylaniline (DMA), dibutyltin dilaurate (DBTDL) and all the monomers were chemically pure and used as received. Benzoyl peroxide (BPO) was dried in a vacuum desiccator. 2,4-Toluene diisocyanate (TDI) was analytical grade.

Synthesis of Simultaneous IPN. Synthesis was carried out as follows: Castor oil was first reacted with TDI at a molar ratio of NCO:OH = 2.2 at room temperature while stirring for 1 h. The resultant prepolymer was mixed with vinyl or acrylic monomer, castor oil, DBTDL (as catalyst), and BPO and DMA (as redox initiators) for 10 min, then poured into a mold and cured at room temperature for 24 h.

Comparison of Formation Rates of Polyurethane Network and Poly(methyl methacrylate) Graft. The formation rates of polyurethane (PU) network and poly(methyl methacrylate) (PMMA) graft were compared by coating a mixture of the prepolymer, castor oil, methyl methacrylate (MMA), BPO, DMA, and DBTDL with molar ratio of NCO:OH = 1 and weight ratio of PU:PMMA = 60:40 onto KBr disks and measuring with an IR spectrophotometer (PE-580B) in the range of 400–4000 cm^{-1} at time intervals.

Gelation. The time of gelation was determined by observation of the fluidity of a reaction mixture of the prepolymer, castor oil, methyl acrylate (MA) or styrene (ST), BPO, DMA, and DBTDL in a dried capped bottle at room temperature. The fluidity of the reaction mixture was lost when it reached the gel point. The time interval from mixing of the components to the gel point was

recorded as the gelation time. The gel content was determined by weighing the dried insoluble residue of the sample that was removed from the reaction mixture and placed into toluene for 48 h.

Testing and Characterization. The mechanical properties of IPN specimens that had been cured at room temperature for 72 h were measured on a tensile tester (XQ-250) with a stretching rate of 250 mm/min. Dynamic mechanical spectra were measured on viscoelastometer apparatus (Rheovibron model DDV-III-EA) with a heating rate of 3 °C/min at 35 Hz in the temperature range of -50 to +150 °C. Transmission electron micrographs of the IPNs were taken with a transmission electron microscope (Phillips 300). The IPN sample was first stained with OsO₄ vapor and cut with a microtome.

Results and Discussion

Comparison of the Formation Rates of Castor Oil Polyurethane and Poly(methyl methacrylate). The spectra in Figure 1 show the change of IR absorption for the IPN-forming reaction mixture at different time intervals. An absorption peak at 2278 cm⁻¹ represents the NCO group, whereas an absorption peak at 965 cm⁻¹ represents the double bonds

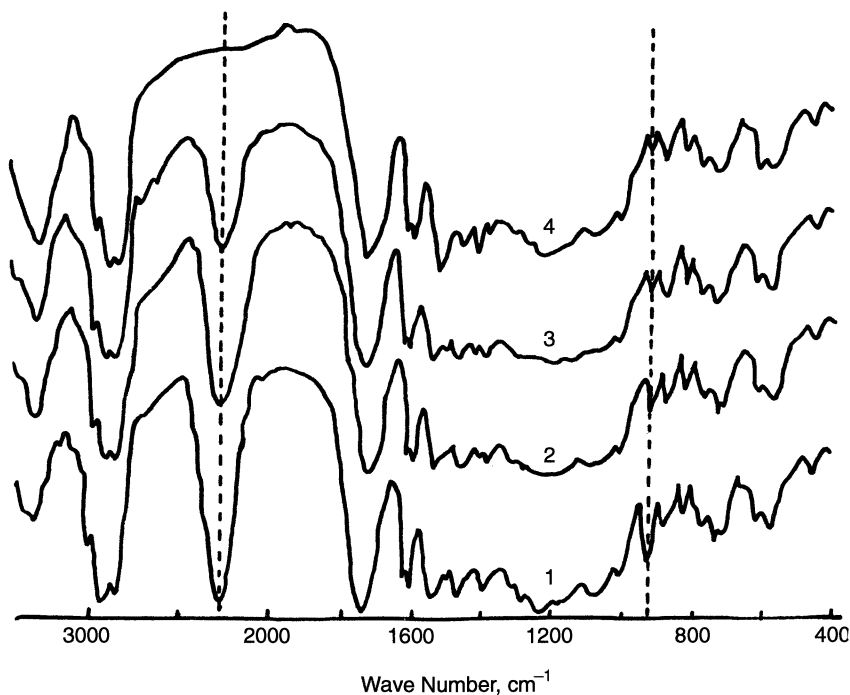


Figure 1. Change of IR spectrum of the reaction mixture during synthesis of the grafted semi-IPN. Reaction times for curves 1, 2, 3, and 4 are 2, 10, 20, and 45 min, respectively.

in MMA. The spectra in Figure 1 reveal that the rate of disappearance of the NCO peak at 2278 cm^{-1} is higher than the rate of the double bond peak at 965 cm^{-1} . This observation indicates that the formation rate of the polyurethane network is higher than the formation rate of the PMMA graft. This difference is the result of an induction period of the free radical polymerization of MMA, which was then accelerated by the heat of formation of the castor oil polyurethane network (20).

Because the final product contained over 95% gel content, MMA was not merely homopolymerized, but copolymerized with the double bonds of castor oil to form grafts. Because castor oil reacted with TDI to form the PU network, the grafts do not dissolve in toluene and remain in gel form.

Gel Point and Gel Content. The time of gelation changed in relation to monomer content in the IPN formation (Figure 2). Increased gelation time corresponded to increased styrene content especially above 60% styrene content. This relationship also demonstrates that the formation

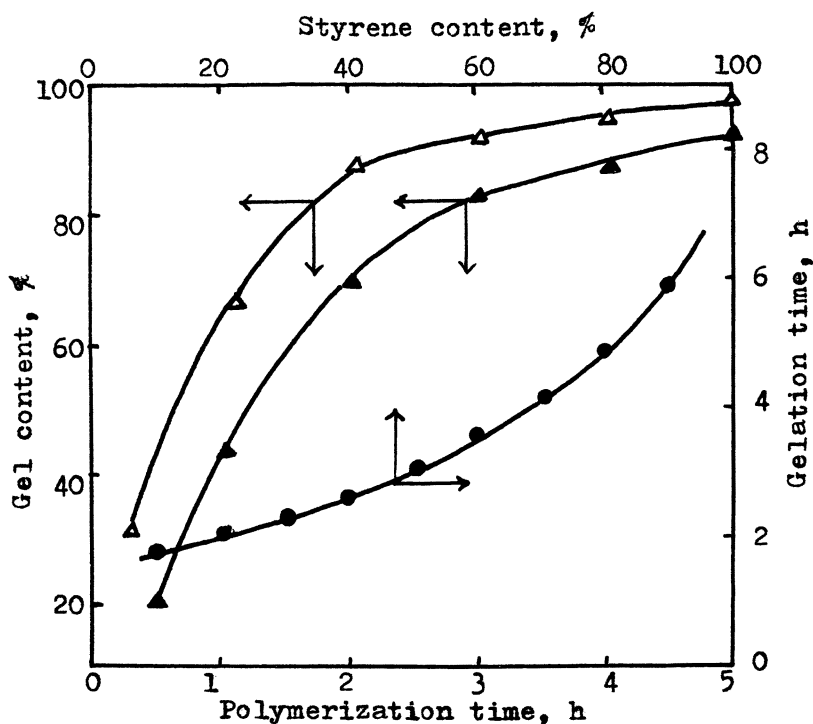


Figure 2. Gelation time vs. vinyl content in the reaction mixture (●) and gel content vs. reaction time for synthesis of IPNs: PU:PS = 60:40 (▲) and PU:PMA = 60:40 (△).

rate of the polyurethane network is higher than the rate of free radical polymerization of styrene. The rate of gel formation is higher in the PU-PMA IPN than in the PU-polystyrene (PS) IPN (Figure 2). This difference is probably due to the greater steric hindrance of styrene compared with MA.

The gel content at the gel point (P_c) for different grafted IPNs with different NCO-OH ratios was compared with the predicted value from the Carother equation (21):

$$P_c = 0.5 + (rf_0)^{-1} \quad (1)$$

or the Flory-Stockmayer equation (21):

$$P_c = [r(f_0 - 1)]^{-1/2} \quad (2)$$

where f_0 is the hydroxyl functionality of the castor oil (equal to 2.7) and r is the NCO-OH ratio.

Table I indicates that the experimental value of P_c for PU-PS IPNs agrees better with the value predicted from the Flory-Stockmayer equation than with the Carothers equation. This preferential agreement is probably because the Flory-Stockmayer equation is based on a statistical approach, whereas the Carothers equation assumes that gelation takes place when the number average molecular weight approaches infinity. The experimental value for PU-PMA IPNs lies between the values predicted by the two equations.

Effect of Different Compositions on the Tensile Strength of IPNs. Figure 3 shows that both monomer and polyurethane content affect the tensile strength of the IPNs. All the IPN samples were prepared at a NCO:OH = 1.5 molar ratio. Most of the IPNs exhibit a maximum tensile strength with PU content of about 50% that may be attributed to the maximum interpenetrating degree and enhanced compatibility at equal weights of polyurethane and acrylic or vinyl polymer, which results in a synergistic effect. For PU-poly(vinyl acetate) (PVAc) IPNs the maximum tensile strength occurred at a PU content of about 35%.

Table I. Comparison of the Experimental and Predicted Values of Gel Content at Gel Point

IPN	NCO:OH	Exp.	Eq 1	Eq 2
PU-PMA	1.1	0.780	0.837	0.731
PU-PMA	1.0	0.805	0.870	0.767
PU-PS	1.1	0.740	0.837	0.731
PU-PS	1.0	0.760	0.870	0.767

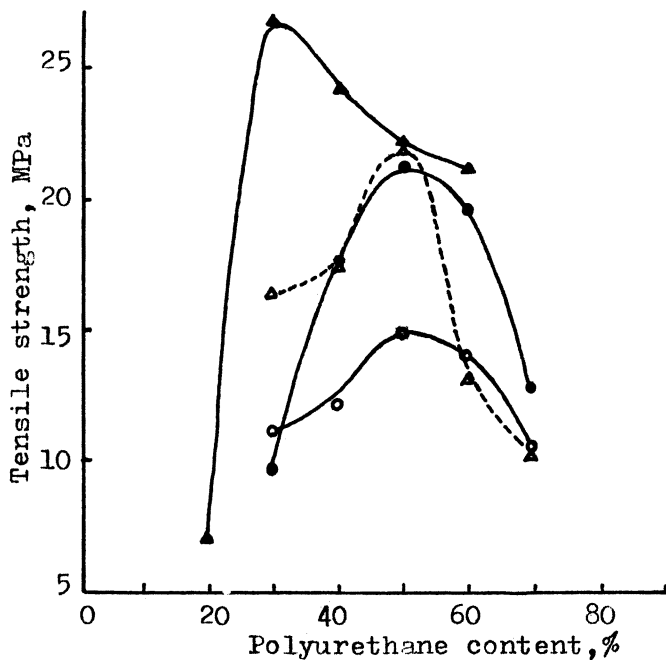


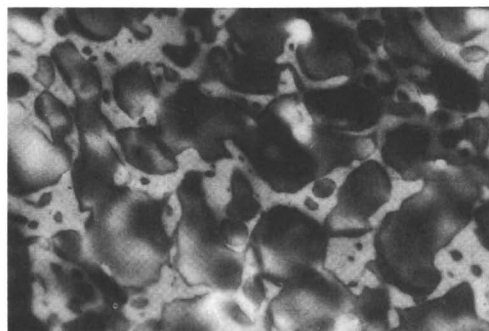
Figure 3. Tensile strength of the IPNs with different compositions: ○, methyl acrylate; ●, butyl acrylate; ▲, vinyl acetate; △, acrylonitrile.

The maximum tensile strength of IPNs that contain different acrylic or vinyl polymers decreases in the following order:

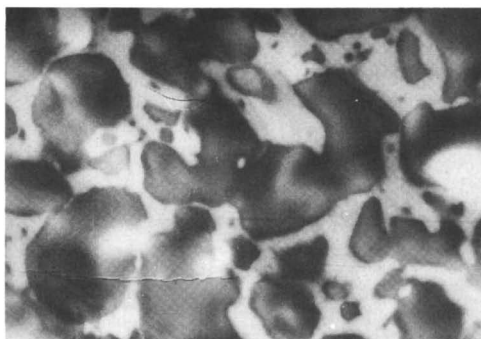
poly(vinyl acetate) > poly(acrylonitrile)

= poly(butyl acrylate) > poly(methyl acrylate)

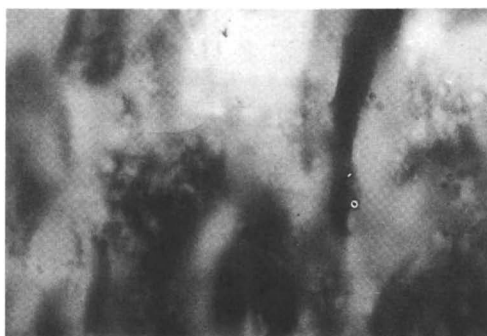
Morphology of the IPNs. Transmission electron micrographs of the PU–PMA IPN stained with OsO_4 show that castor oil polyurethane exists as dark domains (the unreacted double bonds of castor oil can be stained with OsO_4) and PMA grafts exist as a bright continuous phase (Figure 4a). This morphology can be explained by the fact that PU formed earlier and exhibited higher viscosity in the reaction mixture than PMA and, thus, tended to form domains. Preliminary reaction of the prepolymer with castor oil for 20 min and then addition of MA to the reaction mixture results in larger polyurethane domains as shown in Figure 4b. Use of methacrylic acid (MAA) as one of the monomers significantly changes the morphology; almost no domains except cocontinuous phases can be observed (Figure 4c). This change occurs because MAA can react with the NCO groups of the prepoly-



a



b



c

Figure 4. Micrographs of the PU-PMA IPN (20,000 \times): a, simultaneous reactions; b, MA added after 20 min of reaction; c, MAA added with MA at the beginning of the reaction.

mer and, thus, the PMA-PMAA graft can also cross-link with the PU network.

Dynamic Mechanical Properties of the IPNs. The dynamic mechanical spectrum of the PU-PMA IPN shows a broad glass-transition temperature, as illustrated in Figure 5, that is due to the partial compatibility between PMA and PU and the enhanced compatibility due to the interpenetrating network. Table II indicates the temperature range for $\tan \delta > 0.3$ and the maximum $\tan \delta$ in the dynamic mechanical spectra of different IPNs, all of which show a broad glass-transition temperature. In the case of the IPN that contains PMA, the temperature range above $\tan \delta = 0.3$ is only 50 °C, whereas for the IPN that contains poly(butyl acrylate-butyl methacrylate) the temperature range is wider and the maximum $\tan \delta$ higher. The inclusion of acrylic acid in the monomers in the formation of IPNs causes the tempera-

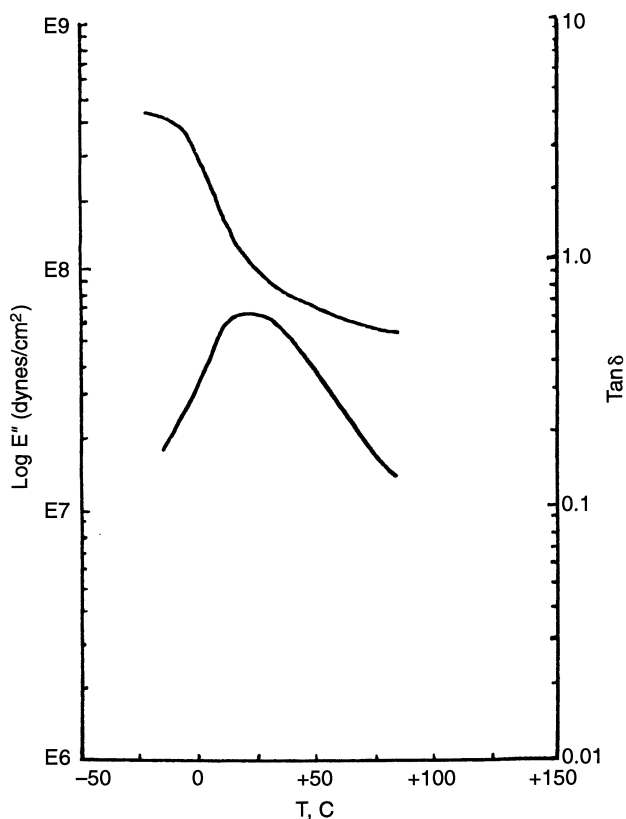


Figure 5. Dynamic mechanical spectrum of the PU-PMA IPN. (PU:PMA = 60:40 wt%).

Table II. Damping Properties of the IPNs

Composition of IPN	Temperature Range at $\tan \delta > 0.3$ ($^{\circ}\text{C}$)	ΔT ($^{\circ}\text{C}$)	Max. $\tan \delta$
PU:PMA = 60:40	- 2 to + 50	52	0.61
PU:PBA-PBMA = 60:40; BA:BMA = 1	- 10 to + 65	75	0.78
PU:PMA-PBA-PAA = 60:40; MA:BA:AA = 5.5:2	+10 to + 85	75	0.65

ture range to shift to higher temperatures. This shift may be attributed to the cross-linking reaction of acrylic acid units in the grafts with some NCO groups of the castor oil prepolymer used to form the PU network during IPN synthesis.

Conclusion

During the formation of simultaneous castor oil polyurethane-acrylic or vinyl polymer grafted IPN, IR spectrophotometry analysis showed that the formation rate of the polyurethane network was higher than the graft polymerization rate of methyl methacrylate. The time of gelation increased with increased styrene content and the higher rate of gel formation in the PU-PMA IPN compared with the PU-PS IPN agreed well with the rate predicted from the Flory-Stockmayer equation. The maximum tensile strength of the IPN occurred when the polyurethane content was about 50%. Transmission electron micrographs indicated that the polyurethane existed as domains in the continuous phase of poly(methyl acrylate). When methacrylic acid was used with methyl acrylate in the formation of IPNs, almost no domains except cocontinuous phases could be observed. The dynamic mechanical spectrum of the IPN that contained poly(butyl acrylate-butyl methacrylate) showed a broad glass-transition temperature with a temperature range above $\tan \delta = 0.30$ from -10 to $+65$ $^{\circ}\text{C}$ and with a maximum $\tan \delta$ of 0.78.

Acknowledgment

Financial support from the National Natural Science Foundation Committee of China is gratefully acknowledged.

References

1. Klempner, D. *Angew. Chem.* **1978**, *90*, 104.
2. Sperling, L. H. *Interpenetrating Polymer Networks and Related Materials*; Plenum: New York, 1981.
3. Yenwo, G. M.; Manson, J. A.; Pulido, J.; Sperling, L. H. *J. Appl. Polym. Sci.* **1977**, *21*, 1531.

4. Yenwo, G. M.; Sperling, L. H.; Pulido, J.; Manson, J. A.; Conde, A. *Polym. Eng. Sci.* **1977**, *17*, 251.
5. Devia, N.; Manson, J. A.; Sperling, L. H.; Conde, A. *Macromolecules* **1979**, *12*, 360.
6. Devia, N.; Manson, J. A.; Sperling, L. H.; Conde, A. *Polym. Eng. Sci.* **1979**, *19*, 869.
7. Devia, N.; Manson, J. A.; Sperling, L. H. *Polym. Eng. Sci.* **1979**, *19*, 878.
8. Devia, N.; Manson, J. A.; Sperling, L. H.; Conde, A. *J. Appl. Polym. Sci.* **1979**, *24*, 569.
9. Jordhamo, G. M.; Manson, J. A.; Sperling, L. H. *Polym. Mater. Sci. Eng.* **1984**, *50*, 362.
10. Xie, H. Q.; Tan, P. W. *China Synth. Rubber Industry* **1984**, *7*, 180.
11. Kumar, V. G.; Rao, M. R.; Guruprasad, T. R.; Rao, K. V. C. *J. Appl. Polym. Sci.* **1983**, *34*, 1803.
12. Patel, M.; Patel, P.; Suthar, B. *Makromol. Chem.* **1986**, *187*, 525.
13. Patel, M.; Suthar, B. *Angew. Makromol. Chem.* **1987**, *149*, 111.
14. Patel, M.; Suthar, B. *J. Polym. Sci., Polym. Chem. Ed.* **1987**, *25*, 2251.
15. Patel, M.; Suthar, B. *Eur. Polym. J.* **1987**, *23*, 399.
16. Patel, P.; Suthar, B. *Polym. Eng. Sci.* **1988**, *28*, 901.
17. Patel, P.; Suthar, B.; Patel, M. *Brit. Polym. J.* **1988**, *20*, 525.
18. Liu, J. J.; Liu, W. Z.; Zhou, U. R. *China Synth. Rubber Industry* **1989**, *12*, 395.
19. Natchimuthu, W.; Rajalingam, P.; Radhakrishnan, G.; Francis, D. J. *J. Appl. Polym. Sci.* **1990**, *41*, 3059.
20. Xie, H. Q.; Tan, P. W.; Guo, J. S. In *Advances in Interpenetrating Polymer Networks*; Klempner, D.; Frisch, K. C., Eds.; Technomic: Lancaster, PA, 1991; Vol. 3, p 187.
21. Odian, G. P. *Principles of Polymerization*; McGraw-Hill: New York, 1970; p 99.

RECEIVED for review November 11, 1991. ACCEPTED revised manuscript August 12, 1992.

Structure and Properties of AB Cross-Linked Polymers

Wenzhong Liu, Xiaozu Han*, Jingjiang Liu, and Huarong Zhou

Changchun Institute of Applied Chemistry, Academia Sinica,
Changchun, People's Republic of China 130022

Hydroxy-terminated oligomers, such as polyester, polyether, or castor oil, were reacted with toluene diisocyanate to form isocyanate-terminated prepolymers, which were then reacted with 2-hydroxyethyl acrylate to obtain vinyl-terminated prepolymer (VTP). A series of AB cross-linked polymers (ABCP) was synthesized by free radical copolymerization of these VTPs and vinyl monomers using photo- or redox initiators. The effects of the cross-link density, component ratio, network structure and defect, hydrogen bond, and monomer structure on the glass-transition temperature, relaxation, and mechanical properties of ABCPs were studied. The morphologies and dynamic mechanical properties of an ABCP and an interpenetrating polymer network (IPN) with the same composition were compared. The results showed that the degree of phase separation of the ABCP is lower than that of the IPN.

THE PHYSICAL PROPERTIES AND THE PROCESSABILITY OF POLYMERIC materials can be improved by physical or chemical combination of two or more structurally different polymers. The simplest combination method involves mechanical blending of two polymers in an extruder or roll mill. These blending techniques generally lead to polymer A–polymer B systems that are not bonded to each other. In the important cases, soluble and thermoplastic polymer materials are prepared from more than one type of monomer unit in

* Corresponding author.

which monomer units are attached in long sequences. These materials include certain types of copolymers and their blends with one or more homopolymers. Examples of the simplest and most relevant copolymer species in this category that are based on two monomers, A and B, are linear AB and ABA block copolymers and nonlinear block copolymer of A_2B . There are two different ways to prepare thermoset combinations of polymers. One case, where two different networks, A and B, are synthesized, is called an interpenetrating polymer network (IPN). In the second case, two polymers are grafted together to form one network. Polymer B is bonded to polymer A at both ends or at various points along the chains. This network is called an AB cross-linked polymer (ABCP). Thus, ideally, one network is generated for ABCP compared to two different networks ideally synthesized for IPN. In ABCPs, although polymer A is bonded primarily to polymer B, it is not cross-linked to itself. Ideal IPNs are unique blends of two cross-linked polymers that contain essentially no covalent bonds or grafts between networks (1–3). To distinguish the type of bonding in ABCPs from the case where the product remains thermoplastic, we designated it conterminous linking.

Bamford and Eastmond (4–8) described a general preparation method for ABCPs of known structure: react a preformed polymer (the A component) that has reactive halogen in side chains with a metal carbonyl in the presence of a monomer. The metal carbonyl specifically removes halogen atoms from the preformed polymer to produce radical sites on the side groups of the A chains. These macroradicals initiate polymerization of the monomer that produces growing chains of polymer B attached to the A chains. Combination termination of the propagating grafts produces B cross-links, whereas disproportionation termination generates B branches on A chains.

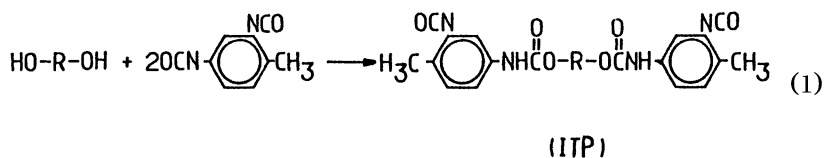
In another case of ABCP preparation, a precursor polymer A that has reactive functions, such as organometallic sites, alcohol functions, and vinyl or hydrosilane groups, at both ends is coupled with a multifunctional polymer B. A typical example of the chain-joined ABCP (random ABCP) is the graft copolymer of unsaturated ester and styrene monomer. This copolymer has been available commercially as a composite material binder for a long time. The regular ABCP is formed by the copolymerization of vinyl-terminated oligomer and vinyl monomer (9). In other publications (10, 11), we have described the syntheses, morphology, and dynamic mechanical properties of ABCPs based on polyurethanes. Although ABCPs have been investigated and reviewed during the past 20 years (5, 12), the details of the relationship between structure and properties of ABCPs are still incomplete.

We have synthesized and studied a series of ABCPs with different structures. The effects of cross-link density, component ratio, network structure and defect, main chain structure, side chain structure, and hydrogen bonding on the properties of some ABCPs are presented in this chapter.

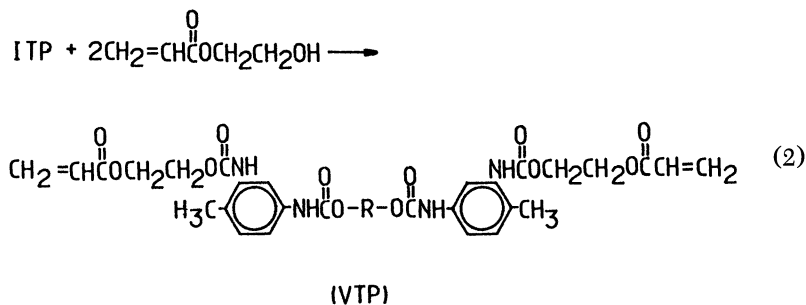
Experimental Details

Materials. The names and properties of the materials, as well as the acronyms used in the text to designate the materials, are listed in Table I. Some of the materials were purified before utilization.

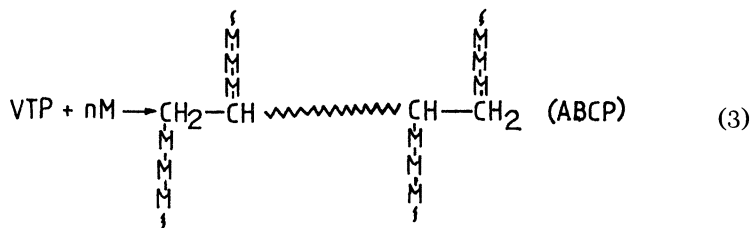
Syntheses. Isocyanate-Terminated Prepolymer (ITP). A hydroxy-terminated polymer (PEA, PPG, or CO) was heated to 100 °C while stirring in a triple-neck flask and degassed under vacuum for 1 h. After cooling to 60 °C under N₂ atmosphere for 1 h, the polymer was reacted with a calculated amount of TDI (NCO-OH = 2):



Vinyl-Terminated Prepolymer (VTP). The previously synthesized ITP was reacted with a calculated amount of HEA (OH-NCO = 1.2) using 0.1 DBTDL as a catalyst at 60 °C for 1.5 h, to yield VTP:



ABCP. VTP, M, and a proper amount of BEE were weighed into a beaker, mixed thoroughly, degassed under vacuum, and then poured into a 3-× 10-mm mold and irradiated with 400-W UV lamp for 10 min. Then the obtained samples were heated at 100 °C for 1 h:



IPN. A PEAPU-PMMA IPN was synthesized according to the following procedure: MMA, DVB, and CHP were weighed into a vessel and mixed. Then suitable amounts of PEA, THMP, and DBTDL were added and dissolved. TDI

Table I. Materials

<i>Acronym</i>	<i>Name and Properties</i>
PEA	Hydroxy-terminated polyethylene glycol adipate; molecular weight 2083 or 1345; OH value = 9.6×10^{-4} or 14.87×10^{-4} mol/g
PPG	Hydroxy-terminated polypropylene glycol; molecular weight 1295; OH value = 14.39×10^{-4} mol/g
CO	Castor oil
TDI	2,4-Toluene diisocyanate
PI	Phenyl isocyanate
HEA	2-Hydroxyethylene acrylate
DBTDL	Dibutyltin dilaurate
DVB	Divinyl benzene
THMP	1,1,1-Tris-(hydroxymethyl)-propane
BEE	Benzoin ethyl ether
CHP	Cyclohexanone peroxide
CoN	Cobalt(II) naphthenate
M	Vinyl monomer
MMA	Methyl methacrylate
PMMA	Poly(methyl methacrylate)
BMA	Butyl methacrylate
PBMA	Poly(butyl methacrylate)
AA	Acrylic acid
MA	Methyl acrylate
BA	Butyl acrylate
ST	Styrene
VAc	Vinyl acetate
AN	Acrylonitrile
MEK	Methyl ethyl ketone
PEAPU	Polymerized vinyl-terminated prepolymer of PEA
PPGPU	Polymerized vinyl-terminated prepolymer of PPG
COPU	Polymerized vinyl-terminated prepolymer of castor oil

and CoN were then added with stirring. The mixture was degassed, poured into a mold, and cured at room temperature for 24 h and at 80 °C for another 2 h.

Solvent Extraction. In some cases, ABCP samples were extracted with benzene in a Soxhlet extractor for 24 h. The extracted solution was distilled under vacuum and the residue was analyzed by IR spectroscopy.

Measurements. Dynamic Mechanical Properties. Dynamic mechanical properties (e.g., storage modulus E' , loss modulus E'' , and $\tan \delta$) were measured using a viscoelastometer (Rheovibron model DDV-II-EA) with a frequency of 3.5 Hz and a heating rate of 3 °C/min. The test specimens were cast and cut into 25- × 4- × 0.3-mm slabs. The temperature that corresponds to the peak of $\tan \delta$ was considered as the glass-transition temperature determined by dynamic mechanical method, T_{gd} . When there were two T_{gd} s, the T_{gd} at higher temperature was defined as T_{gd1} and the T_{gd} at lower temperature was defined as T_{gd2} .

Morphology. The morphology was studied on a transition electron microscope (Hitachi H-500). The sample was cut under refrigeration and stained with OsO_4 .

Mechanical Properties. Stress-strain measurements were carried out on a tensile tester (Instron 1121) at 20 °C with a crosshead speed of 500 mm/min.

Results and Discussion

Cross-Link Density. The cross-linking reactions in the syntheses of PEAPU-PMMA ABCPs take place at the ends of VTP. This linking is different from the more common unsaturated polyester ABCPs. If the preceding reactions 1-3 were all completed and reaction 3 were terminated by combination, a perfect ABCP network would be formed as shown schematically in Figure 1. One PEAPU segment and two PMMA segments can form a repeat unit. The molecular weight of the PEAPU segment, which is equal to that of VTP (M_{VTP}), can be calculated from the molecular weight of the PEA used. The ratio of weight fraction of the two components of an ABCP is expressed as r . When the r value is known, the cross-link density of an ABCP that is exhibited by the average molecular weight between cross-links (\bar{M}_c) can be calculated from the equation

$$\bar{M}_c = (1 + r) M_{\text{VTP}}/3 \quad (4)$$

\bar{M}_c was also determined by both swelling and plateau modulus methods. ABCP based on PEAPU and PMMA was swelled in MEK. The relationship

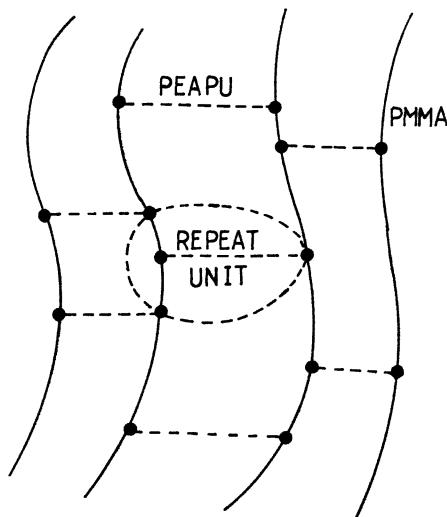


Figure 1. Schematic diagram of ABCP network.

between the equilibrium swelling and the cross-link density can be expressed by the Flory–Rehner equation (13):

$$-\ln(1 - \phi_1) - \phi_1 - X\phi_1^2 = \rho V_s / M_c (\phi^{1/3} - 2\phi_1 / f) \quad (5)$$

where ρ is the density of ABCP after extraction, V_s is the molar volume of solvent, ϕ_1 is the volume fraction of the gel in the swollen ABCP, X is the polymer–solvent interaction parameter, and f is the cross-linking functionality. The X value in eq 5 can be calculated (13) from

$$X = \beta_1 + V_s / RT (\delta_s - \delta_p)^2 \quad (6)$$

where β_1 is the lattice constant (usually $0.35 + 0.1$), R is the gas constant, T is the absolute temperature, δ_s is the solubility parameter of the solvent with a value of $19.0 \text{ J}^{1/2}/\text{mL}^{1/2}$ for MEK (14), and δ_p is the solubility parameter of the ABCP. The measured δ value of PEAPU was $21.08 \text{ J}^{1/2}/\text{mL}^{1/2}$ and the reported δ value of PMMA is $19.44 \text{ J}^{1/2}/\text{mL}^{1/2}$ (14). The δ value of the PEAPU–PMMA ABCP, which is an approximately compatible system, can be obtained according to the simple addition principle:

$$\delta_p = \delta_{\text{PEAPU}} \phi_{\text{PEAPU}} + \delta_{\text{PMMA}} \phi_{\text{PMMA}} \quad (7)$$

where ϕ is the volume fraction. The \bar{M}_c of the PEAPU–PMMA ABCPs with different component ratios, determined from eq 5 and shown in Figure 2, are lower than the values calculated from eq 4.

The shear plateau modulus (G) of an elastomer has the following relationship with cross-link density (N) and absolute temperature (15):

$$G = NRT = (\rho / \bar{M}_c) RT \quad (8)$$

Because Young's modulus (E') is $3G$,

$$E' = 3\rho RT / \bar{M}_c \quad (9)$$

where ρ is the density of the elastomer, which can be calculated from the volume expansion coefficient, β , according to

$$\rho = \rho_0 / (1 + \beta(T - T_0)) \quad (10)$$

where $T_0 = 293 \text{ K}$ and ρ_0 is the density of the sample at T_0 . Figure 3 shows the $E' - T$ dependence for PEAPU–PMMA ABCPs with differing compositions. Samples I–IV all have rubber plateaus, which indicates the existence of network structure. The plateau moduli decrease with increasing MMA content, which reduces the cross-link density. The \bar{M}_c values were calculated using eq 9 from the plateau Young's moduli at the plateaus; the temperature

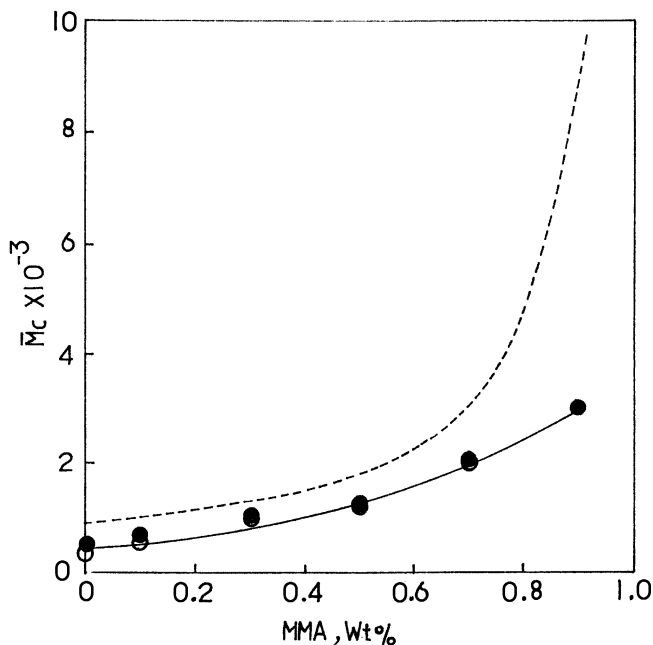


Figure 2. Relationship between \bar{M}_c and MMA content in PEAPU-PMMA ABCPs. ---, calculated from eq 4; ●, measured by the swelling method; ○, measured by the plateau method.

at the inflection point plus 10 K was taken as the reference temperature. These \bar{M}_c values are also lower than the values calculated from eq 4, but coincide with the values measured by the swelling method (see Figure 2).

For the calculation of \bar{M}_c , it was assumed that all of the VTP and MMA entered into the network; in reality, this is impossible. In the experiments about 3% MMA monomer did not polymerize and 9% MMA formed soluble polymer (sol). When the ABCP samples were swollen in solvent, unreacted monomer and sol were extracted. Thus the \bar{M}_c values measured by both the swelling method and the plateau modulus method are values of effective molecular chains. These values agree well with each other, but are lower than the calculated values.

Effects of Cross-Link Density and Component Ratio on Dynamic Mechanical Properties. The most convenient method to study the effect of the cross-link density of the PEAPU-PMMA ABCPs on the dynamic mechanical properties is to change the molecular weight of PEA. The results are shown in Figure 4. The damping peaks are at higher temperatures of 98 and 115 °C for ABCPs with PEA molecular weight of 2083 and 1345, respectively. The T_{gd2} in the lower temperature range, which

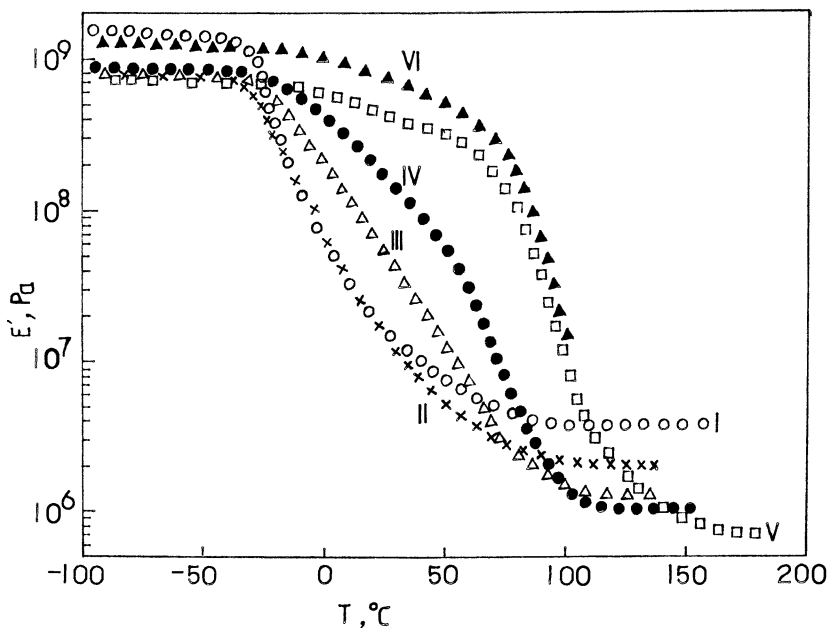


Figure 3. E' - T spectra of PEAPU-PMMA ABCPs. MMA:VTP: curve I, 0:100; curve II, 10:90; curve III, 30:70; curve IV, 50:50; curve V, 70:30; curve VI, 90:10.

corresponds to the T_{gd} of the PEAPU phase, is not obvious and is superimposed on the high-temperature peak. All the results show that the ABCPs exhibit some phase separation and significant interpenetration.

To investigate the effect of the component ratio of PEAPU and PMMA, the ABCP that is used must have the same cross-link density, which can be calculated from the equation

$$N = \rho/\bar{M}_c = 3\rho/[(1+r)(M_{PEA} + 2M_{TDI} + 2M_{HEA})] \quad (11)$$

where N is the cross-link density and M_{PEA} , M_{TDI} , and M_{HEA} are the molecular weights of PEA, TDI, and HEA, respectively. Keeping N constant, the desired molecular weights of PEA were calculated from eq 11 with differing r values. The results are listed in Table II. The PEA samples in Table II with average molecular weights of 1785 and 1486 were obtained by mixing PEA samples with molecular weights of 2083 and 1345.

From the data in Table II, the N values of the three prescribed samples (measured by the swelling method) were found to be approximately equal to each other, but the measured values were higher than desired. The reason may be that the cross-linking reaction was not completed and the gel fraction was only 84–90%.

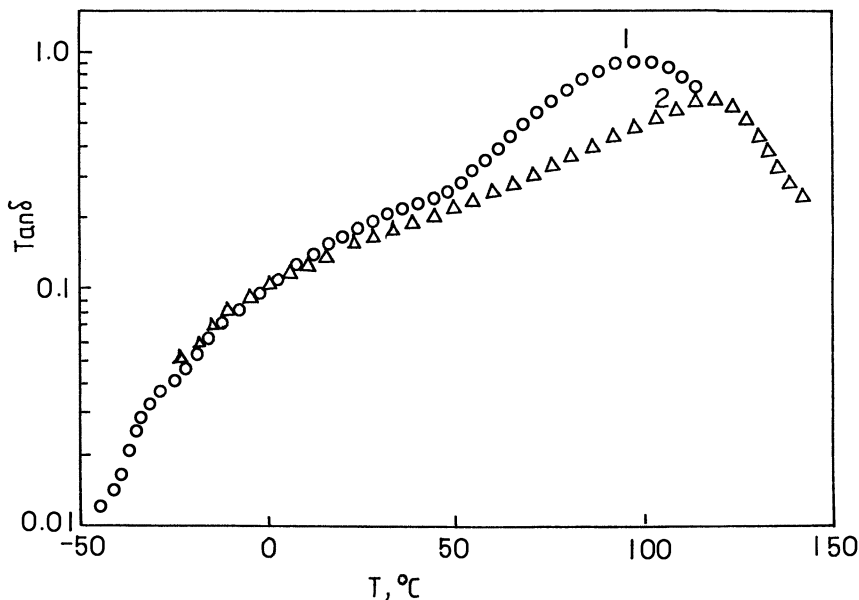


Figure 4. Effects of PEA molecular weight on dynamic mechanical properties of PEAPU-PMMA ABCPs. VTP:MMA = 50:50; M_{PEA} : curve 1, 2083; curve 2, 1345.

Table II. Some Prescribed and Measured Values of PEAPU-PMMA ABCPs

No.	Prescribed Value ^a			Measured Value	
	$N \times 10^3$ mol/mL	r	M_{PEA}	$N \times 10^3$ mol/mL	Gel Content (wt%)
1	1.25	10:90	2083	1.90	89.7
2	1.25	20:80	1785	1.74	84.1
3	1.25	30:70	1486	1.63	84.7

^a Measured by the swelling method.

The effects of MMA content on the dynamic mechanical properties and miscibility with the same cross-link density are shown in Figure 5. The T_{gd1} of the sample with 10% MMA disappears and superimposes upon the damping peak of PEAPU to form a smooth damping curve. The peak that corresponds to PMMA is more obvious when the MMA content increases to 30% and the damping peak for PEAPU forms a shoulder from the superimposition of the PMMA peak. This shoulder formation reveals that the miscibility of the two components decreases with increasing MMA content. Increasing MMA content also resulted in an increase in T_{gd} and the $\tan \delta$ maximum. A plateaulike damping peak in the wide temperature range (from -10 to $+100$ °C) is formed in curve 2 of Figure 5. This damping peak indicates extensive but incomplete mixing in the system.

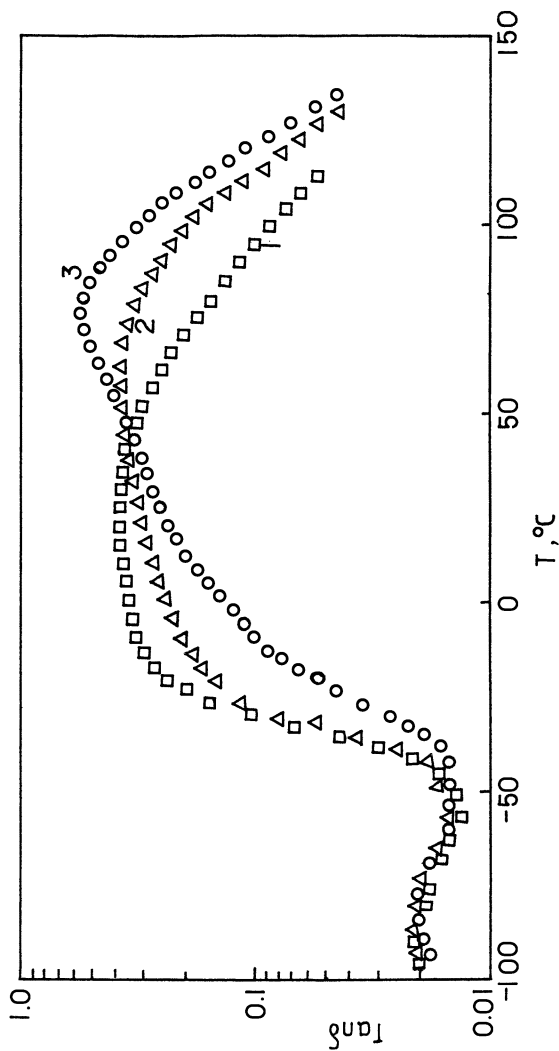


Figure 5. Effects of MMA-VTP ratio (r) on dynamic mechanical properties of PEAPU-PMMA ABCPs (similar cross-link densities). MMA:VTP: curve 1, 10:90; curve 2, 20:80; curve 3, 30:70.

Transition and Relaxation of PEAPU–PMMA ABCP. Generally, network cross-link densities change with the network components. As mentioned previously, cross-link density decreases with increasing MMA content. The increase of MMA content and decrease of cross-link density results in an increase in the $\tan \delta$ maximum as shown in Figure 6. The $\tan \delta$ maximum increased from 0.37 to 1.65 when the MMA content changed from 0 to 100%. The foregoing two factors have different effects on the T_{gd1} value. The total effect results in increased T_{gd1} with increasing MMA content, which indicates that MMA content plays the main role in increasing T_{gd1} (Figure 7).

In Figure 6, a secondary relaxation of PEAPU was found at the -100 to -70 °C range, whereas that of PMMA was at room temperature. The secondary relaxation of ABCPs with different components at lower temperature range are all due to the local movement of PEAPU segments and show that the secondary relaxation is not affected by component or cross-link density. The damping peaks of samples with 10 and 30% MMA that correspond to the T_g s of PEAPU and PMMA are superimposed on each other to form a plateau damping peak (curves 2 and 3 in Figure 6). The T_{gd} shifts inward and the half-peak width is at 96 °C. When the MMA content is increased (curves 4 and 5 in Figure 6), a damping peak that corresponds to PMMA and a shoulder at about 35 °C appear. This situation shows that the peaks of PEAPU and PMMA could not superimpose well. The secondary relaxation of PMMA appears at room temperature and affects the relaxation behavior of ABCPs. When the main glass transitions of PEAPU and PMMA are superimposed at room temperature, the secondary relaxation of PEAPU and PMMA enhances the main transition of ABCP, whereas the secondary relaxation of PMMA is manifest when the superimposition takes place at the elevated temperature.

Dynamic Mechanical Properties of ABCP and IPN. ABCP and IPN are two kinds of networks with different structures. In the PEAPU–PMMA IPN, two independent networks are formed with no chemical cross-linking between them, whereas in PEAPU–PMMA ABCP the ends of PEAPU are joined to PMMA by chemical bonds to form one network.

As previously described, cross-link density is a more important influence on the dynamic mechanical properties of the cross-linked polymers. Therefore, it is important to keep the cross-link densities constant for ABCP and IPN with the same compositions to enable a comparison of their properties. The \bar{M}_c of PEAPU–PMMA ABCP with a PEAPU–PMMA ratio of 50:50 was calculated from eq 4 to be 1895. In PEAPU–PMMA IPN with the same components, the \bar{M}_c of the two networks could be controlled to be 1895. To keep the \bar{M}_c at 1895 for the PEAPU network, with THMP as the cross-link-

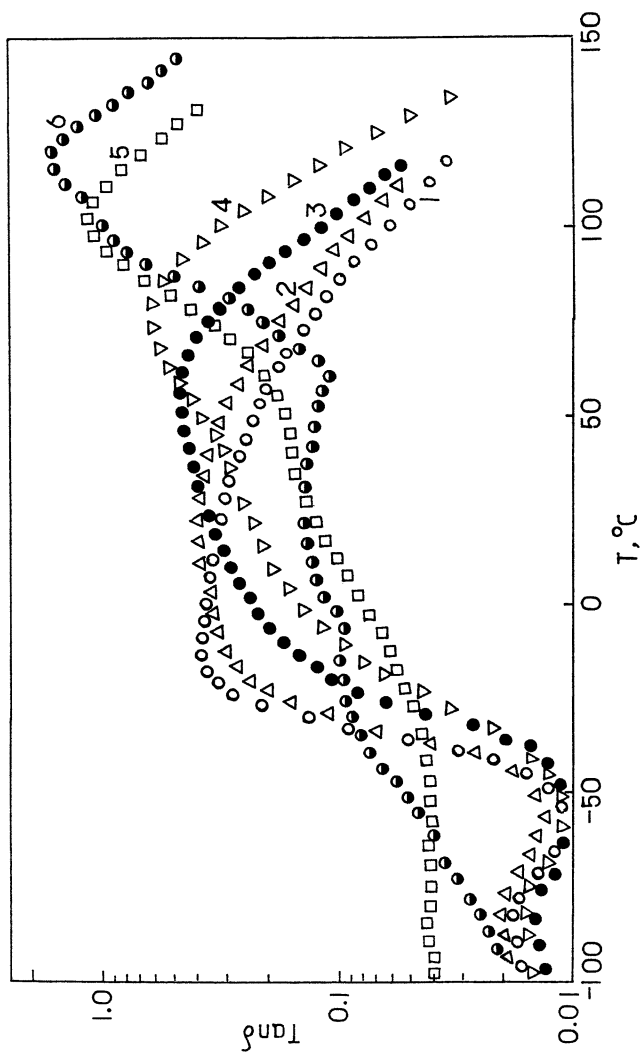


Figure 6. $\tan \delta$ - T spectra of PEAPU-PMMA ABCPs. MMA:VTP: curve 1, 0:100; curve 2, 10:90; curve 3, 30:70; curve 4, 50:50; curve 5, 70:30; curve 6, 100:0.

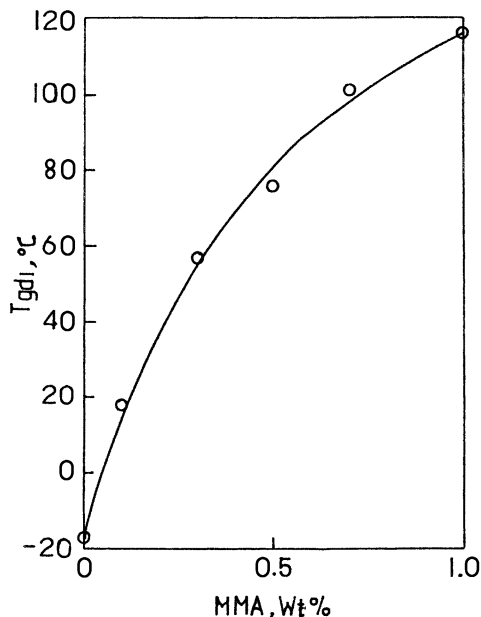


Figure 7. Relationship between T_{gd1} and the composition of PEAPU-PMMA ABCPs.

ing agent, the PEA used must have a molecular weight of 1458. Use of the proper amount of DVB as the cross-linking agent yields $\bar{M}_c = 1895$ for the PMMA network. The dynamic mechanical properties of ABCPs and IPNs with the same compositions and the same cross-link densities are shown in Figure 8. The glass-transition and relaxation behavior of ABCPs and IPNs are quite different. The IPN has two obvious T_{gd} s, which appear at temperatures that correspond to the T_g s of PEAPU and PMMA, and a plateau between them. This configuration indicates that phase separation occurred between the two networks. However, the PEAPU-PMMA ABCP shows one T_{gd} (at 95 °C) with a shoulder, which indicates a higher degree of miscibility (more homogeneous) than IPN.

The dynamic mechanical spectra in Figure 8 reveal that the Young's moduli of the IPNs are smaller than the moduli of ABCP over a wide temperature range (-100 to +70 °C), especially around T_{gd1} . Such a great difference between the Young's moduli of ABCP and IPN reveals that PEAPU is the continuous phase in the IPN, but PMMA is continuous in ABCP.

A secondary relaxation between -100 and -80 °C in ABCP, as well as in the IPN, that is due to the local movements of PEAPU segments that are unrelated to the network structure can be seen in Figure 8.

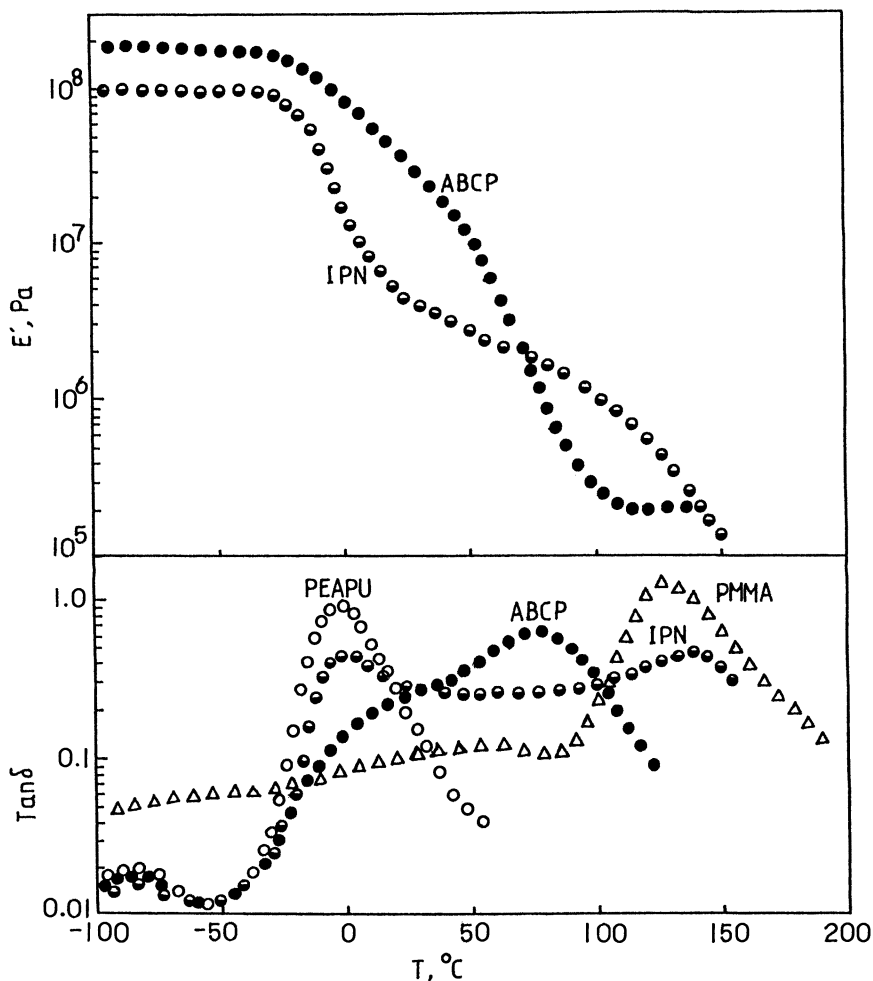


Figure 8. Comparison of dynamic mechanical spectra between ABCP and IPN of PEAPU-PMMA. MMA:VTP = 50:50; calculated $\bar{M}_c = 1895$.

Morphologies of ABCP and IPN. Transmission electron micrographs (TEM) of ABCPs and IPNs with the same composition show a two-phase nature (Figure 9). In the IPN, the PEAPU phase is continuous (dark areas) and the PMMA phase is dispersed (light areas), which is in agreement on the foregoing results. The dispersed phase appears to be spherical structures with quite different domain sizes ranging from 0.03 to 0.55 μm ; most spheres are from 0.08 to 0.15 μm . The domains do not have clear boundaries, especially the larger domains, which reveals that interpenetration may occur at the boundary. A PEAPU fine structure was found in the

matrix and across the smaller dispersed domains, which implies that interpenetration occurred not only at the boundaries, but also inside the domains.

In PEAPU–PMMA ABCP, PMMA is the continuous phase and PEAPU is the dispersed phase with irregular shapes (Figure 9B). During the formation of the ABCP network, the aggregation of PEAPU segments is impeded by the chemically bonded PMMA segments because the PEAPU is joined at the tail to PMMA. Phase separation occurs over a limited range, which results in the formation of smaller domains with sizes less than 0.01 μm . These morphologies are completely in agreement with the results of the dynamic mechanical studies.

Effects of Sol in PPGPU–PST ABCP. A viscous material was obtained from the extract phase of PPGPU–PST ABCP extraction. IR analysis showed that the sol content primarily came from PPG. The functionality of PPG used here was 1.9, so some PPG molecules, especially those with monohydroxyl groups or with no hydroxyl groups, cannot enter the cross-linked network.

The dynamic mechanical properties of ABCP samples before and after sol extraction are illustrated in Figure 10A and B, respectively. The original sample had a primary glass transition at 55 $^{\circ}\text{C}$ and another at -70 $^{\circ}\text{C}$. The existence of two T_{gd} s is evidence for phase separation. If PPGPU and PST were mixed at a molecular level in each phase, then the components of each phase could be estimated from the Fox equation (16):

$$1/T_{\text{g}} = W_1/T_{\text{g}1} + W_2/T_{\text{g}2} \quad (12)$$

where T_{g} , $T_{\text{g}1}$, and $T_{\text{g}2}$ represent the glass-transition temperatures of a certain phase of ABCP and two homopolymers, respectively, and W_1 and W_2 represent the weight fractions of the two components in this phase, respectively. The calculated results are listed in Table III. The T_{gd} at the higher temperature corresponds to the dynamic glass-transition temperature of the PPGPU–plasticized polystyrene (PST) phase, whereas the lower T_{gd} corresponds to the PST–reinforced PPGPU phase. The sample after sol extraction (Figure 10B) has a primary glass transition at 96 $^{\circ}\text{C}$ (41 $^{\circ}\text{C}$ higher than before extraction) and a shoulder at 75 $^{\circ}\text{C}$, as well as another glass transition at -12 $^{\circ}\text{C}$ (5 $^{\circ}\text{C}$ lower than before extraction). Clearly, sol extraction enhances the phase separation of PPGPU–PMMA ABCP.

Effects of Free End on the Properties of COPU–PBMA ABCP. When ABCP is prepared, some free ends in the network are formed due to such complex factors as lower functionality of the oligomer diol, chain transfer, and termination by disproportionation in reaction 3. To control the free-end content easily, castor oil (CO) was used as the polyhy-

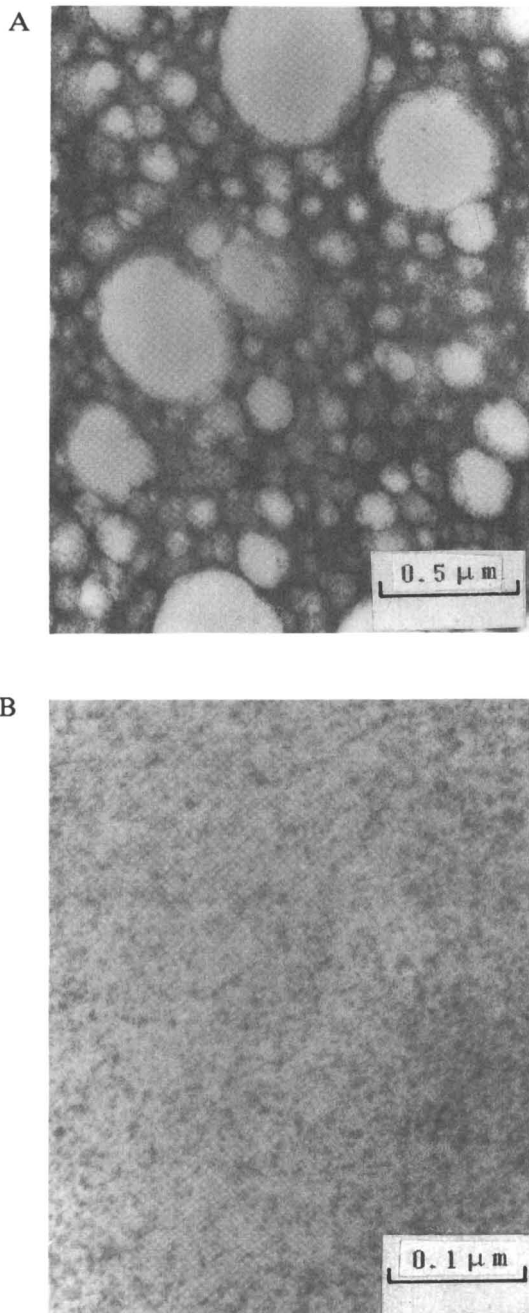


Figure 9. Transition electron micrographs of ABCP and IPN of PEAPU-PMMA.
A, IPN; B, ABCP.

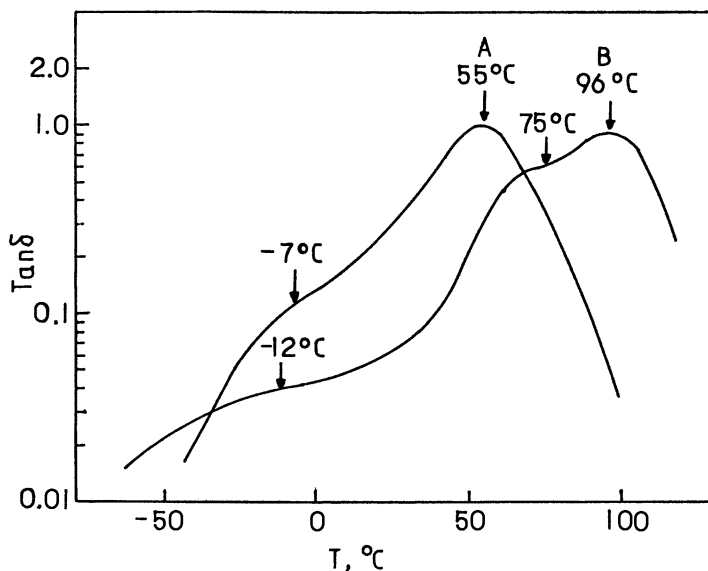


Figure 10. Effect of sol extraction on $\tan \delta$ - T spectra of PPGPU-PMMA ABCP. PPGPU:PMMA = 50:50; A, original; B, after sol extraction.

Table III. Phase Components of PPGPU-PMMA ABCP

Phase (wt%)	Spectrum A		Spectrum B	
	PPGPU at -70 °C	PST at 55 °C	PPGPU at -12 °C	PST at 96 °C
PPGPU	72.6	24.8	77.4	2.0
PST	27.4	75.2	22.6	96.0

droxyl compound to obtain COPU-PBMA ABCP. Castor oil has three hydroxyl groups, and if it reacts with the proper amount of phenyl isocyanate (PI), chains capped with PI cannot enter the network and have a free end. Then the amount of PI added will be the concentration of free ends in ABCP.

Five samples with free-end concentrations of 0, 1.5, 3.2, 5.0, and 7.2×10^{-4} mol/mL were obtained by changing the PI amounts. The effects of the free-end concentration on the stress-strain behavior of ABCPs are illustrated in Figure 11. The rubber elasticity theory states that only the effective chains cross-linked in the network respond to the stress when the network is stretched, whereas the free-end chains do not respond. Therefore, the Young's moduli are decreased and the elongations are increased with increasing concentrations of free ends in the network. Figure 11 also shows that yield points in the stress-strain curves disappear gradually with increas-

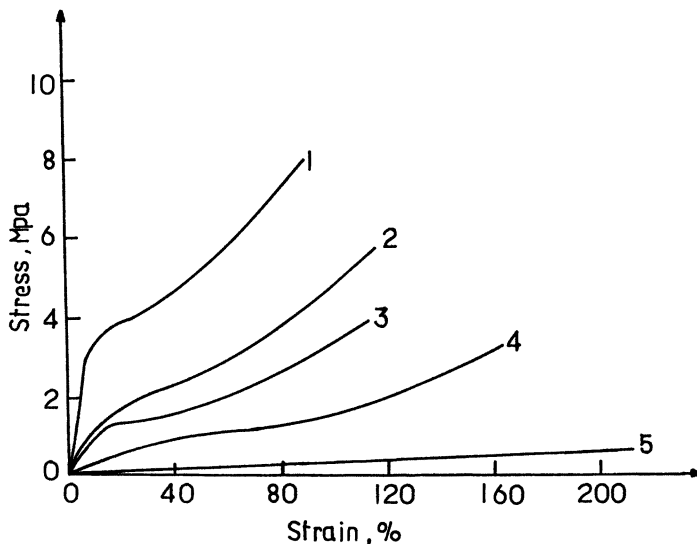


Figure 11. Effect of free ends on the stress-strain behavior of COPU-PBMA ABCPs. COPU:PBMA = 50:50. Concentration of free end (10^{-4} mol/mL): curve 1, 0; curve 2, 1.5; curve 3, 3.2; curve 4, 5.0; curve 5, 7.2.

ing concentration of free ends; the ABCP with a concentration of 7.2×10^{-4} mol/mL become a typical elastomer.

The dynamic mechanical properties of the four samples with given concentrations of free ends are shown in Figure 12. All of the COPU-PBMA ABCPs have one T_{gd} that shifts to the lower temperature region with increasing free-end concentration. The thermodynamic theory implies that COPU-PBMA ABCPs with different concentrations of free ends at their glass-transition temperatures have approximately equal free volume fractions, 0.025 (17). The free-ended chains in COPU-PBMA ABCPs have larger free volume than the effective chains in the network at the same temperature. The free volume increases with increasing temperature. Therefore, the ABCPs with higher concentrations of free ends can get the same free volume at a lower temperature, which means they have lower T_{gd} s.

In Figure 12 it is also shown that $\tan \delta$ values at any temperature below the T_{gd} s increase with increasing concentrations of free ends and the damping factors ($\tan \delta$ maximum) increase from 1.02 to 1.42 because the E' value is decreased from 11.0×10^{-6} to 4.6×10^{-6} Pa with increasing concentrations from 1.5×10^{-4} to 7.2×10^{-4} mol/mL.

Effects of Structures of Hard Segments on the Properties of ABCPs. Vinyl monomers form the hard segments of ABCPs after copolymerization with VTPs. The structure of the vinyl monomers effects the properties of the ABCPs. In the $\tan \delta$ - T spectra of ABCPs that contain

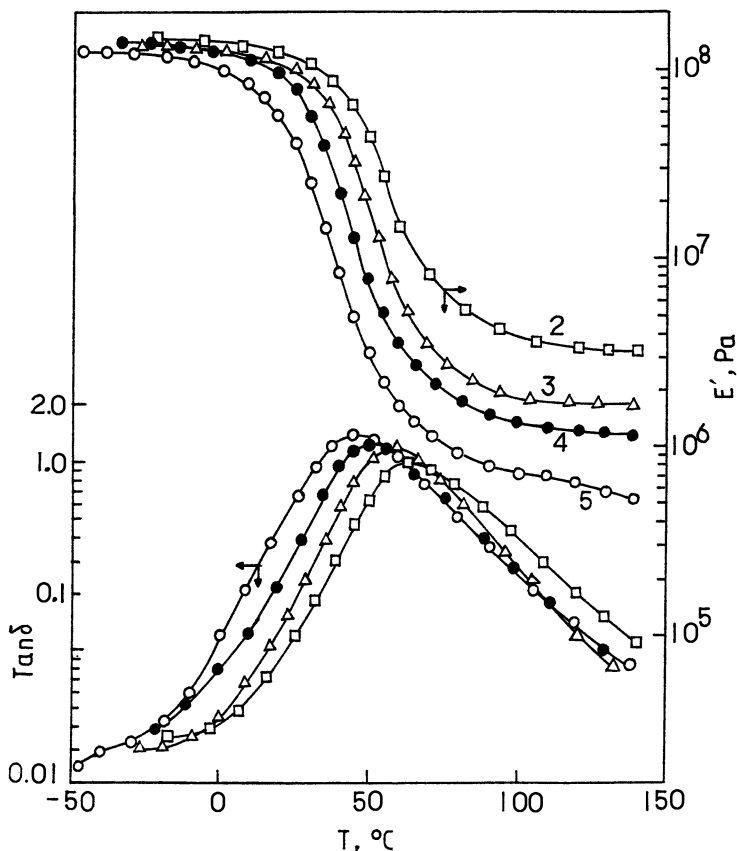


Figure 12. Effect of free ends on the dynamic mechanical properties of COPU-PBMA ABCPs. Curves 2-5 have the same concentration values as in Figure 11.

PEAPU and acrylic esters (curves 1 and 2 in Figure 13), one T_{gd} was found in each curve. However, the microscopic phase separation observed from the TEM results shows the immiscibility at the molecular level of the two components in PEAPU-poly(acrylic ester) ABCPs. The T_{gd} of PEAPU-PBA ABCP is lower than that of PEAPU-PMA ABCP because PBA has longer and more flexible side groups.

When methacrylates were used as a component in the ABCPs, for example, PEAPU-PMMA ABCP, a $\tan \delta-T$ curve quite different from the curve of PEAPU-PMA ABCP (see curves 3 and 1 in Figure 13) results because the presence of a methyl group in the monomer. PEAPU-PMMA ABCP has a higher T_{gd} and a wider damping peak range than PEAPU-PMA ABCP.

MA and VAc are isomers. In ABCPs of PPGPU-PMA and PPGPU-PVAc, PMA and PVAc show obvious differences in miscibility with PPGPU

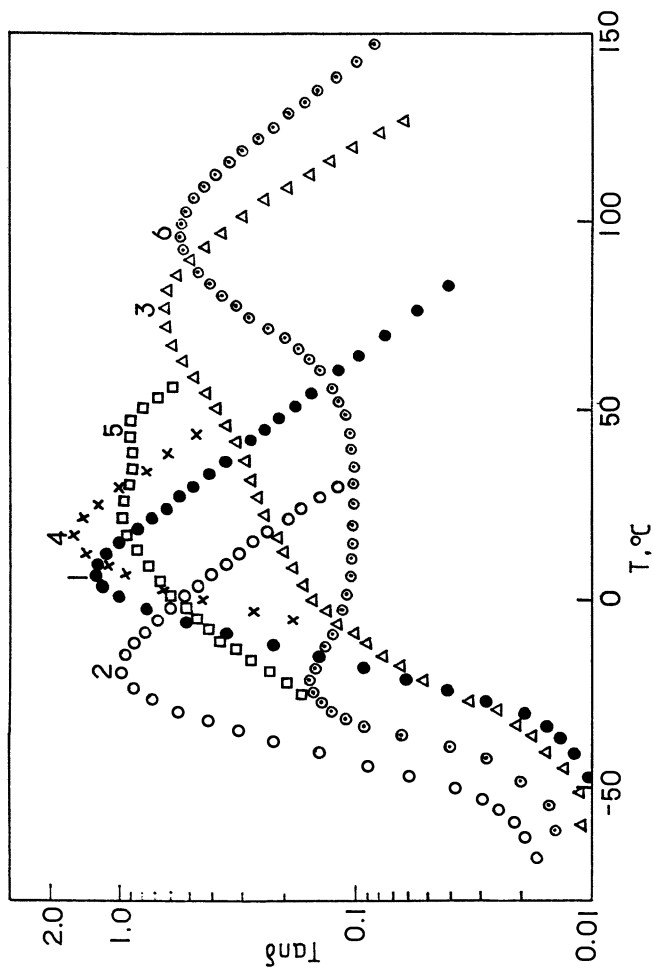


Figure 13. $\tan \delta$ - T spectra of ABCFs. VTP:vinyl monomer = 50:50. Composition: curve 1, PEAPU-PMA; curve 2, PEAPU-PBA; curve 3, PEAPU-PMMA; curve 4, PPGPU-PMA; curve 5, PPGPU-PVAc; curve 6, PEAPU-PAN.

(see curves 4 and 5 in Figure 13). A single glass transition at 28 °C is found in curve 4, whereas two T_{gd} s at 21 and 42 °C are found in curve 5 and a plateau appears in a 64 °C temperature span. The $\tan \delta$ maximum of PPGPU–PMA is much higher than the $\tan \delta$ maximum of PPGPU–PVAc. All the facts demonstrate that the sequence of the side-chain atoms can affect the mechanical damping and the miscibility seriously.

Curve 6 in Figure 13 demonstrates that ABCP obtained from PEA and AN have two independent T_{gd} s: T_{gd2} is –21 °C, which corresponds to the T_g of PEAPU (–27 °C), and T_{gd1} is 98 °C, which corresponds to the T_g of PAN (104 °C) (18). The existence of the two definite T_{gd} s shows the PEAPU–PAN ABCP is an immiscible system.

Effect of Hydrogen Bonding in PEAPU–PMMA + AA ABCP.

The chemical components and the main side-chain structures are the major factors that influence the properties of polymer materials, but the effects from secondary valence force may not be ignored in the polar polymers. The hydrogen bond is the most important representative of secondary valence force. The urethane groups in polyurethane have high cohesive energy (36.6 KJ/mol) (19) and form hydrogen bonds with each other. This important factor effects the mechanical properties of the materials (20). To study the effects of hydrogen bonding in ABCP, another vinyl monomer, acrylic acid, that has a stronger ability to form hydrogen bonds was added to the PEAPU–PMMA system. The compositions of these ABCPs are listed in Table IV and the corresponding $\tan \delta$ – T spectra are shown in Figure 14. The parameters obtained from data shown in the figure are also listed in Table IV.

No obvious change of the main glass-transition temperature (T_{gd1}) is seen in Table IV and Figure 14 when the AA content is increased gradually to 10%. This stability is because the T_g s of PAA (106 °C) and PMMA (105 °C) are approximately equal (18).

The addition of AA to PEAPU–PMMA ABCP changes the miscibility significantly. An obvious shoulder is found at 45 °C beside the main T_{gd} in the $\tan \delta$ – T curve of PEAPU–PMMA ABCP without AA (curve 1 in Figure 14). The shoulder is the result of partial superimposition of the damping curves 1a and 1b. (The dashed lines of curves 1a and 1b are drawn according to the symmetry principle.) The shoulder indicates that PEAPU–PMMA ABCP is a two-phase system. The miscibilities of PEAPU–PMMA + AA ABCPs with

Table IV. Compositions and Some Parameters of PEAPU–PMMA + AA ABCPs

No.	VTP:(MMA + AA)	T_{gd1} (°C)	T_{gd2} (°C)	$\tan \delta$ maximum
1	50:(50 + 0)	72	45	0.79
2	50:(45 + 5)	72	—	0.92
3	50:(40 + 10)	73	—	0.98

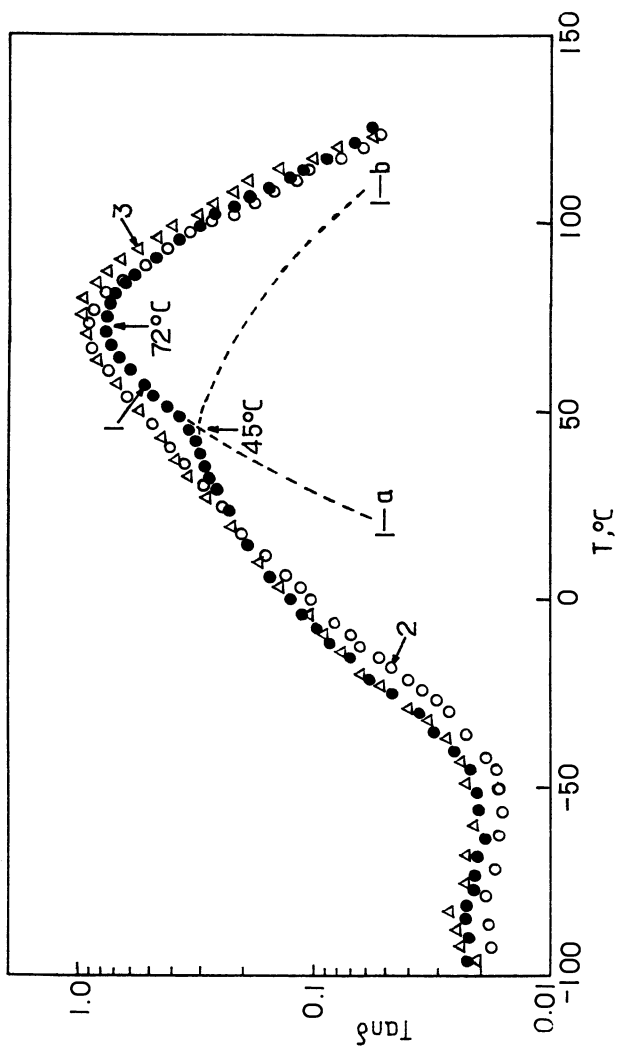


Figure 14. Effects of AA content on the dynamic mechanical properties of PEAPU-PMMA + AA ABCPs. VTP;(MMA + AA) = 50:50, AA content (%): curve 1, 0; curve 2, 5; curve 3, 10.

less than 10% AA are increased significantly and the shoulder at 45 °C disappears. The main reason for this change is the hydrogen bonds formed between soft and hard segments, $\text{—COOH} \cdots \text{O}=\text{CNH—}$, by the addition of AA monomer. Another reason may be that the solubility parameter of the hard segment is enhanced by the addition of polar monomer AA and is closer to that of the PEAPU soft segment.

Hydrogen bonds can absorb mechanical energy and can be broken by external forces; they can also regenerate with release heat energy. Therefore, the damping factor, $\tan \delta$ maximum slightly increases with the introduction of AA, which forms stronger hydrogen bonds in ABCP.

Summary

A series of ABCPs with differing compositions and cross-link densities was synthesized by copolymerization of vinyl-terminated oligomers and vinyl monomers.

The cross-link density was found to be one of the most important factors that effects the dynamic mechanical properties and the miscibility. The increase of cross-link density enhanced the T_{gd} values and decreased the $\tan \delta$ maxima of PEAPU-PMMA ABCPs. The T_{gd} can be varied in a wide temperature range by alteration of the component ratio.

A comparison of the dynamic mechanical properties and the morphologies of the PEAPU-PMMA ABCPs and IPNs with the same composition and cross-link density revealed that the degree of phase separation of ABCPs is lower than the degree of phase separation of IPNs.

The sol fraction in PPGPU-PST ABCPs improved the interphase miscibility and enhanced the $\tan \delta$ maximum. The free ends in COPU-PBMA ABCP networks also increased the damping factor.

Addition of a certain amount of AA monomer to PEAPU-PMMA ABCPs significantly increased the miscibility of the two components due to the formation of hydrogen bonds between carboxyl groups in AA and carbonyl groups in polyurethane segments.

The ABCPs studied here have a two-phase structure with very small size domains.

Acknowledgments

The authors are very grateful to Jin Guiping, Lin He, and Wang Deli for performing some experiments and preparing the manuscript.

References

1. Sperling, L. H. *Interpenetrating Polymer Networks and Related Materials*; Plenum: New York, 1981; p 1.

2. Klempner, D.; Frisch, K. C. *Polymer Alloys II: Blends, Blocks, Grafts and Interpenetrating Networks*; Plenum: New York, 1980; p 185.
3. Frisch, K. C.; Klempner, D.; Xiao, H. X.; Cassidy, E.; Frisch, H. L. *Polym. Eng. Sci.* **1985**, *25*, 12.
4. Bamford, C. H.; Eastmond, G. C. In *Recent Advances in Polymer Blends, Grafts and Blocks*; Sperling, L. H., Ed.; Plenum: New York, 1974; p 165.
5. Manson, J. A.; Sperling, L. H. *Polymer Blends and Composition*; Plenum: New York, 1976, Chapter 8.
6. Bamford, C. H.; Eastmond, G. C.; Whittle, D. *Polymer* **1969**, *10*, 771.
7. Bamford, C. H.; Eastmond, G. C.; Whittle, D. *Polymer* **1971**, *12*, 147.
8. Eastmond, G. C. *Pure Appl. Chem.* **1981**, *53*, 657.
9. Kanamori, K.; Kakeyama, K.; Kikuchi, H. *Jpn. Kokai* **1975**, *75*, 39374.
10. Liu, J.; Liu, W.; Zhou, H.; Hou, C.; Ni, S. *Polymer* **1991**, *32*, 1361.
11. Liu, J.; Ni, S.; Liu, W.; Zhou, H.; Hou, C. In *Advances in Interpenetrating Polymer Networks*; Klempner, D.; Frisch, K. C., Eds.; Technomic: Lancaster, PA, 1991; Vol. III, p 117.
12. Eastmond, G. C.; Smith, E. G. *Polymer* **1976**, *17*, 367.
13. Renwo, G. M.; Sperling, L. H.; Manson, J. A. In *Chemistry and Properties of Crosslinked Polymers*; Labana, S. S., Ed.; Academic: New York, 1977; p 261.
14. Burrell, H. In *Polymer Handbook*; Brandrup, J.; Immergut, E. H., Eds.; Wiley: New York, 1962; p 23.
15. Katz, D.; Tobolsky, A. J. *Polym. Sci. A* **1964**, *2*, 1595.
16. Fox, T. G. *Bull. Am. Phys. Soc.* **1956**, *1*, 123.
17. Aklonis, J. J.; MacKnight, W. J.; Shen, M. *Introduction to Polymer Viscoelasticity*; Wiley-Interscience: New York, 1972; p 60.
18. Nielsen, L. E. *Mechanical Properties of Polymers*; Reinhold: New York, 1962; p 23.
19. Bunn, C. W. *J. Polym. Sci.* **1956**, *16*, 323.
20. Liu, W.; Zhang, X.; Yang, X.; Chang, Q. *China Synth. Rubber Ind.* **1988**, *11*, 225.

RECEIVED for review October 9, 1991. ACCEPTED revised manuscript August 13, 1992.

Interpenetrating Polymer Networks from Castor Oil Polyurethane and Vinyl Copolymers

Peiwen Tan

Institute of Organic Chemistry, Polymer Division, University of Ghent, Krijgslaan 281, 9000 Ghent, Belgium

Interpenetrating polymer networks (IPNs) composed of castor oil polyurethane and vinyl copolymer were synthesized by the simultaneous polymerization technique. The synthesis, kinetics, and characteristics of the systems involved and the effect each has on the resulting two-phase morphology are described. The kinetic considerations indicate that castor oil not only reacts with diisocyanate in the formation of polyurethane networks, but also participates in the formation of vinyl copolymer chains. The IPN obtained is a grafted IPN. The morphology studies throughout the course of the polymerization showed that a phase inversion occurs for composition up to about 50% (w/w) castor oil elastomer content. Dynamic mechanical spectroscopy (DMS) was used to study the glass-transition behavior of IPNs. Phase separation occurs by two mechanisms: (1) multiple precipitation of vinyl copolymers at progressive levels of polymerization and (2) microsineresis processes of polyurethane networks. The thermodynamics of mixing and phase separation in polymerizing grafted IPNs is examined in some detail.

INTERPENETRATING POLYMER NETWORKS (IPNs) are a special type of polymer alloy parallel to blends, blocks, and grafts. IPNs from polyurethane and epoxy or polyurethane and methacrylate polymers have been reported by many investigators (1–12). Grafted IPNs have been reported also (8, 13, 14), but have not been studied as widely as other polymer alloys.

A clear understanding of the effect that synthetic details have on morphological features and subsequent correlation to engineering properties promises improved polyblends that are tailored to meet specific requirements.

The present energy shortage has stimulated scientific interest in renewable resources as feedstock raw materials for the chemical industries because of potential substitution for petrochemical derivatives, for example, the use of a vegetable oil based component in the synthesis of novel polyblends.

Among all the vegetable oils, castor oil stands out because it is composed of triglycerides of a hydroxy acid. Also, castor oil is one of the few naturally occurring oils that is almost a pure compound. The three hydroxyl groups, three double bonds, and three ester linkages per castor oil molecule constitute the reactive sites commonly used in the synthesis of many useful industrial derivatives.

Introduction to Phase Separation

Like most other multiphase systems, phase separation in simultaneous IPNs occurs primarily because of the small entropy gain on mixing large molecules, coupled with a positive heat of mixing. The occurrence of phase separation is controlled by the sign of the Gibbs free energy of mixing ΔG_m . For an isothermal mixing process,

$$\Delta G_m = \Delta H_m - T \Delta S_m \quad (1)$$

where ΔH_m and ΔS_m are the molar enthalpy and entropy of mixing, respectively, at the absolute temperature T . Before polymerization, the components are soluble in each other because of the high ΔS_m value. As polymerization proceeds, ΔS_m decreases and eventually ΔG_m becomes positive, which means that the system is no longer thermodynamically stable and undergoes phase separation.

In most cases of partial miscibility, the free energy composition curve changes with temperature and, thus, temperature regions of complete miscibility, partial miscibility, and complete immiscibility are formed for the same components. In the systems presented here, the extensive phase separation encountered is interpreted to mean that ΔG_m is positive for the full polymerized IPN.

The rarity of the perfect IPN lies in thermodynamics. Mixing two kinds of long polymer chains produces little change in entropy simply because the monomeric units are coupled in polymer chains and chains cannot cut through each other. The heat of mixing of two polymers is usually positive unless some specific interaction, such as hydrogen bonding, occurs between them (15). In most cases, the free energy of mixing will be positive and phase separation will occur. This occurrence is fortunate for the caused mechanical

relaxations in viscoelastic materials, because a broadened region for damping will result if the glass-transition temperatures of the components are different.

One of the advantages of IPNs in damping applications is their ability to damp sound and vibration over broad temperature ranges. This ability is a result of the development of a microheterogeneous morphology in which very small domains, on the order of from 100 to 200 Å in size, are formed. Actually, IPNs are comprised mostly of interphase material and no clearly identifiable "domains" are observed (16).

Because the smallest unit of polymer chain involved in damping motions contains 10–50 backbone atoms, these microheterogeneous domains contain only a few such units. With the statistics of small numbers, the composition of each unit of space is highly variable, and a multitude of regions that exhibit wide variations in the glass-transition temperature are produced within the same material.

Like other compositions of matter, multicomponent polymer systems have phase diagrams and free energies of mixing, with properties similar to a statistical copolymer with the same composition. A material of this type exhibits good damping over a narrow temperature range only. When the material has a positive free energy of mixing, the phase-separated region exists clearly and damping peaks that correspond to the individual phases are observed. However, if the free energy of mixing is nearly zero and much of the material exists near the phase boundary, a microheterogeneous morphology arises as a stable structure.

Another important aspect of the development of microheterogeneous morphology is the kinetics of phase separation. If polymer gelation takes place before phase separation, cross-linking will restrict phase separation. However, if phase separation precedes gelation, the domains will be large and the cross-links will stabilize the phase-separated morphology. Obviously, if the thermodynamics are favorable, phase separation will occur late in the polymerization and produce the desired morphology.

Highly phase-separated IPNs may have interpenetration only at the interface of the separate domains or have interpenetrating phases. However, to the extent that interpenetration exists, adhesion between domains must still be affected and, therefore, mechanical properties are altered as well.

The extent to which the ideal IPN is approached in these materials is highly dependent on the manner in which the mixtures are made. Unless there is some specific interaction between the unlike chains, phase separation can occur up to the point at which cross-linking fixes the final morphology of the material. Often, the result will be a combination of the phase-separated components with additional mixed phases of varying composition. A further complication arises when specific interactions lead to partial miscibility between the components.

The purpose of this chapter is to describe the synthesis and formation kinetics of grafted IPNs of polyurethane and vinyl copolymers, as well as to describe the role of processing on the morphology of IPNs. A detailed study of morphology, mechanical behavior, and general properties is included also.

Experimental Details

Materials. A description of the raw materials employed is given in Table I. The monomers styrene (S), methyl methacrylate (MMA), acrylonitrile (AN), and *n*-butyl acrylate (BA) were purified prior to use with 10-wt% NaOH aqueous solution to remove the inhibitor, washed with deionized water, dried using anhydrous calcium sulfate, and, finally, distilled under a vacuum. Castor oil was dried by azeotropic distillation with toluene and benzoyl peroxide (BPO) was dried in a vacuum desiccator. Dimethylaniline (DMA), 2,4-tolylene diisocyanate (TDI), dibutyltin dilaurate (DBTL), and epoxide resin (EP) were used as received.

Polymerization. Castor oil is reacted first with TDI at a molar ratio of NCO:OH = 2.2 at 20 °C under stirring for 1 h to form isocyanate-terminated prepolymer. The prepolymer then is mixed with vinyl monomers (S, MMA, AN, or BA) or vinyl monomers and EP, castor oil, DBTL (as a catalyst), and BPO and DMA (as initiators) for 10 min, poured into a mold, and cured at room temperature. The IPN is thus synthesized.

Table I. Description of Raw Materials and Technical Data

<i>Material</i>	<i>Source</i>	<i>Technical Data and Notes</i>
Styrene	Zhong Nan Medicine Co. or Aldrich Co.	Purity 99%; density at 20 °C, 0.909; stabilized with 4- <i>tert</i> -butylcatechol
Methyl methacrylate	Zhong Nan Medicine Co. or Aldrich Co.	Purity 99%; density at 20 °C, 0.936; stabilized with hydroquinone monomethyl ether
Acrylonitrile	Zhong Nan Medicine Co. or Aldrich Co.	Purity 99%; density at 20 °C, 0.806; stabilized with hydroquinone monomethyl ether
<i>n</i> -Butyl acrylate	Zhong Nan Medicine Co. or Aldrich Co.	Purity 99%; density at 20 °C, 0.894; stabilized with hydroquinone monomethyl ether
Castor oil	Zhong Nan Medicine Co. or Aldrich Co.	71001 DB grade; density at 20 °C, 0.957 g/cm ³ ; 925.8; hydroxyl functionality, 2.7; moisture < 0.4%
2,4-Tolylene diisocyanate	Haven Industries Inc.	Regent grade; density at 25 °C, $M_w = 174$; functionality, 2.0
Benzoyl peroxide	Aldrich Co.	Purity 97%
Dimethylaniline	Aldrich Co.	Purity 98%; density at 20 °C, 0.972; used as received
Dibutyltin dilaurate	Aldrich Co.	Purity 98%; used as received
Epoxide resin	Dow Chemical Co.	Used as received

The polyurethane formed from castor oil and TDI is called the soft network and the vinyl copolymer formed from castor oil, MMA, S, AN, and other monomers is called the hard network.

Measurement of the Formation Amount. For measurement of the formation amounts of the linear and network polymers, the sample is precipitated in ethanol and toluene, respectively. The precipitate in ethanol is the sum amount of the linear and network polymer, and the precipitate in toluene is the amount of network polymer.

Physical Measurement. The ultimate tensile strength, tear strength, E modulus, and elongation at break were measured at room temperature with a tensile tester (Hounsfield H10KM) at a start speed of 10 mm/min.

Glass-transition temperature was determined by dynamic mechanical thermal analyzer (DMTA). The measurement was carried out from -100 to 150 °C under nitrogen at a heating rate of 2 °C/min.

Results

Ultimate Mechanical Properties. The ultimate mechanical properties of IPNs as a function of variant composition are shown in Table II. The tensile strength of the sample showed significant enhancement when the amount of styrene and acrylonitrile was equal. The tensile strength of IPNs in a S-MMA-AN tercopolymer decreases in the following order of composition: $13.3:20.0:6.7 > 20.0:6.7:13.3 > 13.3:6.7:20.0$. The tensile strength would be better if the IPN system contained epoxy groups. The IPN from a Novolac epoxy resin did not contain charged groups. These IPNs without charged groups showed modulus, ultimate tensile strength, hardness, and tear strength two times higher than IPNs without epoxy resin. The Shore A hardness for a series of IPNs with 60-wt% polyurethane (PU) is also shown in Table II. Clearly, Shore A hardness increases with AN amount. Therefore, the enhancement of the mechanical strength of IPNs in a phase-separated system is a combined result of reinforcement by the glassy dispersed phase and increased physical entanglement, and adhesion at phase boundaries because of interpenetration.

Composition and Morphology. Figure 1 shows stress-strain curves for IPNs of various composition. The IPN with 60-wt% PU showed characteristics of rubber, but had a plasticlike behavior at 45-wt% PU. Obviously, the continuous phase of the system changes from rubber to plastic at 50-wt% PU. The ultimate properties are affected by what happens at the actual phase-inversion point because there the domains are fixed. The IPN at room temperature can be either glassy or rubbery depending on which phase

Table II. Ultimate Mechanical Properties of IPNs

<i>Hard Network Composition (60% PU)</i>	<i>Ultimate Tensile Strength (MPa)</i>	<i>Modulus (MPa)</i>	<i>Tear Resistance (N/M)</i>	<i>Elongation at Break (%)</i>	<i>Shore A Hardness</i>
P(S-MMA-AN)					
13.3:13.3:13.3	9	112		100	80
13.3:6.7:20.0	15	187	10,399	120	
13.3:20.0:6.7	17	196		120	76
20.0:13.3:6.7	10	141		100	
6.7:13.3:20.0	8	150		100	
20.0:6.7:13.3	14	170		100	
6.7:20.0:13.3	11	142		100	
P(S-AN) = 20:20	22	231	19,620	100	91
P(S-BA) = 20:20	7	68	9,810	130	
P(S-BA) = 10:30	3	45	5,886	130	
P(S-BA-AN)					
13.3:13.3:13.3	13	90	9,810	100	
13.3:20.0:6.7	7	78	9,123	130	
P(S-MMA-AN-EP)					
13.3:13.3:7:6.7	12	170	17,658	130	63
13.3:13.3:10:3.4	15	189	14,715	160	
13.3:13.3:3.4:10	18	180	23,152	120	67
P(S-MMA-AN-EP)					
13.3:13.3:6.4:7	13	295	17,658	110	
13.3:13.3:10:3.4	18	230	17,952	100	
13.3:13.3:3.4:10	12	198	14,225	140	

is continuous. If the phases are completely mixed, the mechanical properties are enhanced. The interpenetration of the morphology and the mechanical properties of IPNs is related to phase compatibility, component variance within the multicomponent copolymer, intermolecular forces, secondary movement of chains, and the graft of one network with the other network.

Formation Mechanism of Simultaneous IPNs. Formation of the Polyurethane Network Polymer in the Presence of Vinyl Monomers.

Castor oil reacts with excess TDI (2 mol of TDI for 1 mol castor oil) at room temperature. In 1 h, the linear polymer content is 7% and that of the network is very low. After castor oil, S, MMA, and DBTL are added, mainly network polymer is formed. If S and MMA do not take part in the formation of polyurethane, the conversion to network polymer is lower than 10% in 1 h, but can approach 40% in 10 h. The general rule for the process is as follows: The linear polymer increases with time at first, but later decreases until only 1% is left after 48 h. At this time, the formation of network polymer is nearly 100%.

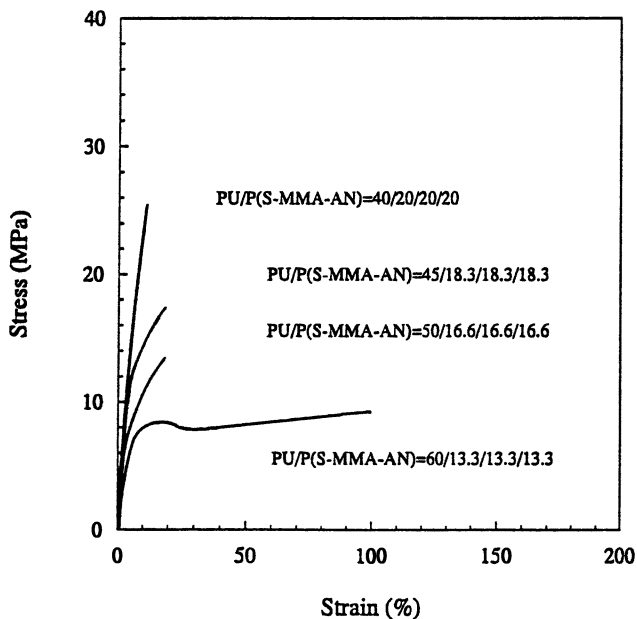


Figure 1. Stress-strain curves for PU-P(S-MMA-AN) IPNs.

Formation of the Polyurethane Network in the Presence of Individual Reagents.

The reaction of castor oil with TDI to form the soft network in the presence of DBTL is a hydrogen transfer reaction, whereas the reaction of castor oil with the vinyl copolymers to form the hard network in the presence of BPO initiator is a free radical reaction. In the present work, the possible effect of individual components was considered in the reaction of castor oil with TDI and DBTL in the presence of individual reagents. Figure 2 shows that the formation rate of polyurethane in the presence of the vinyl monomers is lower than the rate without these monomers. The formation rate with BPO or DMA is higher than the rate without BPO and DMA. Vinyl monomer, as a solution, can dilute the concentration and reaction heat and, therefore, slow down the formation rate of polyurethane. The amine may act as a catalyst and increase the formation rate of polyurethane. When BPO is added, castor oil not only reacts with TDI in the formation of the polyurethane network, but also takes part in the free radical reaction.

The Possibility That Castor Oil Takes Part in the Free Radical Polymerization.

Castor oil is difficult to polymerize at room temperature via the radical reaction in the presence of an initiator. However, it is possible for castor oil to take part in free radical polymerization at higher temperature without TDI. For example, the formation amount of a castor oil network will

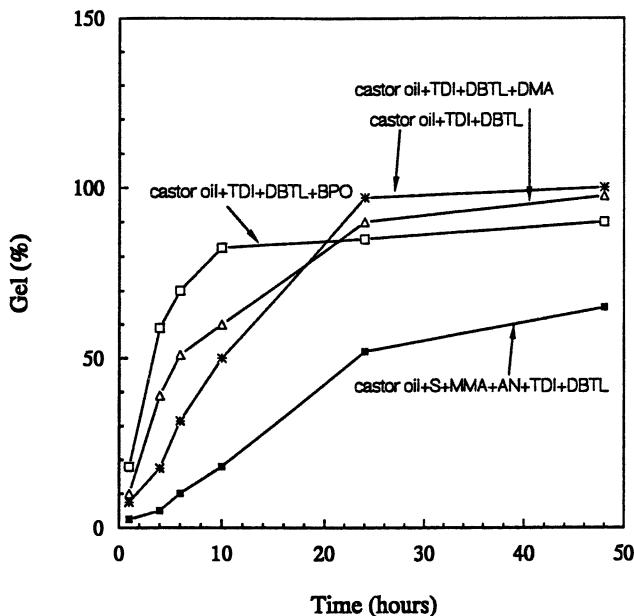


Figure 2. Formation of polyurethane in the presence of individual reagents.

approach 5% if the temperature rises to 35 °C for 48 h to 50% if the temperature is increased to 60 °C for 120 h (Figure 3).

Grafted IPN. Figure 4 shows the formation kinetic of the linear polymer and the IPN from castor oil, styrene, and methyl methacrylate. The conversion approaches 37% in 12 h, but changes remarkably in 24 h: The gel amount of the network increases because most of the linear polymer is transferred to the network. The gel amount of the network is close to 95% after 48 h. Clearly, IPNs are formed from both the polyurethane soft network and the hard network. The temperature of the system rises due to the reaction heat. Therefore, the double bond of castor oil is opened, and castor oil with S and MMA takes part in free radical polymerization to form the hard network (17). This IPN is the grafted IPN because castor oil simultaneously takes part in the formation reaction of both kinds of networks. An IPN would be semi-interpenetrating if castor oil did not take part in the formation of the hard network (see Figure 5). The hard network and the soft network mix fairly well. At this time, the phase of the soft network is predominant and its domain size is mainly controlled by the cross-link graft density that is formed because castor oil in the soft network participates in free radical polymerization. The greater the degree of graft cross-linking, the finer the domain size of the second network. Therefore, it is quite likely that the

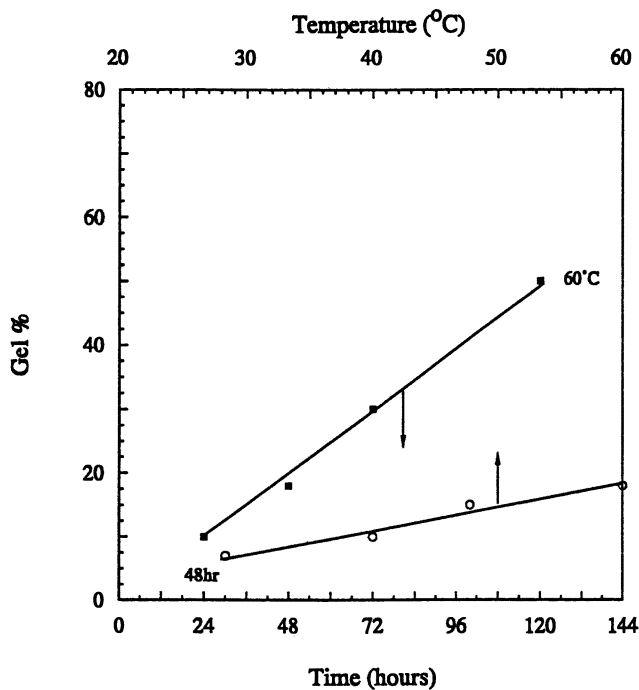


Figure 3. Influence of time and temperature on castor oil polymerization.

structure and properties of IPNs depend largely on the synthetic method rather than on the mutual immiscibility of the individual polymers.

Effect of the Catalyst. Figure 6 shows the formation rate of IPNs. The formation rate increases with DBTL content and there is a similar influence on the network. The increasing amount of DBTL favors the formation of the network, whereas the decreasing amount of DBTL increases formation of the linear polymer. For higher amounts of DBTL the linear polymer cross-links quickly with double bonds of castor oil and transforms to the network. The result is high tensile strength. However, if the amount of DBTL is too high, the tensile strength of the IPN decreases because molecular weight decreases (18).

Effect of the Temperature. Figure 7 illustrates the effect of temperature on the conversion to the network and Figure 8 shows a similar dependence for the linear polymer in the PU-P(S-MMA) IPN. The maximum conversion to the linear polymer depends on the temperature.

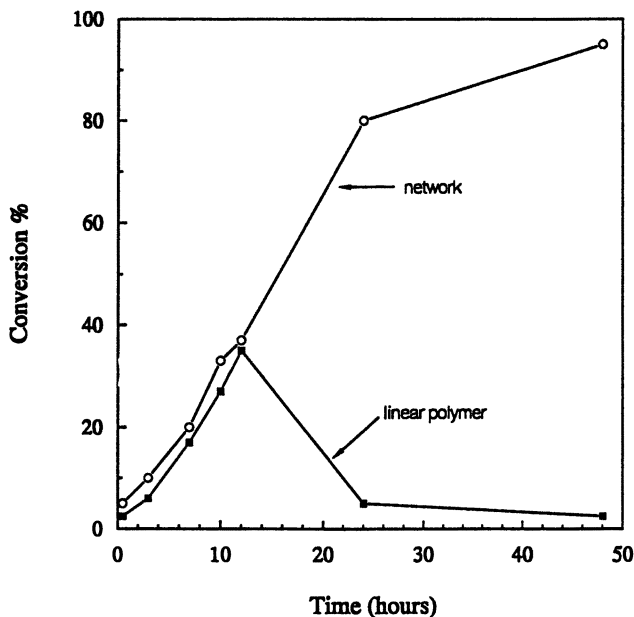


Figure 4. Conversion to PU-P(S-MMA) grafted IPN.

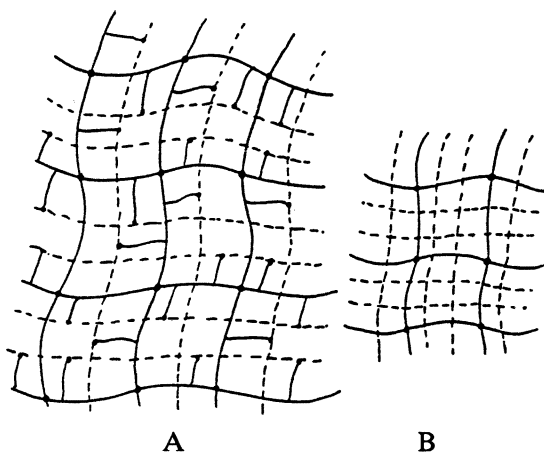


Figure 5. Grafted IPN (A) and semi-IPN (B).

Morphology Change during the Synthesis of Grafted IPNs.

The characteristic morphologies are found in PU-P(S-MMA-AN) simultaneous IPNs that contain 60% PU network during the reaction (see Table III). The sample is prepared with rapid mixing (PU prepolymer, vinyl monomers, catalyst, and initiator) and then poured into test tubes. Both networks of

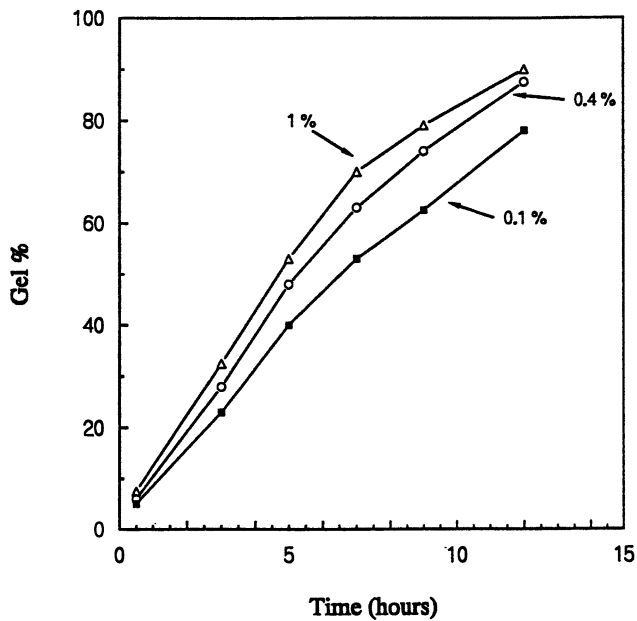


Figure 6. Influence of DBTL on the degree of conversion of IPN.

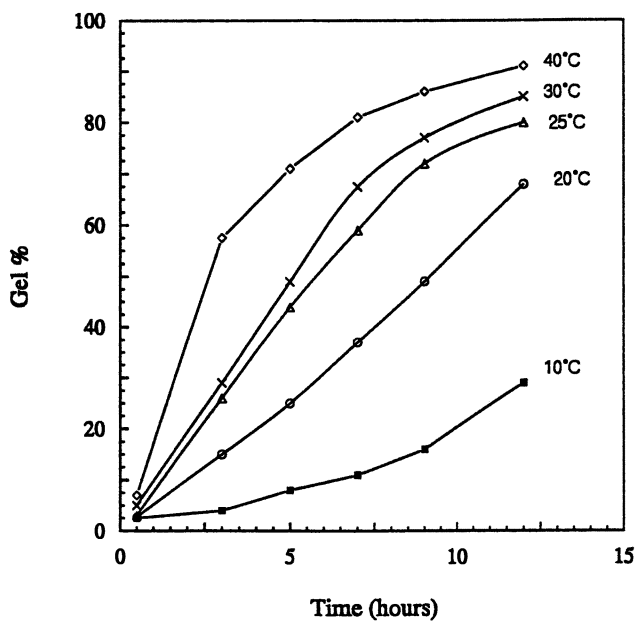


Figure 7. Influence of temperature on the gel content of the network.

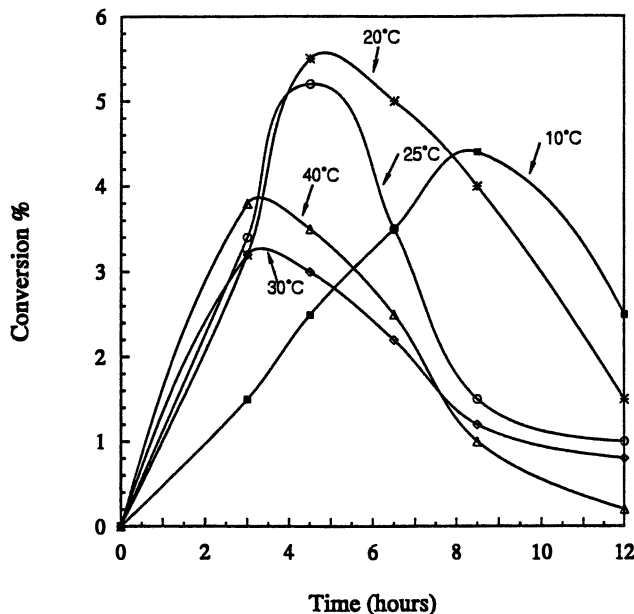


Figure 8. Influence of temperature on conversion to the linear polymer.

these IPNs are formed at the same time but not at the same rate. Phase separation of PU-P(S-MMA-AN) IPNs occurs at several different times. At first, the mixing solution is clear liquid, but it begins to cloud in the test tube after 15 min, which shows that polyurethane prepolymer starts to form gel. After 30 min, the cloudiness increases and a separated gray-brown boundary appears in 60 min. The solution is transformed to an oil-in-oil emulsion in which a poly(S-MMA-AN) solution forms the disperse phase and the elastomer forms the polyurethane component solution in the continuous phase. The point of phase separation is observed experimentally by the onset of turbidity, due to the Tyndall effect. The polyurethane gel slowly becomes macroscopically homogeneous with the precipitation of vinyl copolymer. After 70 min, the phase boundary disappears, and the reaction follows a similar path to secondary, tertiary, and possibly higher order precipitations of vinyl copolymer. Finally, when almost all the vinyl monomers are polymerized, a small molecular amount may remain dissolved in the polyurethane elastomer phase. At this time, the two networks are closely linked and interpenetrated because castor oil participates in both network-forming reactions. At the end of the reaction, the phase boundary nearly disappears. We suggest that this phenomenon depends mainly on the elastomer concentration and compatibility of the two polymers.

Table III. The Phase State of PU–P(S-MMA-AN) Grafted IPNs at Different Temperature

<i>Cure Time (min) 7 °C</i>	<i>Phase-Separated Phenomenon</i>	<i>Cure Time (min) 25 °C</i>	<i>Phase-Separated Phenomenon</i>
5–30	Clear liquid	5	Clear liquid
30–40	Begins to cloud	15	Begins to cloud
> 40	Increased cloudiness	30	Increasing cloudiness
60	Separated layer appears brown boundary	60	Separated layer is not clearly formed; light color boundary appears
90–300	Boundary changes	70	Boundary disappears
350	Phase separation disappears	70–180	Phase separation appears again
360	Phase separation appears again	200	Phase boundary appears, color is lighter than that of first.
420	Phase boundary appears, the color is lighter than that of first.	220	Phase separation disappears
> 430	Phase separation disappears	220–400	Phase separation eventually appears again
450–900	Phase separation eventually appears	420	Phase boundary appears again
1000	Phase boundary appears, the color is lighter than that of the second	540	Phase boundary disappears
1060	Phase boundary nearly disappears		

Dynamic Mechanical Analysis. The dynamic mechanical properties over a range of temperatures are shown in Figures 9 and 10 for varied IPN compositions. The PU–PAN and PU–PMMA IPNs show a significant broad transition peak and a flat modulus. The important observation here is that several samples that contain PU–PMMA at 45:55 and 35:65 have $\tan \delta$ values that are nearly temperature invariant over the range from -80 to 150 °C. Although the performance of any sound damping system is ultimately determined by its application, relative performance evaluation and ranking for materials of interest can be obtained from dynamic mechanical analysis techniques designed to provide vibration damping property information. All polymer systems exhibit a maximum value for $\tan \delta$ and, hence, maximum damping efficiency at their glass-transition temperature, T_g , whereas the homopolymer and statistical copolymers damp effectively over a narrow temperature range. Typically 20 – 30 °C IPNs constitute a class of multicomponent polymeric materials that are capable of damping over a broad

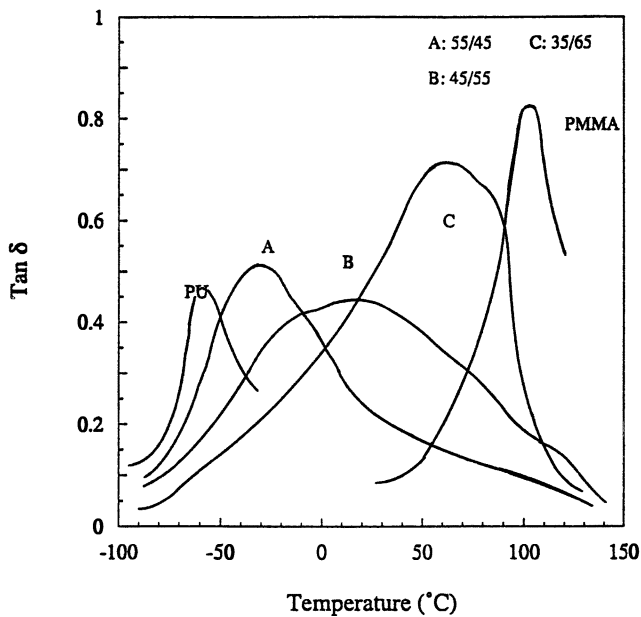


Figure 9. Temperature vs. $\tan \delta$ for PU-PMMA IPNs, PU, and PMMA.

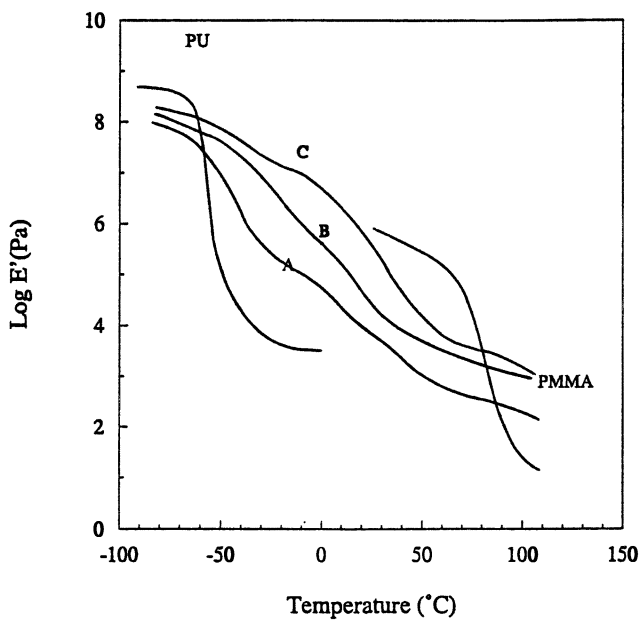


Figure 10. Temperature vs. $\log(E')$ for PU-PMMA IPNs, PU, and PMMA.

temperature range in excess of 100 °C. The results of applied experiments proved that the hard network of IPNs that contain methyl methacrylate or acrylonitrile has an excellent ability to damp sound and vibration.

Applications. Hydrolysis Resistance. Figure 11 shows the results of hydrolysis resistance. The tensile strength will increase rapidly if the synthesized IPN sample is placed in 50 °C water. The tensile strength of the original sample is 12 MPa. After the sample has been immersed in hot water for 14 days, the tensile strength and elongation are increased to 18 MPa and 150%, respectively. After 28 days, the tensile strength is increased to 25 MPa and elongation reverts to 100%. The results indicate that hot water makes IPNs stronger. These IPNs are different from polyester–polyurethane elastomers, which are not hot water resistant.

Abrasion Resistance. The IPN sample that contains PU–P(S-MMA-AN) at 60:13.3:13.3:13.3 was tested with jetting sand. The jetting velocity of sand is 64.6 m/s. In a 150- × 150-mm sample area, the abrasion rate is 8 g/h, whereas the abrasion rate is 80 g/h for polyester concrete. Abrasion resistance for the IPN sample is much better than most polymer concrete and any other material.

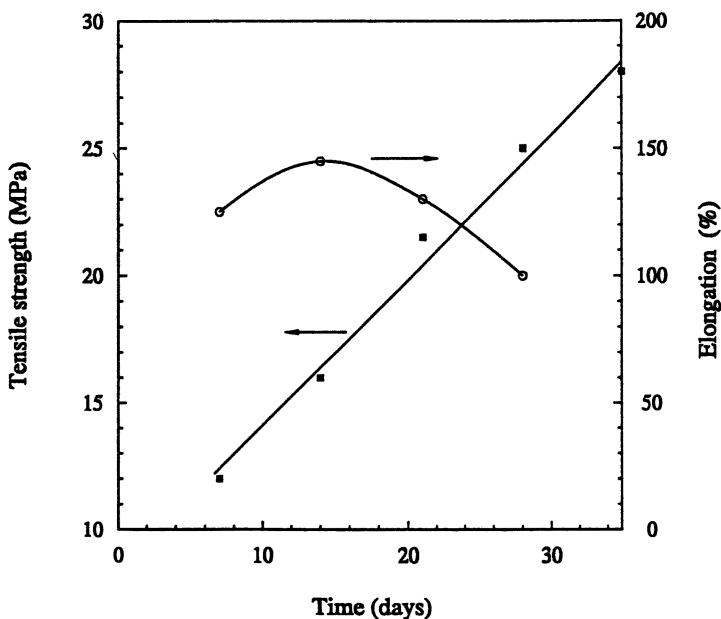


Figure 11. Influence of hot water on the mechanical properties of the IPN.

In another abrasion test, the IPN sample was not abraded at all when it contained 3% sand and the water velocity was 14 m/s. Under the same condition, the abrasion is about 27 g/h for granite, steel, and iron, 8 g/h for cast stone, 77 g/h for limestone, and 86–109 g/h for resin concrete. This IPN material has been satisfactorily applied in Ge Zhou Ba hydroelectrical power station in China (19).

Peel Strength. Table IV shows the effect of temperature on the peel strength of an IPN that was cast on a cement lump. The result indicates that the peel strength did not change in the temperature range from 10 to 30 °C in 6 months. In addition, the peel strength of the adhesion of the IPN with steel was over 30 kN/m.

Acid and Base Resistance. The resistance of these graft IPNs to acid, base, and salt at 50 °C is shown in Table V. The IPN sample that contains PU–P(S-AN) at 60:20:20 demonstrates a good resistance to acid from low to high concentration (from 3 to 50%). This will expand the applications of IPNs. In the petroleum industry and environment protection, the IPNs have far-reaching and widespread applications, and some satisfactory results have been obtained. The IPN is also corrosion resistant to microorganisms in seawater. These grafted IPNs are superior to any other material when applied to ocean-going vessels. Accelerated aging tests indicate that the coated surfaces of vessels could resist corrosion and microbe adhesion for 10 years (20). Table VI shows the resistance of IPNs to organic solvents and oils. PU–P(S-AN) is the best and PU–P(S-MMA) is the worst among the IPNs.

Table IV. The Peel Strength of Concrete IPN in Different Temperatures of Water

<i>T</i> (°C)	<i>Peel Strength</i> (<i>N/m</i>)	<i>Time</i> (<i>month</i>)
10	764	6
20	803	6
30	777	6

Table V. Resistance of IPN to Acid, Base, and Salt

<i>Component</i>	<i>2% HCl</i>	<i>2% NaOH</i>	<i>3% NaCl</i>	<i>36% HCl</i>
PU–P(S-MMA-AN) = 60:13.3:13.3:13.3	0	0	0	0
PU–P(S-MMA) = 60:16:24	0	0	0	21
PU–P(S-AN) = 60:20:20	0	0	0	0

NOTE: All values are weight loss in percent.

Table VI. Effect of Solvent on IPNs

<i>Solvent</i>	<i>PU-P(S-MMA-AN)</i> 60:13.3:20.0:6.7	<i>PU-P(S-MMA)</i> 60:16:24	<i>PU-P(S-AN)</i> 60:20:20
Toluene	95	150	33
CCl ₄	170	295	45
Acetone	85	74	17
Machine oil	0	1	0
Diesel oil	16	28	0
Gasoline	13	16	0

NOTE: All values are weight gain in percent.

Observations indicate that the hard network containing AN has an excellent resistance to solvents and oil.

Corrosion Resistance in Vacuum. The use of IPN material for vacuum corrosion resistance on turbines has been studied. The body and leaf wheel of a turbine were seriously corroded after 2–3 years because of vacuum corrosion and collisions from stone and sand. After being coated with IPN material, the turbine has worked for 5 years. This IPN material is believed to have high resilience, high impact strength, and good adhesive force on the surface of steel.

Discussion

Morphology of Phase Domain Formation. The formation mechanism of the polyurethane soft network and vinyl copolymer hard network can be understood by the morphology study of the IPNs that contain 60% polyurethane network. The present study indicates that the bimodal distribution of domain size in these systems and phase separation occur at several different times, but the final sample has complete molecular mixing or dual phase continuity. This phenomenon is similar to the one suggested by Devia et al. (21, 22). The bimodal distribution of domain size in these systems is expected to arise from phase separation originated by the combination of the following two processes:

1. Multiple precipitation of vinyl copolymer chains at different times.
2. Microsyneresis of the soft network before any vinyl monomer and castor oil take part in the free radical polymerization.

For the first process, the free energy of mixing of the system is negative and, therefore, a homogeneous solution forms as polymerization proceeds. Thus, ΔG_m increases and eventually becomes positive; then primary precipi-

tation occurs (in Table III, cloudiness observed from 35 to 60 min) and the free energy of the system drops to a negative value again. On continuous polymerization, ΔG_m follows a similar path to the second and third precipitation; finally, all vinyl monomers are polymerized.

The second process is built on the basis of the formation mechanism of the polyurethane soft network. At the first precipitation, the soft network (elastomer) at gel point swells with vinyl monomer mixture; this point represents a maximum ability to hold vinyl monomers. As the elastomer network formation proceeds, the increased cross-linking density reduces the ability of the network to hold the liquid. Vinyl monomers begin to polymerize and the molecular weight of vinyl copolymer eventually increases. The inhomogeneity of the network in regions with a substantially different cross-linking density and high viscosity of vinyl copolymer solution provides a favorable condition for IPN synthesis. The concentration of vinyl copolymer increases locally in some regions and a phase separation develops on a microscopic scope (microsyneresis). The double bonds of castor oil take part in the free radical polymerization. The graft points are formed at this moment, and the formation rate of vinyl copolymer increases in these graft pockets. The difference in size appears among vinyl copolymer domains because of the concentration effect and the different grafting.

Dynamic Mechanical Properties. While the dynamic mechanical properties of PU-PMMA, PU-PAN, and PU-P(S-MMA-AN) are under study, it is of interest to note that the broader transitions associated with the PU-PMMA and PU-PAN IPNs as compared to PU-P(S-MMA-AN) IPNs strongly suggest differences in the degree of molecular mixing for the three IPNs.

Microheterogeneous morphologies on the order of 100 Å, which were first observed by Huelck et al. (23), result in large interfacial areas, or interphase regions, with small or excluded pure phase regions. Because each region then has a slightly different composition and a correspondingly different T_g , a spectrum of glass transitions is obtained that results in the observed broadening of the glass transition (24). Similarly, for small compositional fluctuations in PU-PMMA and PU-PAN, broadening of the glass transition would also be expected.

The Simultaneity Problem of Grafted IPN. The formation kinetic considerations for each component in castor oil grafted IPNs is very useful in the design of synthetic procedures for each simultaneous IPN system, as well as in understanding the different phenomena observed during polymerization of such materials. As far as the polyurethane elastomers are concerned, it is clear that use of prepolymers allows the formation of homogeneous co-monomer mixtures, that is, clear solutions. However, the reaction rates for network formation under the same conditions differ signif-

icantly, and simultaneity of formation of both networks is possible (for grafted IPN systems). The gel times for polyurethane networks are comparable to the gel times of vinyl copolymers (hard network). Provided that an appropriate set of conditions such as composition and catalyst concentrations is achieved, both networks can be forced to gel simultaneously. Although this interesting possibility has attracted considerable scientific interest (25), the present study focused mainly on synthesis and characterization of materials that exhibited improved properties with nonsimultaneous reaction rate and simultaneous gel time.

Summary and Conclusions

Grafted IPNs from castor oil polyurethane soft networks and vinyl copolymers (hard network) give more or less phase-separated morphologies. For systems where the elastomer forms particles embedded in a plastic matrix, the content of PU is < 50 wt%. The elastomer domain and vinyl copolymer domain size distributions depend on the phase separation and compatibility of composition and the relative reaction rates for both networks. However, for simultaneous IPNs the reaction rate of the polyurethane network is also an important control factor. PU-PMMA and PU-PAN IPNs exhibit broad glass transitions and flat modulus curves with increased level of molecular mixing.

Morphology studies suggest the existence of two mechanisms of phase domain formation: (1) multiple precipitation and (2) microsineresis.

The results of these studies indicate that IPNs have high strength, good resilience, and high resistance to abrasion, hydrolysis, acids, bases, salts, organic solvents, and vacuum corrosion. The IPNs can also dampen noise and vibration.

Acknowledgments

The author expresses appreciation to H. Xie of Hubei Research Institute of Chemistry and Eric J. Goethals of University of Ghent for their instruction during the research work.

References

1. Sperling, L. H.; Friedman, D. W. *J. Polym. Sci.* **1969**, *7*, 425.
2. Frisch, H. L.; Klempner, D.; Frisch, K. C. *J. Polym. Sci.* **1969**, *7*, 775.
3. Sperling, L. H.; Sarge, III, D. H. *J. Appl. Polym. Sci.* **1972**, *16*, 3041.
4. Frisch, K. C.; Klempner, D.; Mukherjee, S. K.; Frisch, H. L. *J. Appl. Polym. Sci.* **1974**, *18*, 683.
5. Sperling, L. H.; George, H. F.; Huelck, V.; Thomas, D. A. *J. Appl. Polym. Sci.* **1970**, *14*, 2815.
6. Sperling, L. H.; Mihalakis, E. N. *J. Appl. Polym. Sci.* **1973**, *17*, 3811.

7. Kim, K. C.; Klemptner, D.; Frisch, K. C. *J. Appl. Polym. Sci.* **1977**, *21*, 1289.
8. Cassidy, E. F.; Xiao, H. X.; Frisch, K. C.; Frisch, H. L. *J. Polym. Sci.* **1984**, *22*, 1839.
9. Jin, S. R.; Meyer, G. C. *Polymer* **1986**, *27*, 592.
10. Jin, S. R.; Widmaier, J. M.; Meyer, G. C. *Polymer* **1988**, *29*, 346.
11. Frisch, H. L.; Wang, L.; Huang, W. Y.; Hua, Y. H.; Xiao, H. X.; Frisch, K. C. *J. Appl. Polym. Sci.* **1991**, *43*, 475.
12. Lipatov, Y. S.; Alekseeva, T. T.; Rosovitsky, V. F.; Babkina, N. V. *Polymer* **1992**, *33*, 610.
13. Scarito, P. R.; Sperling, L. H. *Polym. Eng. Sci.* **1979**, *19*, 297.
14. Djomo, H.; Morin, A.; Damyanidu, M.; Meyer, G. C. *Polymer* **1983**, *24*, 65.
15. Kim, K. C.; Kwei, T. K.; Pearce, E. M. *Polym. Prepr. (Am. Chem. Soc., Div. Polym. Chem.)* **1987**, *28*, 177.
16. Sperling, L. H. *Sound and Vibration Damping with Polymers*; American Chemical Society: Washington, DC, 1990.
17. Tan, P.; Xie, H. *Acta Polym. Sinica* **1988**, *3*, 186.
18. Tan, P.; Xie, H. *Hecheng Xiangjiao Gongye* **1984**, *7*, 180.
19. The report of application result of IPN materials, Institute of Science Research of the Engineering Bureau of Ge Zhou Ba, China, 1987.
20. The report of experimental results of coating materials, Laboratory of Yangzen River Shipping Company, Wuhan, China, 1990.
21. Devia, N.; Manson, J. A.; Sperling, L. H. *Polym. Eng. Sci.* **1979**, *19*, 869.
22. Devia, N.; Manson, J. A.; Sperling, L. H. *Macromolecules* **1979**, *12*, 360.
23. Huelck, V.; Thomas, D. A.; Sperling, L. H. *Macromolecules* **1972**, *5*, 340.
24. Couchman, P. R.; Karasz, F. E. *J. Polym. Sci., Polym. Symp.* **1978**, *63*, 271.
25. Sperling, L. H. *Macromol. Rev.* **1977**, *12*, 141.

RECEIVED for review October 9, 1991. ACCEPTED revised manuscript November 20, 1992.

Author Index

- Alexandratos, Spiro D., 197
Allcock, H. R., 157
An, Jeong Ho, 463
André, J.-J., 143
Barrett, L. W., 489
Bauer, Barry J., 179
Beauvais, Robert, 197
Briber, Robert M., 179
Burford, R. P., 285
Carraher, Jr., Charles E., 221
Chou, Y. C., 305
Crick, Darrell W., 197
Derrough, S., 143
Dickens, Brian, 179
Dillon, Mark E., 393
Dirlikov, Stoil, 517, 539
Eschbach, F. O., 205
Frisch, H. L., 269
Frisch, K. C., 39
Frischinger, Isabelle, 517, 539
Gilmer, J. W., 489
Grady, Corinne E., 197
Guo, J. S., 557
Han, Xiaozu, 571
Holdsworth, A. K., 449
Hourston, D. J., 449
Hsieh, K. H., 427
Huang, S. J., 205
Jones, J. J., 285
Kim, Sung Chul, 463
Klempner, Daniel, 39
Lee, Doo Sung, 463
Lee, L. J., 305
Lee, S. T., 427
Liao, D. C., 427
Lipatov, Yuri S., 125
Liu, Jingjiang, 571
Liu, Wenzhong, 571
Liucheng, Zhang, 373
Ma, C. C. M., 427
Ma, Song, 405
Mai, Y.-W., 285
Manners, I., 157
Meyer, G. C., 143
Muturi, Patrick, 539
Mylonakis, S. G., 489
Narkis, Moshe, 353
Nemirovski, Naum, 353
Pandya, Bhoomin, 221
Posthuma de Boer, A., 333
Ree, Moonhor, 247
Reiff, William, 221
Ridgway, Thomas H., 221
Rouf, C., 143
Sendjarevic, Vahid, 39
Sophiea, Daniel, 39
Sperling, L. H., 3, 489
Sterling, Dorothy C., 221
Suthar, B., 39
Tan, Peiwan, 595
Tang, Xinyi, 405
Tianchang, Liu, 373
Utracki, L. A., 77
Verhoogt, H., 333
Visscher, K. B., 157
Widmaier, J.-M., 143
Wu, D. W., 427
Xie, H. Q., 557
Xiucuo, Li, 373
Yamamoto, K., 233
Yoon, Do Y., 247
Zhang, C. X., 557
Zhou, Huarong, 571
Zhou, Peiguang, 269
van Dam, J., 333

Affiliation Index

- Bio Med Sciences, Inc., 393
 Changchun Institute of Applied Chemistry, 571
 Delft University of Technology, 333
 Eastern Michigan University, 517, 539
 EniChem America, Inc., 489
 Florida Atlantic University, 221
 Hebei Institute of Technology, 373
 Hitachi Chemical Co., Ltd., 233
 Huazhong University of Science and Technology, 557
 IBM Almaden Research Center, 247
 IBM Technology Products, 247
 Institut Charles Sadron (CNRS–ULP), 143
 Jilin University, 405
 Kenya Industrial Research and Development Institute, 539
 Korea Advanced Institute of Science and Technology, 463
 Lancaster University, 449
 Lehigh University, 1, 489
 Mössbauer Spectroscopy Consultants, 221
 National Institute of Standards and Technology, 179
 National Research Council Canada, 77
 National Taiwan University, 427
 National Tsing Hua University, 427
 The Ohio State University, 305
 The Pennsylvania State University, 157
 Pohang Institute of Science and Technology, 463
 State University of New York at Albany, 269
 Sung Kyun Kwan University, 463
 Sydney University, 285
 Technion–Israel Institute of Technology, 353
 Ukrainian Academy of Sciences, 125
 University of Cincinnati, 221
 University of Connecticut, 205
 University of Detroit Mercy, 39
 University of Ghent, 595
 University of New South Wales, 285
 University of Strathclyde, 405
 University of Tennessee, 197

Subject Index

A

- AB–cross-linked copolymers
 castor oil polyurethane and poly(butyl methacrylate–divinyl benzene), 561
 copolymerization of vinyl-terminated oligomer and vinyl monomer, 572
 definition, 4
 general preparation method, 572
 schematic diagram of network, 575*f*
 structure and properties, 571–594
 synthesis, 573
 ABA block copolymers, reaction with hydroxyl-capped poly(ethylene oxide) to form simultaneous IPN, 221–232
 ABCP, *See* AB–cross-linked copolymers
 Abrasion resistance, jetting sand, 609–610
 Absorbance, internal calibration standard, 148
 Acid and base resistance, graft IPN, 610
 Acoustic absorbing materials, transitions that result from microstructures, 329
 Acoustic impedance, 45–46
 Acoustic theory, 45–48
 Acrylic acid
 dynamic mechanical properties of PEAPU–PMMA + AA ABCP, 592*f*
 Acrylic acid—*Continued*
 miscibility of PEAPU–PMMA ABCP, 591, 593
 Acrylic–epoxy bichain reaction, simultaneous interpenetrating polymer networks, morphology, 405–426
 Additive rule, large positive deviation in annealed samples, 478
 Additivity, homopolymer loss areas, 44*f*
 Adhesion
 molecular interdiffusion, 264–265
 properties of composite films, 262–265
 two-phase coatings, 550, 552
 Airborne noise, acoustic wave transmission, 46
 Allylic monomer, polymerization, 143–156
 Anisotropic domain morphology, interpenetrating polymer networks, 296
 Annealing
 determining factors, 483
 gas transport in IPN membranes, 463–485
 membranes, effect on permeability coefficient and selectivity, 477–482
 Application visualization system, three-dimensional pictures of blend morphology, 341

Affiliation Index

- Bio Med Sciences, Inc., 393
 Changchun Institute of Applied Chemistry, 571
 Delft University of Technology, 333
 Eastern Michigan University, 517, 539
 EniChem America, Inc., 489
 Florida Atlantic University, 221
 Hebei Institute of Technology, 373
 Hitachi Chemical Co., Ltd., 233
 Huazhong University of Science and Technology, 557
 IBM Almaden Research Center, 247
 IBM Technology Products, 247
 Institut Charles Sadron (CNRS-ULP), 143
 Jilin University, 405
 Kenya Industrial Research and Development Institute, 539
 Korea Advanced Institute of Science and Technology, 463
 Lancaster University, 449
 Lehigh University, 1, 489
 Mössbauer Spectroscopy Consultants, 221
 National Institute of Standards and Technology, 179
 National Research Council Canada, 77
 National Taiwan University, 427
 National Tsing Hua University, 427
 The Ohio State University, 305
 The Pennsylvania State University, 157
 Pohang Institute of Science and Technology, 463
 State University of New York at Albany, 269
 Sung Kyun Kwan University, 463
 Sydney University, 285
 Technion-Israel Institute of Technology, 353
 Ukrainian Academy of Sciences, 125
 University of Cincinnati, 221
 University of Connecticut, 205
 University of Detroit Mercy, 39
 University of Ghent, 595
 University of New South Wales, 285
 University of Strathclyde, 405
 University of Tennessee, 197

Subject Index

A

- AB-cross-linked copolymers
 castor oil polyurethane and poly(butyl methacrylate-divinyl benzene), 561
 copolymerization of vinyl-terminated oligomer and vinyl monomer, 572
 definition, 4
 general preparation method, 572
 schematic diagram of network, 575*f*
 structure and properties, 571-594
 synthesis, 573
 ABA block copolymers, reaction with hydroxyl-capped poly(ethylene oxide) to form simultaneous IPN, 221-232
 ABCP, *See* AB-cross-linked copolymers
 Abrasion resistance, jetting sand, 609-610
 Absorbance, internal calibration standard, 148
 Acid and base resistance, graft IPN, 610
 Acoustic absorbing materials, transitions that result from microstructures, 329
 Acoustic impedance, 45-46
 Acoustic theory, 45-48
 Acrylic acid
 dynamic mechanical properties of PEAPU-PMMA + AA ABCP, 592*f*
 Acrylic acid—*Continued*
 miscibility of PEAPU-PMMA ABCP, 591, 593
 Acrylic-epoxy bichain reaction, simultaneous interpenetrating polymer networks, morphology, 405-426
 Additive rule, large positive deviation in annealed samples, 478
 Additivity, homopolymer loss areas, 44*f*
 Adhesion
 molecular interdiffusion, 264-265
 properties of composite films, 262-265
 two-phase coatings, 550, 552
 Airborne noise, acoustic wave transmission, 46
 Allylic monomer, polymerization, 143-156
 Anisotropic domain morphology, interpenetrating polymer networks, 296
 Annealing
 determining factors, 483
 gas transport in IPN membranes, 463-485
 membranes, effect on permeability coefficient and selectivity, 477-482
 Application visualization system, three-dimensional pictures of blend morphology, 341

Artificial teeth, homo-IPN of poly(methyl methacrylate), 31
 Artificial tissue material, PHEMA hydrogels, 219
 Average molecular weight between cross-links, calculation, 575

B

Barrier textile, protective clothing, 403
 Batch or bulk monomer addition, morphology of three-stage latex particles, 383, 385*f*
 Biaxial expansion, definition, 395
 Bichain simultaneous interpenetrating polymer networks, morphology, 405–426
 Bicontinuous structure, latex PS–XPS systems, 363
 Bifunctional interpenetrating polymer networks (IPN), 197–203
 Bimodal behavior, elongation at break of physical blend, 364–367
 Bimodal particle size distribution, DGEBA–DDM–VR thermosets, 526
 Binary interaction parameter, calculation, 92
 Binding constants
 calculation, 200–201
 changes in the microenvironment, 199
 imidazole–acid IPN, 197
 Biocompatibility, PTFE–silicone sheets, 401
 Biodegradable PCL, applications, 206
 Biomedical devices, silicon-based IPN, 394
 Blend(s)
 incorporating block copolymers, 287–288
 size of phase domains, 254
 styrene–ethylene butylene–styrene block copolymer and poly(ether ester), 333–351
 Blend and IPN definitions, 79*t*
 Blend extruded through a convergent die, scanning electron micrograph, 116*f*
 Blend films
 dynamic mechanical relaxation behavior, 256*f*, 257*f*
 properties, 255–262
 Blend morphology
 experimental determination, 336
 variety of modification, 117
 Blend viscosity, concentration dependence, 110–112
 Block copolymers
 definition, 3–4
 immiscible block chains, 287
 in blends, 287–288
 low mixing temperature, 293
 microstructural aspects of interpenetrating polymer networks, 285–303
 morphology, 286–293
 Block lengths, miscibility between component polymers, 4

Blood oxygenation devices, perfusion membranes, 403
 Blow holes, IPN laminates, 241
 Bond interchange reactions
 castor oil, reduction in molecular weight of PET, 499
 copolymer formation, miscibility, 492
 ester–ester interchange and hydroxyl–ester interchange, 510*f*
 PET and castor oil, 511
 Bridging particles, cavitation and shear banding of small particles, 525
 Brittleness, phenolic resins, 234

C

Cahn–Hilliard theory, phase separation, 89, 92
 Castor oil
 advantages for industrial use, 596
 analysis and reactions, 491
 control of free-end content, 585–587
 free radical polymerization, 601–602
 grafted IPN, 602
 influence of time and temperature on polymerization, 603*f*
 semi-interpenetrating IPN, 602
 triglyceride-based IPN, 22–24
 use in IPN research, 490
 Castor oil and poly(ethylene terephthalate) (PET), semi-interpenetrating networks, 489
 Castor oil–polystyrene IPN,
 glass-transition temperature, 80–81*f*
 Castor oil polyurethane–acrylic IPN, room temperature cured, 557–570
 Castor oil polyurethane and poly(methyl methacrylate), formation rates, 563–564
 Castor oil polyurethane and vinyl copolymers, interpenetrating polymer networks, 595–614
 Catalyst, effect of DBTL on formation rate of IPN, 603
 Catenanes, phase morphology, 275*t*
 Cavitation
 DGEBA–DDM and DGEBA–DDS thermosets, 544
 epoxy toughening mechanism, 523
 rubbery particles at fracture surface, 523
 two-phase coatings, 551
 Cell structure, sound attenuation, 48–49
 Cellular plastic foams, sound attenuation, 48
 Cellular structure, IPN phase domains, 25*f*
 Chain extension, phase separation, 11–12
 Chain-joined ABCP, graft copolymer of unsaturated ester and styrene monomer, 572
 Chain mobility
 formation of IPN, 270
 rubbery polymers, 468
 Chain orientation, extrudate swell, 368–369
 Characterization, IPN system, 168–175

- Chemical and physical kinetics, superposition, 128–129
- Chemical blending, interpenetrating polymer blends, 335
- Chemical structure, semi-IPN, 511
- Clusters, microphase structure of IPN, 132
- Co-continuity
 asymmetric composition ranges, 344
 experimental determination, 336
 total over wide range of blend compositions, 346
 wide range of compositions, 333
- Co-continuous compositions, wide range left after annealing, 349
- Co-continuous networks, description, 19–20
- Co-continuous structure, thermoplastic polymer blend, 108
- Coalescence, convergent flow, 114
- Coarsening, later stages of phase separation, 100–102
- Coating failure, two-phase epoxy coatings, 552
- Commercial epoxy resins
 toughening, 542–549
 water absorption, 546
- Compatibility
 definition and example, 428
 interpenetration and grafting, 442–443
 molecular weight of components, 436
- Compatibilization, definition, 77
- Complex moduli, definition, 319
- Component polymers, DSC data and T_g , 169*t*
- Component ratio, effects on dynamic mechanical properties, 577–578*f*
- Component segregation
 temperature dependence, 131*f*, 132*t*
 two-phase polymer system, 130
- Composite films
 dimensional stability, 256
 dynamic mechanical relaxation behavior, 256*f*, 257*f*
 self-adhesion behavior, 262–265
- Compositional quenching process, demixing, 254
- Compression force, flexural strength of composites, 439
- Compression molding, interparticle chain penetration depth, 366
- Concavities, crack-tip propagation, 365
- Condensation cross-linking, free radical cross-linked networks, 271
- Condensation reaction, phase separation, 181
- Configurational effects, entropy, 87
- Confocal laser scanning microscopy (CLSM), computer-aided reconstruction of video images, 336
- Constrained layer dampers, engineering mechanisms, 24
- Conterminous linking, definition, 572
- Conversion profiles, polymerization, 148
- Copolymer, morphology, 285
- Copolymerization
 conversion profile, 151*f*
 conversion vs. time curves, 150*f*
 variable extent, 495
 vinyl-terminated oligomer and vinyl monomer, ABCP, 572
- Core-shell morphology
 amounts of cross-linking agent, 383
 latex particles, 381
 latex PS-XPS systems, 371
 use of water-soluble $K_2S_2O_8$ initiator, 388
- Corrosion resistance
 graft IPN, 610
 in vacuum, 611
- Crack pinning, rubber toughening mechanism, 354
- Crack resistance, two-phase epoxy coatings, 553
- Crack-tip propagation, presence of XPS particles, 365
- Craze formation, 365, 366
- Critical and off-critical mixtures, time dependence, 103*f*
- Cross-link(s)
 miscibility, 180
 morphology of an IPN, 14
 polymer miscibility, 11
- Cross-link density
 average molecular weight per cross-link, 407
 calculation, 578
 domain size, 19
 dynamic mechanical properties, 577–578*f*
 dynamic mechanical properties and miscibility of ABCP, 593
 flexural strength, 364
 gelation time, 415–420
 interpenetration and entanglement, 415–420
 PEAPU-PMMA ABCP, 575–577
 phase domain size, 15
 phase separation, 181
 scattering intensity, 183
 size of polystyrene domains, 297
 swelling of SIN, 412–415
- Cross-link level, domain size of IPN, 4
- Cross-linked components, phase separation, 474
- Cross-linked polymer(s)
 flexible, properties, 249
 nomenclature, 7
 structure and properties, 571–594
- Cross-linked polymer matrix, thermal or radiation techniques, 165
- Cross-linked PU-UPE, radical spectra, 315, 318*f*
- Cross-linked state, effect on gas transport in IPN membranes, 463–485
- Cross-linked systems, miscibility, 87
- Cross-linking
 castor oil with sulfur or diisocyanate, 558
 ^{60}Co gamma radiation, 162

Cross-linking—*Continued*
 epoxy matrix, 443
 exposure to gamma irradiation, 188
 final morphology, 597
 influence on emulsion polymerization, 383
 limit the phase separation process, 355
 silicone polymers, 396
 simultaneous crystallization, 513
 transition peaks, 440–444
 Cross-linking effect, tensile strength, 436
 Cross-linking mechanism, peroxide free radical initiator, 208*f*
 Cryosectioned bulk samples, microstructure of block copolymers, 296
 Crystalline–crystalline thermoplastic IPN, scanning electron micrograph, 115*f*
 Crystalline PET, properties required for an engineering plastic, 490
 Crystallinity
 blends and semi-IPN, 512–513
 PCL network, 217*t*
 semi-IPN morphology, 490
 Crystallization
 extent, 512–513
 melt and glassy state, 506*f*
 phase separation, 512
 poly(ethylene terephthalate), 492–494
 range broadened by addition of castor oil polyurethane, 505
 simultaneous cross-linking, 513
 Crystallization behavior, PET–castor oil–HMDI polyurethane semi-IPN, 503–508*f*
 Crystallization kinetics, PET, 489
 CTBN, ionic content and bulk price, 547*t*
 Curing
 growth in conversion degree, 129
 relevant factors, 235–240
 Curing catalyst, influence of amount, 239, 241*t*
 Cylinders
 polymer II embedded in a continuous matrix of polymer I, 18
 polystyrene, 16, 18*f*
 supporting evidence, 19
 Cylindrical domains
 SBS triblock, 293
 Solprene morphologies, 290

D

Damping
 domain size, 19
 engineering mechanisms, 24
 glass-transition temperatures of components, 597
 kinetic aspects of IPN formation, 49
 optimization, 25–28
 simplified theory, 40–45
 sound and vibration, 24–29, 39–40, 597
 Damping ability, microstructure formation, 329
 Damping materials, IPN, 46–48
 Damping performance, calculation, 42–45
 Damping properties, IPN, 569*t*
 Damping vibrations, energy transfer, 60
 DBTL catalyst, influence on degree of conversion of IPN, 605*f*
 Deformation zone, stress, 525
 Demixing
 compositional quenching process, 254
 polyimide composites, 250
 stress-related, 107
 Density
 measurement, 410
 morphological change in polystyrene IPN, 476
 PnBA–epoxy SIN, 420–424
 Density behavior, free-volume change, 476–478
 Density vs. PS content
 IPN membranes, 476*f*
 varying cross-linked state of the membranes, 477*f*, 478*f*
 Deuterium atoms, contrast in SANS, 189
 DGEBA, veronia rubber particles, rigid occlusions, 536–537
 DGEBA–DDM–VR coating cross-section, fracture surface, 549*f*–556*f*
 DGEBA–DDM–VR formulations
 fracture surfaces, 522*f*
 morphology and particle size distribution, 523*t*
 DGEBA–DDM–VR thermosets, DMA temperature dependence, 532*f*
 Dielectric properties, DGEBA–DDM and DGEBA–DDS thermosets, 546, 547*t*
 Differential scanning calorimetry, miscibility of IPN components, 168
 Diffusion coefficient
 calculation, 89
 temperature dependence, 99*f*
 Diglycidyl ether of bisphenol A (DGEBA), structure, 519
 Dimensional stability, composite films, 256
 Dispersed drops, measured vs. calculated diameters, 80*f*
 Dispersed phase diameter, calculation, 79
 Dispersed phase–matrix morphology, description, 333
 Dispersion
 drop size, 113
 simultaneous interpenetrating network, 79
 Displacement, glass-transition temperature, 169
 Dissipation factor, definition, 319
 Domain contraction, erroneous conclusion, 296
 Domain shapes and sizes, 13–22
 Domain size
 bimodal distribution, 611
 damping, 19
 interpenetrating polymer networks, 18–19
 phase-separated domains, 265
 sequential IPN, 16–17

- Domain size—*Continued*
 simultaneous IPN based on elastomeric polymers, 559
- Drop(s), deformation, 107
- Drop deformation, shear flow, 110
- Drop size
 rate of shear, 114*f*
 time dependence, 102*f*
- Dropwise monomer addition, morphology of three-stage latex particles, 383, 384*f*
- Drug delivery systems, PTFE–silicone semi-IPN, 402–403
- Drying process, phase separation, 248–249
- Dual-mechanism bifunctional polymers, sequential synthesis of IPN, 199
- Dual-phase continuity
 definition, 334
 loss area, 27*f*
 modulus behavior, 321
 supporting evidence, 19
 thermoplastic IPN, 21
 wide range of compositions, 333
- Dual-sorption model, glassy polymers, 452
- Dynamic mechanical analysis
 complex moduli or compliances, 319
 degree of phase mixing, 320
 experimental procedure, 518
 sound damping system, 607
 temperature range, 608*f*
- Dynamic mechanical properties
 ABCP and IPN, 581
 determination, 375
 IPN, 568–569
 LIPN PBA–PS, 378–380
 MMA content, 579, 580*f*
 polyurethane–epoxy composites, 440–444
 torsion braid analysis, 410
- Dynamic mechanical spectra, ABCP and IPN, 584*f*
- Dynamic mechanical spectroscopy, group contribution analysis, 43*f*

E

- Echoes, reflected from a single finite layer of material, 46*f*
- Elastic behavior, PTFE–silicone sheets, 398, 401
- Elastic energy, homogenization, 106
- Elasticity
 contributions to free energy by polymer network, 182
 formation of continuous SEBS structures, 349
 immiscibility of the IPN, 9–11
 unfavorable contribution to free energy, 11
- Elastomer(s)
 polyurethane, epoxy, and unsaturated polyester IPN, 67
 two-component polyurethane–epoxy IPN, 66
- Elastomer network, cross-linking density, 612
- Elastomeric block copolymers, strain-induced plastic-to-rubber transitions, 297
- Electron density, contrast in SANS, 189
- Electron microscopy, PTFE–silicone sheets, 399
- Electron spin resonance spectroscopy, copolymerization, 150–154
- Ellipsoids of revolution, supporting evidence, 19
- Elongation at break
 composite films, 258
 latex PS–XPS systems in tension, 364*f*
 PTFE–silicone sheets, 398
- Emulsifying agent, influence of dose on particle diameters, 378
- Emulsion effect, temperature and shear stress, 112
- Emulsion polymerization
 degree of cross-linking, 383
 three-stage, 373–389
 three-stage LIPN, experimental procedure, 374–376
- Emulsion viscosity, concentration dependence, 109*f*
- Encapsulation, steady state flow through a tube, 114
- Energy-absorbing materials, interpenetrating polymer networks, 39–75
- Energy-damping materials, IPN, 47–49
- Energy dissipation
 crack and impact resistance, 542
 mechanisms, superior toughness, 354
- Entanglements
 contribution to tensile strength, 277
 effective weight fraction, 277
 PnBA–epoxy SIN, 422–424
 polymer network formation, 269–270
- Enthalpy of fusion
 PET–castor oil semi-IPN, 507
 synthesized series of semi-IPN, 505
- Entropy, configurational effects, 87
- Entropy of mixing
 miscibility, 179
 order of magnitude, 270
- Epoxidized soybean liquid rubber compared with the effect of CTBN, 547–549
- toughening commercial epoxy resins, 542
- Epoxidized soybean oil
 commercial availability, 539
 ionic content and bulk price, 547*t*
 sodium and chloride ions, 546
 source and characteristics, 520
 structure, 520
- Epoxidized soybean rubber, polarity and miscibility, 530–531
- Epoxidized triglyceride oils, two-phase interpenetrating epoxy thermosets, 517–556
- Epoxidized vegetable oil, attempts to toughen epoxy resins, 520

- Epoxy resins
 high-performance structural composites, 427–428
 IPN mechanical properties, 599
 toughened, 542–549
- Equilibrium and nonequilibrium microphase structures, 125–139
- Equilibrium domain structure, segment molecular weight, 287
- Equilibrium thermodynamics, phase separation, 81–88
- Equilibrium water content, PHEMA hydrogels, 218
- Ethylene–propylene–diene monomer (EPDM) in combination with isotactic polypropylene (PP), commercial IPN system, 21
- Expansion phenomenon, microporous PTFE sheets, 395
- Extension ratio, calculation, 182
- Extensional dampers, engineering mechanisms, 24
- Extraction
 determination of miscible blend or copolymer, 509–511
 SEBS from polymer blend, 340, 341*f*, 344*f*
- Extrudate swell, 368–369
- Extruder, mechanical blending of two polymers, 571
- Extrusion of PTFE, process, 395
- F**
- Factice, cross-linked triglyceride, 490
- Fiber-reinforced polymeric composites
 longitudinal stress on fibers, 435
 polyurethane and epoxy interpenetrating polymer networks, 427–446
- Fibrillation, deformed drops, 114
- Fillers
 effect on IPN foams, 68
 sound-absorbing materials, 45
 sound-absorption properties, 60
 two-component polyurethane–epoxy IPN, 66
- Film(s), transport of gases, 449–461
- Film drying, phase separation, 248–249
- Filtration systems, PTFE–silicone semi-IPN, 403
- First-formed polymer, behavior, 11
- Flexibility
 reaction products of lignin and organostannane halides, 222
 two-phase coatings, 550, 552
- Flexibility groups
 examples and use, 222
 film-forming characteristics of organostannane products, 231*t*
- Flexible polyurethane and polyurethane–poly(vinyl ester) IPN foams, formulations and properties, 59*t*
- Flexural modulus, latex PS–XPS systems, 363*f*
- Flexural strength
 effect of cross-link density, 364*f*
 latex PS–XPS systems, 361–362
 length of chain segments, 440
 polyurethane–epoxy composites, 439–440
 PU–cross-linked epoxy composites, 433*t*
 PU–epoxy graft–IPN composites, 434*t*
- Flow, homogenizing effect, 106
- Flow behavior
 differences between IPB and IPN, 337
 mixing and mold-filling stage, 307
 SEBS polymer and poly(ether ester), 339*f*
- Flow type, classification, 104*t*
- Foams, two-component polyurethane and epoxy, 67–68
- Forced compatibility, IPN phase separation, 132
- Formation mechanism, simultaneous IPN, 600–603
- Fracture energy, soybean liquid rubber vs. CTBN, 547
- Fracture surfaces
 DGEBA–DDM–VR thermosets with increasing content of vernonia rubber, 522–535*f*
 SEBS–Armitel blends, 348
- Fracture toughness
 DGEBA–DDM and DGEBA–DDS thermosets, 544
 experimental procedure, 540
 phase separation, 354
 polystyrene and styrene–butadiene block copolymers, 287
- Free end, effect on properties of COPU–PBMA ABCP, 585–589*f*
- Free-end concentration, stress–strain behavior of ABCPs, 587, 588*f*
- Free energy, elastic stretching, 9
- Free energy of mixing
 concentration dependence, 135*f*
 layers of gradient IPN, 137*f*
 polymers, 596
- Free radical cross-linking, component of SIN, 271
- Free radical initiators, 211*t*
- Free radical polymerization, castor oil, 601–602
- Free volume
 concentrations of free ends, 588
 permeability in samples synthesized at low temperature, 470
- Free-volume change, density behavior, 476–478
- Free volume effect, PU and PS membrane system, 465
- Free volume–permeability coefficient relationship, IPN membrane, 469
- Freeze-drying, IPN-type molecular polyimide composite, 255

Functionalized triglyceride oils, toughness and crystallization rate of semi-IPN, 490

G

Gas permeability

experimental procedure, 454–455, 467
 latex interpenetrating polymer network films, 449–461

Gas permeation, homopolymer–copolymer blends, 453

Gas permeation and selectivity characteristics, IPN membranes, 467–470

Gas sorption, multiphase acrylic polymer, 454

Gas transport, polyurethane–polystyrene IPN membranes, 463–485

Gel formation, effects of components, 324

Gel particles, viscosity of poly(ethyl acrylate), 357

Gel point and gel content, IPN formation, 564–565

Gelation

IPN, 313–315

phase domain sizes, 14–15

relationship to phase separation, 597

Gelation sequence, IPN, 313–314

Gelation time

cross-linking density, 415–420

selected IPN varnishes, 241, 242*t*

structure, morphology, and properties of SIN, 407

vinyl content and reaction time, 564*t*

vinyl copolymers and polyurethane networks, 613

Gelled domains, role in mechanical performance, 367

Gibbs free energy of mixing

determining factors, 464

sign and magnitude, 270

Glass-fiber composites, polyurethane and epoxy interpenetrating polymer networks, 427–446

Glass IPN, phase morphology, 272–276

Glass-transition behavior

ABCP and IPN, 583

composition of SIN, 415–420

PET–castor oil–HMDI polyurethane semi-IPN, 500–503

Glass-transition temperature

composite films, 255–256

composition dependence, 81*f*

definition, 319–320

depression before cross-linking, 508

DGEBA–DDM and DGEBA–DDS thermosets, 542–544

DGEBA–DDM–VR thermosets, 525

displacement, 168

linear polymer chains found in IPN, 273*t*

Glass-transition temperature—*Continued*

miscibility, 169, 181

phase morphology of simultaneous interpenetrating polymer networks, 269–283

phase separation, evidence, 87, 88*f*

polymer alloys and blends, 80

polymer compositions, 411*t*

shifts, 7–8, 407

simultaneous IPN based on elastomeric polymers, 559

small and large rubbery particles, 528–529

sol extraction, 585

Glass transition(s), impact-resistant plastics, 19

Glassy–glassy IPN, applications, 31

Glassy polymers

dual sorption model, 452

stiff chain structures, 468

Glassy state, rapid crystallization, 512

Gradient IPN, definition, 5

Graft copolymer

blend miscibility, 453

definition, 3

unsaturated ester and styrene monomer, chain-joined ABCP, 572

Graft cross-linking, domain size, 602

Grafted chains, determine clarity or opaque appearance, 190

Grafted IPN, 179–195

castor oil, 602, 604*f*

morphology change during synthesis, 604–607*t*

polyurethane and epoxy interpenetrating polymer networks, 427–446

simultaneity problem, 612–613

Grafted semi-II IPN, TMA scan, 192*f*

Grafted semi-IPN

IR spectrum of the reaction mixture

during synthesis, 563*f*

without castor oil, 604*f*

Grafted SIPN, 561, 562

Grafting

IPN miscibility, 182

phase separation, 324

Grafting efficiency, strong phase

separation to high miscibility, 191

Grafting monomers, IPN morphology, 306–307

Grafting reactions, rubber and

polystyrene, 293

Group contribution analysis, evaluation of damping performance, 42–45

H

Hard and soft nonpolar polymers, range of possible blends, 287

Hard network

formation of IPN, 602

vinyl copolymers, 599, 611

Hard segments, effects of structures on properties of ABCP, 588–591
 Hardness, two-phase coatings, 550, 552
 Heat of mixing, polymers, 596
 Heterogeneities, cross-link concentration fluctuations, 183
 Heterogeneous state, rate of IPN chemical reaction, 464
 High-impact materials, source of superior properties, 356
 Homo-IPN, definition, 31
 Homogeneity
 determining factors, 483
 gas transport characteristics, 463
 membrane properties, 482
 permeability characteristics, 474
 Homogeneity enhancement, application of reaction conditions, 464–465
 Homogeneous nucleation, batch processes, 378
 Homogeneous state, rate of IPN chemical reaction, 464
 Homogenization mechanism, block polymers and blends, 106
 Homopolymer–copolymer blends, gas permeation, 453
 Hot water, influence on the mechanical properties of IPN, 609*f*
 Hybrid molecule, castor oil monosodium terephthalate, 505
 Hybrid systems, urethane and unsaturated polyester in one material, 306
 Hydrogel, 205
 Hydrogen bonding, effect in PEAPU–PMMA + AA ABCP, 591–593
 Hydrolysis resistance, tensile strength, 609
 Hydrophilic–hydrophobic interpenetrating and semi-interpenetrating polymer networks, 205–219
 Hydrostatic pressure, effect on miscibility, 12
 Hydroxyl-capped poly(ethylene oxide), reaction with ABA block copolymers to form simultaneous IPN, 221–232

I

Image analysis, microstructure, 297–299
 Image enhancement, distance vs. intensity, 302*f*
 Immiscibility, definition, 18
 Immiscible blends, effect of varying content on miscibility, 451
 Immiscible polymers, glass-transition temperature shift, 7–8
 Impact loading behavior, simultaneous IPN based on elastomeric polymers, 559
 Impact resistance, shear yielding and craze formation, 356
 Impact-resistant plastics, glass transitions, 19

Impact strength
 polyurethane–epoxy composites, 437–439
 two-phase coatings, 550, 552
 In situ sequential IPN, definition, 144
 Incipient microphase separation, scattering curves with prominent peaks, 188
 Initiator(s)
 in situ sequential IPN, 144
 influence on curing speed, 239, 240*f*
 influence on morphology of three-stage latex particles, 380–381
 polymerization of methyl methacrylate, 146
 synthesis of networks, 145–146
 Initiator concentration, influence on LIPN PBA–PS particle diameters, 378
 Initiator dose, influence on particle distribution width, 388
 Inorganic fillers, rigid particulate phase, 354
 Inorganic–organic polymers, syntheses of interpenetrating polymer networks, 157
 Interchange reactions, possible resulting structures, 509
 Interconnected cylinders, spinodal decomposition, 13
 Interdiffusion coefficient, calculation, 89
 Interfacial polycondensation, formation of simultaneous IPN, 221–232
 Interlayer slip, telescopic pipe flow, 115–118
 Interlayer slip parameter, temperature and shear stress, 112
 Intermediate transition peak, interface between two networks, 420
 Intermolecular interactions
 component materials, 168
 limited swelling behavior, 171–175
 phosphazene polymer and organic polymer, 169–171
 Internal fracture process, microporous PTFE sheets, 395
 Internal reinforcement, polyurethane-based IPN, 306
 Interparticle diffusion, latex PVC particles, 357
 Interparticle interaction, latex PS–XPS systems, 365–366
 Interpenetrating elastomer network, definition, 5
 Interpenetrating epoxy thermosets, two-phase, 517–556
 Interpenetrating polymer blend (IPB)
 chemical blending, 335
 formation, experimental procedure, 337–339
 physical blending, 334
 properties, 334
 Interpenetrating polymer network (IPN)
 anisotropic domain morphology, 296
 applications, 78, 328
 basic synthesis methods, 6*f*, 406
 capabilities of composite structures, 397
 castor oil polyurethane and vinyl copolymers, 595–614

Interpenetrating polymer network (IPN)—

Continued

- commercial materials, 30*t*
- composition and turbidity of pseudo-IPN, 52*t*
- definitions, 3, 7*t*, 198, 206, 305
- degree of mixing, 464
- dynamic mechanical data of pseudo-IPN, 56*t*
- dynamic mechanical spectrum, 50*f*
 - polyurethane, 53*f*–55*f*, 57*f*
- energy-absorbing materials, 39–75
- equations for estimating domain size, 16–17
- history, 32–33
- interconnected cylinders, 18
- linear blend, and pure cross-linked components, transmission electron micrographs, 278*f*–279*f*
- methods of formation, 491–492
- morphological study, 318–326
- nomenclature, 7
- nonequilibrium structure, 132–138
- overview, 3–38
- PCU–PMMA, glass-transition temperatures and tensile strength, 275*f*
- PCU–PVP, glass-transition temperatures and tensile strength, 276*f*
- phase diagrams, 12, 58*f*
- phenolics and vinyl compounds, 233–243
- PMMA–PCU, DSC spectra, 274*f*
- polystyrene and block copolymers, 288
- polyurethane-based, 28–29
- resistance to acid, base, and salt, 610*t*
- structure, 448
- studies, 49–70
- synthesis, 165–167, 573–574
- temperature, effect on miscibility, 8
- transmission electron micrographs, 324*f*–325*f*
- Interpenetration
 - hard and soft segments, Solprene, 297
 - highly phase-separated IPN, 597
 - PnBA–epoxy SIN, 420–424
- Interpenetration and entanglement, cross-linking density, 415–420
- Interpenetration effects, phase separation, 474
- Interpenetration network, longitudinal impact strength, 438
- Interpolymer complex, definition, 7
- Interstitial polymerization, vinyl monomers, 29
- Inverted core–shell morphology
 - latex particles, 381
 - use of oil-soluble AIBN as an initiator, 388
- Ion exchange resins
 - charged networks within the same suspension particle, 30–31
 - networks oppositely charged, 33
- Ion fragments
 - indulin AT–dibutyltin dichloride–PEG product, 228*t*
 - indulin AT–dibutyltin dichloride–silol product, 229*t*, 230*t*

Ion fragments—*Continued*

- reaction of organostannane dihalides with lignin and hydroxyl-capped flexibilizing agents, 226
- relative isotopic ion fragmentation, 228*t*
- tin-containing, 227*t*
- Ionic selectivity, acid–base theory, 198
- IPN, *See* Interpenetrating polymer network
- IPN compounds, applications, 306
- IPN elastomers, dynamic mechanical spectroscopy results, 70*t*, 71*t*
- IPN formation, morphological changes, 293–297
- IPN membranes, gas permeation and selectivity characteristics, 467–470
- IPN micrograph, computerized image enhancement, 301*f*
- IPN morphology, cross-link density, 198
- IPN synthesis, sequential method, 198
- IPN technology, applications, 29–31
- IPN varnish
 - DSC thermogram, 237*f*
 - materials and suppliers for preparation, 235*t*
 - measurement with various kinds of initiators, 239, 240*t*
 - preparation, 234, 236*f*
- Isocyanate-terminated prepolymer (ITP), synthesis, 573
- IUPAC Commission on Macromolecular Nomenclature, proposed nomenclature, 7
- Izod impact strength
 - polyurethane–epoxy composites, 437–439
 - PU–cross-linked epoxy composites, 432*t*
 - PU–epoxy graft–IPN composites, 433*t*

K

- Kinetics measurements, 147–149

L

- Laminate
 - appearance, 241, 242*t*
 - evaluation, 241–243
 - measurement of general properties, 239*t*
 - preparation, 235, 238*f*
 - properties, 241, 242*t*
 - time to gelation point of acrylate component, 239
- Laminate applications, phenolic interpenetrating polymer networks, 233–243
- Latex blend(s), improvements in properties, 356–358
- Latex blend membranes, permeability coefficients, 457
- Latex-interpenetrated systems, sequential emulsion polymerization method, 355

- Latex interpenetrating polymer networks
 characteristics, 355
 commercial series, 31–32
 definitions, 5, 78
 gas permeability, 449–461
 model, spheres embedded in matrix, 457–460
 PBA–PS, dynamic mechanical spectra, 378*f*
 PBA–PS–PMMA, dynamic mechanical spectra, 379*f*
 PBSM–CSS, dynamic mechanical spectra, 379*f*, 380*f*
 three-stage emulsion polymerization, 373–389
- Latex particle(s)
 competition between thermodynamic and kinetic factors, 385–386
 polymerization temperature, effect on morphology, 387*f*
- Latex particle morphology, characterization, 375–376
- Latex polystyrene–cross-linked polystyrene (PS–XPS), generated via sequential emulsion polymerization, 353
- Latex PS–XPS systems
 experimental details of polymerization, 359–360
 mechanical properties, 361–367
 mixture of the two phases by three different routes, 359*f*
 particle size, 361*f*
 sequential emulsion polymerization, 358
- Latex semi-interpenetrating polymer networks, polystyrene–cross-linked polystyrene blends, 353–371
- Latex XPS, typical formulation, 360*t*
- Lesquerella oil, triglyceride-based IPN, 23
- Ligands within polymer network, substrate-complexing properties, 202
- Lightly cross-linked IPN, 300*f*, 301*f*
- Lignin
 abundance, 221
 applications, 221–222
 reaction with organostannane dihalides to form simultaneous IPN, 221–232
- Lignin–PEG–B₂SnCl₂ and associated compounds, Mössbauer results, 231*t*
- Linear chain molecular weight, phase separation, 181
- Linear loss modulus
 methods of correcting, 27*f*
 morphology control, 25–26
- Linear thermal expansion coefficients, polyurethane–polystyrene IPN, 470
- LIPN, *See* Latex interpenetrating polymer networks
- Liquid composite molding, use of PU–UPE IPN as matrix resins, 328
- Liquid rubber, characteristics, 521
- Logarithmic permeability coefficient, polyurethane–polystyrene IPN, 470
- Longitudinal impact strength, interpenetrating network structure with one-phase matrix, 438
- Longitudinal waves, coating of solid viscoelastic polymer, 40
- Loss area
 calculation, 42–45
 dual phase continuity, 27*f*
 morphology control, 25–26
- Loss factor, function of temperature, 41*f*
- Loss modulus and storage modulus, polyurethane foams, 63*f*, 65*f*
- Loss modulus curves
 polyurethane foams, 61*f*
 PU foam compositions, 56–57, 61*f*
- Low-temperature synthesis, reduced permeability, 470

M

- Macromonomers
 characteristics, 185*t*
 homogeneity, 187
 microuniformity of samples, 188
 polymerizable end group, 189
 reactivity ratios, 190
- Matrix, co-continuous phase, 322
- Matrix resins
 IPN-based, 328
 toughening in transverse direction, 438
- Matrix toughness, interpenetrating polymer networks, 428
- Mechanical blend
 effect of varying content on miscibility, 451
 molten state, interpenetrating polymer blends, 334
 two polymers, extruder and roll mill, 571
- Mechanical drawing operations, effect on gas barrier properties, 454
- Mechanical energy absorption, IPN foams, 67
- Mechanical loss, temperature dependence, 133*f*
- Mechanical properties
 composite films, 258*t*
 cured blend films, 255–262
 PET–castor oil–HMDI polyurethane semi-IPN, 498–500
- Medical applications, PTFE–silicone semi-IPN, 402–403
- Medication, gradient IPN used for constant rate of delivery, 31
- Melt, rapid crystallization, 512
- Melt fracture, critical shear rate, 370*f*
- Membrane-moderated transdermal drug delivery systems, selectively permeable matrix, 403
- Membranes, transport of gases, 449–461
- Mesophase, nonequilibrium IPN phase, 134
- Mesophase matrix, embedded microphase regions, 134

- Metal ions, interaction with ligands, 202
- Metallic alloys, spinodal decomposition, 89
- Methacrylic-allylic interpenetrating polymer networks, 143–156
- Methacrylic radical, polymerization, 143–156
- Microelectronic devices, commercial polyimide precursor solutions, 254
- Microgels, polymeric radicals, 314
- Microheterogeneous domains, composition, 597
- Microheterogeneous morphology copolymer of PET and castor oil segments, 511
- interphase material, 24
- IPN phase domains, 25*f*
- semi-IPN, 502, 513
- spectrum of glass transitions, 612
- Microphase separation kinetic conditions of reactions, 127
- TEM micrographs, 299
- volume changes, 127
- Microphase structure, equilibrium and nonequilibrium, 125–139
- Microporous materials, expanded PTFE, 394
- Microporous membranes, 328–329
- Microporous PTFE sheets extraction of silicone, 398
- physical characterization, 395
- Microporous semi-IPN, applications, 404
- Microrheological processes, morphological changes, 336–337
- Microscopic phase separation, PEAPU–poly(acrylic ester) ABCP, 589
- Microstructure image analysis, 297–299
- interpenetrating polymer networks, 285–303
- Microsyneresis, vinyl copolymer, 612
- Miscibility broad glass transition, 171–175
- castor oil and PET, 508–512
- comparison of blends with IPN, 7–12
- comparison of systems, 10*t*
- component and hybrid properties, 175–176
- component polymers, 4
- composition of SIN, 415–420
- cross-link density and grafting, 191
- cross-linked systems, 87
- cross-links, 180
- entropy of mixing, 179
- flow-induced, 106
- free energy of mixing, 134
- full SIN and semi-SIN systems, 419
- grafted and ungrafted polymer combinations, 184
- Huggins–Flory theory, 83–84
- interpenetrating polymer networks, 282
- inward shift of glass-transition temperature, 422
- linear blends, 273–274
- newer theories, 84–85
- Miscibility—*Continued*
- PMDA–PDA blends with 6FDA–APB and BTDA–APB, 253*t*
- (PMDA–PDA)–(6FDA–APB) blends, 254*t*
- polyimide precursors, 265
- polymer–monomer combinations, 180
- polymer–polymer interactions, 85–88
- semi-IPN structure, 508–512
- simultaneous interpenetrating polymer networks, 406–407
- SIN from bichain reactions and from chain reaction–step reaction combinations, 420
- small-angle neutron scattering, 179
- stress field, 105–106
- temperature regions, 596
- three regions, 81–82
- Miscibility behavior, ternary homogeneous solutions, 252–255
- Miscibility window, blends of homopolymers with copolymers, 509
- Miscible blends development, 180–181
- relationship between permeability and composition, 449–450
- simple mixture rules for gas permeation, 468
- sorption and transport of small molecules, 451
- MMA feeding type, influence on diameter and distribution of latex particles, 376*t*, 377*f*
- MMA–VTP ratio, effect on dynamic mechanical properties, 580*f*
- Mobility enhancer castor oil, 512
- PET molding, 493–494
- Modulus behavior, prediction, 321
- Modulus of elasticity, function of temperature, 41*f*
- Moisture uptake, stress relaxation, 266
- Moisture vapor emission, PTFE–silicone sheets, 398–399
- Molecular demixing, polyimide composites, 250
- Molecular interactions between chains, nonequilibrium states, 136
- Molecular interdiffusion, high adhesion strength, 264
- Molecular interpenetration, similar gelation times and the resultant extension of chains, 560
- Molecular mixing castor oil urethane–polystyrene IPN, 558
- quasiequilibrium, 134
- Molecular recognition, shape selectivity, 198
- Molecular sieve, PTFE–silicone semi-IPN, 403
- Molecular tuning, polyphosphazene system, 159
- Molecular weight distribution, polymers, 407, 408
- Monomer(s), conversion to polymers, 408
- Monomer feed type emulsion polymerization, 383–385
- particle distribution width, 388

Morphological study, interpenetrating polymer networks, 318–326

Morphology
 ABCP and IPN, 584–586*f*
 control, 102
 experimental procedure, 518
 extrusion through a capillary, 115*f*
 flow-imposed, 113–118
 IPN, 118, 566–568
 LIPN particles, determining factors, 355
 materials, effect on manufacturing processes, 307
 PnBa–epoxy SIN, transmission electron micrographs, 424
 simultaneous IPN based on elastomeric polymers, 558–559

Morphology and particle size distribution
 DGEBA–DDM–ESR formulation, 536*t*
 DGEBA–DDS–ESR formulation, 536*t*
 DGEBA–DDS–VR formulation, 535*t*

Morphology and physicochemical properties, DGEBA–DDM–VR coatings, 548*t*

Morphology development, polymerization of IPN, 13–22

Morphology–processing relationship, interpenetrating polymer blends of a SEBS block copolymer and a poly(ether ester), 333–351

Multicomponent polymer systems
 basic combinations, 3
 damping over a narrow temperature range, 597

Multiphase polymer systems, 353–354

Multiphase polymeric mixtures, PAB and IPN, 78

Multiple necking behavior, composite films, 258

Multipolymer assemblies, nomenclature, 7

Mutual solvent, polymer mixture, 248

N

Network dominance, sequential IPN, 21

Network formation, sequence, 322

Network ratio, rate of cross-linking, 127

Network segregation, degree in each layer, 138

Newtonian plateau, entangled continuous phase behavior, 358

Nitrogen, cross-linked state and annealing, effect on permeability and selectivity, 466–482

Noise isolation, airborne and structure-borne noise, 46

Nomenclature, interpenetrating polymer networks, 7

Nonequilibrium structure
 interpenetrating polymer networks, 132–138
 thermodynamic description, 135–136

Nonequilibrium transition zone, phase separation, 134

Nucleating agents
 compared to castor oil, 503–505
 loss of effectiveness, 494
 PET molding, 493–494
 transferability to other polymers, 494

Nucleation, sodium benzoate, 512

Nucleation and growth
 kinetics of phase separation, 8
 off-critical shallow quenching into the metastable region, 97
 phase separation, 90*f*, 91*f*, 97–100

O

Oil-soluble initiator, morphology of three-stage latex particles, 380–381

Opposite charged groups, IPN morphology, 307

Optical clarity, phased separation in films, 252–254

Optical properties, PTFE–silicone sheets, 399

Organostannane dihalides
 dichlorides, reaction results for model and SIN systems, 224*t*
 product produced from reaction with lignin and hydroxyl-capped flexibilizing agents, 225*f*
 reaction with lignin to form simultaneous IPN, 221–232

Osmium tetroxide, stain for vernonia rubber, 550

Oxygen, effect of cross-linked state and annealing on permeability and selectivity, 466–482

P

Paper-based phenolic laminates, IPN varnishes, 233

Parallel flux model, permeability of incompatible two-component systems, 469

Parallel model, modulus behavior, 321

Particle size and distribution
 determination, 374–375
 DGEBA–DDM–VR thermosets, 524, 530–534
 imposition of flow, 101
 influence of monomer feeding type and initiator concentration, 376–378
 MMA feeding type, 376*t*
 number and weight average, 376*t*
 rubber content, 531–533

PEAPU–PMMA + AA ABCP, compositions and some parameters, 591*t*

PEAPU–PMMA ABCP, transition and relaxation, 581, 582*f*

Peel strength
 adhesion of IPN with steel, 610
 composite films, 262–263
 concrete IPN in different temperatures of water, 610*t*

- Percolation threshold, phase co-continuity, 110
- Perfusion membranes, blood oxygenation devices, 403
- Permeability
 gaseous molecules, 452
 immiscible polymer blend, 453
 incompatible two-component systems, parallel flux model, 469
 incorporation of graft copolymer, 453
- Permeability characteristics,
 PTFE-silicone semi-IPN, 402
- Permeability coefficient
 change in homogeneity, 465
 determining factors, 483
 polymer blend membranes, 457
 polyurethane-polystyrene IPN, 470
 relationship to separation factor, 474
 synthesis temperature and cross-linked state, 470-476
 temperature, 466
 thermal annealing, 477-482
- Permeability coefficient vs. PS content
 IPN membranes, 471*f*
 linear blend membranes, 473*f*
 semi-IPN membranes, 472*f*
 varying cross-linked state of membranes, 475*f*
- Permeation behavior of IPN, Maxwell and Bottcher theories, 457-460
- Permeation characteristics, effect of cross-linked state, 482
- Permeation data, modeling equations, 454
- PET, *See* Poly(ethylene terephthalate)
- PET and PET compositions, extent of crystallinity vs. temperature, 504*f*
- PET-castor oil-HMDI polyurethane semi-IPN
 crystallization behavior, 503-508*f*
 derivative heat flow plots, 502*f*
 glass-transition behavior, 500-503
 mechanical properties, 498-500
 peak glass-transition temperature vs. weight percentage PET, 503*f*
 peak melting temperature, 508*f*
 stress-strain curves, 498*f*, 500*f*
 tensile stress-strain calculated values, 499*f*
- PET-castor oil-HMDI urethane network semi-IPN, synthetic procedure used in production, 497*f*
- PET crystallization data, castor oil or sodium benzoate compositions, 507*t*
- PET semi-IPN, brittle when crystallized, 499
- Phase co-continuity, blends, 110
- Phase composition
 calculations based on heat capacity change, 511
 phase ratio, 137-138
- Phase continuity, swelling degree of SIN, 413, 415
- Phase demixing, polyimide composites, 250
- Phase diagrams
 interpenetrating polymer networks, 12
 multicomponent polymer materials, 13*f*
 polymer I-polymer II-monomer II, 14*t*
- Phase domain
 comparison of blends with IPN, 8
 formation
 kinetic mechanisms, 9*f*
 morphology, 611-612
- Phase inversion
 calculations, 108-112
 castor oil-polyester-polystyrene, 23*f*
 continuous rubbery phase and randomly distributed small DGEBA rigid particles, 529
 definition, 20
 DGEBA-DDM-ESR mechanism, 537
 DGEBA-DDM-VR thermosets, 523, 534-538
 epoxidized soybean rubber, 537
 isoviscous conditions, 109
 large rubbery particles, small occlusions of rigid DGEBA resin, 528
 latex PS-XPS systems, 363
 phase continuity diagram, during polymerization, 20*f*
 polymer blends, 21
 rubber content, 527-530
 shearing, 20-21
 small particles, cross-linked vegetable rubber, 528
 stirred during polymerization, 14
 two-phase coatings, 551
- Phase inversion point, viscosity ratio of the blend components, 335-336
- Phase morphology
 glass and rubber series of IPN, 272-276
 simultaneous interpenetrating polymer networks, 269-283
- Phase percolation, phase inversion process, 108
- Phase-separated biodegradable network, applications, 206
- Phase separation
 Cahn-Hilliard theory, 89, 92
 chain extension, 11-12
 cloudy appearance, 13
 conditions, 81-82
 cross-linked components, 474
 cross-linked polymers, 47
 cross-linking of the PU component, 53
 crystallization, 512
 developmental stages, 606
 DGEBA epoxy thermosets, evaluation of formulations, 521-538
 driving force, 326
 dynamics, 89-102
 excess Gibbs free energy, 270
 free energy of mixing, 129, 408
 heat of mixing, 180
 incomplete, 129-132

- Phase separation—*Continued*
introduction, 596–598
kinetics, 597
microheterogeneous morphology, 57
mismatch in solubility parameters and t_g , 273–274
modes of blending, 455
nucleation and growth followed by spinodal decomposition, 18
onset, 464
opacity of PHEMA–PCL networks, 210, 212
phase domain sizes, 14–15
polarity of components, 529–530, 533
rate, 464
reaction kinetics, 327
small angle X-ray scattering, 179
suppressed, 270
surface segregation, 264
thermodynamic immiscibility, 125
thermodynamics and kinetics, 77–124
time dependence on reaction conditions and composition of the system, 126
two-phase interpenetrating epoxy thermosets, 517–538
two-stage (condensation) polymerization, 554
variation of light scattering intensity, 94f
vernonia rubber, 536
viscosity, 385–386
- Phase structure
determination, 321
indicated by glass transition, 500
- PHEMA hydrogels, 206
- PHEMA network
characterization, 210
cross-linked, 207f
- PHEMA–PCL network
dry-state mechanical properties, 213t
mechanical properties, 218t
stress-at-break in the dry state, 213f
- Phenol–formaldehyde compositions,
phonograph records, 32
- Phenolic–epoxy equivalent ratio, influence
on curing speed, 239, 240t
- Phenolic interpenetrating polymer networks,
laminate applications, 233–243
- Phenolic laminates, applications, 233
- Phenolic resin, problematic properties, 234
- Phonograph records, phenol–formaldehyde
compositions, 32
- Physical blending, interpenetrating
polymer blends, 334
- Physicochemical parameters of SIPN, 129t
- Pinning, coarsening process, 101–102
- Plastic deformation
matrix, appearance of numerous striations, 526
matrix surrounding particles, 523
toughening mechanism, 526
- Plasticization
CO₂ in polymer blends, 453
- Plasticization—*Continued*
DGEBA–DDM–ESR formulations, 543
soybean rubber, 544
- Plastic-to-rubber transition,
strain-induced, 297
- PnBA–epoxy semi-SIN, transmission
electron micrographs, 424f
- Polar polymers, effects from secondary
valence force, 591
- Polarity
partition of DGEBA monomer, 537
phase separation of components, 529–530, 533
- Poly(butyl acrylate)–polystyrene–poly(methyl
methacrylate), three-stage emulsion
polymerization, 373–389
- Polycaprolactone (PCL), PHEMA network, 206
- Polyester or polyurethane networks,
advantages over factice, 491
- Poly(ether ester), blends with SEBS block
copolymer, 333–351
- Polyethylene blends, temperature gradient
of viscosity vs. composition, 105f
- Poly(ethylene terephthalate)
constraints on IPN formation process, 492
crystallization rate, 492–493
moldability, 492–493
- Poly(ethylene terephthalate) and castor oil,
semi-interpenetrating polymer networks,
489–516
- Poly(ethylene terephthalate)–castor oil
semi-IPN, synthesis, experimental
procedure, 495–498
- Poly(2-hydroxyethyl methacrylate) (PHEMA),
use as a biomaterial, 205–219
- Polyimide precursor blends, solid content, 254
- Polyimide semi-interpenetrating polymer
network (SIPN) composites, rodlike–flexible,
247–267
- Polyimides
applications, 248
self-adhesion behavior, 262–265
- Polymer alloy, definition, 77
- Polymer blend(s)
characterization, 251–252
definitions, 3, 77
excess heat of mixing vs. composition, 88f
mechanical loss and modulus behavior, 47f
methods of mixing, 143–144
phase inversion, 21
photographs of morphologies, 345f
rodlike–flexible, 247–267
- Polymer blend membranes, permeability
coefficients, 457
- Polymer dimensions, theories that relate
to changes, 288
- Polymer–monomer combinations, miscibility,
180
- Polymeric microenvironment, role in
complexation reaction, 202

- Polymerization
 characterized by segregation degree, 130
 cross-linked network IPN component, 180
 sequential IPN, 180
- Polymerization kinetics, differences in
 morphology and properties, 189
- Polymerization of monomers, refractive
 index of the reaction medium, 146
- Polymerization process, transmission
 electron micrograph, 15*f*, 16*f*
- Polymerization temperature, influence on
 emulsion polymerization, 385–386
- Polymers, basic combinations, 4*f*
- Poly(organophosphazene)
 derivatives, 159
 interpenetrating polymer networks,
 synthesis and characterization, 157–178
 physical properties and applications,
 158–159, 161
 shock-absorbing denture liner, 162*f*
 synthesis, 159, 161–165
- Polyphosphazene(s), physical properties, 157
- Polyphosphazene–organic polymer IPN,
 specific descriptions, 171–175
- Polystyrene
 interconnected cylinders, 16, 18*f*
 PS content, effect on permeability
 coefficient, 474
 transparent modified grades, 287
- Polystyrene blends, morphologies, 17*f*
- Polystyrene–cross-linked polystyrene
 blends, latex semi-interpenetrating
 polymer networks, 353–371
- Poly(tetrafluoroethylene)
 applications, 393–394
 interpenetrating polymer networks, 393–404
 molded and sintered, 395
 physical characterization, 394–395
- Polyurethane(s)
 effects on formation of acrylic phase, 29
 improvement of physical properties, 305–306
- Polyurethane and epoxy interpenetrating
 polymer networks, glass-fiber
 composites, 427–446
- Polyurethane and IPN foams, formulation, 72*t*
- Polyurethane and polyurethane–epoxy IPN
 foams, properties, 72*t*
- Polyurethane-based IPN, methods of
 synthesis, 28–29
- Polyurethane elastomers, homogeneous
 comonomer mixtures, 612
- Polyurethane–epoxy IPN elastomers,
 formulations, 69*t*
- Polyurethane–epoxy–unsaturated polyester
 IPN elastomers, formulations, 70*t*
- Polyurethane–epoxy–unsaturated polyester
 two- and three-component IPN, 62–70
- Polyurethane formation, kinetic
 curves, 128*f*
- Polyurethane–modified epoxy system
 effect of matrix properties on mechanical
 properties of composites, 428–429
 experimental procedure, 429–432
- Polyurethane network, formation in
 presence of individual reagents, 601, 602
- Polyurethane network and poly(methyl
 methacrylate) grafts, 562–569
- Polyurethane network polymers, formation
 in the presence of vinyl polymers, 600
- Polyurethane–polyepoxide IPN, permeability
 coefficient, 465
- Polyurethane–polystyrene IPN membranes,
 gas transport, 463–485
- Polyurethane–poly(vinyl chloride)
 semi-IPN, 49–54
- Polyurethane–poly(vinyl ester) hybrid-IPN
 foams, 54–62
- Polyurethane soft network, formation
 mechanism, 612
- Polyurethane–unsaturated polyester IPN,
 kinetic, rheological, and
 morphological changes, 305–331
- Poly(vinyl methyl ether), interaction
 parameter vs. temperature, 86*f*
- Post-mixing relaxation, morphological
 changes, 336–337
- Power law relations, scattering intensity, 101
- PPGPU–PMMA ABCP, phase components, 587*t*
- Precursor film, stress level, 259
- Preferential migration, styrene monomer, 293
- Pressure–composition phase diagram,
 polymerization, 12, 13*f*
- Price difference, soybean liquid rubber
 vs. CTBN, 549
- Processing conditions, morphology and
 physical properties of IPN, 306
- Protective clothing, barrier textile, 403
- Pseudo-IPN, physical and chemical
 properties, 394
- PTFE, *See* Poly(tetrafluoroethylene)
- PTFE–silicone semi-IPN
 drug delivery systems, 402–403
 filtration systems, 403
 medical applications, 402–403
 molecular sieve, 403
 wound dressing, 402
- PTFE–silicone sheets, physical properties,
 398–399
- PU gelation
 effect of styrene or UPE, 313*t*
 effect of UPE components, 313
- PU–PMA IPN
 dynamic mechanical properties, 568*f*
 micrographs, 567*f*
- PU–P(S–MMA), conversion to grafted IPN,
 604*f*
- PU–UPE IPN, reaction mechanism and
 structure, 312*f*

Q

- Quasiequilibrium
 independent phases, 138
 IPN and molecular level of mixing, 125
 microheterogeneous two-phase system, 134
 microphase structure of IPN, 134

R

- Radiation cross-linked system, miscibility, 11
 Radical(s), 151, 152
 Radical chain growth polymerizations, UPE
 gelation, 314
 Radical concentrations of PU-UPE,
 cross-linked and linear, 315, 319f
 Radical spectra, related to gelation, 314–315
 Reaction injection molding, morphology and
 physical properties of IPN, 306
 Reaction kinetics, effect on manufacturing
 processes, 307
 Reaction mechanisms, in situ IPN, 144
 Reactivity, UPE resins, 315–317
 Reactivity ratios, uniformity of copolymers, 188
 Refractive index
 measurements, selectivity of
 free-radical initiators, 146–147
 methyl methacrylate, 147f
 Repulsive interactions, source of
 miscibility, 86–87
 Residual stress behavior, composite films,
 258–261f
 Resin, entropy of mixing, 536
 Rheogoniometry, steady shear in cone and
 plate geometry, 368f
 Rheological considerations, phase
 separation, 102–118
 Rheological properties, latex PS-XPS
 systems, 367–370
 Rheology
 manufacturing processes, 307
 storage shear modulus vs. temperature, 104f
 thermodynamics, 105–108
 Ripening process, imposition of flow, 101
 Rodlike and semirigid polyimides, chemical
 structures, 249f
 Rodlike-cross-linked flexible polyimide
 SIPN composites, miscibility and
 properties, 247–267
 Rodlike-flexible polyimide composites,
 schematic representation, 250f
 Roll mill, mechanical blending of two
 polymers, 571
 Rubber content
 DGEBA particle size, 534
 particle size, 531–533
 phase inversion, 527–530
 Rubber IPN, phase morphology,
 272–276

- Rubber modification, employed to toughen
 polymers, 354
 Rubber-modified thermosets
 DMA lower and higher temperature
 transitions, 543f
 soybean particle size distribution, 543f
 Rubber plateaus, network structure, 576
 Rubber-toughened plastic, invention, 32
 Rubbery polymers, chain mobility, 468

S

- Salami-type morphology, DGEBA-DDM-VR
 thermosets, 524
 SAXS and SANS, difference between the two
 techniques, 189
 Scattering, calculation, 182
 Scattering intensity
 calculated, 185
 grafted and ungrafted semi-II IPN, 187f
 grafted semi-II IPN, 188f
 time dependence, 101f
 SEBS and poly(ether ester)
 interface, 346f
 SEM micrographs of blends after triple
 extrusion, 347f
 SEBS-Arnitel blends, SEM micrographs,
 342f, 343f
 Secondary valance force, effects in polar
 polymers, 591
 Seed latex
 polymerization process, 358
 polystyrene, 353
 Seed particles, hydrophobic initiator, 381
 Seeded emulsion polymerization,
 three-stage, 373–389
 Segregation degree, function of reaction
 conditions, 138
 Self-adhesion
 composite films, 262–265
 molecular interdiffusion, 264–265
 surface composition, 263–266
 Semicrystalline PET, properties
 required for an engineering plastic,
 490
 Semi-II IPN, TMA scan, 193f
 Semi-interpenetrating polymer networks,
 393–404
 castor oil, 602
 castor oil polyurethane and cellulose
 nitrate, 561
 chemical structure, 511
 definitions, 6, 78–79, 206, 508
 formation mechanism, 513
 morphology, 356
 physical and chemical properties, 394
 synthesis, 207–208
 ultrathin sections, 298f–299f

- Semi-interpenetrating polymer networks and simultaneous IPN in the swollen state, 217–218
- Semipermeable membranes, PTFE and silicones, 394
- Separation factor
change in homogeneity, 465
definition, 468
permeability coefficient, 474
synergistic effect with increasing polystyrene content, 469
synthesis temperature and cross-linked state, 470–476
thermal annealing, 477–482
- Separation factor vs. PS content
IPN membranes, 471*f*
linear blend membranes, 473*f*
semi-IPN membranes, 472*f*
varying cross-linked state of the membranes, 475*f*
- Sequential emulsion polymerization
latex-interpenetrated systems, 355
latex PS–XPS systems, 358
- Sequential formation, interpenetrating polymer networks, 491–492
- Sequential initiation of monomers, two distinct networks, 145–146
- Sequential IPN
castor oil-based polyurethane and various polyacrylates, 560
definition, 5, 77–78
dry state, mechanical properties, 214–217
formation, 180
mechanical properties, 214*t*
morphology, 198
synthesis, 208, 209*f*, 289
- Series model, modulus behavior, 321
- Shape selectivity, polymerizing monomers around a template, 197
- Shear deformation, matrix surrounding particles, 523
- Shear flow, deformation of dispersed drops, 110
- Shear plateau modulus of an elastomer, calculation, 576
- Shear rate
effect of viscosity, 367
onset of melt fracture, 370
- Shear stress, PTFE ability to fuse and coalesce at room temperature, 395
- Shear viscosity
concentration dependence, 112*f*, 113*f*
dynamic and capillary, 117*f*
measurement conditions, 117
SEBS polymer and poly(ether ester), 339, 340*f*
- Shearing, 20–21
- Side groups, phosphazene polymers, 159
- Silent paint, 48
- Silicone(s)
extraction studies, 398
- Silicone(s)—*Continued*
history, 394
interpenetrating polymer networks, 393–404
- Silicon-containing SIN products, infrared band assignments, 226*t*
- Silicone elastomers, 396–397
- Simultaneous formation, interpenetrating polymer networks, 491–492
- Simultaneous interpenetrating polymer networks
castor oil, TDI, and vinyl or acrylic monomer without cross-linking agent, 561
castor oil-based polyurethane and divinyl benzene–styrene copolymer, 560
castor oil polyurethane and cross-linked poly(methyl methacrylate), 560
castor oil polyurethane and poly(butyl methacrylate–divinyl benzene), 561
definitions, 5, 78
derived from reaction of organostannane dihalides with lignin and hydroxyl-capped poly(ethylene oxide) and ABA block copolymers, 221–232
elastomeric polymers, synthesis, 558
kinetics of formation, 130*f*
phase morphology, 269–283
radical copolymerization of liquid prepolyesters, 560
synthesis, 208–210
synthesized by two chain reactions, 405–426
synthesized from castor oil polyurethane and copolymers of vinyl monomers, 559–560
synthetic methods, 409–411
synthetic routes and extent of miscibility, 406
- Simultaneous polymerization, definition, 143
- SIN, *See* Simultaneous interpenetrating polymer networks
- Sintered poly(tetrafluoroethylene), amorphous structure, 394
- SIPN, *See* Semi-interpenetrating polymer networks
- Small-angle neutron scattering, plots, 183*f*
- Sodium and chlorine content
DGEBA–DDM and DGEBA–DDS thermosets, 546
soybean liquid rubber vs. CTBN, 549
- Soft network
formation of IPN, 602
polyurethane, 611
polyurethane formed from castor oil and TDI, 599
- Sol, effects in PPGPU–PST ABCP, 585
- Sol extraction
dynamic mechanical properties of ABCP samples, 585
effect on PPGPU–PMMA ABCP, 587*f*

- Sol fraction, interphase miscibility of
PPGPU–PST ABCPs, 593
- Solprene
morphology, 289–293
transmission electron microscopy, 290*f*–292*f*
ultrathin section, 294*f*–296*f*
- Solubility parameters
linear polymer chains found in IPN, 273*t*
phase morphology of SInS, 269–283
- Solvent, effect on IPN, 611*t*
- Sound-absorbing foams, mechanism, 45
- Sound absorption
IPN foams, 67–68
parallel to foam rise, 49*f*
polyurethane:epoxy ratio, 73*f*
solid elastomers, 40
- Sound absorption coefficients
effect of chemical structure, 60*f*
polyurethane foam(s), 62*f*, 64*f*, 66*f*
polyurethane foam compositions, 56–57, 60*f*
- Sound absorption measurement, properties
of foam, 50*t*
- Sound and vibration damping
IPN, 24–29
research teams, 26*t*
viscoelastic nature of polymers, 39–40
- Sound attenuation
IPN morphology, 59–60
mechanisms, 39–40
- Sound power transmission coefficient,
calculation, 45
- Soybean liquid rubber
dielectric properties, 546
toughening effect, 545
- Spherical concavities, crack-tip
propagation, 365
- Spinodal decomposition
appearance of two similar phases, 127
calculation, 93–95
initial rates, 100*f*
interconnected cylinders, 13
phase separation, 90*f*, 91*f*
scattering pattern from phase separation of a
polybutadiene–polystyrene blend, 93*f*
variation of scattering intensity, 95*f*
- Spinodal decomposition kinetics, phase
separation, 8
- Spinodal decomposition process,
competition with the compositional
quenching process, 254–255
- Spinodal temperature, planar flow strain
effect, 106*t*
- Spinodal values, grafted and nongrafted
polymer vs. polydispersity index, 184*f*
- Spontaneous cross-links, soybean liquid
rubber vs. CTBN, 549
- Stiff chain structures, glassy polymers, 468
- Strain at break
sequential IPN, 217*f*
- Strain at break—*Continued*
sequential IPN synthesis, 215–216
swollen SIPN, 218
- Strain at yielding, sequential IPN, 217*f*
- Strain behavior, composite films, 257–262
- Strain compatibilization, steady-state stress, 106
- Strain-induced plastic-to-rubber transitions,
elastomeric block copolymers, 297
- Strength reinforcement, latex PS–XPS
systems, 365
- Stress, deformation zone, 525
- Stress at break
cross-linked PCL particulate-filled
composites, 214
nonadhering composites, 212
sequential IPN, 215*f*
swollen SIPN, 218
- Stress behavior, polyimides and their
composite films, 266
- Stress field, response of heterogeneous
systems, 105–106
- Stress intensity factor, DGEBA–DDM and
DGEBA–DDS thermosets, 544*t*
- Stress relaxation, 261–262
- Stress resistance, two-phase epoxy coatings, 553
- Stress-resistant coatings, two-phase epoxy
thermosets, 549–553
- Stress–strain behavior, simultaneous IPN
based on elastomeric polymers, 559
- Stress–strain curves, PU–P(S–MMA–AN)IPN,
599, 601*f*
- Stress–strain properties, PU–epoxy matrix,
432–437
- Stress–temperature behavior, composite
films, 257–262
- Structural heterogeneity, thermodynamic
immiscibility, 126
- Structural re-formation, orientation of
elastomer segments, 297
- Structure factor, determination, 92–93
- Styrene
influence on PU gelation, 313
swollen cross-linked block copolymer, 293
- Styrene–butadiene block copolymers, hard
and soft segments, 287
- Styrene–divinylbenzene–poly(butyl
methacrylate) network copolymer, phase
diagrams, 127*f*
- Styrene–ethylene butylene–styrene (SEBS)
block copolymer, blends with
poly(ether ester), 333–351
- Substrate recognition, ligand ratios in
bifunctional IPN, 202
- Substrate-selective reagents, bifunctional
network, 199
- Supermolecular flow unit, mechanism, 357
- Surface chemistry, PTFE–silicone sheets,
399–402
- Surface composition, composite films, 262–265

Surface imperfections, cross-linked polystyrene, 33
 Surface segregation, high adhesion strength, 264
 Sustained release devices, semipermeable materials, 403
 Swelling behavior, 411–415
 Swelling ratios, latex PS–XPS systems, 368–369
 Synergistic effect
 forced compatibility of components, 557
 properties of IPN, 306
 Synergistic toughening effect, bimodal particle size distribution, 526
 Synthesis temperature, effect on permeability coefficient and separation factors, 470
 Synthetic method, structure and properties of IPN, 603

T

Teflon, *See* Poly(tetrafluoroethylene)
 Temperature
 influence on conversion to linear polymer, 606f
 influence on gel content of the network, 605f
 Temperature transition, active frequency range of damping, 24
 Template polymerization, selectivity based on size, 197
 Tensile elongation, significant crazing, 366
 Tensile modulus
 cross-linked PCL particulate-filled composites, 214
 latex PS–XPS systems, 363–364
 particulate-filled composites, 212
 sequential IPN, 216f
 swollen SIPN, 218
 Tensile properties, DGEBA–DDM and DGEBA–DDS thermosets, 545
 Tensile strength
 cross-linking structure, 436
 effect of different IPN compositions, 565–566
 hot water, 609
 IPN in S–MMA–AN tercopolymer, 599
 latex PS–XPS systems, 361–362
 maximum, 276–282
 polyurethane content in matrix, 435
 PTFE–silicone sheets, 398, 401
 PU–cross-linked epoxy composites, 432t
 PU–epoxy graft–IPN composites, 433t
 PU–epoxy matrix, 434f, 435f
 transverse direction, 436–437
 Tensile strength to break vs. weight percent PPO, 282f
 Tensile stress to break, pure network components, 280
 Tension force, flexural strength of composites, 439
 Tenter frame, extrusion of PTFE, 395
 Thermal annealing, effect on permeability coefficient and selectivity, 477–482
 Thermal characterization, sequential IPN synthesis, 216
 Thermal curing, phase-separated domains, 255
 Thermal imidization
 rodlike–flexible polyimide composites, 248
 stress level of precursor film, 259
 Thermal polymerization of DACBA, spectra, 151
 Thermal properties, effect of macromonomers, 191
 Thermal stability, soybean liquid rubber vs. CTBN, 549
 Thermodynamic immiscibility
 development, 126–128
 phase separation, 125
 Thermodynamics
 influence on rheology, 103–105
 IPN, 182
 Thermoplastic elastomers, definition, 286
 Thermoplastic interpenetrating polymer networks, definition, 334
 Thermoplastic IPN
 chemically blended, 21
 definition, 5–6, 78
 mechanically blended, 21
 patents, 22f
 Thermoplastic matrix, individual embedded inclusions, 365
 Thermoset(s), rigid DGEBA epoxy matrix and vegetable rubbery particles, 517–538
 Thermoset polymers, preparation methods, 572
 Thin films, images from cryosectioned bulk samples, 285
 Three-stage latex interpenetrating polymer networks (LIPN), 373–389
 Three-stage latex particles, influence of initiators on morphology, 380–381
 Tin-containing materials
 ion fragments, 227t–230t
 Mössbauer spectroscopy, 226
 Torsion braid analysis, dynamic mechanical properties, 410
 Toughened plastics, characteristics, 558
 Toughened polymer, changes in properties, 354
 Toughening, commercial epoxy resins, 542–549
 Toughening mechanisms, 526
 Transition peaks, cross-linking, 440–444
 Transition zone, nonequilibrium IPN phase, 134
 Transmission electron microscopy
 adequate transparency and contrast, 289
 image contrast between phases, 289
 Transparency
 phased separation in films, 252–254
 very small domain size, 464
 Transport behavior, gaseous molecules, 452
 Transport properties, multiphase acrylic polymer, 454

- Transverse tensile strength, composites, 436–437
- Trapped radicals, microgels, 314
- Triglyceride oil(s), functionalized, 490
- Triglyceride oil IPN
 - description, 22–24
 - naturally functionalized, 490–492
- Tung oil, flexibilizer for phenolic laminates, 234
- Turbines, corrosion resistance, 611
- Two-component systems, construction of
 - phase diagram, 82*f*
- Two-phase epoxy coatings
 - model studies, 550
 - stress-resistant, 549–553
- Two-phase epoxy thermosets
 - physicomechanical properties, 555
 - preparation, 518
 - two-stage addition polymerization, 554
- Two-phase interpenetrating epoxy thermosets
 - epoxidized triglyceride oils, 517–556
 - epoxidized vegetable liquid rubbers, 521
 - preparation, 520–521
- Two-stage polymerization, 355–356

U

- Ultimate mechanical properties of IPN, 599, 600*r*
- Uniaxial tensile test, experimental
 - procedure, 540–541
- UPE, influence on PU gelation, 313
- UPE blends and IPN, DSC isothermal runs, 322*f*–323*f*
- UPE cross-linking reaction, polymeric radicals, 314
- UPE gelation
 - effect of MDI, 311*t*
 - effect of PU components, 310–313
 - radical chain growth polymerizations, 314
- UPE–MDI blends
 - DSC isothermal runs, 320*f*
 - kinetic study, 315–317
- UPE network formation, cross-linked and linear PU–UPE IPN, 319*f*
- UPE resins, 310, 311*f*
- UPE with 1% DMB, radical concentration profile and radical spectra, 316*f*–317*f*
- Urethane and amide linkages, formation between functional end groups, 324

V

- Varnishes
 - curing time, 234–243
 - materials and suppliers for preparation, 235*t*
 - phenolic IPN, 233, 234
- Vascular grafts, prosthetic or bypass applications, 403

- Vegetable liquid rubber, characteristics, 521
- Vegetable rubber, epoxidized, 517
- Vegetable rubbery particles, thermosets, 539
- Vegetable rubbery phase, two-phase epoxies, 539
- Vernonia liquid rubber, homogeneous cross-linked rubber, 527
- Vernonia oil
 - combined with PET to make semi-IPN, 491
 - ionic content and bulk price, 547*t*
 - source and characteristics, 520
 - structure, 519
 - triglyceride-based IPN, 23
- Vernonia phase, stainability, 550
- Vernonia rubber
 - fracture surface of DGEBA–DDM–VR thermosets, 522–535*f*
 - glass-transition temperatures, 525
 - phase separation, 536
 - polarity and miscibility, 530
 - solubility in matrix, 530
- Vibration damping, solid elastomers, 39–40
- Vibration-damping polymers, maximizing properties, 42
- Vinyl and castor oil polyurethane copolymers, interpenetrating polymer networks, 595–614
- Vinyl monomers, hard segments of ABCPs after copolymerization with VTPs, 588
- Vinyl-terminated prepolymer, synthesis, 573
- Viscoelastic foams, energy absorption, 40
- Viscoelastic polymer, damping, 29–30
- Viscosity
 - dropwise or batch addition, 383–385
 - kinetics of phase separation, 385–386
 - shear rate, 367
- Viscosity–composition curve, interlocked morphology of polymer blends, 337
- Viscosity–concentration behavior, 108
- Viscosity ratio, phase inversion, 108
- Voids, formation in thermosets, 523
- Volume contraction, varying content of blends, 452
- Vulcanization, silicone polymers, 396

W

- Water absorption, DGEBA–DDM and DGEBA–DDS thermosets, 546
- Water barrier effectiveness, PTFE–silicone sheets, 398–399
- Water-soluble initiator, 380–381
- Water uptake, composite films, 262
- Wave propagation, coating of solid viscoelastic polymer, 40
- Weatherability, soybean liquid rubber vs. CTBN, 549
- Wicking, PTFE–silicone semi-IPN, 402

Window of miscibility,
homopolymer-copolymer blends, 86
Wound-care systems, PTFE-silicone
semi-IPN, 402

Young's modulus
DGEBA-DDM and DGEBA-DDS thermosets,
545*t*
soybean liquid rubber vs. CTBN, 547

Y

Yield stress, interrelation between
morphology and flow, 113
Yielding behavior, composite films, 257-262
Yielding strain, sequential IPN synthesis,
215-216

Z

Zero angle scattering, calculation, 182
Zinc and rubber fillers, effect on sound
absorption coefficients, polyurethane
foams, 67*f*